RADIOLOGY AND ONCOLOGY

vol.60 no.3
september 2026

RADIOLOGY AND ONCOLOGY

September 2026
Vol. 60 No. 3
Pages 307-470
ISSN 1318-2099
UDC 616-006
CODEN: RONCEM
eISSN: 1581-3207

Publisher
Association of Radiology and Oncology

Aims and Scope
Radiology and Oncology (ISSN 1318-2099) is a multidisciplinary journal devoted to the publishing original and high-quality scientific papers and review articles, pertinent to oncologic imaging, interventional radiology, nuclear medicine, radiotherapy, clinical and experimental oncology, radiobiology, medical physics, and radiation protection. Papers on more general aspects of interest to the radiologists and oncologists are also published (no case reports).

Editorial office
Radiology and Oncology
Zaloška cesta 2
P. O. Box 2217
SI-1000 Ljubljana
Slovenia
Phone: +386 1 5879 369
Phone/Fax: +386 1 5879 434
E-mail: gsersa@onko-i.si

The publication of the journal Radiology and Oncology is financially subsidized by Slovenian Research and Innovation Agency (ARIS).

Reader for English
Vida Kološa

Secretary
Mira Klemenčič, Zvezdana Vukmirović, Vijoleta Kaluža, Uroš Kuhar

Design
Monika Fink-Serša, Samo Rovan, Ivana Ljubanović

Layout
Matjaž Lužar

Printed by
Tiskarna Ozimek, Slovenia

Published quarterly in 300 copies

Beneficiary name: DRUŠTVO RADIOLOGIJE IN ONKOLOGIJE
Zaloška cesta 2
1000 Ljubljana
Slovenia

Beneficiary bank account number: SI56 02010-0090006751
IBAN: SI56 0201 0009 0006 751
Our bank name: Nova Ljubljanska banka, d.d.,
Ljubljana, Trg republike 2,
1520 Ljubljana; Slovenia

SWIFT: LJBASI2X

Subscription fee for institutions EUR 100, individuals EUR 50

Indexed and abstracted by:

- *Baidu Scholar*
- *Case*
- *Chemical Abstracts Service (CAS) - CAplus*
- *Chemical Abstracts Service (CAS) - SciFinder*
- *CNKI Scholar (China National Knowledge Infrastructure)*
- *CNPIEC - cnpLINKer*
- *Dimensions*
- *DOAJ (Directory of Open Access Journals)*
- *EBSCO (relevant databases)*
- *EBSCO Discovery Service*
- *Embase*
- *Genamics JournalSeek*
- *Google Scholar*
- *Japan Science and Technology Agency (JST)*
- *J-Gate*
- *Journal Citation Reports/Science Edition*
- *JournalGuide*
- *JournalTOCs*
- *KESLI-NDSL (Korean National Discovery for Science Leaders)*
- *Medline*
- *Meta*
- *Microsoft Academic*
- *Naviga (Softweco)*
- *Primo Central (ExLibris)*
- *ProQuest (relevant databases)*
- *Publons*
- *PubMed*
- *PubMed Central*
- *PubsHub*
- *QOAM (Quality Open Access Market)*
- *ReadCube*
- *Reaxys*
- *SCImago (SJR)*
- *SCOPUS*
- *Sherpa/RoMEO*
- *Summon (Serials Solutions/ProQuest)*
- *TDNet*
- *Ulrich's Periodicals Directory/ulrichsweb*
- *WanFang Data*
- *Web of Science - Current Contents/Clinical Medicine*
- *Web of Science - Science Citation Index Expanded*
- *WorldCat (OCLC)*

This journal is printed on acid- free paper

On the web: ISSN 1581-3207
https://reference-global.com/journal/RAON
http://www.radioloncol.com

contents

experimental oncology

clinical oncology

review

Non-thermal ablation and drug delivery by electroporation: expanding current indications beyond cancer and cardiac treatment

Damijan Miklavcic[1], Helena Cindric[1], Rafael V Davalos[2], Frederic Deschamps[3], Julie Gehl[4,5], Bor Kos[1], Peter Kramar[6], Dimitrij Kuhelj[7,8,9], Martijn R Meijerink[10], Declan Soden[11], Miha Stabuc[7], Gregor Sersa[8,12]

[1] University of Ljubljana, Faculty of Electrical Engineering, Ljubljana, Slovenia
[2] Department of Biomedical Engineering, Georgia Tech – Emory University, Atlanta, United States
[3] Department of Anaesthesia, Surgery and Interventional Procedures (DACI), Gustave Roussy, Villejuif, France
[4] Centre for Experimental Drug and Gene Electrotransfer (C*EDGE), Department of Clinical Oncology and Palliative Care, Zealand University Hospital, Roskilde, Denmark
[5] Department of Clinical Medicine, Faculty of Health and Medical Sciences, University of Copenhagen, Copenhagen, Denmark
[6] SIQ | Slovenian Institute of Quality and Metrology, Ljubljana, Slovenija
[7] Clinical Institute of Radiology, University Medical Centre Ljubljana, Ljubljana, Slovenia
[8] University of Ljubljana, Medical Faculty, Ljubljana, Slovenia
[9] University of Novo mesto, Faculty of Health Sciences, Novo mesto, Slovenia
[10] Department of Radiology and Nuclear Medicine, Amsterdam University Medical Centre, Amsterdam, Netherlands
[11] Mirai Medical, Galway, Ireland
[12] Department of Experimental Oncology, Institute of Oncology Ljubljana, Ljubljana, Slovenia

Radiol Oncol 2026; 60(3): 307-322.

Received 17 June 2026
Accepted 13 July 2026

Correspondence to: Prof. Damijan Miklavčič, Ph.D., University of Ljubljana, Faculty of Electrical Engineering, Ljubljana, Tržaška c 25, SI-1000 Ljubljana, Slovenia. E-mail: damijan.miklavcic@fe.uni-lj.si

Disclosure: Damijan Miklavčič is a retained consultant for Medtronic and receives research funding from Medtronic. In addition, he received consulting fees from Inomagen Therapeutics and speakers' honoraria and travel/accommodation compensation from Boston Scientific, Johnson&Johnson Medtech and Field Medical. Rafael Davalos has research funding from startup companies and Angiodynamics. He received speaker/consulting honoraria or travel support from Biosense-Webster, Angiodynamics, and Boston Scientific. Bor Kos is a retained consultant for Medtronic and received research funding from RadioClash. Gregor Serša received travel grants from IGEA. All other authors declare no conflicts of interest.

Background. Electroporation-Based Treatments and Therapies (EBTTs) – electrochemotherapy, irreversible electroporation, pulsed field ablation, and gene electro-transfer – use short, high-voltage electric pulses to permeabilize cell membranes, enabling non-thermal tissue ablation and enhanced local drug delivery. Although EBTTs have been used clinically for over three decades, primarily in oncology, their adoption remains limited compared to thermal ablation modalities. In contrast, cardiac pulsed field ablation (PFA) has seen rapid adoption since the first FDA device approval in December 2023.

Conclusions. This expert opinion paper reviews the current clinical landscape of EBTTs in oncology and cardiac arrhythmia treatments, and focuses on emerging non-oncological and non-cardiac applications, including endoscopic pulsed electric field therapy for type 2 diabetes, bronchial rheoplasty for chronic bronchitis, bleomycin electrosclerotherapy for vascular malformations, nanosecond PFA for benign thyroid nodules, and electroporation-mediated gene delivery – and identifies key barriers to wider adoption: insufficient randomized evidence, lack of validated treatment planning tools, fragmented reimbursement, and limited standardization. We outline measures to facilitate clinical translation.

Key words: electroporation; pulsed field ablation; electrochemotherapy; irreversible electroporation; gene electrotransfer.

Introduction

Electroporation is a biophysical phenomenon in which the application of short, high-voltage electric pulses disrupts the lipid bilayer of the cell membrane. Depending on pulse parameters, namely amplitude, duration, number, and repetition rate, the effect is either reversible or irreversible.[1] This allows for a family of clinically distinct treatment modalities. In electrochemotherapy (ECT), reversible electroporation potentiates the cytotoxic effect of chemotherapeutic agents such as bleomycin and cisplatin, increasing their intracellular uptake by orders of magnitude.[2,3] In a similar manner, gene electro-transfer (GET) facilitates intracellular delivery of therapeutic nucleic acids.[4,5] In irreversible electroporation (IRE) ablation, the cell membrane is disrupted, causing irreversible cell damage through a predominantly non-thermal mechanism, while preserving the extracellular matrix, vascular scaffolding, and critical anatomical structures.[6,7] The same physical principle, when applied as pulsed field ablation (PFA) via intracardiac catheters, now constitutes the fastest-growing treatment modality in cardiac electrophysiology for the treatment of atrial and ventricular fibrillation.[8,9]

Electroporation Based Treatments and Therapies (EBTTs) offer several inherent advantages over conventional thermal ablation modalities such as radiofrequency ablation (RFA), microwave ablation (MWA), and cryoablation (Cryo). Because cell death is driven primarily by electric field mediated membrane disruption rather than heating, EBTTs can be used in proximity to heat-sensitive critical structures, including bile ducts, bowel walls, and major nerves, without the thermal collateral damage that limits conventional ablation in these anatomical locations.[10,11] EBTTs are also not subject to the heat-sink effect that compromises thermal ablation efficacy near large vessels, and they produce a vascular lock effect that reduces intraprocedural bleeding.[12,13] Emerging evidence further suggests that electroporation-based ablation releases tumour-associated antigens in their native, non-denatured state, eliciting a more robust pro-immunogenic response than thermal modalities and thereby opening a therapeutic window for combination with immune checkpoint inhibitors.[14-17]

Despite these advantages and a clinical track record spanning more than 30 years, the first ECT clinical trial was published in 1991[18], EBTTs remain underutilised in clinical practice. ECT remains primarily applied to cutaneous and subcutaneous tumours, and both ECT and IRE ablation are expanding into interventional oncology for deep-seated tumours; however, both remain niche techniques compared with thermal ablation modalities, which constitute the current standard of care for most tumour indications. In striking contrast, cardiac PFA has experienced explosive growth: following the first FDA clearance of Medtronic's (Minneapolis, MN, USA) PulseSelect system in December 2023 and Boston Scientific's (Marlborough, MA, USA) Farapulse system in February 2024, approximately one million patients have been treated worldwide within two years, fuelled by substantial research and development investment and corporate acquisitions. The cardiac PFA experience demonstrates both the translational potential of electroporation and the conditions required for rapid clinical adoption: a large, homogeneous patient population, compelling randomised evidence, sustained industrial investment, and a clear regulatory pathway.

This expert opinion paper examines whether and how these treatments can be adapted for other non-cardiac and non-oncological applications of electroporation. We review the current clinical landscape of EBTTs, explore emerging indications beyond oncology and cardiology, analyse the barriers to wider clinical adoption, and propose concrete steps to accelerate clinical translation.

Current clinical landscape of electroporation-based treatments

Electrochemotherapy

Electrochemotherapy (ECT) has the longest clinical history among EBTTs. Following the pivotal 1991 clinical trial by Mir *et al*., the 2006 Standard Operating Procedure (SOP) and its 2018 update[19,20] and the NICE (National Institute for Health and Care Excellence) approval of ECT for skin metastases in the UK in 2013 (IPG446), the treatment is now routinely performed in Europe. The Insp-ECT (International Network for Sharing Practices on Electrochemotherapy) registry (https://www.inspect.org/), encompassing more than 40 treatment centres and over 1,000 analysed patients, treated with Cliniporator devices (IGEA, S.p.A., Carpi, Italy), has demonstrated overall response rates exceeding 80% across diverse tumour histologies, with complete response rates of approximately 71%.[21,22] Mirai Medical's ePORE® platform has also been applied to cutaneous malignancies through

the CUTIS probe. In a case series (25 patients), high-frequency electroporation with the ePORE® generator and CUTIS probe, combined with bleomycin, achieved a 91.3% overall lesion response at 12 weeks across 97 lesions of five histological subtypes, with good tolerability under local anaesthesia.[23]

Beyond cutaneous disease, ECT is increasingly applied to deep-seated targets including liver, prostate, bone, colorectal, vulvar, and brain tumours.[21,24-31] A particularly compelling application is ECT for metastatic epidural spinal cord compression, a devastating condition with few therapeutic options beyond palliative radiotherapy. The largest published series of ECT for metastatic epidural spinal cord compression, reported by Deschamps *et al*., included 40 consecutive patients who had failed radiotherapy; 46% achieved complete MRI response and the median pain score fell from 7/10 to 1/10 at one month.[32,33] These results represent a promising change in quality of life for a patient population with previously no treatment options.

ECT has also been delivered endoscopically for gastrointestinal indications. The EndoVE® platform (Mirai Medical, Galway, Ireland) has accumulated the most extensive clinical experience in endoscopic, intraluminal gastrointestinal electroporation. Following the first-in-human colorectal study[34], independent groups have since reported endoscopic calcium electroporation and ECT with this platform across colorectal, gastric and oesophageal cancer, principally for palliation of bleeding and obstructive symptoms in frail patients unfit for surgery, with a consistent safety profile and high rates of symptomatic response.[35-41] A standardised implementation protocol for an endoscopic electroporation service in colorectal cancer has also been published.[36]

A few CE-marked clinical electroporators are currently approved for ECT in Europe. Cliniporator (IGEA S.p.A., Carpi, Italy), which received CE marking for ECT in 2008, remains the most widely used system and is the device employed across the Insp-ECT registry. A higher-output variant, the Cliniporator VITAE, which extended ECT to deep-seated and larger tumours such as those of the liver, bone, and spine, received a CE mark in 2011. The SENNEX System (BionMed Technologies, Saarbrücken, Germany) is also CE-marked for ECT of cutaneous and subcutaneous tumours.[42] Mirai Medical (Galway, Ireland) has developed the ePORE® high-frequency biphasic generator and the EndoVE® endoscopic electrode[34], both CE-approved for ECT and calcium electroporation in the EU, UK and Australia, enabling endoscopic delivery of ECT for gastrointestinal indications.

Irreversible electroporation in interventional oncology

Irreversible electroporation (IRE) was first suggested as a non-thermal ablation modality in 2005[6], demonstrated in vivo in 2007[43] and finally introduced to the market by AngioDynamics (Latham, NY, USA), whose NanoKnifeÒ electroporator received FDA clearance for soft tissue ablation in 2008. IRE has been most extensively studied in the liver, pancreas, and prostate, organs where proximity to critical structures such as the hepatic hilum, bile ducts, and neurovascular bundles, or the heat-sink effect of adjacent vasculature, limits the effectiveness of thermal ablation techniques.[10,44-49] Retrospective and prospective studies have demonstrated technical feasibility and acceptable safety profiles of the procedure.

Clinical interest in IRE for prostate cancer is increasing, as preservation of the neurovascular bundles is essential for maintaining continence and potency. The PRESERVE study (NCT04972097), a recent clinical trial, demonstrated the safety and effectiveness of IRE for treatment of prostate. Most recently, Angiodynamics' NanoKnifeÒ system received FDA clearance in December 2024 for ablation of prostate tissue in intermediate-risk prostate cancer, further expanding the approved indications for IRE.

There is also growing interest in early-stage non-small cell lung cancer, where the proximity to major airways and vessels limits the use of thermal approaches. Recent regulatory milestones reflect this momentum: Galvanize Therapeutics' (Redwood City, CA, USA) Aliya system received FDA clearance in 2022, and the INUMI Flex endoscopic needle in 2024, both supporting soft tissue ablation, including endobronchial treatment of early-stage non-small cell lung cancer. Beyond lung, regulatory clearances continue to expand into other soft tissues; Pulse Biosciences' (Hayward, CA, USA) CellFX nsPFA technology, which received FDA 510(k) clearance in March 2024 for ablation of soft tissue in percutaneous and intraoperative surgical procedures.

Cardiac pulsed field ablation

IRE has also gained momentum with its evolution to Pulsed Field Ablation (PFA), a non-thermal modality for intracardiac catheter-based ablation,

unlocking new possibilities for the treatment of cardiac arrhythmias.[50-52] In cardiology, PFA has achieved rapid regulatory approval and clinical adoption for the treatment of atrial fibrillation. Medtronic's (Minneapolis, MN, USA) PulseSelect system was the first PFA device approved by the FDA for the treatment of atrial fibrillation in December 2023. This was followed in 2024 by FDA approvals for Boston Scientific's (Marlborough, MA, USA) Farapulse, Affera/Medtronic's Sphere 9, and Johnson & Johnson's (New Brunswick, NJ, USA) VARIPULSE, and in 2025 by approvals for Kardium's (Burnaby, BC, Canada) Globe System and Abbott's (Abbott Park, IL, USA) Volt PFA System.

Substantial investment in research and development has supported large-scale randomised trials such as ADVENT, CHAMPION, and BEAT PAROX-AF[53-55], along with prospective pivotal studies such as PULSED AF and ADVANTAGE AF[51,56], which have validated the technology platform.[57,58] PFA is now being evaluated across a broader range of cardiac arrhythmias. In ventricular arrhythmias, PFA's ability to potentially penetrate fibrotic and fatty myocardium makes it mechanistically attractive for ventricular tachycardia ablation. Early multicentre registry data (126 patients) reported approximately 78% freedom from recurrence for premature ventricular contractions and 70% for ventricular tachycardia at a mean follow-up of 5.6 ± 3.7 months.[58] A subsequent single-centre US registry (59 patients) using the Sphere-9 catheter reported acute VT non-inducibility in 78% of patients and complete suppression in all PVC cases, with 6-month VT-free survival of 69.8%.[59] For supraventricular tachycardias, acute procedural success rates exceeding 99% have been reported in early multicentre studies.[58]

The trajectory of cardiac PFA offers both inspiration and a sobering reality check for non-cardiac electroporation. The heart is an anatomically consistent target across patients, the global atrial fibrillation population is vast, and the existing catheter ablation infrastructure could be readily adapted; allowing a single catheter and technique to be applied across the population. Oncological targets, by contrast, span every tumour histology and anatomical site, each demanding different electrodes, specialists, and procedural approaches. This heterogeneity makes a single pivotal trial for oncological EBTTs impractical and calls for alternative trial design. It also carries a regulatory cost: each indication must be evaluated separately, so the evidentiary burden scales with the number of target conditions rather than being shared across one large population, as in atrial fibrillation.

Emerging applications beyond oncology and cardiology

The success of cardiac PFA has demonstrated that electroporation is a viable treatment platform for non-oncological conditions. Several new clinical applications are now at various stages of development, each leveraging the unique properties of pulsed electric fields, cell selectivity ablation, preservation of tissue architecture, and enhanced drug delivery for conditions that were not traditionally considered targets for electroporation.

This section examines the emerging applications of electroporation beyond oncology and cardiology. The variety of terms in use (e.g., pulsed electric field therapy, pulsed field ablation, (ir)reversible electroporation, nanosecond pulsed field ablation), reflect the clinical discipline and context of origin rather than mechanistic distinction; all share electroporation of the cell membrane as their underlying mode of action.

Endoscopic pulsed electric field therapy for type 2 diabetes

Type 2 diabetes mellitus (T2D) affects more than 400 million people worldwide and is responsible for approximately two million deaths annually.[60] The duodenal mucosa plays a central role in metabolic regulation. Structural and functional abnormalities of the duodenal mucosa are increasingly recognised as contributors to insulin resistance and dysglycaemia, suggesting that endoscopic restoration of the mucosal layer may complement existing pharmacotherapy. Recellularization via electroporation therapy (ReCET) is a novel endoscopic procedure that uses an endoscope-mounted electrode, the Endogenex System (Endogenex Inc., Plymouth, MN, USA), to deliver pulsed electric fields to the duodenal mucosa and submucosa, inducing controlled cellular apoptosis and subsequent re-epithelialisation aimed at restoring normal metabolic signalling (Figure 1).[60,61]

Two clinical studies have generated encouraging early feasibility data. In the EMINENT[60] first-in-human study (n = 14), insulin-dependent T2D patients underwent a single ReCET procedure. At 12 months, 86% of patients remained off exogenous insulin with HbA1c maintained below 7.5%, and this effect was durable through 24 months

of follow-up. No serious adverse events were observed in the studies.

Separately, the REGENT-1 programme[61] (two parallel multicentre studies in Australia and the United States, n = 71) evaluated ReCET across multiple energy doses in patients on non-insulin glucose-lowering medications. No device- or procedure-related serious adverse events occurred; in the highest-dose group using a second-generation endoscope electrode, mean HbA1c decreased from 8.8% to 7.2% at 24 weeks, with a clear dose-response relationship observed across treatment groups.

These are single-arm studies, and the relative contributions of ReCET and concomitant pharmacotherapy cannot yet be separated. Two randomised, sham-controlled trials are now underway, the pivotal ReCET study (NCT06267391) and the EMINENT-2 trial in Europe (NCT05984238), which aims to provide the comparative evidence needed for regulatory approval. The Endogenex System has received FDA Breakthrough Device Designation, and the company has secured Series C financing to support its pivotal study and regulatory path to FDA approval.

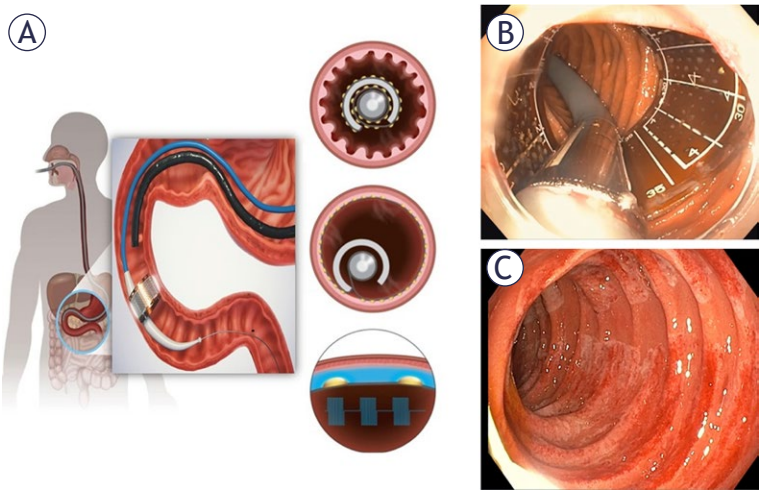

FIGURE 1. Recellularization via electroporation therapy (ReCET) is a novel endoscopic procedure that uses an endoscope-mounted electrode to deliver pulsed electric fields to the duodenal mucosa and submucosa. **(A)** A schematic of the positioning of the flexible electrode and its unfolding and expansion within the duodenum. **(B)** Intraprocedural endoscopic view of the expanded electrode within the duodenum. **(C)** A post-treatment endoscopic view of the resulting circumferential, nonthermal treatment effect. Figure is reproduced from.[62]

Bronchial rheoplasty for chronic bronchitis

Chronic bronchitis, a phenotype of Chronic Obstructive Pulmonary Disease (COPD), is characterised by goblet cell hyperplasia and mucus hypersecretion, leading to persistent cough, sputum production, impaired quality of life and increased exacerbation risk. Currently available pharmacotherapies do not adequately target the underlying mucus hypersecretion, leaving many patients symptomatic despite optimal medical therapy.

Bronchial rheoplasty is a bronchoscopic procedure that uses the RheOx system (Galvanize Therapeutics, Redwood City, CA, USA) to deliver non-thermal pulsed electric fields (PEF) to the airway epithelium and submucosa via an endobronchial endoscope electrode (Figure 2). PEF leaves the extracellular matrix and collagenous structures intact, thereby allowing re-epithelialisation with a normalised distribution of mucus-producing cells.[63-65]

A US multicentre feasibility study (n = 21, 6 centres) with 2-year follow-up reported statistically significant improvements in COPD Assessment Test (CAT) and St George's Respiratory Questionnaire (SGRQ) scores, with no procedure-related serious adverse events.[64] Mean changes from baseline in CAT score were 9.0 ± 6.7 at 12 months and 5.6 ± 7.1 at 24 months, and in SGRQ 16.6 ± 13.2 and 11.8 ± 19.2, respectively. Both scores exceeded twice the minimal clinically important difference at 24 months. There was also a 34% reduction in moderate and a 64% reduction in severe COPD exacerbation rates compared with the year prior to treatment.

A real-world European registry (n = 54, 106 procedures across 8 centres in Austria and Germany) confirmed these findings[65], with CAT score improvements of 5.5 ± 8.0 at 6 months and 4.2 ± 7.4 at 12 months, and SGRQ improvements of 9.5 ± 17.5 and 12.4 ± 16.3, respectively. Notably, patients with a CB-dominant phenotype demonstrated substantially higher responder rates than those with a mixed emphysema/CB phenotype (81.6% vs. 36.3% at 6 months), suggesting that patient selection may be important for optimising outcomes.

The RheOx system holds CE certification in the European Union (since 2019) and has been granted FDA Breakthrough Device designation in the United States, where it remains investigational. The pivotal RheSolve trial (NCT04677465), a prospective, randomised, double-blind, sham-controlled, multicentre study enrolling 270 patients at up to 50 centres in the US, Canada and Europe is currently underway to confirm these findings and support a future FDA approval application.

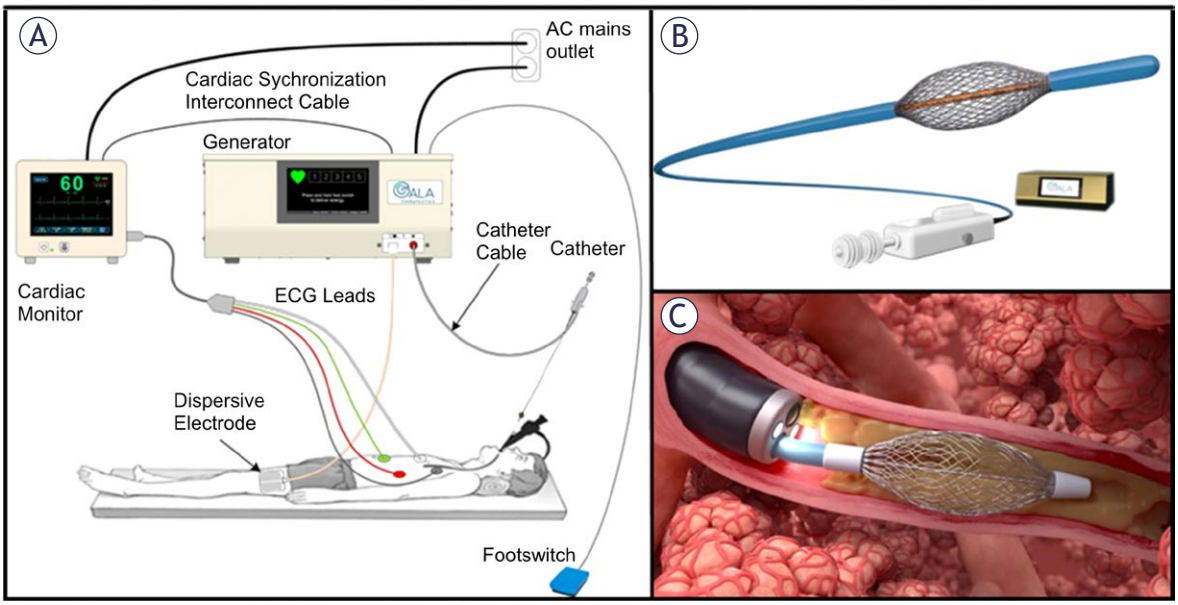

FIGURE 2. (A) The RheOx system (Galvanize Therapeutics, Redwood City, CA, USA) for the treatment of the symptoms of chronic bronchitis consists of a proprietary electrosurgical generator and **(B)** a single use endoscope with an expandable basket electrode. **(C)** The minimally invasive bronchoscopic therapy delivers short bursts of Pulsed Electric Field (PEF) energy to induce non-thermal ablation of the abnormal mucus-producing cells in the airways, leaving the extracellular matrix intact so that the epithelium may rapidly regenerate. Figure is reproduced from.[66]

Bleomycin electrosclerotherapy for vascular malformations

Vascular malformations are congenital anomalies arising from defective vascular morphogenesis and affect approximately 1.5% of the general population.[67] Slow-flow venous and lymphatic malformations are the most common subgroup, typically presenting during childhood with pain, swelling, functional impairment, and recurrent infections.[68] Currently available treatments (embolization, bleomycin sclerotherapy, laser therapy, and surgery) are not reliably curative for larger or infiltrative lesions, and recurrence is common.[67,69]

Bleomycin ElectroScleroTherapy (BEST) combines intralesional bleomycin with reversible electroporation, exploiting the vascular disrupting mechanism as identified and described in ECT (illustrated in Figure 3 A).[12,70] Electric pulses transiently permeabilise endothelial cells, substantially increasing intracellular bleomycin uptake; the resulting mitotic cell death preferentially affects proliferating endothelium, a feature shared by tumour vasculature and the dysplastic endothelium of vascular malformations.[67,69,71]

An early cohort of therapy-resistant venous malformations (n = 17, who had previously undergone at least two unsuccessful invasive treatments) reported a median 86% MRI-derived volume reduction after a single BEST session in most cases.[72] Figure 3 B–C) shows an example of a vascular malformation in the foot that exhibited an approximately 75% volume reduction after BEST. The largest published cohort to date (n = 233 patients, 325 procedures) confirmed positive subjective outcomes in mobility, aesthetics, and pain in most patients. Importantly, children and adolescents performed significantly better than adults across all patient-reported parameters.[73]

Loeser *et al.*[74] reported BEST outcomes specifically in lymphatic malformations (12 patients, 21 procedures) with mean volume reduction of 54.8% and symptom improvement achieved in all patients after a mean follow-up of 8.36 months. Haehl *et al.*[68] in the largest dedicated paediatric cohort (45 children, 68 procedures), demonstrated significant improvement in physician-rated symptom severity, with no patient remaining in the severe grade after treatment.

The most common side effect is skin hyperpigmentation (approximately 69%), which frequently fades over time; serious complications, such as skin necrosis, nerve injury, and haemorrhage, are uncommon but not negligible, the reported major complication rate in the largest cohort was 8.9%.[73] The first consensus-driven Current Operating

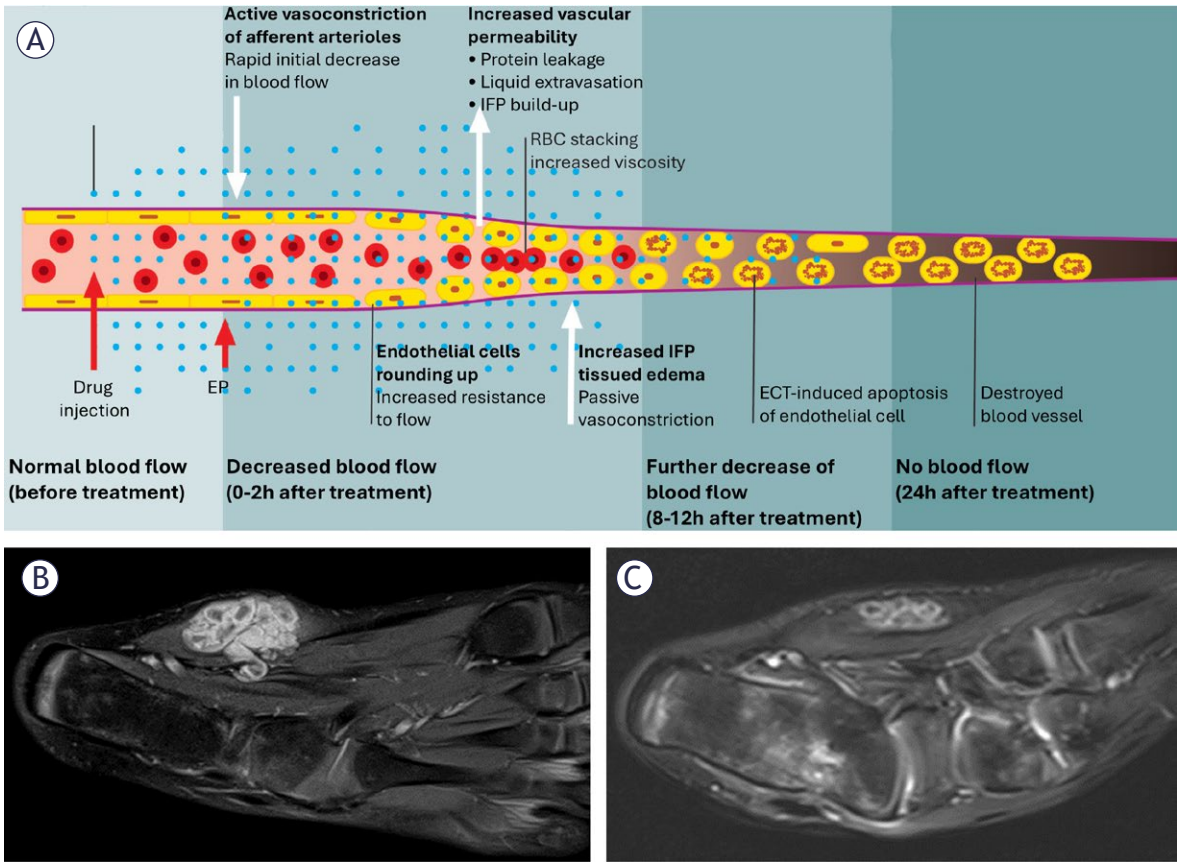

FIGURE 3. Bleomycin ElectroScleroTherapy (BEST) combines intralesional bleomycin with reversible electroporation, exploiting the same vascular-disrupting mechanism described for electrochemotherapy (ECT). **(A)** An illustration of blood-flow changes induced by electrochemotherapy (ECT) at the level of a microcirculatory vessel; from normal flow before treatment to vascular destruction by 24 h. Adapted from.[12] An example of BEST treatment of a vascular malformation in the foot: **(B)** T2-weighted MRI of a vascular malformation in the foot before BEST treatment, showing the hyperintense malformation. **(C)** MRI of the same region 3 months after BEST, demonstrating a 75% volume reduction.

Procedure for BEST was published in 2024.[69] Building on this, a dedicated working group within the Insp-ECT consortium has since been established to develop Standardised Operating Procedures through a prospective clinical trial (NCT07579962). A randomised comparison with conventional sclerotherapy has yet to be initiated.

Nanosecond pulsed field ablation for benign thyroid nodules

Benign thyroid nodules causing compressive symptoms such as difficulty breathing, swallowing, and neck pain are conventionally managed by thyroidectomy, which leads to loss of thyroid function and lifelong hormone replacement.[75] Thermal ablation techniques (RFA, laser, and MWA) are alternative treatment options in specialist centres. However, their use near the recurrent laryngeal nerve, carotid artery, and trachea requires high operator skill, and approximately 20% of patients need retreatment within one year due to incomplete ablation and nodule regrowth. The fibrotic scarring caused by thermal ablation also complicates any subsequent surgery.

Nanosecond pulsed field ablation (nsPFA) is an emerging non-thermal technology developed by Pulse Biosciences (Hayward, CA, USA) for ablation of soft tissue in percutaneous and intraoperative procedures, such as treatment of benign thyroid nodules. The system delivers bipolar nanosecond-duration electric pulses that induce regulated cell death rather than thermal necrosis.[75] Treated cells release danger-associated molecular patterns that recruit immune cells to phagocytose the ablated material, leaving no residual fibrotic mass.

The results of the first-in-human feasibility study were published in 2025.[75] The study enrolled 30 patients across three cohorts, treated with the: ablate and resect, partial nodule treatment, and full nodule treatment. Results showed that nsPFA caused cell death without heat-related damage or scarring, indicating the ability to treat tissue immediately adjacent to critical neurovascular structures.

In the five patients who received full-nodule treatment with therapeutic intent, mean volume reductions were 71.1% at one month and 85.8% at 12 months. Symptom relief was reported as early as two weeks post-procedure, with no serious adverse events in any cohort. Notably, this rate of shrinkage exceeded that typically observed with RFA, as four large clinical trials demonstrated that six months were required to achieve comparable volume reduction.[75] nsPFA has tremendous promise for certain applications but the lesion size is limited by the potential thermal damage from the higher applied fields.

In March 2024, Pulse Biosciences announced FDA 510(k) clearance for the CellFX nsPFA Percutaneous Electrode System for soft tissue ablation. An ongoing multicentre clinical trial (NCT07226804) is further characterising the safety and efficacy profile of nsPFA in a larger cohort.

Electroporation-mediated gene delivery

Electroporation-mediated gene delivery, commonly termed Gene Electro-Transfer (GET), represents a distinct application of reversible electroporation in which pulsed electric fields transiently permeabilise cell membranes to facilitate intracellular delivery of nucleic acids (plasmid DNA, RNA, or CRISPR constructs) without the use of viral vectors.[4,76,77]

Skin and skeletal muscle are the primary target tissues owing to their accessibility, and GET has progressed to clinical investigation across a broad range of indications including cancer immunotherapy, DNA vaccination against infectious diseases, and treatment of heritable conditions.[5,78-81] For transdermal delivery, the stratum corneum presents a substantial barrier to delivery of hydrophilic and high-molecular-weight molecules. Advances in electrode design and pulse protocols, including non-invasive surface applicators, heat-assisted delivery, and combined electrode-reservoir devices, have progressively improved delivery depth, efficiency, and tolerability.[82-84]

Electroporation-mediated gene delivery to the myocardium (i.e. cardioporation) has shown feasibility for cardiac regeneration applications following myocardial infarction. In a rat model of cardiac ischemia, GET of VEGF-B encoding plasmid DNA, delivered directly to the ischemic myocardium, produced the first direct histological evidence of cardiomyogenesis post-infarction.[85] Subsequent work further optimised cardioporation parameters, including electrode configuration and plasmid vector size, to increase expression efficiency while reducing ventricular fibrillation risk and tissue damage.[86]

Another opportunity of GET lies in the in vivo production of monoclonal antibodies (mAbs). Conventional mAbs are well established across oncology, autoimmune disease, and infectious disease, but their costly manufacture and need for repeated administration constrain accessibility.[87] In DNA-based antibody therapy, rather than administering the antibody protein, plasmid DNA encoding the mAb is instead delivered to a tissue, such as skeletal muscle, which then serves as an in-situ source of sustained expression. Preclinical studies in small and large animals have demonstrated feasibility across diverse targets[88-90], and the approach has recently progressed to first-in-human evaluation.[91]

Barriers to wider clinical adoption

Despite almost three decades of clinical experience, EBTTs remain outside mainstream treatment guidelines for most indications and are inconsistently reimbursed across geographical jurisdictions. Three interrelated categories of barriers account for this gap. First, the evidence base consists predominantly of single-arm series and registries, which are insufficient to drive guideline change or secure reimbursement decisions; the randomised comparative trials that regulators and health technology assessment bodies require have, with few exceptions, not been conducted. Second, the absence of validated treatment planning tools and consensus-based operating procedures limits reproducibility across centres and creates a practical expertise barrier that restricts dissemination beyond specialised institutions. Third, the regulatory and reimbursement landscape, particularly in Europe, is deeply fragmented, imposing a disproportionate burden on technologies addressing heterogeneous or rare indications.

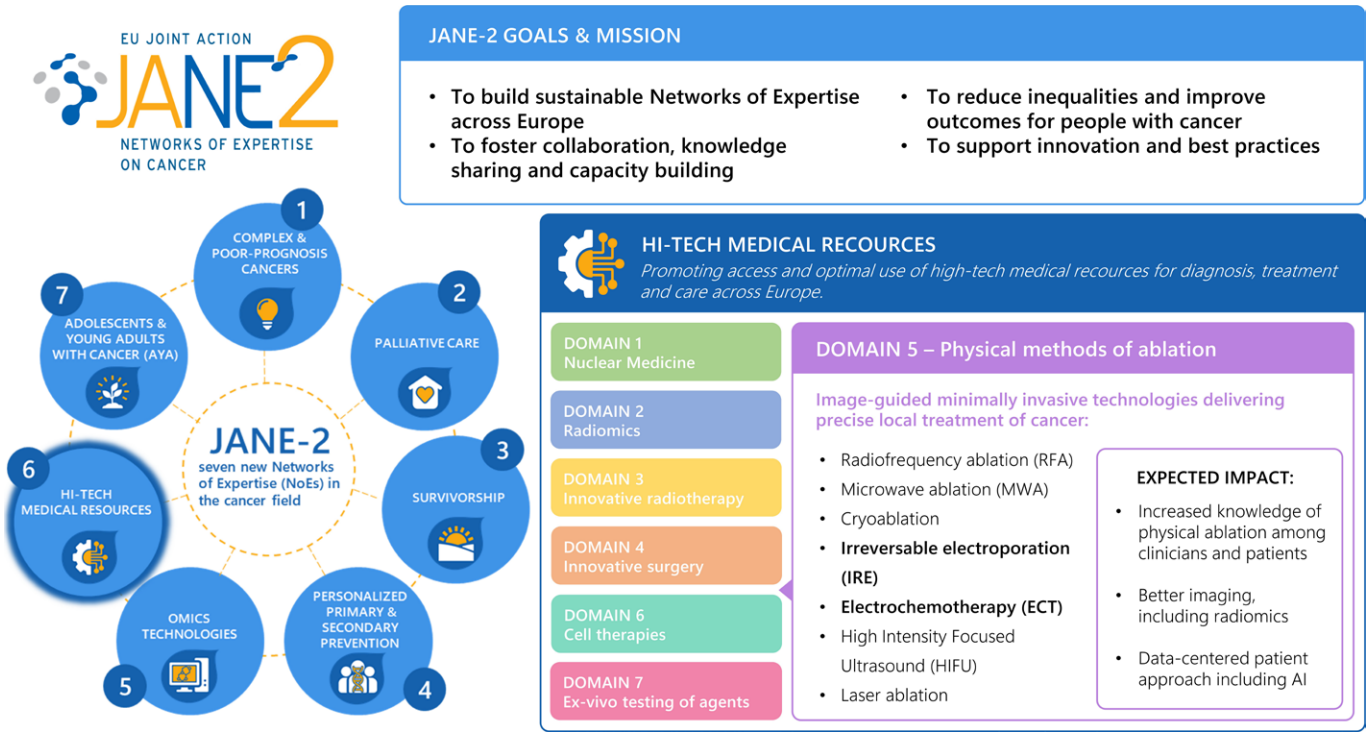

FIGURE 4. Overview of the JANE-2 (Joint Action on Networks of Expertise on Cancer) framework, highlighting WP10 – High-Tech Medical Resources and Domain 5 - Physical Methods of Ablation. The figure illustrates the position of Domain 5 within the broader network of JANE-2 and emphasizes its expected impact on advancing equitable access to innovative cancer treatment technologies across Europe.

Randomised evidence and guideline integration

The most significant barrier to wider adoption of EBTTs is the scarcity of high-quality comparative evidence. After almost 30 years of promising single-arm data, oncological EBTTs remain on the margins of mainstream clinical practice, primarily because randomised trials were not conducted early enough. Registries, however valuable for safety surveillance and hypothesis generation, are insufficient to drive guideline changes or reimbursement decisions.

The challenge is compounded by the heterogeneity of oncological indications. For example, cardiac PFA benefits from an anatomically consistent target, the same catheter and technique apply across the patient population, whereas ECT or IRE ablation address tumours of various histology and sites, requiring different electrodes, different specialists, and different procedural approaches. A single pivotal trial is therefore impractical for oncological EBTTs. A pragmatic alternative is to design disease-specific trials that compare focal ablation (allowing centres to choose their preferred energy) against standard of care and then dissect the contributions of individual modalities in post-hoc analyses. For rare cancers such as cholangiocarcinoma, multi-centre and potentially global collaboration is essential to accrue sufficient patient numbers.

The need for coordination of electroporation research across Europe was recognised more than a decade ago. COST Action TD1104 (2012–2016), the European Network for Development of Electroporation-Based Technologies and Treatments, united 73 researchers from 25 countries with the aims of streamlining European research and development activities, integrating multidisciplinary teams, providing comprehensive training for early-stage researchers, disseminating existing clinical applications, developing new applications, and standardising clinical protocols.[92]

Integration into Multidisciplinary Tumour Boards (MTBs) represents another critical gap. MTBs are the centrepiece of modern cancer care, yet EBTT expertise is not systematically represented; oncologists unfamiliar with ECT or IRE do not refer patients, and the technologies remain invisible

at the point where treatment decisions are made. The EU Joint Action on Networks of Expertise in Cancer (JANE; https://jane-project.eu/) directly addresses this structural problem. Launched in 2022 under Europe's Beating Cancer Plan, JANE has since expanded into JANE-2 (Figure 4) (https://jane-2.eu/), now encompassing 133 organisations from 29 EU countries and co-financed by the EU with €40.5 million.[93]

JANE is establishing Networks of Expertise across EU countries, with physical methods of ablation designated as one of seven priority medical resources (Figure 4). The initiative explicitly targets access inequities: patients across EU countries have widely unequal access to specialised ablation centres, and the absence of EBTTs from disease-specific guidelines compounds this disparity. By embedding EBTT expertise within a formal network structure, JANE-2 creates the institutional conditions under which guideline inclusion, structured real-world data collection, and harmonised standard operating procedures become feasible at a European scale.[94]

Treatment planning and monitoring

Adequate treatment planning remains an unresolved operational barrier for deep-seated EBTT targets. For cutaneous and subcutaneous ECT, fixed-geometry applicators and well-established standard operating procedures, most recently updated in 2018[20], make the treatment zone predictable and the procedure reproducible across centres. No equivalent SOPs exist for ECT or IRE ablation of deep-seated tumours. Physicians performing these procedures must adhere or rely on guidelines developed for superficial targets, on institutional custom, or on the simplified 2D planning tools integrated into commercial electroporators (e.g., IGEA's Cliniporator and Angiodynamics' NanoKnifeÒ), which assume homogeneous tissue and perfectly parallel electrode placement, conditions that are rarely met in practice. In reality, tissue heterogeneity renders electric field distribution difficult to predict and anatomical constraints cause needle deflection.[27,95-97]

The clinical consequences of inadequate treatment planning are well illustrated in spinal ECT, where a 7.5% paraplegia rate has been attributed to uncontrolled current distribution near the spinal cord.[33] Patient-specific 3D numerical models, constructed from CT or MRI data, can optimise electrode positioning and pulse parameters to achieve complete target coverage while minimising thermal injury and damage to sensitive structures (Figure 5).[98-101] However, no treatment planning software for EBTTs is currently approved for clinical use, and prospective validation is lacking.

Furthermore, real-time and post-procedural assessment of the ablated zone constitutes a related unmet need. Unlike thermal ablation, where the necrotic zone is clearly demarcated on imaging and stable over time, the ablation zone after IRE undergoes rapid dynamic changes: it may transiently overestimate the true treatment volume in the first 24 hours, as both reversibly and irreversibly electroporated tissue can accumulate contrast agent, before shrinking considerably over the following weeks.[101-103] The zone is also not internally uniform: histopathologic–radiologic correlation has shown that it comprises concentric layers of coagulative necrosis, congestion, and peripheral inflammation, each with distinct enhancement behaviour, such that different contrast phases over- or underestimate the true extent of cell death.[104,105] Together, these dynamic changes make it difficult to determine with certainty the region of actual irreversible cell death on follow-up imaging, and there is currently no consensus on optimal post-treatment imaging timing or protocol.

Addressing these gaps in treatment planning and monitoring will require investment on several fronts: prospective clinical validation of treatment planning models, development of reliable intraprocedural monitoring, and integration of real-time planning with navigation systems. A further requirement is regulatory clearance for treatment planning software as a clinical-grade medical device. This is a demanding process that neither device manufacturers nor independent developers have so far pursued, leaving available tools confined to research use.[107–111]

Regulatory pathways, reimbursement, and market fragmentation

The regulatory landscape for EBTT devices, while navigable, imposes significant time and cost burdens that disproportionately affect emerging applications and rare disease indications. EU Medical Device Regulation (MDR) certification through a Notified Body takes an average of 14 months (range 6 months to over 2 years), and each new clinical indication requires a separate body of clinical evidence, an obstacle for technologies that potentially address several different tumour types but cannot afford a clinical study for each. In the United States, the mean cost of bringing

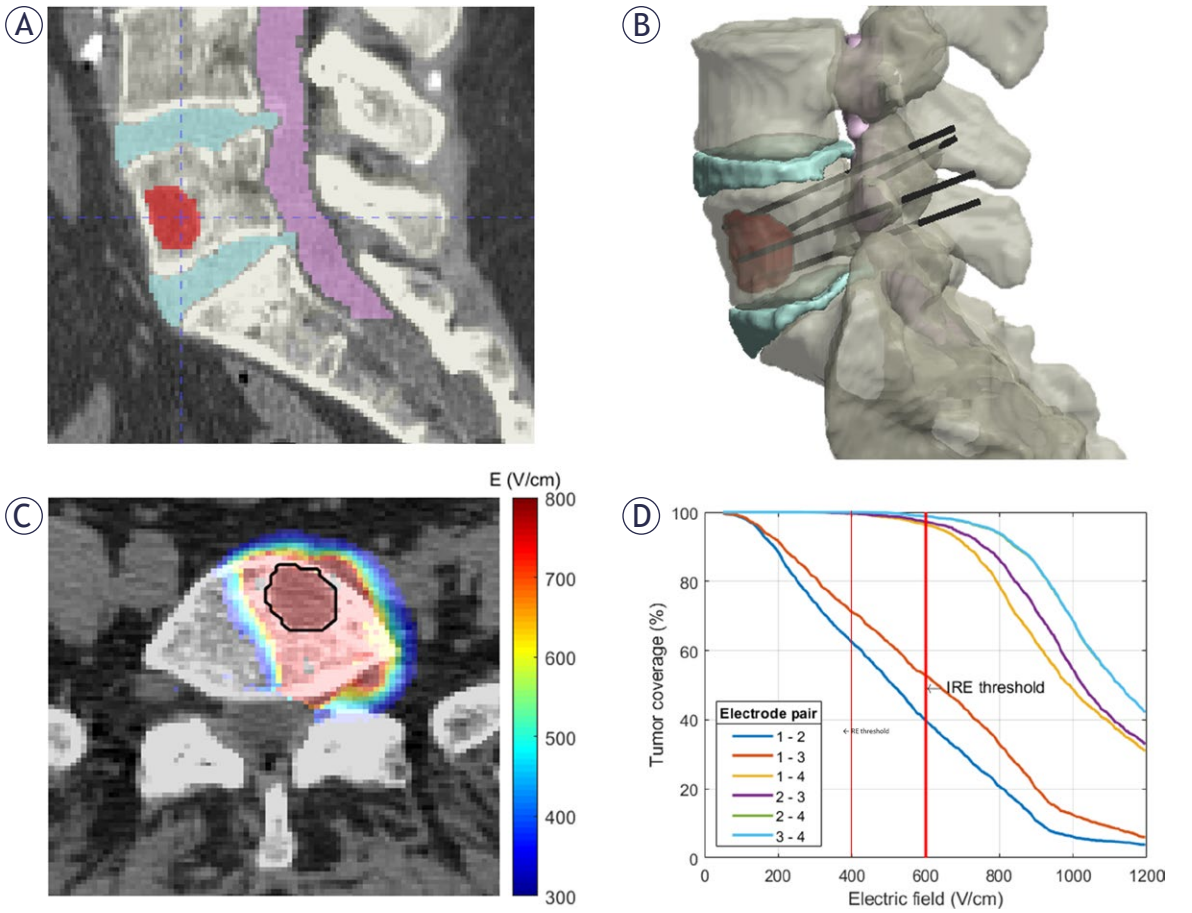

FIGURE 5. Illustration of a computer-assisted patient-specific treatment plan for electrochemotherapy of a spinal metastasis. **(A)** Segmentation of the tissues of interest (vertebrae, intervertebral discs, spinal cord, tumour) from the patient's CT image. **(B)** Patient-specific 3D model developed from image segmentation showing the electrode placement for the selected treatment plan. **(C)** Predicted electric field distribution for the selected treatment plan, overlaid on the CT image (tumour outlined in black). **(D)** Cumulative tumour coverage as a function of electric field for the candidate electrode pairs; vertical lines mark the reversible (RE) and irreversible (IRE) electroporation thresholds. Adapted from.[106]

a novel Class III device to market has been estimated at approximately $54 million, with the pivotal clinical trial alone averaging around $31 million.[112]

In addition, reimbursement across Europe is deeply fragmented. Paradoxically, France, where ECT was pioneered, remains one of the most restrictive markets for the technology. Each country requires its own evidence package, business case, and often local clinical data. Clinical adoption in one jurisdiction does not automatically transfer to another, and evidence generated in one EU member country may not satisfy the reimbursement authorities of another. This fragmentation stands in contrast to the single FDA national approval pathway in the United States and constitutes a significant barrier for small and medium sized companies developing EBTT devices.

The cardiac PFA market illustrates how sufficient investments can overcome these barriers: companies routinely raise successive financing rounds in the tens to hundreds of millions of dollars, supported by the enormous global atrial fibrillation patient pool. Oncological and non-oncological EBTT populations are smaller and more heterogeneous, requiring creative approaches to clinical trial design (adaptive, basket, or platform trials) that can generate sufficient evidence across multiple indications without requiring prohibitive investment for each.

Conclusions and recommendations

Electroporation-based treatments and therapies represent a promising but underutilised family of clinical modalities. They can provide treatment opportunities for diseases that have not been adequately addressed so far and can improve patients' quality of life (e.g. in patients with vascular malformations or with COPD) and offer disruptive treatments (e.g. for type 2 diabetes and cardiac arrhythmia treatment). The explosive growth of cardiac PFA has renewed interest in this platform technology and demonstrated that electroporation can achieve mainstream clinical adoption when the necessary conditions are met. The emerging applications reviewed here confirm that the technology's translational potential extends well beyond its traditional oncological and cardiac domains. Based on the collective expert opinion of the authors, we offer the following recommendations to facilitate wider clinical adoption of EBTTs.

1. **Pursue targeted randomised trials.** Comparative evidence is the main barrier to guideline inclusion. Trials should be prioritised for indications where randomisation is ethical and feasible, such as ECT versus palliative radiotherapy for spinal metastases. Designs comparing focal ablation with standard care can generate actionable evidence.
2. **Develop indication-specific standard operating procedures.** The ECT SOP model has been instrumental in enabling reproducible results across centres. Equivalent consensus-based SOPs are needed for IRE of deep-seated tumours, ECT of spinal metastases, and the emerging non-oncological applications; a recent example is the publication of Current Operating Procedures for BEST with a prospective trial currently underway to evaluate it in clinical practice.
3. **Invest in treatment planning infrastructure.** Reliable patient-specific treatment planning remains a critical gap for deep-seated tumour ablation and complex non-oncological procedures. Validated, regulatory-compliant software is urgently needed, and academic groups should collaborate with device manufacturers to pursue bundled device–software submissions that can streamline the regulatory pathway for both.
4. **Embed EBTTs in multidisciplinary decision-making.** Electroporation expertise must be systematically represented in multidisciplinary oncology boards and, for non-oncological applications, in the relevant disease-specific clinical forums. The EU JANE initiative provides a ready framework for embedding this expertise at the European level.
5. **Harmonise European reimbursement pathways.** The current country-by-country fragmentation of reimbursement criteria discourages investment and limits patient access. European-level harmonisation of evidence requirements for physical ablation modalities would substantially lower the adoption barrier for both established and emerging EBTT applications.

The tools exist, the evidence of biological efficacy is compelling, and the clinical need is clear. The task now is institutional: building the evidentiary, regulatory, and organisational infrastructure to deliver electroporation-based treatments to patients who stand to benefit most.

Acknowledgments

The authors acknowledge the Electroporation-Based Technologies and Treatments International Scientific Workshop and Postgraduate Course (EBTT 2025, Ljubljana, November 2025), which organized and hosted the round table "Non-thermal ablation and drug delivery by electroporation: expanding current indications" that provided the basis for this paper. The authors also thank Mitch Levinson and Steven Mickelsen for their contributions to the round table discussion.

AI disclosure

During the preparation of this paper, the authors used Claude (Anthropic) in two specific capacities: (1) screening the transcript of the round table on Non-thermal ablation and drug delivery by electroporation: expanding current indications held at Electroporation-Based Technologies and Treatments (EBTT 2025, Ljubljana, November 2025), in which the authors participated as panellists, to identify key discussion points and themes; and (2) assisting with language editing and phrasing during manuscript preparation. The literature search, selection and interpretation of sources, clinical judgements, and all substantive intellectual content are the sole work of the authors. After using this tool, the authors reviewed and edited the content as required and take full responsibility for the publication's content.

References

1. Kotnik T, Rems L, Tarek M, Miklavčič D. Membrane electroporation and electropermeabilization: mechanisms and models. *Annu Rev Biophys* 2019; **48:** 63-91. doi: 10.1146/annurev-biophys-052118-115451
2. Serša G, Miklavcic D, Cemazar M, Rudolf Z, Pucihar G, Snoj M. Electrochemotherapy in treatment of tumours. *Eur J Surg Oncol* 2008; **34:** 232-40. doi: 10.1016/j.ejso.2007.05.016
3. Orlowski S, Belehradek J, Paoletti C, Mir LM. Transient electropermeabilization of cells in culture: increase of the cytotoxicity of anticancer drugs. *Biochem Pharmacol* 1988; **37:** 4727-33. doi: 10.1016/0006-2952(88)90344-9
4. Heller R, Heller LC. Chapter Eight - Gene Electrotransfer Clinical Trials. In: Huang L, Liu D, Wagner E, editors *Advances in Genetics*. Academic Press; 2015. p. 235-62. doi: 10.1016/bs.adgen.2014.10.006
5. Sachdev S, Potočnik T, Rems L, Miklavčič D. Revisiting the role of pulsed electric fields in overcoming the barriers to *in vivo* gene electrotransfer. *Bioelectrochemistry* 2022; **144:** 107994. doi: 10.1016/j.bioelechem.2021.107994
6. Davalos RV, Mir ILM, Rubinsky B. Tissue ablation with irreversible electroporation. *Ann Biomed Eng* 2005; **33:** 223-31. doi: 10.1007/s10439-005-8981-8
7. Geboers B, Scheffer HJ, Graybill PM, Ruarus AH, Nieuwenhuizen S, Puijk RS, et al. High-voltage electrical pulses in oncology: irreversible electroporation, electrochemotherapy, gene electrotransfer, electrofusion, and electroimmunotherapy. *Radiology* 2020; **295:** 254-72. doi: 10.1148/radiol.2020192190
8. Ekanem E, Neuzil P, Reichlin T, Kautzner J, Van Der Voort P, Jais P, et al. Safety of pulsed field ablation in more than 17,000 patients with atrial fibrillation in the MANIFEST-17K study. *Nat Med* 2024; **30:** 2020-9. doi: 10.1038/s41591-024-03114-3
9. Miklavčič D, Verma A, Krahn PRP, Štublar J, Kos B, Escartin T, et al. Biophysics and electrophysiology of pulsed field ablation in normal and infarcted porcine cardiac ventricular tissue. *Sci Rep* 2024; **14:** 32063. doi: 10.1038/s41598-024-83683-y
10. Cannon R, Ellis S, Hayes D, Narayanan G, Martin RCG. Safety and early efficacy of irreversible electroporation for hepatic tumors in proximity to vital structures. *J Surg Oncol* 2013; **107:** 544-9. doi: 10.1002/jso.23280
11. Sutter O, Calvo J, N'Kontchou G, Nault J-C, Ourabia R, Nahon P, et al. Safety and efficacy of irreversible electroporation for the treatment of hepatocellular carcinoma not amenable to thermal ablation techniques: a retrospective single-center case series. *Radiology* 2017; **284:** 877-86. doi: 10.1148/radiol.2017161413
12. Jarm T, Cemazar M, Miklavcic D, Sersa G. Antivascular effects of electrochemotherapy: implications in treatment of bleeding metastases. *Expert Rev Anticancer Ther* 2010; **10:** 729-46. doi: 10.1586/era.10.43
13. Brinton M, Mandel Y, Schachar I, Palanker D. Mechanisms of electrical vasoconstriction. *J Neuroeng Rehabil* 2018; **15:** 43. doi: 10.1186/s12984-018-0390-y
14. Calvet CY, Mir LM. The promising alliance of anti-cancer electrochemotherapy with immunotherapy. *Cancer Metastasis Rev* 2016; **35:** 165-77. doi: 10.1007/s10555-016-9615-3
15. Scheffer HJ, Stam AGM, Geboers B, Vroomen LGPH, Ruarus A, de Bruijn B, et al. Irreversible electroporation of locally advanced pancreatic cancer transiently alleviates immune suppression and creates a window for antitumor T cell activation. *Oncoimmunology* 2019; **8:** 1652532. doi: 10.1080/2162402X.2019.1652532
16. Zhao J, Wen X, Tian L, Li T, Xu C, Wen X, et al. Irreversible electroporation reverses resistance to immune checkpoint blockade in pancreatic cancer. *Nat Commun* 2019; **10:** 899. doi: 10.1038/s41467-019-08782-1
17. Kesar U, Markelc B, Jesenko T, Valentinuzzi KU, Cemazar M, Strojan P, et al. Effects of electrochemotherapy on immunologically important modifications in tumor cells. *Vaccines* 2023; **11:** doi: 10.3390/vaccines11050925
18. Mir LM, Belehradek M, Domenge C, Orlowski S, Poddevin B, Belehradek J, et al. [Electrochemotherapy, a new antitumor treatment: first clinical trial]. [French]. *C R Acad Sci III* 1991; **313:** 613-8. PMID: 1723647
19. Mir LM, Gehl J, Sersa G, Collins CG, Garbay J-R, Billard V, et al. Standard operating procedures of the electrochemotherapy: instructions for the use of bleomycin or cisplatin administered either systemically or locally and electric pulses delivered by the CliniporatorTM by means of invasive or non-invasive electrodes. *Eur J Cancer Suppl* 2006; **4:** 14-25. doi: 10.1016/j.ejcsup.2006.08.003
20. Gehl J, Sersa G, Matthiessen LW, Muir T, Soden D, Occhini A, et al. Updated standard operating procedures for electrochemotherapy of cutaneous tumours and skin metastases. *Acta Oncol* 2018; **57:** 874-82. doi: 10.1080/0284186X.2018.1454602
21. Campana LG, Edhemovic I, Soden D, Perrone AM, Scarpa M, Campanacci L, et al. Electrochemotherapy - emerging applications technical advances, new indications, combined approaches, and multi-institutional collaboration. *Eur J Surg Oncol* 2019; **45:** 92-102. doi: 10.1016/j.ejso.2018.11.023
22. Clover AJP, de Terlizzi F, Bertino G, Curatolo P, Odili J, Campana LG, et al. Electrochemotherapy in the treatment of cutaneous malignancy: outcomes and subgroup analysis from the cumulative results from the pan-European International Network for Sharing Practice in Electrochemotherapy database for 2482 lesions in 987 patients (2008–2019). *Eur J Cancer* 2020; **138:** 30-40. doi: 10.1016/j.ejca.2020.06.020
23. Lyons P, Polini D, Russell-Ryan K, Clover AJP. High-frequency electroporation and chemotherapy for the treatment of cutaneous malignancies: evaluation of early clinical response. *Cancers (Basel)* 2023; **15:** 3212. doi: 10.3390/cancers15123212
24. Linnert M, Iversen HK, Gehl J. Multiple brain metastases - current management and perspectives for treatment with electrochemotherapy. *Radiol Oncol* 2012; **46:** 271-8. doi: 10.2478/v10019-012-0042-y
25. Djokic M, Cemazar M, Popovic P, Kos B, Dezman R, Bosnjak M, et al. Electrochemotherapy as treatment option for hepatocellular carcinoma, a prospective pilot study. *Eur J Surg Oncol* 2018; **44:** 651-7. doi: 10.1016/j.ejso.2018.01.090
26. Izzo F, Granata V, Fusco R, D'Alessio V, Petrillo A, Lastoria S, et al. Clinical Phase I/II study: local disease control and survival in locally advanced pancreatic cancer treated with electrochemotherapy. *J Clin Med* 2021; **10:** 1305. doi: 10.3390/jcm10061305
27. Luerken L, Doppler M, Brunner SM, Schlitt HJ, Uller W. Stereotactic percutaneous electrochemotherapy as primary approach for unresectable large HCC at the hepatic hilum. *Cardiovasc Intervent Radiol* 2021; **44:** 1462-6. doi: 10.1007/s00270-021-02841-1
28. Campanacci L, Cevolani L, De Terlizzi F, Saenz L, Alì N, Bianchi G, et al. Electrochemotherapy is effective in the treatment of bone metastases. *Curr Oncol* 2022; **29:** 1672-82. doi: 10.3390/curroncol29030139
29. Granata V, Fusco R, D'Alessio V, Simonetti I, Grassi F, Silvestro L, et al. Percutanous electrochemotherapy (ECT) in primary and secondary liver malignancies: a systematic review. *Diagnostics* 2023; **13:** 209. doi: 10.3390/diagnostics13020209
30. Stevanovic M, Heringer M, Hjouj M, Zanasi A, Terlizzi F de, Stehling MK. Prostate cancer treatment with electrochemotherapy (ECT): safety, efficacy and clinical experience in 144 patients. *Radiol Oncol* 2025; **59:** 597-606. doi: 10.2478/raon-2025-0061
31. Vivod G, Cilensek I, Kovacevic N, Sersa G, Cemazar M, Merlo S. Quality of life of women with recurrent vulvar cancer treated with electrochemotherapy. *Radiol Oncol* 2025; **59:** 267-76. doi: 10.2478/raon-2025-0019
32. Deschamps F, Tselikas L, Yevich S, Bonnet B, Roux C, Kobe A, et al. Electrochemotherapy in radiotherapy-resistant epidural spinal cord compression in metastatic cancer patients. *Eur J Cancer* 2023; **186:** 62-8. doi: 10.1016/j.ejca.2023.03.012
33. Deschamps F, Tselikas L, Cazzato RL, Facchini G, Granata V, Bonnet B, et al. Electrochemotherapy in metastatic epidural spinal cord compression: a review and technical update. *Br J Radiol* 2025; **98:** 828-39. doi: 10.1093/bjr/tqae219
34. Falk Hansen H, Bourke M, Stigaard T, Clover J, Buckley M, O'Riordain M, et al. Electrochemotherapy for colorectal cancer using endoscopic electroporation: a phase 1 clinical study. *Endosc Int Open* 2020; **8:** E124-32. doi: 10.1055/a-1027-6735
35. Broholm M, Vogelsang R, Bulut M, Gögenur M, Stigaard T, Orhan A, et al. Neoadjuvant calcium electroporation for potentially curable colorectal cancer. *Surg Endosc* 2024; **38:** 697-705. doi: 10.1007/s00464-023-10557-1

36. Adeyeye A, Haji A. Establishing a salvage endoscopic electroporation (SEE) service for colorectal cancer: the King's protocol for clinical implementation. *J Clin Med* 2025; **14:** 8436. doi: 10.3390/jcm14238436

37. Adeyeye A, Olabintan O, Ayubi H, Gao H, Saini A, Emmanuel A, et al. Palliative luminal treatment of colorectal cancer using endoscopic calcium-electroporation: first case series from United Kingdom. *J Clin Med* 2025; **14:** 4138. doi: 10.3390/jcm14124138

38. Bonura GF, Gualandi N, Soriani P, Cortegoso Valdivia P, Gabbani T, Zadro V, et al. Pioneering endoscopic calcium-electroporation in gastric cancer: a case series of an emerging therapeutic approach. *Diseases* 2025; **13:** 340. doi: 10.3390/diseases13100340

39. Pellegrino R, Nacca V, Paragliola F, Martinelli E, Federico A, Gravina AG. Endoscopic calcium electroporation for unfit-for-surgery bleeding colorectal cancer: the dawn of a new treatment? *Minerva Med* 2026; **117:** 55-7. doi: 10.23736/S0026-4806.24.09270-X

40. Egeland C, Baeksgaard L, Johannesen HH, Löfgren J, Plaschke CC, Svendsen LB, et al. Endoscopic electrochemotherapy for esophageal cancer: a phase I clinical study. *Endosc Int Open* 2018; **6:** E727-34. doi: 10.1055/a-0590-4053

41. Egeland C, Baeksgaard L, Gehl J, Gögenur I, Achiam MP. Palliative treatment of esophageal cancer using calcium electroporation. *Cancers (Basel)* 2022; **14:** 5283. doi: 10.3390/cancers14215283

42. Cvetkoska A, Pírc E, Reberšek M, Magjarević R, Míklavčič D. Towards standardization of electroporation devices and protocols. *IEEE Instrum Meas Mag* 2020; **23:** 74-81. doi: 10.1109/MIM.2020.9062692

43. Al-Sakere B, André F, Bernat C, Connault E, Opolon P, Davalos RV, et al. Tumor ablation with irreversible electroporation. *PLoS One* 2007; **2:** e1135. doi: 10.1371/journal.pone.0001135

44. Narayanan G, Gentile NT, Eyshi J, Schiro BJ, Gandhi RT, Peña CS, et al. Irreversible electroporation in treating colorectal liver metastases in proximity to critical structures. *J Vasc Interv Radiol* 2024; **35:** 1806-13. doi: 10.1016/j.jvir.2024.08.021

45. van den Bos W, Scheltema MJ, Siriwardana AR, Kalsbeek AMF, Thompson JE, Ting F, et al. Focal irreversible electroporation as primary treatment for localized prostate cancer. *BJU Int.* 2018; **121:** 716-24. doi: 10.1111/bju.13983

46. Niessen C, Thumann S, Beyer L, Pregler B, Kramer J, Lang S, et al. Percutaneous irreversible electroporation: Long-term survival analysis of 71 patients with inoperable malignant hepatic tumors. *Sci Rep* 2017; **7:** 43687. doi: 10.1038/srep43687

47. Martin RCG, Durham AN, Besselink MG, Iannitti D, Weiss MJ, Wolfgang CL, et al. Irreversible electroporation in locally advanced pancreatic cancer: a call for standardization of energy delivery. *J Surg Oncol* 2016; **114:** 865-71. doi: 10.1002/jso.24404

48. Narayanan G, Hosein PJ, Beulaygue IC, Froud T, Scheffer HJ, Venkat SR, et al. Percutaneous image-guided irreversible electroporation for the treatment of unresectable, locally advanced pancreatic adenocarcinoma. *J Vasc Interv Radiol* 2017; **28:** 342-8. doi: 10.1016/j.jvir.2016.10.023

49. Ruarus AH, Vroomen LGPH, Geboers B, van Veldhuisen E, Puijk RS, Nieuwenhuizen S, et al. Percutaneous irreversible electroporation in locally advanced and recurrent pancreatic cancer (PANFIRE-2): a multicenter, prospective, single-arm, phase II study. *Radiology* 2019; **294:** 212-20. doi: 10.1148/radiol.2019191109

50. Reddy VY, Koruth J, Jais P, Petru J, Timko F, Skalsky I, et al. Ablation of atrial fibrillation with pulsed electric fields: an ultra-rapid, tissue-selective modality for cardiac ablation. *JACC Clin Electrophysiol* 2018; **4:** 987-95. doi: 10.1016/j.jacep.2018.04.005

51. Verma A, Haines DE, Boersma LV, Sood N, Natale A, Marchlinski FE, et al. Pulsed field ablation for the treatment of atrial fibrillation: PULSED AF pivotal trial. *Circulation* 2023; **147:** 1422-32. doi: 10.1161/CIRCULATIONAHA.123.063988

52. Della Rocca DG, Cespón-Fernández M, Keelani A, Raffa S, Pannone L, Almorad A, et al. Focal pulsed field ablation for premature ventricular contractions: a multicenter experience. *Circ Arrhythm Electrophysiol* 2024; **17:** e012826. doi: 10.1161/CIRCEP.124.012826

53. Reddy VY, Gerstenfeld EP, Natale A, Whang W, Cuoco FA, Patel C, et al. Pulsed field or conventional thermal ablation for paroxysmal atrial fibrillation. *N Engl J Med* 2023; **389:** 1660-71. doi: 10.1056/NEJMoa2307291

54. Reichlin T, Kueffer T, Badertscher P, Jüni P, Knecht S, Thalmann G, et al. Pulsed field or cryoballoon ablation for paroxysmal atrial fibrillation. *N Engl J Med* 2025; **392:** 1497-507. doi: 10.1056/NEJMoa2502280

55. Jais P, Neuzil P, Scherr D, Frison E, Knecht S, Boveda S, et al. Pulsed field vs radiofrequency ablation for paroxysmal atrial fibrillation: the BEAT PAROX-AF trial. *Eur Heart J* 2026; **47:** 1527-37. doi: 10.1093/eurheartj/ehaf1115

56. Reddy VY, Gerstenfeld EP, Schmidt B, Nair D, Natale A, Saliba W, et al. Pulsed field ablation for persistent atrial fibrillation: 1-Year Results of ADVANTAGE AF. *J Am Coll Cardiol* 2025; **85:** 1664-78. doi: 10.1016/j.jacc.2025.03.515

57. Kühne M, Badertscher P, Andrade JG, Anic A, Chun J, Dello Russo A, et al. Pulsed field ablation for the interventional treatment of atrial fibrillation. A scientific statement of the European Heart Rhythm Association (EHRA) of the ESC, the Heart Rhythm Society (HRS), the Asia Pacific Heart Rhythm Society (APHRS), the Latin American Heart Rhythm Society (LAHRS) and the Canadian Heart Rhythm Society (CHRS). *Europace* 2026; **28:** euag080. doi: 10.1093/europace/euag080

58. Verma A, Hocini M, Andrade J, Gerstenfeld E, Kapa S, Lakkireddy D, et al. 2026 HRS/EHRA scientific statement on pulsed field ablation for cardiac arrhythmias. *Heart Rhythm* 2026; **13:** S1547-5271(26)00124-4. doi: 10.1016/j.hrthm.2026.02.006

59. Dasa O, Younis A, Higuchi K, Sroubek J, Lee JZ, Chung R, et al. Early U.S. experience with catheter ablation of ventricular arrhythmias with a dual-energy lattice-tip catheter: insights from the CLEAR-VT registry. *JACC Clin Electrophysiol* 2026; **6:** S2405-500X(26)00238-0. doi: 10.1016/j.jacep.2026.03.002

60. Busch CBE, Meiring S, van Baar ACG, Holleman F, Nieuwdorp M, Bergman JJGHM. Recellularization via electroporation therapy of the duodenum combined with glucagon-like peptide-1 receptor agonist to replace insulin therapy in patients with type 2 diabetes: 12-month results of a first-in-human study. *Gastrointest Endosc* 2024; **100:** 896-904. doi: 10.1016/j.gie.2024.04.2904

61. O'Neal DN, Sartoretto A, Holt BA, Abu Dayyeh BK, Vaughan R, Cameron G, et al. Safety, feasibility, and dose-dependent metabolic effects of endoscopic duodenal pulsed electric field therapy in adults with type 2 diabetes: results from two multicentre proof-of-concept studies. *Diabetes Obes Metab* 2026; **28:** 3367-76. doi: 10.1111/dom.70533

62. Abu Dayyeh BK, Asirvatham SJ. Nonthermal pulsed electric field recellularization in the duodenum for type 2 diabetes mellitus. *VideoGIE* 2024; **9:** 530-2. doi: 10.1016/j.vgie.2024.08.013

63. Valipour A, Fernandez-Bussy S, Ing AJ, Steinfort DP, Snell GI, Williamson JP, et al. Bronchial rheoplasty for treatment of chronic bronchitis. Twelve-month results from a multicenter clinical trial. *Am J Respir Crit Care Med* 2020; **202:** 681-9. doi: 10.1164/rccm.201908-1546OC

64. Sciurba FC, Dransfield MT, Kim V, Marchetti N, Comellas A, Hogarth DK, et al. Bronchial rheoplasty for chronic bronchitis: 2-year results from a US feasibility study with RheOx. *BMJ Open Respir Res* 2023; **10:** e001710. doi: 10.1136/bmjresp-2023-001710

65. Brock J, Herth F, Darwiche K, Hübner R-H, Skowasch D, Schwick B, et al. Bronchial rheoplasty for chronic bronchitis: real-world evidence of safety and performance. *ERJ Open Res* 2025; **11:** doi: 10.1183/23120541.00480-2025

66. Meininger GR, Neal RE, Hunter DW, Krimsky WS. Absence of arrhythmogenicity with biphasic pulsed electric fields delivered to porcine airways. *Ann Biomed Eng* 2024; **52:** 1-11. doi: 10.1007/s10439-023-03190-5

67. Muir T, Bertino G, Groselj A, Ratnam L, Kis E, Odili J, et al. Bleomycin electrosclerotherapy (BEST) for the treatment of vascular malformations. An International Network for Sharing Practices on Electrochemotherapy (InspECT) study group report. *Radiol Oncol* 2023; **57:** 141-9. doi: 10.2478/raon-2023-0029

68. Haehl J, Haeberle B, Muensterer O, Hartel A, Fröba-Pohl A, Dussa CU, et al. Bleomycin electrosclerotherapy (BEST) of slow-flow vascular malformations (SFVMs) in children. *J Pediatr Surg* 2025; **60:** 162631. doi: 10.1016/j.jpedsurg.2025.162631

69. Muir T, Wohlgemuth WA, Cemazar M, Bertino G, Groselj A, Ratnam LA, et al. Current Operating Procedure (COP) for Bleomycin ElectroScleroTherapy (BEST) of low-flow vascular malformations. *Radiol Oncol* 2024; **58:** 469-79. doi: 10.2478/raon-2024-0061

70. Sersa G, Krzic M, Sentjurc M, Ivanusa T, Beravs K, Kotnik V, et al. Reduced blood flow and oxygenation in SA-1 tumours after electrochemotherapy with cisplatin. *Br J Cancer* 2002; **87:** 1047-54. doi: 10.1038/sj.bjc.6600606

71. Lisec B, Cemazar M, Muir T, Omerzel M, Jesenko T, Markelc B, et al. Bleomycin ElectroScleroTherapy (BEST): mechanistic parallels to electrochemotherapy, experimental models, and unresolved questions. *Radiol Oncol* 2026; 60(3): 307-322.; **60:** 1-14. doi: 10.2478/raon-2026-0017

72. Wohlgemuth WA, Müller-Wille R, Meyer L, Wildgruber M, Guntau M, Heydt S von der, et al. Bleomycin electrosclerotherapy in therapy-resistant venous malformations of the body. *J Vasc Surg Venous Lymphat Disord* 2021; **9:** 731-9. doi: 10.1016/j.jvsv.2020.09.009

73. Schmidt VF, Cangir Ö, Meyer L, Goldann C, Hengst S, Brill R, et al. Outcome of bleomycin electrosclerotherapy of slow-flow malformations in adults and children. *Eur Radiol* 2024; **34:** 6425-34. doi: 10.1007/s00330-024-10723-6

74. Loeser JH, Guntau M, Bidakov O, von der Heydt S, Gussew A, Schob S, et al. Therapy of lymphatic malformations or isolated lymphatic components in combined slow-flow malformations with bleomycin electrosclerotherapy (BEST). *Rofo* 2025; **198:** 624-34. doi: 10.1055/a-2648-6555

75. Spiezia S, Offi C, Misso C, Antonelli G, Nuccitelli R, Tufano RP, et al. First-in-human clinical feasibility study of ablation of benign thyroid nodules using nanosecond pulsed field ablation. *Thyroid* 2025; **35:** 1024-9. doi: 10.1177/10507256251372166

76. Lambricht L, Lopes A, Kos S, Sersa G, Préat V, Vandermeulen G. Clinical potential of electroporation for gene therapy and DNA vaccine delivery. *Expert Opin Drug Deliv* 2016; **13:** 295-310. doi: 10.1517/17425247.2016.1121990

77. Rosazza C, Meglic SH, Zumbusch A, Rols M-P, Miklavcic D. Gene Electrotransfer: a Mechanistic Perspective. *Curr Gene Ther* 2016; **16:** 98-129. doi: 10.2174/1566523216666160331130040

78. Heller LC, Singh JS, Synowiec JC, Cherukuri PK, Phan N, Shi G, et al. Effective gene immunotherapy for melanoma utilizing an advanced *in vivo* electrotransfer system. *Mol Ther Oncol* 2025; **33:** 201035. doi: 10.1016/j.omton.2025.201035

79. Strojan P, Jesenko T, Omerzel M, Jamsek C, Groselj A, Tratar UL, et al. Phase I trial of phIL12 plasmid intratumoral gene electrotransfer in patients with basal cell carcinoma in head and neck region. *Eur J Surg Oncol* 2025; **51:** 109574. doi: 10.1016/j.ejso.2025.109574

80. Daud AI, DeConti RC, Andrews S, Urbas P, Riker AI, Sondak VK, et al. Phase I trial of interleukin-12 plasmid electroporation in patients with metastatic melanoma. *J Clin Oncol* 2008; **26:** 5896-903. doi: 10.1200/JCO.2007.15.6794

81. Spanggaard I, Snoj M, Cavalcanti A, Bouquet C, Sersa G, Robert C, et al. Gene electrotransfer of plasmid antiangiogenic metargidin peptide (AMEP) in disseminated melanoma: safety and efficacy results of a phase I first-in-man study. *Hum Gene Ther Clin Dev* 2013; **24:** 99-107. doi: 10.1089/humc.2012.240

82. Bulysheva A, Heller L, Francis M, Varghese F, Boye C, Heller R. Monopolar gene electrotransfer enhances plasmid DNA delivery to skin. *Bioelectrochemistry* 2021; **140:** 107814. doi: 10.1016/j.bioelechem.2021.107814

83. Edelblute C, Mangiamele C, Heller R. Moderate heat-assisted gene electrotransfer as a potential delivery approach for protein replacement therapy through the skin. *Pharmaceutics* 2021; **13:** 1908. doi: 10.3390/pharmaceutics13111908

84. Simon J, Jouanmiqueou B, Rols M-P, Flahaut E, Golzio M. Transdermal delivery of macromolecules using two-in-one nanocomposite device for skin electroporation. *Pharmaceutics* 2021; **13:** 1805. doi: 10.3390/pharmaceutics13111805

85. Bulysheva AA, Burcus N, Lundberg CG, Francis MP, Heller R. VEGF-B electrotransfer mediated gene therapy induces cardiomyogenesis in a rat model of cardiac ischemia. *Bioelectrochemistry* 2018; **124:** 105-11. doi: 10.1016/j.bioelechem.2018.07.007

86. Boye C, Arpag S, Burcus N, Lundberg C, DeClemente S, Heller R, et al. Cardioporation enhances myocardial gene expression in rat heart. *Bioelectrochemistry* 2021; **142:** 107892. doi: 10.1016/j.bioelechem.2021.107892

87. Aboul-Ella H, Gohar A, Ali AA, Ismail LM, Mahmoud AEE-R, Elkhatib WF, et al. Monoclonal antibodies: from magic bullet to precision weapon. *Mol Biomed* 2024; **5:** 47. doi: 10.1186/s43556-024-00210-1

88. Hollevoet K, De Smidt E, Geukens N, Declerck P. Prolonged in vivo expression and anti-tumor response of DNA-based anti-HER2 antibodies. *Oncotarget* 2018; **9:** 13623-36. doi: 10.18632/oncotarget.24426

89. Esquivel RN, Patel A, Kudchodkar SB, Park DH, Stettler K, Beltramello M, et al. In vivo delivery of a DNA-encoded monoclonal antibody protects non-human primates against Zika virus. *Mol Ther* 2019; **27:** 974-85. doi: 10.1016/j.ymthe.2019.03.005

90. Cuypers M-L, Geukens N, Hollevoet K, Declerck P, Dewilde M. Exploring the fate of antibody-encoding pDNA after intramuscular electroporation in mice. *Pharmaceutics* 2023; **15:** 1160. doi: 10.3390/pharmaceutics15041160

91. Tebas P, Patel A, Agnes JT, Parzych EM, Baer A, Caturla M, et al. Safety and pharmacokinetics of SARS-CoV-2 DNA-encoded monoclonal antibodies in healthy adults: a phase 1 trial. *Nat Med* 2025; **31:** 4150-9. doi: 10.1038/s41591-025-03969-0

92. Miklavčič D. Network for development of electroporation-based technologies and treatments: COST TD1104. *J Membr Biol* 2012; **245:** 591-8. doi: 10.1007/s00232-012-9493-8

93. Gehl J, Pereira PL, Cantwell CP, Deschamps F, Kocijancic A, Schmidt N, et al. Tumor ablation: emerging uses, challenges, and strategic implementation. A green paper by the Network of Expertise in Cancer (JANE-2), High Tech Medical Resources, network on Physical Methods of Tumor Ablation. *Radiol Oncol* 2026; 60(3): 307-322.; **60:** 153-65. doi: 10.2478/raon-2026-0030

94. Casali PG, Antoine-Poirel H, Berrocoso S, Blay J-Y, Dubois T, Ferrari A, et al. Health networking on cancer in the European Union: a 'green paper' by the EU Joint Action on Networks of Expertise (JANE). *ESMO Open* 2025; **10:** 104126. doi: 10.1016/j.esmoop.2024.104126

95. Mathy RM, Tinoush P, da Florencia RD, Braun A, Ghamarnejad O, Radeleff B, et al. Impact of needle positioning on ablation success of irreversible electroporation: a unicentric retrospective analysis. *Sci Rep* 2020; **10:** 21902. doi: 10.1038/s41598-020-78660-0

96. Cindrič H, Kos B, Miklavčič D. Electrodes and electric field distribution in clinical practice. In: Impellizeri JA, editor. *Electroporation in veterinary oncology practice: electrochemotherapy and gene electrotransfer for immunotherapy*. Cham: Springer International Publishing; 2021. p. 21-59. doi: 10.1007/978-3-030-80668-2_2

97. Andrade DLLS, Guedert R, Pintarelli GB, Rangel MMM, Oliveira KD, Quadros PG, et al. Electrochemotherapy treatment safety under parallel needle deflection. *Sci Rep* 2022; **12:** 2766. doi: 10.1038/s41598-022-06747-x

98. Grošelj A, Kos B, Čemažar M, Urbančič J, Kragelj G, Bošnjak M, et al. Coupling treatment planning with navigation system: a new technological approach in treatment of head and neck tumors by electrochemotherapy. *Biomed Eng Online* 2015; **14 (Suppl 3)**: S2. doi: 10.1186/1475-925X-14-S3-S2

99. Kos B, Voigt P, Miklavcic D, Moche M. Careful treatment planning enables safe ablation of liver tumors adjacent to major blood vessels by percutaneous irreversible electroporation (IRE). *Radiol Oncol* 2015; **49:** 234-41. doi: 10.1515/raon-2015-0031

100. Garcia PA, Kos B, Rossmeisl JH, Pavliha D, Miklavčič D, Davalos RV. Predictive therapeutic planning for irreversible electroporation treatment of spontaneous malignant glioma. *Med Phys* 2017; **44:** 4968-80. doi: 10.1002/mp.12401

101. Cindrič H, Mariappan P, Beyer L, Wiggermann P, Moche M, Miklavčič D, et al. Retrospective study for validation and improvement of numerical treatment planning of irreversible electroporation ablation for treatment of liver tumors. *IEEE Trans Biomed Eng* 2021; **68:** 3513-24. doi: 10.1109/TBME.2021.3075772

102. Padia SA, Johnson GE, Yeung RS, Park JO, Hippe DS, Kogut MJ. Irreversible electroporation in patients with hepatocellular carcinoma: immediate versus delayed findings at MR imaging. *Radiology* 2016; **278:** 285-94. doi: 10.1148/radiol.2015150031

103. Barabasch A, Distelmaier M, Heil P, Krämer NA, Kuhl CK, Bruners P. Magnetic resonance imaging findings after percutaneous irreversible electroporation of liver metastases: a systematic longitudinal study. *Invest Radiol* 2017; **52:** 23. doi: 10.1097/RLI.0000000000000301

104. Felker ER, Dregely I, Chung DJ, Sung K, Osuagwu FC, Lassman C, et al. Irreversible electroporation: defining the MRI appearance of the ablation zone with histopathologic correlation in a porcine liver model. *AJR Am J Roentgenol* 2017; **208:** 1141-6. doi: 10.2214/AJR.16.17207

105. Granata V, Fusco R, Salati S, Petrillo A, Bernardo ED, Grassi R, et al. A Systematic review about imaging and histopathological findings for detecting and evaluating electroporation based treatments response. *Int J Environ Res Public Health* 2021; **18:** 5592. doi: 10.3390/ijerph18115592

106. Cindrič H, Kos B, Tedesco G, Cadossi M, Gasbarrini A, Miklavčič D. Electrochemotherapy of spinal metastases using transpedicular approach - a numerical feasibility study. *Technol Cancer Res Treat* 2018; **17:** 1533034618770253. doi: 10.1177/1533034618770253

107. Pavliha D, Kos B, Marčan M, Zupanič A, Serša G, Miklavčič D. Planning of electroporation-based treatments using Web-based treatment-planning software. *J Membr Biol* 2013; **246:** 833-42. doi: 10.1007/s00232-013-9567-2

108. Marčan M, Pavliha D, Kos B, Forjanič T, Miklavčič D. Web-based tool for visualization of electric field distribution in deep-seated body structures and planning of electroporation-based treatments. *Biomed Eng Online* 2015; **14 (Suppl 3):** S4. doi: 10.1186/1475-925X-14-S3-S4

109. Perera-Bel E, Yagüe C, Mercadal B, Ceresa M, Beitel-White N, Davalos RV, et al. EView: an electric field visualization web platform for electroporation-based therapies. *Comput Methods Programs Biomed* 2020; **197:** 105682. doi: 10.1016/j.cmpb.2020.105682

110. Perera-Bel E, Aycock KN, Salameh ZS, Gómez-Barea M, Davalos RV, Ivorra A, et al. PIRET - a platform for treatment planning in electroporation-based therapies. *IEEE Trans Biomed Eng* 2022; **70:** 1902-10. doi: 10.1109/TBME.2022.3232038.

111. Paffi A, Apollonio F, Cadossi M, D'Alessio V, Fusco R, Giannini A, et al. A fast 3-D approach for electroporation treatment planning: optimal electrodes configuration. *IEEE J Electromagn RF Microw Med Biol* 2024; **8:** 393-400. doi: 10.1109/JERM.2024.3409678

112. Sertkaya A, DeVries R, Jessup A, Beleche T. Estimated cost of developing a therapeutic complex medical device in the US. *JAMA Netw Open* 2022; **5:** e2231609. doi: 10.1001/jamanetworkopen.2022.31609

review

The role of particle therapy in the treatment of locally recurrent rectal cancer: a systematic review

Ana Perpar[1], Petra Georg[2,3], Ajra Secerov Ermenc[1,4]

[1] Department of Radiation Oncology, Institute of Oncology Ljubljana, Ljubljana, Slovenia
[2] Department of Radiation Oncology, University Clinic Krems, Krems an der Donau, Austria
[3] Karl Landsteiner University of Health Sciences, Krems an der Donau, Austria
[4] Medical Faculty, University of Ljubljana, Ljubljana, Slovenia

Radiol Oncol 2026; 60(3): 323-331.

Received 25 November 2025
Accepted 22 May 2026

Correspondence to: Ana Perpar, M.D., Ph.D., Institute of Oncology Ljubljana, Department of Radiation Oncology, Zaloška cesta 2, SI-1000 Ljubljana, Slovenia. E-mail: aperpar@onko-i.si

Disclosure: No potential conflicts of interest were disclosed.

Background. Colorectal cancer is a common malignancy. Advancements in multimodality treatment have improved outcomes. About 2–10% of patients will have a local recurrence even after optimal treatment. Salvage surgical treatment is the treatment of choice, however, in posterior and lateral recurrences, surgery is linked to a high rate of treatment-related morbidity. Some recurrences remain unresectable even after neoadjuvant treatment.

Materials and methods. A systematic literature review was performed to search for studies on curative-intent radiation therapy (RT) with photons, stereotactic body radiation therapy (SBRT) and particle beam therapy. The aim of the literature search was to define the role of particle therapy in the treatment of patients with unresectable or inoperable local recurrences of rectal cancer where neoadjuvant treatment is unlikely to result in downstaging, leaving patients with RT as the only curative treatment option.

Results. 32 studies which fulfil the criteria were identified. In general, SBRT and particle beam therapy permitted the application of significantly higher doses to the target without a concomitant increase in treatment-related toxicities.

Conclusions. For unresectable and inoperable locally recurrent rectal cancer ablative radiotherapy techniques such as SBRT and particle beam therapy offer a curative treatment approach as an alternative to surgery. SBRT can be offered for small local and nodal recurrences, while particle beam therapy can be offered for larger recurrences and complex shapes spanning several anatomical compartments as well. Further research is needed to stratify patients according to their need and eligibility for the different possible modalities of curative-intent RT.

Key words: rectal cancer; inoperable local recurrence; unresectable recurrence; particle therapy; ion beam therapy; SBRT; curative RT

Introduction

Colorectal cancer is the third commonest cancer in men and the second commonest cancer in women in the European Union.[1] With improvements in treatment, e.g. the use of total mesorectal excision in surgical treatment, the use of neoadjuvant and later total neoadjuvant treatment combining radiotherapy and systemic treatment, including immunotherapy, the risk for local and pelvic recurrence has been significantly reduced, the 5-year follow-up of the RAPIDO trial yielded a 10% rate of locoregional failure in the experimental group and may be as low as 2%, according to some results.[2-9]

However, for patients experiencing a pelvic recurrence, curative treatment options are limited.

Rokan *et al*. have published a review grouping local recurrences according to anatomical site of recurrence: central (18%), lateral (15%), posterior (13%), anterior below peritoneal reflection (10%), infralevator/anterior urogenital triangle (4%), and anterior above peritoneal reflection (1%), unknown 39%.[10]

The preferred treatment for pelvic recurrences is salvage surgery which must be undertaken with the aim of achieving negative margins, since complete (R0) resections have been consistently linked to significantly better survival outcomes than non-radical resections.[11-13]

Unfortunately, not all sites of recurrence have the same resectability and prognosis. Central recurrences have consistently been shown to result in the highest rate of R0 resection, lateral and posterior recurrences are the least likely to be successfully treated with an R0 resection and even worse results have been reported for recurrences involving more than one compartment.[12,14-17]

Additionally, aggressive surgical treatment of lateral and posterior recurrences results in a higher rate of severe impairments, including severe neurological dysfunction of bladder and bowel in high sacral resection, while extensive lateral resection is linked to a 82% rate of postoperative complications.[18] And though exenteration may offer patients with locally advanced rectal cancer the chance of long-term survival with acceptable levels of morbidity, it remains a major operation associated with significant morbidity and mortality where the R1 resection rate remains high, especially in recurrent cancers (median 28.26%, upper range 68.2%).[19,20]

The use of neoadjuvant chemoradiation in locally recurrent rectal cancer is recommended by both ESMO and Beyond TME guidelines, with the aim of downstaging and improving resectability.[21,22] In patients who had already received a radiation course to the pelvis, the prescribed dose must be individualized to reach a compromise between maximum safe dose and the dose constraints of pelvic organs. The Dutch national guidelines for the management of locally recurrent rectal cancer report the use of intensity-modulated radiation therapy / volumetric modulated arc therapy (IMRT/VMAT) use as the standard of care in the Netherlands both for primary and reirradiation of locally recurrent rectal cancer.[23]

There is however a significant proportion of patients with locally recurrent rectal cancer who either remain unresectable after neoadjuvant treatment or are not candidates for surgical treatment due to other reasons (e.g. the patients' poor general condition, comorbidities or refusal to consent to treatment which may leave them with life-long functional compromise). If lateral and posterior recurrences from Rokan *et al*. are grouped together, we have over a quarter (28%) of all local recurrences with a significant likelihood of unresectable disease even after neoadjuvant treatment.[10]

There is evidence that local recurrences after radiation therapy shift from central and anterior to more lateral and posterior.[24] This means that an even larger proportion of patients who received neoadjuvant radiation as part of their primary treatment have recurrences in unfavourable locations.

For these patients, curative-intent radiation therapy (RT) presents the only chance of cure. The development of modern treatment techniques – stereotactic body radiation therapy (SBRT) and intensity-modulated radiation therapy (IMRT) – as well as the use of charged particles with a more favourable dose distribution profile makes the application of a curative dose possible.

The risk of severe radiation-induced toxicity depends on where the recurrence is located. In posterior and lateral recurrences, the major risks are radiation-induced damage to the rectum (with possible haemorrhage, perforation and fistulas) and neurotoxicity (with sensorimotor impairments and neuropathic pain), while high-dose radiation therapy of central and anterior recurrences, while still linked with increased risk of rectal damage, also carries the risk of bladder toxicity (haemorrhage, perforation and fistulas). Any recurrence abutting the bony structures of the pelvis also increases the risk of bone fractures.

For the purposes of this article, we have focused on unresectable or inoperable local recurrences of rectal cancer where neoadjuvant treatment is unlikely to result in any significant downstaging, leaving patients with definitive RT as the only curative treatment option. In this narrative review we wish to summarize the current state of the art in the treatment of these patients and establish the role of particle therapy in their treatment of patients.

Materials and methods

This review was conducted using the Preferred Reporting Items for Systematic Reviews and Meta-

Analyses (PRISMA) guidelines.[25] Eligible sources included published and peer-reviewed work evaluating

(1) clinical outcomes (including local control and overall survival was mandatory, data on toxicities was desired, but not necessary for inclusion) of
(2) conformal photon, SBRT or particle beam therapy with curative intent for
(3) pelvic recurrences of rectal cancer in
(4) both radiation-naïve and pre-irradiated patients, reported in
(5) English with
(6) a minimum number of 10 reported cases.

Studies had to report on the

(7) radiation dose applied,
(8) any concomitant or additional treatment the patients received, e.g. concomitant chemotherapy, hyperthermia or surgery,
(9) pelvic control outcomes (including local and regional control, if reported) and
(10) survival.

We have searched PUBMED, EMBASE, SCOPUS, Clinicaltrials.gov and COCHRANE, those found in references from the major articles identified, and articles known to the authors. To avoid missing potentially relevant publications, sources were excluded by individual screening of reports rather than screening of titles and abstracts. We have also scanned the references of included articles for missed publications.

The first search was conducted in December 2023, then updated in September / October 2024.

An initial screening was performed using citations and titles, to filter studies duplicated among databases or studies that were not clinical trials, such as reviews, letters, editorials, and in vivo or in vitro studies. A second screening of abstracts and excluded studies with irrelevant subjects, fewer than 10 patients with rectal cancer receiving reirradiation, and studies that were not clinical trials was conducted. Finally, a full-text review to identify studies meeting the above inclusion criteria was performed. In cases of multiple studies from a single institution, the following criteria were applied and prioritized in the following order: (1) studies with the largest number of patients with rectal cancer who received reirradiation, and (2) the most recent publication. Even if studies were published by the same institution, multiple studies were included if the patient cohorts could safely be assumed to be different.

Only articles that report patient outcomes on the usual timepoints were included, i.e. full years.

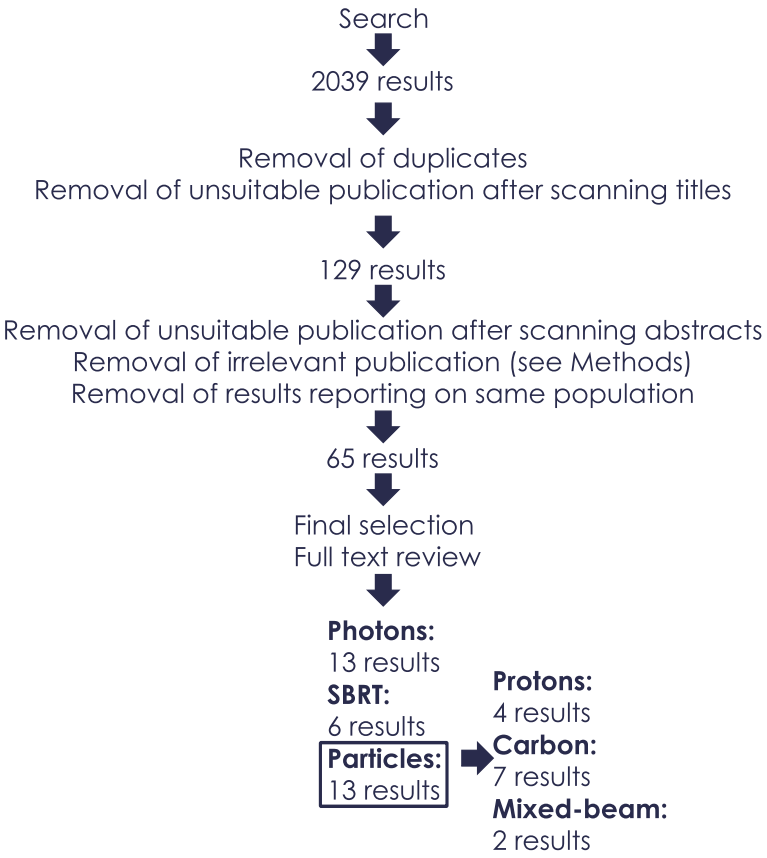

FIGURE 1. Process of article selection.

The report by Habermehl *et al*. was excluded for this reason.[26]

Studies on conventional photon radiation therapy were excluded if they reported results on older treatment techniques used before the adoption of 3-dimensional conformal radiation therapy (3D-CRT), or if no definite information was available in the article and it could safely be assumed the cohort was treated with older techniques.

Studies reporting on locally recurrent rectal cancer amongst other pelvic malignancies (e.g. together with locally advanced rectal cancer or together with recurrent urological and/or gynaecological malignancies) were included only if the results of treatment of locally recurrent rectal cancer were reported separately from the other entities and if the number of the included patients with locally recurrent rectal cancer was 10 or more. Moningi *et al*. and Shirai *et al*. were excluded for this reason.[27,28]

The above screening processes was performed by AP and checked by PG & AŠE, final inclusion was confirmed upon mutual consent.

The following terms were used:

((carbon[Title/Abstract]) OR (hadron[Title/Abstract]) OR (hadrons[Title/Abstract]) OR (carbon ion beam[Title/Abstract]) OR (carbon ion[Title/Abstract]) OR (proton[Title/Abstract]) OR (protons[Title/Abstract]) OR (proton beam[Title/Abstract]) OR (charged particle[Title/Abstract]) OR (charged particles[Title/Abstract]) OR (particle[Title/Abstract]))	OR	((SBRT[Title/Abstract]) OR stereotactic[Title/Abstract]) OR stereotaxy[Title/Abstract]))	OR	((radiation[Title/Abstract]) OR radiotherapy[Title/Abstract]) OR (radiation therapy[Title/Abstract]) OR (reirradiation[Title/Abstract]) OR (irradiation[Title/Abstract]) OR (actinotherapy[Title/Abstract]))
AND				
(rectal[Title/Abstract] OR (rectum[Title/Abstract]))				
AND				
((recurrence[Title/Abstract]) OR (relapse[Title/Abstract]) OR (local recurrence[Title/Abstract]) OR (pelvic recurrence[Title/Abstract]) OR (pelvic relapse[Title/Abstract]) OR (local relapse[Title/Abstract]) OR (locally recurrent[Title/Abstract]) OR (recurrent[Title/Abstract]) OR (pelvis[Title/Abstract]) OR (pelvic[Title/Abstract]) OR (pelvic[Title/Abstract]))				

SBRT = stereotactic body radiation therapy

For Clinicaltrials.gov the terms were: rectal and rectum for condition/disease and particle, carbon or proton for other terms.

A search for currently active studies on radiation therapy of locally recurrent rectal cancer was performed.

Results

32 studies which fulfil the criteria were identified, 12 studies reporting on the results of photon RT, 6 studies reporting on the results of SBRT, 13 studies reporting on the results of particle beam therapy. The process of selection is depicted in Figure 1.

Multimodality treatment

Several studies have reported improved outcomes in patients treated with multimodality therapy and in which an R0 resection could be achieved.[29,30]

The results of photon RT are presented in Supplementary Table 1.[31-42]

Surgery after radiation has been shown to result in superior outcomes, including local control as well as survival, in addition, tumour size and total dose applied were predictive of improved outcomes. However, in some reports, surgery as well as higher applied dose have also been linked with a higher risk of severe late toxicity.[31,34,36,39-41,43-45]

Patients unlikely to have resectable disease even after neoadjuvant chemo(re)irradiation are unlikely to benefit from surgical treatment and for them, the outcomes for definitive radiation therapy with photons remain dismal, please see Supplementary Table 1 for further details. These patients urgently require a treatment alternative, since for most of them, their survival is determined by local control of the recurrence.[31,39,41]

Numerous strategies to enhance the therapeutic ratio have been explored, including concomitant systemic treatment, alterative fractionation regimes, to the use of intraoperative RT which, owing to the physical characteristics of the beams used, electrons, kilovoltage photons, or brachytherapy, can facilitate the application of a higher cumulative dose without significantly increasing the risk for late toxicities.[31-33,36,39,41-43,46,47] Photons, given their physical limitations, cannot apply a curative dose to the recurrent tumour outside of stereotactic radiation modalities and are used in a neoadjuvant setting or a means of palliation.

It should also be pointed out that several of the studies included patients with metastatic disease, which undoubtedly had an impact on overall survival. In the studies reporting on the results of definitive RT, only Cai *et al*. report including patients with metastatic disease.[31,33,34,36,40,41]

Definitive radiation therapy

The results of definitive RT with SBRT or particle beams are presented in Supplementary Table 2.[48-66]

Stereotactic body radiation therapy (SBRT)

The included studies report clinical results for various follow-up intervals; thus an esti mate of expected local control is difficult. In addition, dose prescription regimes within individual publications are highly variable as most publications report only a mean dose or biologically equivalent dose (BED) or alternatively a range of doses and fractions.[48,49,51,52] The results of a uniform dose prescription protocol (30 Gy in 5 fractions) are reported only by Johnstone *et al*. and Smith *et al*.[50,53]

2-year local control can be expected to be 68.2–93.7%, while 2-year survival was reported to be 65.9-84.4%.[48-50,53] Minecci *et al*.[52] report 5-year local control rates of 82.6%, Kim *et al*. report 5 year-survival 23.2%.[51,] The incidence of late grade 3 or more toxicities ranges from 0–13%.[49,52]

In the studies reported, the median tumour size ranges from 13.4 to 90.1 cm^3 or up to 136.5 cm^3 for the median planning target volume (PTV) volume.[48,50,52] The vast majority of treated patients were treated for pelvic nodal rectal cancer recurrences, which confirms that SBRT is the radiation modality of choice for delivering high dose to a smaller volume of relatively simple shape.

Particle beam therapy

The usual dose regimes used in the Japanese centres for carbon ion beam therapy consists of 16 fractions with a total dose of 67.2–73.6 Gy. 5-year local control rates are reported to be between 35–88% with a clear dose-response relationship, which is also mirrored in the reported 5-year overall survival.[54]

Other centres using carbon ion beams have more heterogeneous dose prescription, however Cai *et al*. have also observed a dose-response relationship with the cutoff at 66 Gy.[64]

It is difficult to compare the results of proton beam therapy since the publications we have included report outcomes at different time intervals and do not use uniform dose prescription regimes, however, 1-year and 3-year local control is reported as between 66.3-70% and 55-80.2%.[56,57,60,62]

The volumes of treated targets are variable, but from the studies that report volumes of targets, the median gross target volume (GTV) volume ranges from 57.1–154 cm^3 for carbon ions and 26.1-86.4 cm^3 for protons, with maximum volumes over 300 cm^3. Others report only median target diameters which range from 30–63 mm.[56,58,60,65,66]

In RT-naïve patients, the toxicity profile is very favourable and in general late toxicities of particle beam therapy grade 3 or higher are reported in up to 5% of cases, with rare grade 4 toxicities, though Takagawa *et al*. report grade 4 gastrointestinal toxicities in 3 patients in 2 of whom reirradiation was associated with further local recurrence after proton beam therapy.[54,57,62,67,68] In patients treated with reirradiation severe toxicities are reported more frequently, up to 21%.[55] There is also mention of grade 5 toxicities, in particular Koroulakis *et al*. report a fatal presacral haemorrhage in patient previously treated with radiation for ovarian cancer in the 1970s who developed a grade 4 presacral skin ulcer.[60]

Clinical trials

The ongoing studies are summarized in Supplementary Table 3.[69-77]

There are several studies currently recruiting patients with locally recurrent rectal cancer for particle beam RT.

Combs *et. al* published the protocol of the PANDORA-01 study in 2012[78], describing the protocol for their prospective phase I/II study for carbon ion beam therapy for recurrent rectal cancer. As of now, no clinical results have been published.

Discussion

Since the majority of the included studies were retrospective, non-controlled studies, there is an inherent risk of bias in our publication.

As is evident from this review, patients with locally recurrent rectal cancer who do not receive a complete resection have dismal outcomes after conformal photon radiation therapy. However, both SBRT as well as particle therapy offer a curative non-invasive treatment option for these patients, both RT-naïve and preirradiated. Both SBRT as well as particle beam therapy allow for the application of ablative doses to the target in contrast to conformal photon RT. The application of sufficient dose in the context of ablative radiation therapy is crucial to the curative intent.[61,63,64] Yamada *et al*. have demonstrated that raising the prescribed dose from 67.2 Gy relative biological effectiveness (RBE) to 73.6 Gy RBE more than doubles both 5-year local control as well as 5-year overall survival.[54]

The main limiting factors to the use of SBRT are target size and shape; while small local and nodal recurrences are good candidates for SBRT, larger recurrences with complex shapes spanning several anatomical compartments are not optimal candidates for SBRT. The definitions of SBRT treatment almost never include the maximum size of the target, specifying only that an ablative dose must be safely applied to the target, the commonly used cut-off for lung tumours is 5 cm (with acceptable results published for larger tumours) and 6 cm for liver tumours, both of which usually have simple, circular shapes.[79,80] Any attempt at generalizing these results to tumours with complex concave shapes is difficult if not impossible. In our review,

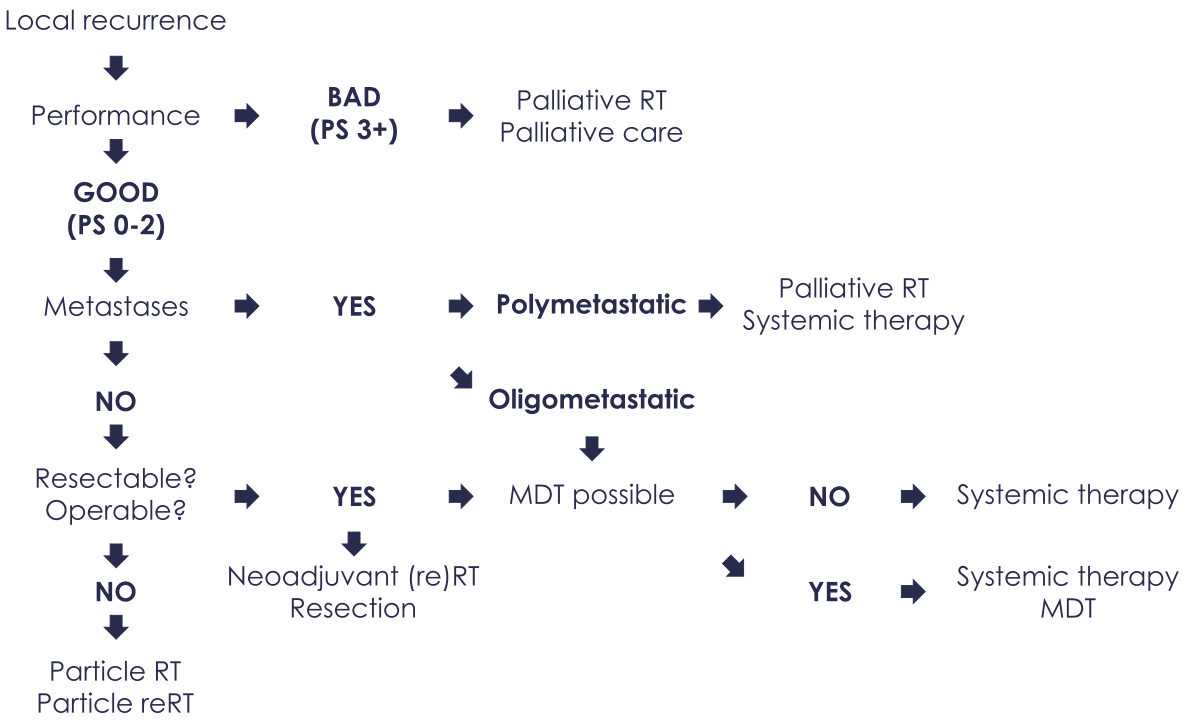

FIGURE 2. Patient selection for particle therapy of locally recurrent rectal cancer.

MDT = metastasis-directed treatment; PS = performance status; reRT = reirradiation; RT = radiation therapy; SBRT = stereotactic body radiation therapy

studies that reported the range of tumour volumes reported maxima under 150 cm^3, with Dagoglu *et al*. as the only exception, where the maximum size of lesions was over 1 litre, with the median under 100 cm^3, meaning that most targets were still relatively small.[48]

The favourable dose distribution characteristics of particle beams and the potential for dose escalation would increase the chances of cure of macroscopic radioresistant disease without significantly increasing the rate of severe toxicity. Thus, particle beam therapy would present a curative alternative for surgery in patients with unresectable or inoperable locally recurrent rectal cancer.

As regards the selection of patients for each curative-intent RT modality, tumour size and shape may provide useful criteria. Some centres set an upper limit for particle therapy at tumour sizes above 15 x 15 cm, there is still a significant number of patients which are not candidates for SBRT due to the size of the recurrent tumours which would be considered treatable with particles.[54,58] Thus, particle beams can offer curative treatment to patients with recurrent tumours too large or too complex-shaped for SBRT.

While patients with recurrent tumours abutting or invading the gastrointestinal and urinary tract are routinely counselled against ablative RT, case reports show that in select cases, even such patients may be treated curatively with the application of ablative dose if all reasonable measures are taken to mitigate the risk of late, severe, possibly life-threatening toxicities, including resecting bowel loops at risk of radiation-induced necrosis.[81,82] However, it should be stressed that these cases are exceptions to the rule and that such decisions lie exclusively in the domain of an experienced, well-versed multidisciplinary team that operates in a high-volume comprehensive cancer centre.

An alternative mitigation strategy in the case of hollow organ abutment is the use of spacers, which displace the hollow organs from the high-dose area and thus both render the application of ablative dose possible and significantly reduce the risk of severe late toxicities.[83-85] Though it should be noted that Shinoto *et al*. report that out of 224 patients in the J-CROS-1404 trial 12 patients developed grade 3 or more late toxicities and all 7 patients who developed pelvic abscesses had undergone spacer insertion before particle beam RT, so this method

may have a risk of toxicities independent of ablative RT.[58]

A randomized trial between surgery and particle beam therapy for patients with unresectable locally recurrent rectal cancer is neither practicable nor is it acceptable from an ethical point of view, given that according to the literature, patients who were treated with an incomplete resection with macroscopic residual tumour (R2 resection) had at best comparable and at worst worse outcomes than those who had not been surgically treated and received only palliative / conservative treatment.[11-13]

Similarly, comparing the results of conformal photon radiation therapy and ablative radiation therapy (either SBRT or particle therapy) is meaningless, since their roles in the management of this diverse patient group are different: the former is an adjunct to surgical treatment while the latter, with the possibility of dose escalation, is an alternative for surgery when surgery is not possible.[61,63] While retrospective studies have shown that certain patients are better candidates for one over the other, until we have more robust, prospective data, no definitive recommendations can be made for patient selection.

Particle therapy avoids mutilating surgical procedures in patients with posterior and lateral recurrences, in extensive recurrent tumours spanning more than one compartment, as well as offering the chance of cure for patients with unresectable disease and contraindications to surgery with acceptable toxicity.

The authors propose the following algorithm for the selection of candidates for particle therapy of locally recurrent rectal cancer:

In conclusion, for unresectable and inoperable locally recurrent rectal cancer ablative radiotherapy techniques such as SBRT and particle beam therapy offer a curative treatment approach. Further research is needed to stratify patients according to their need and eligibility for the different possible modalities of treatment.

Currently running prospective studies will furnish us with more robust results to facilitate patient stratification towards optimal modes of treatment as well as optimizing treatment protocols to achieve optimal results.

References

1. Cancer Factsheets in EU-27 countries - 2020 | ECIS - European Cancer Information System [Internet]. [cited 2023 Nov 12]. Available at: https://ecis.jrc.ec.europa.eu/cancer-factsheets-eu-27-countries-2020
2. Heald RJ, Ryall RDH. Recurrence and survival after total mesorectal excision for rectal cancer. *Lancet* 1986; **327:** 1479-82. doi: 10.1016/S0140-6736(86)91510-2
3. Sauer R, Liersch T, Merkel S, Fietkau R, Hohenberger W, Hess C, et al. Preoperative Versus postoperative chemoradiotherapy for locally advanced rectal cancer: results of the German CAO/ARO/AIO-94 Randomized Phase III Trial after a median follow-up of 11 years. *J Clin Oncol* 2012; **30:** 1926-33. doi: 10.1200/JCO.2011.40.1836
4. Folkesson J, Birgisson H, Pahlman L, Cedermark B, Glimelius B, Gunnarsson U. Swedish Rectal Cancer Trial: long lasting benefits from radiotherapy on survival and local recurrence rate. *J Clin Oncol* 2005; **23:** 5644-50. doi: 10.1200/JCO.2005.08.144
5. Conroy T, Castan F, Etienne PL, Rio E, Mesgouez-Nebout N, Evesque L, et al. Total neoadjuvant therapy with mFOLFIRINOX versus preoperative chemoradiotherapy in patients with locally advanced rectal cancer: long-term results of the UNICANCER-PRODIGE 23 Trial. *Ann Oncol* 2024; **35:** 873-81. doi: 10.1016/j.annonc.2024.06.019
6. Fokas E, Schlenska-Lange A, Polat B, Klautke G, Grabenbauer GG, Fietkau R, et al. Chemoradiotherapy plus induction or consolidation chemotherapy as total neoadjuvant therapy for patients with locally advanced rectal cancer: long-term results of the CAO/ARO/AIO-12 Randomized Clinical Trial. *JAMA Oncol* 2022; **8:** e215445. doi: 10.1001/jamaoncol.2021.5445
7. Ciseł B, Pietrzak L, Michalski W, Wyrwicz L, Rutkowski A, Kosakowska E, et al. Long-course preoperative chemoradiation versus 5 × 5 Gy and consolidation chemotherapy for clinical T4 and fixed clinical T3 rectal cancer: long-term results of the randomized Polish II study. *Ann Oncol* 2019; **30:** 1298-303. doi: 10.1093/annonc/mdz186
8. Li H, Tang Y, Zhou H, Hu C, Wei L, Zhang Y, et al. Preoperative short-course radiotherapy followed by chemotherapy and PD-1 inhibitor administration for locally advanced rectal cancer: the initial results of a Randomized Phase II/III Trial (STELLAR II study). *Int J Radiat Oncol Biol Phys* 2024; **120:** e462. doi: 10.1016/j.ijrobp.2024.07.1025
9. Dijkstra EA, Nilsson PJ, Hospers GAP, Bahadoer RR, Meershoek-Klein Kranenbarg E, Roodvoets AGH, et al. Locoregional failure during and after short-course radiotherapy followed by chemotherapy and surgery compared with long-course chemoradiotherapy and surgery: a 5-year follow-up of the RAPIDO Trial. *Ann Surg* 2023; **278:** e766-72. doi: 10.1097/SLA.0000000000005799
10. Rokan Z, Simillis C, Kontovounisios C, Moran B, Tekkis P, Brown G. Locally recurrent rectal cancer according to a Standardized MRI Classification System: a systematic review of the literature. *J Clin Med* 2022; **11:** 3511. doi: 10.3390/jcm11123511
11. Bhangu A, Ali SM, Darzi A, Brown G, Tekkis P. Meta-analysis of survival based on resection margin status following surgery for recurrent rectal cancer. *Colorectal Dis* 2012; **14:** 1457-66. doi: 10.1111/j.1463-1318.2012.03005.x
12. Bhangu A, Ali M, Cunningham D, Brown G, Tekkis PP. Comparison of long-term survival outcomes of operative versus nonoperative management of recurrent rectal cancer. *J Clin Oncol* 2012; **30:** e14132. doi: 10.1200/jco.2012.30.15_suppl.e14132
13. Hagemans JAW, Van Rees JM, Alberda WJ, Rothbarth J, Nuyttens JJME, Van Meerten E, et al. Locally recurrent rectal cancer; long-term outcome of curative surgical and non-surgical treatment of 447 consecutive patients in a tertiary referral centre. *Eur J Surg Oncol* 2020; **46:** 448-54. doi: 10.1016/j.ejso.2019.10.037
14. Bird TG, Ngan SY, Chu J, Kroon R, Lynch AC, Heriot AG. Outcomes and prognostic factors of multimodality treatment for locally recurrent rectal cancer with curative intent. *Int J Colorectal Dis* 2018; **33:** 393-401. doi: 10.1007/s00384-018-2985-y
15. Zhao J. Patterns and prognosis of locally recurrent rectal cancer following multidisciplinary treatment. *World J Gastroenterol* 2012; **18:** 7015. doi: 10.3748/wjg.v18.i47.7015
16. Yamada K, Ishizawa T, Niwa K, Chuman Y, Akiba S, Aikou T. Patterns of pelvic invasion are prognostic in the treatment of locally recurrent rectal cancer. *Br J Surg* 2001; **88:** 988-93. doi: 10.1046/j.0007-1323.2001.01811.x
17. Moore HG, Shoup M, Riedel E, Minsky BD, Alektiar KM, Ercolani M, et al. Colorectal cancer pelvic recurrences: determinants of resectability. *dis colon rectum* 2004; **47:** 1599-606. doi: 10.1007/s10350-004-0677-x
18. Gao Z, Gu J. Surgical treatment of locally recurrent rectal cancer: a narrative review. *Ann Transl Med* 2021; **9:** 1026. doi: 10.21037/atm-21-2298

19. Fahy MR, Hayes C, Kelly ME, Winter DC. Updated systematic review of the approach to pelvic exenteration for locally advanced primary rectal cancer. *Eur J Surg Oncol* 2022; **48:** 2284-91. doi: 10.1016/j.ejso.2021.12.471

20. Platt E, Dovell G, Smolarek S. Systematic review of outcomes following pelvic exenteration for the treatment of primary and recurrent locally advanced rectal cancer. *Tech Coloproctol* 2018; **22:** 835-45. doi: 10.1007/s10151-018-1883-1

21. Beyond TME Collaborative; Ali SM, Antoniou A, Beynon J, Bhangu A, Bose P, et al. Consensus statement on the multidisciplinary management of patients with recurrent and primary rectal cancer beyond total mesorectal excision planes. *Br J Surg* 2013; **100:** 1009-14. doi: 10.1002/bjs.9192

22. Glynne-Jones R, Wyrwicz L, Tiret E, Brown G, Rödel C, Cervantes A, et al. Rectal cancer: ESMO Clinical Practice Guidelines for diagnosis, treatment and follow-up. *Ann Oncol* 2017; **28:** iv22-40. doi: 10.1093/annonc/mdx224

23. Piqeur F, Creemers DMJ, Banken E, Coolen L, Tanis PJ, Maas M, et al. Dutch national guidelines for locally recurrent rectal cancer. *Cancer Treat Rev* 2024; **127:** 102736. doi: 10.1016/j.ctrv.2024.102736

24. Enríquez-Navascués JM. Patterns of local recurrence in rectal cancer after a multidisciplinary approach. *World J Gastroenterol* 2011; **17:** 1674. doi: 10.3748/wjg.v17.i13.1674

25. Page MJ, McKenzie JE, Bossuyt PM, Boutron I, Hoffmann TC, Mulrow CD, et al. The PRISMA 2020 statement: an updated guideline for reporting systematic reviews. *BMJ* 2021; **n71.** doi: 10.1136/bmj.n71

26. Habermehl D, Wagner M, Ellerbrock M, Büchler MW, Jäkel O, Debus J, et al. Reirradiation using carbon ions in patients with locally recurrent rectal cancer at HIT: first results. *Ann Surg Oncol* 2015; **22:** 2068-74. doi: 10.1245/s10434-014-4219-z

27. Moningi S, Ludmir EB, Polamraju P, Williamson T, Melkun MM, Herman JD, et al. Definitive hyperfractionated, accelerated proton reirradiation for patients with pelvic malignancies. *Clin Transl Radiat Oncol* 2019; **19:** 59-65. doi: 10.1016/j.ctro.2019.08.004

28. Shirai K, Ohno T, Saitoh J ichi, Okamoto M, Katoh H, Murata K, et al. Prospective study of isolated recurrent tumor re-irradiation with carbon-ion beams. *Front Oncol* 2019; **9:** 181. doi: 10.3389/fonc.2019.00181

29. Bird TG, Ngan SY, Chu J, Kroon R, Lynch AC, Heriot AG. Outcomes and prognostic factors of multimodality treatment for locally recurrent rectal cancer with curative intent. *Int J Colorectal Dis* 2018; **33:** 393-401. doi: 10.1007/s00384-018-2985-y

30. Tang Z, Liu L, Liu D, Wu L, Lu K, Zhou N, et al. Clinical Outcomes and Safety of Different Treatment Modes for Local Recurrence of Rectal Cancer. *Cancer Manag Res* 2020; **12:** 12277-86. doi: 10.2147/CMAR.S278427

31. Al-Haidari G, Skovlund E, Undseth C, Rekstad BL, Larsen SG, Åsli LM, et al. Re-irradiation for recurrent rectal cancer - a single-center experience. *Acta Oncol* 2020; **59:** 534-40. doi: 10.1080/0284186X.2020.1725111

32. Bosman SJ, Holman FA, Nieuwenhuijzen GAP, Martijn H, Creemers GJ, Rutten HJT. Feasibility of reirradiation in the treatment of locally recurrent rectal cancer. *Br J Surg* 2014; **101:** 1280-9. doi: 10.1002/bjs.9569

33. Cai G, Zhu J, Palmer JD, Xu Y, Hu W, Gu W, et al. CAPIRI-IMRT: a phase II study of concurrent capecitabine and irinotecan with intensity-modulated radiation therapy for the treatment of recurrent rectal cancer. *Radiat Oncol* 2015; **10:** 57. doi: 10.1186/s13014-015-0360-5

34. Chung SY, Koom WS, Keum KC, Chang JS, Shin SJ, Ahn JB, et al. Treatment outcomes of re-irradiation in locoregionally recurrent rectal cancer and clinical significance of proper patient selection. *Front Oncol* 2019; **9:** 529. doi: 10.3389/fonc.2019.00529

35. Jo S, Choi Y, Park SK, Kim JY, Kim HJ, Lee YH, et al. Efficacy of dose-escalated radiotherapy for recurrent colorectal cancer. *Ann Coloproctol* 2016; **32:** 66. doi: 10.3393/ac.2016.32.2.66

36. Kishan AU, Voog JC, Wiseman J, Cook RR, Ancukiewicz M, Lee P, et al. Standard fractionation external beam radiotherapy with and without intraoperative radiotherapy for locally recurrent rectal cancer: the role of local therapy in patients with a high competing risk of death from distant disease. *Br J Radiol* 2017; **90:** 20170134. doi: 10.1259/bjr.20170134

37. Park Y, Kim K, Park HJ, Jeong SY, Park KJ, Han SW, et al. Results of re-irradiation for pelvic recurrence in anorectal cancer patients. *Br J Radiol* 2019; **92:** 20180794. doi: 10.1259/bjr.20180794

38. Sun DS, Zhang JD, Li L, Dai Y, Yu JM, Shao ZY. Accelerated hyperfractionation field-involved re-irradiation combined with concurrent capecitabine chemotherapy for locally recurrent and irresectable rectal cancer. *Br J Radiol* 2012; **85:** 259-64. doi: 10.1259/bjr/28173562

39. Susko M, Lee J, Salama J, Thomas S, Uronis H, Hsu D, et al. The use of re-irradiation in locally recurrent, non-metastatic rectal cancer. *Ann Surg Oncol* 2016; **23:** 3609-15. doi: 10.1245/s10434-016-5250-z

40. Tanaka H, Yamaguchi T, Hachiya K, Okada S, Kitahara M, Matsuyama K, et al. Radiotherapy for locally recurrent rectal cancer treated with surgery alone as the initial treatment. *Radiat Oncol J* 2017; **35:** 71-7. doi: 10.3857/roj.2016.02005

41. Tao R, Tsai CJ, Jensen G, Eng C, Kopetz S, Overman MJ, et al. Hyperfractionated accelerated reirradiation for rectal cancer: an analysis of outcomes and toxicity. *Radiother Oncol* 2017; **122:** 146-51. doi: 10.1016/j.radonc.2016.12.015

42. Watanabe J, Shoji H, Hamaguchi T, Miyamoto T, Hirano H, Iwasa S, et al. Chemoradiotherapy for local recurrence of rectal cancer: a single center study of 18 patients. *In Vivo* 2019; **33:** 1363-8. doi: 10.21873/invivo.11612

43. Youssef FF, Parikh PJ, DeWees TA, Mutch MG, Tan BR, Grigsby PW, et al. Efficacy and toxicity of rectal cancer reirradiation using IMRT for patients who have received prior pelvic radiation therapy. *Adv Radiat Oncol* 2016; **1:** 94-100. doi: 10.1016/j.adro.2016.02.002

44. Koom WS, Choi Y, Shim SJ, Cha J, Seong J, Kim NK, et al. Reirradiation to the pelvis for recurrent rectal cancer. *J Surg Oncol* 2012; **105:** 637-42. doi: 10.1002/jso.23023

45. Das P, Delclos ME, Skibber JM, Rodriguez-Bigas MA, Feig BW, Chang GJ, et al. Hyperfractionated accelerated radiotherapy for rectal cancer in patients with prior pelvic irradiation. *Int J Radiat Oncol Biol Phys* 2010; **77:** 60-5. doi: 10.1016/j.ijrobp.2009.04.056

46. Cai G, Zhu J, Hu W, Zhang Z. Accelerated hyperfractionated intensity-modulated radiotherapy for recurrent/unresectable rectal cancer in patients with previous pelvic irradiation: results of a phase II study. *Radiat Oncol* 2014; **9:** 278. doi: 10.1186/s13014-014-0278-3

47. Holman FA, Bosman SJ, Haddock MG, Gunderson LL, Kusters M, Nieuwenhuijzen GAP, et al. Results of a pooled analysis of IOERT containing multimodality treatment for locally recurrent rectal cancer. *Eur J Surg Oncol* 2017; **43:** 107-17. doi: 10.1016/j.ejso.2016.08.015

48. Dagoglu N, Mahadevan A, Nedea E, Poylin V, Nagle D. Stereotactic body radiotherapy (SBRT) reirradiation for pelvic recurrence from colorectal cancer. *J Surg Oncol* 2015; **111:** 478-82. doi: 10.1002/jso.23858

49. DeFoe S, Bernard M, Rwigema JC, Heron D, Ozhasoglu C, Burton S. Stereotactic body radiotherapy for the treatment of presacral recurrences from rectal cancers. *J Can Res Ther* 2011; **7:** 408. doi: 10.4103/0973-1482.92000

50. Johnstone P, Okonta L, Aitken K, Holmes J, Harrison M, Harji D, et al. A multicentre retrospective review of SABR reirradiation in rectal cancer recurrence. *Radiother Oncol* 2021; **162:** 1-6. doi: 10.1016/j.radonc.2021.06.030

51. Kim MS, Choi C, Yoo S, Cho C, Seo Y, Ji Y, et al. Stereotactic Body radiation therapy in patients with pelvic recurrence from rectal carcinoma. *Jpn J Clin Oncol* 2008; **38:** 695-700. doi: 10.1093/jjco/hyn083

52. Minneci M, Baclay JRM, Von Eyben R, Vitzthum L, Pollom E, Chang DT. The utility of stereotactic body radiotherapy for pelvic recurrences after prior radiation therapy. *Int J Radiat Oncol Biol Phys* 2021; **111:** e59-60. doi: 10.1016/j.ijrobp.2021.07.405

53. Smith T, O'Cathail SM, Silverman S, Robinson M, Tsang Y, Harrison M, et al. Stereotactic body radiation therapy reirradiation for locally recurrent rectal cancer: outcomes and toxicity. *Adv Radiat Oncol* 2020; **5:** 1311-9. doi: 10.1016/j.adro.2020.07.017

54. Yamada S, Kamada T, Ebner DK, Shinoto M, Terashima K, Isozaki Y, et al. Carbon-ion radiation therapy for pelvic recurrence of rectal cancer. *Int J Radiat Oncol Biol Phys* 2016; **96:** 93-101. doi: 10.1016/j.ijrobp.2016.04.022

55. Yamada S, Takiyama H, Isozaki Y, Shinoto M, Ebner DK, Koto M, et al. Carbon ion radiotherapy for locally recurrent rectal cancer of patients with prior pelvic irradiation. *Ann Surg Oncol* 2022; **29:** 99-106. doi: 10.1245/s10434-021-10876-4

56. Takagawa Y, Suzuki M, Seto I, Azami Y, Machida M, Takayama K, et al. Proton beam reirradiation for locally recurrent rectal cancer patients with prior pelvic irradiation. *J Radiat Res* 2024; **65:** 379-86. doi: 10.1093/jrr/rrae019

57. Takagawa Y, Suzuki M, Yamaguchi H, Seto I, Azami Y, Machida M, et al. Outcomes and prognostic factors for locally recurrent rectal cancer treated with proton beam therapy. *Adv Radiat Oncol* 2023; **8:** 101192. doi: 10.1016/j.adro.2023.101192

58. Shinoto M, Yamada S, Okamoto M, Shioyama Y, Ohno T, Nakano T, et al. Carbon-ion radiotherapy for locally recurrent rectal cancer: Japan Carbon-ion Radiation Oncology Study Group (J-CROS) Study 1404 Rectum. *Radiother Oncol* 2019; **132:** 236-40. doi: 10.1016/j.radonc.2018.10.007

59. Shiba S, Okamoto M, Shibuya K, Kobayashi D, Miyasaka Y, Ohno T. Five-year outcomes in carbon-ion radiotherapy for postoperative pelvic recurrence of rectal cancer: a prospective clinical trial (GUNMA 0801). *Clin Transl Radiat Oncol* 2024; **44:** 100701. doi: 10.1016/j.ctro.2023.100701

60. Koroulakis A, Molitoris J, Kaiser A, Hanna N, Bafford A, Jiang Y, et al. Reirradiation for rectal cancer using pencil beam scanning proton therapy: a single institutional experience. *Adv Radiat Oncol* 2021; **6:** 100595. doi: 10.1016/j.adro.2020.10.008

61. Jeans EB, Ebner DK, Takiyama H, Qualls K, Cunningham DA, Waddle MR, et al. Comparing oncologic outcomes and toxicity for combined modality therapy vs. carbon-ion radiotherapy for previously irradiated locally recurrent rectal cancer. *Cancers* 2023; **15:** 3057. doi: 10.3390/cancers15113057

62. Hiroshima Y, Ishikawa H, Murakami M, Nakamura M, Shimizu S, Enomoto T, et al. Proton beam therapy for local recurrence of rectal cancer. *Anticancer Res* 2021; **41:** 3589-95. doi: 10.21873/anticanres.15147

63. Chung SY, Takiyama H, Kang JH, Chang JS, Min BS, Tsuji H, et al. Comparison of clinical outcomes between carbon ion radiotherapy and X-ray radiotherapy for reirradiation in locoregional recurrence of rectal cancer. *Sci Rep* 2022; **12:** 1845. doi: 10.1038/s41598-022-05809-4

64. Cai X, Du Y, Wang Z, Li P, Yu Z, Zhang Q, et al. The role of carbon ion radiotherapy for unresectable locally recurrent rectal cancer: a single institutional experience. *Radiat Oncol* 2020; **15:** 209. doi: 10.1186/s13014-020-01653-w

65. Cai X, Li P, Zhao J, Wang W, Cheng J, Zhang G, et al. Definitive carbon ion re-irradiation with pencil beam scanning in the treatment of unresectable locally recurrent rectal cancer. *J Radiat Res* 2023; **64:** 933-9. doi: 10.1093/jrr/rrad068

66. Barcellini A, Vitolo V, Cobianchi L, Peloso A, Vanoli A, Mirandola A, et al. Re-irradiation with carbon ion radiotherapy for pelvic rectal cancer recurrences in patients previously irradiated to the pelvis. *In Vivo* 2020; **34:** 1547-53. doi: 10.21873/invivo.11944

67. Hamauchi S, Yamazaki K, Yasui H, Boku N, Onozawa Y, Fukutomi A, et al. Safety and efficacy of proton-beam radiation therapy for patients with locally recurrent rectal cancer. *Ann Oncology* 2012; **23:** xi160. doi: 10.1016/S0923-7534(20)32506-0

68. Shiba S, Okamoto M, Kiyohara H, Ohno T, Kaminuma T, Asao T, et al. Prospective observational study of high-dose carbon-ion radiotherapy for pelvic recurrence of rectal cancer (GUNMA 0801). *Front Oncol* 2019; **9:** 702. doi: 10.3389/fonc.2019.00702

69. Shioyama Y. A phase II clinical trial of carbon-ion radiotherapy for patients with local recurrence after primarily resected rectal cancer (HIMAT1351) [Internet]. Clinical trial registration. [cited 2025 Sep 13]. Available at: https://center6.umin.ac.jp/cgi-open-bin/ctr/ctr.cgi?function=brows&action=brows&type=summary&language=J&recptno=R000015979

70. Yamada S. A phase II clinical trial of carbon-ion radiotherapy for pelvic recurrent rectal cancer in patients with prior pelvic carbon-ion irradiation. [Internet]. UMIN Clinical Trials Registry U. [cited 2025 Sep 13]. Available at: https://center6.umin.ac.jp/cgi-open-bin/ctr_e/ctr_view.cgi?recptno=R000025839

71. Cai X. A Prospective Phase II clinical study of carbon ion re-irradiation in unresectable locally recurrent rectal cancer [Internet]. [Clinical trial registration] clinicaltrials.gov; 2023 [cited 2025 Sep 13]. Available at: https://clinicaltrials.gov/study/NCT05807984

72. Wan J, Wu R, Fu M, Shen L, Zhang H, Wang Y, et al. TORCH-R trial protocol: hypofractionated radiotherapy combined with chemotherapy and toripalimab for locally recurrent rectal cancer: a prospective, single-arm, two-cohort, phase II trial. *Front Oncol* 2023; **13:** 1304767. doi: 10.3389/fonc.2023.1304767

73. Kim HC. Concurrent chemo-proton radiotherapy with or without resection and spacer insertion for loco-regional recurrence of previous irradiated rectal cancer (RECCPT) [Internet]. [cited 2025 Sep 14]. Available at: https://clinicaltrials.gov/study/NCT03098108. clinicaltrials.gov; 2018.

74. Washington University School of Medicine. Hypofractionated pencil-beam scanning intensity-modulated proton therapy (IMPT) in recurrent rectal cancer (IMPARC) [Internet]. [cited 2025 Sep 14]. Available at: https://clinicaltrials.gov/study/NCT04827732. 2025.

75. Truelsen CG, Rønde HS, Kallehauge JF, Szpejewska JE, Bahij R, Diness LV, et al. Acute toxicity and quality of life in dose-escalated proton reirradiation for locally recurrent rectal cancer: the prospective ReRad II trial. *Clin Transl Radiat Oncol* 2025; **54:** 100999. doi: 10.1016/j.ctro.2025.100999

76. Gambacorta MA, Romano A, Caravatta L, Macchia G, Chiloiro G, Galofaro E, et al. Radiotherapy & total neoadjuvant therapy for recurrent rectal cancer in previously irradiated patients, (RETRY): a multicenter prospective observational study. *Radiat Oncol* 2024; **19:** 174. doi: 10.1186/s13014-024-02555-x

77. Denost Q, Frison E, Salut C, Sitta R, Rullier A, Harji D, et al. A phase III randomized trial evaluating chemotherapy followed by pelvic reirradiation versus chemotherapy alone as preoperative treatment for locally recurrent rectal cancer – GRECCAR 15 trial protocol. *Colorectal Dis* 2021; **23:** 1909-18. doi: 10.1111/codi.15670

78. Combs SE, Kieser M, Habermehl D, Weitz J, Jäger D, Fossati P, et al. Phase I/II trial evaluating carbon ion radiotherapy for the treatment of recurrent rectal cancer: the PANDORA-01 trial. *BMC Cancer* 2012; **12:** 137. doi: 10.1186/1471-2407-12-137

79. Peterson J, Niles C, Patel A, Boujaoude Z, Abouzgheib W, Goldsmith B, et al. Stereotactic body radiotherapy for large (> 5 cm) non–small-cell lung cancer. *Clin Lung Cancer* 2017; **18:** 396-400. doi: 10.1016/j.cllc.2016.11.020

80. Dawson LA, Hashem S, Bujold A. Stereotactic body radiation therapy for hepatocellular carcinoma. *Am Soc Clin Oncol Educ Book* 2012; **32:** 261-4. doi: 10.14694/EdBook_AM.2012.32.171

81. Shiba S, Okamoto M, Shibuya K, Okazaki S, Miyasaka Y, Ohtaka T, et al. Carbon Ion radiation therapy for postoperative pelvic recurrence of rectal cancer with a large tumor infiltrating and compressing the rectum: a case report. *Adv Radiat Oncol* 2021; **6:** 100774. doi: 10.1016/j.adro.2021.100774

82. Nagata K, Takiyama H, Tashiro K, Yamadera M, Okamoto K, Kajiwara Y, et al. Multidisciplinary management of locally recurrent rectal cancer with carbon ion radiotherapy followed by prophylactic removal of the irradiated bowel: a case report. *Surg Case Rep* 2024; **10:** 13. doi: 10.1186/s40792-024-01811-2

83. Kobayashi T, Sekimoto M, Miki H, Yamamoto N, Harino T, Yagyu T, et al. Laparoscopic polyglycolic acid spacer placement for locally recurrent rectal cancer. *Colorectal Dis* 2024; **26:** 760-5. doi: 10.1111/codi.16882

84. Sasaki R, Demizu Y, Yamashita T, Komatsu S, Akasaka H, Miyawaki D, et al. First-In-human phase 1 study of a Nonwoven Fabric Bioabsorbable Spacer for Particle Therapy: Space-Making Particle Therapy (SMPT). *Adv Radiat Oncol* 2019; **4:** 729-37. doi: 10.1016/j.adro.2019.05.002

85. Trifiletti DM, Garda AE, Showalter TN. Implanted spacer approaches for pelvic radiation therapy. *Expert Rev Med Devices* 2016; **13:** 633-40. doi: 10.1080/17434440.2016.1195682

The role of particle therapy in the treatment of locally recurrent rectal cancer: a systematic review

Ana Perpar, Petra Georg, Ajra Secerov Ermenc

doi: 10.2478/raon-2026-0036

SUPPLEMENTARY TABLE 1. The results of photon RT of locally recurrent rectal cancer.

Author	Year	# pts	mFU (months)	Techn	Median dose (Gy)	IORT	FRACT	CT	M1	Target size	Surgery	Local control (%, median in months)						Overall survival (%, median in months)					
												1Y	2Y	3Y	4Y	5Y	Median	1Y	2Y	3Y	4Y	5Y	Median
Al-Haidari[31]	2020	67		3DCRT	45	N	N	67,0%	25%	107 ccm	Y									32,0			15,6
	SURGERY NO SURGERY																			62 16			39,2 8,9
Bosman[32]	2014	135	28	IMRT	25	100,0%	N	N	0%		Y											35,2	
Cai[33]	2015	71	31	IMRT	55	N	N	Y	32%		19,7%							80,1		36,5			29,0
	SURGERY																	92,3		53,3			
Chung[34]	2019	41	53,7	IMRT	50	N	N	N	12%	3,3 cm	21,9%		49,9				23,3		55,3				33,8
Jo[35]	2016	22	24,9	3DCRT	57,6	N	N	50,0%	0%		N	88,4	74,6					89,4	82,0				
Kishan[36]	2017	25	36,9	3DCRT	49,6	33,3%	N	92,0%	40%		64,0%			73,3	68,6	68,6				51,6	32,9	28,2	35,8
Park[37]	2019	25	21,5	3DCRT	45	N	N	56,0%	0%	191,1 ccm	44,0%		44,6	29,7					54,6	49,7			
Sun[38]	2012	72	24	3DCRT	36	N	Y	Y	0%	≤ 5 cm 34,7% > 5 cm 65,3%	N			31,1			17,0			45,1			32,0
Susko[39]	2016	33	13,9	2D-3D	30	N	N	75,0%	0%		42,0%		15,7						47,8				23,1
	SURGERY NO SURGERY																						32,3 13,3
Tanaka[40]	2017	32	16	3DCRT	60	N	N	N	56%	39 mm	N	51,5	24,5	19,6	19,6	13,1		82,6	56,5	45,2	38,7	23,2	
	HIGH BED LOW BED																	100 77,9					
Tao[41]	2017	102	28	3DCRT	39	21,6%	Y	91,0%	YES[2]		45,0%		51,0	40,0					61,0	39,0			30,0
	SURGERY NO SURGERY																			62 20			47 17
Watanabe[42]	2020	18	42	3DCRT	59,4	N	N	56,0%	0%	49 mm	N					34,8						54,4	

1Y = 1-year outcomes; 2D-3D = 2-dimensional and 3- dimensional conformal radiation therapy; 3DCRT = 3-dimensional conformal radiation therapy; BED = biologically effective dose; CT = chemotherapy; FRACT = altered fractionation regimes; IMRT = intensity-modulated radiation therapy; IORT = intraoperative RT; M1 = proportion of metastatic patients; mFU = median follow-up; Pts = patients; reRT = reirradiation; Tech = RT technique.

White background for studies with radiation-naïve cohort, blue background for studies with reirradiated cohort, orange background for mixed radiation-naïve and reirradiated cohort.

* The study only reports that metastatic patients were included in the analysis. It does not report how many were included.

SUPPLEMENTARY TABLE 2. Results of definitive RT of locally recurrent rectal cancer (stereotactic body radiation therapy [SBRT] and particle therapy)

Author	Year	# pts	mFU	Tech	Dose (med, Gy/fx)	Size	G3+	Local control (%, median in months)						Overall survival (%, median in months)					
								1Y	2Y	3Y	4Y	5Y	Median	1Y	2Y	3Y	4Y	5Y	Median
Dagoglu[48]	2015	18	38	SBRT	25/5	90,1 ccm	2 pts	100,0	93,7	85,9			38,0	76,8	65,9	59,3			40,0
DeFoe[49]	2011	14	16,5	SBRT	36/3/3	52,5 ccm	0%	90,9	68,3					90,0	78,8				
Johnstone[50]	2021	69	28	SBRT	30/5	13,4 ccm	NR								77,0				38,7
Kim[51]	2008	23	31	SBRT	39/3	26 ccm	1 pt				74,3						24,9	23,2	37,0
Minneci[52]	2021	23	91	SBRT	40/5	GTV 13,4 ccm	13%			95,6		82,6							
Smith[53]	2020	30	24,5	SBRT	30/5	14,3 ccm	1 pt	84,9	69,0					95,0	84,4				28,3
Yamada[54]	2016	186	42	C12	73,6/16	34 mm	2%	100,0								72,0		53,0	69,0
		10	42	C12	67,2							35,0				20,0		20,0	
		21	42	C12	70,4							77,0				53,0		26,0	
		155	42	C12	73,6							88,0				78,0		59,0	
Yamada[55]	2022	77	45	C12	70,4/16	40 mm	21%			69,0		62,0				61,0		38,0	47,0
Takagawa[56]	2024	10	28,7	p+	72/36	34 mm 26,1 ccm	10%	70,0	58,3					100,0	60,0				26,0
Takagawa[57]	2023	23	37,4	p+	70/35	37 mm	13%			55,0		47,2				72,1		44,6	54,4
Shinoto[58]	2019	224	62	C12	73,6/16	30 mm	5%			93,0		88,0				73,0		51,0	
Shiba[59]	2024	28	51,2	C12	73,6/16	44 mm	11%			88,0		83,0	NR			89,0		50,0	75,6
Koroulakis[60]	2021	28	28,6	p+	44,4/?[2]	86,4 ccm	14%	66,3						81,8					29,2
Jeans[61]	2023	86	49,2	IMRT	45/15	50 mm	10,5/15%		73,3			63,3			62,5			25,7	31,2
		85	92,4	C12	70,4/16	29 mm	14,1/0%		58,2			53,6			83,1			46,8	54,0
Hiroshima[62]	2021	13	42,9	p+	72/24	63 mm	0%			80,2						71,3			67,1
Chung[63]	2022	35	45,7	C12	70,4/16	25 mm	19/6%	93,3		87,3				97,0		86,4			
		31	22,8	IMRT	50/25	30 mm	13/0%	89,3		43,7				88,9		54,5			
Cai[64]	2020	25	19,6	C12	72/20	84,5 ccm	12%	90,4	71,8					82,9	65,1				
		9	19,6	C12	< 66			76,2	30,5					77,8	55,6				
		16	19,6	C12	≥ 66			100,0	100,0					86,5	69,2				
Cai[65]	2023	24	23,8	C12	72/20	GTV 57,1 ccm	12,5%	100,0	93,3					86,7	81,3				
Barcellini[66]	2020	14	18	C12	60/16	GTV 154 ccm	0%	78,0	52,0					100,0	76,2				

[1] 1Y = 1-year outcomes; C12 = carbon ion beam; G3+ - proportion of patients with grade 3 or above toxicities; GTV = gross target volume; IMRT = intensity-modulated radiation therapy; med = median; mFU = median follow-up in months; NR = not reported; p+ = proton beam; Pts = patients; reRT = reirradiation; SBRT = stereotactic body radiation therapy; Tech = RT technique

White background for studies with radiation-naïve cohort, blue background for studies with reirradiated cohort, orange background for mixed radiation-naïve and reirradiated cohort.

SUPPLEMENTARY TABLE 3. Ongoing studies on radiation therapy (RT) in locally recurrent rectal cancer

Country	Study Name / ID	Diagnosis	Beam type	ReRT	Outcome
Japan[69]	HIMAT 1351	locally recurrent rectal cancer	C12	NO	Primary: 3-year local control Secondary: response rate, survival rate, progression-free survival, complication rate and pain response
Japan[70]	UMIN000022731	locally recurrent rectal cancer	C12	YES	Primary: 3-year local control
China[71]	SPHIC-TR-CRC2021-01 NCT05807984	locally recurrent rectal cancer	C12[1]	YES (> 1 course)	Primary: local control Secondary: overall and progression-free survival
China[72]	TORCH-R	locally recurrent rectal cancer oligometastatic patients included	EBRT[2] SBRT	BOTH	Primary: local objective response rate
S. Korea[73]	RECCPT	locally recurrent rectal cancer	p+[3]	YES	Primary: 3-year local control
USA[74]	IMPARC	locally recurrent rectal cancer	p+	YES	Primary: maximum tolerated dose (MTD) of hypofractionated IMPT (3 groups based on dose level)
Denmark[75]	ReRAD II	locally recurrent rectal cancer	p+[4]	YES	Primary operable: rate of pathological resection Primary definitive: 1-year local control. Secondary: local re-recurrence 6, 12 and 24 months after treatment, disease-free and overall survival, toxicity and quality of life.
Italy[76]	RETRY	locally recurrent rectal cancer oligometastatic patients included	ANY[5]	YES	Primary: local control
France[77]	GRECCAR-15	locally recurrent rectal cancer	EBRT[6]	YES	Primary: R0 resection rate

[1] 74 Gy in 20 fractions

[2] Primary RT to 25–40 Gy in 5 fractions, reirradiation to 15–30 Gy in 5 fractions, followed by 18 weeks of various regimes of chemotherapy and immunotherapy (toripalimab). Further management determined by multidisciplinary team.

[3] Proton therapy with simultaneous integrated boost technique to gross tumor volume to a dose of 70.4 Gy in 16 fractions and dose to clinical target volume 44.8 Gy in 16 fractions with Capecitabine in a salvage setting with or without surgery

[4] Neoadjuvant (55 Gy RBE à 1.25 Gy RBE twice daily) or definitive (57.5-65 Gy RBE à 1.25 Gy RBE twice daily)

[5] The protocol does not decidedly prescribe local treatment aside from it being reirradiation in a neoadjuvant context.

[6] Randomized phase III trial comparing neoadjuvant chemotherapy followed by pelvic RT (30.6 Gy with capecitabine) versus neoadjuvant chemotherapy alone

C12 = carbon ion beams, p+ = proton beams

RADIOLOGY AND ONCOLOGY Radiology and Oncology | Ljubljana | Slovenia | www.radioloncol.com

review

Clinical impact of trace elements as potential biomarkers for diagnosis and prediction of response to systemic treatment in gastrointestinal cancers

Martina Rebersek[1,2], Radmila Milacic Scancar[3,4], Janez Scancar[3,4], Nezka Hribernik[1,2]

[1] Department of Medical Oncology, Institute of Oncology Ljubljana, Ljubljana, Slovenia
[2] Medical Faculty, University of Ljubljana, Ljubljana, Slovenia
[3] Jožef Stefan Institute, Ljubljana, Slovenia
[4] Jožef Stefan International Postgraduate School, Ljubljana, Slovenia

Radiol Oncol 2026; 60(3): 332-338.

Received 22 January 2026
Accepted 13 April 2026

Corresponence to: Assoc. Prof. Martina Reberšek, M.D., Ph.D., Department of Medical Oncology, Institute of Oncology Ljubljana, Zaloška 2, SI-1000 Ljubljana, Slovenia. E-mail: mrebersek@onko-i.si.

Disclosure: No potential conflicts of interest were disclosed.

Background. Gastrointestinal cancers are among the most common malignancies worldwide and, at advanced stages, remain incurable. Currently used biomarkers, such as tumour markers, have limited diagnostic value for early detection and relapse, highlighting the urgent need for more sensitive and specific markers. Trace elements are involved in numerous physiological and metabolic processes, and deregulation of their homeostasis is implicated in the carcinogenesis of various cancers, including gastrointestinal malignancies. Several basic and preclinical studies have identified the importance of trace elements in key biological processes. Recent clinical studies and retrospective analyses suggest that fluctuations in trace element levels may be associated with the development and progression of many cancers. Thus, quantitative and dynamic determination of serum trace element concentrations during treatment and follow-up represents a promising option for monitoring treatment efficacy and disease prognosis.

Conclusions. Trace elements may serve as potential prognostic and predictive biomarkers for diagnosis and response to systemic treatment.

Key words: trace elements; prognostic and predictive biomarkers; gastrointestinal cancers; systemic therapy

Introduction

Gastrointestinal (GI) cancers comprise a heterogeneous group of diseases affecting the gastrointestinal tract, including cancers of the oesophagus, stomach, liver, biliary tract, pancreas, small intestine, colorectal (CRC), and anus. These cancers vary in aetiology and clinical management and are among the most prevalent malignancies globally, representing a leading cause of cancer-related death.[1] According to the Cancer Registry of the Republic of Slovenia, nearly 3,000 new cases of gastrointestinal cancer are diagnosed annually.[2] Prognosis has improved significantly over the past decade due to successful screening programmes, advances in surgical and local ablative techniques, radiation therapy, and systemic treatments for both early and advanced disease. In Slovenia, the incidence of CRC has declined in re-

cent years, primarily due to increased awareness and preventive screening.[2]

Despite these advances, cancer remains a leading cause of death worldwide.[1] Metastatic GI cancers are still incurable for most patients, with prognosis varying by cancer type, location, and extent of metastases. Pancreatic cancer has the poorest prognosis, while metastatic CRC has a better survival rate, largely due to combined surgical and systemic treatments, especially new systemic treatment possibilities.[3,4]

Early diagnosis greatly improves survival and treatment outcomes, making reliable biomarkers essential. Widely accepted biomarkers for GI cancers are still lacking. Currently used serum tumour markers, carbohydrate antigen 19-9 (CA 19-9) and carcinoembryonic antigen (CEA), have limited diagnostic value due to low sensitivity and specificity.[3-5] CA 19-9 has higher specificity than CEA (92.7% *vs*. 79.2%) but lower sensitivity (50% *vs*. 79.4%).[5] Elevated CA 19-9 is associated with poorer prognosis and may serve as a predictive biomarker for systemic treatment response, but it is not cancer-specific and can be elevated in benign liver diseases and other metastatic cancers.[3-5] Serum CEA is also insufficiently sensitive or specific for GI cancer diagnosis and can be elevated in other cancers and non-malignant diseases. Improved understanding and application of traditional tumour biomarkers, alongside identification of new biomarkers, is crucial for personalized cancer treatment.

Trace elements

Essential trace elements, including iodine (I), copper (Cu), iron (Fe), manganese (Mn), zinc (Zn), selenium (Se), cobalt (Co), and molybdenum (Mo), are required in minute amounts for normal physiology.[6] Alterations in levels and changes in the expression of proteins involved in trace element metabolism have been demonstrated in various cancers, including GI malignancies.[6-8] Cu, Zn, and Fe are particularly important for normal bodily function.[6-8] They participate in numerous biochemical reactions, act as enzyme cofactors, and regulate biological processes by binding to specific receptors and transcription factors. Deregulation of trace metal homeostasis at the cellular and tissue level is implicated in cancer pathology, accelerating the transformation of normal cells into cancerous cells and altering immune responses.[6-8]

Cu is an essential trace element that is tightly regulated in the body.[9] It is present in all tissues, stored mainly in the liver, and transported in the blood, mostly bound to ceruloplasmin (Cp).[9-11] It acts as a coenzyme for several enzymes, including Cu/Zn superoxide dismutase, Cp, cytochrome oxidase, tyrosinase, dopamine hydroxylase, lysine oxidase, catalase, and Se-dependent peroxidase, all of which are crucial for cellular respiration and defines against free radicals. Cu also affects glutathione function, and its deficiency impairs cellular respiration and the regulation of reactive oxygen species. Excessive oxidative stress, due to the overproduction of reactive oxygen species, impairs deoxyribonucleic acid (DNA) repair mechanisms and is a key factor in cancer development.[11]

Cu and Zn are essential micronutrients involved in antioxidant functions, immune regulation, and DNA repair. Cu can promote oxidative stress and inflammation, while Zn has antioxidative properties. Imbalances in Cu and Zn disrupt homeostasis, increasing oxidative stress and inflammation, which are implicated in CRC development. Cancer patients often exhibit higher serum Cu and lower Zn levels than healthy individuals.[11-17] These differences vary with diet, sex, age, cancer type, and other factors. Low Zn and elevated Cu can increase oxidative stress and impair antioxidant enzyme activity.[17] Increased Cu/Zn ratios have been observed in various malignancies, including GI, gynaecological, breast, and lung cancers, and correlate with disease stage.[11-17] The Cu/Zn ratio reflects the balance between Cu and Zn, is crucial for regulating oxidative stress and inflammation, and may serve as a clinical diagnostic and prognostic biomarker for treatment response. Fe is a key mineral for survival, as it helps cells in transport of oxygen and to function properly.[6] It is essential for the activity of enzymes involved in cellular respiration and the conversion of food into energy. Fe helps the body respond to infections and maintain a healthy immune system. It plays a crucial role in brain development, cognitive function, hormone synthesis, and connective tissue health. The body stores Fe in the liver, spleen, and bone marrow in the form of a protein called ferritin. Se is an essential mineral that acts as a powerful antioxidant and is essential for the smooth functioning of several body processes.[6] It is necessary for the conversion of thyroid hormones into their active form, strengthens the body's natural resistance and protects cells from oxidative stress. Se also plays a role in fertility and in hair and nail health.

Methods for determining trace element concentrations in biological samples

The determination of trace elements in biological samples is essential for under-standing their role in human health and disease. Various analytical techniques are used for analysing trace element concentrations in biological matrices, such as blood, tissue, and urine.[18] Among these, inductively coupled plasma mass spectrometry (ICP-MS) is the most sensitive and versatile.[18] It enables rapid simultaneous detection of nearly all elements in the periodic table at extremely low concentrations (below 0.01 μg/L). ICP-MS combines an inductively coupled plasma with a mass spectrometer, which identifies ions based on their mass-to-charge ratio (m/z). This technique can also be used for isotope ratio measurements. The advantages of ICP-MS include its ability to perform rapid, simultaneous multi-elemental analysis, high sensitivity and selectivity, and a wide operational dynamic range (up to 10^9). To ensure accurate determination of elemental concentrations, it is crucial to minimize or eliminate spectral interferences, such as polyatomic and isobaric interferences, as well as non-spectral interferences that arise from compounds in the sample. These interferences can affect transport efficiency and nebulization. Due to its exceptional performance, ICP-MS has become the fastest growing analytical technique for trace element analysis, particularly for elements in biological matrices.[18]

Similarly, to ICP-MS, inductively coupled plasma atomic emission spectrometry (ICP-AES) also uses a high-temperature argon plasma to excite atoms and ions in a sample, which emit element-specific radiation that is measured for quantitative analysis.[18] It offers moderate to high sensitivity, typically in the μg/L to low mg/L range, making it suitable for routine multi-element determination. Although it is less sensitive than ICP-MS, it can also be used for trace element determination in biological matrices. The method is primarily affected by spectral interferences from overlapping emission lines and by matrix effects that can influence signal intensity. However, careful selection of alternative emission lines and mathematical correction techniques can minimize these interferences.

Flame and electrothermal atomic absorption spectrometry (FAAS and ETAAS) are much less sensitive than ICP-MS, with typical detection limits in the mg/L range for FAAS and μg/L range for ETAAS, and they allow the determination of only a single element per analysis.[18] For this reason, they are less commonly used for trace element analysis in biological samples compared with ICP-MS. The technique is based on the ability of atoms in the atomization medium (flame or electrothermally heated graphite furnace) to absorb the characteristic light of the element. The most common interferences are chemical and spectral interferences, as well as background non-specific absorption caused by scattering or absorption from other matrix components. These effects can be minimized by using matrix modifiers, optimized furnace programs, or background correction techniques such as continuum source or Zeeman correction.[18]

Total Reflection X-ray Fluorescence (TXRF) enables direct analysis of liquids, slurries, and solid tissues with minimal sample preparation, providing moderate sensitivity in the μg/L to mg/L range, which makes it suitable for trace element determination in biological samples.[18]

Neutron activation analysis (NAA) is a highly sensitive, matrix-independent technique, often achieving ng/L to μg/L detection limits, and offers absolute quantification, making it particularly

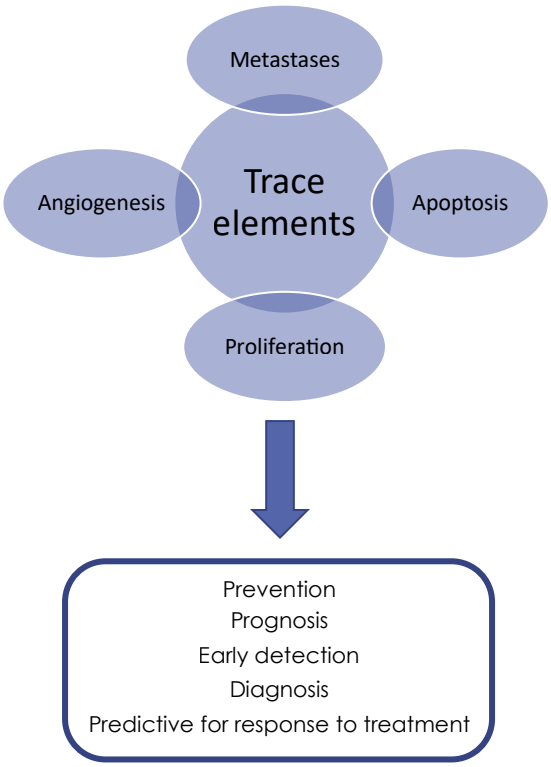

FIGURE 1. Potential roles of trace elements in oncology.

TABLE 1. Overview of the data on the clinical impact of trace elements in gastrointestinal (GI) cancers

Author, year of publication, Ref	GI cancer type	Clinical study	Trace elements and analytical methods	Summary of main findings
Lossow *et al.*, 2021[21]	Colorectal	Retrospective	Se, Cu, Fe, Zn ICP-MS, SRXRF	Elevated Cu and low Zn serum concentrations in four cancer types (CRC, lung, prostate, breast) studied. Analysis of Cu and Zn could contribute to an early cancer diagnosis.
Yang *et al.*, 2021,[22]	Liver, gastric, colorectal	Prospective, closed	Cu, Zn, Fe, Se ICP-MS	OXs exists in the occurrence and development of cancer, related to the changes of trace element concentrations.
Stepien *et al.*, 2017[23]	Colorectal	Prospective, closed	Cu, Zn XRF	Cu/Zn ratio may be associated with increased CRC risk, particularly within two years of diagnosis, and could serve as an early indicator of CRC development. Zn showed a potential protective effect, especially in women.
Baszuk *et al.*, 2021[24]	Colorectal	Retrospective	Cu ICP-MS	A high blood Cu level (>900 µg/L) is associated with a significantly increased risk of colorectal cancer in the Polish population. Cu concentrations has the potential as a marker for identifying of patients for further surveillance with colonoscopy.
Nawi *et al.*, 2019[25]	Colorectal	Retrospective	Ca, Cu, Mg, Mn, Se, Si, Zn, Co, S, Cd, Cr, Cu, Mg, Mn, Pb AAS	Serum concentrations of Ca, Cu, Mg, Mn, Se, Si, and Zn were lower in CRC patients, whereas Co and S the levels were higher. Concentrations of Cd, Cr, Cu, Mg, Mn, Pb and Zn were elevated in patients with metastasis.
Lener *et al.*, 2016[26]	Pancreatic cancer	Prospective, closed	Se, Cu ICP-MS	Low Se and elevated Cu levels may contribute to PC development, higher Se concentrations are associated with longer survival in affected patients.
Yanjun *et al.*, 2024[27]	Pancreatic cancer	Prospective, closed	Cu, Fe, Zn, Mn ICP-MS	High concentration levels of Cu may increase the risk of PC. Fe can promote ferroptosis, Excessive Fe levels may elevate PC risk. High Zn intake is associated with a reduced risk of PC and can inhibit tumour growth. Mn contributes to anti-PC effects primarily by promoting ferroptosis and suppressing excessive cell proliferation.
Türkdoğan *et al.*, 2022[28]	Oesophageal, gastric, colorectal	Prospective, closed	Cd, Co, Cu, Fe, Mg, Mn, Pb, Zn, Ni FAAS	Cd, Co, Ni, Fe, and Mn were significantly lower in cancer patients compared to healthy controls. Serum Zn levels were lower in cancer patients, the difference was not statistically significant. No significant differences were observed for Cu, Mg, Pb, and Zn between cancer patients and controls.
Kocak *et al.*, 2025[29]	Oesophageal squamous cell carcinoma	Prospective, closed	Al, Cr, Mn, Fe, Co, Cu, Zn, Se, Sb, Hg Pb ICP-MS	Significant increases in Cu, and Fe levels, as well as total oxidant status, alongside a marked decrease in Se levels in cancerous tissues.

valuable for trace element analysis in biological ma-trices.[18] However, it is time-consuming and requires access to a nuclear reactor, which, for most of the laboratories, is not available.

Trace elements as potential biomarkers in oncology

Recent findings highlight the potential of trace element identification as a cancer biomarker.[17] Imbalances in the Cu/Zn ratio may be used for clinical diagnosis and as a predictive biomarker for treatment response. Cp correlates with immune infiltration and serves as a prognostic biomarker in breast cancer.[17] Elevated serum Cu-Cp levels have been found in lung, colon, ovarian, and bile duct cancers, while Cp expression is downregulated in adrenocortical and hepatocellular carcinoma.[17] Serum Cu levels increase in several cancers. In hepatocellular carcinoma, blood Cu and sulphur (S) are enriched in light isotopes compared to healthy individuals, and isotopic ratios of Cu ($^{65}Cu/^{63}Cu$) and S ($^{34}S/^{32}S$) may serve as disease biomarkers.[19] Changes in the isotopic compositions of Fe, Cu, and Zn and their plasma concentrations in haematological malignancies can be measured for prognostic assessment.[20] Further investigation is needed to fully evaluate the biomarker potential of trace metal concentrations, speciation, and isotopic fractionation. The potential roles of trace elements in oncology are shown in Figure 1.

Author, year of publication, Ref	GI cancer type	Clinical study	Trace elements and analytical methods	Summary of main findings
Yan *et al.*, 2024[30]	Hepatocellular cancer, gastric cancer	Prospective, closed	As, Cd, Co, Cr, Cu, Fe, Mn, Ni, Pb, Se, Zn ICP-MS	Tissue concentrations of As, Cd, Co, Cr, Cu, Fe, Mn, Ni, Pb, Se, and Zn in patients with liver cancer were significantly lower than those in healthy controls. Patients with gastric cancer exhibited lower levels of Cd, Co, Cr, Mn, Ni, and Zn, but higher levels of Cu and Se compared to the controls. Patients with liver and gastric cancers who had poorly differentiated tumours and positive lymph node metastases showed lower levels of trace elements.
Gupta *et al.*, 2005[31]	Gallbladder cancer	Prospective, closed	Cu, Zn FAAS	Mean serum Zn levels, biliary and tissue Zn levels were significantly lower in gallbladder carcinoma patients comparing to patients with cholelithiasis, and healthy controls. Mean serum Cu levels, biliary and tissue Cu levels were significantly higher in gallbladder carcinoma patients comparing to those with cholelithiasis, and healthy controls. Serum Cu/Zn ratio showed a gradual and significant increase, rising from healthy controls to patients with cholelithiasis and patients with carcinoma of the gallbladder. Biliary and tissue Cu/Zn ratios were significantly higher in gallbladder carcinoma patients than in patients with cholelithiasis.
Basu *et al.*, 2013[32]	Biliary tract cancers	Prospective, closed	Se, Zn, Cu, Mg, Cd, Cr, Pb, Ni FAAS	Se and Zn levels were significantly reduced, and Cu levels were significantly higher in serum, bile, and gallbladder tissue from gallbladder carcinoma patients. Pb, Cd, Cr and Ni levels were increased in serum and bile of these patients.
Stepien *et al.*, 2017[33]	Hepatocellular cancer, biliary tract cancers	Prospective, closed	Cu, Zn XRF	Zn may play a role in preventing liver cancer development. An inverse association between pre-diagnostic Zn levels, but not Cu levels, and the risk of HCC is shown. An imbalance of Cu relative to Zn, indicated by a higher Cu/Zn ratio, was positively associated with HCC risk.
Reberšek *et al.*, 2024[34]	Biliary tract cancers	Prospective, ongoing	Cu, Zn, Fe, se, Mn ICP-MS	Serum levels of trace elements, their proportion of free Cu and Cu-Cp, and its isotopic fractionation (Cu^{65}/Cu^{63}) are being investigated as potential predictive biomarkers of response to systemic therapy.
Kozlica *et al.*, 2025[35]	Biliary tract cancers	Retrospective - prospective	Cu, Cu-Cp ICP-MS	Analytical methodologies for studying metabolic disorders affecting Cu metabolism. Accurate interpretation of disease states related to Cu disorders and detailed information obtained through advanced analytical techniques. Immunological assays, ultrafiltration procedures, and speciation techniques based on ICP-MS including Cu isotopic analysis for identification of metabolic abnormalities in different diseases and types of cancer, including BTCs.

Al = aluminium; As = arsenic, AAS = atomic absorption spectrometry; BTCs = biliary tract cancers; Ca = calcium; Cd = cadmium; Cr = chromium; Co = cobalt; CRC = colorectal cancer; Cu-Cp = copper bound ceruloplasmin; Cu = copper; FAAS = flame atomic absorption spectrometry; HCC = hepatocellular cancer; Hg = mercury; ICP-MS = inductively coupled plasma mass spectrometry; Fe = iron-Fe; Mg = magnesium; Mn = manganese; Ni = nickel; OxS = oxidative stress; Pb = lead; PC = pancreatic cancer; Sb = antimuon; SE = selenium; Si = silicon; SRXRF = synchrotron radiation based X-ray fluorescence; XRF = X-ray fluorescence; Zn = zinc-Zn

Trace elements as biomarkers of gastrointestinal (GI) cancers in clinical trials

Much research has focused on the role of trace elements in biochemical and physiological processes and their involvement in tumour growth, invasion, and metastasis. However, there are few published clinical studies examining the role of trace elements as prognostic and predictive biomarkers in GI cancer patients. Key clinical studies are summarized in Table 1.

Conclusions and future directions

Predictive and prognostic biomarkers are essential for personalized medicine and optimal treatment of cancer patients. Trace elements as biomarkers in oncology represent a promising field for the detection, diagnosis, and prediction of treatment response. Currently, serum determination of trace elements as prognostic or predictive biomarkers has not been integrated into routine clinical practice. Few clinical studies have examined the role of

trace element concentrations in predicting prognosis, survival, and treatment response in GI cancer patients or their potential as therapeutic targets.

Trace elements such as Cu, Zn, and Fe, including exchangeable and Cp-bound copper and isotope ratios in serum, are emerging as promising biomarkers for prognostic and predictive purposes in systemic cancer treatment. However, the evidence remains inconsistent and varies by cancer type. Future research should focus on developing accurate, reliable, and optimized analytical and imaging methods for the quantitative determination of serum trace elements and investigating their role in cancer diagnosis and treatment. More clinical research is needed to define the significance of trace elements in relation to prognosis, cancer characteristics, disease stage, and treatment outcomes.

Acknowledgement

Supported by the Slovenian Research and Innovation Agency (ARIS), programmes P3-0321 of Institute of Oncology Ljubljana, P1-0143, Project No. J7-50128 of Jožef Stefan Institute, and internal project OI-1-24 funded by the Institute of Oncology Ljubljana. The funder was not involved in the study design, data collection, analysis, interpretation, writing, or publication decisions. Manuscript edited by AJE Digital/Curie.

References

1. World Health Organization International Agency for Research on Cancer (IARC). GLOBOCAN 2020: Estimated cancer incidence, mortality and prevalence worldwide in 2020. [internet]. [cited 2026 Jan 19]. Available at: http://globocan.iarc.fr
2. Cancer in Slovenia 2022. Ljubljana: Institute of Oncology Ljubljana, Epidemiology and Cancer Registry, Slovenian Cancer Registry; 2025.
3. National Comprehensive Cancer Network: NCCN Clinical Practice Guidelines in Oncology: Colon cancer. V 2. 2025 [internet]. [cited 2026 Jan 15]. Available at: https://www.nccn.org/professionals/physician_gls/pdf/colon.pdf
4. Cervantes A, Adam R, Roselló S, Arnold D, Normanno N, Taïeb J, et al; ESMO Guidelines Committee. Metastatic colorectal cancer: ESMO Clinical Practice Guideline for diagnosis, treatment and follow-up. *Ann Oncol* 2023; **34:** 10-32. doi: 10.1016/j.annonc.2022.10.003
5. Lowe RC, Anderson CD. Clinical presentation, diagnosis, and staging of cholangiocarcinoma. *UpToDate*, [internet], last updated: Sep 10, 2025. [cited 2026 Jan 15]. Available at: https://www.uptodate.com/contents/clinical-presentation-diagnosis-and-staging-of-cholangiocarcinoma
6. Ferreira CR, Gahl WA. Disorders of metal metabolism. *Transl Sci Rare Dis* 2017; **2:** 101-39. doi: 10.3233/TRD-170015
7. Morales M, Xue X. Targeting iron metabolism in cancer therapy. *Theranostics* 2021; **11:** 8412-29. doi: 10.7150/thno.59092
8. Stojsavljević A, Vujotić L, Rovčanin B, Borković-Mitić S, Gavrović-Jankulović, Manojlović D. Assessment of trace metal alterations in the blood, cerebrospinal fluid and tissue samples of patients with malignant brain tumors. *Sci Rep* 2020; **10:** 3816. doi: 10.1038/s41598-020-60774-0
9. Lelièvre P, Sancey L, Coll JL, Deniaud A, Busser B. The multifaceted roles of copper in cancer: a trace metal element with dysregulated metabolism, but also a target or a bullet for therapy. *Cancers* 2020; **12:** 3594. doi: 10.3390/cancers1212359
10. Chen F, Han B, Meng Y, Han Y, Liu B, Zhang B, et al. Ceruloplasmin correlates with immune infiltration and serves as a prognostic biomarker in breast cancer. *Aging (Albany NY)* 2021; **13:** 20438-67. doi: 10.18632/aging.203427
11. Wang B, Wang XP. Does ceruloplasmin defend against neurodegenerative diseases? *Curr Neuropharmacol* 2019; **17:** 539-49. doi: 10.2174/1570159X16666180508113025
12. Linder MC. Ceruloplasmin and other copper binding components of blood plasma and their functions: an update. *Metallomics* 2016; **8:** 887-905. doi: 10.1039/c6mt00103c
13. Mukae Y, Ito H, Miyata Y, Araki K, Matsuda T, Aibara N, et al. Ceruloplasmin levels in cancer tissues and urine are significant biomarkers of pathological features and outcome in bladder cancer. *Anticancer Res* 2021; **41:** 3815-23. doi: 10.21873/anticanres.15174
14. Sogabe M, Kojima S, Kaya T, Tomioka A, Kaji H, Sato T, et al. Sensitive new assay system for serum wisteria floribunda agglutinin-reactive ceruloplasmin that distinguishes ovarian clear cell carcinoma from endometrioma. *Anal Chem* 2022; **94:** 2476-84. doi: 10.1021/acs.analchem.1c04302
15. Michalczyk K, Cymbaluk-Płoska A. The Role of zinc and copper in gynecological malignancies. *Nutrients* 2020; **12:** 3732. doi: 10.3390/nu12123732
16. Lossow K, Schwarz M, Kipp AP. Are trace element concentrations suitable biomarkers for the diagnosis of cancer? *Redox Biol* 2021; **42:** 101900. doi: 10.1016/j.redox.2021.101900
17. Chen F, Han B, Meng Y, Han Y, Liu B, Zhang B, et al. Ceruloplasmin correlates with immune infiltration and serves as a prognostic biomarker in breast cancer. *Aging (Albany NY)* 2021; **13:** 20438-67. doi: 10.18632/aging.203427
18. Bolann BJ, Rahil-Khazen R, Henriksen H, Isrenn R, Ulvik RJ. Evaluation of methods for trace-element determination with emphasis on their usability in the clinical routine laboratory. *Scand J Clin Lab Invest* 2007; **67:** 353-66. doi: 10.1080/00365510601095281
19. Balter V, Nogueira da Costa A, Bondanese VP, Jaouen K, Lamboux A, et al. Natural variations of copper and sulphur stable isotopes in blood of hepatocellular carcinoma patients. *Proc Natl Acad Sci U S A* 2015; **112:** 982-5. doi: 10.1073/pnas.1415151112
20. Hastuti AAMB, Costas-Rodríguez M, Matsunaga A, Ichinose T, Hagiwara S, Shimura M, et al. Cu and Zn isotope ratio variations in plasma for survival prediction in hematological malignancy cases. *Sci Rep* 2020; **10:** 16389. doi: 10.1038/s41598-020-71764-7
21. Lossow K, Schwarz M, Kipp AP. Are trace element concentrations suitable biomarkers for the diagnosis of cancer? *Redox Biol* 2021; **42:** 101900. doi: 10.1016/j.redox.2021.101900
22. Yang YW, Dai CM, Chen XH, Feng JF. The relationship between serum trace elements and oxidative stress of patients with different types of cancer. *Oxid Med Cell Longev* 2021; **2021:** 4846951. doi: 10.1155/2021/4846951
23. Stepien M, Jenab M, Freisling H, Becker NP, Czuban M, Tjønneland A, et al. Prediagnostic copper and zinc biomarkers and colorectal cancer risk in the European Prospective Investigation into Cancer and Nutrition cohort. *Carcinogenesis* 2017; **38:** 699-707. doi: 10.1093/carcin/bgx051
24. Baszuk P, Marciniak W, Derkacz R, Jakubowska A, Cybulski C, Gronwald J, et al. Blood copper levels and the occurrence of colorectal cancer in poland. *Biomedicines* 2021; **9:** 1628. doi: 10.3390/biomedicines9111628
25. Nawi AM, Chin SF, Azhar Shah S, Jamal R. Tissue and serum trace elements concentration among colorectal patients: a systematic review of case–control studies. *Iran J Public Health* 2019; **48:** 632-43. PMID: 31110973
26. Lener MR, Scott RJ, Wiechowska-Kozłowska A, Serrano-Fernández P, Baszuk P, Jaworska-Bieniek K, et al. Serum concentrations of selenium and copper in patients diagnosed with pancreatic cancer. *Cancer Res Treat* 2016; **48:** 1056-64. doi: 10.4143/crt.2015.282

27. Yanjun Y, Jing Z, Yifei S, Gangzhao G, Chenxin Y, Qiang W, et al. Trace elements in pancreatic cancer. *Cancer Med* 2024; **13**: e7454. doi: 10.1002/cam4.7454

28. Türkdoğan MK, Karapinar HS, Kilicel F. Serum trace element levels of gastrointestinal cancer patients in an endemic upper gastrointestinal cancer region. *J Trace Elem Med Biol* 2022; **72:** 126978. doi: 10.1016/j.jtemb.2022.126978

29. Kocak OF, Yaman ME, Eroglu A. An integrated analytical approach for biomarker discovery in esophageal cancer: combining trace element and oxidative stress profiling with machine learning. *J Trace Elem Med Biol* 2025; **89:** 127678. doi: 10.1016/j.jtemb.2025.127678

30. Yan J, Zhang H, Zhang M, Tian M, Nie G, Xie D, et al. The association between trace metals in both cancerous and noncancerous tissues with the risk of liver and gastric cancer progression in northwest China. *J Pharm Biomed Anal* 2024; **242:** 116011. doi: 10.1016/j.jpba.2024.116011

31. Gupta SK, Singh SP, Shukla VK. Copper, zinc, and Cu/Zn ratio in carcinoma of the gallbladder. *J Surg Oncol* 2005; **91:** 204-8. doi: 10.1002/jso.20306

32. Basu S, Singh MK, Singh TB, Bhartiya SK, Singh SP, Shukla VK. Heavy and trace metals in carcinoma of the gallbladder. *World J Surg* 2013; **37:** 2641-6. doi: 10.1007/s00268-013-2164-9

33. Stepien M, Hughes DJ, Hybsier S, Bamia C, Tjønneland A, Overvad K, et al. Circulating copper and zinc levels and risk of hepatobiliary cancers in Europeans. *Br J Cancer* 2017; **116:** 688-96. doi: 10.1038/bjc.2017.1

34. Rebersek M, Hribernik N, Markovic K, Markovic S, Valentinuzzi KU, Cemazar M, et al. Determination of copper and other trace elements in serum samples from patients with biliary tract cancers: prospective noninterventional nonrandomized clinical study protocol. *Radiol Oncol* 2024; **58:** 300-10. doi: 10.2478/raon-2024-0026

35. Kozlica K, Milačič Ščančar R, Reberšek M, Čemažar, M, Uršič Valenzinuzzi K, Ščančar J. Advances in copper speciation, isotopic ratio measurement, bioimaging, and single-cell analysis – a critical review. *TrAC trends in analytical chemistry* 2025; **184:** 1-24. doi: 10.1016/j.trac.2025.118152

research article

Timed saliva sampling as a new reliable marker for assessing iodine intake

Adrijana Oblak[1,2], Jernej Imperl[3], Mitja Kolar[3], Gregor Marolt[3], Blaz Krhin[1], Katja Zaletel[1,2], Simona Gaberscek[1,2]

[1] Division of Nuclear Medicine, University Medical Centre Ljubljana, Ljubljana, Slovenia
[2] Faculty of Medicine, University of Ljubljana, Ljubljana, Slovenia
[3] Faculty of Chemistry and Chemical Technology, University of Ljubljana, Ljubljana, Slovenia

Radiol Oncol 2026; 60(3): 339-345.

Received 11 March 2026
Accepted 6 July 2026

Correspondence to: Adrijana Oblak, Ph.D., Division of Nuclear Medicine, University Medical Centre Ljubljana, Zaloška 7, SI-1000 Ljubljana, Slovenia. E-mail: adrijana.oblak@kclj.si

Disclosure: No potential conflicts of interest were disclosed.

Background. Iodine is an essential component of thyroid hormones. Therefore, sufficient iodine intake is important for adequate thyroid function. Measuring the urinary iodine concentration (UIC) is the recommended method for assessing population iodine intake, but it has certain drawbacks. In addition to urine, iodine is also excreted into saliva. Therefore, the aim of our work was to determine whether salivary iodine concentration (SLIC) measurement could replace UIC measurements, even a gold standard, urinary iodine excretion (UIE) in the 24-hour urine. We also evaluated the influence of saliva collection time on SLIC measurements.

Subjects and methods. We invited adult volunteers who first provided 24-hour urine and saliva samples collected on the same day at home, strictly according to the protocol. UIC and SLIC before and after meals were measured using the Sandell-Kolthoff method, comparable to inductively coupled plasma mass spectrometry.

Results. The study included 104 healthy participants from whom all biological samples were completely collected. Importantly, none of them was taking thyroid medication or iodine supplements and all were without thyroid disease. A very good correlation of SLIC values at 60 and 120 min after the first and second meal and 30 min after the second, third, and fourth meals with UIE was observed ($P>0.05$).

Conclusions. We found an excellent correlation between SLIC values and UIE, where the SLIC value depends on the sampling timing and/or number of meals. SLIC measurement could replace UIE measurement and represents an important and possible new biomarker for assessing iodine intake.

Key words: Sandell-Kolthoff reaction; salivary iodine concentration; iodine excretion in the 24-hour urine; ICP-MS; saliva; iodine intake; iodine concentration

Introduction

Approximately one-third of the world's population does not consume enough iodine[1], leading to an increased risk of developing iodine deficiency disorders[2] and a higher risk of thyroid disease.[3] With adequate iodine intake, people with healthy thyroid glands excrete approximately 90% of the ingested iodine in their urine.[2] Therefore, measurement of urinary iodine concentration (UIC) is recommended to assess iodine intake. UIC can be measured from a single urine sample or from a 24-hour urine collection, assessing daily urinary iodine excretion (UIE), the latter being considered the gold standard.[1] Consequently, most population-based studies have used urine as the primary sample matrix for the assessment of iodine intake. However, owing to the drawbacks of urine sam-

pling, such as fluid intake, diuresis, dietary factors, and (patho)physiological factors (pregnancy, renal function)[4,5], UIC and UIE measurements should be interpreted with caution, especially at the individual level. In light of these limitations, the presence of sodium iodide symporter molecules in the salivary glands[6], which enables iodine excretion into saliva, highlights saliva as a promising alternative sample for the assessment of iodine intake.

Several methods have been developed to determine iodine content.[7] In common practice, we normally use two methods for iodine measurement in biological samples: method using the Sandell-Kolthoff (S-K) reaction with various pretreatment steps and inductively coupled plasma mass spectrometry (ICP-MS).[8] While the S-K method is easier to handle and less expensive than ICP-MS, owing to the toxic effect of arsenic, which is used in the S-K reaction, careful waste disposal is required.[9] On the other hand, although the ICP-MS method is more accurate, it is more complex to handle and requires more trained personnel. The S-K method is also suitable for the measurement of salivary iodine concentration (SLIC) and yields results comparable to those obtained using ICP-MS.[10] In addition, thiocyanate, present in the saliva of tobacco smokers[11], and caffeine, which is abundant in caffeinated drinks, do not interfere with SLIC measurements. Previous studies on schoolchildren have shown that the amount of iodine in saliva increases during the course of the day.[12]

The aim of our work was to determine whether SLIC measurement could replace UIE measurement in the 24-hour urine collection to assess population iodine intake. Furthermore, we also wanted to establish a correct time window for saliva collection to measure the SLIC.

Subjects and methods

Study design and institutional review board approval

This cross-sectional study was conducted between May 2022 and February 2023. One hundred and forty-five adult participants from the local population were invited to participate in the study, approved by the Slovenian National Medical Ethics Committee (identification number 0120-271/2021/3). The study was completed in accordance with the Declaration of Helsinki as revised in 2013. All the participants provided informed consent. Only participants without known thyroid diseases were included in the study. The exclusion criteria were: presence of thyroid antibodies, failure at providing of all saliva and urine samples, consuming iodine-containing supplements or water treated with iodine. Blood samples were collected from each participant on the day of the study. After clotting, the samples were centrifuged at 1800 x G for 10 min at room temperature, followed by thyroid-stimulating hormone (TSH), thyroglobulin antibodies (anti-Tg), and thyroid peroxidase antibodies (anti-TPO) measurement. On the same day, all participants collected 24-hour urine samples and all saliva samples before (0 min) and 30, 60, and 120 min after each meal, regardless of the time and number of meals consumed. For the 24-hour urine sample collection, 3.3-liter bottles (Becton Dickinson, USA) were used. Subsequently, two urine samples were aliquoted using Vacuette® (10mL, Greiner Bio One, GmbH, Austria) for UIC and creatinine determination, and the volume of urine collected was determined. Salivettes® (Sarstedt, Germany) were used for the saliva samples. Each sample was stored in a freezer and transported to the laboratory within 24 hours. The saliva samples were centrifuged at 1800 x G for 10 min at room temperature, and all urine and saliva samples were frozen at -80°C before analysis.

The participants completed a questionnaire in which they stated their smoking status, intake of dietary supplements and medication, and use of (non-)iodized salt.

Methods

TSH, anti-Tg and anti-TPO levels were measured using Atellica® IM 1600 Solution according to the manufacturer's instructions (Siemens Healthineers, Germany). TSH was measured using the TSH3-Ultra assay, with intra- and inter-assay coefficients of variation (CV) ranging from 1.2%–3.6% and 2.6%–4.5%, respectively. The TSH reference interval for the adult population was defined by the laboratory.[13] Anti-Tg was measured using the analyte-bridging immunoassay aTgII, with intra- and inter-assay CV ranging from 1.5%–2.5% and 2.0%–3.7%, respectively. Anti-TPO was measured using the competitive immunoassay aTPO, with intra- and inter-assay CV ranging from 1.5%–4.1% and 3.4%–7.4%, respectively. Urinary creatinine was measured using the Dimension Vista® 1500 Inteligent Lab System (Siemens Healthineers, Germany) using enzymatic quantitative creatinine determination. The intra- and inter-assay CV

ranged from 0.8%–2.9% and 1.7%–4.4%, respectively.

UIC and SLIC were measured by the spectrophotometric method on microplates based on the S-K reaction with ammonium peroxydisulfate digestion of samples prior to analysis, both comparable to ICP-MS.[10,14] The S-K reaction utilizes the catalytic activity of iodide ions in the reaction of arsorous acid and ammonium cerium (IV) sulfate in sulfuric acid solution. The presence of iodide increases the reaction rate, which is directly proportional to the concentration of iodide in the solution.[15] For UIC, the intra- and inter-assay CV were 2.3%–2.5% and 4.9%–6.3%, respectively[14], while for SLIC, the intra- and inter-assay CV were 2.8%–18.4% and 4.3%–20.7%, respectively.[10] In brief, 1 mL of 1 mol/L ammonium peroxydisulfate solution was added to 250 µL of the standards, controls, and samples. The solution was mixed and incubated for 1 h at 95°C in a dry bath. After cooling to room temperature, 50 µL of the standards, controls, and samples were transferred in duplicates to the microplate. An arsorous acid solution (100 µL) was added to each well. The microplate was then sealed and incubated for 60 s on a microplate shaker. Subsequently, 50 µL of ammonium cerium (IV) sulfate solution was added to each well within 40 s. The microplate was sealed and incubated on the microplate shaker for exactly 30 min. Immediately after shaking, the absorbance was measured at 405 nm using a spectrophotometer (SunriseTM, Tecan, Switzerland).

The Kolmogorov-Smirnov test was used to assess the normality of the data distribution. None of the data were normally distributed; therefore, all data are presented as medians with interquartile ranges (IQR), except for age, which is presented as the mean and associated range. Inferential statistics were performed using the Mann-Whitney test. Statistical analysis was performed using MedCalc Statistical Software version 22.021 (MedCalc Software bvba, Ostend, Belgium) with statistical significance set at $P < 0.05$.

TABLE 1. Participant characteristics

Demographic data		N = 104
Age (y) (range)		43 (23-74)
Gender (%)	Men	32 (30.8)
	Women	72 (69.2)
TSH (mIU/L) (IQR)		1.68 (1.22-2.30)
Smoking (%)	Smokers	7 (6.7)
	Non-smokers	97 (93.3)
Salt (%)	Iodized	98 (94.2)
	Non-iodized	6 (5.8)

IQR = interquartile range; TSH = thyroid-stimulating hormone

Results

In total, 145 participants were included in this study. Three participants declined participation in the study, 20 participants had antibodies against anti-TPO and/or anti-Tg and were later removed from the study. Fifteen participants failed to provide all saliva and/or urine samples, and 3 participants consumed iodine-containing supplements and were therefore excluded from the analysis. The characteristics of the study population are summarized in Table 1.

The results of all measurements and calculations for iodine and creatinine in 24-hour urine are shown in Table 2. All 24-hour urine samples had a creatinine concentration above 0.2 g/L and volume of urine above 0.5 L and were thus suitable for further measurements.

TABLE 2. Median volume, measured and calculated values of iodine and creatinine in 24-hour urine

N = 104	Median (IQR)
Volume of 24-hour urine (L)	2.0 (1.4-2.7)
Measured iodine concentration in 24-hour urine (µg/L) - UIC	70.6 (50.7-95.2)
Measured creatinine concentration in 24-hour urine (g/L)	0.61 (0.47-0.86)
Calculated amount of iodine in 24-hour urine (µg) – UIE	137.1 (103.3-173.2)
Calculated amount of creatinine in 24-hour urine (g)	1.18 (0.98-1.59)
Calculated amount of iodine/creatinine in 24-hour urine (µg/g)	108.6 (82.5-134.0)

IQR = interquartile range; UIC = urinary iodine concentration; UIE = urinary iodine excretion

TABLE 3. Median SLIC per meal, including different time points of saliva sampling, before (0 min) and 30, 60, and 120 min after the meal. The median SLIC was also compared among the different time points of saliva sampling, and a comparison was made with UIE

Meal	N	Time of sampling (min)		SLIC (µg/L)	[1]P	[2]P	[3]P	[4]P	[5]P	[6]P
1	104	0	median (IQR)	92.7 (60.2-166.1)	P = 0.994	P = 0.208	P = 0.013	P = 0.005	P = 0.002	P = 0.001
		30		100.3 (73.3-136.4)						P < 0.001
		60		119.7 (90.7-168.9)	P = 0.533					P = 0.138
		120		123.2 (90.9-178.7)						P = 0.491
2	104	0	median (IQR)	76.7 (53.7-115.3)	P < 0.001	P < 0.001	P < 0.001	P = 0.003	P = 0.006	P < 0.001
		30		110.0 (83.7-182.6)						P = 0.064
		60		141.1 (102.4-237.5)	P = 0.925					P = 0.176
		120		159.9 (87.9-235.5)						P = 0.116
3	92	0	median (IQR)	98.3 (62.5-146.7)	P = 0.001	P < 0.001	P < 0.001	P = 0.007	P =0.002	P < 0.001
		30		127.3 (97.1-183.7)						P = 0.981
		60		163.0 (116.2-237.5)	P = 0.590					P = 0.002
		120		163.0 (120.6-276.5)						P< 0.001
4	26	0	median (IQR)	108.2 (66.1-163.6)	P = 0.464	P = 0.001	P = 0.002	P = 0.006	P = 0.004	P=0.040
		30		112.2 (98.9-154.2)						P = 0.163
		60		173.8 (136.1-237.9)	P = 0.714					P = 0.012
		120		183.8 (120.9-268.6)						P = 0.012

[1]P-value, comparison of SLIC before (0) meal and 30 min (above) after, and 60, and 120 min (below) after meal, [2]P-value, comparison of SLIC before (0) meal and 60 min after meal, [3]P-value, comparison of SLIC before (0) meal and 120 min after meal, [4]P-value, comparison of SLIC 30 and 60 min after meal, [5]P-value, comparison of SLIC 30 and 120 min after meal, [6]P-value, comparison of SLIC before (0) meal and after meal (30 min, 60 min and 120 min, respectively) with UIE.

IQR = interquartile range; SLIC = salivary iodine concentration; UIE = urinary iodine excretion

Participants consumed 2–4 meals per day, with 2 meals consumed by 12/104 (11.5%) participants, 3 meals consumed by 66/104 (63.5%) and 4 meals consumed by 26/104 (25.0%) participants. The results of the individual SLIC medians per meal are shown in Table 3.

Looking at the first meal, the results showed no statistical difference in the SLIC values between before (0 min) and 30 and 60 min after the meal. A statistical difference was found between 0 and 120 min after the meal. Additionally, there were also statistical differences in the SLIC values between 30 and 60 min after the meal and between 30 and 120 min after the meal. In contrast, there were no statistical differences in the SLIC values between 60 and 120 min after the meal. For the second and third meals, there was a statistical difference in SLIC values before the meal and at all other times after the meal, whereas there was no difference in SLIC values between 60 and 120 min after the meal. At the fourth meal, there was no statistical difference in the SLIC values between the pre-meal and 30 min post-meal measurements or between the 60- and 120-minute post-meal measurements. However, comparisons among post-meal time points showed a statistical difference in the SLIC values. After comparing all SLIC values at different times with UIE, the SLIC values at 60 and 120 min after the first and second meal and 30 min after the second, third, and fourth meals were comparable with UIE ($P > 0.05$), while all other values were not comparable ($P < 0.05$).

The comparison of the SLIC values before the meal (0 min) showed that there were no statistically significant differences between the first and third meal and between the first and fourth meal ($P = 0.860$ and $P = 0.942$, respectively), and the same applies to the second and fourth meals and between the third and fourth meals ($P = 0.106$ and $P = 0.884$, respectively). At the same time, statistical differences were observed between the first and second meals and between the second and third meals ($P = 0.008$ and $P = 0.014$, respectively). Similarly, comparison of all 120-minute post-meal SLIC values showed no statistical differences between the first and second, between the second and third, between the second and fourth and between the third and fourth meals ($P = 0.081$, $P = 0.125$, $P = 0.200$, $P = 0.974$, respectively), but there was a statistical difference between the first and third meals and between the first and fourth meals ($P < 0.001$ and $P = 0.009$, respectively).

SLIC values increased with number of meals. The median SLIC value increased after each meal, regardless of meal time. In addition, the median SLIC value also increased with the number of

meals per day and was the highest 120 min after the fourth meal. Importantly, a statistical difference in SLIC values was also observed 120 min after each meal and immediately before the next meal (i.e., 0 min), namely, between the first and second meal ($P < 0.001$), between the second and third meal ($P < 0.001$), and between the third and fourth meal ($P = 0.004$). Additionally, SLIC values were compared according to the number of meals consumed. There was a statistically significant difference between the first meal and 120 min after the last meal if a participant had consumed 2 meals/day ($P = 0.002$), three meals/day ($P < 0.001$) or four meals/day ($P < 0.001$). In addition, there was also a statistical difference between participants who ate three or four meals/day ($P = 0.001$).

Discussion

In recent years, some studies have assessed the suitability of SLIC for iodine intake estimation.[12,16] To our knowledge, this is the first study to compare excreted iodine in saliva before and at different times after each meal with UIE to determine the dynamics of iodine excretion into saliva. Our research showed an important breakthrough in this field, namely, an excellent correlation between the SLIC value and UIE. The results showed that the SLIC value at 60 min and 120 min after the first and second meal, as well as SLIC value 30 min after the second, third, and fourth meal, is comparable to UIE, which is currently the gold standard method and is therefore suitable for assessing iodine intake.

Adequate iodine intake is essential for normal thyroid function. This is usually achieved by adequate iodization of table salts.[17] However, in some countries, this can also be achieved through dietary habits.[18] The WHO recommends assessing iodine intake at the population level by measuring UIC in a single urine sample; however, the timing of urine collection is not suggested.[1] UIC measurements should be interpreted with caution, considering the influence of diuresis (urine sample dilution effect) and the timing of urine sample collection[19], especially at the individual level. As iodine is also excreted in saliva, this biological sample offers an additional option for assessing iodine intake. Among 104 adults, 32 (30.8%) men and 72 (69.2%) women participated in our study. As already shown, there are no differences in gender in UIC determination[19]; therefore, gender should not influence the SLIC values. Most (94.2%) participants consumed iodized salt or at least a combination of iodized/non-iodized salt, which is consistent with research in our country, where only limited non-iodized salt is available or used.[20]

The gold standard method for assessing population iodine intake is currently UIE, which is why all SLIC measurements were compared with it. Creatinine concentration was measured in all urine samples to determine the quality of the sample and to reduce the possible impact of diuresis on UIC results. The median UIC value in 24-hour urine was 70.6 μg/L. However, this value indicates little about the daily iodine intake in our participant group, as this value also depends on the fluid intake and volume of collected urine. Considering the median volume of 24-hour collected urine, which was 2.0 L and corresponds to normal urine excretion per day[21], the calculation of UIE yields a median value 137.1 μg iodine/day. It is known from the literature that in healthy people, 90% of the daily iodine intake is excreted via urine.[2] Accordingly, the median iodine intake of our group was approximately 150 μg iodine/day, which corresponds to WHO recommendations.[1]

Due to the disadvantage of time-consuming collection and the possibility of improper sampling of 24-hour urine[22], our aim was to evaluate the results of SLIC at different individual time points of saliva sampling with UIE in healthy individuals.

The comparison of SLIC values at different sampling times before/after a meal and independent of the number of meals per day showed that SLIC values between pre-meal and 30 min after a meal were statistically different from SLIC values between 60 and 120 min after a meal ($P < 0.05$), with only one exception, the first meal, where there was no difference in SLIC value before and 60 min after the meal ($P = 0.208$). Interestingly, there are statistical differences in the SLIC before and 30 min after the second and third meals, but not after the first and fourth meals. This could be due to a time lag between iodine absorption via the intestine and iodine transfer to the salivary glands during the first half of the day. According to literature data, iodine is excreted into saliva approximately 10–15 min after food intake[23], and SLIC increases with time after all meals. The increased salivary excretion (along with iodine) after a meal may be related to antimicrobial protection of the oral and gastric mucosa.[24,25] Importantly, there was a statistically significant difference in SLIC levels after (120 min) a meal and before (0 min) the next meal ($P < 0.05$). The reason for this could be that iodine requirements and its effect on the oral cavity decrease

with time after food intake (at least 120 min). Interestingly, the SLIC increased after each meal throughout the day, and not only after each meal. The highest SLIC was observed in the evening. Similar findings have been reported in children.[12] Notably, the results showed that SLIC levels at 60 and 120 min after the first and second meals, as well as 30 min after the second meal, were comparable to UIE. Therefore, saliva could replace iodine measurement in 24-hour urine, which is very difficult to collect, especially for elderly individuals.[22] Furthermore, SLIC values at 30 min after the third and fourth meals were comparable to those of excreted iodine in 24-hour urine. This could be consistent with the increase in iodine concentration throughout the day, which could lead to a more rapid increase in SLIC levels when healthy individuals consume more than 2 meals per day. The advantage of saliva sampling is that it is a faster and simpler protocol for assessing iodine intake, allowing sampling at any point in time, regardless of the number of meals per day. The results showed that the timing of saliva sampling could be related to meals and not to a specific time of day. In addition, individuals can collect saliva sample at home/work at their own pace and send the sample to the laboratory instead of traveling to a medical facility. Only a small group of smokers (7) participated in our study and were included in the analysis because thiocyanate and coloured saliva, which are present in smokers, do not affect SLIC measurements using the S-K method.[10]

The advantage of our work was that the collection of urine and saliva sampling took place on the same day in the participants' own environment, which allowed simultaneous monitoring of iodine excretion in saliva and the 24-hour collected urine. In addition, all participants taking dietary supplements that affect iodine measurements were excluded from calculations. More than 100 participants took part in this study. A disadvantage of saliva sampling could be the poor hydration of the individual, which could lead to lower saliva volume and consequently higher SLIC values[26], especially in the elderly.[27] This problem could be solved by using constantly secreted analytes in saliva as an internal standard, such as amylase[28], which is also used in forensics.[29]

For the additional support of the research, it would be important to extend the study to population-based groups of people to confirm the data at a national level, and to study groups of people with known thyroid disease, as well as those who deliberately avoid iodized salt or iodine intake. It would also be important to investigate any possible interferences affecting SLIC measurements, particularly in participants taking medication, determine relevant cut-offs for SLIC, and, to assess inter- and intraindividual variability of SLIC.

Acknowledgments

We thank Darinka Levstek at University Medical Centre Ljubljana, Slovenia, for her technical assistance and Eva Fliser at University Medical Centre Maribor, Slovenia, for the creatinine measurements. Additionally, we thank prof. Marjan Veber for his assistance that led to collaboration between both working groups and all the support he showed throughout the research. We also thank all participants for their efforts in collecting biological samples.

References

1. WHO, UNICEF, ICCIDD. Assessment of iodine deficiency disorders and monitoring their elimination: a guide for programme managers. 3rd edition. [Internet]. *WHO Library Cataloguing-in-Publication Data*; 2007. [cited 2025 Oct 30]. Available at: https://www.who.int/publications/i/item/9789241595827
2. Zimmermann MB. Iodine deficiency. *Endocr Rev* 2009; **30:** 376-408. doi: 10.1210/er.2009-0011
3. Hetzel BS. Iodine Deficiency Disorders (IDD) and their eradication. *Lancet* 1983; **322:** 1126-9. doi: 10.1016/S0140-6736(83)90636-0
4. Sallsten G, Barregard L. Variability of urinary creatinine in healthy individuals. *Int J Environ Res Public Health* 2021; **18:** 1-12. doi: 10.3390/ijerph18063166
5. Gaberšček S, Zaletel K. Thyroid physiology and autoimmunity in pregnancy and after delivery. *Expert Rev Clin Immunol* 2011; **7:** 697-707. doi: 10.1586/eci.11.42
6. Portulano C, Paroder-Belenitsky M, Carrasco N. The Na+/I- Symporter (NIS): mechanism and medical impact. *Endocr Rev* 2014; **35:** 106-49. doi: 10.1210/er.2012-1036
7. Shelor CP, Dasgupta PK. Review of analytical methods for the quantification of iodine in complex matrices. *Anal Chim Acta* 2011; **702:** 16-36. doi: 10.1016/j.aca.2011.05.039
8. Jooste PL, Strydom E. Methods for determination of iodine in urine and salt. *Best Pract Res Clin Endocrinol Metab* 2010; **24:** 77-88. doi: 10.1016/j.beem.2009.08.006
9. Sandell EB, Kolthoff IM. Micro determination of iodine by a catalytic method. *Mikrochim Acta* 1937; **1:** 9-25. doi: 10.1007/BF01476194
10. Oblak A, Imperl J, Kolar M, Marolt G, Krhin B, Zaletel K, et al. Introduction of a spectrophotometric method for salivary iodine determination on microplate based on Sandell-Kolthoff reaction. *Radiol Oncol* 2024; **58:** 357-65. doi: 10.2478/raon-2024-0035
11. Flieger J, Kawka J, Tatarczak-Michalewska M. Levels of the thiocyanate in the saliva of tobacco smokers in comparison to e-cigarette smokers and non-smokers measured by HPLC on a phosphatidylcholine column. *Molecules* 2019; **24:** 3790. doi: 10.3390/molecules24203790
12. Guo W, Dong S, Jin Y, Pan Z, Pearce ENe, Wuet W, et al. Evaluation of variation of saliva iodine and recommendations for sample size and sampling time: Implications for assessing iodine nutritional status. *Clin Nutr* 2021; **40:** 3559-66. doi: 10.1016/j.clnu.2020.12.010

13. Oblak A, Biček A, Pirnat E, Zaletel K, Gaberšček S. First estimation of reference intervals for thyroid-stimulating hormone and thyroid hormones in Slovenian population. *Acta Chim Slov* 2021; **68:** 488-93. doi: 10.17344/acsi.2020.5922

14. Oblak A, Arohonka P, Erlund I, Kuzmanovska S, Zaletel K, Gaberšček S. Validation of a spectrophotometric method for urinary iodine determination on microplate based on Sandell-Kolthoff reaction. *Lab Med* 2022; **53:** 376-80. doi: 10.1093/labmed/lmab117

15. Pino S, Fang SL, Braverman LE. Ammonium persulfate: a safe alternative oxidizing reagent for measuring urinary iodine. *Clin Chem* 1996; **42:** 239-43. doi: 10.1093/clinchem/42.2.239

16. Guo W, Pan Z, Zhang Y, Jin Y, Dong S, Wu W, et al. Saliva iodine concentration in children and its association with iodine status and thyroid function. *J Clin Endocrinol Metab* 2020; **105:** 3451-9. doi: 10.1210/clinem/dgaa471

17. Zimmermann MB, Andersson M. Global endocrinology: Global perspectives in endocrinology: coverage of iodized salt programs and iodine status in 2020. *Eur J Endocrinol* 2021; **185:** R13-21. doi: 10.1530/EJE-21-0171

18. Gunnarsdóttir I, Brantsæter AL. Iodine: a scoping review for Nordic Nutrition Recommendations 2023. *Food Nutr Res* 2023; **67:** 10369. doi: 10.29219/fnr.v67.10369

19. Oblak A, Hribar M, Hristov H, Gregorič M, Blaznik U, Osredkar J, et al. Interpreting urinary iodine concentration: effects of urine dilution and collection timing. *Eur J Clin Nutr* 2024; **78:** 1105-10. doi: 10.1038/s41430-024-01492-y

20. Žmitek K, Pravst I. Iodisation of salt in Slovenia: Increased availability of non-iodised salt in the food supply. *Nutrients* 2016; **8:** 434. doi: 10.3390/nu8070434

21. Kugler S, Blaznik U, Rehberger M, Zaletel M, Korošec A, Somrak M, et al. Twenty-four hour urinary sodium and potassium excretion in adult population of Slovenia: results of the Manjsoli.si/2022 study. *Public Health NutR* 2024; **27:** e163. doi: 10.1017/S1368980024001605

22. Miler M, Šimundić AM. Low level of adherence to instructions for 24-hour urine collection among hospital outpatients. *Biochem Medica* 2013; **23:** 316-20. doi: 10.11613/bm.2013.038

23. Bruger M, Member S. On the excretion of iodine in the saliva. *Am J Physiol Content* 1943; **139:** 212-6. doi: 10.1152/ajplegacy.1943.139.2.212

24. Venturi S, Venturi M. Iodine in evolution of salivary glands and in oral health. *Nutr Health* 2009; **20:** 119-34. doi: 10.1177/026010600902000204

25. Akiba Y, Leung AM, Bashir MT, Ebrahimi R, W Currier JW, Neverova N, et al. Excess iodine exposure acutely increases salivary iodide and antimicrobial hypoiodous acid concentrations in humans. *Sci Rep* 2022; **12:** 20935. doi: 10.1038/s41598-022-23803-8

26. Ship JA, Fischer DJ. The relationship between dehydration and parotid salivary gland function in young and older healthy adults. *J Gerontol Ser A Biol Sci Med Sci* 1997; **52:** M310-9. doi: 10.1093/gerona/52a.5.m310

27. Rosinger A Herrick K. U.S. Department of health and human services. Centers for Disease Control and Prevention. National Center for Health Statistics. Daily water intake among U.S. men and women, 2009-2012. *NCHS Data Br* 2016; **242:** 1-8.

28. Noble RE. Salivary alpha-amylase and lysozyme levels: A non-invasive technique for measuring parotid vs submandibular/sublingual gland activity. *J Oral Sci* 2000; **42:** 83-6. doi: 10.2334/josnusd.42.83

29. Hedman J, Dalin E, Rasmusson B, Ansell R. Evaluation of amylase testing as a tool for saliva screening of crime scene trace swabs. *Forensic Sci Int Genet* 2011; **5:** 194-8. doi: 10.1016/j.fsigen.2010.03.003

RADIOLOGY AND ONCOLOGY Radiology and Oncology | Ljubljana | Slovenia | www.radioloncol.com

research article

^{18}F-FDG PET/CT-based recurrence patterns and survival outcomes in esophageal carcinoma: a single center experience

Milica Kotur[1], Strahinja Odalovic[1,2], Jelena Petrovic[1,2], Nikola Pantic[1], Isidora Grozdic Milojevic[1,2], Dragana Sobic Saranovic[1,2], Predrag Sabljak[2,3], Vera Artiko[1,2]

[1] Center for Nuclear Medicine with PET, University Clinical Center of Serbia, Belgrade, Serbia

[2] Faculty of Medicine, University of Belgrade, Belgrade, Serbia

[3] Clinic for Digestive Surgery, University Clinical Center of Serbia, Belgrade, Serbia

Radiol Oncol 2026; 60(3): 346-355.

Received 7 June 2026
Accepted 26 July 2026

Correspondence to: Milica Kotur, M.D., Center for Nuclear Medicine with PET, University Clinical Center of Serbia, Belgrade, Serbia.
E-mail: koturmilica99@gmail.com

Disclosure: No potential conflicts of interest were disclosed.

Background. This study aimed to evaluate differences among three patient groups with suspected recurrent esophageal carcinoma, defined by ^{18}F-fluorodeoxyglucose positron emission tomography/computed tomography (^{18}F-FDG PET/CT) findings, in quantitative and semiquantitative PET/CT parameters and serum tumor markers, and to assess their impact on progression-free survival (PFS) and overall survival (OS).

Patients and methods. This retrospective cohort study included 77 patients with positive ^{18}F-FDG PET/CT findings between January 2014 and December 2025. Based on ^{18}F-FDG PET/CT findings, patients were classified into three groups: G1 (isolated locoregional recurrence), G2 (isolated metastases), and G3 (both locoregional disease and metastases). Semiquantitative and quantitative ^{18}F-FDG PET/CT parameters, histopathological characteristics, and blood tumor marker levels were compared among the groups. For survival analysis, patients were stratified into low and high groups according to the median value of each parameter.

Results. Elevated carcinoembryonic antigen (CEA) levels were significantly more frequent in G2 and G3 compared with G1 ($p = 0.005$), while no significant difference was observed for carbohydrate antigen 19-9 (CA19-9) levels ($p = 0.280$). Significant differences in all analyzed ^{18}F-FDG PET/CT parameters were found among the three groups, with the highest values in G3. Patients with lower maximal standardized uptake values (SUVmax) and SUVmean values demonstrated significantly longer PFS and OS. Lower metabolic tumor volume (MTV) and total lesion glycolysis (TLG) values were associated with significantly longer progression-free survival (PFS), while overall survival (OS) was also longer, although without statistical significance.

Conclusions. Studies stratifying patients by isolated locoregional recurrence, isolated metastases, and combined locoregional/metastases on ^{18}F-FDG PET/CT remain limited. Our findings suggest that disease spread patterns and semiquantitative/quantitative ^{18}F-FDG PET/CT parameters may provide important prognostic value in patients with esophageal carcinoma.

Key words: recurrence of esophageal carcinoma; ^{18}F-FDG PET/CT; semiquantitative and quantitative ^{18}F-FDG PET/CT parameters; progression-free survival; overall survival

Introduction

Esophageal carcinoma (EC) is one of the leading causes of cancer mortality worldwide.[1] The two main histopathological subtypes of this malignancy are esophageal squamous cell carcinoma (ESCC) and esophageal adenocarcinoma (EAC).[1,2] The distribution of these subtypes shows marked geographical variation, with EAC being more prevalent in Europe and North America, while ESCC predominates in Asia and Africa.[3]

The treatment of esophageal carcinoma depends on histopathological subtype, tumor location, disease stage, and the patient's overall clinical condition and includes surgery, chemotherapy (CHT), and radiotherapy (RT). Despite advances in therapeutic strategies, the prognosis remains poor, primarily due to the high rate of disease recurrence.[4] After initial treatment, early detection of disease recurrence, accurate localization, and timely initiation of therapy are crucial for disease course and patient outcome.[5,6]

Different studies have classified esophageal carcinoma recurrence in different ways. Different approaches have been proposed, with relapse most commonly categorized as: (1) local, (2) regional, and (3) metastases.[7] In addition, some studies have classified esophageal carcinoma relapse based on ^{18}F-FDG PET/CT findings, distinguishing between local recurrence and metastatic disease, as well as more complex categories, including isolated locoregional disease, locoregional disease associated with lymph node metastases (without distant metastases), and disease with simultaneous lymph node and distant metastases. In general, regardless of how esophageal carcinoma recurrence is classified, patients with metastases have worse progression free survival (PFS) and overall survival (OS) than those with isolated locoregional recurrence.[7-9]

Although previous studies have highlighted the high sensitivity of ^{18}F-FDG PET/CT in detecting recurrent disease[10], there is still a clear gap in understanding the prognostic value of quantitative and semiquantitative ^{18}F-FDG PET/CT parameters, including standardized uptake values (SUVmax, SUVpeak, and SUVmean), metabolic tumor volume (MTV), and total lesion glycolysis (TLG), across different recurrence patterns identified by ^{18}F-FDG PET/CT isolated locoregional recurrence, metastatic relapse, and combined locoregional and metastatic relapse. Furthermore, these parameters have not been systematically evaluated and compared among these three groups.

Therefore, the aim of this study was to evaluate differences among three specific patient groups, defined solely on the basis of ^{18}F-FDG PET/CT findings, with regard to key quantitative and semiquantitative ^{18}F-FDG PET/CT parameters, as well as to assess their impact on PFS and OS.

Patients and methods

Patients

This retrospective cohort study included 77 patients with suspected relapse of esophageal carcinoma and positive ^{18}F-FDG PET/CT findings between January 2014 and December 2025. Inclusion criteria were: (1) patients with histologically confirmed primary esophageal carcinoma; (2) positive ^{18}F-FDG PET/CT findings; (3) available data on histopathological type; (4) previously received therapy (surgical resection, CHT, and/or RT); (5) a minimum interval of three months following surgery or RT, or four weeks after the last cycle of CHT; and (6) available values of tumor markers carcinoembryonic antigen (CEA) and CA 19-9 obtained within one month prior to the ^{18}F-FDG PET/CT scan. Exclusion criteria were: (1) negative ^{18}F-FDG PET/CT findings; (2) glycemia above 11 mmol/L; and (3) history of another malignancy. ^{18}F-FDG PET/CT was performed due to suspected locoregional recurrence and/or metastatic disease.

Medical data collected included demographic characteristics (age and sex), tumor characteristics (histopathological type), and details of prior treatment (surgery, CHT, and/or RT). Serum tumor marker levels (CEA and CA 19-9), measured within one month prior to the ^{18}F-FDG PET/CT examination, were also recorded.

Clinical and imaging follow-ups for at least one year after the ^{18}F-FDG PET/CT examination were used as a gold standard for assessment of the progression of the disease.

Written informed consent was obtained from all participants. The study was approved by the Institutional Ethics Committee (approval No. 1500/45).

^{18}F-FDG PET/CT protocol, acquisition, and interpretation

All patients fasted for at least six hours prior to ^{18}F-FDG PET/CT imaging (Biograph True64 hybrid scanner, Siemens). Blood glucose levels were measured before tracer administration, and only patients with values below 11 mmol/L proceeded

with the examination. ^{18}F-FDG was administered intravenously at a dose of 5.5 MBq/kg.

Image acquisition started 60 minutes after tracer injection. Initially, a low-dose, non-contrast-enhanced CT scan was performed (120 kV, 45 mAs, slice thickness 5 mm, pitch 1.5, rotation time 0.5 s), followed by a three-dimensional whole-body PET acquisition extending from the skull to the proximal femur (6–7 bed positions, 3 minutes per position). PET images were reconstructed using the ordered subset expectation maximization (OSEM) algorithm.

All images were analyzed on a dedicated workstation (syngo.via, version 2008B, Siemens Healthineers). The evaluation included both visual (qualitative) and semiquantitative/quantitative assessments. Any focal ^{18}F-FDG uptake exceeding physiological distribution and not attributable to benign processes was interpreted as pathological. For each suspicious lesion, parameters including SUVmax, SUVpeak, SUVmean, MTV, and TLG were recorded.

Positive findings on ^{18}F-FDG PET/CT were classified as either locoregional recurrence or metastatic disease. Locoregional lesions were defined as pathological ^{18}F-FDG uptake within the surgical field and anastomosis in patients who underwent surgery or at the primary esophageal tumor site in non-operated patients. All other sites of pathological focal uptake were considered metastatic.

Patient groups based on ^{18}F-FDG PET/CT findings

Based on ^{18}F-FDG PET/CT findings, patients were classified into three groups (G1–G3). Group G1 included patients with isolated locoregional disease on ^{18}F-FDG PET/CT. Group G2 included patients with metastases without evidence of locoregional recurrence on ^{18}F-FDG PET/CT. Group G3 included patients with both locoregional disease and metastases detected on ^{18}F-FDG PET/CT. Semiquantitative and quantitative ^{18}F-FDG PET/CT parameters—SUVmax, SUVmean, SUVpeak, MTV, and TLG values—were recorded for the locoregional lesion in the G1 group; the most metabolically active metastatic lesion in the G2 group; and separately for both the locoregional and the most metabolically active metastatic lesions in the G3 group. For comparisons of semiquantitative and quantitative ^{18}F-FDG PET/CT parameters between groups, the higher value of each parameter obtained either from the locoregional lesion or from the most metabolically active metastatic lesion was selected for patients in the G3 group. These values were subsequently compared with the corresponding parameter values in the G1 and G2 groups.

Patient groups based on the therapy administered before the ^{18}F-FDG PET/CT examination

Patients were also divided in relation to the previously applied therapeutic modality into three groups: therapeutic group 1 (Th1), therapeutic group 2 (Th2) and therapeutic group 3 (Th3). The Th1 includes patients who underwent only surgical resection, without the use of CHT or RT. The therapeutic group Th2 consisted of patients who, in addition to surgical intervention, also underwent CHT and/or RT. The Th3 included patients who received CHT and/or RT, without previous surgical resection.

Follow-up and survival analysis

Patients were followed for at least one year after the ^{18}F-FDG PET/CT examination. During the follow-up period, disease progression was recorded. Progression is defined as the appearance of new lesions, an increase in the dimensions of existing lesions, or an increase in their metabolic activity, detected by conventional radiological methods (CT or magnetic resonance imaging) or on subsequent ^{18}F-FDG PET/CT, as well as death due to the underlying disease or from other causes (based on data from medical records). PFS was calculated from the date of the ^{18}F-FDG PET/CT examination to the date of confirmed disease progression, or until the end of the follow-up period if no progression was recorded. OS was defined as the time from the date of the ^{18}F-FDG PET/CT examination to death from any cause or to the last follow-up. For survival analysis, patients were further stratified into two groups based on the median value of each ^{18}F-FDG PET/CT parameter (low ≤ median and high > median).

Statistical analysis

Statistical analysis was performed using EZR (Easy R) software, version 1.70, a graphical user interface for the R statistical programming language (version 4.5.2; The R Foundation for Statistical Computing, Vienna, Austria). Continuous variables were expressed as median and range, while categorical variables were presented as absolute numbers and percentages. Differences between two independent groups were assessed using the Mann-Whitney U test, whereas comparisons among three groups

TABLE 1. Baseline demographic, clinical, and tumor characteristics of patients stratified by ^{18}F-FDG PET/CT group classification

Parameter	G1	G2	G3	P
N	10	34	33	-
Age Med (range)	61.5 (46-76)	63.5 (35-78)	63.0 (32-73)	0.765
Sex Male/female	8/2	29/5	27/6	0.894
Histopathology type EAC/ESCC	9/1	12/22	19/14	**0.007**
CEA Normal/elevated	8/2	11/23	8/25	**0.005**
CA19-9 Normal/elevated	5/5	12/22	8/25	0.280
Therapy Th1/Th2/Th3	6/2/2	10/17/7	4/16/13	**0.030*F**

^{18}F-FDG PET/CT = ^{18}F-fluorodeoxyglucose positron emission tomography/computed tomography; CA19-9 = Carbohydrate antigen 19-9; CEA = carcinoembryonic antigen; EAC = esophageal adenocarcinoma; ESCC = esophageal squamous cell carcinoma; *F = Fisher's exact test; G1 = isolated locoregional disease; G2 = metastases without locoregional recurrence; G3 = locoregional disease and metastases; Th1 = surgery only; Th2 = surgery plus chemotherapy and/or radiotherapy; Th3 = chemotherapy and/or radiotherapy without prior surgery

P values were calculated using the Chi-square or Fisher's exact test; age was analyzed using the Kruskal-Wallis test

were performed using the Kruskal-Wallis test. When statistically significant, post-hoc pairwise comparisons were conducted using the Mann-Whitney U test with Holm correction for multiple testing. Categorical variables were compared using the Chi-square test or Fisher's exact test, as appropriate. PFS and OS were analyzed using the Kaplan–Meier method, and differences between survival curves were assessed using the log-rank test. A p value < 0.05 was considered statistically significant.

Results

Patient characteristics and clinical findings

The study included 77 patients with previously histopathologically confirmed esophageal carcinoma and positive ^{18}F-FDG PET/CT findings, performed due to suspected disease relapse after therapy. The mean age of the patients was 60.3 years (32–77). Of the total number of subjects, EAC was identified in 40 patients (51.9%), while 37 patients (48.1%) had ESCC. Detailed demographic characteristics, tumor marker levels, and data on previously applied therapeutic modalities according to group classification are presented in Table 1.

A total of 10 patients were assigned to the G1 group, 34 to the G2 group, and 33 to the G3 group (representative cases from each group are illustrated in Figure 1). No statistically significant differences in age and sex were observed among the G1, G2, and G3 groups (p = 0.765 and p = 0.894, respectively). A statistically significant difference was

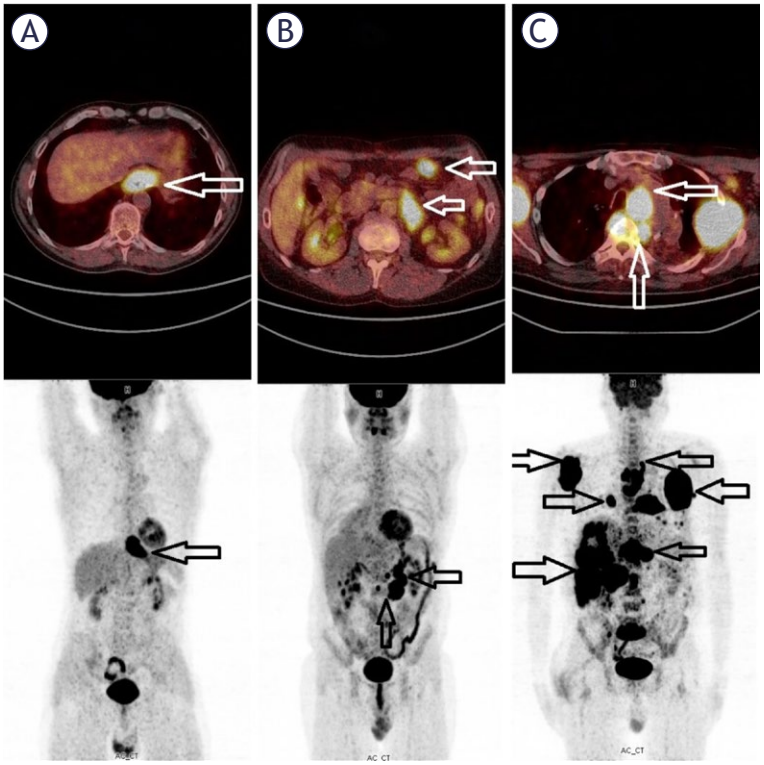

FIGURE 1. Representative imaging examples of patients from each study group (G1–G3). **(A)** Patient from the G1 group on ^{18}F-FDG PET/CT demonstrating isolated locoregional esophageal recurrence. The white arrow indicates the locoregional lesion on the fused ^{18}F-FDG PET/CT image, while the black arrow indicates the locoregional lesion on the MIP image. **(B)** Patient from the G2 group on ^{18}F-FDG PET/CT demonstrating metastatic sites of esophageal recurrence without locoregional recurrence. The white arrows indicate metastatic lesions on the fused ^{18}F-FDG PET/CT image, while the black arrows indicate metastatic lesions on the MIP image. **(C)** Patient from the G3 group on ^{18}F-FDG PET/CT demonstrating metastatic sites of esophageal recurrence with locoregional recurrence. The white arrows indicate lesions on the fused ^{18}F-FDG PET/CT images, while the black arrows indicate metastatic lesions on the MIP image.

TABLE 2. Semiquantitative and quantitative ^{18}F-FDG PET/CT parameters according to group classification

Parameter	G1	G2	G3	P
SUVmax	5.9 (4.2-33.7)	7.8 (1.9-29.3)	12.7 (3.6-30.5)	**0.001**
SUVpeak	4.3 (3.1-30.1)	6.1 (1.3-24.7)	9.9 (3.3-23.2)	**0.001**
SUVmean	3.1 (2.2-21.5)	3.9 (1.6-14.9)	6.7 (2.3-20.3)	**<0.001**
MTV	8.4 (0.9-313.3)	13.2 (0.5-121.0)	24.4 (3.8-292.5)	**0.007**
TLG	9.7 (3.3-74.4)	19.5 (0.7-1768.5)	30.1 (2.9-790.5)	**0.042**

^{18}F-FDG PET/CT = ^{18}F-fluorodeoxyglucose positron emission tomography/computed tomography; G1 = isolated locoregional disease; G2 = metastases without locoregional recurrence; G3 = locoregional disease and metastases; MTV = metabolic tumor volume; SUV = standardized uptake value; TLG = total lesion glycolysis.

Continuous variables are expressed as median (range). Differences between groups were assessed using the Kruskal-Wallis test. Post-hoc pairwise comparisons using the Mann–Whitney U test with Holm correction showed significant differences for SUVmax between G2 and G3 ($p = 0.002$), for SUVpeak between G2 and G3 ($p = 0.002$), for SUVmean between G1 and G3 ($p = 0.008$) and between G2 and G3 ($p < 0.001$), and for MTV between G2 and G3 ($p = 0.007$). Although TLG differed significantly in the Kruskal–Wallis test, post-hoc pairwise comparisons did not reach statistical significance.

TABLE 3. ^{18}F-FDG PET/CT metabolic parameters by histopathology and treatment groups

Parameter	EAC med (range)	ESCC med (range)	P	Th1 med (range)	Th2 med (range)	Th3 med (range)	P
N	40	37	-	20	35	22	-
SUVmax	10.2 (1.9-33.7)	9.9 (3.6-29.3)	1.000	11.2 (4.2-33.7)	7.6 (1.9-23.7)	11.9 (4.2-30.5)	0.124
SUVpeak	8.3 (1.3-30.1)	8.2 (2.4-24.7)	0.943	8.7 (3.1-30.1)	6.4 (1.3-20.1)	9.4 (3.6-23.2)	0.089
SUVmean	5.3 (1.6-21.5)	5.4 (1.9-14.9)	0.874	5.9 (1.9-21.5)	4.2 (1.6-14.5)	6.5 (2.8-20.3)	0.889
MTV	16.8 (0.5-313.3)	15.5 (1.5-118.8)	0.984	16.7 (0.9-118.3)	14.2 (0.5-121.0)	21.8 (1.5-313.3)	0.417
TLG	26.1 (0.7-1768.5)	25. 9(5.1-900.1)	0.915	28.7 (3.3-900.1)	21.7 (0.7-1768.5)	25.4 (2.9-70.5)	0.853

^{18}F-FDG PET/CT = ^{18}F-fluorodeoxyglucose positron emission tomography/computed tomography; EAC = esophageal adenocarcinoma; ESCC = esophageal squamous cell carcinoma; MTV = metabolic tumor volume; SUV = standardized uptake value; TLG = total lesion glycolysis; Th1 = therapeutic group 1 (surgical resection only); Th2 = therapeutic group 2 (surgical resection plus chemotherapy and/or radiotherapy); Th3 = therapeutic group 3 (chemotherapy and/or radiotherapy without prior surgical resection).

Continuous variables are presented as median (range). Differences between histopathological groups (EAC and ESCC) were assessed using the Mann-Whitney U test. Differences between therapeutic groups (Th1–Th3) were assessed using the Kruskal-Wallis test.

found in histopathological type ($p = 0.007$), with EAC being more prevalent in the G1 group, while ESCC predominated in the G2 group.

Elevated CEA levels were significantly more frequent in the G2 and G3 groups compared to G1 ($p = 0.005$). In addition, a statistically significant difference in the applied therapeutic modalities was observed among the groups ($p = 0.030$). Although elevated blood carbohydrate antigen 19-9 (CA19-9) values were more common in G2 and G3 groups, this difference was not statistically significant ($p = 0.280$).

Semiquantitative and quantitative ^{18}F-FDG PET/CT analysis

Analysis of semiquantitative and quantitative ^{18}F-FDG PET/CT parameters revealed statistically significant differences among the groups (G1-G3) for all examined parameters, with the highest level of significance observed for SUVmean ($p < 0.001$). The highest values of all analyzed parameters were recorded in the G3 group (Table 2).

Further analysis showed that ^{18}F-FDG PET/CT parameters (SUVmax, SUVpeak, SUVmean, MTV, and TLG) did not differ significantly according to histopathological tumor type (EAC vs. ESCC; $p > 0.05$ for all parameters). Additionally, no statistically significant differences were observed in ^{18}F-FDG PET/CT parameter values with respect to the applied therapeutic modalities (Th1, Th2, and Th3) (Table 3).

Table 4 shows the most common metastatic sites in patients classified into the G2 and G3 groups, based on the metabolically most active lesion detected on ^{18}F-FDG PET/CT.

Follow-up

Of the total 77 patients initially included in the study, 72 completed all study phases and were included in the final analysis. Median follow-up for the cohort was 70 months (95% CI: 26–105 months), estimated using the reverse Kaplan–Meier method. Median PFS was 10 months (95% CI: 9–14 months). Median OS was 27 months (95% CI: 15–40 months). Progression of disease was present in 55/72 (76.4%). Death was present in 43/72 (59.7%).

In this phase of the study, the final analysis consisted of 10 subjects in group G1, 32 subjects in group G2, and 30 subjects in group G3. The frequency of disease progression and death in each group was analyzed individually, and then their mutual comparison was made. A statistically significant difference was observed in the frequency of disease progression, which was significantly higher in groups G2 and G3 compared to group G1 (p = 0.001). On the other hand, there was no statistically significant difference in the frequency of death among the observed groups (P = 0.112). At the same time, the medians for PFS and OS were calculated and compared for each group individually, whereby no statistically significant difference was observed in median values for either PFS (p = 0.190) or OS (p = 0.707) (Table 5).

Association of ^{18}F-FDG PET/CT parameters with survival outcomes

Higher values of SUVmax, SUVmean, MTV, and TLG were associated with significantly shorter median PFS (p = 0.019, p = 0.016, p = 0.024, and p = 0.036, respectively). Although a difference in median PFS was observed for SUVpeak, it did not reach statistical significance (p = 0.085) (Figures 2A-E) (Table 6).

Higher values of SUVmax, SUVpeak, and SUVmean were associated with shorter median OS (p = 0.016, p = 0.036, and p = 0.048, respectively). In contrast, MTV and TLG did not show a statistically significant association with OS (p = 0.115 and p = 0.238, respectively) (Figures 2F-J) (Table 6).

Discussion

The main innovation of our study is reflected in a specific approach to the classification of patients with suspected recurrence esophageal carcinoma based on ^{18}F-FDG PET/CT findings, which differs

TABLE 4. Distribution of metastatic sites in G2 and G3 groups

Site of metastasis	G2 (n=34)	G3 (n=33)
Supradiaphragmatic lymph node	11	10
Lungs/pleura	8	3
Abdominal solid organs	6	6
Infradiaphragmatic lymph nodes	3	6
Bones	5	5
Small intenstine/large intestine	1	2
Peritoneum	-	1

^{18}F-FDG PET/CT = ^{18}F-fluorodeoxyglucose positron emission tomography/computed tomography; G2 = metastases without locoregional recurrence; G3 = locoregional disease and metastases

TABLE 5. Clinical outcomes according to ^{18}F-FDG PET/CT groups

Outcome	G1	G2	G3	P
N	10	32	30	-
Progression Yes/No	3/7	27/5	25/5	**0.001**
Mortality Yes/No	3/7	20/12	20/10	0.112
PFS median (range)	18.0 (7-105)	11.0 (6-125)	10.0 (6-116)	0.190
OS median (range)	21.0 (10-105)	18.5 (6-132)	15.5 (6-126)	0.707

^{18}F-FDG PET/CT = ^{18}F-fluorodeoxyglucose positron emission tomography/computed tomography; G1 = isolated locoregional disease; G2 = metastases without locoregional recurrence; G3 = locoregional disease and metastases; OS = overall survival; PFS = progression-free survival

P values were calculated using the Chi-square test for categorical variables. Continuous variables (PFS and OS) were analyzed using the Kruskal-Wallis test. Pairwise post hoc comparisons are not presented when the overall P value was not statistically significant.

TABLE 6. Median progression-free and overall survival times according to low and high ^{18}F-FDG PET/CT parameters

Parameter	Cut-off (median)	Median PFS Low vs. high (months)	Median OS Low vs. high (months)
SUVmax	9.9	8.5 vs. 16.0	15.0 vs. 33.0
SUVpeak	8.2	10.0 vs. 16.0	15.0 vs. 30.0
SUVmean	5.4	9.0 vs. 16.0	15.0 vs. 30.0
MTV	16.5	8.5 vs. 19.0	15.0 vs. 30.0
TLG	25.9	9.5 vs. 14.0	22.0 vs. 30.0

^{18}F-FDG PET/CT = ^{18}F-fluorodeoxyglucose positron emission tomography/computed tomography; MTV = metabolic tumor volume; OS = overall survival; PFS = progression-free survival; SUV = standardized uptake value; TLG = total lesion glycolysis

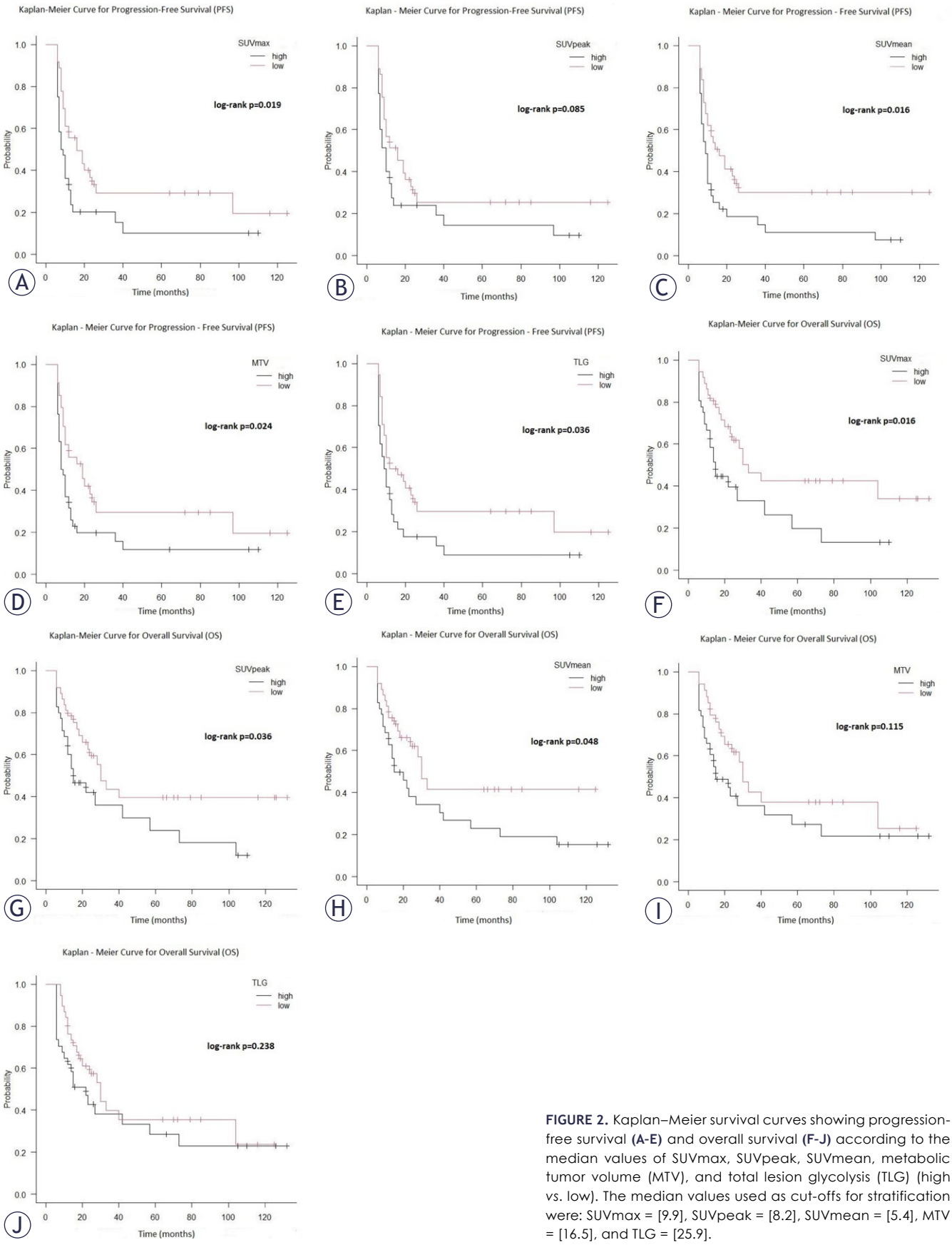

FIGURE 2. Kaplan–Meier survival curves showing progression-free survival **(A-E)** and overall survival **(F-J)** according to the median values of SUVmax, SUVpeak, SUVmean, metabolic tumor volume (MTV), and total lesion glycolysis (TLG) (high *vs.* low). The median values used as cut-offs for stratification were: SUVmax = [9.9], SUVpeak = [8.2], SUVmean = [5.4], MTV = [16.5], and TLG = [25.9].

from the approaches used in previous studies. To our knowledge, studies that specifically stratified patients according to isolated locoregional recurrence, isolated metastases, and the simultaneous presence of locoregional recurrence and metastases on ^{18}F-FDG PET/CT are still rare. In our study, patients with positive ^{18}F-FDG PET/CT findings in the form of metastases or a combination of metastases and local recurrence (groups G2 and G3) significantly more frequently had elevated CEA blood levels compared to patients with isolated locoregional findings (G1). This result is in accordance with literature data showing that high serum CEA levels in esophageal carcinoma are more frequently associated with the presence of metastases.[11,12]

On the other hand, no statistically significant difference in the frequency of elevated CA19-9 levels was observed among the groups. Das *et al*., in a study that included patients with ESCC who had not previously undergone treatment, demonstrated that CA19-9 had higher sensitivity compared to CEA.[13] In contrast, Ansari *et al*. reported that CEA blood levels have higher sensitivity than CA19-9.[14] It is important to note that the participants in our study were more similar to the patients included in the study by Ansari *et al*., as that cohort consisted of post-treatment patients, including both EAC and ESCC cases. These results may suggest that CA19-9 has greater diagnostic value in patients before any treatment, while CEA may be more important for identifying and monitoring esophageal carcinoma recurrence after treatment.

Our results showed that disease progression was significantly more frequent in groups G2 and G3 compared to group G1. This finding may be explained by the fact that patients in group G1 had isolated locoregional recurrence, which potentially allows for better disease control through the applied therapeutic modalities and a lower chance of disease progression.[15,16] In our study, ^{18}F-FDG PET/CT parameters of the metastatic lesion with the highest metabolic activity were used, reflecting the metabolic characteristics of the biologically most aggressive tumor lesion. Accordingly, group G3 showed the highest values for all ^{18}F-FDG PET/CT parameters evaluated. Increased glycolytic activity, accompanied by high values of ^{18}F-FDG PET/CT parameters, was more often reported in more aggressive forms of the disease and advanced stages of malignancy.[17]

In our investigation, SUVmean demonstrated the highest statistical significance ($p < 0.001$) among all analyzed semiquantitative and quantitative ^{18}F-FDG PET/CT parameters when comparing the three groups. This observation may be explained by the fact that SUVmean reflects the average metabolic activity across the tumor lesion, unlike SUVmax, which represents only the single voxel with the highest ^{18}F-FDG uptake within the tumor.[18]

Semiquantitative and quantitative ^{18}F-FDG PET/CT parameters were similar in patients with EAC and ESCC, with no statistically significant differences in median values according to histopathological tumor type. In previous studies analyzing these parameters in primary esophageal carcinoma before therapy, ESCC generally showed higher values.[19,20] On the other hand, comparison of our results with the study by Korkmaz *et al*., which included patients after therapy, revealed a substantial similarity in findings.[21]

Progression-free survival and OS were shortest in patients from the G3 group; however, these differences did not reach statistical significance. Similarly, Kahraman *et al*. also stratified patients into three groups according to ^{18}F-FDG PET/CT findings and evaluated differences in OS.[9] Nevertheless, their classification was not entirely comparable to ours. In their study, OS was longest in patients with isolated locoregional disease and shortest in those with metastatic involvement, with statistically significant differences between the groups. Although our findings demonstrate a similar trend, the lack of statistical significance in our study may be attributed to differences in patient stratification criteria, sample size and the potential heterogeneity of the study population.

Our patients, who were classified into the "low" group according to SUVmax and SUVmean values, demonstrated statistically significantly longer PFS as well as OS. Patients with lower values of volumetric parameters (MTV and TLG) also had a statistically significantly higher median PFS. It is interesting that patients with lower values of volumetric parameters had longer OS, but without statistical significance compared to patients with higher values of these parameters. These results indicate that volumetric parameters better reflect the biological dynamics of the disease and the probability of earlier progression, while overall survival is additionally influenced by numerous other factors, including the therapeutic approach, the general condition in the patient, and the presence of comorbidities.

The prognostic significance of MTV and TLG parameters remains controversial in the literature, as some studies have demonstrated a significant

association with survival outcomes, whereas others have failed to confirm such results.[22,23] These discrepancies may be attributed to heterogeneity among study populations, differences in disease stage and therapeutic approaches, as well as methodological variations between studies, population heterogeneity, and a variable number of subjects.

However, the results of this study should be interpreted in the context of certain limitations. The study had a retrospective design and was conducted in one center, with a relatively small number of subjects. Additionally, the number of patients was not evenly distributed between all three groups, which could affect the comparison of the parameters analyzed among them.

Despite the mentioned limitations, our results provide a new approach to the classification of patients with esophageal carcinoma based on ^{18}F-FDG PET/CT findings and open the possibility for further research into the prognostic significance of different disease patterns on ^{18}F-FDG PET/CT. Based on the obtained results, it may be worth considering whether the standard classifications of esophageal cancer recurrence should be supplemented by this or a similar classification, and whether its potential value could be assessed through comparison with existing systems in future studies. Future prospective multicenter studies with a larger number of subjects are necessary to confirm the obtained findings.

Conclusions

The main innovation of our study is reflected in a specific approach to the classification of patients with suspected recurrence esophageal carcinoma based on ^{18}F-FDG PET/CT findings, which differs from the approaches used in previous studies. To our knowledge, studies that specifically stratified patients according to isolated locoregional recurrence, isolated metastases, and the simultaneous presence of locoregional recurrence and metastases on ^{18}F-FDG PET/CT are still rare. The results of our study indicate that the pattern of disease spread on ^{18}F-FDG PET/CT, in combination with semiquantitative and quantitative ^{18}F-FDG PET/CT parameters, may have significant prognostic value in patients with esophageal carcinoma. Patients with simultaneous locoregional recurrence and metastases are particularly distinguished, in whom the highest values of ^{18}F-FDG PET/CT parameters, more frequent disease progression, and the shortest survival were registered.

References

1. Jiang W, Zhang B, Xu J, Xue L, Wang L. Current status and perspectives of esophageal cancer: a comprehensive review. *Cancer Commun* 2025; **45:** 281-331. doi: 10.1002/cac2.12645
2. Lander S, Lander E, Gibson MK. Esophageal cancer: overview, risk factors, and reasons for the rise. *Curr Gastroenterol Rep* 2023; **25:** 275-9, doi: 10.1007/s11894-023-00899-0
3. Sung J, Lin D, Fitzgerald R, Sharma P, Law S, Ilson D. Carcinoma of esophagus. *J Gastroenterol Hepatol* 2025; **40:** 1861-75. doi:10.1111/jgh.16990
4. National Comprehensive Cancer Network. *NCCN Clinical Practice Guidelines in Oncology: Esophageal and Esophagogastric Junction Cancers* [Internet]. [cited 2026 Mar 5]. Available at: https://www.nccn.org/guidelines/guidelines-detail?category=1&id=1433
5. National Cancer Institute. *Esophageal Cancer Treatment (PDQ®)–Patient Version* [Internet]. Bethesda (MD): National Cancer Institute; [cited 2026 Mar 15]. Available at: https://www.cancer.gov/types/esophageal/patient/esophageal-treatment-pdq.
6. Samoylova ML, Rajaram R. The evolving role of systemic therapy in locoregionally advanced esophageal cancer: a narrative review. *Ann Esophagus* 2025; **8:** 20. doi: 10.21037/aoe-25-11
7. Mariette C, Balon JM, Piessen G, Fabre S, Van Seuningen I, Triboulet JP. Pattern of recurrence following complete resection of esophageal carcinoma and factors predictive of recurrent disease. *Cancer* 2003; **97:** 1616-23. doi: 10.1002/cncr.11228
8. Kim N, Cho H, Yun M, Park KR, Lee CG. Prognostic values of mid-radiotherapy ^{18}F-FDG PET/CT in patients with esophageal cancer. *Radiat Oncol* 2019; **14:** 27. doi: 10.1186/s13014-019-1232-1
9. Karahan Şen NP, Aksu A, Çapa Kaya G. Volumetric evaluation of staging ^{18}F-FDG PET/CT images in patients with esophageal cancer. *Mol Imaging Radionucl Ther* 2022; **31:** 216-22. doi: 10.4274/mirt.galenos.2022.38980
10. Goense L, van Rossum PS, Reitsma JB, Lam MG, Meijer GJ, van Vulpen M. Diagnostic performance of ^{18}F-FDG PET and PET/CT for the detection of recurrent esophageal cancer after treatment with curative intent: a systematic review and meta-analysis. *J Nucl Med* 2015; **56:** 995-1002. doi: 10.2967/jnumed.115.155580
11. Clark GW, Ireland AP, Hagen JA, Collard JM, Peters JH, De Meester TR. Carcinoembryonic antigen measurements in the management of esophageal cancer: an indicator of subclinical recurrence. *Am J Surg* 1995; **170:** 597-601. doi: 10.1016/s0002-9610(99)80023-3
12. Mao YS, Zhang DC, Zhao XH, Wang LJ, Qi J, Li XX. [Significance of CEA, SCC and Cyfra21-1 serum test in esophageal cancer]. [Chinese]. *Zhonghua Zhong Liu Za Zhi* 2003; **25:** 457-60. doi: 10.3760/cma.j.issn.0253-3766.2003.05.112
13. Das S, Kakoti LM, Ahmed S, Sarma A, Kataki AC. Study of serum CEA and CA 19-9 in esophageal squamous carcinoma and ROC curve analysis. *Asian Pac J Cancer Biol* 2020; **5:** 141-5. doi: 10.31557/APJCB.2020.5.4.141
14. Ansari F, Rai A, Shukla S. Study of carcinoma embryonic antigen and carbohydrate antigen 19-9 levels in patients of esophageal cancer. *Int Surg J* 2021; **8:** 3274-8. doi: 10.18203/2349-2902.isj20214060
15. Ter Veer E, van Kleef JJ, Schokker S, van der Woude SO, Laarman M, Haj Mohammad N, et al. Prognostic and predictive factors for overall survival in metastatic oesophagogastric cancer: a systematic review and meta-analysis. *Eur J Cancer* 2018; **103:** 214-26. doi: 10.1016/j.ejca.2018.07.132
16. Al-Batran SE, Homann N, Pauligk C, Goetze TO, Meiler J, Kaspe S, et al. Perioperative chemotherapy with fluorouracil plus leucovorin, oxaliplatin, and docetaxel versus fluorouracil or capecitabine plus cisplatin and epirubicin for locally advanced, resectable gastric or gastro-oesophageal junction adenocarcinoma (FLOT4): a randomised, phase 2/3 trial. *Lancet* 2019; **393:** 1948-57, doi: 10.1016/S0140-6736(18)32557-1
17. Mantziari S, Pomoni A, Prior JO, Winiker M, Allemann P, Demartines N, et al. ^{18}F- FDG PET/CT-derived parameters predict clinical stage and prognosis of esophageal cancer. *BMC Med Imaging* 2020; **20:** 7. doi: 10.1186/s12880-019-0401-x
18. Kinahan PE, Fletcher JW. Positron emission tomography-computed tomography standardized uptake values in clinical practice and assessing response to therapy. *Semin Ultrasound CT MR* 2010; **31:** 496-505. doi: 10.1053/j.sult.2010.10.001

19. Kommi S, Rallapeta RP, Subramanian BV, Yadagiri LA, Hulikal N, Chandramaliteeswaran C, et al. Utility of [18F]FDG- PET/CT in initial staging and management of patients with esophageal carcinoma: a tertiary care center experience. *Indian J Nucl Med* 2024; **39:** 329-34. doi: 10.4103/ijnm.ijnm_118_23

20. Al-Taan OS, Eltweri A, Sharpe D, Rodgers PM, Ubhi SS, Bowrey DJ. Prognostic value of baseline FDG uptake on PET-CT in esophageal carcinoma. *World J Gastrointest Oncol* 2014; **6:** 139-44. doi: 10.4251/wjgo.v6.i5.139

21. Korkmaz U, Hacioglu MB, Kostek O, Sut N, Kodaz H, Erdogan B, et al. The relationship between FDG PET/CT-defined metabolic parameters and the histopathological subtype of oesophageal carcinomas. *Pol J Radiol* 2020; **85:** e254-e60. doi: 10.5114/pjr.2020.95945

22. Hatt M, Visvikis D, Albarghach NM, Tixier F, Pradier O, Cheze-le Rest C. Prognostic value of 18F-FDG PET image-based parameters in oesophageal cancer and impact of tumour delineation methodology. *Eur J Nucl Med Mol Imaging* 2011; **38:** 1191-202. doi: 10.1007/s00259-011-1755-7

23. Martínez A, Infante JR, Quirós J, Rayo JI, Serrano J, Moreno M, et al. Baseline ^{18}F-FDG PET/CT quantitative parameters as prognostic factors in esophageal squamous cell cancer. *Rev Esp Med Nucl Imagen Mol* 2022; 41: 164-70. doi: 10.1016/j.remnie.2021.07.006

RADIOLOGY AND ONCOLOGY Radiology and Oncology | Ljubljana | Slovenia | www.radioloncol.com

research article

Breast DCE-MRI morphological features and semi-quantitative parameters associated with upgrade to invasive carcinoma in biopsy-proven DCIS

Vladimir Urban[1], Zorica Milosevic[2], Zoran Bukumiric[2,3], Katarina Obradovic[1], Nina Adzic[1], Dragana Pavlovic-Stankovic[1], Ivana Petkovic[1], Ivana Sovic[1], Irena Jovanic[4], Igor Spurnic[2,5]

[1] Department of Diagnostic Radiology, Institute for Oncology and Radiology of Serbia, Belgrade, Serbia
[2] School of Medicine, University of Belgrade, Belgrade, Serbia
[3] Institute for Medical Statistics and Informatics, Belgrade, Serbia
[4] Department of Pathology, Institute for Oncology and Radiology of Serbia, Belgrade, Serbia
[5] Department of Surgery, Institute for Oncology and Radiology of Serbia, Belgrade, Serbia

Radiol Oncol 2026; 60(3): 356-366.

Received 7 February 2026
Accepted 19 July 2026

Correspondence to: Vladimir Urban, M.D., Institute for Oncology and Radiology of Serbia, Serbia. E-mail: vladimir.urban@ncrc.ac.rs

Disclosure: No potential conflicts of interest were disclosed.

Background. The aim of this study was to identify imaging predictors of upgrade to invasive carcinoma (IC) in patients with biopsy-proven ductal carcinoma *in situ* (DCIS) based on morphological features and semi-quantitative parameters derived from dynamic contrast-enhanced breast magnetic resonance imaging (DCE-MRI).

Patients and methods. Ninety consecutive patients with biopsy-proven DCIS who had positive findings on standard full-protocol breast DCE-MRI and subsequently underwent surgical excision with final postoperative histopathological diagnosis were included. Patients with final postoperative IC were compared with those without IC. Morphological features (lesion type, size, multifocality/multicentricity, T2-weighted (T2W) and turbo inversion recovery magnitude [TIRM] characteristics) and semi-quantitative parameters (wash-in, peak enhancement, delayed phase of the time-intensity curve [TIC], time to peak [TTP], and positive enhancement integral [PEI]) were analyzed.

Results. Fifty-five patients (61.1%) had no IC, while 35 patients (38.9%) had IC on final histopathology. Patients with IC more frequently demonstrated non-mass enhancement (NME) combined with a mass, larger lesion size, multifocal or multicentric disease, T2W/TIRM hyperintensity, fast wash-in, higher peak enhancement, plateau and washout TIC patterns, higher PEI, and shorter TTP. Multivariate analysis identified NME combined with a mass, delayed-phase TIC characteristics, and TIRM hyperintensity as independent predictors of IC.

Conclusions. Our study confirmed that prediction models incorporating breast DCE-MRI morphological features and semi-quantitative parameters can stratify patients with biopsy-proven DCIS by their probability of upgrade to IC. TIRM hyperintensity emerged as one of three independent predictors of IC and, to the best of our knowledge, has not been previously reported in this context.

Key words: DCIS; breast biopsy; breast MRI; semi-quantitative; upgrade; invasive carcinoma

Introduction

The World Health Organization defines ductal carcinoma *in situ* (DCIS) as a neoplastic proliferation of epithelial cells confined to the mammary ductal-lobular system, characterized by subtle to marked cytological atypia and an inherent, though not necessarily obligate, tendency to progress to inva-

sive cancer.[1,2] When the integrity of the basement membrane is disrupted and the tumor extends beyond the ductal-lobular system into adjacent tissue, it is classified as invasive carcinoma (IC). Because DCIS is considered a non-obligate precursor of IC, timely detection and treatment may prevent progression to invasive disease. Currently, in the era of widespread screening mammography, most newly diagnosed cases of DCIS are asymptomatic (80–85%) and are detected incidentally.[2] Mammography remains the standard modality for DCIS detection due to its high sensitivity for suspicious microcalcifications, which are present in about 75% of DCIS cases.[3]

DCIS can be unifocal or involve multiple segments of one or more ductal systems, with intervening normal breast tissue.[4] In addition, DCIS may coexist with IC, reflecting the heterogeneous nature of malignant lesions. Consequently, percutaneous biopsy may underestimate the presence of invasive disease due to sampling limitations and intralesional heterogeneity. In clinical practice, the identification of IC on final postoperative histopathology following a percutaneous biopsy diagnosis of DCIS is regarded as an "upgrade". Preoperative identification of a possible concomitant IC in the cases of percutaneously diagnosed DCIS is important, as it guides further patient management, particularly the need for sentinel lymph node biopsy (SLNB).

In this context, dynamic contrast-enhanced breast magnetic resonance imaging (DCE-MRI) may provide additional information. Following intravenous administration of a low-molecular-weight gadolinium-based contrast agent to assess tumor angiogenesis, DCE-MRI detects areas of pathological enhancement that cannot be visualized on mammography or ultrasound.[4] By combining morphological features and dynamic enhancement parameters, DCE-MRI offers the greatest potential among breast imaging modalities for excluding IC.[5] According to the literature, the sensitivity of DCE-MRI for detecting DCIS ranges from 88% to 92%, while sensitivity for detecting IC ranges from 91% to 95%.[5-9] However, considerable controversy remains regarding the usefulness of breast DCE-MRI in patients with preoperatively biopsy-proven DCIS, as published results are highly variable and sometimes conflicting.[5,10-22]

In this article, we focused on the morphological features of preoperatively biopsy-proven DCIS and the time-intensity curve (TIC) of its most enhancing part as a semi-quantitative parameter, both derived from a standard full breast DCE-MRI protocol and interpreted in accordance with the ACR BI-RADS lexicon.[23] We also analyzed two additional semi-quantitative parameters derived from TIC – the positive enhancement integral (PEI) and time to peak (TTP). These parameters are readily available in vendor-provided software packages. PEI and TTP can be expressed both numerically and graphically (as color maps), reflecting different aspects of tissue perfusion. Although they are not part of the BI-RADS framework, PEI and TTP are suitable for research purposes and may also be applicable in routine clinical practice, as they can assist radiologists in identifying areas of suspicious enhancement.[24]

All semi-quantitative parameters are based on the premise that malignant lesions tend to take up and release the contrast agent earlier and faster than benign lesions. TIC represents the change in signal intensity (%) over time (s). It is generated for each voxel or a selected region of interest (ROI) and is derived from multiple serial images that are obtained after contrast agent injection. TIC comprises an initial phase (wash-in), representing the initial rate of contrast enhancement (slow, medium, or fast), and a delayed phase, during which signal intensity (SI) may continue to rise (type 1 – persistent), reach a steady level (type 2 – plateau), or decrease (type 3 – washout).[23] PEI is defined as the integral of the area under the TIC and above the baseline and reflects the concentration of contrast agent within the selected ROI at a given time point.[22,25,26] TTP is the time (s) required for SI to reach its peak value after contrast agent injection; therefore, more avid contrast uptake is associated with shorter TTP values.[18] For both parameters, color maps can be automatically generated for each slice of a breast DCE-MRI examination, providing a clear overview of areas with suspicious enhancement.

On DCE-MRI, DCIS most commonly appears as areas of clumped non-mass enhancement (NME), usually with a linear or segmental distribution, similar to microcalcifications on mammography.[27] Less common presentations include focal or regional NME, foci, masses, or architectural distortion. The TIC of contrast enhancement in DCIS typically demonstrates fast wash-in during the initial phase; however, in the delayed phase, all three curve types may be observed, most commonly plateau, but also persistent and washout patterns.[4,28] Nevertheless, because DCIS lacks intrinsic vascularity and enhances predominantly by diffusion of gadolinium contrast agent, its enhancement pattern differs from that of IC, with slower wash-in and rare washout.[29] Consequently, DCIS is associated with longer TTP values and lower PEI values compared with IC.[22,30]

The aim of this study was to: (1) compare morphological features and semi-quantitative breast DCE-MRI parameters in patients with preoperatively biopsy-proven DCIS, stratified by final postoperative histopathology (without IC *vs*. with IC); (2) identify independent imaging predictors of IC and to develop a predictive model for detecting coexistent IC.

Patients and methods

Patients

This retrospective study included patients with DCIS diagnosed by percutaneous breast biopsy between January 2013 and December 2022 at the Institute for Oncology and Radiology of Serbia (Belgrade, Serbia). All patients provided written informed consent prior to the DCE-MRI examination. The study was approved by the institutional Ethics Committee (approval No. 3926-01).

The inclusion criteria were: (1) availability of a preoperative standard full-protocol breast DCE-MRI demonstrating an enhancing lesion; (2) imaging-guided percutaneous biopsy performed either after DCE-MRI or at least 14 days before DCE-MRI; (3) biopsy performed using one of the following techniques: ultrasound-guided 14-gauge core-needle biopsy (CNB), stereotactic or digital breast tomosynthesis–guided 9-gauge vacuum-assisted biopsy (SVAB or DBT-VAB), or magnetic resonance–guided 9-gauge vacuum-assisted biopsy (MR-VAB); (4) a mean of five cores for CNB and twelve for vacuum-assisted biopsy techniques[14]; (5) subsequent surgical excision of the lesion; (6) availability of a final postoperative histopathological diagnosis; and (7) histopathological evaluation performed by specialized oncologic pathologists at the same institution.

The exclusion criteria were: (1) inability to tolerate the DCE-MRI examination; and (2) severe image artifacts that reduced the sensitivity and specificity of diagnostic interpretation.

According to these criteria, 90 consecutive patients with DCIS diagnosed by percutaneous breast biopsy were included. Based on the final postoperative histopathological diagnosis, patients were divided into two groups: those without IC and those with IC, the latter being defined as upgrade to IC. The group without IC comprised patients with pure DCIS on final histopathology as well as patients without residual DCIS or IC, as confirmed by the postoperative multidisciplinary board.

Standard full breast DCE-MRI protocol and postprocessing

All breast DCE-MRI examinations were performed using 1.5 T Siemens scanners (Siemens Medical Solutions, Erlangen, Germany): a Magnetom Avanto system until February 2018 and a Magnetom Avanto Fit system from April 2018 onward, both equipped with a dedicated bilateral breast coil. Premenopausal patients were scanned during the second week of their menstrual cycle to minimize false-positive findings. Images were acquired in the prone position using a 2-mm slice thickness according to the following protocol: axial turbo-spin-echo (TSE) T2-weighted (T2W) without fat suppression (FS) (echo time 70 ms, repetition time 5900 ms, flip angle 180°, field of view 340 × 340 mm, image matrix 384 × 319), turbo inversion recovery magnitude (TIRM, echo time 60 ms, repetition time 7690 ms, inversion time 150 ms, flip angle 150°, field of view 340 × 340 mm, image matrix 320 × 256), axial TSE T1-weighted (T1W) without FS (echo time 12 ms, repetition time 910 ms, flip angle 90°, field of view 340 × 340 mm, image matrix 320 × 234), and dynamic three-dimensional fast low-angle shot (3D FLASH) sequences without FS (echo time 4.8 ms, repetition time 9.1 ms, flip angle 25°, field of view 340 × 340 mm, image matrix 576 × 564), comprising one pre-contrast acquisition followed by five successive acquisitions every 1 min 23 s after intravenous contrast agent administration. The gadolinium-based contrast agents used were gadopentetate dimeglumine (Magnevist, Bayer Schering Pharma, Berlin, Germany) during the initial study period (until June 2014) and gadobutrol (Gadovist, Bayer Schering Pharma, Berlin, Germany) thereafter. This transition from a linear to a macrocyclic gadolinium-based contrast agent reflected evolving safety recommendations regarding gadolinium retention.[31] Contrast agents were administered as a bolus injection at a dose of 0.1 mmol/kg using an automatic injector (Mississippi, Ulrich Medical, Ulm, Germany) at a rate of 2 ml/s, followed by a 20 ml saline flush.

The indications for breast DCE-MRI were determined by the institutional preoperative multidisciplinary board in accordance with national guidelines for breast cancer diagnosis and treatment.[32]

Image analysis

Images were analyzed using Syngo or Syngo Via software (Siemens Medical Solutions, USA).

Postprocessing was performed to generate subtraction images, multiplanar reconstructions, TICs, and parametric colour maps, including wash-in, TTP, and PEI maps. Additionally, PEI values were normalized by calculating a lesion-to-normal parenchyma (L/NP) ratio, defined as the ratio of lesion PEI to the PEI measured at the corresponding location in the contralateral normal breast parenchyma. The normalization was applied to minimize inter-patient and inter-scan variability related to differences in MRI scanners and contrast agents.[22] All DCE-MRI examinations were independently reviewed by two radiologists with 8 years (V. U.) and 12 years (D. P. S.) of clinical experience in breast DCE-MRI, who were blinded to all patient-related information, including histopathological diagnosis. Discrepancies were resolved by consensus, and the final consensus assessment was used for statistical analysis.

The following DCE-MRI data were evaluated: morphological features (lesion type – mass, NME or both; lesion size; multifocality/multicentricity; and T2W and TIRM signal characteristics) and semi-quantitative parameters, including TIC characteristics (wash-in, peak enhancement, and delayed phase), TTP, PEI, and the PEI L/NP ratio. For wash-in analysis, enhancement thresholds were defined as ≥ 50% for medium enhancement and ≥ 100% for fast enhancement.[23] A freehand ROI (14.37 ± 9.68 mm^2) was placed over the fastest enhancing part of the lesion, as assessed on the wash-in map – a parametric color map reflecting enhancement behavior across the dynamic post-contrast acquisition, with higher signal intensity corresponding to faster wash-in – and was then copied onto the PEI and TTP maps to calculate the corresponding values. For the purpose of semi-quantitative analysis, in cases of lesion multiplicity, the dominant lesion was defined as the lesion with the highest signal intensity on the wash-in map, corresponding to the fastest wash-in. In cases of discrepancies in ROI placement and/or dominant lesion selection, consensus was used to determine the final ROI and/or dominant lesion for statistical analysis.

Statistical analysis

Statistical analysis was performed using IBM SPSS Statistics version 21 (IBM Corp., Armonk, NY, USA) and R software version 4.5.0 (R Foundation for Statistical Computing, Vienna, Austria). Normally distributed variables were expressed as mean ± standard deviation, whereas non-normally distributed variables were presented as median and interquartile range (IQR). Categorical variables were described using frequencies and percentages. Depending on variable type, between-group differences were assessed using appropriate parametric (Student's t-test) or non-parametric tests (χ^2, Fisher's exact test, or Mann-Whitney U test). The least absolute shrinkage and selection operator (LASSO) algorithm was used for variable selection prior to multivariate logistic regression analysis. Model fit was evaluated using the likelihood ratio test, Hosmer-Lemeshow goodness-of-fit test, and Nagelkerke's pseudo-R^2. Diagnostic performance was assessed using receiver operating characteristic (ROC) analysis and area under the curve (AUC). The optimal cut-off value was determined using the Youden index, and sensitivity and specificity were calculated accordingly. P-values < 0.05 were considered statistically significant.

Results

Based on final postoperative histopathology, among patients without IC, pure DCIS was confirmed in 49 of 90 patients (54.4%), while no residual DCIS was identified in 6 patients (6.7%). IC was found in 35 of 90 patients (38.9%), including 7 cases (7.8%) of microinvasive carcinoma. Regarding histological types, intracystic papillary carcinoma was present in 2 cases (2.2%), while tubular, tubulo-lobular, mucinous, mixed ductal and mucinous, lobular and metaplastic carcinoma were each identified in 1 case (1.1%). The remaining invasive carcinomas were of no special type (NST). These 35 patients (38.9%) therefore represented an upgrade from the initial percutaneous biopsy diagnosis of DCIS.

Patient characteristics, as well as morphological and semi-quantitative breast DCE-MRI findings for these two groups and their corresponding statistical comparisons, are presented in Table 1 and Figures 1 and 2.

Compared with patients without IC, patients with IC showed a significantly higher prevalence of the following morphological DCE-MRI features: NME combined with a mass ($p < 0.001$), larger lesion size ($p = 0.015$), multifocal or multicentric disease ($p < 0.001$), T2W hyperintensity ($p = 0.023$), and TIRM hyperintensity ($p = 0.003$).

Regarding semi-quantitative parameters, patients with IC more frequently exhibited plateau and washout TIC patterns ($p < 0.001$), fast wash-in

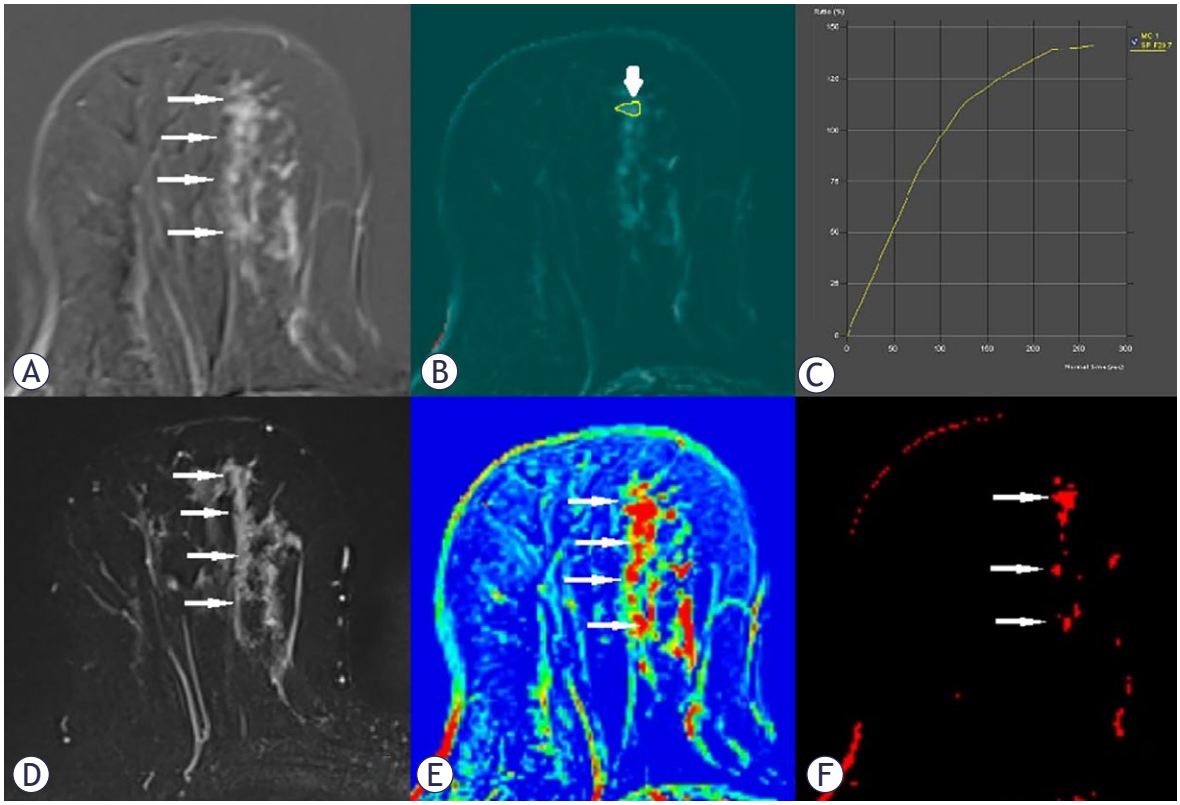

FIGURE 1. A 69-year-old woman with biopsy-proven ductal carcinoma *in situ* (DCIS) presenting as segmental clumped non-mass enhancement (NME) on breast dynamic contrast-enhanced magnetic resonance imaging (DCE-MRI) (thin arrows). The upper row shows the dynamic contrast-enhanced study: subtracted postcontrast image demonstrating the extent and distribution of NME **(A)**, wash-in parametric map **(B)**, and time-intensity curve (TIC) analysis **(C)**. On the wash-in map, the freehand region of interest (ROI) was placed over the fastest enhancing part of the lesion, corresponding to the area with the highest signal intensity (thick arrow). TIC analysis demonstrated medium initial enhancement and a persistent delayed phase, corresponding to type 1 kinetics. The lower row shows the corresponding turbo inversion recovery magnitude (TIRM) image with no hyperintense areas **(D)**, positive enhancement integral (PEI) map **(E)**, and time to peak (TTP) map **(F)**, illustrating the semi-quantitative parameters used for lesion assessment. Final postoperative histopathology confirmed pure DCIS without invasive carcinoma (IC).

($p < 0.001$), higher peak enhancement ($p = 0.023$), higher PEI values ($p = 0.009$), and shorter TTP ($p = 0.003$).

No significant differences between the two groups were observed with respect to age ($p = 0.141$), biopsy type ($p = 0.256$), or the PEI L/NP ratio ($p = 0.493$).

After application of the LASSO variable selection algorithm to all tested variables, four predictors were selected for inclusion in multivariate logistic regression analysis: lesion type (NME, mass, or NME combined with a mass), multifocality/multicentricity, delayed-phase TIC characteristics, and TIRM characteristics. These variables were entered into the multivariate logistic regression model, which identified NME combined with a mass, delayed-phase TIC characteristics, and TIRM hyperintensity as independent predictors of IC (Table 2).

The overall model was statistically significant ($p < 0.001$), with no evidence of relevant multicollinearity among predictors. Nagelkerke's R^2 indicated that approximately 50.5% of the variance in invasive disease status was explained by the model.

ROC analysis yielded an AUC of 0.872 (Figure 3). The optimal probability cut-off was 0.31, corresponding to a sensitivity of 88.6% and specificity of 72.7%.

Discussion

The results of our study suggest that morphological and dynamic features described in the

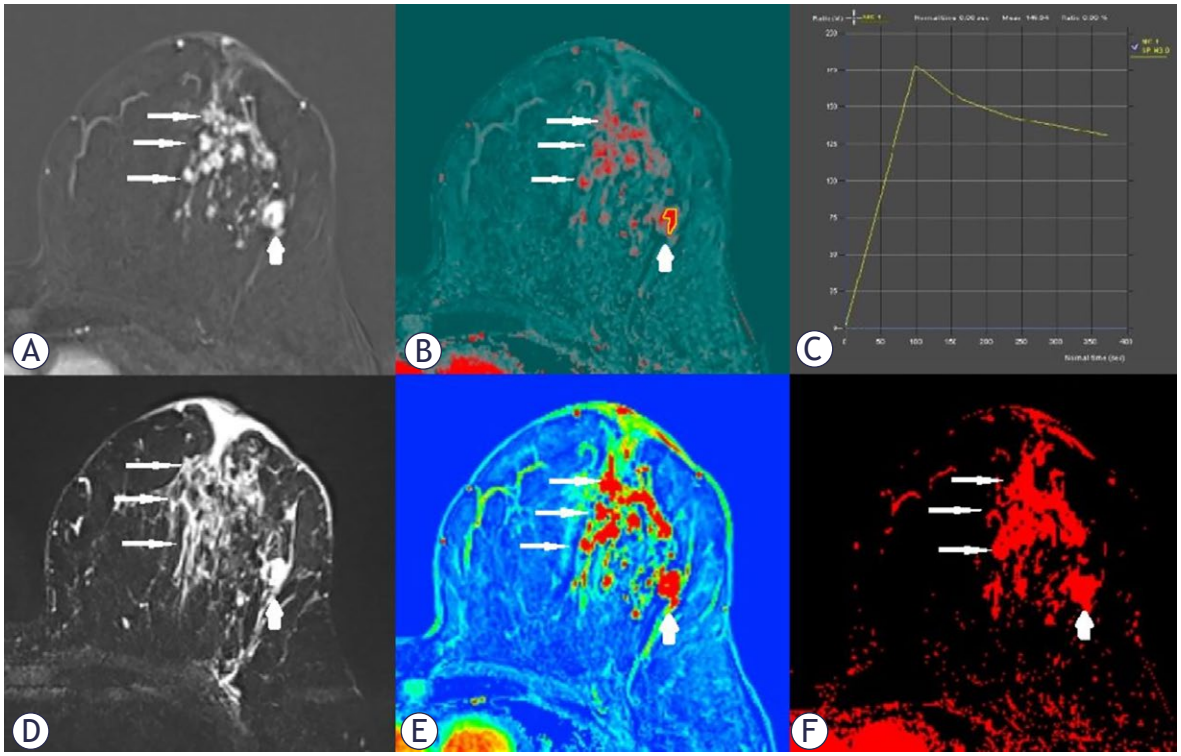

FIGURE 2. A 56-year-old woman with biopsy-proven ductal carcinoma *in situ* (DCIS) presenting as segmental non-mass enhancement (NME) (thin arrows) with an associated irregular mass in the inner quadrants (thick arrow) on breast dynamic contrast-enhanced magnetic resonance imaging (DCE-MRI). The upper row shows the dynamic contrast-enhanced study: subtracted postcontrast image demonstrating the extent of NME and the associated irregular mass **(A)**, wash-in parametric map **(B)**, and time-intensity curve (TIC) analysis **(C)**. On the wash-in map, the freehand region of interest (ROI) was placed over the irregular mass, which represented the fastest enhancing part of the lesion and corresponded to the area with the highest signal intensity (thick arrow). TIC analysis demonstrated fast initial enhancement and washout delayed-phase kinetics, corresponding to type 3 kinetics. The lower row shows the corresponding turbo inversion recovery magnitude (TIRM) image, where the lesion appears conspicuously hyperintense **(D)**, positive enhancement integral (PEI) map **(E)**, and time to peak (TTP) map **(F)**, illustrating the semi-quantitative parameters used for lesion assessment. Final postoperative histopathology revealed DCIS with an associated invasive carcinoma (IC).

BI-RADS atlas, as well as additional semi-quantitative parameters derived from breast DCE-MRI, may contribute to the preoperative prediction of upgrade to IC in patients with biopsy-proven DCIS. The comparison between patients with and without IC was based on postoperative histopathology as the reference standard for defining upgrade, reflecting the clinical aim of identifying patients at increased risk of upgrade before surgery. These findings are discussed in relation to previous studies addressing the same clinical question.

In our study, 38.9% of patients with biopsy-proven DCIS were upgraded to IC after surgery, which falls within the range reported in previous studies. Postoperative upgrade rates of 25–43% have been described, including 25% reported by Wisner *et al*., 40.7% by Takada *et al*., 36.4% underestimation of invasive disease on ultrasound-guided CNB reported by Park M *et al*., 38% by Miceli *et al*., and 33% by Dillon *et al*., who additionally reported microinvasive carcinoma in 14%, and suspected microinvasion in 7.5% of cases.[5,10-13] Yoon *et al*. reported pure DCIS in 54.4% of patients, microinvasive carcinoma in 24.3%, and IC in 21.4%, while Lee CW *et al*. reported IC in 43% of patients and noted a broad upgrade range of 3.5–56% in the literature.[14,15]

In our cohort, 6 patients (6.7%) had no residual DCIS on final histopathology, reflecting complete removal of the lesion at biopsy, as confirmed by the multidisciplinary board. Similar findings have been reported previously, with Wisner *et al*. observing no residual DCIS or invasion in 8% of patients and Lee KH *et al*. reporting this outcome in 2% of cases.[5,16]

TABLE 1. Comparison of findings between patients with and without invasive carcinoma

	Without IC (n = 55)	With IC (n = 35)	p-value
Age	55.29 ± 11.13	51.91 ± 9.42	0.141
Type of biopsy CNB SVAB/DBT-VAB MR-VAB	 19 (34.5%) 34 (61.8%) 2 (3.6%)	 17 (48.6%) 18 (51.4%) 0	0.256
DCE-MRI lesion type NME Mass NME + mass	 45 (81.8%) 6 (10.9%) 4 (7.3%)	 14 (40%) 6 (17.1%) 15 (42.9%)	< 0.001*
Lesion size (mm)	25 (52)	48 (46)	0.015*
Multifocality/multicentricity No Yes	 37 (67.3%) 18 (32.7%)	 10 (28.6%) 25 (71.4%)	< 0.001*
Wash-in Slow Medium Fast	 13 (23.6%) 18 (32.7%) 24 (43.6%)	 3 (8.6%) 2 (5.7%) 30 (85.7%	< 0.001*
Peak enhancement (%)	253.49 ± 168.06	343.14 ± 195.26	0,023*
Delayed phase Persistent Plateau Washout	 34 (61.8%) 14 (25.5%) 7 (12.7%)	 5 (14.3%) 16 (45.7%) 14 (40%)	< 0.001*
T2W TSE Hypointense Isointense Hyperintense	 19 (34.5%) 32 (58.2%) 4 (7.3%)	 8 (22.9%) 17 (48.6%) 10 (28.6%)	0.023*
TIRM Hypointense Isointense Hyperintense	 14 (25.5%) 23 (41.8%) 18 (32.7%)	 6 (17.1%) 5 (14.3%) 24 (68.6%)	0.003*
PEI	988 (733)	1391 (1307)	0.009*
PEI L/NP	10.83 (7.61)	11 (11.92)	0.493
TTP	470 (343)	359 (182)	0.003*

CNB = core-needle biopsy; DBT-VAB = digital breast tomosynthesis-guided vacuum-assisted biopsy; DCE-MRI = dynamic contrast-enhanced magnetic resonance imaging; IC = invasive carcinoma; L/NP = lesion-to-normal parenchyma; MR-VAB = magnetic resonance-guided vacuum-assisted biopsy; NME = non-mass enhancement; PEI = positive enhancement integral; SVAB = stereotactic vacuum-assisted biopsy; T2W TSE = T2-weighted turbo-spin-echo; TIRM = turbo inversion recovery magnitude; TTP = time to peak.

Normally distributed numeric variables are presented as mean ± standard deviation, non-normally distributed variables as median (interquartile range), and categorical variables as frequencies (percentages). Statistically significant differences are marked with an asterisk (*).

TABLE 2. Multivariate regression analysis with independent predictors of invasive carcinoma

Variable	OR	95% CI	p-value
NME + mass	4.494	1.078–18.742	0.039*
Multifocality/multicentricity	2.407	0.716–8.096	0.156
Delayed phase	3.915	1.665–9.205	0.002*
TIRM-hyperintensity	6.754	1.448–31.506	0.015*

CI = confidence interval; NME = non-mass enhancement; OR = odds ratio; TIRM = turbo inversion recovery magnitude.

Statistically significant independent predictors are marked with an asterisk (*).

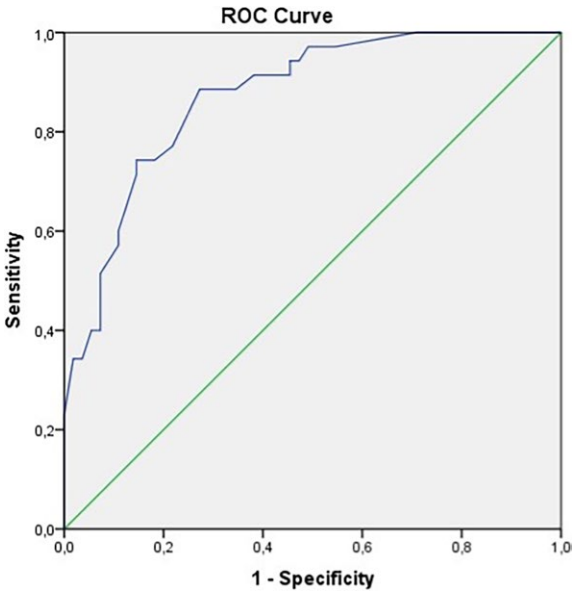

FIGURE 3. Receiver operating characteristic (ROC) curve for the multivariate regression model (area under the curve [AUC] = 0.872).

The upgrade rate was higher among patients who underwent ultrasound-guided CNB (47.2%) compared with those who underwent vacuum-assisted biopsy (33.3%), although this difference did not reach statistical significance (p = 0.185). In contrast, other studies have demonstrated statistically significant differences. Takada *et al*. reported a significantly higher postoperative upgrade rate in CNB compared with VAB, with biopsy method identified as an independent predictor of invasion on multivariate analysis.[10] Dillon *et al*. similarly reported a higher upgrade rate after ultrasound-guided CNB than after stereotactic techniques, with a statistically significant difference, while Brennan *et al*., in a meta-analysis, found higher underestimation rates with 14-gauge automated biopsy devices than with 11-gauge VAB.[13,17] This may be partly explained by differences in lesion presentation and sampling volume. Ultrasound-guided CNB is more often performed for larger lesions or palpable masses, which are more likely to be associated with IC, whereas SVAB/DBT-VAB and MR-VAB are frequently performed for microcalcifications or NME, which are more commonly associated with pure DCIS. In addition, the smaller tissue volume obtained with CNB may increase the risk of sampling error and missing an invasive component.[17]

In our study, patients with IC (mean age 51.91 ± 9.42) were younger than patients without IC (mean

age 55.29 ± 11.13), but the difference was not statistically significant (p = 0.141). Similar findings of younger age in patients with IC than in patients without IC, but without a statistically significant difference, were reported by Ko *et al*. and Park M *et al*.[11,18]

In contrast, lesion size was significantly larger in patients with IC (median 48 mm *vs*. 25 mm, p = 0.015). This is consistent with several previous studies and may be explained by the greater likelihood of unsampled invasive foci within larger areas of DCIS.[13,18,19] Dillon *et al*. reported that lesions ≥ 5 cm on postoperative histopathology were more likely to harbor invasive disease.[13] Ko *et al*. found that the longest tumor diameter was significantly larger in IC than in pure DCIS and identified DCIS size as an independent predictor of IC on multivariate analysis.[18] Takada *et al*. reported a significantly higher probability of IC when tumor diameter exceeded 20 mm, Goto *et al*. observed larger lesions in patients with IC, while Park AY *et al*. found a significantly higher upgrade rate in lesions ≥ 30 mm.[10,19,20] In contrast, Lee CW *et al*. found no significant difference in lesion size measured by DCE-MRI, although tumor volume was significantly greater in patients with IC, while Park M *et al*. reported larger lesions in patients without underestimation, without statistical significance.[11,15]

Multifocal and multicentric lesions were significantly more frequent in patients with IC than in those without IC (71.4% *vs*. 32.7%, p < 0.001); however, this parameter was not an independent predictor in the multivariate regression model (OR = 2.407, 95% CI = 0.716–8.096, p = 0.156). In contrast, Lee CW *et al*. found no significant difference in the frequency of multifocal/multicentric disease between IC and pure DCIS.[15]

In our study, lesion type on DCE-MRI differed significantly between patients with and without IC (p < 0.001), and the combined presence of a mass and NME emerged as an independent predictor of IC on multivariate analysis (OR = 4.494, 95% CI = 1.078–18.742, p = 0.039). Wisner *et al*. showed that the presence of a mass was strongly associated with invasion for both independent readers, whereas NME was negatively associated with invasion for only one reader.[5] Lee CW *et al*. also found a significantly higher rate of mass-like lesions in patients with IC than in those with pure DCIS.[15] In contrast, Yoon *et al*. reported that both masses and NME were independent predictors of histological upgrade, with NME being the stronger predictor, while Goto *et al*. found no statistically significant difference in lesion type between DCIS and IC.[14,20]

In our study, both T2W and TIRM hyperintensity were more prevalent in patients with IC, reaching statistical significance (p = 0.023 and p = 0.003, respectively). TIRM hyperintensity was also identified as an independent predictor on multivariate analysis (OR = 6.754, 95% CI = 1.448–31.506, p = 0.015). A possible explanation is that invasive lesions tend to have higher tissue water content due to necrosis, edema, and/or inflammatory changes, and TIRM is more sensitive to increased water content than conventional T2W TSE imaging. Data from previous studies are conflicting. Goto *et al*. reported that high signal intensity (SI) on fat-suppressed T2W TSE (similar to TIRM) was significantly more common in patients with IC.[20] In contrast, Park AY *et al*. reported that lower signal intensity on fat-saturated T2W imaging was associated with a significantly higher underestimation rate.[19] Wisner *et al*. and Lee CW *et al*. found no significant correlation between T2W signal characteristics and invasion.[5,15]

To the best of our knowledge, TIRM hyperintensity has not previously been specifically evaluated as an independent predictor of upgrade to IC in patients with biopsy-proven DCIS. Although conventional DCE-MRI descriptors, including lesion morphology and enhancement kinetics, have been associated with invasive disease or upgrade in previous studies, TIRM provides information derived from a non-contrast, fluid-sensitive sequence and may therefore reflect tissue characteristics not fully captured by dynamic enhancement analysis. In the present study, TIRM hyperintensity remained an independent predictor in the multivariate regression model together with lesion type and delayed-phase TIC characteristics, suggesting that it may provide complementary information beyond established morphological and kinetic DCE-MRI descriptors. This finding may be clinically relevant because TIRM is routinely available as part of standard breast DCE-MRI protocols, requires no additional contrast administration or advanced postprocessing, and may contribute to preoperative risk stratification in patients with biopsy-proven DCIS. However, given the limited sample size and retrospective design of our study, this observation should be regarded as hypothesis-generating and requires validation in larger prospective cohorts.

Three aspects of TIC were analyzed in our study: wash-in, peak enhancement, and delayed phase kinetics. Fast wash-in, higher peak en-

hancement, and plateau or washout delayed-phase patterns were more frequent in patients with IC ($p < 0.001$, $p = 0.023$, and $p < 0.001$, respectively), whereas persistent enhancement was more common in patients without IC. Delayed-phase TIC characteristics were additionally identified as an independent predictor of IC on multivariate regression analysis (OR = 3.915, 95% CI = 1.665–9.205, $p = 0.002$). These findings are largely consistent with previous studies. Wisner *et al*. reported that fast wash-in and washout delayed-phase kinetics were positively associated with invasion, while persistent delayed enhancement showed a negative association; however, all three parameters reached statistical significance for only one of the two independent readers.[5] Ko *et al*. found that a higher signal enhancement ratio (SER), reflecting faster wash-in and washout, was an independent predictor of IC with a cut-off value > 0.7, together with larger DCIS size.[18] Deurloo *et al*. demonstrated that the absence of enhancement or a persistent TIC were the strongest predictors for excluding invasive disease on multivariate analysis.[21] In contrast, Park M *et al*. and Lee CW *et al*. did not find statistically significant differences in peak or initial enhancement, although some trends toward stronger enhancement in upgraded lesions were observed.[11,15]

To date, PEI and the L/NP ratio for PEI have not been extensively evaluated as predictors of upgrade from biopsy-proven DCIS to IC. In our study, PEI values were significantly higher in patients with IC (median 1391 *vs*. 988; $p = 0.009$), whereas the L/NP ratio for PEI did not differ significantly between groups ($p = 0.493$). Nadrljanski *et al*. reported higher PEI values in invasive ductal carcinoma than in DCIS, as well as significant differences between lesions and contralateral normal breast parenchyma.[22] However, their study was based on diagnoses obtained after biopsy rather than final postsurgical histopathology, which may partly explain differences between studies.

In our cohort, TTP values were significantly lower in patients with IC, reflecting faster enhancement (median 359 *vs*. 470; $p = 0.003$). Ko *et al*. evaluated TTP among other DCE-MRI parameters and observed shorter TTP values in patients with IC, although the difference was not statistically significant.[18]

It is worth noting that our study focused on semi-quantitative parameters that are part of widely available software packages and easily applicable in routine clinical practice. In contrast, there is growing interest in fully quantitative parameters, which require more demanding technical implementation and are currently used primarily in research settings.[33,34]

As discussed above, from a clinical standpoint, the ability to identify patients at higher risk of upgrade prior to surgery remains highly relevant, regardless of whether the invasive component was not sampled at biopsy or whether the imaging findings overlap with general imaging characteristics of invasive carcinoma. In this context, the identified DCE-MRI features may provide useful information for preoperative risk stratification and surgical planning. Literature data on the predictive value of individual DCE-MRI morphological features and semi-quantitative parameters for detecting IC in biopsy-proven DCIS are highly variable, and no single parameter allows sufficiently accurate prediction. However, when combined in a multivariate regression model, their predictive performance may improve. In our study, we developed a statistically significant model ($p < 0.001$) with a strong overall fit (Nagelkerke's $R^2 = 50.5\%$) and an AUC of 0.872, indicating excellent discrimination between cases with and without IC. In this model, the presence of both NME and a mass, delayed-phase TIC characteristics, and TIRM hyperintensity emerged as independent predictors of upgrade to IC.

This study had several limitations. First, the sample size was relatively small, which limits the robustness and generalizability of the findings, particularly in the context of multivariable prediction modeling. Second, the study was retrospective, and potential selection bias cannot be excluded. Third, although all DCE-MRI examinations were independently reviewed by two radiologists and final assessments were established by consensus, interobserver variability was not formally analyzed. Fourth, clinical, mammographic, ultrasound, and detailed histopathological data were not analyzed, as the focus of this study was on multiparametric breast DCE-MRI with additional semi-quantitative parameters.

In conclusion, DCE-MRI-based prediction models incorporating morphological features and semi-quantitative parameters may help stratify patients according to the risk of upgrade at surgery. In our cohort, the combined presence of NME and a mass, delayed-phase TIC characteristics, and TIRM hyperintensity were independent predictors of upgrade to IC. Notably, TIRM hyperintensity has not, to the best of our knowledge, been specifically evaluated as an independent predictor of upgrade to IC in this context. Although PEI and

TTP differed significantly between patients with and without IC, their independent predictive value was limited. Given the paucity of existing literature data on these parameters, further prospective cohort studies are warranted to validate their role in breast DCE-MRI assessment and to evaluate whether incorporation of multimodal clinical, mammographic, ultrasound, and histopathological parameters could further improve preoperative prediction of upgrade.

AI disclosure

During the preparation of this manuscript, the authors used ChatGPT (OpenAI, USA) for improving readability and language clarity. After using this tool/service, the authors reviewed and edited the content as necessary and take full responsibility for the content of the manuscript.

References

1. Tomlinson-Hansen SE, Khan M, Cassaro S. Breast ductal carcinoma in situ. In: *StatPearls* [Internet]. Treasure Island, FL: StatPearls Publishing; 2025. PMID: 33620843
2. Jatoi I, Shaaban AM, Jou E, Benson JR. The biology and management of ductal carcinoma in situ of the breast. *Curr Probl Surg* 2023; **60:** 101361. doi: 10.1016/j.cpsurg.2023.101361
3. Barreau B, de Mascarel I, Feuga C, MacGrogan G, Dilhuydy MH, Picot V, et al. Mammography of ductal carcinoma in situ of the breast: review of 909 cases with radiographic-pathologic correlations. *Eur J Radiol* 2005; **54:** 55-61. doi: 10.1016/j.ejrad.2004.11.019
4. Raza S, Vallejo M, Chikarmane SA, Birdwell RL. Pure ductal carcinoma in situ: a range of MRI features. *AJR Am J Roentgenol* 2008; **191:** 689-99. doi: 10.2214/AJR.07.3779
5. Wisner DJ, Hwang ES, Chang CB, Tso HH, Joe BN, Lessing JN, et al. Features of occult invasion in biopsy-proven DCIS at breast MRI. *Breast J* 2013; **19:** 650-8. doi: 10.1111/tbj.12201
6. Menell JH, Morris EA, Dershaw DD, Abramson AF, Brogi E, Liberman L. Determination of the presence and extent of pure ductal carcinoma in situ by mammography and magnetic resonance imaging. *Breast J* 2005; **11:** 382-90. doi: 10.1111/j.1075-122X.2005.00121.x
7. Kuhl CK, Schrading S, Bieling HB, Wardelmann E, Leutner CC, Koenig R, et al. MRI for diagnosis of pure ductal carcinoma in situ: a prospective observational study. *Lancet* 2007; **370:** 485-92. doi: 10.1016/S0140-6736(07)61232-X
8. Bluemke DA, Gatsonis CA, Chen MH, DeAngelis GA, DeBruhl N, Harms S, et al. Magnetic resonance imaging of the breast prior to biopsy. *JAMA* 2004; **292:** 2735-42. doi: 10.1001/jama.292.22.2735
9. Berg WA, Gutierrez L, NessAiver MS, Carter WB, Bhargavan M, Lewis RS, et al. Diagnostic accuracy of mammography, clinical examination, US, and MR imaging in preoperative assessment of breast cancer. *Radiology* 2004; **233:** 830-49. doi: 10.1148/radiol.2333031484
10. Takada K, Kashiwagi S, Asano Y, Goto W, Morisaki T, Takahashi K, et al. Factors predictive of invasive ductal carcinoma in cases preoperatively diagnosed as ductal carcinoma in situ. *BMC Cancer* 2020; **20:** 513. doi: 10.1186/s12885-020-07001-1
11. Park M, Kim EK, Kim MJ, Moon HJ. Preoperative prediction of ductal carcinoma in situ underestimation of the breast using dynamic contrast enhanced and diffusion-weighted imaging. *J Korean Soc Magn Reson Med* 2013; **17:** 101-9. doi: 10.13104/jksmrm.2013.17.2.101
12. Miceli R, Gao Y, Qian K, Heller SL. Predicting upgrade of ductal carcinoma in situ to invasive breast cancer at surgery with ultrafast imaging. *AJR Am J Roentgenol* 2023; **221:** 34-43. doi: 10.2214/AJR.22.28698
13. Dillon MF, McDermott EW, Quinn CM, O'Doherty A, O'Higgins N, Hill AD. Predictors of invasive disease in breast cancer when core biopsy demonstrates DCIS only. *J Surg Oncol* 2006; **93:** 559-63. doi: 10.1002/jso.20445
14. Yoon GY, Choi WJ, Cha JH, Shin HJ, Chae EY, Kim HH. The role of MRI and clinicopathologic features in predicting the invasive component of biopsy-confirmed ductal carcinoma in situ. *BMC Med Imaging* 2020; **20:** 95. doi: 10.1186/s12880-020-00494-z
15. Lee CW, Wu HK, Lai HW, Wu WP, Chen ST, Chen DR, et al. Preoperative clinicopathologic factors and breast magnetic resonance imaging features can predict ductal carcinoma in situ with invasive components. *Eur J Radiol* 2016; **85:** 780-9. doi: 10.1016/j.ejrad.2015.12.027
16. Lee KH, Han JW, Kim EY, Yun JS, Park YL, Park CH. Predictive factors for the presence of invasive components in patients diagnosed with ductal carcinoma in situ based on preoperative biopsy. *BMC Cancer* 2019; **19:** 1201. doi: 10.1186/s12885-019-6417-3
17. Brennan ME, Turner RM, Ciatto S, Marinovich ML, French JR, Macaskill P, et al. Ductal carcinoma in situ at core-needle biopsy: meta-analysis of underestimation and predictors of invasive breast cancer. *Radiology* 2011; **260:** 119-28. doi: 10.1148/radiol.11102368
18. Ko MS, Kim SH, Kang BJ, Choi BG, Song BJ, Cha ES, et al. A method to quantify breast MRI for predicting tumor invasion in patients with preoperative biopsy-proven ductal carcinoma in situ (DCIS). *J Korean Soc Magn Reson Med* 2013; **17:** 73-82. doi: 10.13104/jksmrm.2013.17.2.73
19. Park AY, Gweon HM, Son EJ, Yoo M, Kim JA, Youk JH. Ductal carcinoma in situ diagnosed at US-guided 14-gauge core-needle biopsy for breast mass: preoperative predictors of invasive breast cancer. *Eur J Radiol* 2014; **83:** 654-9. doi: 10.1016/j.ejrad.2014.01.010
20. Goto M, Yuen S, Akazawa K, Nishida K, Konishi E, Kajihara M, et al. The role of breast MR imaging in pre-operative determination of invasive disease for ductal carcinoma in situ diagnosed by needle biopsy. *Eur Radiol* 2012; **22:** 1255-64. doi: 10.1007/s00330-011-2357-2
21. Deurloo EE, Sriram JD, Teertstra HJ, Loo CE, Wesseling J, Rutgers EJ, et al. MRI of the breast in patients with DCIS to exclude the presence of invasive disease. *Eur Radiol* 2012; **22:** 1504-11. doi: 10.1007/s00330-012-2394-5
22. Nadrljanski M, Maksimovic R, Plesinac-Karapandzic V, Nikitovic M, Markovic-Vasiljkovic B, Milosevic Z. Positive enhancement integral values in dynamic contrast enhanced magnetic resonance imaging of breast carcinoma: ductal carcinoma in situ vs. invasive ductal carcinoma. *Eur J Radiol* 2014; **83:** 1363-7. doi: 10.1016/j.ejrad.2014.05.006
23. D'Orsi CJ, Sickles EA, Mendelson EB, Morris EA, Creech WE, Butler PF, et al. *ACR BI-RADS® Atlas, Breast Imaging Reporting and Data System.* 5th ed. Reston, VA: American College of Radiology; 2013
24. Verma S, Turkbey B, Muradyan N, Rajesh A, Cornud F, Haider MA, et al. Overview of dynamic contrast-enhanced MRI in prostate cancer diagnosis and management. *AJR Am J Roentgenol* 2012; **198:** 1277-88. doi: 10.2214/AJR.12.8510
25. Khiat A, Gianfelice D, Amara M, Boulanger Y. Influence of post-treatment delay on the evaluation of the response to focused ultrasound surgery of breast cancer by dynamic contrast enhanced MRI. *Br J Radiol* 2006; **79:** 308-14. doi: 10.1259/bjr/23046051
26. Gelezhe PB, Blokhin IA, Marapov DI, Morozov SP. Quantitative parameters of MRI and ^{18}F-FDG PET/CT in the prediction of breast cancer prognosis and molecular type: an original study. *Am J Nucl Med Mol Imaging* 2020; **10:** 279-92. PMID: 33329930
27. Marcotte-Bloch C, Balu-Maestro C, Chamorey E, Ettore F, Raoust I, Flipo B, et al. MRI for the size assessment of pure ductal carcinoma in situ (DCIS): a prospective study of 33 patients. *Eur J Radiol* 2011; **77:** 462-7. doi: 10.1016/j.ejrad.2009.09.003
28. Greenwood HI, Heller SL, Kim S, Sigmund EE, Shaylor SD, Moy L. Ductal carcinoma in situ of the breasts: review of MR imaging features. *Radiographics* 2013; **33:** 1569-88. doi: 10.1148/rg.336125055

29. Kuhl CK. Why do purely intraductal cancers enhance on breast MR images? *Radiology* 2009; **253:** 281-3. doi: 10.1148/radiol.2532091401

30. Newstead GM. MR imaging of ductal carcinoma in situ. *Magn Reson Imaging Clin N Am* 2010; **18:** 225-40. doi: 10.1016/j.mric.2010.02.004

31. Kanda T, Ishii K, Kawaguchi H, Kitajima K, Takenaka D. High signal intensity in the dentate nucleus and globus pallidus on unenhanced T1-weighted MR images: relationship with increasing cumulative dose of a gadolinium-based contrast material. *Radiology* 2014; **270:** 834-41. doi: 10.1148/radiol.13131669

32. Milosevic Z, Bogdanovic D. Breast imaging and percutaneous interventional procedures. In: Dzodic R, editor. *Guidelines of Good Clinical Practice for the Diagnosis and Treatment of Breast Cancer* [Serbian]. Belgrade: Ministry of Health of the Republic of Serbia; 2013. Available at: http://www.azus.gov.rs. Accessed 25 Dec 2025

33. Moloney B, Li X, Hirano M, Saad Eddin A, Lim JY, Biswas D, et al. Initial experience in implementing quantitative DCE-MRI to predict breast cancer therapy response in a multi-center and multi-vendor platform setting. *Front Oncol* 2024; **14:** 1395502. doi: 10.3389/fonc.2024.1395502

34. Ochoa-Albiztegui RE, Sevilimedu V, Horvat JV, Thakur SB, Helbich TH, Trattnig S, et al. Pharmacokinetic analysis of dynamic contrast-enhanced magnetic resonance imaging at 7T for breast cancer diagnosis and characterization. *Cancers* 2020; **12:** 3763. doi: 10.3390/cancers12123763

research article

Is there a correlation between signal intensity ratio of 3T MRI and molecular subtypes of breast cancer?

Yuanping Tao[1], Hongyan Chao[1], Yue Ren[1], Wanjun Zheng[2], Yuyou Chen[2], Liang Du[1], Huanguo Li[1], Feng Cui[1]

[1] Department of Radiology, Hangzhou TCM Hospital Affiliated to Zhejiang Chinese Medical University, Hangzhou, China
[2] School of Economics, Center for Economic Behavior and Decision-making (CEBD), Zhejiang University of Finance and Economics, Hangzhou, China

Radiol Oncol 2026; 60(3): 367-377.

Received: 23 January 2026
Accepted: 11 April 2026

Correspondence to: Feng Cui, M.D., Department of Radiology, Hangzhou TCM Hospital Affiliated to Zhejiang Chinese Medical University, Hangzhou, China. E-mail address: feng6812@163.com.

Disclosure: No potential conflicts of interest were disclosed.

Background. The study aimed to test whether tumoral signal intensity ratio (SIR) and other indicators of 3T MRI provides information related to molecular subtypes of breast cancer.

Patients and methods. Between January 2022 and August 2025, 256 patients with breast cancer underwent 3T MRI. MRI morphological features and quantitative parameters (T1 SIR, T2 SIR, mean apparent diffusion coefficient [ADC] from diffusion-weighted imaging [DWI] and tumor diameter) were compared and measured according to molecular subtypes. Logistic regression was performed to find the related MRI parameters and establish combined parameters. A receiver operating characteristic (ROC) analysis was finally performed to test the diagnostic power of multivariate logistic regression model.

Results. 263 lesions were considered. Triple-negative (TN) subtype exhibited the highest T2 SIR and lowest T1 SIR ($p < 0.05$). Mean ADC values in TN were the lowest and highest in human epidermal growth factor receptor 2 (HER2)-enriched type ($p < 0.001$). Tumor diameter of HER2-enriched was the smallest, and that of triple-negative subtype was the largest ($p < 0.001$). Independent influencing factors were higher T2 SIR ($p = 0.017$) and larger tumor diameter ($p = 0.011$) associated with triple-negative subtype, and T1 SIR ($p = < 0.01$) was the only quantitative parameter associated with HER2-enriched subtype. The combined parameter (mean ADC + tumor diameter) achieved a largest area under the ROC curve (AUC = 0.781) for separating luminal A subtype.

Conclusions. Quantitative MRI parameters are correlated with the molecular subtypes of breast cancer. Combined parameters incorporating T1 SIR and T2 SIR exhibit potential diagnostic utility for differentiating HER2-enriched and triple-negative subtypes, respectively. T1 SIR and T2 SIR can enrich quantitative descriptors from breast MRI.

Key words: breast cancer; signal intensity ratio; molecular subtype; MRI

Introduction

Magnetic resonance imaging (MRI) has very high sensitivity in detecting breast cancer, with detection rates ranging from 95% to 99%.[1] Breast MRI is also the most accurate imaging method for evaluating tumours size, multifocality and multicentricity.[2] The morphological and contrast-enhanced features, diffusion-weighted imaging (DWI) and T2 weight imaging (T2WI) in MRI are helpful for diagnosing lesions.[3] In addition to the complete diagnostic protocol, simplified rapid breast MRI also

has certain diagnostic accuracy and sensitivity in detecting breast cancer.[4,5] In recent years, MRI-based quantitative metrics, including dynamic contrast-enhanced MRI (DCE-MRI) and DWI, as well as derived parameters such as T1 and T2 relaxation time and proton density (PD) image, have shown great potential in the non-invasive diagnosis and evaluation of breast cancer.[6-10] The MRI signal intensity ratio (SIR) has been used as a quantitative measure in the other diseases.[11-14] However, there are still few studies on the SIR of breast cancer.[15] Therefore, we attempted to analyse the correlation between T1 SIR, T2 SIR, ADC values, lesion diameters combining with other morphological and enhanced scanning characteristics and the different molecular subtypes of breast cancer.

Patients and methods

Study participants

From January 2022 to August 2025, we consecutively collected 534 patients who underwent 3T breast MRI in the radiology department of one hospital. These patients were derived from routine breast cancer screening, those with breast lesions of uncertain nature, and individuals with previously confirmed breast cancer. All patients had no MRI contraindications, and breast lesions were classified as breast imaging reporting and data system (BI-RADS) category 4A or 5 on mammography or ultrasound. A total of 332 cases of breast cancer (from 325 patients, including 7 patients with bilateral breast cancer) were pathologically diagnosed with breast cancer. This study was approved by the institutional review boards of our centre (ethics committee approval number: 202310130922000244065), and the requirement for informed consent was waived. This study complied with the principles of the Declaration of Helsinki. The inclusion criteria were as follows: (1) breast cancer confirmed by pathological assessment of the resection specimen or biopsy; (2) molecular subtype validated by immunohistochemistry (IHC) and human epidermal growth factor receptor 2 (HER2) gene amplification status validated by fluorescence in-situ hybridization (FISH); (3) breast MRI examination completed less than 1 month prior to biopsy or resection. The exclusion criteria were as follows: (1) incomplete clinical and pathological data; (2) breast-related invasive procedure (such as biopsy less than 2 weeks interference of bleeding and inflammation on imaging features) and treatment (chemotherapy, radiotherapy, or hormone therapy) before MRI examination; (3) pregnant or lactation period and (4) poor image quality or small lesion (e.g., motive artifacts, smaller than 5mm lesion). Based on the exclusion criteria, 69 patients were excluded because of incomplete clinical and pathological data (n= 31), breast-related invasive procedure and treatment before MRI examination (n = 28), lactation period (n = 1), poor image quality (n = 6) and small lesions could not be measured (n = 3). A flowchart of study population is shown in Figure 1. Thus, 256 patients with a total of 263 lesions (7 patients with bilateral

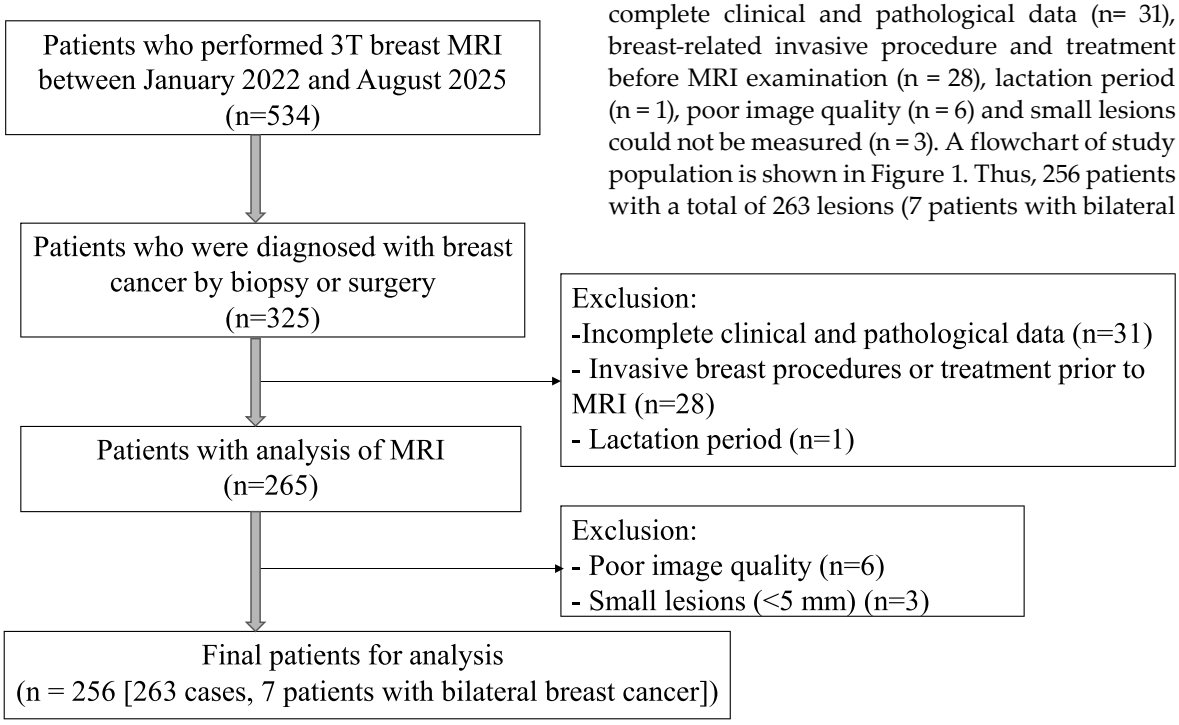

FIGURE 1. Inclusion and exclusion criteria and the data collection flowchart showing the study population.

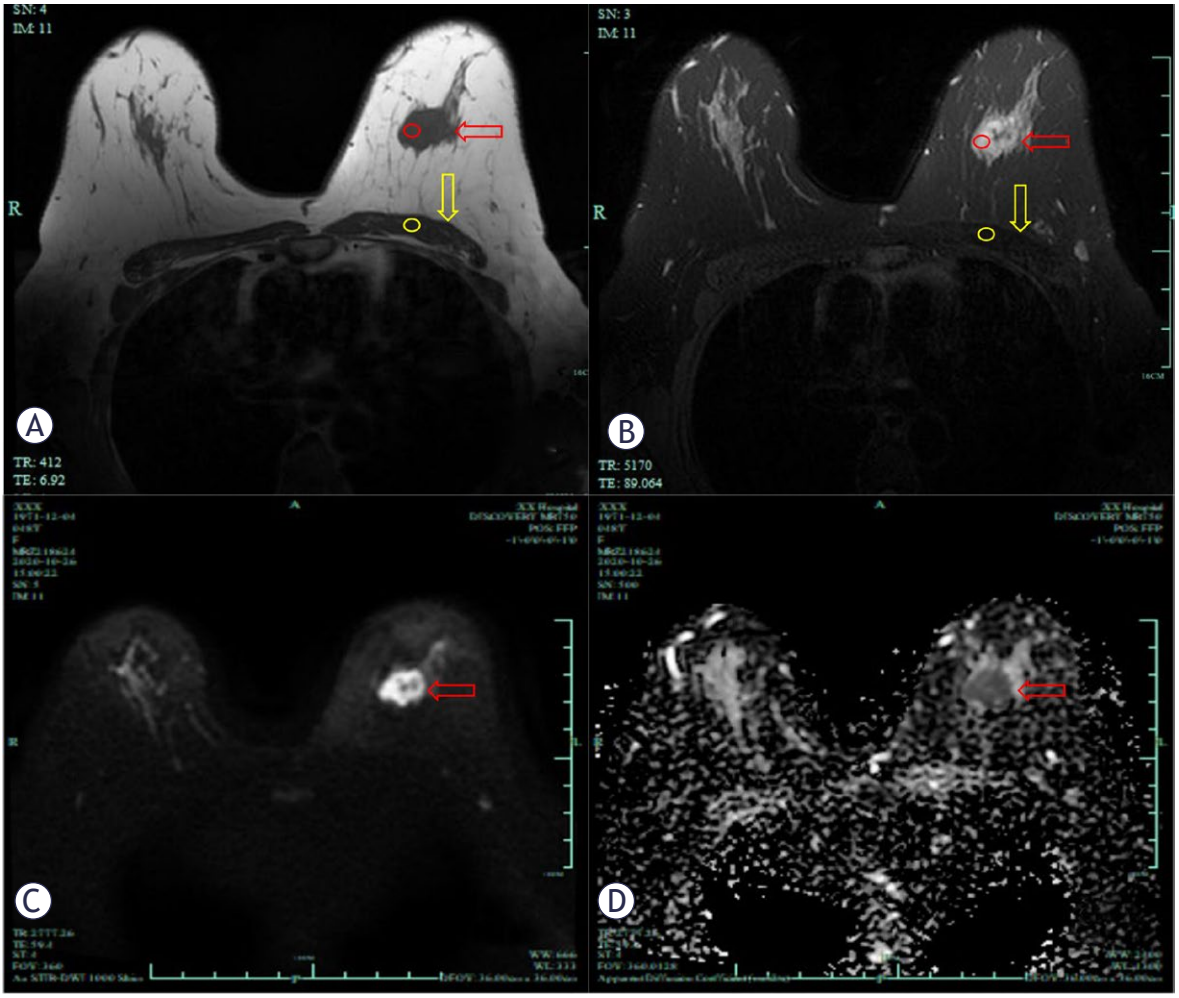

FIGURE 2. MR images of a 48 years-old patient diagnosed with luminal B subtype breast cancer. T1 weight image **(A)**, T2 fat-suppression sequence image **(B)**, DWI image **(C)** and ADC map **(D)** was shown. T1 and T2 signal intensity ratio **(A** and **B)** were calculated by proportioning the average signal intensity of the lesion (red circle) to the average signal intensity of the pectoral muscle (yellow circle). Red arrows show the lesions and yellow arrows show the pectoral muscles.

ADC = apparent diffusion coefficient; DWI = diffusion-weighted imaging

lesions) of breast cancer were ultimately enrolled in this study.

MRI protocol

3.0T MRI scanner (Discovery 750 3.0T, GE Healthcare, Milwaukee, USA) was used, with a dedicated eight-channel phased-array coil for the breast. The patient was placed in a prone position, with both arms raised, keeping the body basically parallel to the scanning bed. The two breasts were adjusted to hang naturally in the coil, with the head first. The following sequences were scanned in turn: axial T1 and T2 weighted fat-suppressed sequence, DWI, and axial T1WI dynamic enhanced scan. The scanning parameters of axial T1WI were: repetition time (TR) = 425 m s, echo time (TE) = 8.384 m s, slice thickness = 4 mm, field of view (FOV) = 320 mm × 320 mm; the scanning parameters of T2WI fat-suppressed sequence were: TR = 5762 m s, TE = 89.408 m s, slice thickness = 4 mm, FOV = 320 mm × 320 mm; the scanning parameters of DWI sequence were: TR = 2777.26 m s, TE = 60.6 m s, slice thickness = 4 mm, FOV = 320 mm × 320 mm; the scanning parameters of T1WI dynamic enhancement were: TR = 4.537 m s, TE = 1.798 m s, slice thickness = 1 mm, FOV = 320 mm × 320 mm. Plain scan was performed as a mask before injecting the contrast agent. After the plain scan, gadolinium contrast agent (Gd - DTPA, 0.1 mmol/kg, 2.0 mL/s) was injected through the elbow vein, followed by a rapid injection of 20ml of 0.9% so-

TABLE 1. Clinical characteristics of patients and MRI morphological features for different molecular subtypes

Parameters	Luminal A (n = 52)	Luminal B (n = 135)	HER2-enriched (n = 31)	TN (n = 45)	p
ALNM					**0.010**
Yes	9 (17.3)	58 (43.0)	12 (38.7)	14 (31.1)	
No	43 (82.7)	77 (57.0)	19 (61.3)	31 (68.9)	
History of hormone use					**0.038**
Yes	3 (5.8)	2 (1.5)	3 (9.7)	0 (0.0)	
No	49 (94.2)	133 (98.5)	28 (90.3)	45 (100.0)	
Tumor morphology					0.053
Mass	43 (82.7)	114 (84.4)	20 (64.5)	39 (86.7)	
Non-mass	9 (17.3)	21 (15.6)	11 (35.5)	6 (13.3)	
Margin					0.206
Circumscribed	21 (40.4)	39 (28.9)	13 (41.9)	19 (42.2)	
Not-circumscribed	31 (59.6)	96 (71.1)	18 (58.1)	26 (57.8)	
Dynamic curve curve					0.248
type I	8 (15.4)	13 (9.6)	4 (12.9)	7 (15.6)	
type II	9 (17.3)	30 (22.2)	12 (38.7)	8 (17.8)	
type III	35 (67.3)	92 (68.1)	15 (48.4)	30 (66.7)	

Categorical variables are numbers with percentages in parentheses. Bolded text indicates statistical significance ($p < 0.05$).

ALNM = axillary lymph node metastasis; HER2 = human epidermal growth factor receptor 2; TN = triple-negative

dium chloride. The enhanced scan started at the 23rd second, and parallel acquisition was used to continuously scan 8 times without interruption.

Imaging analysis

Two radiologists with 10 and 11 years of experience in diagnosing breast disease evaluated all lesions based on the BI-RADS diagnostic criteria respectively, who were blinded to histopathological results. If there was any disagreement, a consensus was finally reached through negotiation. The final quantitative parameters were the mean values of two readers. The diameter of the lesion was measured during the fourth phase of enhancement and non-mass-like lesions were excluded.

TABLE 2. Intraclass correlation coefficient (ICC) analysis between the two readers

Parameters	ICC (95%CI)
T1 SIR	0.970 (0.961–0.976)
T2 SIR	0.967 (0.957–0.974)
Mean ADC ($\times 10^{-3}$ mm^2/ s)	0.898 (0.871–0.919)
Tumor diameter (cm)	0.923 (0.900–0.940)

ADC = apparent diffusion coefficient; T1 SIR = T1 signal intensity ratio; T2 SIR = T2 signal intensity ratio

Quantitative parameters

For T1 and T2 signal intensity ratio (SIR) analysis, signal intensities were obtained from the lesion and the pectoral muscle, which was used as an internal reference. The SIR was calculated as the ratio of lesion-to-pectoral muscle signal intensity. Region of interests (ROIs) drawn in the lesion and pectoral muscle were of identical size. On T1 and T2 weighted axial image, ROI of the lesion was adjusted based on contrast enhancement in DCE-MRI, and non-enhancing, necrotic, and cystic areas were carefully disregarded to include only solid tumour components. ROI of the pectoral muscle was obtained at the thickest layer of the pectoralis major muscle, avoiding fatty tissue (Figure 2).

ADC values

ROI was drawn within the tumour lesion on the ADC map based on the DWI image with b-value of 800. The location of the ROI was adjusted accord-

TABLE 3. MRI quantitative parameters for molecular subtypes of breast cancer

Parameters	Luminal A (n = 52)	Luminal B (n = 135)	HER2-enriched (n = 31)	TNBC (n = 45)	p
T1 SIR	1.318 (1.179–1.630)	1.366 (1.209–1.620)	1.515 (1.268–1.788)	1.254 (1.141–1.401)	**0.026**
T2 SIR	3.137±1.156	3.163±1.186	3.280±1.289	3.689±1.093	**0.009**
Mean ADC ($\times 10^{-3}$ mm^2/s)	1.037±0.291	0.912±0.211	1.102±0.297	0.900±0.164	**0.000**
Tumor diameter (cm)	1.200 (0.887–1.762)	1.900 (1.325–2.725)	1.150 (0.600–2.750)	2.550 (1.700–3.750)	**0.000**

Normally distributed variables are expressed as the mean ± SD, and abnormally distributed variables are expressed as the median with the first and third interquartile range (IQR). Bolded text indicates statistical significance ($p < 0.05$).

ADC = apparent diffusion coefficient; HER2 = human epidermal growth factor receptor 2; T1 SIR = T1 signal intensity ratio; T2 SIR = T2 signal intensity ratio; TN = triple-negative

ing to the higher region on DWI and enhancement on DCE-MRI, and the mean ADC values were recorded for each lesion.

Histopathological analysis

The pathologist with 10 years of experience in breast disease, who was blinded to the results of MRI. ER and/or PR positivity was considered hormone receptor (HR)-positive, while both ER and PR negativity was considered HR-negative. A HER2 status of 0 or 1+ was considered negative, 2+ was considered ambiguous, and 3+ was considered positive. Patients with an ambiguous HER2 status were evaluated using fluorescence in situ hybridization (FISH); if HER2 gene amplification was observed, they were considered positive. The Ki-67 expression was classified as high if the staining positivity was more than 14% and low if it was equal to or less than 14%. Tumor subtypes were categorized as follows: Luminal A(HR-positive and Ki-67≤14% and HER2-negative), luminal B (HR-positive with either ki-67≥14% and/or HER2-positive), HER2-enriched (HR-negative and HER2-positive) and triple-negative (TN) (ER- and PR-negative and HER2-negative).[16]

Data and statistical analysis

The normality of continuous variables was evaluated by using the Shapiro–Wilk test. Normally distributed variables are expressed as the means ± standard deviations; abnormally distributed variables are expressed as the median with the first and third interquartile range (IQR). Levels of inter-reader agreement were assessed via the intraclass correlation coefficient (ICC) test. The Kruskal-Wallis H test for continuous variables and the Chi-square test or Fisher's exact test for categorical variables were used to evaluate the relationship between MRI findings and clinical data with molecular subtypes. Benjamini-Hochberg method was invoked to correct p values for multiple testing. Receiver operating characteristic (ROC) curve analysis was performed to evaluate the performance of the binary classifier system and was compared by DeLong tests. Univariate and multivariate logistic regression analysis were performed to screen the independent risk factors associated with one specific subtype and establish combined parameters. Variables with $p < 0.1$ in the univariate analysis were used in the multivariate analysis. The Stata 16.0 was used for statistical analysis. $p < 0.05$ was considered statistically significant.

Results

Clinical data of patients and MRI morphological features with different molecular subtype

All 263 cases breast cancer patients were female, including 52 (19.8%) cases of luminal A type, 135(51.3%) cases of luminal B type, 31 (11.8%) cases of HER2-enriched type and 45 (17.1%) cases of triple-negative type. For clinical characteristics, there were significant differences in axillary lymph node metastasis (ALNM) ($p = 0.01$) and history of hormone use ($p = 0.038$) for four molecular subtypes, and no statistical differences in age, uterine fibroid, menopause and fertility. For MRI morphological features, there were slightly significant differences in tumor morphology ($p = 0.053$), and no statistical differences in margin and dynamic curve (Table 1).

TABLE 4. ROC analysis of MRI quantitative parameters for separating one subtype from all other subtypes

Parameters	AUC	Cutoff value	Sensitivity (%)	Specificity (%)	p*
Luminal A *vs.* all others					
T1 SIR	0.506	≤ 1.270	46.15 (40.1, 52.2)	61.61 (55.7, 67.5)	0.640
T2 SIR	0.550	≤ 3.000	59.62 (53.7, 65.6)	54.50 (48.5, 60.5)	0.397
Mean ADC (×10^{-3} mm^2/s)	0.612	> 0.980	46.15 (40.3, 52.0)	70.62 (65.3, 76.0)	**0.022**
Tumor diameter(cm)	0.768	≤1.900	80.00 (73.1, 86.9)	64.2 (57.0, 71.4)	**0.016**
Luminal B *vs.* all others					
T1 SIR	0.510	>1.291	62.96 (56.2, 69.7)	48.44 (41.7, 55.2)	0.181
T2 SIR	0.563	≤ 3.298	65.93 (59.6, 72.3)	45.31 (38.6, 52.0)	0.169
Mean ADC (×10^{-3} mm^2/s)	0.624	≤ 0.978	77.78 (71.6, 84.0)	44.53 (37.8, 51.3)	**0.012**
Tumor diameter(cm)	0.540	>1.550	78.63 (71.7, 85.6)	35.58 (28.2, 42.9)	0.829
HER2-enriched *vs.* all others					
T1 SIR	0.631	> 1.503	58.06 (50.3, 65.8)	69.40 (61.9, 76.9)	**0.000**
T2 SIR	0.517	> 2.815	67.74 (60.0, 75.5)	44.40 (36.6, 52.2)	0.927
Mean ADC (×10^{-3} mm^2/s)	0.713	> 0.903	87.10 (81.5, 92.7)	53.02 (45.1, 60.9)	**0.002**
Tumor diameter(cm)	0.543	> 2.190	60.00 (52.4, 67.6)	60.20 (52.6, 67.8)	0.697
TN *vs.* all others					
T1 SIR	0.608	≤ 1.286	64.44 (58.6, 70.2)	62.84 (57.0, 68.7)	0.176
T2 SIR	0.655	>3.157	68.89 (61.8, 76.0)	59.63 (51.9, 67.4)	**0.020**
Mean ADC (×10^{-3} mm^2/s)	0.562	≤ 0.869	51.11 (44.1, 58.1)	62.39 (54.9, 69.9)	0.087
Tumor diameter(cm)	0.706	>2.050	74.36(65.3, 83.4)	57.69 (49.3, 66.1)	**0.040**

* Corrected p values by Benjamini-Hochberg method. Data are values with 95% confidence interval in parentheses. Bolded text indicates statistical significance ($p < 0.05$).

ADC = apparent diffusion coefficient; AUC = area under the ROC curve; HER2 = human epidermal growth factor receptor 2; ROC = receiver operating characteristic; T1 SIR = T1 signal intensity ratio; T2 SIR = T2 signal intensity ratio; TN = triple-negative

Interobserver agreement of quantitative parameters

T1 SIR, T2 SIR, mean ADC values and tumor diameter showed excellent interobserver agreements with ICC > 0.8 (Table 2).

Comparison of MRI quantitative parameters for molecular subtypes

Comparison of MRI quantitative parameters according to molecular subtypes are summarized in Table 3. T1 SIR was the lowest in triple-negative type and highest in HER2-enriched type, with statistically significant difference ($p = 0.026$). T2 SIR was the lowest in luminal A type and the highest in triple-negative type, with significant statistical difference ($p = 0.009$). Mean ADC values had significant difference in four molecular subtypes ($p < 0.001$), in triple-negative type were the lowest and highest in HER2-enriched type. Tumor diameter of HER2-enriched type was the smallest, and that of triple-negative type was the largest, with significant statistical difference ($p < 0.001$).

Univariate and multivariate logistic regression analysis

In the univariate regression analysis, mean ADC values (OR = 4.259, $p = 0.022$), tumor diameter (OR = 0.593, $p = 0.016$) and ALNM (OR = 0.316, $p = 0.012$) were associated with luminal A. Mean ADC values (OR = 0.176, $p = 0.012$) and ALNM (OR =2.002, $p = 0.018$) were associated with luminal B. T1 SIR (OR = 3.277, $p < 0.01$), mean ADC values (OR = 7.815, $p = 0.002$) and non-mass (OR = 0.334, $p = 0.036$) were associated with HER2-enriched. T2 SIR (OR = 1.384, $p = 0.02$) and tumor diameter (OR = 1.256, $p = 0.04$) were associated with TN.

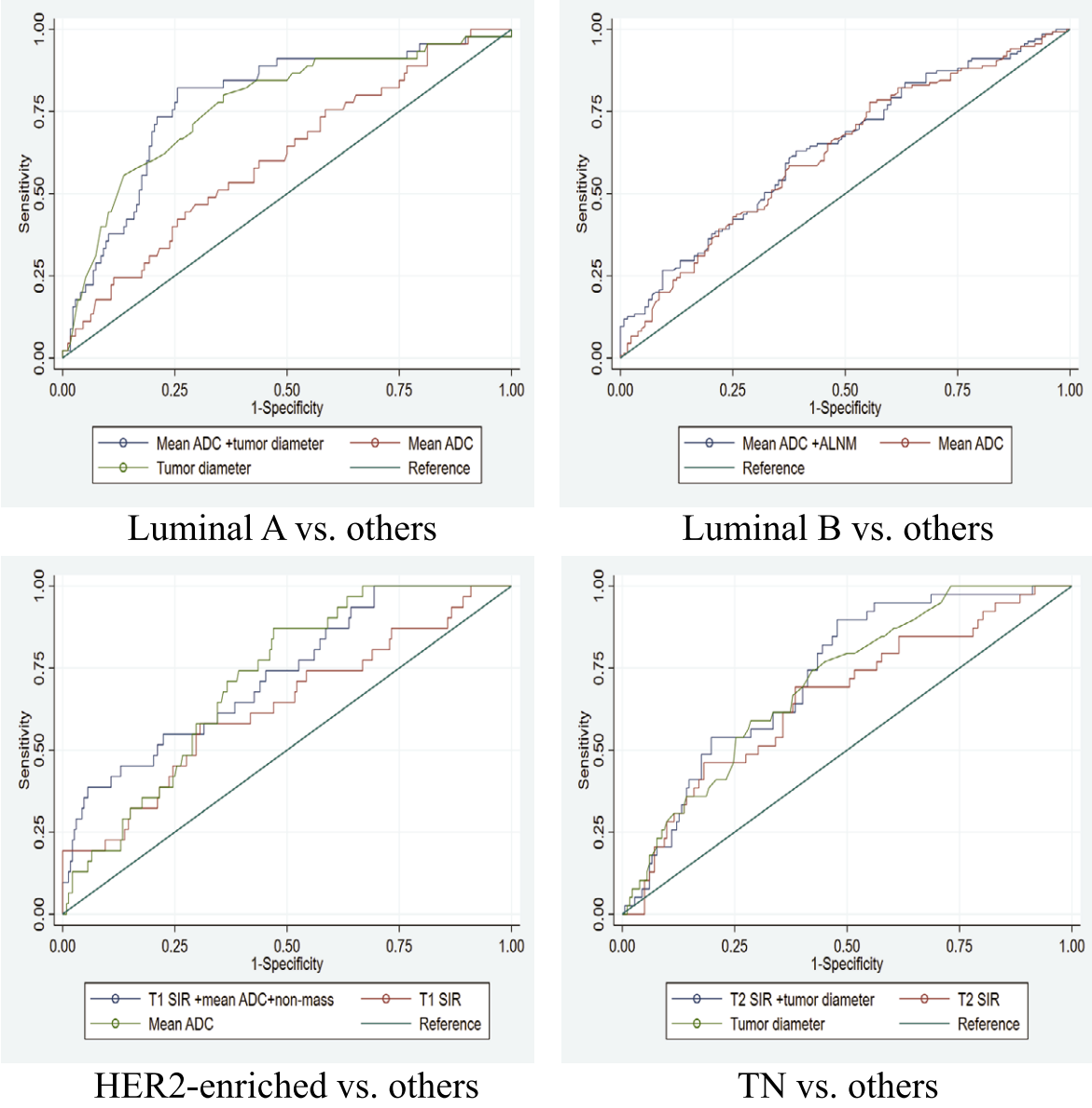

FIGURE 3. The comparison of receiver operating characteristic (ROC) curve of single and combined parameters for distinguishing one subtype from all other subtypes.

ADC = apparent diffusion coefficient; ALNM = axillary lymph node metastasis; TN: triple-negative; T1 SIR = T1 signal intensity ratio; T2 SIR = T2 signal intensity ratio

In the multivariate regression analysis, mean ADC (OR = 3.121; p = 0.041) and tumor diameter (OR = 0.652; p = 0.019) were associated with luminal A. Mean ADC (OR = 0.193; p = 0.005) and ALNM (OR = 1.908; p = 0.016) were associated with luminal B; T1 SIR (OR = 2.907; p = 0.002), non-mass (OR = 0.373, p = 0.028) and mean ADC (OR = 3.732; p = 0.069) were associated with HER2-enriched. T2 SIR (OR = 1.395; p = 0.017) and tumor diameter (OR = 1.245; p = 0.011) were associated with TN.

Parameters for discriminating molecular subtypes

Detailed results of ROC analysis of MRI quantitative parameters for separating one subtype from

TABLE 5. ROC analysis of combined parameters for separating one subtype from all other subtypes

	AUC	Sensitivity (%)	Specificity (%)	p
Luminal A *vs.* all others				
Mean ADC+ tumor diameter	0.781	82.22 (76.57, 87.87)	74.43 (68.99, 79.87)	< 0.001
Luminal B *vs.* all others				
Mean ADC+ALNM	0.639	62.96 (57.12, 68.80)	60.94 (55.04, 66.84)	< 0.001
HER2-enriched *vs.* all others				
T1 SIR + mean ADC+ non-mass	0.728	38.71(21.56, 55.86)	94.4(91.44, 97.36)	< 0.001
TN *vs.* all others				
T2SIR+ tumor diameter	0.724	89.74 (85.64, 93.84)	52.20 (45.68, 58.72)	0.002

Bolded text indicates statistical significance ($p < 0.05$). Data are values with 95% confidence interval in parentheses.

ADC = apparent diffusion coefficient; ALNM = axillary lymph node metastasis; AUC = area under the ROC curve; HER2 = human epidermal growth factor receptor 2; TN = triple-negative; T1 SIR = T1 signal intensity ratio; T2 SIR = T2 signal intensity ratio

all other subtypes are summarized in Table 4. To distinguish luminal A and TN from other subtypes respectively, tumor diameter achieved the largest area under the ROC curves (AUC = 0.768, p = 0.016; AUC = 0.706, p = 0.04). Mean ADC showed a largest AUC (AUC = 0.713, p =0.002) in the differentiation between HER2-enriched and other subtypes. The other quantitative parameters only showed poor discrimination or no significant difference.

MRI parameters associated with each molecular subtype in multivariate logistic regression analysis were used to establish combined parameters. The comparison of ROC curves of single and combined parameters was shown in Figure 3. The AUCs of combined parameters (Table 5) were higher than any single quantitative parameter (Table 4). Delong tests showed the diagnostic efficiency of combined parameters and single quantitative parameters were no significant difference. For separating luminal A subtype from others, the combined parameter (mean ADC+ tumor diameter) achieved a largest AUC (AUC = 0.781).

Discussion

Breast cancer is a highly heterogeneous disease, and the 2017 edition of the St. Gallen Consensus divided breast cancer into 4 molecular pathological subtypes based on its gene expression profile, and stated that the four subtypes of breast cancer require different treatments.[16] These subtypes differ significantly in clinical behaviour, prognosis, and response to treatment. Other researchers used the above four subtypes of classification[17-19], thus we also categorized breast cancer into four subtypes in our study.

Histopathological analysis is currently the gold standard for diagnosing molecular subtypes of breast cancer in clinical practice. However, pathologists only perform hot-spot studies on surgical specimens and do not routinely evaluate all areas of the tumor. Furthermore, this is an invasive examination that may lead to complications (hematoma, inflammation, oedema), and due to the longitudinal heterogeneity of tumour volume, there may be discordance in biomarker status (ER, PR, HER2) between biopsy and surgical specimen.[20] In contrast, with MRI, a minimally invasive procedure, evaluating all areas of the tumor and repeating these measurements is significantly easier and more advantageous than in pathology practice. MRI especially advanced quantitative MRI techniques as highly sensitive non-invasive imaging technology, can provide overall information on tumour morphology, angiogenesis, cell density and microstructure[21,22], compensating for the limitations of biopsy or histopathological examination in tumour heterogeneity. Nevertheless, these quantitative parameters require additional image post-processing, radiomics feature extraction, selection, and model construction. The quantitative parameters in our study can be directly measured from the scan images without needing additional image post-processing, making the process simple, quick, and conducive to widespread clinical application.

The present study attempts to compare multiple quantitative parameters including (T1 SIR, T2 SIR,

mean ADC values and tumor diameter) of breast cancer for discriminating molecular subtypes. We found triple-negative type had the lowest T1 SIR and highest T2 SIR, similar with some studies.[23,24] Triple-negative breast cancer exhibits higher levels of VEGF compared to non-triple-negative type, which promotes angiogenesis, leading to increased microvascular density, indicating lower T1 signal intensity and higher T2 signal intensity. Moreover, the higher angiogenesis levels in triple-negative breast cancer may lead to local tissue oedema, further decreasing T1 SIR and increasing T2 SIR.[15,25] Furthermore, the T2 SIR in luminal A type were the lowest in our study. This aligns with some findings. Luminal A breast cancer was related homogeneous iso/hypointense features on T2W[26], compared to heterogeneous hypointense ones, exhibited lower proliferation, correlating with better prognosis.[27]

In our study, we also revealed that mean ADC values were the lowest in triple-negative and highest in HER2-enriched type, consistent with some studies.[28,29] In contrast, another study indicated that ER or PR-positive tumors had lower mean ADC values.[30] Variations in mean ADC values or diffusion restriction may result from differences in luminal A proportions across studies and the changing thresholds distinguishing luminal B from luminal A subtypes. Another contributing factor may be the inherent heterogeneity within luminal A breast cancer.

Additionally, we observed that tumor diameters in luminal A and luminal B type were smaller than triple-negative, similar with previous findings.[19] This highlights the faster growth and invasive capability of triple-negative breast cancer compared to the relatively slow-growing luminal A and luminal B subtype.

HER2-enriched subtype had a higher proportion of non-mass lesions (35.5%) and hormone use history (9.7%) in our cohort. This observation is comparable with the study of Navarro *et al*.[31], which reported frequent non-mass enhancement in HER2-positive breast cancer. This supports the theory of intraductal development in this subtype. Kazama T *et al*.[32] and Coskun B A *et al*.[33] also revealed that HER2-enriched type is closely related to high hormone level.

Our study quantified the subjective signal intensity as T1 SIR and T2 SIR and found that independent influencing factors were higher T2 SIR and larger tumor diameter associated with triple-negative subtype, and T1 SIR was the only quantitative parameter associated with HER2-enriched subtype. The combined parameters (mean ADC + tumor diameter) achieved a largest AUC (AUC = 0.781) for separating luminal A subtype. The result is similar with Chen *et al*.[34], the AUC of combined model (mean kurtosis value + perfusion fraction + pseudo diffusion coefficient) was 0.785, and higher than that of another study combining the T2, mean ADC and tumor volume parameters to distinguish luminal A subtype (AUC= 0.765).[3] A recent study regarding the identification of luminal A/B breast cancer subtypes[35] demonstrated that the hybrid model significantly outperformed the individual approaches, achieving an excellent AUC (0.921) and the most important contributors were radiomic features related to shape and texture and high-level deep features.

Breast fibroglandular tissue content varies in individuals. Identification of suitable fibroglandular tissue for T1 and T2 signal measurement is challenging in extremely fatty breasts. So, the patient's own pectoral muscle was selected as the internal control for T1 and T2 SIR.[15] Interindividual variation in the pectoralis muscle among patients may be associated with sex, body habitus, lesion invasion, as well as age-related fatty infiltration and muscle atrophy. However, age exerts no impact on the contractility or fatigue resistance of the pectoralis muscle.[36] In the present study, when placing ROIs in the pectoralis muscle as an internal reference, the slice with the greatest thickness of the pectoralis muscle was selected, and areas with visually evident fatty infiltration were carefully avoided to minimize the confounding effect of adipose tissue on the signal intensity of the muscle. Furthermore, for patients with tumor invasion of the pectoralis muscle, the contralateral pectoralis muscle was used as an internal control.

This study has the following limitations that need to be addressed. First, we used the signal value of the pectoralis muscle within the same patient as a reference for calculation, ignoring inter-patient difference in pectoralis major muscle signal value, which might be a factor affecting T1 SIR and T2 SIR. Second, this was a single centre study with limited number of patients and unbalanced molecular subtypes. When measuring lesion size, only mass-like lesions were included, and lesions smaller than 5 mm were excluded, because excessively small lesions may compromise the accuracy of SIR. Future studies should include more patients and conduct multi-centre research to explore the combined application of MRI novel imaging technologies, and biomarkers. By extracting more refined imaging features, non-invasive assessment

of intra-tumoral heterogeneity in breast cancer is expected to be achieved.

In conclusion, quantitative MRI parameters are correlated with the molecular subtypes of breast cancer. Combined parameters incorporating T1 SIR and T2 SIR exhibit potential diagnostic utility for differentiating HER2-enriched and triple-negative subtypes, respectively. T1 SIR and T2 SIR can enrich quantitative descriptors from breast MRI.

Acknowledgments

This study has received funding by Zhejiang Medical and Health Science and Technology Program (Grant No. 2023KY990), Hangzhou Medical and Health Science and Technology Project (Grant No. A20220619) and Hangzhou Science and Technology Development Program (Grant No. 202204B07).

References

1. Orel SG, Schnall MD. MR imaging of the breast for the detection, diagnosis, and staging of breast cancer. *Radiology* 2001; **220:** 13-30. doi: 10.1148/radiology.220.1.r01jl3113
2. Telegrafo M, Rella L, Stabile Ianora AA, Angelelli G, Moschetta M. Unenhanced breast MRI (STIR, T2-weighted TSE, DWIBS): an accurate and alternative strategy for detecting and differentiating breast lesions. *Magn Reson Imaging* 2015; **33:** 951-5. doi: 10.1016/j.mri.2015.06.002
3. Du S, Gao S, Zhang L, Yang X, Qi X, Li S. Improved discrimination of molecular subtypes in invasive breast cancer: comparison of multiple quantitative parameters from breast MRI. *Magn Reson Imaging* 2021; **77:** 148-58. doi: 10.1016/j.mri.2020.12.001
4. Heacock L, Lewin AA, Toth HK, Moy L, Reig B. Abbreviated MR imaging for breast cancer. *Radiol Clin North Am* 2021; **59:** 99-111. doi: 10.1016/j.rcl.2020.09.001
5. Yamaguchi K, Ichinohe K, Iyadomi M, Fujiki K, Yoshinaga Y, Egashira R, et al. Abbreviated and ultrafast dynamic contrast-enhanced (DCE) MR imaging. *Magn Reson Med Sci* 2025; **24:** 315-31. doi: 10.2463/mrms.rev.2024-0158
6. Kousi E, O'Flynn EAM, Borri M, Morgan VA, deSouza NM, Schmidt MA. Pre-treatment functional MRI of breast cancer: T2* evaluation at 3 T and relationship to dynamic contrast-enhanced and diffusion-weighted imaging. *Magn Reson Imaging* 2018; **52:** 53-61. doi: 10.1016/j.mri.2018.05.014
7. Meng T, He N, He H, Liu K, Ke L, Liu H, et al. The diagnostic performance of quantitative mapping in breast cancer patients: a preliminary study using synthetic MRI. *Cancer Imaging* 2020; **20:** 88. doi: 10.1186/s40644-020-00365-4
8. Malikova MA, Tkacz JN, Slanetz PJ, Guo CY, Aakil A, Jara H. Evaluation of T1/T2 ratios in a pilot study as a potential biomarker of biopsy: proven benign and malignant breast lesions in correlation with histopathological disease stage. *Future Sci OA* 2017; **3:** FSO197. doi: 10.4155/fsoa-2016-0063
9. Li Q, Xiao Q, Yang M, Chai Q, Huang Y, Wu PY, et al. Histogram analysis of quantitative parameters from synthetic MRI: correlations with prognostic factors and molecular subtypes in invasive ductal breast cancer. *Eur J Radiol* 2021; **139:** 109697. doi: 10.1016/j.ejrad.2021.109697
10. Matsuda M, Kido T, Tsuda T, Okada K, Shiraishi Y, Suekuni H, et al. Utility of synthetic MRI in predicting the Ki-67 status of oestrogen receptor-positive breast cancer: a feasibility study. *Clin Radiol* 2020; **75:** 398 e1-398 e8. doi: 10.1016/j.crad.2019.12.021
11. Kim TH, Ha Y, Shin JJ, Cho YE, Lee JH, Cho WH. Signal intensity ratio on magnetic resonance imaging as a prognostic factor in patients with cervical compressive myelopathy. *Medicine (Baltimore)* 2016; **95:** e4649. doi: 10.1097/MD.0000000000004649
12. Duvnjak S, Ravn P, Green A, Andersen PE. Magnetic resonance signal intensity ratio measurement before uterine artery embolization: ability to predict fibroid size reduction. *Cardiovasc Intervent Radiol* 2017; **40:** 1839-44. doi: 10.1007/s00270-017-1721-2
13. Shetty AS, Sipe AL, Zulfiqar M, Tsai R, Raptis DA, Raptis CA, et al. In-phase and opposed-phase imaging: applications of chemical shift and magnetic susceptibility in the chest and abdomen. *Radiographics* 2019; **39:** 115-35. doi: 10.1148/rg.2019180043
14. Priola AM, Priola SM, Ciccone G, Evangelista A, Cataldi A, Gned D, et al. Differentiation of rebound and lymphoid thymic hyperplasia from anterior mediastinal tumors with dual-echo chemical-shift MR imaging in adulthood: reliability of the chemical-shift ratio and signal intensity index. *Radiology* 2015; **274:** 238-49. doi: 10.1148/radiol.14132665
15. Durhan G, Poker A, Settarzade E, Karakaya J, Kösemehmetoğlu K, Akpınar MG, et al. Magnetic resonance imaging findings of invasive breast cancer in different histological grades and different histopathological types. *Clin Imaging* 2021; **76:** 98-103. doi: 10.1016/j.clinimag.2021.01.039
16. Curigliano G, Burstein HJ, Winer EP, Gnant M, Dubsky P, Loibl S, et al. De-escalating and escalating treatments for early-stage breast cancer: the St. Gallen International Expert Consensus Conference on the Primary Therapy of Early Breast Cancer 2017. *Ann Oncol* 2017; **28:** 1700-12. doi: 10.1093/annonc/mdx308
17. Guvenc I, Akay S, Ince S, Yildiz R, Kilbas Z, Oysul FG, et al. Apparent diffusion coefficient value in invasive ductal carcinoma at 3.0 Tesla: is it correlated with prognostic factors? *Br J Radiol* 2016; **89:** 20150614. doi: 10.1259/bjr.20150614
18. Suo S, Cheng F, Cao M, Kang J, Wang M, Hua J, et al. Multiparametric diffusion-weighted imaging in breast lesions: association with pathologic diagnosis and prognostic factors. *J Magn Reson Imaging* 2017; **46:** 740-50. doi: 10.1002/jmri.25612
19. Montemezzi S, Camera L, Giri MG, Pozzetto A, Caliò A, Meliadò G, et al. Is there a correlation between 3T multiparametric MRI and molecular subtypes of breast cancer? *Eur J Radiol* 2018; **108:** 120-7. doi: 10.1016/j.ejrad.2018.09.024
20. Eisenhauer EA, Therasse P, Bogaerts J, Schwartz LH, Sargent D, Ford R, et al. New response evaluation criteria in solid tumours: revised RECIST guideline (version 1.1). *Eur J Cancer* 2009; **45:** 228-47. doi: 10.1016/j.ejca.2008.10.026
21. Yin H, Bai L, Jia H, Lin G. Noninvasive assessment of breast cancer molecular subtypes on multiparametric MRI using convolutional neural network with transfer learning. *Thorac Cancer* 2022; **13:** 3183-91. doi: 10.1111/1759-7714.14673
22. Leithner D, Mayerhoefer ME, Martinez DF, Jochelson MS, Morris EA, Thakur SB, et al. Non-invasive assessment of breast cancer molecular subtypes with multiparametric magnetic resonance imaging radiomics. *J Clin Med* 2020; **9:** 1853. doi: 10.3390/jcm9061853
23. Linderholm BK, Hellborg H, Johansson U, Elmberger G, Skoog L, Lehtiö J, et al. Significantly higher levels of vascular endothelial growth factor (VEGF) and shorter survival times for patients with primary operable triple-negative breast cancer. *Ann Oncol* 2009; **20:** 1639-46. doi: 10.1093/annonc/mdp062
24. Mohammed RA, Ellis IO, Mahmmod AM, Hawkes EC, Green AR, Rakha EA, et al. Lymphatic and blood vessels in basal and triple-negative breast cancers: characteristics and prognostic significance. *Mod Pathol* 2011; **24:** 774-85. doi: 10.1038/modpathol.2011.4
25. Ozturk VS, Polat YD, Soyder A, Tanyeri A, Karaman CZ, Taskin F. The Relationship between MRI findings and molecular subtypes in women with breast cancer. *Curr Probl Diagn Radiol* 2020; **49:** 417-21. doi: 10.1067/j.cpradiol.2019.07.003
26. Nguyen VT, Duong DH, Nguyen QT, Nguyen DT, Tran TL, Duong TG. The association of magnetic resonance imaging features with five molecular subtypes of breast cancer. *Eur J Radiol Open 2024*; **13:**100585. doi: 10.1016/j.ejro.2024.100585
27. Yuen S, Monzawa S, Yanai S, Matsumoto H, Yata Y, Ichinose Y, et al. The association between MRI findings and breast cancer subtypes: focused on the combination patterns on diffusion-weighted and T2-weighted images. *Breast Cancer* 2020; **27:** 1029-37. doi: 10.1007/s12282-020-01105-z

28. Surov A, Chang YW, Li L, Partridge SC, Kim JY, Wienke A. Apparent diffusion coefficient cannot predict molecular subtype and lymph node metastases in invasive breast cancer: a multicenter analysis. *BMC Cancer* 2019; **19:** 1043. doi: 10.1186/s12885-019-6298-5

29. Ab Mumin N, Ramli Hamid MT, Wong JHD, Rahmat K, Ng KH. Magnetic resonance imaging phenotypes of breast cancer molecular subtypes: a systematic review. *Acad Radiol* 2022; **29 (Sppl 1):** S89-106. doi: 10.1016/j.acra.2021.07.017

30. Suo S, Zhang D, Cheng F, Cao M, Hua J, Lu J, et al. Added value of mean and entropy of apparent diffusion coefficient values for evaluating histologic phenotypes of invasive ductal breast cancer with MR imaging. *Eur J Radiol* 2018; **29:** 1425-34. doi: 10.1007/s00330-018-5667-9

31. Navarro Vilar L, Alandete German SP, Medina Garcia R, Blanc Garcia E, Camarasa Lillo N, Vilar Samper J. MR imaging findings in molecular subtypes of breast cancer according to BIRADS system. *Breast J* 2017; **23:** 421-8. doi: 10.1111/tbj.12756

32. Kazama T, Takahara T, Hashimoto J. Breast cancer subtypes and quantitative magnetic resonance imaging: a systemic review. *Life (Basel)* 2022; **12:** 490. doi: 10.3390/life12040490

33. Coskun Bilge A, Yaltirik Bilgin E, Bulut ZM, Esen Bostanci I, Bilgin E. Preoperative dynamic contrast-enhanced and diffusion-weighted breast magnetic resonance imaging findings for prediction of lymphovascular invasion of the lesions in node-negative invasive breast cancer. *Can Assoc Radiol J* 2024; **75:** 386-96. doi: 10.1177/08465371231212893

34. Chen K, Yu C, Pan J, Xu Y, Luo Y, Yang T, et al. Prediction of the Nottingham prognostic index and molecular subtypes of breast cancer through multimodal magnetic resonance imaging. *Magn Reson Imaging* 2024; **108:** 168-75. doi: 10.1016/j.mri.2024.02.012

35. Shangguan J, Shchukina E, Monov D, Larina S. Integrating deep learning and radiomics for precise identification of luminal A/B breast cancer subtypes on dynamic contrast-enhanced MRI. *Cancer Imaging* 2026; **26:** 36. doi: 10.1186/s40644-026-00996-z

36. Fogarty MJ. Age influences the specific force and fatigability of the external abdominal obliques but not pectoralis major muscles. *Resp Physiol Neurobiol* 2024; **320:** 104187. doi: 10.1016/j.resp.2023.104187

RADIOLOGY AND ONCOLOGY Radiology and Oncology | Ljubljana | Slovenia | www.radioloncol.com

research article

Diagnostic performance of whole-body diffusion-weighted imaging for staging esophageal cancer: a comparative study with PET-CT

Xiaohu Xu[1], Rong Yu[1], Qiulian Ma[1], Tingting Yin[1], Haisheng Chen[2], Ye Qian[3], Hong Li[1], Rongxing Qi[4], Yachun Xu[1]

[1] Department of Imaging, Haian People's Hospital, Haian, Jiangsu Province, China
[2] Department of Thoracic Surgery, Haian People's Hospital, Haian, Jiangsu Province, China
[3] Department of Oncology, Haian People's Hospital, Haian, Jiangsu Province, China
[4] Department of Nuclear Medicine, Nantong First People's Hospital Affiliated to Southeast University, Nantong, Jiangsu Province, China

Radiol Oncol 2026; 60(3): 378-393.

Received 27 February 2026
Accepted 5 June 2026

Correspondence to: Yachun Xu, Department of Imaging, Haian People's Hospital, Haian 22660, Jiangsu Province, China.
E-mail: xuyachun4488@hotmail.com

Disclosure: No potential conflicts of interest were disclosed.

Background. Accurate preoperative staging is crucial for selecting treatment strategies and assessing prognosis in esophageal cancer. Positron emission tomography-computed tomography (PET-CT) is currently recognized as an essential staging modality, whereas the value of whole-body diffusion-weighted imaging (WB-DWI), a radiation-free functional magnetic resonance imaging (MRI) technique in esophageal cancer staging remains unclear. The objective of the study was to conduct a head-to-head comparison of the diagnostic accuracy of WB-DWI versus PET-CT in the initial diagnosis of esophageal cancer patients for local T staging, regional lymph node (N) assessment, and distant metastasis (M) detection.

Patients and methods. This study collected data from 96 patients with esophageal cancer who underwent pathological diagnosis and imaging evaluation at Haian People's Hospital between January 2023 and January 2025. Propensity Score Matching (PSM) was employed to balance confounding factors between groups, ultimately forming matched cohorts for analysis: the WB-DWI group (n = 32) and the PET-CT group (n = 32). Using postoperative pathology (PTNM) and/or 6-month follow-up clinical diagnosis as the gold standard, the following metrics were evaluated: T staging accuracy, N staging sensitivity/specificity, distant metastasis (M staging) detection rate, overall staging accuracy, image signal-to-noise ratio (SNR), examination duration, and inter-observer agreement (Kappa value). Sensitivity, specificity, positive predictive value (PPV), negative predictive value (NPV), and accuracy were calculated for both methods. Diagnostic performance was analyzed using ROC curves, and the area under the curve (AUC) was compared via DeLong's test.

Results. WB-DWI and PET-CT demonstrated comparable overall staging accuracy for esophageal cancer (84.4% *vs.* 87.5%, $p > 0.05$). For N staging, PET-CT demonstrated higher sensitivity (90.6% *vs.* 78.1%, $p < 0.05$), while both methods showed identical specificity (87.5%). In detecting distant metastases, PET-CT exhibited marginally higher detection rates and accuracy than WB-DWI, though differences were not statistically significant. WB-DWI demonstrated lower accuracy for T staging (71.9% *vs.* 84.4%, $p < 0.05$). WB-DWI images exhibited significantly lower SNR than PET-CT ($p < 0.01$), but the examination was shorter in duration and showed good inter-observer agreement (Kappa > 0.60, $p < 0.001$).

Conclusions. WB-DWI demonstrates comparable overall efficacy to PET-CT in esophageal cancer staging. Although its sensitivity and efficiency are slightly lower, its radiation-free nature and high specificity make it a viable supplement or alternative to PET-CT for specific patient populations. These findings provide evidence for precise clinical selection.

Key words: esophageal cancer; tumor staging; WB-DWI; PET-CT; diagnostic performance; comparative study

Introduction

Esophageal cancer is one of the most prevalent malignant tumors globally, particularly in East Asia. Its insidious onset and aggressive nature often result in poor patient prognosis.[1,2] Accurate preoperative staging is crucial for developing individualized treatment plans, assessing prognosis, and improving survival rates.[3,4] Currently, clinical staging primarily relies on imaging examinations, aiming to precisely evaluate the depth of primary tumor invasion (T staging), regional lymph node metastasis (N staging), and the presence of distant metastasis (M staging).[5,6] In this field, positron emission tomography-computed tomography (PET-CT), which integrates anatomical and functional information, is widely recognized as a vital staging tool.[7,8] By reflecting glucose metabolic activity in tumor cells, PET-CT demonstrates high sensitivity in detecting lymph node and distant metastases, significantly influencing treatment strategy adjustments.[9,10] However, this technology also has inherent limitations, including relatively high examination costs, exposure to ionizing radiation, and the potential for false-positive results in certain inflammatory or physiological uptake scenarios. These factors have somewhat constrained its routine and repetitive clinical application.[11,12]

With the rapid advancement of magnetic resonance imaging (MRI) technology, whole-body diffusion-weighted imaging (WB-DWI) has gained increasing attention in oncological assessment as a radiation-free functional imaging modality.[13,14] This technique reflects cellular density by detecting the degree of restriction to water-molecule diffusion within tissues, with malignant tissues typically exhibiting higher signal intensity.[15,16] Theoretically, WB-DWI holds the potential to perform whole-body tumor screening and staging in a single examination while avoiding radiation exposure.[17,18] Preliminary studies in recent years have explored the value of WB-DWI in evaluating systemic tumors such as breast cancer and lymphoma. However, systematic evidence supporting its application in staging esophageal cancer, a malignancy with unique anatomical and biological characteristics, remains lacking.[19,20] The existing literature primarily consists of small-sample exploratory studies or those that have not conducted rigorous, methodologically robust direct comparisons with the current gold standard, PET-CT. Therefore, clarifying the specific diagnostic efficacy of WB-DWI across all tumor node metastasis (TNM) stages of esophageal cancer and delineating its advantages and limitations has clear practical significance for enriching clinical imaging options and optimizing diagnostic and therapeutic pathways.

Against this background, this study aims to systematically evaluate the diagnostic performance of WB-DWI in staging newly diagnosed esophageal cancer patients through a retrospective, head-to-head comparative analysis, using PET-CT as the reference standard. The study addresses several key questions: Is there a difference between WB-DWI and PET-CT in overall TNM staging accuracy? How do the sensitivity and specificity of the two imaging techniques perform in specific tasks such as assessing local invasion for T staging, lymph node metastasis for N staging, and distant metastasis for M staging? Beyond diagnostic efficacy, operational metrics such as examination duration, image quality, and consistency in result interpretation are equally important dimensions in clinical practice. Addressing these questions will contribute to a more comprehensive understanding of WB-DWI's clinical applicability.

The innovation of this study lies in its adoption of a more rigorous research design to enhance the reliability of its conclusions. We collected consecutive case records from Hai'an People's Hospital over the past two years. All enrolled patients received pathological confirmation and underwent comprehensive imaging evaluations. To control potential confounding factors affecting comparative outcomes, this study employed Propensity Score Matching (PSM) to balance baseline clinical characteristics between the WB-DWI and PET-CT assessment groups. This approach enabled the construction of a more comparable matched cohort for analysis. For evaluation metrics, we established multidimensional assessment criteria encompassing not only core diagnostic indicators, such as accuracy, sensitivity, and specificity for traditional T, N, M staging, but also parameters reflecting technical utility and stability, such as image signal-to-noise ratio (SNR), examination duration, and inter-observer agreement. Through this comprehensive comparison, we aim not only to validate WB-DWI's fundamental diagnostic capabilities but also to provide more detailed evidence from a clinical practice perspective for its positioning, whether as an effective alternative in specific scenarios (*e.g.*, iodine contrast agent contraindications, radiation avoidance requirements) or as a complementary diagnostic tool to PET-CT. The findings of this study are expected to provide clinically relevant, evidence-based insights from Chinese population

data to develop personalized imaging staging protocols for esophageal cancer.

Patients and methods

Research subjects

This study employed a retrospective cohort design. The subjects were esophageal cancer patients who sought treatment at Hai'an People's Hospital between January 2023 and January 2025. Initially, 108 newly diagnosed patients with pathologically confirmed diseases and complete imaging data were identified. By strictly applying inclusion and exclusion criteria, we established an initial study cohort of 96 patients. All patients underwent WB-DWI and completed one or more conventional CT and/or MRI examinations within a 2-week interval for clinical staging. Among these, 64 patients also underwent 18F-FDG PET-CT examinations concurrently. To fairly compare the diagnostic performance of the two imaging modalities and to control for selection bias and confounding factors, we performed propensity score-matching analysis on the 64 patients with both WB-DWI and PET-CT data. Matching variables included key clinical and pathological factors potentially affecting staging accuracy: age, sex, primary tumor location (cervical, thoracic, abdominal), histological type (squamous cell carcinoma, adenocarcinoma), and preliminary clinical staging (based on conventional imaging). Through 1:1 nearest-neighbor matching with a caliper value of 0.02, a matched cohort of 32 patient pairs was successfully established, comprising a WB-DWI evaluation group and a PET-CT evaluation group, each containing 32 cases. The matched groups demonstrated good balance in the matched variables, as shown in Figure 1.

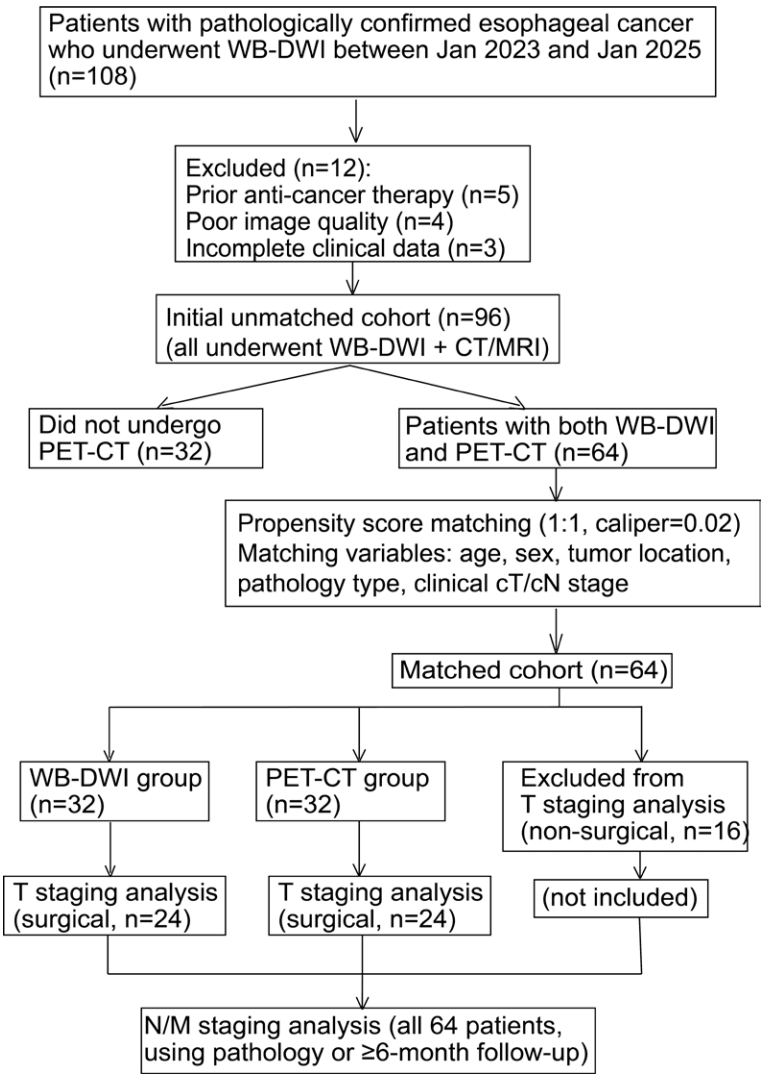

FIGURE 1. Flowchart.

WB-DWI = whole-body diffusion-weighted imaging

Inclusion and exclusion criteria

Inclusion criteria[21]: (1) The biopsy under gastroscopy confirmed it to be esophageal cancer (squamous cell carcinoma or adenocarcinoma), and a complete pathological report was available.; (2) Newly diagnosed and not previously treated with any anticancer therapy; (3) Completed chest and whole-abdominal contrast-enhanced CT, whole-body WB-DWI, and whole-body PET-CT examinations within the same treatment period (interval ≤ 4 weeks); (4) Possesses complete basic clinical information.

Exclusion criteria[22]: (1) History of other active malignancies; Poor image quality with severe artifacts significantly impairing interpretation; Severe deficiencies in clinical or follow-up data preventing determination of final clinical staging; Examination intervals exceeding the specified time window.

Research plan

The PET-CT examination was conducted using the Biograph mCT 64-slice scanner produced by Siemens of Germany. Before the examination, patients were required to fast for more than 6 hours, and their blood sugar levels were controlled within the normal range. They were intravenously injected with ^{18}F-FDG tracer (3.7–4.4 MBq/kg) based

on their weight, and the scan was performed 60 minutes after rest. The scanning range extended from the top of the skull to the middle of the thigh. Unlike conventional PET/CT, the PET/CT examination in this study also included diagnostic contrast-enhanced CT: after injecting the iodine contrast agent (iodiprone, 1.5 mL/kg, injection rate 3 mL/s), images were collected respectively during the arterial phase and the venous phase, with a layer thickness of 1.25 mm and a reconstruction interval of 1.0 mm. This diagnostic CT was used to precisely assess the T stage of the primary tumor (the depth of esophageal wall infiltration, the relationship with the surrounding fat space and adjacent organs) and the morphological characteristics of lymph nodes. The PET data was corrected for attenuation using low-dose CT and fused with the diagnostic CT images.[23,24]

WB-DWI examinations were performed on the Ingenia CX 3.0T MRI system (Philips Healthcare, Netherlands). Patients are positioned supine with a body phased-array coil. The scanning sequence is a single-shot planar echo-planar imaging (EPI) sequence. The scan range covers from the cranial vault to the mid-thigh. Key parameters are as follows: TR/TE 5600/70 ms, field of view (FOV) 380×380 mm, matrix 128×128, slice thickness 6 mm, slice spacing 1 mm. DWI utilized three b-values (0, 800, 1000 s/mm^2). The system automatically generated diffusion-weighted images at a high b-value (b = 1000 s/mm^2) and corresponding apparent diffusion coefficient maps.[25,26]

Regarding imaging interpretation standards, all images were independently analyzed by two senior radiologists under double-blind conditions. Staging was strictly according to the 8th edition of the American Joint Committee on Cancer (AJCC) TNM classification for esophageal and gastroesophageal junction cancers.[27] For PET-CT images, the criterion for determining positive lymph node metastasis is as follows: the maximum standardized uptake value (SUVmax) of the lymph node exceeds 2.5 times the SUVmax of the mediastinal blood pool, or exceeds the background SUVmax of the liver. That is: lymph node SUVmax > 2.5 × SUVmax (mediastinal blood pool) or lymph node SUVmax > SUVmax (liver background). For WB-DWI images, lymph nodes exhibiting marked hyperintensity on high b-value images and hypointensity on ADC maps were considered suspicious for metastasis. For each suspicious lymph node detected by WB-DWI and PET-CT, two physicians jointly measured its short diameter (taking the maximum diameter perpendicular to the long axis on the cross-sectional image), and recorded the measurement in the structured report. For metastatic lymph nodes confirmed by pathology or follow-up, the minimum short diameter value was further recorded to evaluate the detection lower limit of the two imaging techniques for small lymph node metastasis. The determination of T stage of the primary lesion mainly relies on the anatomical morphological features of diagnostic enhanced CT (or MRI), including the degree of esophageal wall thickening, whether the layers of the wall are clear, whether the periphery is smooth, whether there are cord-like shadows or blurring in the surrounding fat space, and whether there is direct invasion of adjacent organs (trachea, aorta, pericardium, vertebrae). At the same time, the abnormal distribution range and pattern of metabolic abnormalities of PET (such as whether FDG uptake exceeds the esophageal contour) serve as supplementary reference information.[28] In cases of diagnostic disagreement, a third senior expert reviewed the findings to reach consensus.

Observation indicators

This study established comprehensive and multilevel evaluation criteria to systematically compare the performance of WB-DWI and PET-CT in esophageal cancer staging across three dimensions: diagnostic accuracy, image quality, and clinical utility. All the T-stage determinations based on imaging examinations were based solely on the postoperative pathological examination (pTNM) results as the gold standard. Therefore, the accuracy analysis of T-stage was limited to patients who underwent radical surgery and received complete pathological specimens. The T-stage of patients who did not undergo surgery was not included in the accuracy analysis. For N-stage and M-stage, the gold standard was defined as follows: For patients who undergo radical surgery and lymph node dissection, the postoperative pathological report shall be taken as the standard; for patients who have not undergone surgery or whose lymph nodes have not been dissected, if they undergo endoscopic ultrasound-guided fine-needle aspiration (EUS-FNA) and obtain a positive pathological result, it is determined as metastasis; if there is no pathological result, the reference standard is the comprehensive judgment based on at least 6 months of clinical follow-up (including subsequent progressive enlargement of lymph nodes on imaging or shrinkage after treatment for the metastatic lesion).

The specific detection indicators and their judgment criteria are as follows: (1) For primary tumors, evaluate the diagnostic accuracy of T staging, specifically the proportion of cases where imaging T staging and pathological T staging are completely consistent.[29] (2) For regional lymph node metastasis, evaluate the diagnostic performance of N staging by calculating its sensitivity (true positive rate), specificity (true negative rate), positive predictive value (PPV), and negative predictive value (NPV). The determination of lymph node metastasis status shall be based on pathological results or comprehensive follow-up diagnosis. (3) For distant metastasis, evaluate the diagnostic performance of M staging by calculating its detection rate, sensitivity, specificity, and accuracy, with the gold standard being distant metastatic lesions confirmed by pathology or follow-up. (4) Assess the overall accuracy of TNM staging, defined as the proportion of cases where imaging-based staging perfectly aligns with the final pathologically confirmed clinical stage in stages I, II, III, and IV.[30]

In addition to the aforementioned core diagnostic indicators, this study introduced an image quality assessment system combining objective and subjective measures. The objective metric was the image SNR, calculated by the operating engineer after measuring the target lesion signal intensity and background noise standard deviation within a fixed region of interest. Subjective evaluation used a specially designed 5-point Likert scale, with two radiologists independently scoring the overall image quality for each examination. The scoring criteria were as follows: 1 point (Poor image quality, extreme noise, unidentifiable anatomical structures, unusable for diagnosis); 2 points (Fairly poor image quality, noticeable noise, blurred anatomical structures, low diagnostic confidence); 3 points (Average image quality, some noise present, but key anatomical structures still recognizable, basic diagnosis possible); 4 points (good image quality, well-controlled noise, clear anatomical structures, high diagnostic confidence); 5 points (excellent image quality, minimal noise, sharp and clear anatomical details, ideal diagnostic image).[31] The two physicians' scores were used to calculate inter-observer agreement, with the average score serving as the final subjective image quality score for each case.

Additionally, this study will document and compare the examination duration for both techniques, defined as the total time from patient entry into the examination room until completion of all image acquisition and exit from the room. Finally, an integrated assessment of interobserver agreement will be conducted, encompassing not only Kappa consistency analysis for T, N, M, and overall staging determinations, but also intraclass correlation coefficient (ICC) analysis for the aforementioned subjective image quality ratings. All statistical analyses will strictly adhere to the predefined protocol to ensure the scientific rigor of comparisons and the reliability of conclusions.

Evaluation process for distant metastases

In this study, the assessment of distant metastatic lesions follows a tiered, gold-standard process anchored by objective evidence independent of the imaging studies being evaluated. The specific criteria are as follows:

First, at the imaging interpretation level, the evaluating physician documents all suspected distant metastatic lesions based on WB-DWI or PET-CT imaging findings, such as abnormal discoveries in the liver, lungs, bones, adrenal glands, or non-regional lymph nodes. On WB-DWI, metastatic lesions typically appear markedly hyperintense on high b-value images and hypodense on corresponding apparent diffusion coefficient maps. On PET-CT, metastatic lesions appear as focal areas of abnormal fluorodeoxyglucose (FDG) metabolism inconsistent with physiological uptake at corresponding anatomical locations.

However, imaging abnormalities alone do not constitute a definitive diagnosis. The gold standard for confirming distant metastasis in this study is established by high-level evidence in the following order of priority: 1. Pathological confirmation: Tissue obtained via needle biopsy or surgical resection, pathologically confirmed as esophageal cancer metastasis, represents the highest level of evidence.[32] 2. Follow-up imaging confirmation: For lesions without pathological confirmation, subsequent imaging studies (*e.g.*, contrast-enhanced CT, contrast-enhanced MRI, or follow-up PET-CT) performed at least 3 months later must demonstrate clear features of malignant progression, such as progressive enlargement, increased number, or emergence of new typical malignant signs (*e.g.*, osteolytic lesions caused by bone metastasis).[33] 3. Confirmation by clinical treatment response: During systemic antitumor therapy (*e.g.*, chemotherapy, targeted therapy, or immunotherapy), the lesion significantly shrinks or disappears in response to effective treatment, and enlarges or recurs when treatment fails or progresses.[34]

Comprehensive Evaluation Process: The study will integrate all available information. For a suspected lesion, if confirmed by either criterion 1 or 2 above, it is definitively diagnosed as a metastatic lesion. If criterion 3 is met and consensus is reached during multidisciplinary consultation, it is also deemed metastatic. Conversely, if an imaging-suspicious lesion remains stable or shows no malignant progression during long-term follow-up (≥ 6 months) and cannot be explained by other benign lesions, it should remain under suspicion and be cautiously excluded. If follow-up confirms benignity (*e.g.*, cyst, hemangioma) or if the lesion remains stable long-term and is determined benign by multidisciplinary discussion, it is classified as negative. The final M stage classification for all cases will be adjudicated using this comprehensive gold standard, which will serve as the basis for evaluating the diagnostic performance of WB-DWI and PET-CT at initial diagnosis.

Sample size calculation

Given the retrospective nature of this study, the sample size was not determined prospectively but rather based on the available eligible consecutive cases in our hospital's imaging database during the study period. We systematically collected all newly diagnosed esophageal cancer patients with pathologically confirmed diagnoses who underwent both WB-DWI and PET-CT examinations between January 2023 and January 2025, resulting in an initial cohort of 96 cases. To control baseline confounding factors, cases were screened and matched using propensity score matching, yielding a matched analysis set comprising 64 patients (32 in the WB-DWI group and 32 in the PET-CT comparison group). A post-hoc power analysis was conducted. Based on Weijun Zhao *et al.'s* reported overall staging accuracy (P1) of approximately 85% for WB-DWI and 90% (P2) for PET-CT.[35] Retrospective calculations were performed using the paired proportion comparison formula at $\alpha = 0.05$ (two-tailed). Analysis indicates that the current matched sample size provides approximately 80% statistical power to detect the observed effect difference, confirming its adequacy for the comparative analysis.

Statistical methods

Statistical analysis methods will be rigorous and comprehensive. Quantitative data will be expressed as mean ± standard deviation or median (interquartile range), and intergroup comparisons will be performed using independent-samples t-tests or Mann-Whitney U tests. Qualitative data will be presented as frequencies (percentages), and intergroup comparisons will be conducted using chi-square tests or Fisher's exact test. Postoperative pathological staging (PTNM) and/or comprehensive clinical follow-up results for at least 6 months (for non-surgical patients) will serve as the diagnostic gold standard. Sensitivity, specificity, PPV, NPV, and accuracy for each staging indicator will be calculated separately for WB-DWI and PET-CT. Receiver operating characteristic (ROC) curve analysis was used to evaluate the diagnostic per-

TABLE 1A. Baseline characteristics before propensity score matching (unmatched cohort, n = 64)

Variable	WB-DWI group (n = 32)	PET-CT group (n = 32)	SMD
Age (years), mean ± SD	62.5 ± 9.1	65.8 ± 8.2	0.38
Gender, male, n (%)	23 (71.9)	25 (78.1)	0.14
Tumor location, n (%)			
Cervical	2 (6.3)	3 (9.4)	0.12
Thoracic	24 (75.0)	23 (71.9)	0.07
Abdominal	6 (18.7)	6 (18.7)	0.00
Pathological type, n (%)			
Squamous cell carcinoma	27 (84.4)	26 (81.3)	0.08
Adenocarcinoma	5 (15.6)	6 (18.7)	0.08
Preliminary clinical T stage, n (%)			
cT1-2	13 (40.6)	15 (46.9)	0.13
cT3-4	19 (59.4)	17 (53.1)	0.13
Preliminary clinical N stage, n (%)			
cN0	10 (31.3)	12 (37.5)	0.13
cN+	22 (68.7)	20 (62.5)	0.13
Tumor length (cm), mean ± SD	4.3 ± 1.6	4.9 ± 1.8	0.35
Degree of differentiation, n (%)			
High	4 (12.5)	5 (15.6)	0.09
Medium	18 (56.3)	19 (59.4)	0.06
Low	10 (31.3)	8 (25.0)	0.14
Body mass index (kg/m²), mean ± SD	21.9 ± 3.0	22.3 ± 2.9	0.14

SMD = standardized mean difference; WB-DWI = whole-body diffusion-weighted imaging

SMD > 0.3 indicates moderate to large imbalance. Before matching, notable imbalances were observed in age (SMD = 0.38) and tumor length (SMD = 0.35).

TABLE 1B. Baseline characteristics after propensity score matching (matched cohort, n = 64)

Variable	WB-DWI group (n = 32)	PET-CT group (n = 32)	SMD
Age (years), mean ± SD	63.2 ± 8.5	64.1 ± 7.9	0.11
Gender, male, n (%)	24 (75.0)	25 (78.1)	0.07
Tumor location, n (%)			
Cervical	2 (6.3)	3 (9.4)	0.12
Thoracic	25 (78.1)	23 (71.9)	0.14
Abdominal	5 (15.6)	6 (18.7)	0.08
Pathological type, n (%)			
Squamous cell carcinoma	28 (87.5)	26 (81.3)	0.17
Adenocarcinoma	4 (12.5)	6 (18.7)	0.17
Preliminary clinical T stage, n (%)			
cT1–2	14 (43.8)	13 (40.6)	0.06
cT3–4	18 (56.2)	19 (59.4)	0.06
Preliminary clinical N stage, n (%)			
cN0	11 (34.4)	10 (31.3)	0.07
cN+	21 (65.6)	22 (68.7)	0.07
Tumor length (cm), mean ± SD	4.5 ± 1.8	4.7 ± 1.6	0.12
Degree of differentiation, n (%)			
High	5 (15.6)	4 (12.5)	0.09
Medium	18 (56.3)	20 (62.5)	0.13
Low	9 (28.1)	8 (25.0)	0.07
Body mass index (kg/m²) mean ± SD	21.8 ± 3.2	22.2 ± 2.9	0.13

SMD = standardized mean difference; WB-DWI = whole-body diffusion-weighted imaging

After 1:1 nearest-neighbor matching with a caliper of 0.02, all variables achieved SMD < 0.2, with most < 0.1, indicating successful balance between the two groups. The matched cohort consisted of 32 patients per group (total n = 64).

TABLE 2. Comparison of diagnostic accuracy in T staging (n = 32, compared with pathology results)

Imaging technology	Number of accurate diagnoses	Diagnostic accuracy (%)
WB-DWI	23	71.9
PET-CT	27	84.4
$\chi^2 = 1.60$, $p = 0.206$		

WB-DWI = whole-body diffusion-weighted imaging

Accurate diagnosis refers to complete concordance between imaging T staging and pathological pT staging.

formance of both methods for N and M staging, with differences in area under the curve (AUC) assessed via DeLong's test. Inter-observer agreement was evaluated using the Kappa coefficient. All statistical analyses were performed using SPSS 26.0, with $p < 0.05$ considered statistically significant.

After propensity score matching, two independent and baseline-balanced groups were formed: the WB-DWI assessment group (n = 32) and the PET-CT assessment group (n = 32). For each diagnostic performance indicator (T stage accuracy, N stage sensitivity/specificity, M stage diagnostic efficacy, overall TNM accuracy), it was independently calculated based on the patients in each group and their corresponding gold standards. For example, the N stage sensitivity of WB-DWI was derived from the comparison of the WB-DWI interpretation results of the 32 patients in this group with the gold standard; the N stage sensitivity of PET-CT was derived from the comparison of the PET-CT interpretation results of the 32 patients in this group with the gold standard. Therefore, in the result table, each technique presents a set of diagnostic parameters, and the total number of diagnostic results is 64 (32 + 32). In Tables 2 to 5, "n = 64" indicates the total of the diagnostic results of the two techniques, rather than calculating a single indicator by mixing the data from the two groups.

Ethics statement

This study strictly adheres to medical ethics standards. The research protocol has been submitted to and approved by the Ethics Review Committee of Hai'an People's Hospital. Given that this study is a retrospective analysis involving no additional invasive procedures, and all data will be analyzed after de-identification, the Ethics Committee has approved an exemption from obtaining patient-informed consent. Throughout the study, patient privacy and data security will be rigorously protected, and all information will be used solely for this research.

Results

Baseline information

Before PSM, there were noticeable differences in several baseline variables between the two groups, particularly in age (SMD = 0.38) and tumor length (SMD = 0.29). After 1:1 nearest-neighbor matching with a caliper of 0.02, all variables achieved SMD <0.1, indicating successful balance (Table 1A and 1B). After propensity score matching (Table 1B), 32 patients were enrolled in each of the WB-DWI and PET-CT groups. As shown in Table 1, no statistically significant differences were observed between

TABLE 3. Comparative diagnostic performance of N staging (n = 64, all lymph node regions)

Imaging technology	Sensitivity (%)	Specificity (%)	PPV (%)	NPV (%)	Accuracy rate (%)
WB-DWI	78.1 (25/32)	87.5 (28/32)	86.2	80.0	82.8
PET-CT	90.6 (29/32)	87.5 (28/32)	87.9	90.3	89.1

PPV = positive predictive value; NPV = negative predictive value; WB-DWI = whole-body diffusion-weighted imaging

Numbers in parentheses indicate sample size. Sensitivity comparison: $c^2 = 4.01$, $p = 0.045$. In this table, the sensitivity of WB-DWI (78.1%, 25/32) is calculated based on the 32 patients in the WB-DWI group; the sensitivity of PET-CT (90.6%, 29/32) is calculated based on the 32 patients in the PET-CT group. The notation "n = 64" at the top of the table merely indicates that there are a total of 64 diagnostic results from both techniques (32 + 32), and it does not mean that the two groups of data are combined.

TABLE 4. Comparative diagnostic performance of M staging (n = 64, patient level)

Imaging Technology	Sensitivity (%)	Specificity (%)	PPV (%)	NPV (%)	Accuracy rate (%)
WB-DWI	83.3 (10/12)	92.3 (48/52)	76.9	94.1	90.6
PET-CT	91.7 (11/12)	94.2 (49/52)	84.6	96.1	93.8

PPV = positive predictive value; NPV = negative predictive value; WB-DWI = whole-body diffusion-weighted imaging

1. The gold standard is pathological confirmation or confirmation via follow-up. The diagnostic parameters for WB-DWI in the table are calculated based on the 32 patients in the WB-DWI group; the diagnostic parameters for PET-CT are calculated based on the 32 patients in the PET-CT group. The notation "n = 32" at the top of the table corresponds to the sample size of each group and does not indicate that data from the two groups have been combined.

2. Sensitivity comparisons were performed using Fisher's exact test, with $p = 1.000$.

3. Explanation of the denominators 12 and 52: Among the 32 patients in the WB-DWI group, 6 were gold standard positive (M1) and 26 were negative (M0); in the PET-CT group of 32 patients, 6 were gold standard positive (M1) and 26 were negative (M0). In the table, 10/12 represents 10 true positives in the WB-DWI group (out of a total of 12 actual positives, *i.e.*, the sum of positives from both groups), and 48/52 represents the sum of true negatives from both groups. To avoid misunderstanding, we clarify: the "12" in 10/12 refers to the total number of positive cases across both groups, and the "52" in 48/52 refers to the total number of negative cases across both groups. The sensitivity and specificity for both techniques were calculated based on data within their respective groups and then presented as aggregated results.

TABLE 5. Comparison of overall accuracy in TNM staging (n = 64)

Imaging technology	Number of accurate diagnoses	Overall staging accuracy rate (%)
WB-DWI	54	84.4
PET-CT	56	87.5

WB-DWI = whole-body diffusion-weighted imaging

Accurate diagnosis refers to complete agreement between the overall radiological staging and the final pathological/clinical staging (Stages I, II, III, or IV). 2. The accuracy rate for the WB-DWI group is calculated based on the 32 patients in that group; the accuracy rate for the PET-CT group is calculated based on the 32 patients in that group. The "n = 64" above the table represents the total number of diagnostic results for both techniques (32+32) and does not indicate a single accuracy rate calculated by combining data from both groups. 3. Intergroup comparisons were performed using the chi-square test: $\chi^2 = 0.22$, $p = 0.639$.

TABLE 6. Objective and subjective evaluation of image quality and examination duration

Evaluation Indicators	WB-DWI group (n = 32)	PET-CT group (n = 32)	F	*p*
Image signal-to-noise ratio, (mean ± SD)	15.2 ± 4.1	22.8 ± 5.6	t = 6.42	< 0.001
Subjective quality rating (5-point scale, mean ± SD)	3.8 ± 0.7	4.5 ± 0.5	t = 4.76	< 0.001
Inspection time (minute, mean ± SD)	28.5 ± 5.2	45.3 ± 8.7	t = 9.83	< 0.001

WB-DWI = whole-body diffusion-weighted imaging

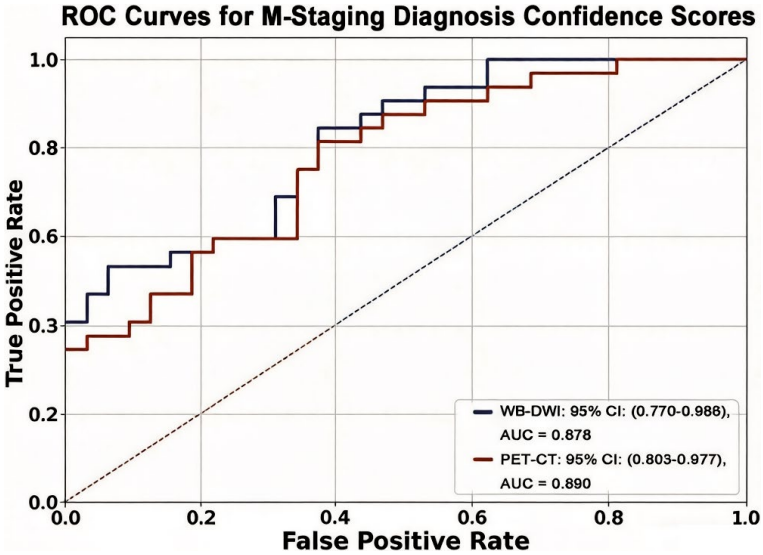

FIGURE 2. ROC curves for M-staging diagnosis confidence score.

AUC = area under the curve; CI = confidence interval; WB-DWI = whole-body diffusion-weighted imaging

the two groups in all 11 baseline characteristics, including age, gender, tumor location, histological type, clinical preliminary staging (cT, cN), tumor length, differentiation grade, macroscopic subtype, clinical symptoms, and body mass index ($p > 0.05$). This indicates successful matching and good comparability between groups.

Primary diagnostic performance indicators

Among the 64 matched patients after PSM, a total of 48 cases (75.0%) underwent radical esophageal cancer resection and achieved complete pathological T staging. Among them, 24 cases were in the WB-DWI group and 24 cases were in the PET-CT group. The remaining 16 patients did not undergo surgery due to distant metastasis (n = 10), locally advanced inoperability (n = 4), or poor general condition making them intolerant to surgery (n = 2). Their T staging was not included in the accuracy analysis. Therefore, the T staging accuracy rate in Table 2 was calculated based on 48 surgical patients (24 cases in each group). Regarding primary diagnostic efficacy indicators, the two imaging modalities exhibit distinct characteristics. The following diagnostic performance indicators were independently calculated for each of the two groups of patients (32 cases in each group) after matching. To facilitate presentation, the results of both techniques are listed in the table, and the total number of diagnostic cases is indicated as 64. As shown in Table 2, PET-CT demonstrated a trend toward higher accuracy (84.4%) in primary tumor T staging compared with WB-DWI (71.9%), though the difference was not statistically significant ($p > 0.05$). For regional lymph node (N staging) assessment, Table 3 data indicate that PET-CT significantly outperformed WB-DWI in sensitivity (90.6% *vs.* 78.1%, $p < 0.05$), while both techniques demonstrated comparable specificity (87.5% each). Regarding the detection of distant metastasis (M staging), Table 4 shows that both techniques performed well. PET-CT showed marginally higher values for sensitivity (91.7% *vs.* 83.3%) and specificity (94.2% *vs.* 92.3%), but the differences were not statistically significant. Regarding overall staging capability, Table 5 shows that WB-DWI and PET-CT demonstrated very similar overall TNM staging accuracy rates of 84.4% and 87.5%, respectively, with no statistically significant difference between them ($p > 0.05$).

Secondary technical and practical performance metrics

The contrast between the two modalities is even more pronounced in secondary technical and practical metrics. As shown in Table 6, PET-CT significantly outperformed WB-DWI in both objective image quality measures (SNR) and subjective ratings (5-point scale) ($p < 0.001$). However, WB-DWI demonstrated a clear advantage in efficiency, with a significantly shorter average scan duration than PET-CT (28.5 minutes *vs.* 45.3 minutes, $p < 0.001$).

The results of the interobserver agreement analysis (Table 7) indicate that both radiologists demonstrated good to excellent agreement when using the two staging techniques (all Kappa values > 0.60, $p < 0.001$). Specifically, the consistency coefficients for PET-CT (Kappa values ranging from 0.78 to 0.85) were generally slightly higher than those for WB-DWI (Kappa values ranging from 0.65 to 0.80) across all staging items.

Ultimately, the combined diagnostic performance for N staging and M staging was quantified via ROC curve analysis (Table 8, Figure 2). Both techniques demonstrated high accuracy for N staging: WB-DWI (AUC = 0.828, 95% CI: 0.715–0.941) and PET-CT (AUC = 0.890, 95% CI: 0.803–0.977) and M staging WB-DWI (AUC = 0.878, 95% CI: 0.770–0.986), PET-CT (AUC = 0.929, 95% CI: 0.850–1.000) both demonstrated high diagnostic value (AUC > 0.8). DeLong's test further confirmed that although PET-CT's AUC values were numeri-

cally higher than WB-DWI's, the diagnostic efficacy (AUC) differences between the two techniques for N staging and M staging were not statistically significant ($p > 0.05$).

Detection of small metastatic lymph nodes by WB-DWI and PET-CT

Among the 32 positive lymph node regions (N+) confirmed by pathology or follow-up, the median short diameter of the 25 metastatic lymph nodes detected by WB-DWI was 8.2 mm (range: 4.5–18.6 mm), while the median short diameter of the 7 false-negative lymph nodes missed by WB-DWI was 5.1 mm (range: 3.2–6.8 mm), and the difference was statistically significant ($p = 0.008$). The minimum short diameter of the metastatic lymph nodes detected by WB-DWI was 4.5 mm. In contrast, among the 29 metastatic lymph nodes detected by PET-CT, the minimum short diameter was 3.8 mm, and the median short diameter of the 3 false-negative lymph nodes was 4.2 mm (range: 3.5–5.0 mm). These results indicate that the size of lymph nodes is an important factor affecting the sensitivity of WB-DWI detection, especially for micro-metastatic lymph nodes with a short diameter of < 5 mm, where WB-DWI has a higher risk of missed diagnosis, as shown in Figure 9. The clinical utility of WB-DWI for dynamic treatment monitoring and restaging is illustrated in Figure 3.

Clinical implication: WB-DWI enables radiation-free, longitudinal assessment of tumor burden and treatment response. It can inform dynamic restaging and guide clinical decision-making, particularly when repeated imaging is required.

Discussion

This study systematically evaluated the diagnostic value of WB-DWI in staging newly diagnosed esophageal cancer through a meticulously designed retrospective comparative analysis, using the widely accepted PET-CT as the reference standard. Our core findings reveal a clinically significant picture: WB-DWI demonstrates diagnostic efficacy comparable to PET-CT for overall TNM staging and detection of distant metastases in esophageal cancer. However, PET-CT retains a certain sensitivity advantage in two critical aspects: precisely determining the local invasion depth of the primary tumor and identifying regional lymph node metastases. This outcome does not simply declare one superior to the other, but provides a nuanced, evidence-based rationale for the differentiated positioning and application of these two imaging modalities in clinical practice. The study's value lies not only in its comparative conclusions but also in its effective control of baseline confounding factors through propensity score matching. Furthermore,

TABLE 7. Inter-observer agreement analysis (Kappa Coefficient)

Evaluation Project	WB-DWI (κ-value)	PET-CT (κ-value)
T-Installment Assessment	0.65	0.78
N-period judgment	0.72	0.81
M-stage determination	0.80	0.85
Overall phasing assessment	0.75	0.82

WB-DWI = whole-body diffusion-weighted imaging

All Kappa values $p < 0.001$. A Kappa value > 0.75 indicates excellent agreement, while 0.60–0.75 indicates good agreement.

TABLE 8. ROC curve analysis results (diagnostic performance of N staging and M staging)

Imaging technology	Evaluation project	AUC (95% CI)	Yorden index
WB-DWI	N installments	0.828 (0.715–0.941)	0.656
PET-CT	N installments	0.890 (0.803–0.977)	0.781
WB-DWI	M installments	0.878 (0.770–0.986)	0.756
PET-CT	M installments	0.929 (0.850–-1.000)	0.859

AUC = area under the curve; CI = confidence interval; WB-DWI = whole-body diffusion-weighted imaging

The DeLong test revealed no statistically significant difference in AUC between the two techniques for N staging ($Z = 1.34$, $p = 0.180$) or for M staging ($Z = 1.12$, $p = 0.263$). # N and M staging diagnoses are based on qualitative assessments and do not utilize a single continuous variable; therefore, numerical cutoff values are not provided.

TABLE 9. Detection of small metastatic lymph nodes: comparison of node size between true-positive and false-negative cases on WB-DWI and PET-CT

Imaging modality	Detection outcome	Number of nodes (n)	Short-axis diameter (mm), median (range)	Statistical comparison (TP vs. FN)
WB-DWI	True-positive	25	8.2 (4.5–18.6)	$p = 0.008$*
	False-negative	7	5.1 (3.2–6.8)	
PET-CT	True-positive	29	— (3.8–†)	$p = 0.278$‡
	False-negative	3	4.2 (3.5–5.0)	

FN = false negative; TP = True positive: WB-DWI = whole-body diffusion-weighted imaging

* Comparison between TP and FN nodes on WB-DWI using Mann-Whitney U test.

† The upper range of TP node size on PET-CT was not systematically recorded; the smallest detected node was 3.8 mm.

‡ Comparison between TP and FN nodes on PET-CT was not statistically significant (Mann-Whitney U test, $p = 0.278$).w

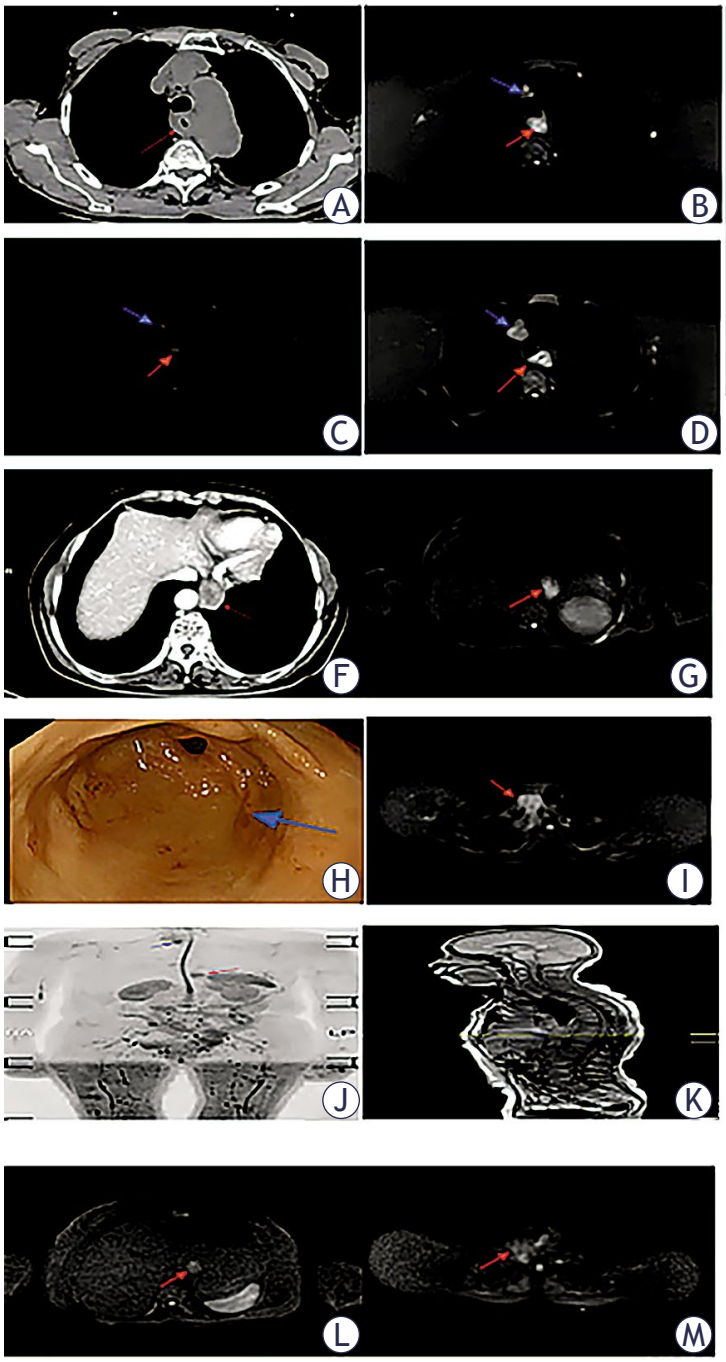

FIGURE 3. Serial whole-body DWI for dynamic treatment monitoring and restaging in two representative esophageal cancer patients.

Case 1 **(A-E)**: An 86-year-old female with newly diagnosed mid-upper esophageal cancer and mediastinal lymph node metastasis. **(A)** Baseline contrast-enhanced CT shows irregular wall thickening of the esophagus (red arrow) and a small pre-tracheal lymph node (blue arrow, indeterminate). **(B)** Baseline axial WB-DWI (b = 800 s/mm²) demonstrates marked hyperintensity of the primary tumor (red arrow) and the lymph node (blue arrow), indicating metastasis. **(C)** Whole-body DWI maximum intensity projection (MIP) delineates the longitudinal extent of the primary tumor (red arrows), correlating well with barium esophagography and endoscopy. **(D)** After 3 months of chemoradiotherapy, WB-DWI shows reduced signal intensity and size of both lesions, indicating partial response. **(E)** After 6 months, both lesions have progressed (increased size and signal), indicating disease progression.

Case 2 **(F-M)**: A 68-year-old female with lower esophageal cancer and right supraclavicular lymph node metastasis. **(F)** Baseline contrast-enhanced CT shows thickening and enhancement of the lower esophagus (red arrow). **(G)** Axial WB-DWI shows a hyperintense primary tumor (red arrow). **(H)** Endoscopy confirms the lower esophageal lesion (blue arrow). **(I)** Axial WB-DWI reveals hyperintense, partially confluent right supraclavicular lymph nodes (blue arrows). **(J)** Whole-body DWI MIP shows the primary tumor (red arrow) and supraclavicular nodes (blue arrows). **(K)** Sagittal WB-DWI localizer image corresponding to **(F)** can guide radiotherapy planning. **(L)** After 8 months of treatment, the primary tumor shows reduced signal and size (red arrow). **(M)** The supraclavicular nodes also show reduced signal (blue arrows), indicating treatment response.

it incorporates multidimensional practical indicators such as image quality, examination duration, and inter-observer consistency, resulting in a more comprehensive and clinically relevant assessment.

Focusing on primary tumor T staging, this study found that PET-CT demonstrated numerically higher accuracy than WB-DWI, although the difference did not reach statistical significance. This trend is closely related to the physical principles of DWI technology and the esophagus's unique anatomical structure. Accurate T staging relies heavily on clear visualization of the esophageal wall's layered structures, particularly infiltration of the submucosal and muscular layers.[36] Although high b-value DWI images can highlight tumor tissue through water diffusion restriction, their rela-

tively low spatial resolution and susceptibility to esophageal artifacts caused by peristalsis, cardiac pulsation, and respiratory motion can obscure fine esophageal wall layers. This may lead to overestimation or underestimation of invasion depth.[37,38] An earlier study by Penny Fang *et al*. indicated that conventional DWI-MRI achieves approximately 70–80% accuracy in T staging for esophageal cancer, with limitations primarily in distinguishing T2 from T3 disease.[39] In contrast, the diagnostic CT component of PET-CT, particularly when employing multi-phase contrast-enhanced scanning, provides superior anatomical detail. This facilitates visualization of esophageal wall thickening, rigidity, and blurred relationships with surrounding fat plane critically important for assessing T3/T4 lesions.[40,41] Our findings align with these technical characteristics. However, it must also be noted that relying solely on the metabolic information from PET-CT has limited value for T staging; its advantage lies more in the fusion interpretation with high-quality CT images. In the future, combining WB-DWI with high-resolution T2-weighted images or even esophagus-specific MRI sequences to construct a multiparametric MRI protocol may be a promising approach to improve the accuracy of local T staging. A similar approach has proven highly successful in the MRI assessment of rectal cancer.

Regarding the diagnosis of regional lymph node metastasis, a critical factor determining treatment strategies – our data demonstrate that PET-CT exhibits significantly higher sensitivity than WB-DWI. This undoubtedly represents one of PET-CT's core advantages as a gold standard for staging. The fundamental reason is that diagnosing lymph node metastasis relies not only on morphological criteria such as size and shape but also, critically, on its functional metabolic state.[42] Numerous studies, including those by Sankari Kommi and colleagues, confirm that 18F-FDG PET-CT can detect metabolically active metastatic lymph nodes before they become macroscopically enlarged. This capability alters N staging in approximately 20% of patients with esophageal cancer and influences treatment planning.[43] Our study observed a PET-CT N staging sensitivity of 90.6%, consistent with findings from multiple prior meta-analyses.[44] While WB-DWI can also suggest metastasis through restricted diffusion of water molecules within lymph nodes (high signal), the specificity of its signal changes remains challenging.[14] Benign lymph node lesions, such as reactive hyperplasia and inflammation, may also cause diffusion restriction, whereas certain micrometastases or lymph nodes with low cell density may not exhibit the typical high signal.[45] In this study, the sensitivity of WB-DWI in N staging was lower than that of PET-CT (78.1% *vs.* 90.6%). Part of the reason can be attributed to the limited detection ability of DWI for small-volume metastatic lymph nodes. Our data indicate that the minimum short diameter of metastatic lymph nodes detected by WB-DWI is 4.5 mm, and for micro-metastatic foci with a short diameter of <5 mm, the missed diagnosis rate significantly increases. This finding is consistent with previous studies: the spatial resolution of DWI (usually 1.5–2.0 mm within-layer resolution) and partial volume effect make it difficult to distinguish the signal of lesions smaller than 3–4 mm from background noise.[46] In contrast, PET-CT can detect lymph nodes with a short diameter of only 3–4 mm and active metabolism, thus having a greater advantage in the detection of early micrometastases. Clinically, for small lymph nodes that are highly suspected but negative in WB-DWI, it is recommended to further evaluate by combining endoscopic ultrasound or PET-CT. Notably, both techniques demonstrated identical specificity in this study, though neither achieved perfection. This suggests that false positives remain an inherent issue across all functional imaging modalities. In clinical practice, suspected lymph nodes identified by PET-CT or WB-DWI, particularly in critical regions, may still require confirmation via endoscopic ultrasound-guided fine-needle aspiration biopsy. This raises a deeper consideration: For N staging, future imaging advancements should not solely pursue higher sensitivity. Equally important may be enhancing specificity through quantitative parameters, such as ADC values, SUVmax ratios, or texture features to reduce unnecessary invasive procedures.

The most compelling and noteworthy finding in this study is the comparable performance of WB-DWI versus PET-CT in detecting distant metastases. No statistically significant differences were observed between the two modalities in sensitivity, specificity, or AUC. This result has significant implications for advancing the clinical application of WB-DWI. The presence of distant metastasis directly determines disease staging and the feasibility of curative treatment goals. WB-DWI inherently offers the advantage of performing whole-body screening in a single examination.[46] Our findings are supported by a series of recent studies. For instance, in a comparative study across multiple malignancies, Mahmoud Rezk *et al*. found that DWI-

based breast imaging (DWIBS) technology demonstrated comparable capability to PET-CT in detecting distant metastases.[47] Specifically for esophageal cancer, some scholars have explored the value of WB-DWI in detecting liver, bone, and non-regional lymph node metastases. Particularly for bone metastases, studies indicate that DWI is highly sensitive to abnormal signals from early intramedullary lesions, sometimes even outperforming bone scans and CT, and effectively complements PET-CT's metabolic detection capabilities.[48,49] The M staging gold standard in this study combined pathology and long-term follow-up, thereby enhancing the robustness of the conclusions. From a pathophysiological perspective, metastatic lesions typically exhibit high cellular density and active proliferation, manifesting on DWI as markedly restricted diffusion with high contrast, making them readily identifiable. Although PET-CT may hold an advantage over WB-DWI in detecting certain specific metastases (*e.g.*, pulmonary micronodules) due to CT's superior spatial resolution, WB-DWI's radiation-free nature and absence of radioactive tracer injection make it particularly suitable for patients requiring multiple follow-up examinations, younger patients, or those with contrast/tracer allergies.[50] This advantage is significant, directly impacting patient safety over the long term and the repeatability of examinations.

Beyond its diagnostic performance in initial staging, WB-DWI demonstrates significant value in longitudinal disease assessment. As shown in Figure 3, serial WB-DWI examinations can visually capture tumor burden changes, from baseline through partial response to progression in a radiation-free manner. This capability allows clinicians to dynamically revise the clinical stage based on treatment response, which is particularly important for patients receiving neoadjuvant therapy or palliative treatment where repeated imaging is required. In contrast, repeated PET-CT is often limited by cumulative radiation exposure and higher costs. Thus, WB-DWI may serve as a practical alternative for treatment monitoring and restaging, especially in resource-limited settings or for patients requiring frequent follow-up.

Beyond the core diagnostic metrics mentioned above, this study's evaluation of image quality, examination efficiency, and observer consistency provides indispensable practical information for clinical decision-making. Objective measurements and subjective ratings of image SNR consistently demonstrate superior image quality in PET-CT, primarily due to its technical maturity and higher spatial resolution.[51] However, a critical balancing factor is examination duration. This study clearly documented that WB-DWI examination times were significantly shorter than PET-CT. In a high-efficiency radiology department, shorter examination times translate to increased patient throughput and reduced appointment backlogs. Simultaneously, shorter examination times enhance patient comfort and cooperation, particularly for advanced cancer patients in poor physical condition. Inter-observer agreement analysis revealed both techniques achieved good to excellent consistency, though PET-CT generally yielded slightly higher Kappa values. This suggests PET-CT interpretation may hold greater potential for standardization due to its distinct imaging features (*e.g.*, hypermetabolic lesions) and accumulated diagnostic expertise. Nevertheless, WB-DWI achieved Kappa values at the "good" level or higher, indicating that radiologists can reliably interpret WB-DWI images with appropriate training, laying the groundwork for its clinical adoption. These "non-diagnostic" yet critical factors collectively paint a more complete picture: PET-CT offers more "refined" diagnostic information in certain aspects, while WB-DWI provides a faster, radiation-free alternative or supplement with reliable diagnostic efficacy, particularly for whole-body screening.

Placing this study within a broader academic context reveals its innovation and significance across multiple dimensions. Methodologically, propensity score matching to address selection bias inherent in retrospective studies provides a more equitable basis for comparing the WB-DWI and PET-CT groups. This approach, not widely adopted in previous comparative studies, enhances the credibility of the conclusions. In terms of research content, we transcended the traditional paradigm of solely comparing diagnostic sensitivity and specificity. By incorporating metrics directly impacting clinical adoption and workflow, such as image quality, examination time, and observer consistency into our systematic evaluation, the study conclusions offer more direct reference value for hospital administrators and clinicians. Clinically, this study provides evidence for individualized imaging pathways in esophageal cancer. For patients seeking a cure and requiring precise N staging to determine the necessity of neoadjuvant therapy, PET-CT may remain the preferred choice. However, for staging evaluation, treatment follow-up, and especially for patient groups needing to avoid radiation exposure, WB-DWI is un-

doubtedly an attractive alternative. Furthermore, considering the high cost and limited availability of PET-CT equipment, WB-DWI emerges as a more accessible MRI technique, highlighting its value in resource-constrained regions.

Looking ahead, several valuable research directions can be extended based on the findings of this study. One is to explore the correlation between WB-DWI quantitative parameters, such as lesion ADC values and their histogram characteristics and tumor pathological grading, treatment response, and prognosis. Preliminary studies exist, such as Qingxue Cong *et al.'s* investigation into the relationship between esophageal cancer ADC values and tumor invasiveness, which will help advance WB-DWI from morphofunctional diagnosis to higher-level applications, such as prognosis prediction and treatment efficacy monitoring.[52] Second, investigating the value of integrating or combining WB-DWI with PET-CT. Rather than choosing one over the other, this considers whether their information complements each other in complex cases, achieving a "1+1>2" diagnostic effect. For instance, combining PET's high metabolic specificity with DWI's high soft tissue contrast may further enhance diagnostic confidence for peritoneal and small lymph node metastases. Third, with the explosive growth of artificial intelligence, particularly deep learning, in medical image analysis, developing automated segmentation, feature extraction, and staging prediction models based on WB-DWI or PET-CT images holds promise. This could partially address interobserver variability and uncover deep imaging biomarkers invisible to the human eye, potentially representing a next-generation technological breakthrough for more precise, objective staging.

Of course, this study also has certain limitations that should be considered when interpreting the results. First, despite the use of propensity score matching (PSM), the retrospective study design itself cannot completely eliminate all potential biases. Second, although the sample size was estimated and met statistical requirements, a larger multicenter sample would provide more robust estimates and enable more meaningful subgroup analyses. As Yousafzai *et al*. noted in their discussion of emerging cancer technologies, standardization of analytical methods and rigorous external validation are critical steps for any diagnostic technology to advance toward routine clinical application.[53] Third, the gold standard pathological TNM staging was not available for all patients. For non-surgical patients, we relied on comprehensive clinical follow-up diagnoses. Despite extended follow-up periods and strict criteria, this approach inherently differs from pathological standards. Fourth, the WB-DWI technical parameters and interpretation experience in this study are based on a single center. Extending these conclusions to other institutions using different MRI equipment, sequences, and parameters may require further validation. Fifth, the accuracy of T staging in this study was derived based on the examination protocol that included diagnostic enhanced CT. This result may not be applicable to the routine PET/CT examinations where only low-dose non-contrast CT is used. For units where diagnostic CT cannot be performed due to equipment limitations, the value of PET/CT for T staging will be significantly reduced. In such cases, it is recommended that patients undergo separate enhanced CT or MRI examinations. Sixth, in this study, the accuracy analysis of T staging only included patients who underwent surgery (accounting for 75.0% of the matched cohort). This may introduce selection bias, as surgical patients are usually staged relatively early or are potentially resectable. For patients with advanced disease who did not undergo surgery, the T staging cannot obtain the pathological gold standard. Therefore, the conclusions of this study have limited value for the assessment of T staging in locally advanced and unresectable esophageal cancer. Seventh, due to the retrospective design and incompatible DICOM archiving formats between PET-CT and WB-DWI workstations, we were unable to retrieve directly comparable PET-CT images for the same patients at identical time points. Therefore, Figure 3 presents only WB-DWI serial images to demonstrate its clinical utility in treatment monitoring, but side-by-side PET-CT/WB-DWI comparisons are not provided. Future prospective studies should include paired imaging to enable direct visual comparison.

Conclusions

In summary, this study rigorously demonstrated, through comparative analysis, that WB-DWI is an effective tool for staging esophageal cancer. It exhibits comparable efficacy to PET-CT in overall staging and detection of distant metastases, while offering distinct advantages of radiation-free imaging and a shorter examination duration. Although slightly less sensitive than PET-CT for local T staging and regional lymph node staging, it performs well overall and is well-suited for its critical appli-

cation in specific clinical scenarios. The findings not only enrich the evidence base for esophageal cancer imaging assessment but also provide practical guidance for clinicians to individualize the selection of optimal imaging protocols based on patient-specific conditions, healthcare resources, and technical capabilities. Advances in imaging technology ultimately serve more precise diagnosis and treatment, and WB-DWI, with its unique value, is securing a solid position within the multidisciplinary diagnostic and therapeutic landscape of esophageal cancer.

Acknowledgment

Scientific research project of Nantong Municipal Health Commission (NO. MSZ2024085)

Author contribution

[Xiaohu Xu, Rong Yu, Qiulian Ma]: Developed and planned the study, performed experiments, and interpreted results. Edited and refined the manuscript with a focus on critical intellectual contributions.

[Tingting Yin, Haisheng Chen, Ye Qian]: Participated in collecting, assessing, and interpreting the date. Made significant contributions to date interpretation and manuscript preparation.

[Hong Li, Yachun Xu]: Provided substantial intellectual input during the drafting and revision of the manuscript.

Data availability statement

The data supporting the findings of this study can be obtained from the corresponding author, upon request.

References

1. Zhang Y, He S, Chen J, Liu G, Luo Y, Song Y, et al. Artificial intelligence-assisted enhancement of prostate volume metrics in the diagnosis of clinically significant prostate cancer: a retrospective analysis. *Quant Imaging Med Surg* 2025; **15:** 1641-52. doi: 10.21037/qims-24-1015
2. Pozaruk A, Atamaniuk V, Pawar K, Carey A, Cheng J, Cholewa M, et al. Correlations between MR apparent diffusion coefficients and PET standard uptake values in simultaneous MR-PET imaging of prostate cancer. *Int J Mol Sci* 2025; **26:** 905. doi: 10.3390/ijms26030905
3. Dai X, Ye X, Ren J, Yang J, Zhou Y, Ma Z, et al. Construction of the preoperative staging prediction model for cervical cancer based on deep learning and MRI: a retrospective study. *Front Oncol* 2025; **15:** 1557486. doi: 10.3389/fonc.2025.1557486
4. Alkarn A, Stapleton LJ, Eleftheriou D, Stewart L, Chalmers GW, Hamed A, et al. Real-life pre-operative nodal staging accuracy in non-small cell lung cancer and its relationship with survival. *Diagnostics (Basel)* 2025; **15:** 430. doi: 10.3390/diagnostics15040430
5. Wang W, Ding Y, Jiang W, Li X. Can cervical lymph node metastasis increase the risk of distant metastasis in papillary thyroid carcinoma? *Front Endocrinol (Lausanne)* 2022; **13:** 917794. doi: 10.3389/fendo.2022.917794
6. Detterbeck FC, Woodard GA, Bader AS, Dacic S, Grant MJ, Park HS, et al. The proposed ninth edition TNM classification of lung cancer. *Chest* 2024; **166:** 882-95. doi: 10.1016/j.chest.2024.05.026
7. Ebner R, Sheikh GT, Brendel M, Ricke J, Cyran CC. ESR essentials: staging and restaging with FDG-PET/CT in oncology—practice recommendations by the European Society for Hybrid, Molecular and Translational Imaging. *Eur Radiol* 2025; **35:** 1894-902. doi: 10.1007/s00330-024-11094-8
8. Dien Esquivel MF, AlMutawa A, Amirabadi A, Weitzman S, Buhtoiarov I, Doria AS, et al. Value of 18F-FDG PET/CT scans in staging and follow-up of pediatric Langerhans cell histiocytosis: comparison to CT and/or MRI. *Children (Basel)* 2025; **12:** 1089. doi: 10.3390/children12081089
9. Gitau SN, Shah J, Olwit W, Saeed S, Mansour MH, Makhdomi K. Supraclavicular nodal metastasis at primary staging of prostate cancer using (18)F-PSMA-1007 PET/CT. *EJNMMI Rep* 2025; **9:** 9. doi: 10.1186/s41824-025-00241-z
10. Pahk K, Ryu KJ, Joung C, Kwon HW, Lee S, Park H, et al. Metabolic activity of visceral adipose tissue is associated with metastatic status of lymph nodes in endometrial cancer: a (18)F-FDG PET/CT study. *Int J Environ Res Public Health* 2021; **19:** 92. doi: 10.3390/ijerph19010092
11. Salehjahromi M, Karpinets TV, Sujit SJ, Qayati M, Chen P, Aminu M, et al. Synthetic PET from CT improves diagnosis and prognosis for lung cancer: proof of concept. *Cell Rep Med* 2024; **5:** 101463. doi: 10.1016/j.xcrm.2024.101463
12. Hussain D, Abbas N, Khan J. Recent breakthroughs in PET-CT multimodality imaging: innovations and clinical impact. *Bioengineering (Basel)* 2024; **11:** 1213. doi: 10.3390/bioengineering11121213
13. Frolli A, Varvello S, Balbo Mussetto A, Gottardi D, Bullo M, Marini S, et al. A radiation-free approach based on whole-body MRI shows high accuracy in the follow-up of lymphoma patients: a single-center retrospective study. *J Clin Med* 2024; **13:** 3637. doi: 10.3390/jcm13133637
14. Yoshida S, Takahara T, Arita Y, Sakaino S, Katahira K, Fujii Y. Whole-body diffusion-weighted magnetic resonance imaging: diagnosis and follow-up of prostate cancer and beyond. *Int J Urol* 2021; **28:** 502-13. doi: 10.1111/iju.14497
15. Mayer P, Kraft A, Witzel HR, Marnet N, Hörner N, Roth W, et al. Restricted water diffusion in diffusion-weighted magnetic resonance imaging in pancreatic cancer is associated with tumor hypoxia. *Cancers (Basel)* 2020; **13:** 89. doi: 10.3390/cancers13010089
16. Messina C, Bignone R, Bruno A, Bruno A, Bruno F, Calandri M, et al. Diffusion-weighted imaging in oncology: an update. *Cancers (Basel)* 2020; **12:** 1493. doi: 10.3390/cancers12061493
17. De Vuysere S, Vandecaveye V, De Bruecker Y, Carton S, Vermeiren K, Tollens T, et al. Accuracy of whole-body diffusion-weighted MRI in diagnosis, staging and follow-up of gastric cancer compared with CT: a pilot study. *BMC Med Imaging* 2021; **21:** 18. doi: 10.1186/s12880-021-00550-2
18. Albano D, Bruno A, Patti C, Micci G, Midiri M, Tarella C, et al. Whole-body magnetic resonance imaging in lymphoma: state of the art. *Hematol Oncol* 2020; **38:** 12-21. doi: 10.1002/hon.2676
19. Balestrucci G, Patanè V, Giordano N, Russo A, Urraro F, Nardone V, et al. Evolving paradigms in gastric cancer staging: from conventional imaging to advanced MRI and artificial intelligence. *Diagnostics (Basel)* 2026; **16:** 284. doi: 10.3390/diagnostics16020284
20. Kataoka M, Iima M, Miyake KK, Honda M. Multiparametric approach to breast cancer with emphasis on magnetic resonance imaging in the era of personalized breast cancer treatment. *Invest Radiol* 2024; **59:** 26-37. doi: 10.1097/rli.0000000000001044
21. Long Y, Shi R. Prognostic value of the cholesterol-dependent nutritional prognostic index in patients receiving adjuvant chemotherapy after radical esophageal cancer treatment. *Eur J Med Res* 2024; **29:** 550. doi: 10.1186/s40001-024-02136-4

22. Xie W, Bai X, Liu M, Shangguan H, Zhan Y, Wu X, et al. Benign and malignant bone lesion diagnosis based on self-supervised and radiomics fusion using SPECT/CT images. *J Bone Oncol* 2025; **55:** 100723. doi: 10.1016/j.jbo.2025.100723

23. Yu X, Wang J, Huang L, Xie L, Su Y. Predictive value of 18F-FDG PET/CT metabolic parameters for lymph node metastasis of non-small cell lung cancer. *Biomark Med* 2025; **19:** 35-41. doi: 10.1080/17520363.2024.2443379

24. Gao J, Shi Y, Niu R, Shao X, Shao X. Association analysis of maximum standardized uptake values based on (18)F-FDG PET/CT and EGFR mutation status in lung adenocarcinoma. *J Pers Med* 2023; **13:** 396. doi: 10.3390/jpm13030396

25. Li S, Liu J, Zhang Z, Wang W, Lu H, Lin L, et al. Added-value of 3D amide proton transfer MRI in assessing prognostic factors of cervical cancer: a comparative study with multiple model diffusion-weighted imaging. *Quant Imaging Med Surg* 2023; **13:** 8157-72. doi: 10.21037/qims-23-324

26. Yang C, Tian S, Du W, Liu M, Hu R, Gao B, et al. Glymphatic function assessment with diffusion tensor imaging along the perivascular space in patients with major depressive disorder and its relation to cerebral white-matter alteration. *Quant Imaging Med Surg* 2024; **14:** 6397-412. doi: 10.21037/qims-24-510

27. Rice TW, Ishwaran H, Ferguson MK, Blackstone EH, Goldstraw P. Cancer of the esophagus and esophagogastric junction: an eighth edition staging primer. *J Thorac Oncol* 2017; **12:** 36-42. doi: 10.21037/qims-24-510

28. Duarte AL, Dias JL, Cunha TM. Pitfalls of diffusion-weighted imaging of the female pelvis. *Radiol Bras* 2018; **51:** 37-44. doi: 10.1590/0100-3984.2016.0208

29. Wang J, Chen B, Zhu J, Zhang J, Jiang R. Intelligent diagnosis value of preoperative T staging of colorectal cancer based on MR medical imaging. *Front Genet* 2023; **14:** 1119990. doi: 10.3389/fgene.2023.1119990

30. Fajardo A, Jara Noel K, Azevedo A, Marcotte E, Darvish M, Rocha G, et al. Concordance between clinical and pathological diagnosis of stromal corneal dystrophies in a large case series. *Cornea* 2025; **44:** 1528-31. doi: 10.1097/ico.0000000000003980

31. Zhong H, Huang Q, Zheng X, Wang Y, Qian Y, Chen X, et al. Generation of virtual monoenergetic images at 40 keV of the upper abdomen and image quality evaluation based on generative adversarial networks. *BMC Med Imaging* 2024; **24:** 151. doi: 10.1186/s12880-024-01331-3

32. Wang CY, Xu G, Gao C, Wang D. Esophageal metastases from primary lung cancer: a case report. *J Med Case Rep* 2021; **15:** 265. doi: 10.1186/s13256-021-02765-x

33. Sakata A, Fushimi Y, Oshima S, Uto M, Mineharu Y, Nakajima S, et al. RANO 2.0: critical updates and practical considerations for radiological assessment in neuro-oncology. *Jpn J Radiol* 2025; **43:** 1557-74. doi: 10.1007/s11604-025-01821-6

34. Matute-González M, Ronot M, Chernyak V, Sangro B, Rimola J. Response evaluation to systemic therapy in HCC: current challenges and future perspectives. *Hepatology* 2025. doi: 10.1097/hep.0000000000001621

35. Zhao W, Huang J, Chen Y, Lu J, Hu W. The clinical value of CT and MRI in preoperative TNM staging of esophageal cancer. *Front Med (Lausanne)* 2025; **12:** 1637764. doi: 10.21037/atm-20-2909

36. Schmidlin EJ, Gill RR. New frontiers in esophageal radiology. *Ann Transl Med* 2021; **9:** 904. doi: 10.3390/cancers17081351

37. Haefliger L, Chapellier P, Vietti Violi N, Ledoux JB, Mantziari S, Schäfer M, et al. Advancing esophageal cancer staging and restaging: the role of MRI in precision diagnosis. *Cancers (Basel)* 2025; **17:** 704. doi: 10.1007/s10388-019-00704-w

38. Shuto K, Kono T, Shiratori T, Akutsu Y, Uesato M, Mori M, et al. Diagnostic performance of diffusion-weighted magnetic resonance imaging in assessing lymph node metastasis of esophageal cancer compared with PET. *Esophagus* 2020; **17:** 239-49. doi: 10.1016/j.ijrobp.2018.02.029

39. Fang P, Musall BC, Son JB, Moreno AC, Hobbs BP, Carter BW, et al. Multimodal imaging of pathologic response to chemoradiation in esophageal cancer. *Int J Radiat Oncol Biol Phys* 2018; **102:** 996-1001. doi: 10.3389/fonc.2022.844702

40. Wang F, Guo R, Zhang Y, Yu B, Meng X, Kong H, et al. Value of (18)F-FDG PET/MRI in the preoperative assessment of resectable esophageal squamous cell carcinoma: a comparison with (18)F-FDG PET/CT, MRI, and contrast-enhanced CT. *Front Oncol* 2022; **12:** 844702. doi: 10.3390/diagnostics15070908

41. Kuhtić I, Mandić Paulić T, Kovačević L, Badovinac S, Jakopović M, Dobrenić M, et al. Clinical TNM lung cancer staging: a diagnostic algorithm with a pictorial review. *Diagnostics (Basel)* 2025; **15:** 908. doi: 10.3390/diagnostics15070908

42. Peng G, Zhan Y, Wu Y, Zeng C, Wang S, Guo L, et al. Radiomics models based on CT at different phases predicting lymph node metastasis of esophageal squamous cell carcinoma (GASTO-1089). *Front Oncol* 2022; **12:** 988859. doi: 10.3398/fonc.2022.988859

43. Kommi S, Rallapeta RP, Subramanian BV, Yadagiri LA, Hulikal N, Chandramaliteeswaran C, et al. Utility of [18F]FDG-PET/CT in initial staging and management of patients with esophageal carcinoma: a tertiary care center experience. *Indian J Nucl Med* 2024; **39:** 329-34. doi: 10.4103/ijnm.ijnm_118_23

44. Yu J, Tan XG, Li F. Evaluation of the efficacy of (18)F-FDG PET-CT combined with CT in detecting lymph node metastasis in liver cancer. *Front Oncol* 2025; **15:** 1636566. doi: 10.3389/fonc.2025.1636566

45. Ingenerf M, Rübenthaler J, Wenter V, Zacherl M, Völter F, Winkelmann M, et al. Evaluation of MRI in the diagnostic accuracy of extrahepatic metastases in neuroendocrine tumors in comparison with the reference standard somatostatin-receptor PET/CT. *Front Oncol* 2023; **13:** 1194152. doi: 10.3389/fonc.2023.1194152

46. Cattabriga A, Renzetti B, Galuppi F, Bartalena L, Gaudiano C, Brocchi S, et al. Multiparametric whole-body MRI: a game changer in metastatic prostate cancer. *Cancers (Basel)* 2024; **16:** 2531. doi: 10.3390/cancers16142531

47. Rezk M, Nasr I, Ali I, Abdelhamed H. Comparative study between (18)F FDG-PET/CT and whole-body MRI DWIBS in assessment of recurrent breast cancer (prospective, comparative, cross-sectional study design). *Indian J Nucl Med* 2019; **34:** 1-9. doi: 10.4103/ijnm.IJNM_121_18

48. Murakami T, Shimizu H, Nojima H, Shuto K, Usui A, Kosugi C, et al. Diffusion-weighted magnetic resonance imaging for the diagnosis of lymph node metastasis in patients with biliary tract cancer. *Cancers (Basel)* 2024; **16:** 3143. doi: 10.3390/cancers16183143

49. Jacobs MA, Macura KJ, Zaheer A, Antonarakis ES, Stearns V, Wolff AC, et al. Multiparametric whole-body MRI with diffusion-weighted imaging and ADC mapping for the identification of visceral and osseous metastases from solid tumors. *Acad Radiol* 2018; **25:** 1405-14. doi: 10.1016/j.acra.2018.02.010

50. Zhang B, Zhang L, Bian B, Lin F, Zhu Z, Wang J. Diagnostic value of WB-DWI versus (18)F-FDG PET/CT for the detection of multiple myeloma. *Indian J Cancer* 2023; **60:** 303-9. doi: 10.4103/ijc.IJC_1129_20

51. Yang H, Chen S, Qi M, Chen W, Kong Q, Zhang J, et al. Investigation of PET image quality with acquisition time/bed and enhancement of lesion quantification accuracy through deep progressive learning. *EJNMMI Phys* 2024; **11:** 7. doi: 10.1186/s40658-023-00607-x

52. Cong Q, Li G, Wang Y, Zhang S, Zhang H. DW-MRI for esophageal squamous cell carcinoma: correlations between ADC values with histologic differentiation and VEGF expression. *Oncol Lett* 2019; **17:** 2770-6. doi: 10.3892/ol.2019.9934

53. Yousafzai U, Najia J, Ali SL, Awais A, Amir H. Computer-aided discovery of novel COX-2 inhibitors for anti-inflammatory therapy using pharmacophore modelling, molecular docking, ADMET, and virtual screening. *Adv Mod Biomed* 2025; **1:** 25-38. doi: 10.64229/md3sjz95

RADIOLOGY AND ONCOLOGY Radiology and Oncology | Ljubljana | Slovenia | www.radioloncol.com

research article

Visual versus automated CT perfusion for outcome prediction in anterior circulation stroke treated with mechanical thrombectomy

Igor Rigler[1], Tina Gspan[1], Alja Longo[2], Janja Pretnar Oblak[1,3]

[1] Clinical Department of Vascular and Intensive Neurology Therapy, Neurology Clinic, University Medical Centre Ljubljana, Ljubljana, Slovenia

[2] Clinical Institute of Radiology, Institute of Neuroradiology, University Medical Centre Ljubljana, Ljubljana, Slovenia

[3] Department of Neurology, Faculty of Medicine, University of Ljubljana, Ljubljana, Slovenia

Radiol Oncol 2026; 60(3): 394-401.

Received 3 March 2026
Accepted 18 April 2026

Correspondence to: Igor Rigler, M.D., Clinical Department of Vascular and Intensive Neurology Therapy, Neurology Clinic, University Medical Centre Ljubljana, Slovenia. E-mail: igor.rigler@kclj.si

Disclosure: No potential conflicts of interest were disclosed.

Background. The prognostic value of simple visual assessment of CT perfusion (CTP) for predicting clinical outcomes has already been demonstrated in stroke patients undergoing mechanical thrombectomy (MT). Automated software, however, has become the dominant method of CTP evaluation. The aim of the study was to compare the prognostic accuracy of visually graded CTP maps with automated CTP analysis on clinical outcomes in anterior circulation stroke patients treated with MT.

Patients and methods. In the single centre we retrospectively analysed consecutive patients with anterior circulation large-vessel occlusion treated with MT. Baseline imaging included non-contrast brain CT, CT angiography (CTA) with collateral status (CS) and CTP. Time to peak (TTP) maps were visually graded on a four-level ordinal scale based on estimated penumbra. Automated CTP was processed with syngo.via (SYV) using default thresholds and classified on a comparable ordinal scale. The primary endpoint was favourable 90-day functional outcome (Rankin Scale (mRS) ≤ 3).

Results. We included 579 patients. Agreement between visual and automated CTP was fair ($\kappa = 0.36$). Both methods were significantly associated with favourable outcome ($p < 0.01$), with visual grading showing a slightly stronger association (Pearson $\chi^2 = 30$ vs. 22). In multivariable models, visual CTP remained an independent predictor, whereas automated CTP lost significance when CS was included.

Conclusions. Visual CTP grading provided a slightly better prognostic performance than automated CTP. Visual CTP assessment is a simple, accessible and clinically meaningful tool for both treatment decision making and outcome prediction in anterior circulation stroke treated with MT.

Key words: CT perfusion; acute stroke; mechanical thrombectomy; prognosis

Introduction

CT perfusion (CTP) is increasingly used in acute ischemic stroke workflow to estimate infarct core and salvageable penumbra. Automated CTP gained importance after DAWN and DEFUSE-3 trials established its role in selecting patients for mechanical thrombectomy (MT) beyond 6 hours and EXTEND trial demonstrated its utility for extending intravenous thrombolysis up to 9 hours or after wake-up stroke.[1-3] More recently, RESCUE-Japan LIMIT, SELECT2 and ANGEL-Alberta Stroke Program Early CT Score (ASPECTS) trials broadened MT eligibility to patients with large

estimated ischemic cores using either automated CTP-derived core volumes or markedly reduced ASPECTS, though outcomes remained considerably poorer than in the small core patients.[4-6]

CTP therefore contributes not only to treatment selection but also enables prognostic assessment, particularly in patients with advanced age, frailty or significant comorbidities. However, automated CTP maps vary substantially between software platforms, reflecting differences in acquisition assumptions, deconvolution models and perfusion thresholds.[7] Comparative studies show only moderate agreement in core and penumbra estimation and limited spatial concordance with final infarction[8-10], raising concerns about the consistency of automated CTP for prognostication.

Visual CTP assessment remains widely used because it is rapid, easily interpretable and independent of software-specific thresholds. Time-to-peak (TTP) maps, in particular, provide a clear contrast between normal and critically delayed perfusion, while TTP »black-hole« regions have been linked with severely impaired hemodynamics.[11] We previously demonstrated that a semi-quantitative TTP grading scale independently predicted 90-day outcome in MT treated anterior circulation stroke.[12]

Nevertheless, direct comparisons between visual and automated CTP remain limited. Given the dominance of automated analysis in clinical trials, evaluation of whether visual assessment retains prognostic impact compared to automated analysis is clinically relevant. This study compares visual TTP grading with automated CTP analysis using syngo.via (SYV) in a large, real-world cohort of anterior-circulation stroke patients treated with MT.

Patients and methods

Study design and patient selection

We performed a retrospective, single-centre observational study of consecutive patients with anterior circulation large-vessel occlusion (LVO) stroke treated with MT between January 2013 and December 2020. All patients were managed according to contemporary international stroke guidelines and were discussed within the hospital multidisciplinary stroke team.

Patients were included if they had an anterior circulation LVO (intracranial internal carotid artery, M1 or proximal M2 segment of the middle cerebral artery) on baseline CT angiography (CTA), underwent MT and had a documented 90-day modified Rankin Scale (mRS). We excluded patients with posterior circulation stroke and isolated distal medium-vessel occlusions. Separate models were constructed for visual and automated CTP, each including only patients with available respective perfusion data.

The National Medical Ethics Committee of Slovenia approved the study (ethical approval number: 0120-354/2019/4). The study adhered to the Declaration of Helsinki.

Imaging protocol

Baseline imaging included non-contrast CT (CT), CTA, and CTP as part of the standard acute ischemic stroke imaging protocol. Imaging parameters and scanner hardware remained stable over the study period. Alberta Stroke Program Early CT Score (ASPECTS) was scored on CT. CTA was used to determine occlusion site and collateral status. CTP covered the supratentorial brain and was performed immediately after CTA.

Radiological studies were performed using a 40-row spiral CT unit (Somatom Sensation Open 40, Siemens Healthineers, Erlangen, Germany). Perfusion CT (80 kVp, 209 mAs) consisted of a 40-second series with 1 rotation/s during intravenous administration of iodinated contrast media. We injected 40 ml of nonionic low-osmolar iodinated contrast iopromide (370 mg/l, Ultravist; Bayer Healthcare, Leverkusen, Germany) antecubitally at a flow rate of 6 ml/s, followed by a 40-ml saline flush. Four 5-mm-thick slices were selected above the orbits at the level of the basal ganglia and the third ventricle. CTA was performed by injecting 80 ml of contrast media at a rate of 5 ml/s, followed by a craniocaudal scan from the vertex to the aortic arch with scanning parameters 120 kV, 150 mAs, gantry rotation time 0.5 s, collimation 40 × 0.6 mm, pitch 1.2 and field of view (FOV) 200 mm. Sections were reconstructed at 0.75 mm with a reconstruction increment of 0.4 mm. Additionally, maximum intensity projection (MIP) images in the coronal and axial planes were produced.

Visual CT perfusion (CTP) assessment

Visual evaluation focused on time-to-peak (TTP) maps reviewed independently by a single reader with specialization in neuroradiology, with at least 5 years of clinical experience, who was blinded to clinical outcomes. Hypoperfusion was graded on a four-level ordinal scale reflecting the estimated

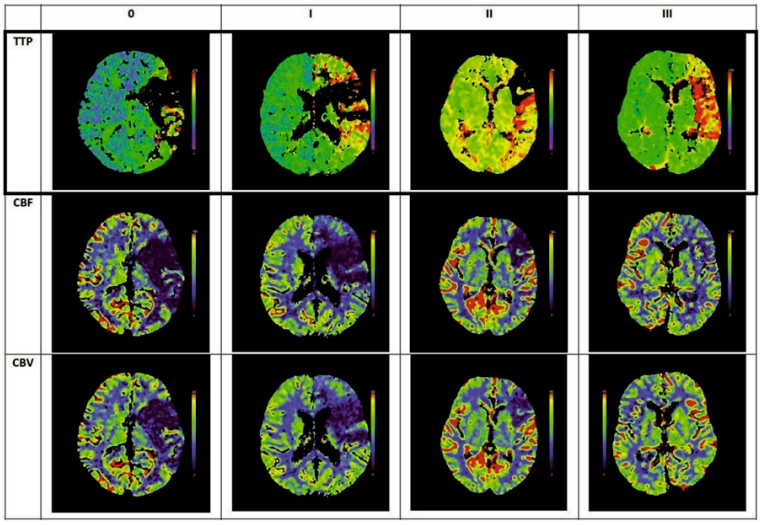

FIGURE 1. Examples of time to peak (TTP) based CT perfusion (CTP) maps divided into four categories, according to the percentage of »black hole« estimation in the hypoperfused region, with their corresponding cerebral blood flow (CBF) and cerebral blood volume (CBV) perfusion images.

TABLE 1. Distribution of patients according to visual CT perfusion (CTP) and outcome

Visual CTP (penumbra category)	mRS ≤ 3	mRS > 3	Total
0–25% penumbra	14	27	41
25–50% penumbra	26	27	53
50–75% penumbra	84	60	144
75–100% penumbra	215	86	301
Total	**339**	**200**	**539**

Pearson $\chi^2 = 29.545$, $p < 0.001$

TABLE 2. Distribution of patients according to automated CT perfusion (CTP) and outcome

Automated CTP (penumbra category)	mRS ≤ 3	mRS > 3	Total
0–25% penumbra	2	7	9
25–50% penumbra	14	18	32
50–75% penumbra	71	65	136
75–100% penumbra	239	112	351
Total	**326**	**202**	**528**

Pearson $\chi^2 = 21.562$, $p < 0.001$

proportion of penumbra within the affected vascular territory (0–25%, 25–50% ,50–75%, 75–100%) (Figure 1). Grading was based on the extent of markedly delayed - »black-hole« - TTP signal. This variable is referred to as *visual CTP.*

Automated CT perfusion (CTP) analysis

Automated perfusion analysis was performed using SYV CT Neuro Perfusion (Siemens Healthineers, version VB40) with unchanged default settings throughout the study. To align with visual assessment, we derived a four-level ordinal measure representing the perfusion abnormality within the affected territory (0–25%, 25–50%, 50–75%, 75–100%). This variable is referred as *automated CTP.*

Collateral assessment

Collateral status (CS) was evaluated on baseline CTA using a three-category visual scale adapted from established collateral grading systems.[13] Collaterals within the affected vascular territory were classified as absent or minimal, reduced or normal/good compared with the contralateral hemisphere.

Clinical data and outcome measures

Baseline variables included age, sex and pre-stroke functional status. Treatment-related variables included the use of IVT prior to MT and time from symptom onset (or last known well) to groin puncture. Recanalization was assessed using the Thrombolysis in Cerebral Infarction (TICI) scale; successful recanalization was defined as TICI ≥ 2b. Routine follow up CT was performed 24 hours after MT.

Functional outcome at 90 days was assessed using the mRS, obtained from outpatient visits, telephone interviews or medical records. Although 47% of patients achieved mRS ≤ 2 at 90 days, which is regarded as excellent outcome, the number of patients with mRS ≤ 2 within individual CTP subgroups was insufficient to allow stable modelling. Therefore, mRS ≤ 3 at 90 days was predefined as primary endpoint for favourable functional outcome.

Statistical analysis

Continuous variables are reported as mean ± SD, categorical variables as counts and percentages.

TABLE 3. Distribution of patients between visual CT perfusion (CTP) and automated CTP

Automated CTP category (rows) /Visual CTP category (columns)	0–25% penumbra	25–50% penumbra	50–75% penumbra	75–100% penumbra	Row total
0–25% penumbra	5	1	0	0	6
25–50% penumbra	13	9	4	5	31
50–75% penumbra	21	25	60	25	131
75–100% penumbra	0	15	70	267	352
Column total	**39**	**50**	**134**	**297**	**520**

Cohen's κ = 0.365 (95% CI 0.299–0.431).

Group comparisons between patients with favourable (mRS ≤ 3) and unfavourable (mRS > 3) outcomes were performed using χ^2 or Fisher's exact test for categorical variables. Agreement between visual CTP and automated CTP ordinal classifications was assessed using Cohen's κ coefficient.

To evaluate the independent prognostic value of visual and automated CTP, we constructed separate multivariable logistic regression models with favourable 90-day outcome (mRS ≤ 3) as the dependent variable. Two sets of models were used for each CTP technique:

Baseline model (without CS): age, baseline ASPECTS, IVT, time from symptom onset to *groin puncture, recanalization success (TICI ≥ 2b vs < 2b), and the respective CTP grade.*

Extended model (with CS): all base variables plus CS.

Odds ratios (ORs) with 95 % confidence intervals (CI) were calculated relative to the CTP category with the biggest estimated penumbra. A two-sided $p < 0.05$ was considered statistically significant. Analyses were performed using SPSS (IBM Corp., Armonk, NY, USA).

Results

We included 579 patients with acute anterior circulation LVO stroke treated with MT (mean age 70.8 years, 51.5% male). The mean onset-to-groin puncture time was 4.2 hours, 45% received IVT, and successful recanalization (TICI ≥ 2b) was achieved in 81%. Favourable 90-day outcome (mRS ≤ 3) was demonstrated in 61.9%. Visual CTP was available in 539 patients, automated CTP in 528 patients and both were available in 520 patients for agreement analysis.

TABLE 4A. Multivariable logistic regression including visual CT perfusion (CTP) (n = 539) for favourable outcome (mRS ≤ 3); baseline model (without CT angiography [CTA] collaterals)

Predictor	OR (95% CI)	p-value
Age (per year)	**0.94 (0.92–0.96)**	**< 0.01**
ASPECTS (per point)	**1.29 (1.09–1.51)**	**< 0.01**
Time to groin puncture	1.01 (0.92–1.11)	0.82
IV thrombolysis	0.75 (0.49–1.15)	0.18
TICI < 2b	**0.31 (0.18–0.54)**	**< 0.01**
Visual CTP 0–25 %	**0.22 (0.10–0.47)**	**< 0.01**
Visual CTP 25–50 %	**0.30 (0.15–0.62)**	**< 0.01**
Visual CTP 50–75 %	**0.51 (0.31–0.83)**	**< 0.01**

Odds ratios (OR) with 95% CI; reference category for CTP = 75–100%

ASPECTS = Alberta Stroke Program Early CT Score; TICI = Thrombolysis in Cerebral Infarction

TABLE 4B. Multivariable logistic regression including visual CT perfusion (CTP) (n = 539) for favourable outcome (mRS ≤ 3); extended model (with CT angiography [CTA] collaterals)

Predictor	OR (95% CI)	p-value
Age (per year)	**0.94 (0.92–0.96)**	**< 0.01**
ASPECTS (per point)	**1.26 (1.07–1.49)**	**< 0.01**
Time to groin puncture	1.01 (0.92–1.10)	0.92
IV thrombolysis	0.71 (0.46–1.10)	0.13
TICI < 2b	**0.33 (0.19–0.57)**	**< 0.01**
Collaterals absent/minimal	0.37 (0.07–2.10)	0.26
Collaterals reduced	**0.56 (0.34–0.92)**	**0.02**
Visual CTP 0–25%	**0.39 (0.16–0.97)**	**0.04**
Visual CTP 25–50%	**0.44 (0.20–0.96)**	**0.04**
Visual CTP 50–75%	0.64 (0.38–1.07)	0.09

Odds ratios (OR) with 95% CI; reference category for CTP = 75–100%

ASPECTS = Alberta Stroke Program Early CT Score; TICI = Thrombolysis in Cerebral Infarction

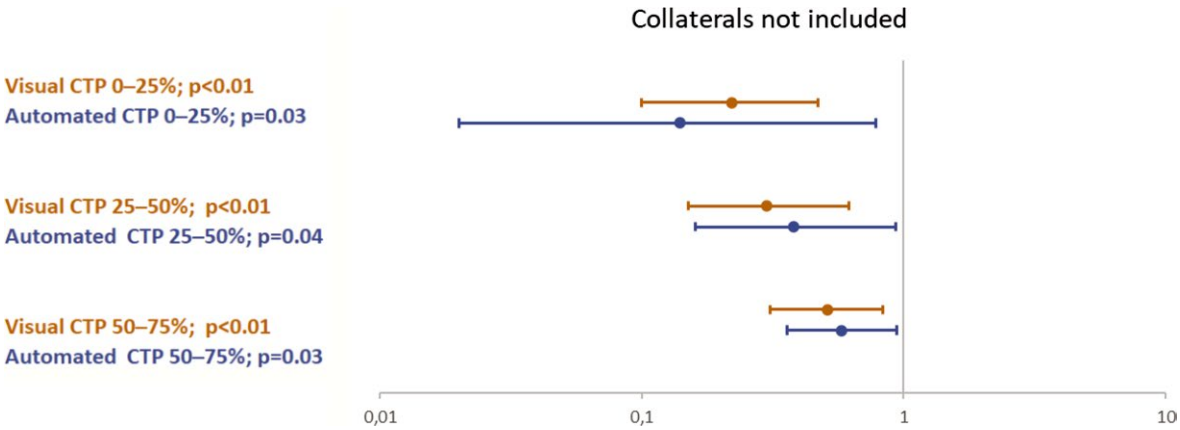

FIGURE 2A. Odds ratios comparisons between automated (n = 528) and visual (n = 539) CT perfusion (CTP) for favourable outcome (mRS ≤ 3) in multivariable logistic regression; baseline model (without CT angiography [CTA] collaterals).

Association between visual CT perfusion (CTP) and functional outcome

Visual CTP categories demonstrated a clear shift toward higher penumbra in patients with favourable outcome (Table 1). The association was significant ($\chi^2 = 29.5$, $p < 0.001$).

Association between automated CT perfusion (CTP) and functional outcome

Automated CTP categories were also associated with outcome ($\chi^2 = 21.6$, $p < 0.001$), although the strength of association was lower than for visual CTP (Table 2).

Agreement between visual and automated CT perfusion (CTP)

Among 520 patients with both visual and automated CTP assessment, agreement between the four-level classifications was only fair ($\kappa = 0.365$; 95% CI 0.299–0.431) (Table 3).

Multivariable models: visual CT perfusion (CTP)

In multivariable logistic regression, visual CTP remained an independent predictor of favourable outcome in both baseline and extended models

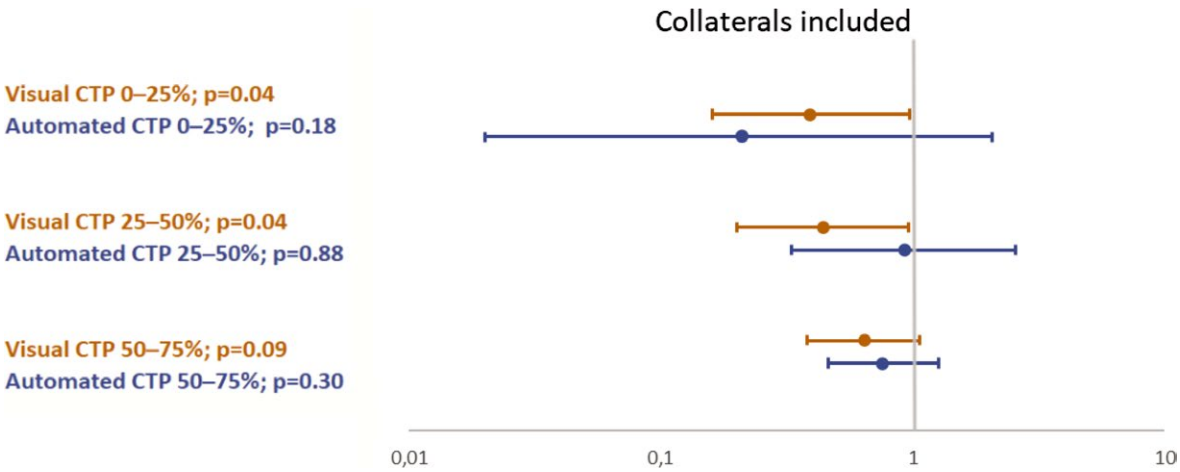

FIGURE 2B. Odds ratios comparisons between automated (n = 528) and visual (n = 539) CT perfusion (CTP) for favourable outcome (mRS ≤ 3) in multivariable logistic regression; extended model (with CT angiography [CTA] collaterals).

(Tables 4A and 4B). Increasing visual penumbra demonstrated a graded, positive association with favourable outcome in both models.

Multivariable models: automated CT perfusion (CTP)

Automated CTP categories contributed significantly to outcome in the baseline model (Table 5A), but the association was attenuated and lost statistical significance after inclusion of CS (Table 5B). In the extended model, age, ASPECTS, recanalization success, and CS quality remained independent predictors, whereas automated CTP did not.

Comparisons of OR for favourable outcome (mRS ≤ 3) according to automated and visual CTP categories in multivariable logistic regression, using the same entry parameters as above, are graphically depicted in Figure 2A (without CS) and 2B (with CS).

TABLE 5A. Multivariable logistic regression including automated CT perfusion (CTP) (n = 528) for favourable outcome (mRS ≤ 3); baseline model (without CT angiography [CTA] collaterals)

Predictor	OR (95% CI)	p-value
Age (per year)	**0.94 (0.92–0.96)**	**< 0.01**
ASPECTS (per point)	**1.29 (1.10–1.52)**	**< 0.01**
Time to groin puncture	1.01 (0.92–1.10)	0.90
IV thrombolysis	0.80 (0.52–1.22)	0.29
TICI < 2b	**0.28 (0.16–0.49)**	**< 0.01**
CTP 0–25%	**0.14 (0.02–0.78)**	**0.03**
CTP 25–50%	**0.38 (0.16–0.93)**	**0.04**
CTP 50–75%	**0.58 (0.36–0.94)**	**0.03**

Odds ratios (OR) with 95 % CI; reference category for CTP = 75–100%

ASPECTS = Alberta Stroke Program Early CT Score; TICI = Thrombolysis in Cerebral Infarction

TABLE 5B. Multivariable logistic regression including automated syngo.via (SYV) CT perfusion (CTP) (n = 528) for favourable outcome (mRS ≤ 3); extended model (with CT angiography [CTA] collaterals)

Predictor	OR (95% CI)	p-value
Age (per year)	**0.95 (0.93–0.97)**	**< 0.01**
ASPECTS (per point)	**1.26 (1.07–1.50)**	**< 0.01**
Time to groin puncture	1.00 (0.92–1.10)	0.98
IV thrombolysis	0.72 (0.47–1.13)	0.15
TICI < 2b	**0.28 (0.16–0.50)**	**< 0.01**
Collaterals absent/minimal	0.22 (0.03–1.50)	0.12
Collaterals reduced	**0.39 (0.24–0.63)**	**< 0.01**
CTP 0–25%	0.21 (0.02–2.07)	0.18
CTP 25–50%	0.93 (0.33–2.57)	0.88
CTP 50–75%	0.76 (0.46–1.27)	0.30

Odds ratios (OR) with 95 % CI; reference category for CTP = 75–100%

ASPECTS = Alberta Stroke Program Early CT Score; TICI = Thrombolysis in Cerebral Infarction

Discussion

In this large single-centre cohort of acute anterior circulation LVO stroke patients treated with MT, a simple visual grading of TTP maps provided prognostic information that was at least comparable to, and in adjusted models even more robust than, automated CTP analysis performed with syngo.via. Although both methods were associated with 90-day outcomes in univariate testing, agreement between them was only fair ($\kappa = 0.36$). In multivariable models, visual CTP remained an independent predictor after adjusting for age, ASPECTS, recanalization success, IVT, time to groin puncture and CS, whereas automated CTP lost significance once CS was included.

CTP has become central to treatment selection and outcome prediction in modern stroke care with major randomized trials demonstrating clinical value of perfusion-based core and penumbra estimates.[1-6] Contemporary studies further highlight that automated CTP metrics not only predict functional independence and malignant infarction but also that their performance varies with software platforms, thresholding strategy and collateral quality.[14]

Our findings extend prior work, showing that visually identified TTP »black-hole« regions reflect severely impaired brain hemodynamics and poor prognosis.[11,12] The only fair concordance between visual and automated CTP categories is in alignment with previous reports of substantial variability across CTP software platforms and limited spatial agreement with follow-up infarction.[7,15,16] Several recent comparisons also suggest that visual or semi-quantitative assessment can match or outperform automated assessment for prognostication, particularly when combined with ASPECTS and CS.[12,14] Consistent with this, visual CTP grading retained prognostic value even after adjusting for CS, whereas automated CTP did not.

CS is a dominant determinant of infarct progression and outcome.[13,17] Its inclusion in our mod-

els reduced the predictive contribution of automated CTP but not visual CTP, possibly because visual CTP captures both the extent and severity of microvascular delay more effectively.

From a practical perspective, these findings support continued use of structured visual CTP assessment in acute stroke workflows. Visual CTP grading is rapid, universally available and independent of software specific thresholds or software versions. This is particularly relevant in centres where automated CTP may be unavailable. Moreover, visual CTP can be useful in clinical decision-making for elderly, frail or severely comorbid patients, where prognosis, not merely treatment eligibility, guides therapeutic choices.

Strengths of the study include the large real-world cohort, parallel four-category scales enabling direct comparison and multivariable models incorporating CS. Study limitations include its retrospective, single-centre design, missing CTP in a subset of patients, absence of inter-rater reliability testing for visual CTP grading and reliance on a single automated platform (syngo.via VB40). Additionally, CTP was performed with an old CT technology, which includes only four 5 mm slices through the affected area. This is in contrast with the modern stroke imaging, which these uses the whole brain CTP imaging as standard, which can influence the interpretation of CTP parameters. Different results might also emerge with alternative thresholds or newer AI-based post-processing methods.[18]

Favourable outcome (mRS ≤ 3) was used as the primary endpoint because the distribution of excellent outcome (mRS ≤ 2) within individual perfusion categories was too sparse to permit stable regression. This limitation reduces direct comparability with some major MT studies, which typically define primary endpoint by excellent outcome. Nonetheless, our study focused on the relative prognostic value of two technical perfusion assessment methods, aiming to evaluate their ability to predict the overall distribution of functional outcomes rather than selective prediction of excellent outcome alone.

Future research should validate these findings across centres, scanners, software packages and directly compare visual CTP with newer automated or AI-driven tools designed specifically for prognostication. It is likely that AI-driven tools are going to guide clinicians in the future, but simple visual CTP evaluation should remain a way of final clinical check-up before final treatment decisions.

Conclusions

Visual CTP evaluated on TTP maps provided a slightly better prognostic performance than automated CTP evaluated by SYV using default settings. Visual CTP assessment is a simple, accessible and clinically meaningful tool for both treatment decision making and outcome prediction in anterior circulation stroke treated with MT.

AI disclosure

During the preparation of this work the authors used ChatGPT (OpenAI) in order to assist with language refinement and structural editing of the manuscript. After using this tool, the authors carefully reviewed, revised, and edited the content as necessary and take full responsibility for the scientific content and conclusions of the published article.

References

1. Albers GW, Marks MP, Kemp S, Christensen S, Tsai JP, Ortega-Gutierrez S, et al. Thrombectomy for stroke at 6 to 16 hours with selection by perfusion imaging. *N Engl J Med* 2018; **378:** 708-18. doi: 10.1056/NEJMoa1713973
2. Nogueira RG, Jadhav AP, Haussen DC, Bonafe A, Budzik RF, Bhuva P, et al. Thrombectomy 6 to 24 hours after stroke with a mismatch between deficit and infarct. *N Engl J Med* 2018; **378:** 11-21. doi: 10.1056/NEJMoa1706442
3. Ma H, Campbell BCV, Parsons MW, Churilov L, Levi CR, Hsu CY, et al. Thrombolysis guided by perfusion imaging up to 9 hours after onset of stroke. *N Engl J Med* 2019; **380:** 1795803. doi: 10.1056/NEJMoa1813046
4. Yoshimura S, Sakai N, Yamagami H, Uchida K, Beppu M, Toyoda K, et al. Endovascular therapy for acute stroke with a large ischemic core. *N Engl J Med* 2022; **386:** 1303-13. doi: 10.1056/NEJMoa2118191
5. Sarraj A, Hassan AE, Savitz SI, Grotta JC, Cai C, Parsha KN, et al. Endovascular thrombectomy for large ischemic strokes. *N Engl J Med* 2023; **388:** 1259-71. doi: 10.1056/NEJMoa2214403
6. Huo X, Ma G, Tong X, Zhang X, Pan Y, Nguyen TN, et al. Endovascular therapy for acute ischemic stroke with a large infarct core. *N Engl J Med* 2023; **388:** 359-70. doi: 10.1056/NEJMoa2213379
7. Hoving JW, Marquering HA, Majoie CBLM, Yassi N, Sprengers MES, Berkhemer OA, et al. Accuracy of CT perfusion ischemic core volume and location estimation: comparison of four core estimation approaches using syngo.via VB40. *PLoS One* 2022; **17:** e0272276. doi: 10.1371/journal.pone.0272276
8. Muehlen I, Kloska SP, Almekhlafi MA, Bendszus M, Möhlenbruch MA, Pham M, et al. Comparison of two automated CT perfusion software packages (syngo.via vs RAPID) for ischemic core indication and clinical impact. *Stroke* 2022; **53:** 1657-64. doi: 10.1161/STROKEAHA.121.036314
9. Suomalainen OP, Martinez-Majander N, Sibolt G, Curtze S, Putaala J, Tatlisumak T, et al. Comparative analysis of core and perfusion lesion volumes between commercially available computed tomography perfusion software. *Eur Stroke J* 2023; **8:** 259-67. doi: 10.1177/23969873221139416
10. Koopman MS, van der Worp HB, Berkhemer OA, Fransen PSS, Beumer D, van Oostenbrugge RJ, et al. Comparison of three commonly used CT perfusion software packages in acute ischemic stroke patients. *J Neurointerv Surg* 2019; **11:** 1249-56. doi: 10.1136/neurintsurg-2019-014822

11. Meagher R, Shankar JJS. CT perfusion in acute stroke: black holes on time-to-peak image maps indicate unsalvageable brain. *J Neuroimaging* 2016; **26:** 605-11. doi: 10.1111/jon.12336

12. Rigler I, Gspan T, Avsenik J, Milosevic Z, Pretnar Oblak J. Independent significance of visual assessment of perfusion CT maps in anterior circulation stroke patients treated with mechanical thrombectomy. *Clin Neuroradiol* 2022; **32:** 829-37. doi: 10.1007/s00062-021-01115-6

13. Maas MB, Lev MH, Ay H, Singhal AB, Greer DM, Smith WS, et al. Collateral vessels on CT angiography predict outcome in acute ischemic stroke. *Stroke* 2009; **40:** 3001-5. doi: 10.1161/STROKEAHA.109.552513

14. Psychogios MN, Sporns PB, Ospel J, Schregel K, Zoubi T, Behme D, et al. Automated perfusion calculations versus visual scoring of collaterals and CBV-ASPECTS: has the machine surpassed the eye? *Clin Neuroradiol* 2021; **31:** 499-506. doi: 10.1007/s00062-020-00934-3

15. Austein F, Riedel C, Kerby T, Meyne J, Binder A, Lindner T, et al. Comparison of perfusion CT software to predict the final infarct volume after thrombectomy. *Stroke* 2016; **47:** 2311-7. doi: 10.1161/STROKEAHA.116.013147

16. Yang W, Hoving JW, Koopman MS, Dankbaar JW, van der Schaaf IC, Niesten JM, et al. Agreement between estimated computed tomography perfusion ischemic core and follow-up infarct on diffusion-weighted imaging. *Insights Imaging* 2022; **13:** 191. doi: 10.1186/s13244-022-01311-8

17. Bang OY, Goyal M, Liebeskind DS. Collateral circulation in ischemic stroke: assessment tools and therapeutic strategies. *Stroke* 2015; **46:** 3302-9. doi: 10.1161/STROKEAHA.115.010508

18. Robben D, Boers AMM, Marquering HA, Berkhemer OA, Yoo AJ, van der Lugt A, et al. Prediction of final infarct volume from native CT perfusion and treatment parameters using deep learning. *Med Image Anal* 2020; **59:** 101589. doi: 10.1016/j.media.2019.101589

RADIOLOGY AND ONCOLOGY Radiology and Oncology | Ljubljana | Slovenia | www.radioloncol.com

research article

Luciferase-induced immune activation prevents orthotopic K7M2luc osteosarcoma establishment in BALB/c mice

Sasa Kupcic[1,2], Urska Kamensek[1,3], Maja Cemazar[1,4], Ursa Lampreht Tratar[1,5]

[1] Department of Experimental Oncology, Institute of Oncology, Ljubljana, Slovenia
[2] Faculty of Medicine, University of Ljubljana, Ljubljana, Slovenia
[3] Biotechnical Faculty, University of Ljubljana, Ljubljana, Slovenia
[4] Faculty of Health Sciences, University of Primorska, Izola, Slovenia
[5] Veterinary Faculty, University of Ljubljana, Ljubljana, Slovenia

Radiol Oncol 2026; 60(3): 402-415.

Received 17 August 2026
Accepted 21 August 2026

Correspondence to: Assist. Prof. Urša Lampreht Tratar, Ph.D., Institute of Oncology Ljubljana, Zaloška 2, SI-1000 Ljubljana, Slovenia.
E-mail: ulampreht@onko-i.si

Disclosure: No potential conflicts of interest were disclosed.

Background. Use of murine orthotopic tumor models dictates utilization of luciferase-expressing cells for *in vivo* bioluminescence imaging. However, luciferase may trigger immune responses that impair tumor establishment.

Materials and methods. We transduced K7M2 cells wild-type (wt) with luciferase gene and evaluated their growth *in vitro*. We then implanted cells orthotopically in BALB/c mice and upon unsuccessful tumor establishment assessed systemical and local mechanism for tumor growth suppression.

Results. All investigated cell lines had a comparative doubling time *in vitro* at 24 and 48h. Despite that, K7M2luc E5 differed from K7M2luc A7 and K7M2 wt by having a much higher proliferation rate at 72h (35x, 15x and 17x). *In vivo,* both luciferase-expressing cell lines failed to establish tumors, whereas K7M2 wt had a 100% success rate. To investigate the underlying mechanism, we assessed systemic and local cell-mediated immunity. Mice in groups K7M2luc A7 and K7M2luc E5 had a higher fold change (5 ± 0.8 and 6 ± 1.05) of GrB secreting splenocytes than naïve mice (1 ± 0.2). In the bone microenvironment, luciferase groups exhibited elevated numbers of GrB-secreting cells and $CD8^+$ T cells relative to K7M2 wt and naïve mice.

Conclusions. These findings indicate that luciferase activates cytotoxic T-cell responses capable of eliminating implanted cells. Tumor establishment was restored in immunodeficient mice lacking $CD8^+$ cells, confirming the immune-mediated rejection.

Key words: mouse orthotopic tumor; luciferase; bioluminescence; osteosarcoma

Introduction

Osteosarcoma is a rare, highly aggressive primary malignant bone tumor that predominantly affects adolescents and young adults. It accounts for approximately 2.4% of all pediatric malignancies.[1,2] Most frequently it arises in metaphyseal regions of long bones, particularly the distal femur, proximal tibia, and proximal humerus.[3] Histopathologically, osteosarcoma is characterized by malignant mesenchymal cells that undergo aberrant osteoblastic differentiation, leading to the production of immature and structurally fragile bone matrix, termed osteoid.[4,5]

Bone microenvironment is a highly complex and dynamic system composed of bone, stromal, endothelial, and immune cells that are closely integrated with the mineralized extracellular matrix.[6] Tumor cells establish intensive communication with this environment through a wide array of cytokines, chemokines, and growth factors, thereby promoting the development of a favorable tumor microenvironment (TME).[7] Given the unique characteristics of the bone niche in which sarcomas develop, use of mouse orthotopic models is strongly recommended and surpasses the use of subcutaneous tumors.[8,9] Their growth and invasiveness are more representative of the clinical course of the disease in patients. Evidence from studies of colorectal, bladder, prostate, and pancreatic cancer have demonstrated that cancer cells implanted in orthotopic sites can acquire a metastatic phenotype, underscoring the importance of these models for investigating the metastatic process.[10-13] Moreover, tumor implantation site can significantly influence antitumor efficacy of experimental therapies. For example, in a study comparing colorectal carcinoma cells implanted subcutaneously versus orthotopically, inhibition of tumor growth following doxorubicin treatment was twice as pronounced in subcutaneous tumors compared with orthotopic tumors.[14]

Orthotopic localization of osteosarcoma tumors poses considerable challenges for their longitudinal monitoring and growth assessment. Non-invasive bioluminescence imaging (BLI) is a widely adopted approach for pre-clinical evaluation. This technique relies on the stable transduction of tumor cell lines with a bioluminescent reporter gene prior to their inoculation into mice.[15] One of the most widely used BLI markers is luciferase (luc), mainly due to its noninvasiveness, sensitivity and affordability. Luciferases are animal-derived enzymes that produce light in presence of an appropriate substrate. Luciferases differ among themselves according to the animal of origin, e.g. sea pen (Renilla luciferase), black prince copepod (Gaussia luciferase) or the most used firefly luciferase, which derives from the common eastern firefly (*Photinus pyralis*).[16] For imaging, animals are administered the substrate (e.g. D-luciferin), typically via intraperitoneal or subcutaneous injection.[17] *In vivo* imaging system (IVIS) subsequently detects and quantifies emitted bioluminescent signal, which is a result of luciferin oxidation due to presence of luciferase enzyme. This method enables sensitive, real-time visualization and quantification of tumor burden without the need for invasive procedures.[18,19]

Despite the widespread use of BLI, some studies utilizing luciferase-expressing cell lines report a delay in tumor growth and subsequent reduced metastatic potential. Such examples include a pancreatic ductal adenocarcinoma model, where a cell line with incorporated red-shifted firefly luciferase failed to establish an orthotopic tumor, whereas a cell line transduced with a click-beetle green luciferase proceeded to establish tumors. Other groups reported similar problems with a firefly luciferase in a glioblastoma tumor model.[20,21] Luciferase can reportedly suppress tumor growth even in cases of subcutaneous implantation, as was reported by Brutkiewicz *et al*., where they demonstrated that in case of subcutaneous implantation luciferase expression levels directly altered *in vivo* tumor growth dynamics, underscoring biological effects beyond imaging.[22] Luciferase has even been deliberately employed as a model immunogen in DNA immunization study, highlighting its intrinsic immunostimulatory potential.[23] In our own earlier work, we also demonstrated that reporter luciferase expression can contribute to antitumor effects.[24] Stated interferences in tumor development can be attributed to the immune response, spearheaded by the expression of intracellular luciferase.[20,22,25]

Codon-optimized and improved firefly luciferase, named luc2, is widely utilized and even though it was shown to be successful in establishing K7M2luc osteosarcoma tumors in relatively small number of syngeneic BALB/c mice, there are several studies on 4T1 mammary tumors and glioblastoma tumors, where luc2 cell lines showed to be detrimental to tumor growth.[25-28]

However, numerous studies, that also described luciferase-based imaging modalities in immunocompetent mice, did not report any detectable immunogenic limitations.[28-30] Furthermore, some reports specifically evaluated the potential adverse effects of luciferase expression on tumor growth and found no evidence of a detrimental impact.[31]

Conflicting or limited evidence has likely contributed to the immunogenicity of reporter genes being underestimated, resulting in this phenomenon remaining insufficiently addressed in routine experimental practice.

Therefore, our aim was to investigate the interference of luc2 with development of murine orthotopic osteosarcoma models in immunocompetent mice which has not been reported yet.

Materials and methods

Establishment of transduced cell line

Murine osteosarcoma (OS) cell line K7M2 wild type (wt) (CRL-28369) was obtained from the American Type Culture Collection (ATCC; Manassas, VA, USA). Cells were cultured in Advanced Dulbecco's Modified Eagle Medium (Advanced DMEM; Gibco, Thermo Fisher Scientific, Waltham, MA, USA), supplemented with 5% (v/v) fetal bovine serum (FBS; Gibco), 100 U/mL penicillin, 100 μg/mL streptomycin (Sigma-Aldrich, Darmstadt, Germany), and 1% (v/v) GlutaMAX (Gibco), in a humidified incubator at 37 °C with 5% CO_2. Mycoplasma contamination was routinely monitored using the MycoAlert™ PLUS Mycoplasma Detection Kit (Lonza Group Ltd., Basel, Switzerland), and all cultures were confirmed to be mycoplasma-free.

The transduced cell lines were established using two different modalities, with in-house preparation of lentivirus particles and by using commercial lentiviral particles.

Plasmid construction and lentiviral transduction

K7M2luc A7 cell line was generated via lentiviral transduction as previously described.[32] Luciferase transfer plasmid was constructed by replacing the enhanced green fluorescent protein (eGFP) gene in pLenti PGK GFP Puro plasmid (w509-5; a gift from Eric Campeau and Paul Kaufman, Addgene plasmid #19070) with luciferase 2 (*Photinus pyralis*) (Luc2 CO) gene fragment (gBlocks™ HiFi Gene Fragments; Integrated DNA Technologies, Coralville, IA, USA). Luc2 CO derived from luc2 gene fragment that was further codon-optimized for mouse expression by the tool for codon optimization (Integrated DNA Technologies). Lentiviral packaging was achieved using plasmids pMDLg/pRRE, pMD2.G, and pRSV-Rev (gifts from Didier Trono; Addgene plasmids #12259, #12251, and #12253, respectively).

All four plasmids were propagated in *Escherichia coli* under ampicillin selection and isolated per manufacturer's instructions, using EndoFree Plasmid Mega Kit (Qiagen, Hilden, Germany). Lentiviral particles were produced in 293T cells (CRL-3216, ATCC) grown to 80% confluence in 6-well plates. Modified transfer plasmid was co-transfected with packaging plasmids pMDLg/pRRE, pMD2.G, and pRSV-Rev using Lipofectamine 2000 (Invitrogen, Thermo Fisher Scientific). At 24 hours post-transfection, medium was replaced with 5 mL of fresh complete medium. Supernatants containing viral particles were harvested 48 and 72 hours after transfection, pooled, centrifuged at 500 × g for 10 minutes, and filtered through a 0.45 μm membrane (Merck Millipore, Burlington, MA, USA).

For transduction, K7M2 wt cells were seeded in 6-well plates and grown to 80% confluence. Culture medium was replaced with afore mentioned virus-containing medium with added polybrene (4 μg/mL; Sigma-Aldrich) and incubated for 24 hours. At 48 hours post-transduction, puromycin (8 μg/mL; Sigma-Aldrich) was added for selection. A monoclonal stable cell line was established by seeding single cells into 96-well plates and maintaining puromycin selection. After 10 days, colonies were harvested and transferred to T75 flasks. Once confluence was achieved in T75 flasks, monoclonal populations were generated and screened for bioluminescent intensity with IVIS Lumina XMRS (Revvity, Waltham, MA, USA). Clone displaying a sufficient bioluminescent intensity was selected (clone K7M2luc A7), expanded under standard conditions with continuous puromycin selection, and stored in liquid nitrogen.

Transduction with commercially available viral particles

K7M2luc E5 cell line was established using IVISbrite Red F-luc-Puromycin Lentiviral Particles (RediFect; Revvity) according to manufacturer's instructions. K7M2 wt cells were seeded into 24-well plates and grown to 80% confluence. Cells were transduced at varying multiplicities of infection (MOIs) in presence of polybrene (4 μg/mL) to enhance transduction efficiency. After 24 hours, medium was replaced, and puromycin (8 μg/mL) was added after another 24 hours for selection. Cells were then seeded to 96-well plates to establish monoclonal populations which were then transferred to T75 flasks. Upon reaching confluence in T75 flasks, clone exhibiting a sufficient bioluminescent intensity was selected (clone K7M2luc E5), expanded under standard conditions with continuous puromycin selection and cryopreserved in liquid nitrogen.

Cell proliferation assay and luciferase expression *in vitro*

For assessment of cell growth kinetics K7M2 wt, K7M2luc E5 and K7M2luc A7 cells were seeded to a 96-well plate ($1.5x10^3$ cells/well). Fluorescence based assay with Presto Blue™ reagent (Thermo Fischer) was performed. At different time points (0, 24, 48 and 72 h) 10 μL of the reagent was added

to wells. Upon 1 h incubation in a CO_2 incubator, fluorescence of a metabolic product resorufin was measured at 530/590 ex/em with a multimodal reader Cytation 1 (BioTek, Winooski, VT, USA).

Luciferase expression *in vitro* was determined by seeding 100 µl of a cell suspension (concentration of 1x10^{5}cells/ml) to a 96-well plate. D-luciferin (30 mg/mL; Thermo Fischer) was added to wells with cell suspensions at different working concentrations. Plates were then incubated for 10 min in a CO_2 incubator and imaged using imaging system IVIS Lumina XMRS.

Animals and tumor induction

6–8 weeks old female 9 BALB/c and 6 NUDE mice from Charles River Laboratories (Lecco, Italy) were used. Animals were housed in cages of 3–6 animals per cage in specific-pathogen-free conditions in a carousel mouse IVC rack system (Animal Care Systems Inc., Revere Parkway, USA) at a temperature of 20–24°C, 55 ± 10% relative humidity, 12 h light/dark cycle, food and water ad libitum and cage enrichment. For tumor induction in BALB/c mice, 1×10^6 K7M2 wt, K7M2luc A7 or K7M2luc E5 cells were resuspended in 25 µL of saline solution. Mice were placed under isoflurane anesthesia (2–3%) and cell suspension was injected intratibially to the shaved proximal site of the anterolateral region of right hind leg. Further on in the animal experiment, confirming the role of immune cells in NUDE mice, the mice were inoculated with 1×10^6 of only K7M2luc A7 cell line.[26] This cell line, which demonstrated lower luciferase expression compared to K7M2luc E5, was chosen based on previous reports showing that cell lines with higher luciferase expression exhibited reduced tumor growth as opposed to similarly produced cell clones with a lower luciferase expression.[22] Buprenorphine (0.1 mg/kg body weight, 0.015 mg/mL) was administered perioperatively and 8 hours postoperatively. Animals were monitored daily for signs of distress and weighed twice a week. All procedures were planned and performed according to PREPARE, ARRIVE and OBSERVE guidelines and approved by the Ministry of Agriculture, Forestry, and Food of the Republic of Slovenia (permit no. U34401-17/2023/1).

Bioluminescence imaging and X-ray imaging

Tumor progression was monitored twice a week using BLI and once a week by X-ray imaging. Substrate D-luciferin (15 mg/mL) (GoldBio, St. Louis, MO, USA) was administered intraperitoneally at a dose of 150 mg/kg body weight. Mice were placed under isoflurane anesthesia (2–3%) and images of the lower half of the body were captured by IVIS Lumina XRMS (Revvity) 15 minutes after D-luciferin administration. Exposure was set to automatic with a maximum time of 2 minutes, binning was set to 8. Images were analyzed with Living Image software (Revvity); regions of interest (ROIs) were drawn over tumor sites, and total photon flux (photons/sec) was quantified after background subtraction.

In all groups, X-ray imaging was utilized once a week as previously mentioned. Mice were placed under isoflurane anesthesia (2–3%), followed by imaging of the inoculated knee joint. Each image was recorded with a 96-s exposure, tube potential 35 kVp and a tube current of 100 µA. Binning was set to 1.

Sample collection

When bioluminescence signal in BALB/c mice dropped below detection threshold (1×10^4 photons/second), mice were placed under anesthesia and blood was collected from the retro-orbital venous sinus and centrifuged (20 min, 2000 × g) to obtain a serum, which was then frozen at −80 °C. Mice were humanely euthanized by a method of cervical dislocation. Spleens were aseptically harvested, mechanically sheared, and strained through a sterile 50 mm strainer to obtain single-cell splenocyte suspension. Cells were centrifuged (5 min, 500 × g, 4°C), washed with chilled PBS and resuspended in chilled red blood cell lysis buffer for 5 min. Reaction was stopped by 4 × dilution with chilled PBS. After centrifugation, pellets were resuspended in chilled serum-free freezing medium (Bulldog Bio, Portsmouth, NH, USA) and frozen at −80 °C.

Tibias, previously inoculated with tumor cells, were removed, fixed in 10% neutral buffered formalin and decalcified in EDTA (MoL-DECALCIFIER, Milestone, Valbrembo, ITA). Upon decalcification, samples were embedded in paraffin and cut in 2 µm thick sections for H&E or immunohistochemical staining. Tissue sections, stained with H&E, were evaluated for necrotic and viable areas, indicated by pink and purple staining, respectively. Samples were also collected from naïve mice without any prior tumor inoculation.

NUDE mice were split into groups for tumor establishment (2 mice) and tumor growth observation (4 mice). Mice from the first group were euthanized at the time of tumor establishment and tumor

samples were collected for immunohistochemical staining. Second group was observed with BLI and X-ray imaging continuously until signal strength started faltering or animals started to exhibit signs of clinical distress (lack of grooming, minimal loss of weight, limping…), at which point they were humanely euthanized with cervical dislocation.

Immunohistochemistry staining

2 μm thick paraffin embedded tissue sections were marked using 2 different primary antibodies: rabbit anti-mouse anti-CD8 alpha Ab (ab209775; Abcam, Danaher, Washington, D.C., DC, USA) and rabbit anti-mouse anti-Granzyme B Ab (ab4059, Abcam). Tissue sections were first incubated at 60° C for an hour, then deparaffinization and antigen retrieval (20 min, 97°C) were performed in a PT Link Pre-Treatment module for Tissue Specimens (Agilent Technologies, Santa Clara, Ca, USA) with a low pH Target Retrieval Solution EnVision FLEX (Dako Omnis, Agilent). Sections were subsequently incubated in a humid chamber with primary antibodies overnight at 4°C. Dilutions of primary antibodies in blocking buffer were as follows: 1/1000 for anti-CD8 and 1/1000 for anti-Granzyme B. Subsequently, biotinylated secondary antibodies (goat anti-rabbit IgG) (Abcam) were added, followed by a chromogenic reaction with rabbit specific HRP/DAB (ABC) detection IHC Kit (ab64261; Abcam) according to manufacturer's instructions. Slides were dried overnight and imaged with NanoZoomer S360MD digital slide scanner (Hamamatsu Photonics, Hamamatsu, Japan).

To quantify infiltration of $CD8^+$ cells and secretion of granzyme B (GrB), ten high-power fields (HPFs) were selected, representing a total area of 1 mm^2 of the entire scanned slide. The number of positively stained objects within each HPF was then counted in blind fashion by 2 independent examiners.

ELISpot GrB assay

An ELISpot assay was performed to assess cytotoxic lymphocyte activity via GrB secretion. Splenocytes were thawed overnight and activated with a luciferase peptide H-GFQSMYTFV-OH (20μg/mL, 20h; Biosynth Ltd., Berkshire, UK), luc2-specific $CD8^+$ epitope in BALB/c mice, that was previously described as being used to activate splenocytes in *ex vivo* studies.[25,33-37] Splenocytes were then seeded to ELISpot plate (5×10^4 cells/well), followed by 48 h incubation. ELISpot assay was then performed according to the manufacturer's instructions. GrB spot-forming cells were counted using a stereomicroscope Zeiss Lumar.V12 (Zeiss, Oberkochen, Germany). Results were normalized to unactivated splenocytes.

ELISA interferon-γ assay

To detect the presence of interferon-γ (IFN-γ), mice serum was thawed and added to the ELISA plate (R&D systems, Minneapolis, MN, USA) along with reagents according to the manufacturer's instructions. Optical density was determined with Cytation 1 multimodal plate reader set to 450 nm, with wavelength correction at 570 nm.

To collect cell culture supernatant, splenocytes were thawed and allowed to recuperate for 24 h in a humidified CO_2 incubator. They were reactivated with a luciferase peptide H-GFQSMYTFV-OH (20 μg/mL, 20 h; Biosynth Ltd., Berkshire, UK) and added to a plate with previously seeded cells at a target:effector ratio of 1:10 and left to incubate for 48 h in a CO_2 incubator. Supernatant was removed, centrifuged to remove cell debris and concentrated 2.5x times in centrifuge tubes with a centrifugal filter (Millipore). 50 μl of each sample was then added to the ELISA plate (R&D systems, Minneapolis, MN, USA) along with reagents according to the manufacturer's instructions. Optical density was determined with Cytation 1 multimodal plate reader set to 450 nm, with wavelength correction at 570 nm.

Statistical analysis

Statistical analysis and graphing were done in GraphPad Prism software 10.4.2 (Graphpad Software, Boston, MA, USA). Results were first tested for normal distribution using the Shapiro-Wilk or D'Agostino-Pearson test. One-way analysis of variance (ANOVA), Student's t-test and Welch's t test were used to determine differences among experimental groups, where data was normally distributed. Differences were considered statistically significant if the p value was below 0.05. Data are presented as arithmetic means (AM) and standard errors of means (SEM).

Results

In vitro evaluation of cell proliferation and luminescence signal

We assessed the effect of luciferase expression on cell proliferation kinetics with a fluorescence-

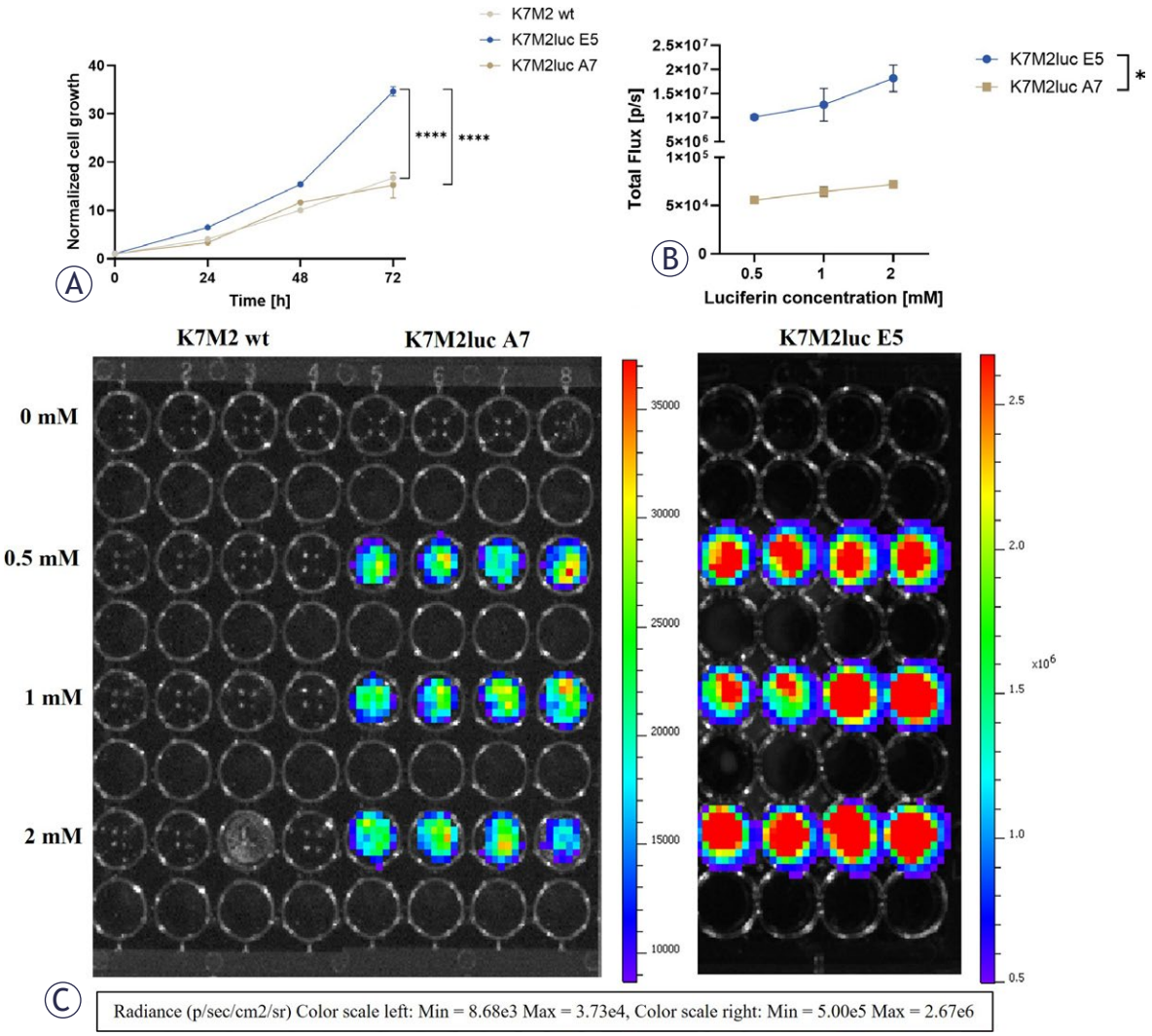

FIGURE 1. (A) All cell lines show exponential growth during time points 24 h, 48 h and 72 h. **(B)** K7M2luc A7 and K7M2luc E5 clonal lines show no dose-dependent statistically significant differences in bioluminescent signal, K7M2luc E5 has a higher bioluminescent signal at all added luciferin doses. **(C)** BLI of cell lines with added luciferin (0 –2 mM). n = 4–12.

Values are presented as Arithmetic Mean (AM) ± Standard Error of the Mean (SEM).

* $p < 0.01$, **** $p < 0.0001$. Where not indicated with *, differences are not significant. Paired t-test, one-way ANOVA.

based assay Presto Blue™. All cell lines exhibited exponential growth during time points of measurement, with similar proliferation rates at time points 24 h (3–6×) and 48 h (10–15×) (Figure 1A). However, at time point 72 h, K7M2luc E5 cell line had the highest proliferation rate, 35×, which significantly differed from proliferation rates of cell lines K7M2luc A7 and K7M2 wt, which were 15× and 17× respectively ($p < 0.0001$). From the measured data, doubling times for each cell line were also calculated. K7M2luc E5 had a doubling time of 19 h, K7M2luc A7 26 h, and K7M2 wt 25 h. Differences in doubling times were not statistically significant.

Expression of luciferase was assessed by adding varying concentrations of D-luciferin substrate (0 mM–2 mM) to K7M2luc clonal lines, with K7M2 wt cells serving as a negative control. No dose-dependent differences in bioluminescent signal intensity were observed across substrate concentrations (Figure 1B). However, statistically significant differences were detected among the luciferase-expressing clones. K7M2luc E5 cell line exhibited

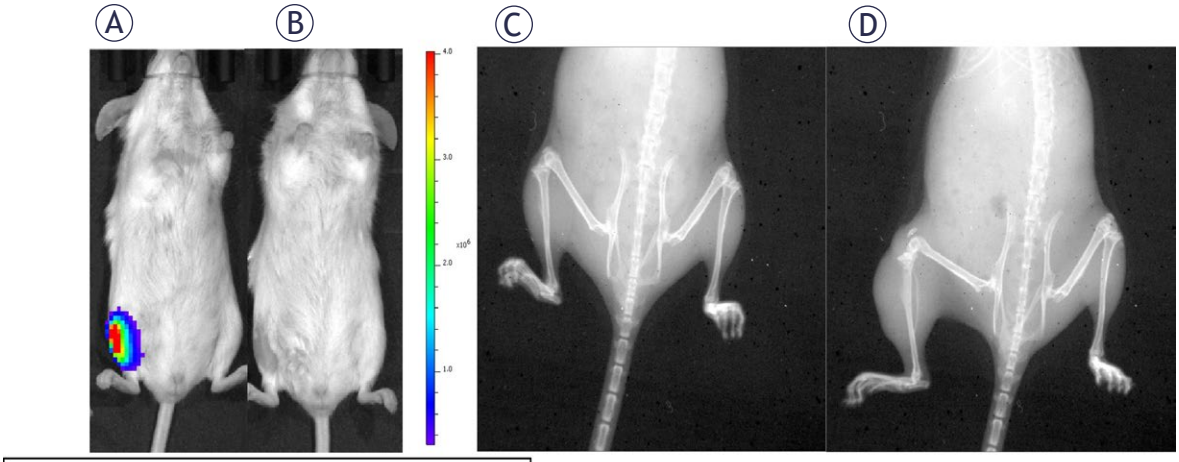

FIGURE 2. Representative images of BLI and X-ray imaging. BALB/c mice, inoculated with K7M2luc A7 at **(A)** day 6 and **(B)** day 8 demonstrating a decrease in signal. BALB/c mice, inoculated with K7M2 wt at **(C)** day 6 and **(D)** day 25 demonstrating progressive tumor growth due to bone lysis.

robust bioluminescence, with signal intensities ranging from 6.5×10^6 to 2.3×10^7 photons/second (p/s), whereas K7M2luc A7 demonstrated markedly lower levels of signal, averaging approximately 6×10^4 p/s ($p = 0.0294$, Figure 1C).

Evaluation of K7M2 wt, K7M2luc A7 and K7M2luc E5 growth rate after tumor inoculation in BALB/c mice

In vivo tumor growth was examined by first implanting K7M2 wt or luciferase-expressing clonal lines to the mice tibia. To observe tumor growth, K7M2 wt group was imaged once a week using X-ray imaging, whereas K7M2luc A7 and E5 mice were imaged twice a week using BLI and X-ray once a week (Figure 2A–D).

K7M2luc A7 group had a strong positive signal on day 3 post inoculation, from 1.5×10^5 to 2.2×10^7 p/s, with a prominent decline in signal strength to 0 p/s on day 6 (Mouse 1) and day 8 (Mouse 2, 3) (Figure 3A), when mice were sacrificed and samples were collected. K7M2luc E5 group also had a positive signal at day 3, between 8.5×10^5 and 9.5×10^8 p/s. Unlike K7M2 A7 group, there was a general increase in signals on day 6 with a subsequent fall (Figure 3B). Mice were sacrificed and samples were taken on day 8 (Mouse 2), day 22 (Mouse 1) and 29

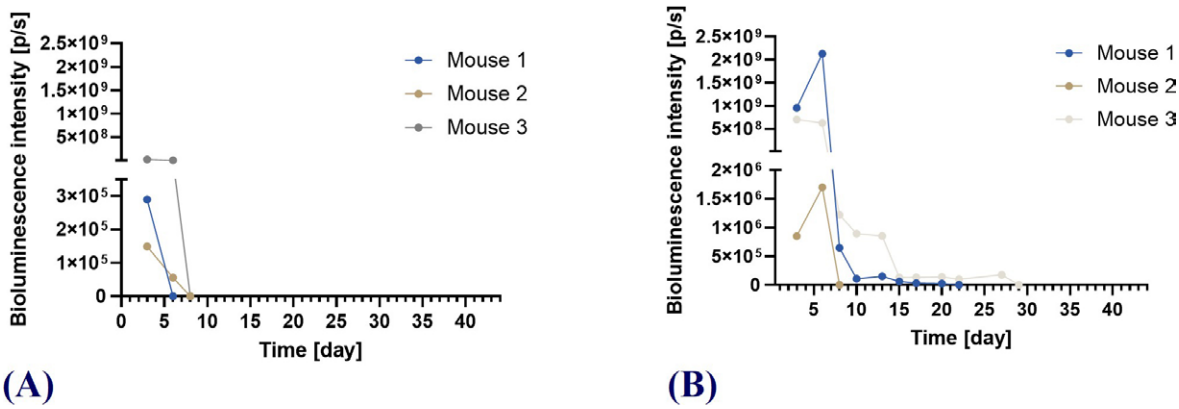

FIGURE 3. **(A)** BALB/c mice, inoculated with K7M2luc A7, showed a strong signal on day 3 with a drastic drop on day 6. **(B)** K7M2luc E5-inoculated BALB/c mice had an increase in signal strength on day 6 and a delayed fall day 8–29. n = 3.

Values are presented as Arithmetic Mean (AM) ± Standard Error of the Mean (SEM).

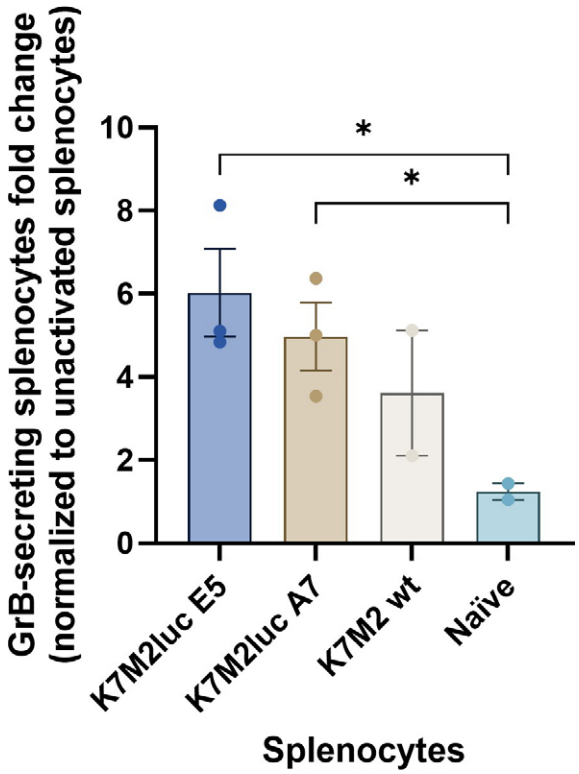

FIGURE 4. GrB positive splenocytes from inoculated mice with unsuccessful tumor growth. Splenocytes underwent secondary activation with luciferin peptide. n = 2–3.

Values are presented as Arithmetic Mean (AM) ± Standard Error of the Mean (SEM).

* $p < 0.05$. Where not indicated with *, differences are not significant. Welch's t test.

(Mouse 3), when the bioluminescence signal was under 1×10^4 p/s. K7M2 wt group was observed for 25 days, with tumor detection due to bone lysis and soft tissue growth at the site of cell inoculation in all three mice (Figure 2D). On day 25, mice were sacrificed, and samples were collected for continuation of studies.

Assaying activation of cytotoxic effector cells in mice on systemic and local level

Activation of cytotoxic effector cells ($CD8^+$ T cells and NK cells) in response to immunogenic properties of luciferase protein was assessed by measuring the amount of GrB-secreting splenocytes by a quantitative ELISpot assay. The highest fold change in GrB-secreting splenocytes was detected in mice inoculated with luciferase-expressing cell lines, with values of 6 ± 1.05 (K7M2luc E5) and 5 ± 0.8 (K7M2luc A7). Lower numbers of GrB-secreting splenocytes were detected in splenocytes isolated from naïve mice with a fold change of 1 ± 0.2. Activation of examined immune cells in mice with K7M2 wt inoculation was lower than in those inoculated with luciferase-expressing cell lines (Figure 4). Statistical analysis indicated differences among groups K7M2luc E5, K7M2luc A7 and Naïve ($p = 0.04$), although the low number of biological replicates limits statistical robustness.

ELISA for secretion of IFN-γ was performed on both serum samples and spleen-derived supernatant samples. No detectable IFN-γ was observed in either the serum or supernatant samples. Secondary activation of splenocytes *in vitro* with the luciferase peptide, as well as subsequent concentrating of supernatant samples, did not yield measurable IFN-γ levels. These findings indicate that IFN-γ production was either absent or below the detection threshold of the assay under tested conditions.

Immunohistochemistry for observation of immune cell infiltration to the tumor site

Immune cell infiltration to the inoculation site was determined by immunohistochemical staining of collected samples. Slides were stained with anti-$CD8^+$ and anti-GrB antibodies to assess the presence of cytotoxic lymphocytes (Figure 5A).

Groups K7M2luc A7 and K7M2luc E5 exhibited the highest $CD8^+$ infiltration, with 120 ± 17 /10 HPF and 106 ± 16 /10 HPF counted spots (Figure 5A,B), respectively. In contrast, the remaining two groups showed markedly lower $CD8^+$ infiltration, with 20-35 /10 HPF $CD8^+$ spots counted ($p = 0.0077$ - 0.0285).

The highest number of GrB-positive cells (218 ± 2 /10 HPF) was observed in the K7M2luc E5 group (Figure 5A,C) which was followed with a reduction (157 ± 9 /10 HPF) in K7M2luc A7 group. K7M2 wt and Naïve groups showed the lowest GrB-positive cell counts (70 ± 11 /10 HPF and 48 ± 3 /10 HPF spots, respectively), which were lower than those observed in K7M2luc A7 ($p < 0.0001$, $p < 0.0001$). K7M2 wt and Naïve group were also lower than K7M2luc E5 group ($p < 0.0001$, $p < 0.0001$). Although differences were statistically significant, interpretation is limited due to small sample sizes.

Establishment and growth curve monitoring of K7M2luc A7 cell line in NUDE mice

To confirm the premise of immunogenic properties of luciferase, six immunocompromised NUDE

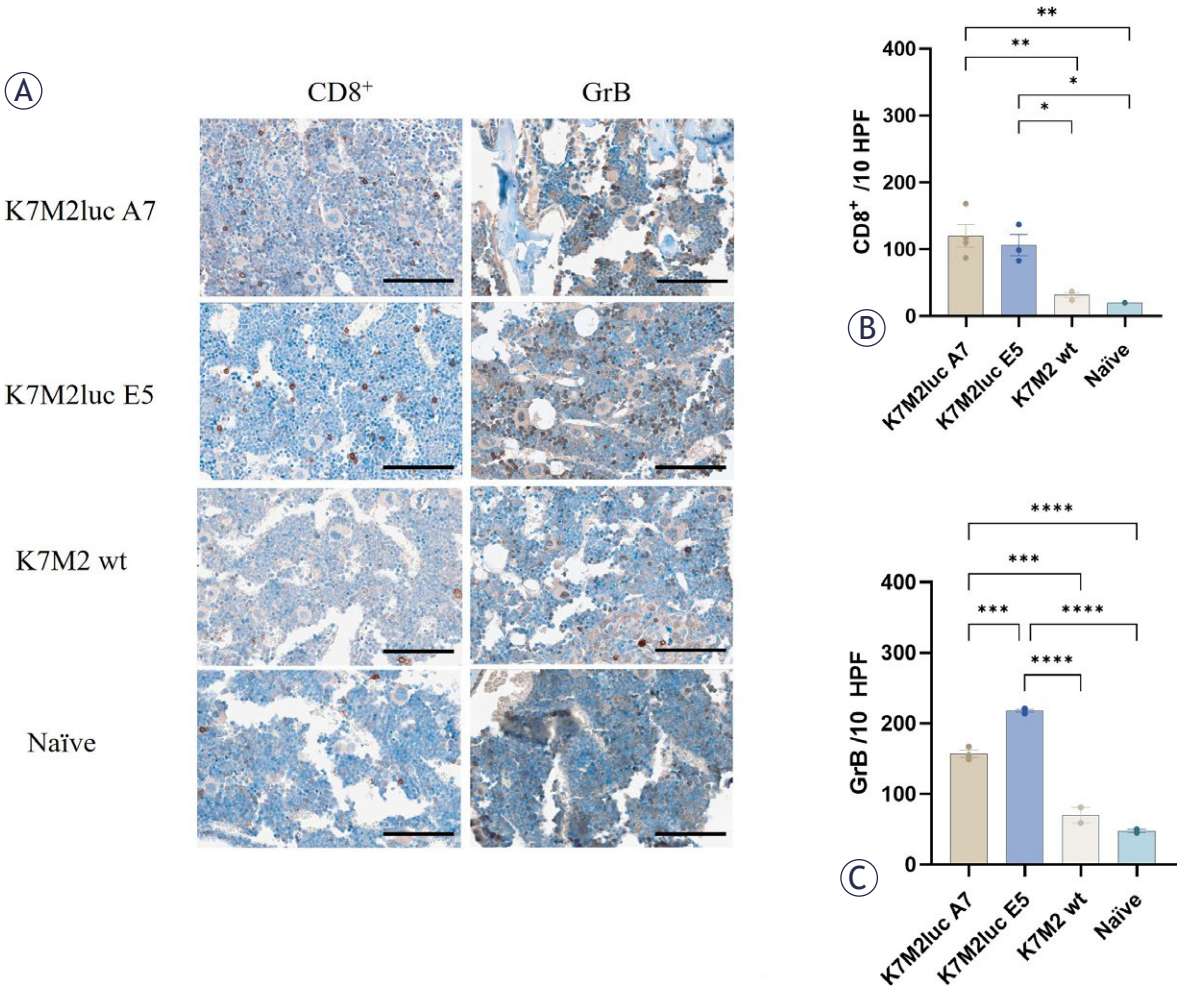

FIGURE 5. (A) Representative images of tibial paraffin sections collected after the bioluminescence signal dropped below the detection threshold and stained with anti-CD8 and anti-GrB antibodies. 40x magnification, scale bar = 100 µm. **(B)** $CD8^+$ positive cells /10 high-perfusion fields (HPF). **(C)** GrB positive cells /10 (HPF). n = 2–3.

Values are presented as Arithmetic Mean (AM) ± Standard Error of the Mean (SEM).

* $p < 0.05$. Where not indicated with *, differences are not significant. One-way ANOVA.

mice were inoculated with 1×10^6 K7M2luc A7 cells. In all six mice establishments of the tumor was confirmed based on previous results from BALB/c mice. In those mice a drastic fall of signal strength on or after day 6 meant a subsequent failed tumor growth. Therefore, tumor establishment was assumed to be marked by stable signal above 1×10^6 p/s at two consecutive BLI starting on day 7. For this reason, 2 mice were euthanized at the time of tumor establishment for histopathological evaluation and another 4 were monitored for further growth monitoring with BLI twice a week and X-ray imaging once weekly. First BLI was performed on day 4 post-inoculation (Figure 6A). From initial values of $2.3 \times 10^6 \pm 9 \times 10^4$ p/s the signal steadily rose until day 50 ($5.9 \times 10^8 \pm 3.3 \times 10^8$ p/s). X-ray imaging showed intact bone on day 8 post-inoculation (Figure 6B), indicating no damage due to surgical implantation of cells. Bone was intact up until day 25 (Figure 6C), when bone lysis was visible, demonstrating a progressive tumor growth. However, mice showed no clinical signs of distress up until day 50, when extensive bone lysis was visible and mice started to exhibit lack of grooming, minimal loss of weight and limping, at which point they were humanely euthanized (Figure 6D).

The histopathological evaluation of two euthanized mice at the time of tumor establishment showed typical pathological changes after K7M2luc inoculation when comparing healthy (Figure 7A,D) and tumor-affected (Figure 7B,E) bone histological sections. Differences included presence of viable tumor cells with enlarged or multiple nuclei (Figure 7E-F: yellow arrows), changes in nucleus:cytoplasm ratio (Figure 7E-F: red arrows) and lace-like malignant osteoid matrix formation (Figure 7E-F: red asterisks). Furthermore, samples taken on day 30 show signs of progressive disease (Figure 7C,F), where bone lysis is visible (Figure 7C: yellow asterisks) and tumor cells invade the surrounding soft tissue (Figure 7F).

Discussion

The aim of this study was to evaluate immunogenic changes after orthotopic implantation of K7M2 luciferase-expressing cells into mouse tibia. One of the main characteristics of osteosarcoma tumors is their microenvironment, therefore there is a need for an orthotopic tumor model as opposed to a more widely used subcutaneous one. Furthermore, to evaluate antitumor effectiveness of novel therapies on orthotopic tumor models, *in vivo* imaging should be employed.[38]

In this study, we successfully transduced mouse osteosarcoma cell line K7M2 wt with luciferase gene using in-house developed plasmid and commercially available viral particles. (K7M2luc A7, K7M2luc E5). When selecting clonal cell lines, clones exhibiting sufficient bioluminescent intensity were chosen, favoring high, but not maximal, expression levels, as excessively high expression has been associated with reduced *in vivo* tumor growth.[22]

Despite slightly shorter doubling time observed in K7M2luc E5 cell line, no statistically significant differences in doubling time were found between wt and luciferase-expressing cell lines. This indicates that luciferase expression does not alter *in vitro* cell proliferation, which was previously also reported by Ferrari *et al*., 2024.[20] Next, we orthotopically implanted these two cell lines to syngeneic BALB/c mice. The results of *in vivo* orthotopic model showed there were differences between luciferase-expressing cell lines and wt. Although luciferase-expressing cells produced a detectable bioluminescent signal at the BLI on day 3, signal rapidly declined to below detection threshold (1 ×

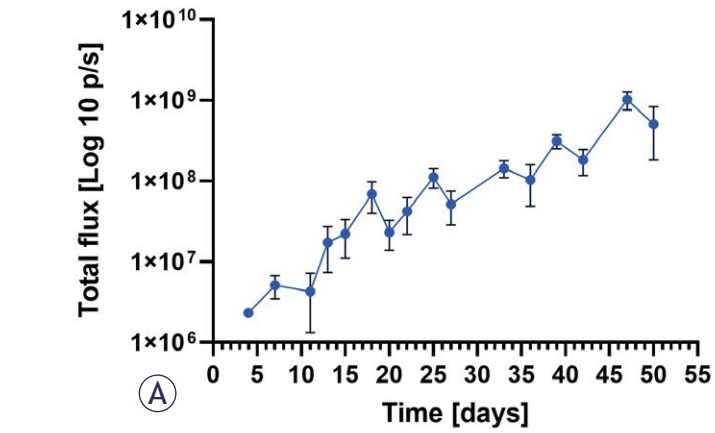

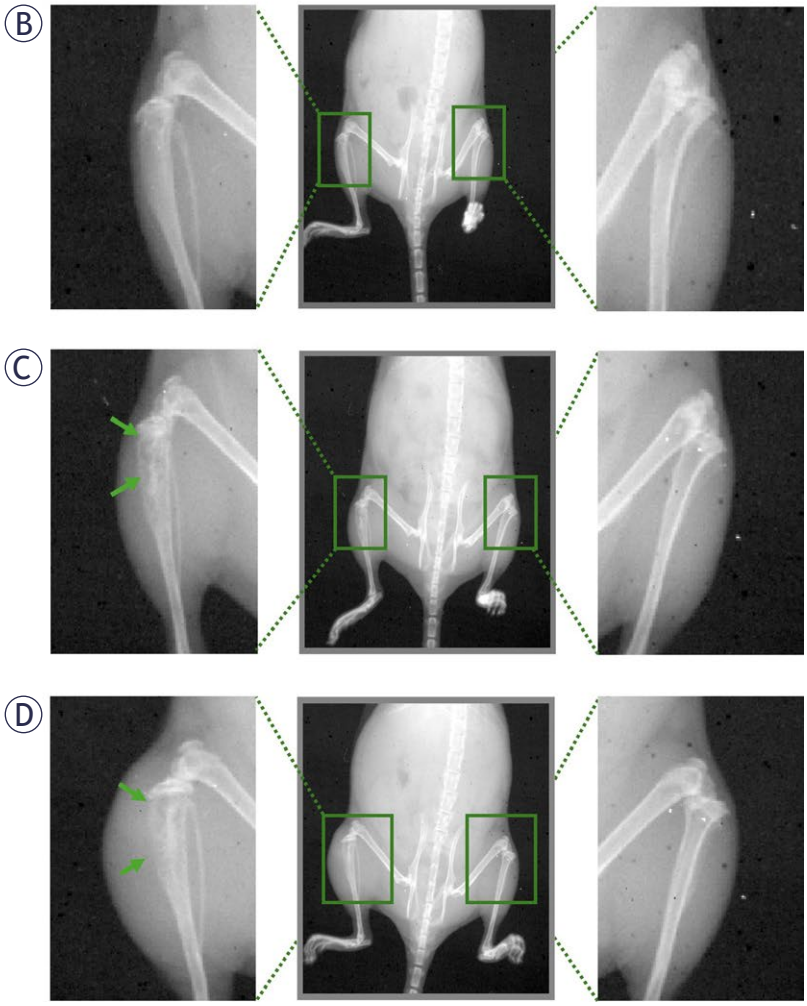

FIGURE 6. (A) Bioluminescent signal growth in NUDE mice, inoculated with K7M2luc A7 cells. **(B-D)** X-ray images of NUDE mice, inoculated with K7M2luc A7 cells on day 8, 25, 50. n = 4.

Arrows mark bone lysis. Values are presented as Arithmetic Mean (AM) ± Standard Error of the Mean (SEM).

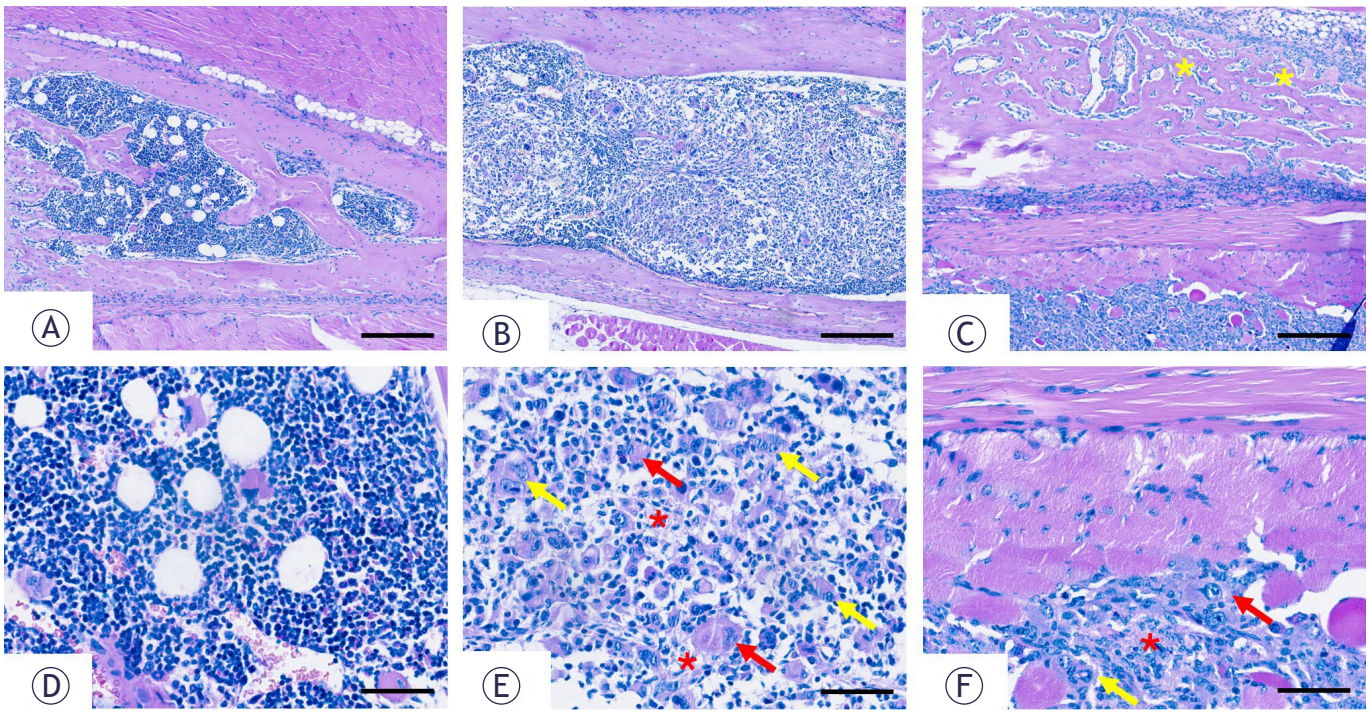

FIGURE 7. Representative images of paraffin tibia samples; **(A, D)** healthy, **(B, E)** established and **(C, F)** progressive tumor with soft tissue invasion. Yellow arrows mark tumor cells with enlarged or multiple nuclei, red arrows mark changed nucleus:cytoplasm ratio in tumor cells, red asterisks mark lace-like malignant osteoid matrix and yellow asterisks mark bone lysis. **(A, D)** 5x magnification, scale bar = 100 µm. **(B, C, E, F)** 40x magnification, scale bar = 60 µm.

10^4 p/s). As a result, inoculation success rate was 0%, which contrasts with previously reported rates of 80% and 90% using similar luciferase-tagged K7M2 lines.[39] Using K7M2 wt cell line, our inoculation rate was 100%, which is consistent with literature, where they reported an inoculation rate of 92%.[39]

One possibility for unsuccessful tumor establishment could be attributed to the immunogenic characteristics of luciferase. There have been several papers published describing induced immunogenicity, which negatively affected the growth of KPC tumors in pancreatic ductal adenocarcinoma models as well as in case of orthotopic 4T1 tumors, where unsuccessful implantation of the tumor in the mammary fat pad was attributed to the development of IFN-ɣ response.[20,25]

Therefore, we examined possible effects of luciferase on inducing antitumor immune response. We focused on investigating cell-mediated immunity, which is activated by intracellular changes and eliminates abnormal cells, including tumor cells.[40] Luciferase as a novel protein expressed in tumor cells supposedly presents as a foreign antigen, which is detected by immune system.[21,25,27] Humoral response, targeting extracellular pathogens, was already proven in previous reports to be inactive in the presence of luciferase.[20] NK cells and $CD8^+$ cells are leading anticancer immune responders, causing tumor suppression by releasing cytokines, granzymes and other effector molecules.[41] Activation of spleen-derived cytotoxic immune cells was tested via GrB and IFN-ɣ secretion. Luciferase-expressing cells showed an activation of cytotoxic lymphocytes, leading to elevated GrB secretion in comparison to samples from naïve mice. This was similar to KPC-luc spleen samples where a significant increase in NK T cell presence was reported, as well as in activated $CD8^+$ cells, expressing IFN-ɣ.[20]

Additionally, we evaluated tumor inoculation site for the presence of immune cells that would be accounted for the local immune response and rejection of the tumor. Immunohistochemical staining for GrB showed increase in K7M2luc samples compared to both wt and naïve mice, indicating presence of activated cytotoxic lymphocytes. Moreover, K7M2luc E5 had a higher number of GrB positive cells in comparison to K7M2luc A7. Such results indicate K7M2luc E5 as being more immunogenic, probably due to a higher luciferase expression, which was observed *in vitro*. Similarly

other groups already reported a connection between higher luciferase expression in a cell line and reduced tumor growth *in vivo*.[22] In order to determine whether GrB is secreted from activated $CD8^+$ or NK cells, we also stained for $CD8^+$ cells. Both K7M2luc exhibited a significantly higher concentration of $CD8^+$ cells as opposed to wt and naïve samples. It can be thus supposed that tumor regression mainly occurs due to localized presence of activated $CD8^+$ cytotoxic cells with limited systemic cytokine elevation. Owyang *et al*. published similar conclusions, where no systemic anti-tumor reactivity was detected in murine colon carcinoma CT26 tumors and tumor regression was limited to changes in TME.[42] Therefore, despite vast usage of luciferase and other imaging markers, considerations must be made as to the possible detrimental impact on tumor model development.

To further confirm the involvement of cytotoxic T lymphocytes in tumor establishment of K7M2luc orthotopic tumors, we inoculated NUDE mice with only K7M2luc A7 cells since K7M2luc E5 cells demonstrated higher immunogenicity, likely associated with their increased luciferase expression observed *in vitro*. Similar associations between high luciferase expression and reduced *in vivo* tumor growth have previously been reported.[22] Immunodeficient NUDE mice lack T lymphocytes, such as $CD8^+$, but still contain innate immune components like NK cells that could act as anti-tumor effectors.[43] Results from histological analysis of tumors in NUDE mice confirmed the chosen criteria for tumor establishment, which was as followed: starting 6 days post inoculation two consecutive BLI signal strengths hold above 1×10^6 p/s. Histochemical staining of samples, taken at the point of tumor establishment confirmed presence of tumor cells and changes in bone tissue, consistent with murine OSA histopathological markers.[44-47] Following tumor growth by BLI showed that tumor establishment occurred 7-11 days after tumor implantation. Further on, on day 15, signal strength was between 2.31×10^6 and 4.13×10^7 p/s, which is comparable to values stated by Grisez *et al*. at day 14 (approximately 2.5×10^6 p/s). They reported further stable signal growth with a peak on day 21 of approximately 1.5×10^7 p/s and subsequent tumor signal stagnation, whereas our model displayed a stable, progressive growth until day 50.[26]

Staining for GrB-secreting and $CD8^+$ cells revealed discrepancies in the number of positively stained cells, with a higher abundance of GrB-secreting cells observed. This difference may be attributable to the presence of NK cells secreting GrB. Hypothesis, that adaptive immunity represents the primary mechanism underlying tumor establishment failure, was based on previous reports.[20] Successful tumor establishment and further stable growth as visible by BLI and X-ray imaging confirmed that although NK cells may be present and could act as tumor suppressors, they are not sufficient for tumor rejection in case of OSA luciferase-expressing orthotopic tumors. Presence of activated $CD8^+$ is crucial for complete tumor regression, which was already shown in our previous studies, where activation of innate immune system effectors such as NK cells in NUDE mice led to tumor growth delay, whereas in immunocompetent mice both arms (NK cells and $CD8^+$ cells) of antitumor immune response were activated and succeeded in complete eradication of the tumor.[48] Our results are also in line with other studies, where they observed faster growth of adaptive immune system inhibiting CT26-TGF-β-R tumors in NUDE mice as opposed to immunocompetent mice.[42] Furthermore, another murine colon adenocarcinoma tumor model CT-26 expressing luciferase exhibited differences in tumor growth between immunocompetent and immunodeficient mice. A notable tumor growth retardation was observed in immunocompetent mice, but not in immunodeficient.[49]

In conclusion, our study demonstrated that luciferase-induced immune responses in syngeneic mice interfered with the establishment of orthotopic osteosarcoma tumors, necessitating the use of NUDE mice. However, immunocompromised models present certain challenges, particularly for evaluation of antitumor effect of novel immunotherapies.

Some limitations of this study should be acknowledged. First, the ELISpot assay did not include an exogenous antigen-specific positive control, which limits direct comparison of the observed responses with well-characterized immunodominant epitopes. However, the assay was intended to assess relative differences in cytotoxic responses across experimental groups under identical conditions. Therefore, conclusions are based on within-assay comparisons rather than absolute benchmarks of antigen-specific immunogenicity. Furthermore, luciferase-specific immune responses were evaluated using only a single luciferase-derived peptide, which may not fully reflect the range of antigenic epitopes generated from luciferase expression *in vivo*. Use of an entire luc2 peptide pool would allow for a more comprehensive

evaluation of luciferase-specific cytotoxic responses. Another limitation was the inability to detect IFN-γ in either serum or supernatant samples, despite secondary in vitro stimulation of splenocytes using a peptide containing the immunodominant luciferase-derived CD8+ epitope in the BALB/c background.[33] These findings contrast with previously published reports demonstrating elevated serum IFN-γ levels in mice bearing luciferase-expressing tumors compared with wt tumors.[25] Several factors may account for this discrepancy. Firstly, IFN-γ production is highly dynamic and often transient during antitumor immune responses. Because samples in our study were collected at experimental endpoints, it is possible that peak cytokine production had already passed by the time of analysis.[50] Another reason for lack of detection could be that the levels produced were below the threshold of our tests. In addition, a limitation of this study is the low number of samples, which reduces statistical robustness. In line with the 3R principles, the results were derived from a study comprising three mice per group, which further limits the strength and generalizability of the conclusions.

Nonetheless, these findings should further raise awareness of this critical yet often overlooked experimental variable and encourage the use and development of alternative models for preclinical cancer research. One such example are luciferase-tolerant transgenic strains (Tol mice). Other possibilities include alternative reporter systems with lower immunogenic potential, like click green beetle luciferase, which reportedly has minimal immunogenic effects in C57BL/6 mice. Precautions can also be taken in preparation of clones of parental cell lines, that express lower levels of luciferase that can still be detected.[21,22,51]

Acknowledgments

We would like to thank Ana Izlakar (Institute of Oncology Ljubljana) and Joni Katarina Knavs (Institute of Oncology Ljubljana) for their technical help.

This work was supported by the Slovenian Research Agency (ARIS); Programme Grant number P3-0003 and Programme Grant number P3-0428.

AI statement

During the preparation of this manuscript, authors used OpenAI 2026 GPT-5.6 Sol for text refinement. After using this tool, the authors reviewed and edited the content as necessary and take full responsibility for the content of the manuscript.

References

1 Ottaviani G, Jaffe N. The epidemiology of osteosarcoma. *Cancer Treat Res* 2009; **152:** 3-13. doi: 10.1007/978-1-4419-0284-9_1

2 Steliarova-Foucher E, Colombet M, Ries LAG, Moreno F, Dolya A, Bray F, et al. International incidence of childhood cancer, 2001-10: a population-based registry study. *Lancet Oncol* 2017; **18:** 719-31. doi: 10.1016/S1470-2045(17)30186-9

3 Bacci G, Longhi A, Fagioli F, Briccoli A, Versari M, Picci P. Adjuvant and neoadjuvant chemotherapy for osteosarcoma of the extremities: 27 year experience at Rizzoli Institute, Italy. *Eur J Cancer* 2005; **41:** 2836-45. doi: 10.1016/J.EJCA.2005.08.026

4 Mohseny AB, Szuhai K, Romeo S, Buddingh EP, Bruijn IB De, De Jong D, et al. Osteosarcoma originates from mesenchymal stem cells in consequence of aneuploidization and genomic loss of Cdkn2. *J Pathol* 2009; **219:** 294-305. doi: 10.1002/path.2603

5 Fletcher CDM, Mertens F, Unni K, editors. *World Health Organization classification of tumours. Pathology and genetics of tumours of soft tissue and bone* [Internet]. IARC Press; 2002. [cited 2026 Jan 05]. Available at: https://portal.research.lu.se/en/publications/world-health-organization-classification-of-tumours-pathology-and/

6 Corre I, Verrecchia F, Crenn V, Redini F, Trichet V. The osteosarcoma microenvironment: a complex but targetable ecosystem. *Cells* 2020; **9:** 1-25. doi: 10.3390/cells9040976.

7 Miyamoto N, Higuchi Y, Mori K, Ito M, Tsurudome M, Nishio M, et al. Human osteosarcoma-derived cell lines produce soluble factor(s) that induces differentiation of blood monocytes to osteoclast-like cells. *Int Immunopharmacol* 2002; **2:** 25-38. doi: 10.1016/S1567-5769(01)00134-5

8 Rubio R, Abarrategi A, Garcia-Castro J, Martinez-Cruzado L, Suarez C, Tornin J, et al. Bone environment is essential for osteosarcoma development from transformed mesenchymal stem cells. *Stem Cells* 2014; **32:** 1136-48. doi: 10.1002/STEM.1647

9 Omerzel M, Markelc B, Kranjc Brezar S, Sersa G, Cemazar M, Čemažar M. Efficient gene transfer by pulse parameters for electrochemotherapy of cells in vitro and in muscle and melanoma tumors in mice. *Radiol Oncol* 2025; **59:** 203-12. doi: 10.2478/raon-2025-0027

10 Killion JJ, Radinsky R, Fidler IJ. Orthotopic models are necessary to predict therapy of transplantable tumors in mice. *Cancer Metastasis Rev* 1999; **17:** 279-84. doi: 10.1023/a:1006140513233

11 Lwin TM, Hoffman RM, Bouvet M. Advantages of patient-derived orthotopic mouse models and genetic reporters for developing fluorescence-guided surgery. *J Surg Oncol* 2018; **118:** 253-64. doi: 10.1002/jso.25150

12 Denda-Nagai K, Fujita K, Fujime M, Nakatsugawa S, Ishigaki T, Irimura T. Absence of correlation of MUC1 expression to malignant behavior of renal cell carcinoma in experimental systems. *Clin Exp Metastasis* 2000; **18:** 77-81. doi: 10.1023/a:1026508402526

13 Fidler IJ. Experimental orthotopic models of organ-specific metastasis by human neoplasms. *Adv Molec Cell Biol* 1994; **9:** 191-215. doi: 10.1016/S1569-2558(08)60385-9

14 Fidler IJ, Wilmanns C, Staroselsky A, Radinsky R, Dong Z, Fan D. Modulation of tumor cell response to chemotherapy by the organ environment. *Cancer Metastasis Rev* 1994; **13:** 209-22. doi: 10.1007/BF00689637

15 Sangeetha B, Leroy KI, Udaya Kumar B. Harnessing bioluminescence: a comprehensive review of in vivo imaging for disease monitoring and therapeutic intervention. *Cell Biochem Funct* 2024; **42:** e70020. doi: 10.1002/CBF.70020

16 England CG, Ehlerding EB, Cai W. NanoLuc: a small luciferase is brightening up the field of bioluminescence. *Bioconjug Chem* 2016; **27:** 1175. doi: 10.1021/acs.bioconjchem.6b00112

17 Amadeo F, Plagge A, Chacko A, Wilm B, Hanson V, Liptrott N, et al. Firefly luciferase offers superior performance to AkaLuc for tracking the fate of administered cell therapies. *Eur J Nucl Med Mol Imaging* 2022; **49:** 796-808. doi: 10.1007/s00259-021-05439-4

18 Garimella R, Eskew J, Bhamidi P, Vielhauer G, Hong Y, Anderson HC, et al. Biological characterization of preclinical Bioluminescent Osteosarcoma Orthotopic Mouse (BOOM) model: a multi-modality approach. *J Bone Oncol* 2013; **2:** 11. doi: 10.1016/J.JBO.2012.12.005

19 Liu S, Su Y, Lin MZ, Ronald JA. Brightening up biology: advances in luciferase systems for in vivo imaging. *ACS Chem Biol* 2021; **16:** 2707. doi: 10.1021/ACSCHEMBIO.1C00549

20 Ferrari DP, Ramos-Gomes F, Alves F, Markus MA. KPC-luciferase-expressing cells elicit an anti-tumor immune response in a mouse model of pancreatic cancer. *Sci Rep* 2024; **14:** 1-12. doi: 10.1038/s41598-024-64053-0

21 Basnet A, Thomas DD, Landreth KM, Damron FH, Liu TW. Immune response to bioluminescence imaging reporters in murine tumor models. *Mol Imaging Biol* 2025; **27:** 341. doi: 10.1007/s11307-025-02010-7

22 Brutkiewicz S, Mendonca M, Stantz K, Comerford K, Bigsby R, Hutchins G, et al. The expression level of luciferase within tumour cells can alter tumour growth upon in vivo bioluminescence imaging. *Luminescence* 2007; **22:** 221-8. doi: 10.1002/BIO.953;CTYPE:STRING:JOURNAL

23 Petkov SP, Heuts F, Krotova OA, Kilpelainen A, Engström G, Starodubova ES, et al. Evaluation of immunogen delivery by DNA immunization using non-invasive bioluminescence imaging. *Hum Vaccin Immunother* 2013; **9:** 2228. doi: 10.4161/hv.25561

24 Kamensek U, Rols M-P, Cemazar M, Golzio M. Visualization of nonspecific antitumor effectiveness and vascular effects of gene electro-transfer to tumors. *Curr Gene Ther* 2016; **16:** 90-7. doi: 10.2174/1566523216666160331125611

25 Baklaushev VP, Kilpeläinen A, Petkov S, Abakumov MA, Grinenko NF, Yusubalieva GM, et al. Luciferase expression allows bioluminescence imaging but imposes limitations on the orthotopic mouse (4T1) model of breast cancer. *Sci Rep* 2017; **7:** 7715. doi: 10.1038/S41598-017-07851-Z

26 Grisez BT, Ray JJ, Bostian PA, Markel JE, Lindsey BA. Highly metastatic K7M2 cell line: a novel murine model capable of in vivo imaging via luciferase vector transfection. *J Orthop Res* 2018; **36:** 2296-304. doi: 10.1002/jor.23868

27 Sanchez VE, Lynes JP, Walbridge S, Wang X, Edwards NA, Nwankwo AK, et al. GL261 luciferase-expressing cells elicit an anti-tumor immune response: an evaluation of murine glioma models. *Sci Rep* 2020; **10:** 11003. doi: 10.1038/s41598-020-67411-w

28 Liang Y, Walczak P, Bulte JWM. Comparison of red-shifted firefly luciferase Ppy RE9 and conventional Luc2 as bioluminescence imaging reporter genes for in vivo imaging of stem cells. *J Biomed Opt* 2012; **17:** 016004. doi: 10.1117/1.jbo.17.1.016004

29 Craft N, Bruhn KW, Nguyen BD, Prins R, Liau LM, Collisson EA *et al.* Bioluminescent imaging of melanoma in live mice. *J Invest Dermatol* 2005; **125:** 159-65. doi: 10.1111/J.0022-202X.2005.23759.X

30 Smakman N, Martens A, Kranenburg O, Borel Rinkes IHM. Validation of bioluminescence imaging of colorectal liver metastases in the mouse. *J Surg Res* 2004; **122:** 225-30. doi: 10.1016/j.jss.2004.05.021

31 Tiffen JC, Bailey CG, Ng C, Rasko JEJ, Holst J. Luciferase expression and bioluminescence does not affect tumor cell growth in vitro or in vivo. *Mol Cancer* 2010; **9:** 299. doi: 10.1186/1476-4598-9-299.

32 Perrone F, Craparo EF, Cemazar M, Kamensek U, Drago SE, Dapas B, et al. Targeted delivery of siRNAs against hepatocellular carcinoma-related genes by a galactosylated polyaspartamide copolymer. *J Control Release* 2021; **330:** 1132-51. doi: 10.1016/j.jconrel.2020.11.020

33 Limberis MP, Bell CL, Wilson JM. Identification of the murine firefly luciferase-specific CD8 T-cell epitopes. *Gene Ther* 2009; **16:** 441. doi: 10.1038/GT.2008.177

34 Petkov S, Starodubova E, Latanova A, Kilpeläinen A, Latyshev O, Svirskis S, et al. DNA immunization site determines the level of gene expression and the magnitude, but not the type of the induced immune response. *PLoS One* 2018; **13:** e0197902. doi: 10.1371/JOURNAL.PONE.0197902

35 Mezzapelle R, De Marchis F, Passera C, Leo M, Brambilla F, Colombo F, et al. CXCR4 engagement triggers CD47 internalization and antitumor immunization in a mouse model of mesothelioma. *EMBO Mol Med* 2021; **13:** e12344. doi: 10.15252/EMMM.202012344

36 Dicks MDJ, Spencer AJ, Coughlan L, Bauza K, Gilbert SC, Hill AVS, et al. Differential immunogenicity between HAdV-5 and chimpanzee adenovirus vector ChAdOx1 is independent of fiber and penton RGD loop sequences in mice. *Sci Rep* 2015; **5:** 16756. doi: 10.1038/srep16756

37 Jansons J, Sominskaya I, Petrakova N, Starodubova ES, Smirnova OA, Alekseeva E, et al. The immunogenicity in mice of HCV core delivered as DNA is modulated by its capacity to induce oxidative stress and oxidative stress response. *Cells* 2019; **8:** 208. doi: 10.3390/CELLS8030208

38 Burgos JS, Rosol M, Moats RA, Khankaldyyan V, Kohn DB, Nelson MD, et al. Time course of bioluminescent signal in orthotopic and heterotopic brain tumors in nude mice. *Biotechniques* 2003; **34:** 1184-8. doi: 10.2144/03346ST01

39 Grisez BT, Ray JJ, Bostian PA, Markel JE, Lindsey BA. Highly metastatic K7M2 cell line: a novel murine model capable of in vivo imaging via luciferase vector transfection. *J Orthop Res* 2018; **36:** 2296-304. doi: 10.2144/03346ST01

40 Bonilla FA, Oettgen HC. Adaptive immunity. *J Allergy Clin Immunol* 2010; **125:** 33-40. doi: 10.1016/j.jaci.2009.09.017

41 Yu S, Yao X. Advances on immunotherapy for osteosarcoma. *Mol Cancer* 2024; **23:** 192. doi: 10.1186/S12943-024-02105-9

42 Owyang SY, Zhang M, Walkup GA, Chen GE, Grasberger H, El-Zaatari M, et al. The effect of CT26 tumor-derived TGF-β on the balance of tumor growth and immunity. *Immunol Lett* 2017; **191:** 47. doi: 10.1016/J.IMLET.2017.08.024

43 Hong ZF, Zhao WX, Yin ZY, Xie CR, Xu YP, Chi XQ, et al. Natural killer cells inhibit pulmonary metastasis of hepatocellular carcinoma in nude mice. *Oncol Lett* 2016; **11:** 2019-26. doi: 10.3892/OL.2016.4170

44 Yao M, Lei Z, Peng F, Wang D, Li M, Zhong G, et al. Establishment of orthotopic osteosarcoma animal models in immunocompetent rats through muti-rounds of in-vivo selection. *BMC Cancer* 2024; **24:** 703. doi: 10.1186/S12885-024-12361-Z

45 Wu H, He Z, Li X, Xu X, Zhong W, Bu J, et al. Efficient and consistent orthotopic osteosarcoma model by cell sheet transplantation in the nude mice for drug testing. *Front Bioeng Biotechnol* 2021; **9:** 690409. doi: 10.3389/FBIOE.2021.690409/BIBTEX

46 Beck J, Ren L, Huang S, Berger E, Bardales K, Mannheimer J, et al. Canine and murine models of osteosarcoma. *Vet Pathol* 2022; **59:** 399-414. doi: 10.1177/03009858221083038

47 Kavirayani AM, Foreman O. Retrospective study of spontaneous osteosarcomas in the nonobese diabetic strain and nonobese diabetic-derived substrains of mice. *Vet Pathol* 2010; **47:** 482-7. doi: 10.1177/0300985810363699

48 Lampreht Tratar U, Kos S, Kamensek U, Ota M, Tozon N, Sersa G, et al. Antitumor effect of antibiotic resistance gene-free plasmids encoding interleukin-12 in canine melanoma model. *Cancer Gene Ther* 2018; **25:** 260-73. doi: 10.1038/S41417-018-0014-5

49 Yong HJ, Choi Y, Joo HK, Chul WK, Jae MJ, Dong SL, et al. Immune response to firefly luciferase as a naked DNA. *Cancer Biol Ther* 2007; **6:** 781-6. doi: 10.4161/CBT.6.5.4005

50 Gonzalez H, Hagerling C, Werb Z. Roles of the immune system in cancer: from tumor initiation to metastatic progression. *Genes Dev* 2018; **32:** 1267. doi: 10.1101/GAD.314617.118

51 Khan KA, Qureshi AA, Xu P, Kuo HY, Schumacher TN, Michael IP, et al. Immunological tolerance to luciferase and fluorescent proteins using Tol mice enables development of improved tumor models for investigating immunity and metastasis. *Cancer Res* 2025; **85:** 2165-78. doi: 10.1158/0008-5472.CAN-24-2418

RADIOLOGY AND ONCOLOGY Radiology and Oncology | Ljubljana | Slovenia | www.radioloncol.com

research article

EPHA3, upregulated in high-risk histological subtypes of gastrointestinal stromal tumor, promotes GIST progression

Han Wei[1], Jia Zhao[2], Hongmei Wang[1], Lihong Guo[3], Yanhong Liu[2], Chuntao Wang[2], Liang Yang[1], Zhi Qi[1,2], Wencong Tian[2], Lei Cao[2], Yang Gao[1]

[1] Department of Molecular Pharmacology, School of Medicine, Nankai University; Tianjin, 300071, China

[2] Department of General Surgery, Tianjin Union Medical Center, The First Affiliated Hospital of Nankai University, Nankai University, Tianjin, 300122, China

[3] Institute of Digestive Disease, Shengli Oilfield Central Hospital, Dongying, 257000, China

Radiol Oncol 2026; 60(3): 416-426.

Received 6 May 2026
Accepted 4 June 2026

Correspondence to:Wencong Tian, Department of General Surgery, Tianjin Union Medical Center, The First Affiliated Hospital of Nankai University, No. 190 Jieyuan Road, Hongqiao District, Tianjin 300122, PR China. E-mail: tianwencong427@163.com; Lei Cao, Department of General Surgery, Tianjin Union Medical Center, The First Affiliated Hospital of Nankai University, No. 190 Jieyuan Road, Hongqiao District, Tianjin 300122, PR China. E-mail: caolei@umc.net.cn; Yang Gao, School of Medicine, Nankai University, No. 94 Weijin Road, Nankai District, Tianjin 300350, PR China. E-mail: Gaoy@nankai.edu.cn

Han Wei, Jia Zhao and Hongmei Wang contributed equally to this work.

Disclosure: No potential conflicts of interest were disclosed.

Background. To explore the expression pattern and functional role of EPH receptor A3 (EPHA3) in high-risk gastrointestinal stromal tumors (GISTs) and its potential relevance to tumor progression.

Materials and methods. Immunohistochemical (IHC) analysis was performed to evaluate EPHA3 expression across a pilot cohort of clinical GIST specimens with different risk stratifications. The biological functions of EPHA3 *in vitro* were assessed using (5-ethynyl-2'-deoxyuridine, EdU) assay, colony formation, apoptosis, wound-healing, and transwell assays in EPHA3-knockout GIST-430 cells. Furthermore, RNA sequencing (RNA-seq) analysis was utilized to identify differentially expressed genes and associated signaling pathways following EPHA3 knockout.

Results. EPHA3 expression was found to be elevated in high-risk GIST specimens compared with intermediate-risk cases. Loss-of-function assays demonstrated that EPHA3 knockout attenuated cell proliferation and migration while promoting apoptosis *in vitro*. Pathway enrichment analysis suggested that EPHA3 expression is associated with cell adhesion, extracellular matrix interaction, and mesenchymal-related phenotypic remodeling.

Conclusions. Our findings suggest that EPHA3 is upregulated in high-risk GIST and contributes to aggressive cellular behavior *in vitro*. These preliminary data indicate that EPHA3 may play a role in the malignant progression of GIST, although its clinical utility as a biomarker requires further validation in larger cohorts.

Key words: EPHA3; gastrointestinal stromal tumors (GISTs); histological subtype; epithelial–mesenchymal transition (EMT)

Introduction

Gastrointestinal stromal tumors (GISTs), the most frequent mesenchymal tumors in the gastrointestinal system, have an annual incidence of 16–20 per million in Asian populations and 10–15 per million in Western countries, with a gradually rising global trend.[1,2] Molecularly, GISTs are associated with mutations in receptor tyrosine kinase (RTK) genes such as *KIT* or *PDGFRA*.[3] Although tyrosine kinase inhibitors like imatinib have significantly improved treatment outcomes, therapeutic resist-

ance and postoperative recurrence remain major clinical challenges.[4]

Accurate recurrence risk assessment is critical for guiding postoperative strategies, and the modified NIH consensus criteria introduced in 2008 are commonly used.[5] According to this framework, gastric GISTs smaller than 5 cm with a mitotic count of < 5 per 50 HPFs are typically classified as low risk. These cases generally carry a favourable prognosis and are often managed successfully with surgery alone. In contrast, tumors that exceed 5–10 cm in size, exhibit elevated mitotic counts (e.g., > 5 or > 10/50 HPFs), or are located in the non-gastric sites (such as the small bowel or colon) are considered intermediate or high-risk. Such features reflect enhanced biological aggressiveness, including increased potential for invasion and metastasis, thereby increasing the likelihood of postoperative recurrence. These patients often require prolonged adjuvant TKI therapy.[6]

Despite the diagnostic utility of immunohistochemical markers such as CD117 and DOG1, their ability to predict tumor behavior remains limited.[7] This underscores the need for novel biomarkers to better characterize GIST aggressiveness. EphA3, a receptor tyrosine kinase in the Eph family, has been reported to be upregulated in various cancers and is associated with aggressive clinical features, including tumor invasion, metastasis, and poor prognosis in gastric and colorectal cancers.[8-11] However, its expression and role in GIST have not yet been thoroughly examined.

This study aimed to investigate EPHA3 expression in GIST samples across different risk groups and evaluate its potential as a biomarker for risk stratification. We further explored the impact of EPHA3 on GIST cell proliferation, migration, and apoptosis, and investigated the underlying molecular mechanisms.

Materials and methods

Patient enrollment and tissue collection

Between 2023 and 2025, a total of 11 patients diagnosed with primary gastrointestinal stromal tumors (GIST) at The First Affiliated Hospital of Nankai University were recruited (Table 1). Eligible participants met the following criteria: (1) newly diagnosed and histologically confirmed GIST; (2) availability of representative tumor tissue blocks for immunohistochemical and molecular analyses; and (3) no prior exposure to neoadjuvant treatments such as radiotherapy, chemotherapy, or targeted therapy. Tumor specimens were excised during radical surgery and promptly frozen in liquid nitrogen to preserve RNA and protein integrity for downstream analyses. Following resection, clinical data and histopathological features were collected for each patient. The study was approved by the Ethics Committee of Nankai University (Approval No. NKUIRB2025078), and written informed consent was obtained from all subjects. All procedures were conducted in accordance with the Declaration of Helsinki.

TABLE 1. Clinicopathological characteristics of the study cohort (n = 11)

Case No.	Gender	Age	Primary site	Mitotic count (per 50 HPFs)	Ki-67 Index	NIH risk category	CD117 / DOG1	Maximum diameter (cm)*
1	Female	72	Stomach	10	5%	Intermediate	+/+	2
2	Female	61	Stomach	≤ 2	<5%	Intermediate	+/+	4
3	Male	39	Stomach	6	8%	Intermediate	+/+	3
4	Female	82	Stomach	< 5	5%	Intermediate	+/+	7
5	Male	51	Stomach	< 5	5%	Intermediate	+/+	3
6	Female	81	Stomach	> 20	15%	High	+/+	5
7	Female	68	Stomach	> 10	20%	High	+/+	3
8	Male	37	Stomach	> 20	10%	High	+/+	4.5
9	Male	61	Stomach	> 20	20%	High	+/+	7
10	Male	67	Rectum	> 10	15%	High	+/+	6.5
11	Female	57	Stomach	14	3%	High	+/-	3.5

HPF = high-power field; NIH = National Institutes of Health

* Tumor size was determined by the maximum diameter from the pathological gross description. Risk stratification was performed according to the modified NIH consensus criteria (2008).

Histopathological evaluation and risk stratification

Histopathological evaluation was performed by two independent pathologists. The risk of recurrence for each GIST case was determined according to the modified National Institutes of Health (NIH) consensus criteria (2008), which integrates tumor size, primary site, and mitotic activity. Mitotic count was assessed by examining 50 consecutive high-power fields (HPFs, total area of 5 mm^2) in the most cellular areas of the tumor. Tumors were specifically categorized into intermediate-risk and high-risk groups to compare the differential expression of EPHA3. For immunohistochemical (IHC) analysis, the scoring was conducted using a semi-quantitative system considering both staining intensity and the percentage of positive cells, as previously described. To ensure objectivity, the pathologists were blinded to the clinical risk stratification of the patients during the evaluation.

Cell culture and transfection

GIST-430 cell line, derived from human gastrointestinal stromal tumor tissue, was generously provided by Professor Wenbing Ou from Zhejiang SciTech University. Cells were maintained in DMEM (High glucose; SparkJade, CA0002), added with fetal bovine serum (Gibco, USA, 10%) and penicillin–streptomycin solution (MCE, HY-K1106, 1%). Cells were maintained at 37°C in a humidified atmosphere with 5% CO_2.

To silence EPHA3 expression, GIST-430 cells were transfected with either EPHA3-specific siRNA (si-EPHA3) or a negative control (NC) siRNA. The siRNA sequences are provided in Supplementary Table S1. The small interfering RNA (siRNA) oligonucleotides were designed and manufactured by Saisofi Biotechnology Co., Ltd. Transient transfections were conducted using GP-transfect-mate reagent (GenePharma, G04008), following the recommended protocol, Cells were collected for further analysis 48 hours later. The efficacy of gene knockdown was subsequently examined with quantitative reverse transcription polymerase chain reaction (qRT-PCR) and Western blotting refer to Supplementary Table S2 (for detailed sequences).

Establishment of EPHA3-knockout GIST-430 cells

To generate an EPHA3-deficient model, GIST-430 cells were genetically edited using a CRISPR/Cas9-based approach. A plasmid construct containing Cas9 nuclease and an sgRNA targeting human EPHA3 (Plasmid ID: L15525; supplier: Beyotime Biotechnology, China) was introduced into the cells using Lipofectamine™ 3000 transfection reagent (Thermo Fisher, L3000001), according to the manufacturer's instructions. Approximately 48 hours after transfection, cells were subjected to puromycin selection at 2 μg/mL for 7–10 days to enrich stable knockout populations. EPHA3 disruption was subsequently validated by Western blotting, confirming the loss of protein expression in the established knockout cells.

Immunohistochemistry (IHC)

Formalin-fixed, paraffin-embedded (FFPE) GIST specimens were sectioned at a thickness of 4 μm. The sections were deparaffinized in xylene and rehydrated through graded ethanol. Antigen retrieval was performed by microwave heating in 10 mM citrate buffer (pH 6.0) at medium power for approximately 10 minutes. Endogenous peroxidase activity was blocked with 3% hydrogen peroxide for 10 minutes at room temperature. After blocking non-specific binding, the sections were incubated overnight at 4°C with a primary monoclonal antibody against EPHA3 (Santa Cruz Biotechnology, sc-514209; dilution 1:1000). After three washes with PBS, an HRP-conjugated secondary antibody (ORIGENE, PV-8000-1) was applied for 1 hour at room temperature. Signal detection was performed using a DAB chromogen substrate, and nuclei were counterstained with hematoxylin. The slides were then dehydrated, mounted, and examined under a light microscope. EPHA3 expression was quantitatively assessed by average optical density (AOD) using ImageJ software.

5-ethynyl-2'-deoxyuridine (EdU) assay

To evaluate cell proliferation, 430-WT and 430-KO cells were seeded into 24-well plates and cultured under standard conditions until reaching appropriate confluence. Cell proliferation was assessed using the BeyoClick™ EdU Cell Proliferation Kit with Alexa Fluor 488 (Beyotime, C0071S) according to the manufacturer's instructions. Briefly, cells were incubated with EdU working solution for an hour, then fixed with 4% paraformaldehyde and permeabilized with 0.3% Triton X-100. After washing with PBS, the cells were subjected to click reaction staining and counterstained with Hoechst 33342 to visualize nuclei. Images were

captured using a fluorescence microscope, and the percentage of EdU-positive cells was quantified using ImageJ software. All experiments were performed in triplicate.

Colony formation assay

For colony formation assays, a total of 300 cells with EPHA3 KO or WT were placed in 6-well plates and grown for 10 to 14 days. The colonies were then fixed using 4% paraformaldehyde and stained with a 0.1% crystal violet solution (Solarbio, G1064) for visualization, and quantified under a microscope.

Apoptosis assay by flow cytometry

To determine apoptotic cell populations, exponentially growing GIST-430 cells were collected and rinsed twice with PBS. Using the Annexin V-FITC/PI staining kit (Yeasen, 40302ES60), apoptosis was detected as per the manufacturer's protocols. Cells were treated with Annexin V-FITC and propidium iodide for 15 minutes at room temperature, keeping them in the dark to prevent photobleaching. Fluorescence signals were then acquired using a BD FACSCalibur flow cytometer. Data analysis and quantification of apoptotic fractions were performed using FlowJo software. All experimental groups were assessed in three independent replicates.

Wound healing assay

In 6-well plates, GIST-430 cells were grown until they reached full coverage. A sterile pipette tip was used to make a scratch, and the cells were then cultured in a serum-free environment. Images were taken initially and after 24 h, and wound closure was quantified using ImageJ.

Transwell assay

Cells were seeded in DMEM (2%FBS) into 8-μm pore Transwell inserts (Corning, 3422), with 10% FBS medium in the lower chamber. Cells that had migrated were fixed with 4% paraformaldehyde after 24 hours, stained with 0.1% crystal violet, and counted in five random areas.

Western blot analysis

Total proteins were isolated using RIPA lysis buffer, and their concentrations were assessed with a BCA protein assay kit. Proteins in equal quantities were resolved on SDS-PAGE gels and then moved to 0.22 μm PVDF membranes provided by Millipore. To reduce nonspecific binding, membranes were incubated in 5% skim milk at room temperature for 1 hour. They were then incubated overnight at 4°C with the following primary antibodies: anti-EPHA3 (Santa Cruz, sc-514209, 1:1000), anti-PCNA (Santa Cruz, sc-71858, 1:1000), anti-Bcl-2 (CST, #3498, 1:1000), anti-Bax (CST, #2772, 1:1000), anti-cleaved Caspase-3 (ZenBio, L13OC01, 1:1000), anti-ZEB1 (CST, #70512T, 1:1000), anti-Vimentin (Proteintech, 10366-1-AP, 1:1000), and anti-N-cadherin (Proteintech, 22018-1-AP, 1:1000). After thorough washing, HRP-conjugated secondary antibodies (Proteintech, 1:1000) were applied for 60 minutes at ambient temperature. SparkJade ECL Super chemiluminescence reagent (ED0015) was used for detection, and ImageJ software counted the signal intensities of the protein bands.

Quantitative real-time PCR (qRT-PCR)

The R1100 reagent from Solarbio was used to isolate total RNA. cDNA synthesis was performed using the EasyScript® All-in-One First-Strand cDNA Synthesis SuperMix for qPCR (TransGen, AE341), following the manufacturer's protocol. Amplification was conducted on a Roche qPCR system utilizing PerfectStart® Green qPCR SuperMix (TransGen, AQ601). The thermal cycling program began with an initial denaturation at 94°C for 30 seconds, followed by 45 amplification cycles consisting of 94°C, 5 seconds and 60°C, 30 seconds. Gene expression was normalized and quantified using the 2^−ΔΔCt method. Supplementary Table S1 provides all the primer sequences utilized in the assay.

RNA sequencing and bioinformatic analysis

Total RNA was obtained from 430-WT and EPHA3-knockout (430-KO) GIST-430 cells and submitted to Hongxu Bio (China) for transcriptome profiling. Library construction and high-throughput paired-end sequencing (150 bp, PE150) were performed on the Illumina NovaSeq platform. To ensure data quality, raw sequencing reads were processed with fastp[12] for filtering and trimming. Clean reads were then aligned to the human reference genome (GRCh38) using HISAT2.[13] Gene-level quantification was performed using featureCounts[14], and differential gene expression analysis was con-

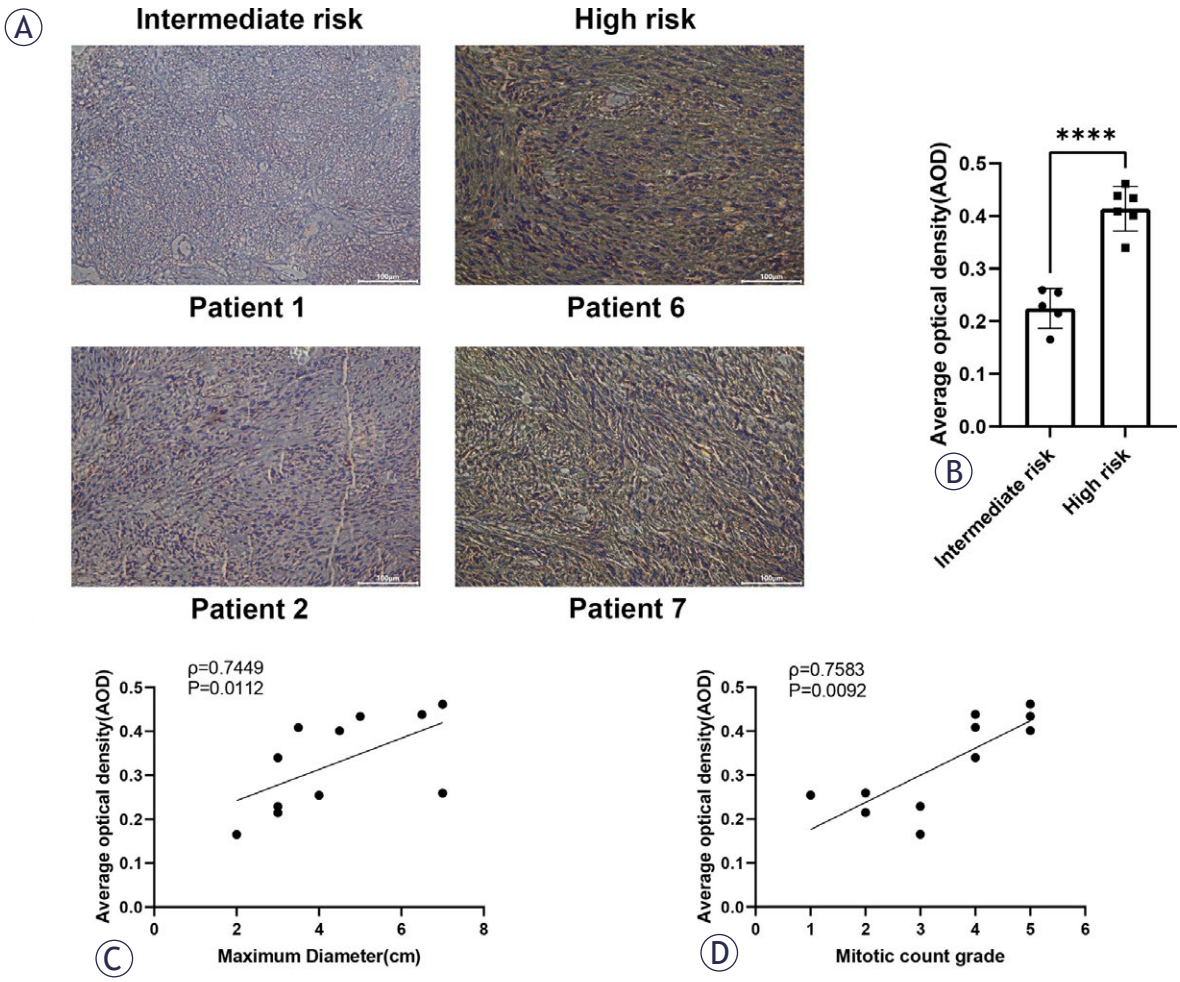

FIGURE 1. EPHA3 expression is elevated in high-risk GIST specimens and correlates with clinicopathological features. **(A)** Representative immunohistochemical (IHC) images of EPHA3 staining in intermediate-risk and high-risk GIST specimens, Scale bar = 100 μm. Full EPHA3 IHC images for all 11 patients are shown in Supplementary Figure S1, and the case numbers correspond to those listed in Table 1. **(B)** Quantification of EPHA3 staining by average optical density (AOD) in intermediate-risk and high-risk GIST specimens. Each dot represents one patient. Data are presented as the mean ± SD. ****$p < 0.0001$. **(C)** Spearman correlation analysis between maximum tumor diameter and EPHA3 AOD values in 11 GIST patients ($\rho = 0.7449$, $p = 0.0112$). **(D)** Spearman correlation analysis between mitotic count grade and EPHA3 AOD values in 11 GIST patients ($\rho = 0.7583$, $p = 0.0092$).

ducted using DESeq2.[15] Differentially expressed genes (DEGs) were filtered using the criteria of an adjusted P value < 0.05 and $|\log_2$ fold change$|$ > 0.585, corresponding to a fold change > 1.5 for upregulated genes or < 0.67 for downregulated genes. Differentially expressed genes were visualized using a volcano plot, and the full list of DEGs was provided in the Supplementary Table S3. To investigate their functional implications, Gene Ontology (GO) and KEGG pathway enrichment analyses were performed using clusterProfiler[16] and KEGG pathway annotation was based on the KEGG database.[17]

Statistical analysis

Data are presented as mean ± SD from three independent experiments. Statistical analyses were performed using GraphPad Prism 9.0. Differences between two groups were assessed using unpaired two-tailed t-tests, and comparisons among multiple groups were analyzed by one-way ANOVA

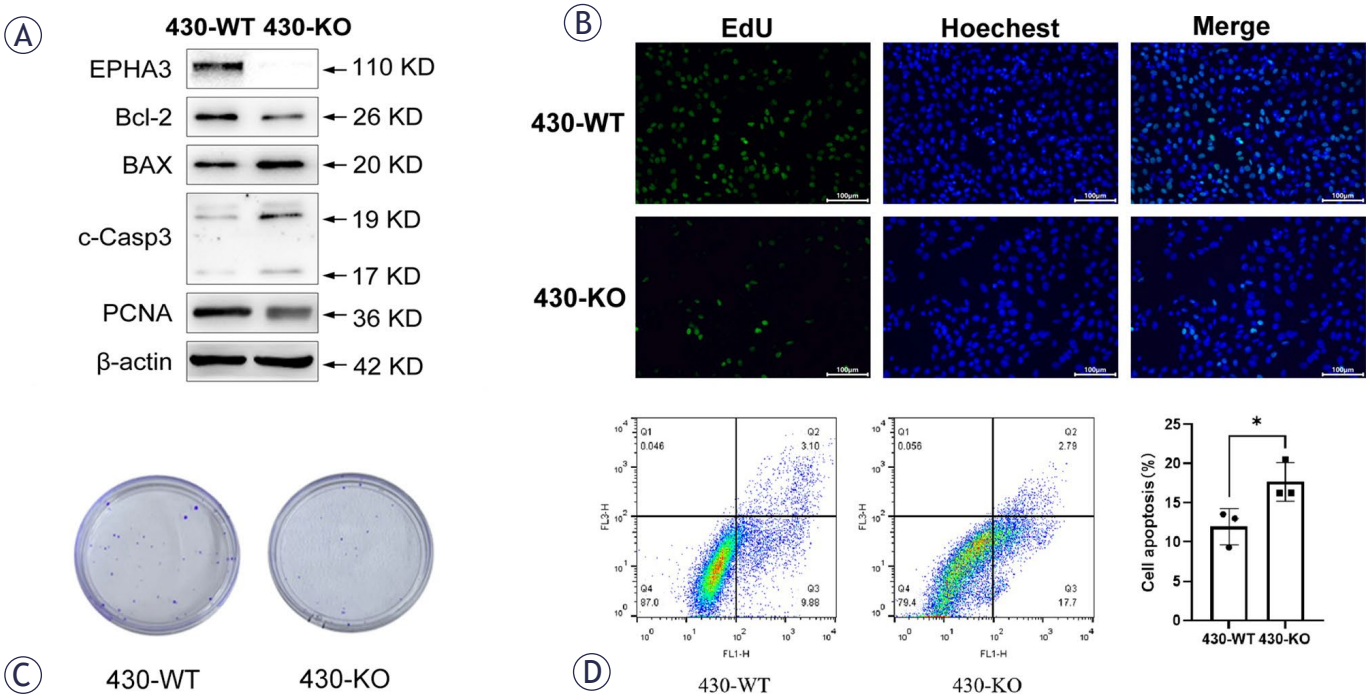

FIGURE 2. EPHA3 promotes the proliferation and survival of GIST-430 cells. **(A)** Representative Western blot images showing showing the expression of EPHA3, Bcl-2, Bax, cleaved caspase-3, and PCNA in 430-WT and 430-KO cells, with β-actin as the loading control. **(B)** 5-ethynyl-2'-deoxyuridine, EdU) assay showing the proliferative capacity of 430-WT and 430-KO cells, Scale bar = 100 μm. **(C)** Colony formation assay of 430-WT and 430-KO cells. **(D)** Representative flow cytometry plots and quantification of apoptotic cells in 430-WT and 430-KO cells using Annexin V/PI staining. Data are presented as mean ± SD from three independent experiments. *$p < 0.05$, **$p < 0.01$, ***$p < 0.001$.

followed by Tukey's post hoc test. Correlations between EPHA3 AOD values and tumor size or mitotic count grade were evaluated using Spearman correlation analysis. A p value < 0.05 was considered statistically significant. Significance levels are indicated as follows: $p < 0.05$ (*), $p < 0.01$ (**), $p < 0.001$ (***), and $p < 0.0001$ (****).

Results

EPHA3 positively correlates with malignant progression in GIST patients

To assess the correlation between EPHA3 expression and GIST progression, immunohistochemistry was performed on tissue specimens from a pilot cohort of 11 patients, including six categorized as high-risk and five as intermediate-risk according to the modified NIH criteria. As shown in Figure 1A, representative IHC images revealed stronger EPHA3 staining in high-risk tumors than in intermediate-risk tumors. Quantitative analysis showed that EPHA3 AOD values were significantly elevated in high-risk tumors compared with intermediate-risk tumors (Figure 1B). Spearman correlation analysis further demonstrated that EPHA3 AOD values were positively correlated with tumor size ($\varrho = 0.7449$, $p = 0.0112$) and mitotic count grade ($\varrho = 0.7583$, $p = 0.0092$) (Figure 1C-D, Table 1). Full EPHA3 IHC images for all 11 patients are shown in Supplementary Figure 1. These results suggest that increased EPHA3 expression is associated with the high-risk clinical features of GIST, potentially reflecting its role in biological aggressiveness.

EPHA3 promotes GIST tumor progression *in vitro*

To elucidate the functional contribution of EPHA3 in GIST, we employed a CRISPR/Cas9-mediated knockout strategy in GIST-430 cells. Representative Western blot images showed the loss of EPHA3 expression in 430-KO cells compared with 430-WT cells (Figure 2A, Supplementary Figure 2). Functional assays, including EdU and colony formation assays, demonstrated that EPHA3 depletion significantly attenuated cell proliferation (Figure 2B-C). In line with these observations, the

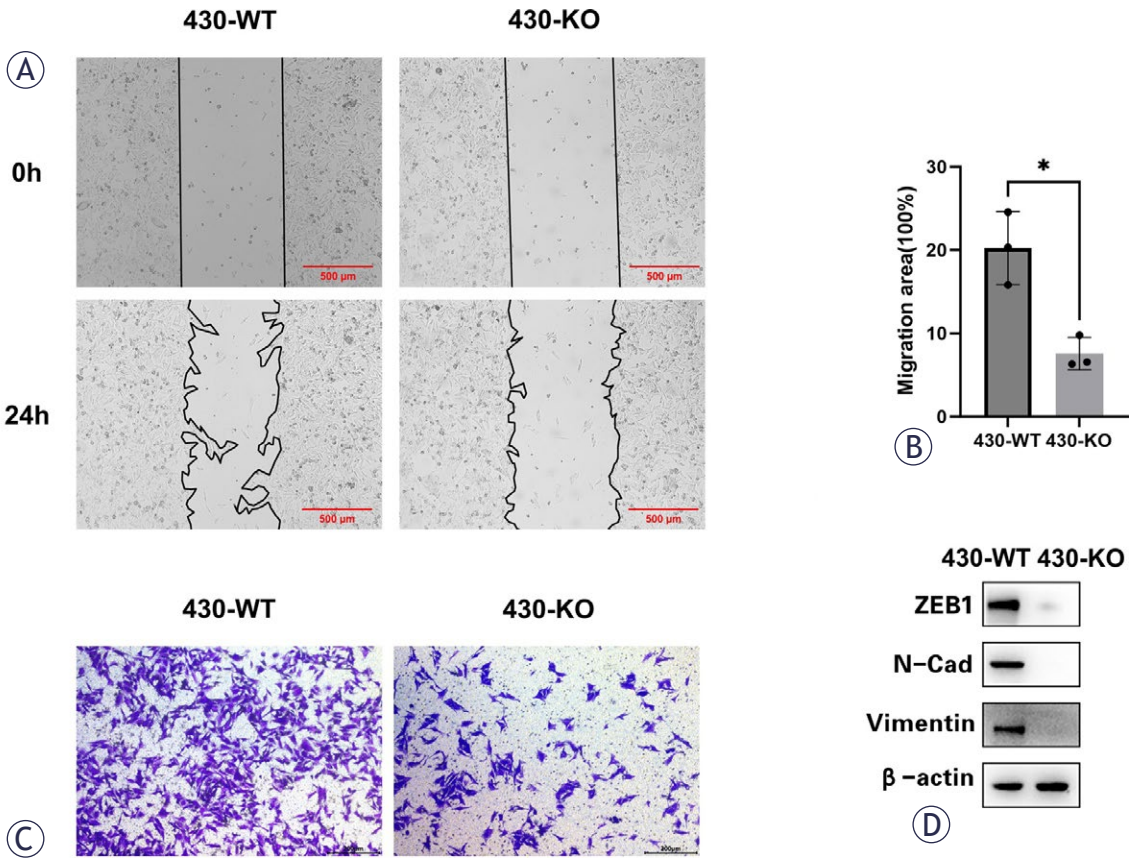

FIGURE 3. EPHA3 promotes the migration of GIST-430 cells. **(A)** Representative images of the wound-healing assay in 430-WT and 430-KO cells at 0 and 24 h. Scale bar = 500 μm. **(B)** Quantification of wound closure in 430-WT and 430-KO cells after 24 h. **(C)** Transwell migration assay showing the migratory ability of 430-WT and 430-KO cells. Scale bar = 200 μm. **(D)** Representative Western blot images showing ZEB1, N-cadherin, and Vimentin expression in 430-WT and 430-KO cells, with β-actin as the loading control. Data are presented as mean ± SD from three independent experiments. *$p < 0.05$, **$p < 0.01$, ***$p < 0.001$.

expression of PCNA was notably decreased in 430-KO cells (Figure 2A, Supplementary Figure 2).

To assess whether EPHA3 loss triggers programmed cell death, we utilized Annexin V/PI double staining followed by flow cytometric analysis. A marked increase in apoptotic cell populations was observed in 430-KO cells relative to 430-WT cells (Figure 2D). Representative Western blot images further supported this finding, as EPHA3-deficient cells exhibited increased levels of cleaved caspase-3 and a reduced Bcl-2/Bax ratio (Figure 2A, Supplementary Figure 2). These data suggest that EPHA3 deficiency may activate the mitochondrial apoptosis pathway, thereby contributing to enhanced apoptotic activity and reduced tumor cell survival in GIST-430 cells.

EPHA3 deficiency impairs migration and invasion of GIST-430 cells *in vitro*

To investigate the impact of EPHA3 in GIST cell mobility and invasive behavior, we conducted both wound healing and Transwell assays after silencing EPHA3 in GIST-430 cells.

As anticipated, EPHA3 knockout significantly reduced the wound-closure rate of GIST-430 cells after 24 h, indicating impaired migratory capacity (Figure 3A–B). Consistently, the number of cells passing through the Transwell membrane was markedly decreased in 430-KO cells compared with 430-WT cells (Figure 3C). In line with these observations, representative Western blot images showed decreased expression of

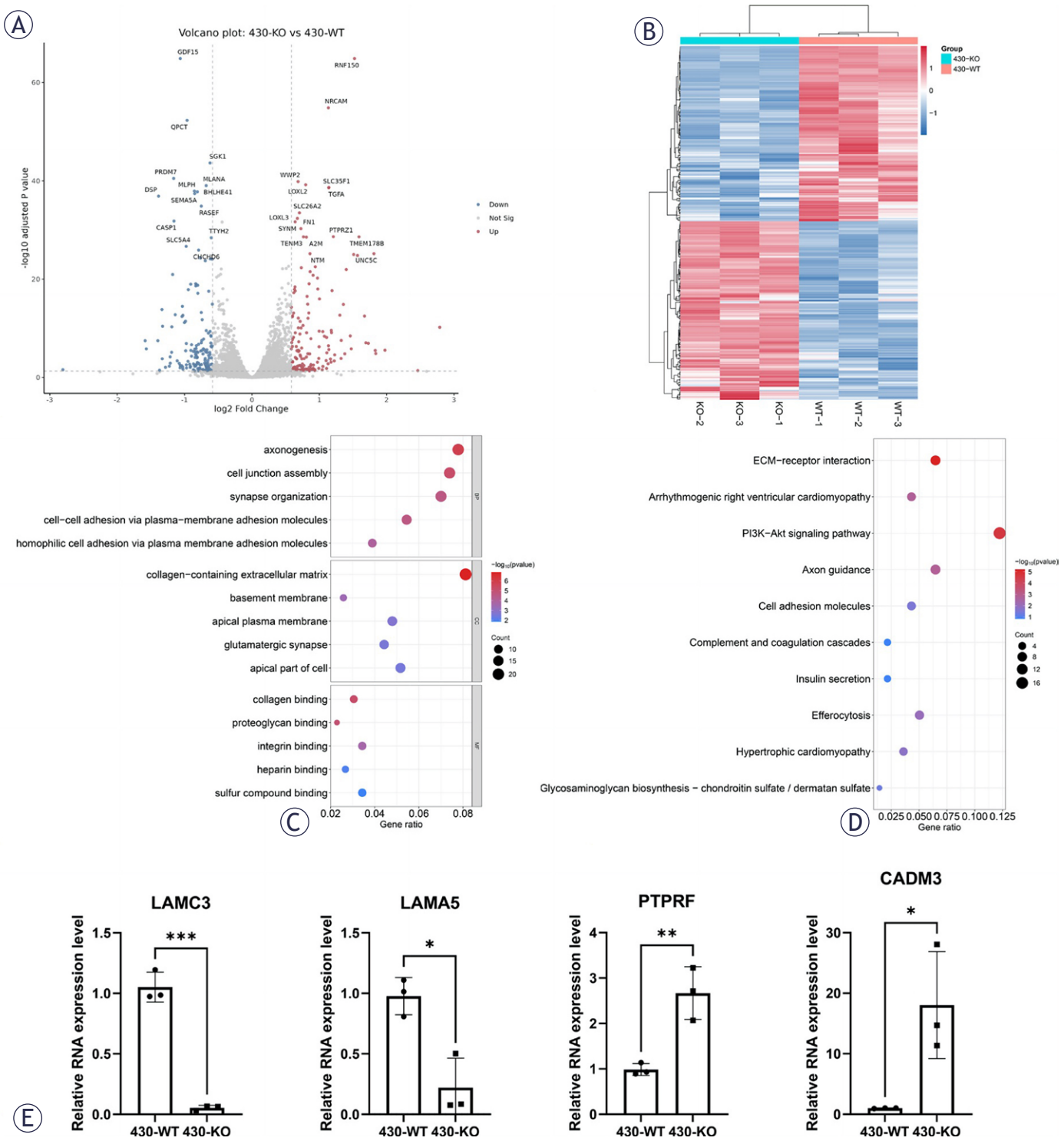

FIGURE 4. RNA sequencing (RNA-seq) analysis of EPHA3-knockout GIST-430 cells. **(A)** Volcano plot showing differentially expressed genes (DEGs) in 430-KO cells relative to 430-WT cells. DEGs were defined using the criteria of an adjusted P value < 0.05 and $|\log_2$ fold change$|$ > 0.585. Red dots indicate upregulated genes, blue dots indicate downregulated genes, and grey dots indicate genes without significant differential expression. **(B)** Hierarchical-clustering heatmap showing the expression patterns of DEGs in 430-WT and 430-KO cells. Rows represent genes, columns represent samples, and the colour scale indicates row-wise Z-score-normalized expression levels. **(C)** Gene Ontology (GO) enrichment analysis showing the top five enriched terms in each GO category, including biological process, cellular component, and molecular function. **(D)** Kyoto Encyclopaedia of Genes and Genomes (KEGG) pathway-enrichment analysis showing the top 10 enriched pathways. (E) RT-qPCR validation of the relative mRNA expression levels of LAMC3, LAMA5, PTPRF, and CADM3 in 430-WT and 430-KO cells. Data are presented as the mean ± SD from three independent experiments. *p < 0.05, **p < 0.01, ***p < 0.001.

ZEB1, N-cadherin, and Vimentin in 430-KO cells (Figure 3D, Supplementary Figure 3). These results suggest that EPHA3 may regulate mesenchymal-related phenotypic remodeling and promote the migratory capacity of GIST-430 cells.

To control for potential off-target effects of EPHA3 depletion, we employed siRNA-mediated knockdown in GIST-430 cells. We also observed both a decreased migratory ability and downregulated expression of relevant marker proteins in GIST-430 cells following EPHA3 knockdown (Supplementary Figure 4). Critically, both approaches yielded consistent phenotypic outcomes, confirming that the observed effects are specifically attributable to EPHA3 depletion rather than off-target or compensatory mechanisms.

EPHA3 modulates the expression of genes associated with cell adhesion and matrix interactions in GIST cells

To elucidate the potential role of EPHA3 in the progression of gastrointestinal stromal tumors (GIST), we conducted a comparative transcriptomic analysis using bulk RNA sequencing in 430-WT cells and their EPHA3-knockout (430-KO) counterparts. Differential expression analysis identified a total of 327 significantly altered genes, including 162 upregulated and 165 downregulated genes, as visualized in the volcano plot (Figure 4A). Hierarchical clustering analysis further revealed distinct gene-expression patterns between 430-WT and 430-KO cells (Figure 4B). The full list of differentially expressed genes is provided in Supplementary Table S2. Functional enrichment through Gene Ontology (GO) analysis indicated that these differentially expressed genes were predominantly involved in biological processes related to cell-cell adhesion, homophilic cell adhesion, and cell junction assembly. Regarding cellular components, enrichment was observed in collagen-containing extracellular matrix and apical plasma membrane. Molecular function categories significantly represented included proteoglycan binding, integrin binding, and collagen binding (Figure 4C). Additionally, KEGG pathway analysis highlighted the enrichment of several pathways associated with tumor invasiveness and mesenchymal remodeling, including extracellular matrix (ECM)-receptor interactions, PI3K-Akt signaling, and cell adhesion (Figure 4D).[18] Among the identified differentially expressed genes, key mediators of cell-matrix interactions and adhesion, including LAMC3, LAMA5, PTPRF and CADM3 were selected, and their altered expression levels were confirmed by RT-qPCR (Figure 4E). Collectively, these data suggest that EPHA3 may regulate signaling pathways associated with cell adhesion, extracellular matrix interaction, and mesenchymal-related phenotypic remodeling in GIST cells.

Discussion

The biological role of EPHA3 in determining phenotypic characteristics across histopathological subtypes of GIST, particularly in high- and intermediate-risk groups, remains poorly understood. In the present study, we found that EPHA3 expression was elevated in high-risk GIST specimens and was associated with larger tumor size and higher mitotic activity. In functional experiments using GIST-430 cells, EPHA3 deficiency significantly suppressed cell proliferation and migration while promoting apoptosis. Furthermore, transcriptomic profiling suggested that EPHA3 may contribute to the malignant phenotype of GIST cells through the regulation of pathways related to cell adhesion, extracellular matrix interaction, and mesenchymal-related phenotypic remodeling. Nevertheless, several limitations should be acknowledged. The clinical cohort in this study was relatively small, and the *in vitro* functional analyses were performed mainly in a single GIST-430 cell model. In addition, although our findings support an association between EPHA3 expression and aggressive clinicopathological features, the prognostic value of EPHA3 still requires validation in larger independent cohorts.

Eph receptors and their cognate ephrin ligands play pivotal roles in diverse biological processes, including cell adhesion, migration[19], and angiogenesis.[20] Although their expression in normal adult tissues is typically restricted, Eph/ephrin family members are frequently overexpressed in human malignancies[21], where they are often associated with aggressive, invasive, and metastatic behavior.[22-24] As cell surface receptors, Eph/ephrin signaling can elicit distinct biological outcomes, ranging from cell adhesion to repulsion, depending on multiple contextual factors. Emerging evidence suggests that these opposing effects are modulated by the intensity of Eph receptor activation, the specific cellular context, and receptor density at the cell surface.[25,26] Crucially, EPHA3 acts as a key signaling hub, transmitting extracellular cues into intracellular responses that drive oncogenic potential across multiple malignancies. In glioblastoma

multiforme (GBM), EPHA3 demonstrates minimal expression in normal brain tissue but is markedly upregulated in glioblastoma stem cells (GSCs), where it critically maintains self-renewal capacity and cell survival. Notably, EPHA3 knockdown induces tumor cell differentiation and apoptosis in GBM models.[27]

The Eph receptor family, including EPHA2, EPHA3, EPHB2, and EPHB4, is frequently dysregulated in breast cancer. Comparative analyses reveal significantly elevated expression of these receptors in malignant versus normal mammary epithelium. Specifically, EPHB2 overexpression occurs in 51% of breast tumors and correlates with unfavorable clinical outcomes. EPHB4 expression similarly associates with advanced tumor stage, higher histological grade, increased proliferation indices, and DNA aneuploidy.[28] Functional studies demonstrate that EPHB4 knockdown reduces cell viability, enhances apoptosis, and sensitizes breast cancer cells to TRAIL-induced cell death.[29] EPHA2 overexpression also portends worse prognosis in breast cancer, where it potentiates HER2-mediated oncogenic signaling cascades. Genetic ablation of EPHA2 in murine models significantly attenuates mammary tumor progression and metastasis.[30] In pancreatic cancer, EPHA2 knockdown has been reported to reduce transwell invasion in specific molecular subtypes.[31] Furthermore, EPHA3 has been identified as a novel effector of RAGE-mediated motility in breast cancer cells.[24] Moreover, higher levels of EPHA4, EPHA7, and EPHA10 expression are linked to adverse clinical outcomes in breast cancer, with EPHA4 specifically promoting tumor progression through TGFβ pathway activation. These collective findings underscore the pivotal role of Eph receptors in driving oncogenic processes across diverse malignancies by orchestrating complex intracellular signaling networks.

Conclusions

In conclusion, our study demonstrates that EPHA3 expression is remarkably elevated in high-risk GISTs compared to intermediate-risk cases, with its overexpression significantly correlating with aggressive features. Functional studies revealed that EPHA3 knockdown limits tumor cell proliferation, invasion, and migration by modulating pathways associated with mesenchymal phenotypic remodeling and cell adhesion. suggest that EPHA3 may serve as a promising novel therapeutic target and a potential candidate biomarker for the risk assessment of GIST.

Acknowledgments

We sincerely appreciate Prof. Wenbing Ou from Zhejiang Sci-Tech University for providing the 430 cell line.

CRediT authorship contribution statement

Han Wei: Conceptualization, Data curation, Investigation, Methodology, Software, Formal analysis, Writing - original draft. Jia Zhao: Conceptualization, Formal analysis, Investigation, Writing-review & editing. Hongmei Wang: Formal analysis, Validation, Visualization, Writing - review & editing. Lihong Guo: Formal analysis, Investigation. Yanhong Liu: Formal analysis, Investigation, Methodology. Chuntao Wang: Data curation, Formal analysis, Investigation. Liang Yang: Data curation, Formal analysis, Investigation, Software. Zhi Qi: Formal analysis, Investigation, Methodology, Resources. Wencong Tian: Formal analysis, Investigation, Writing -review & editing. Lei Cao: Conceptualization, Methodology, Resources, Writing - original draft. Yang Gao: Conceptualization, Data curation, Formal analysis, Funding acquisition, Investigation, Methodology, Project administration, Resources, Supervision, Writing - original draft.

Funding

This study was supported by the Natural Science Foundation of Tianjin (23JCYBJC01810). Tianjin Health Research Project (TJWJ2023XK014), Scientific Research Project of Tianjin Union Medical Center (2022PWXK03, 2022PWXK05).

Availability of data and materials

The raw sequence data reported in this paper have been deposited in the Genome Sequence Archive (Genomics, Proteomics & Bioinformatics 2025) in National Genomics Data Center (Nucleic Acids Res 2025), China National Center for Bioinformation / Beijing Institute of Genomics, Chinese Academy of Sciences (GSA-Human: HRA013608) that are publicly accessible at https://ngdc.cncb.ac.cn/gsa-human.

References

1. Sircar K, Hewlett BR, Huizinga JD, Chorneyko K, Berezin I, Riddell RH. Interstitial cells of cajal as precursors of gastrointestinal stromal tumors. *Am J Surg Pathol* 1999; **23:** 377-89. doi: 10.1097/00000478-199904000-00002
2. Xu Y, Peng XL, East MP, Mccabe IC, Stroman GC, Jenner MR, et al. Tumor-intrinsic kinome landscape of pancreatic cancer reveals new therapeutic approaches. *Cancer Discov* 2025; **15:** 346-62. doi: 10.1158/2159-8290.CD-23-1480
3. Venkataraman V, George S, Cote GM. Molecular advances in the treatment of advanced gastrointestinal stromal tumor. *Oncologist* 2023; **28:** 671-81. doi: 10.1093/oncolo/oyad167
4. Buchdunger E, Cioffi CL, Law N, Stover D, Ohno-Jones S, Druker BJ, et al. Abl protein-tyrosine kinase inhibitor STI571 inhibits in vitro signal transduction mediated by c-kit and platelet-derived growth factor receptors. *J Pharmacol Exp Ther* 2000; **295:** 139-45. doi: 10.1016/S0022-3565(24)38879-2
5. Joensuu H. Risk stratification of patients diagnosed with gastrointestinal stromal tumor. *Hum Pathol* 2008; **39:** 1411-9. doi: 10.1016/j.humpath.2008.06.025
6. Joensuu H, Eriksson M, Sundby Hall K, Hartmann JT, Pink D, Schutte J, et al. One vs three years of adjuvant imatinib for operable gastrointestinal stromal tumor: a randomized trial. **JAMA** 2012; **307:** 1265-72. doi: 10.1001/jama.2012.347
7. Novelli M, Rossi S, Rodriguez-Justo M, Taniere P, Seddon B, Toffolatti L, et al. DOG1 and CD117 are the antibodies of choice in the diagnosis of gastrointestinal stromal tumours. *Histopathology* 2010; **57:** 259-70. doi: 10.1111/j.1365-2559.2010.03624.x
8. Xi H, Wu X, Wei B, Chen L. Aberrant expression of EphA3 in gastric carcinoma: correlation with tumor angiogenesis and survival. *J Gastroenterol* 2012; **47:** 785-94. doi: 10.1007/s00535-012-0549-4
9. Li M, Yang C, Liu X, Yuan L, Zhang F, Wang M, et al. EphA3 promotes malignant transformation of colorectal epithelial cells by upregulating oncogenic pathways. *Cancer Lett* 2016; **383:** 195-203. doi: 10.1016/j.canlet.2016.10.004
10. Nasri B, Inokuchi M, Ishikawa T, Uetake H, Takagi Y, Otsuki S, et al. High expression of EphA3 (erythropoietin-producing hepatocellular a3) in gastric cancer is associated with metastasis and poor survival. *BMC Clin Pathol* 2017; **17:** 8. doi: 10.1186/s12907-017-0047-y
11. Surawska H, Ma PC, Salgia R. The role of ephrins and eph receptors in cancer. *Cytokine Growth Factor Rev* 2004; **15:** 419-33. doi: 10.1016/j.cytogfr.2004.09.002
12. Chen S, Zhou Y, Chen Y, Gu J. Fastp: an ultra-fast all-in-one FASTQ preprocessor. *Bioinformatics* 2018; **34:** i884-i90. doi: 10.1093/bioinformatics/bty560
13. Kim D, Paggi JM, Park C, Bennett C, Salzberg SL. Graph-based genome alignment and genotyping with HISAT2 and HISAT-genotype. *Nat Biotechnol* 2019; **37:** 907-15. doi: 10.1038/s41587-019-0201-4
14. Liao Y, Smyth GK, Shi W. Featurecounts: an efficient general purpose program for assigning sequence reads to genomic features. *Bioinformatics* 2014; **30:** 923-30. doi: 10.1093/bioinformatics/btt656
15. Love MI, Huber W, Anders S. Moderated estimation of fold change and dispersion for RNA-seq data with DESeq2. *Genome Biol* 2014; **15:** 550. doi: 10.1186/s13059-014-0550-8
16. Wu T, Hu E, Xu S, Chen M, Guo P, Dai Z, et al. Clusterprofiler 4.0: a universal enrichment tool for interpreting omics data. *Innovation (N Y)* 2021; **2:** 100141. doi: 10.1016/j.xinn.2021.100141
17. Kanehisa M, Furumichi M, Sato Y, Matsuura Y, Ishiguro-Watanabe M. KEGG: biological systems database as a model of the real world. *Nucleic Acids Res* 2025; **53:** D672-D7. doi: 10.1093/nar/gkae909
18. Kanehisa M, Goto S. KEGG: kyoto encyclopedia of genes and genomes. *Nucleic Acids Res* 2000; **28:** 27-30. doi: 10.1093/nar/28.1.27
19. Park I, Lee H. EphB/ephrinb signaling in cell adhesion and migration. *Mol Cells* 2015; **38:** 14-9. doi: 10.14348/molcells.2015.2116
20. Adams RH, Wilkinson GA, Weiss C, Diella F, Gale NW, Deutsch U, et al. Roles of ephrinb ligands and EphB receptors in cardiovascular development: demarcation of arterial/venous domains, vascular morphogenesis, and sprouting angiogenesis. *Genes Dev* 1999; **13:** 295-306. doi: 10.1101/gad.13.3.295
21. Anderton M, van der Meulen E, Blumenthal MJ, Schafer G. The role of the eph receptor family in tumorigenesis. *Cancers (Basel)* 2021; **13:** 206. doi:10.3390/cancers13020206
22. Chen J. Regulation of tumor initiation and metastatic progression by Eph receptor tyrosine kinases. *Adv Cancer Res* 2012: **114:** 1-20. doi: 10.1016/B978-0-12-386503-8.00001-6.
23. Kandouz M. The eph/ephrin family in cancer metastasis: communication at the service of invasion. *Cancer Metastasis Rev* 2012; **31:** 353-73. doi: 10.1007/s10555-012-9352-1
24. Talia M, Cirillo F, Spinelli A, Zicarelli A, Scordamaglia D, Muglia L, et al. The ephrin tyrosine kinase A3 (EphA3) is a novel mediator of RAGE-prompted motility of breast cancer cells. *J Exp Clin Cancer Res* 2023; **42:** 122-64. doi: 10.1186/s13046-023-02747-5
25. Pasquale EB. Eph receptors and ephrins in cancer: bidirectional signalling and beyond. *Nat Rev Cancer* 2010; **10:** 165-80. doi: 10.1038/nrc2806
26. Nievergall E, Lackmann M, Janes PW. Eph-dependent cell-cell adhesion and segregation in development and cancer. *Cell Mol Life Sci* 2012; **69:** 1813-42. doi: 10.1007/s00018-011-0900-6
27. Offenhauser C, Al-Ejeh F, Puttick S, Ensbey KS, Bruce ZC, Jamieson PR, et al. EphA3 pay-loaded antibody therapeutics for the treatment of glioblastoma. *Cancers (Basel)* 2018; **10:** 519. doi: 10.3390/cancers10120519
28. Wu Q, Suo Z, Risberg B, Karlsson MG, Villman K, Nesland JM. Expression of ephb2 and ephb4 in breast carcinoma. *Pathol Oncol Res* 2004; **10:** 26-33. doi: 10.1007/BF02893405
29. Kumar SR, Singh J, Xia G, Krasnoperov V, Hassanieh L, Ley EJ, et al. Receptor tyrosine kinase EphB4 is a survival factor in breast cancer. *Am J Pathol* 2006; **169:** 279-93. doi: 10.2353/ajpath.2006.050889
30. Brantley-Sieders DM, Zhuang G, Hicks D, Fang WB, Hwang Y, Cates JMM, et al. The receptor tyrosine kinase EphA2 promotes mammary adenocarcinoma tumorigenesis and metastatic progression in mice by amplifying ErbB2 signaling. *J Clin Invest* 2008; **118:** 64-78. doi: 10.1172/JCI33154
31. Duxbury MS, Ito H, Zinner MJ, Ashley SW, Whang EE. Retraction note: EphA2: a determinant of malignant cellular behavior and a potential therapeutic target in pancreatic adenocarcinoma. *Oncogene* 2004; **23:** 1448-56. doi: 10.1038/sj.onc.1207247

EPHA3, upregulated in high-risk histological subtypes of gastrointestinal stromal tumor, promotes GIST progression

Han Wei, Jia Zhao, Hongmei Wang, Lihong Guo, Yanhong Liu, Chuntao Wang, Liang Yang, Zhi Qi, Wencong Tian, Lei Cao, Yang Gao

doi: 10.2478/raon-2026-0042

Radiol Oncol 2026; 60(3): 416-426.

Supplementary tables

SUPPLEMENTARY TABLE S1. siRNA sequences used for transfection

Target gene (Species)	Sequence (5'→3')
si-EPHA3 (*Homo sapiens*)	Forward: CCAGGUUUCUACAAGGCAUTT Reverse: AUGCCUUGUAGAAACCUGGTT
si-NC	Forward: UUCUCCGAACGUGUCACGUTT Reverse: ACGUGACACGUUCGGAGAATT

SUPPLEMENTARY TABLE S2. Primer sequences for quantitative reverse transcription polymerase chain reaction (qRT-PCR)

Gene (Species)	Sequence (5'→3')
EPHA3 (*Homo sapiens*)	Forward: CAGCCTTCCAACGAAGTTAATCT Reverse: TGCACACCTGGTAAGTCCTGA
ZEB1 (*Homo sapiens*)	Forward: GATGATGAATGCGAGTCAGATGC Reverse: ACAGCAGTGTCTTGTTGTTGT
VIM (*Homo sapiens*)	Forward: GACGCCATCAACACCGAGTT Reverse: CTTTGTCGTTGGTTAGCTGGT
CDH1 (*Homo sapiens*)	Forward: ATTTTTCCCTCGACACCCGAT Reverse: TCCCAGGCGTAGACCAAGA
CDH2 (*Homo sapiens*)	Forward: TGCGGTACAGTGTAACTGGG Reverse: GAAACCGGGCTATCTGCTCG
NRCAM (*Homo sapiens*)	Forward: TCCAACCATCACCCAACAGTC Reverse: TGAGTCCCATTACGGGTCCAG
LAMC3 (*Homo sapiens*)	Forward: CCCACCTCGGTCAACATCAC Reverse: GAGGCGCTGTAGAACTGGTA
LAMA5 (*Homo sapiens*)	Forward: GACTGCCAACAGTGCCAAC Reverse: CCACCCTGATAGGTGCCAT
PTPRF (*Homo sapiens*)	Forward: ACAGGACGGGTTGGCTACA Reverse: AAGTTCAGCTCCTTCGTCAGA
CADM3 (*Homo sapiens*)	Forward: CAAGTGCCAAGTGAAAGATCACG Reverse: CCCAAAGTAGAGAGTCTGCTGAG
ACTB (*Homo sapiens*)	Forward: CATGTACGTTGCTATCCAGGC Reverse: CTCCTTAATGTCACGCACGAT

SUPPLEMENTARY TABLE S3. List of differentially expressed genes

Geneid	gene_name	gene_type	mean_norm_430	mean_norm_430_KO	log_2FoldChange	pvalue	padj	change
ENSG00000002586.20	CD99	protein_coding	345.2539762	897.5698055	1.378337928	5.93E-07	1.54E-05	Up
ENSG00000004799.8	PDK4	protein_coding	151.2838665	93.4654943	-0.693056402	0.00022553	0.002365029	Down
ENSG00000005471.19	ABCB4	protein_coding	158.9134479	94.42341444	-0.750226418	0.000228784	0.002388864	Down
ENSG00000023171.20	GRAMD1B	protein_coding	594.973511	371.8604592	-0.677148855	4.01E-12	2.98E-10	Down
ENSG00000030419.17	IKZF2	protein_coding	79.84019267	146.5099774	0.875303268	0.000223591	0.002353664	Up
ENSG00000041515.16	MYO16	protein_coding	127.0564942	79.60404924	-0.671982336	0.000905216	0.007165779	Down
ENSG00000047365.13	ARAP2	protein_coding	164.4379476	249.9371611	0.605474279	5.16E-05	0.000703593	Up
ENSG00000049192.15	ADAMTS6	protein_coding	40.77079228	70.86220976	0.799335513	0.003159224	0.0187421	Up
ENSG00000054793.14	ATP9A	protein_coding	93.6003788	54.95121476	-0.772079879	0.001856632	0.01249308	Down
ENSG00000055163.21	CYFIP2	protein_coding	340.3044991	214.8554005	-0.663731289	2.84E-07	7.99E-06	Down
ENSG00000057294.18	PKP2	protein_coding	145.0050529	92.71302335	-0.644099492	0.000598259	0.005090754	Down
ENSG00000064300.9	NGFR	protein_coding	560.4386346	988.7401142	0.81857115	1.79E-19	3.15E-17	Up
ENSG00000067715.15	SYT1	protein_coding	50.37120931	94.76195874	0.912666458	0.000301316	0.002967377	Up
ENSG00000071073.13	MGAT4A	protein_coding	166.9510832	95.11455667	-0.810807354	4.10E-06	8.22E-05	Down
ENSG00000071991.9	CDH19	protein_coding	699.6697453	1311.585038	0.907462748	6.20E-24	1.66E-21	Up
ENSG00000074047.22	GLI2	protein_coding	95.08232789	189.7327734	0.997064602	1.47E-08	5.66E-07	Up
ENSG00000076356.7	PLXNA2	protein_coding	284.0656858	124.2508905	-1.189436571	5.83E-13	5.02E-11	Down
ENSG00000077238.14	IL4R	protein_coding	137.7799021	79.65286269	-0.792491567	0.000123693	0.001452172	Down
ENSG00000080573.7	COL5A3	protein_coding	432.6367254	650.8325668	0.590052271	1.72E-09	8.00E-08	Up
ENSG00000080709.17	KCNN2	protein_coding	299.6257562	181.7546209	-0.720965612	4.08E-08	1.44E-06	Down
ENSG00000081923.15	ATP8B1	protein_coding	29.99664842	59.62237	0.991969056	0.002135736	0.013989671	Up
ENSG00000082293.13	COL19A1	protein_coding	1506.276312	2288.804128	0.603418882	2.59E-15	2.92E-13	Up
ENSG00000082482.14	KCNK2	protein_coding	50.26947495	84.20166668	0.746369885	0.006984219	0.03452292	Up
ENSG00000082497.12	SERTAD4	protein_coding	151.7832349	401.0302754	1.400623023	3.84E-25	1.12E-22	Up
ENSG00000084636.18	COL16A1	protein_coding	206.7272171	313.9629608	0.60305668	4.22E-05	0.000595958	Up
ENSG00000085276.19	MECOM	protein_coding	156.3068898	445.5058582	1.510192863	2.46E-28	9.87E-26	Up
ENSG00000088038.20	CNOT3	protein_coding	124.2818395	197.7414983	0.668506807	0.000741475	0.006087397	Up
ENSG00000091129.22	NRCAM	protein_coding	3450.481201	7573.101337	1.134150268	3.30E-59	1.41E-55	Up
ENSG00000096696.16	DSP	protein_coding	805.9803697	308.1991581	-1.386316066	1.57E-40	1.34E-37	Down
ENSG00000099139.14	PCSK5	protein_coding	448.5840845	683.2145939	0.607062983	1.38E-10	7.77E-09	Up
ENSG00000100167.21	SEPTIN3	protein_coding	204.255094	129.1565044	-0.658616747	0.000304311	0.002987692	Down
ENSG00000100191.6	SLC5A4	protein_coding	992.3045367	504.0355322	-0.976539367	4.70E-30	2.15E-27	Down
ENSG00000100628.12	ASB2	protein_coding	193.3631215	120.7757116	-0.679606292	0.000685132	0.005694051	Down
ENSG00000101197.13	BIRC7	protein_coding	858.4654403	484.215673	-0.826259404	5.46E-22	1.25E-19	Down
ENSG00000101210.14	EEF1A2	protein_coding	1018.184662	528.8827452	-0.944819815	6.90E-21	1.38E-18	Down
ENSG00000101230.6	ISM1	protein_coding	176.2358491	89.0110982	-0.983713642	1.21E-07	3.77E-06	Down
ENSG00000101265.16	RASSF2	protein_coding	195.6718889	124.2938598	-0.65498685	9.89E-05	0.001205188	Down
ENSG00000101850.13	GPR143	protein_coding	1499.454346	882.4378926	-0.764977349	1.33E-27	5.03E-25	Down
ENSG00000102109.9	PCSK1N	protein_coding	107.0294298	58.49366358	-0.868161805	0.000160363	0.001801905	Down
ENSG00000102313.9	ITIH6	protein_coding	335.9305625	567.9337057	0.758263188	3.00E-13	2.69E-11	Up
ENSG00000103489.12	XYLT1	protein_coding	2720.071205	4235.387013	0.639217838	1.76E-21	3.82E-19	Up
ENSG00000105088.9	OLFM2	protein_coding	242.3104159	138.8541596	-0.801653991	2.65E-07	7.56E-06	Down
ENSG00000105613.10	MAST1	protein_coding	220.104621	144.0801223	-0.613029287	0.000241147	0.002489455	Down
ENSG00000105618.14	PRPF31	protein_coding	27.8719355	153.556756	2.462135765	0.008626885	0.040467676	Up
ENSG00000105708.9	ZNF14	protein_coding	111.9392512	187.1395145	0.740385923	9.43E-06	0.000166182	Up
ENSG00000105711.14	SCN1B	protein_coding	138.9898782	89.34720501	-0.639478992	0.001489553	0.010519509	Down
ENSG00000106069.26	CHN2	protein_coding	716.0573747	472.6525501	-0.597812976	1.62E-08	6.18E-07	Down
ENSG00000106278.12	PTPRZ1	protein_coding	313.3382477	723.676303	1.208071677	4.14E-32	2.31E-29	Up
ENSG00000107281.10	NPDC1	protein_coding	460.22346	285.7009522	-0.685852155	2.16E-07	6.32E-06	Down
ENSG00000107719.10	PALD1	protein_coding	150.1351944	95.25077388	-0.656200989	0.000743662	0.006097555	Down
ENSG00000109738.11	GLRB	protein_coding	28.99428826	52.23735448	0.85133826	0.007911843	0.037981581	Up
ENSG00000111341.10	MGP	protein_coding	38.10001377	85.61702721	1.173155423	5.51E-05	0.000746468	Up
ENSG00000112280.18	COL9A1	protein_coding	104.7877492	268.3732006	1.357138089	9.36E-18	1.40E-15	Up
ENSG00000112294.14	ALDH5A1	protein_coding	88.79707708	38.25024531	-1.214170181	3.09E-06	6.44E-05	Down
ENSG00000112902.12	SEMA5A	protein_coding	4065.499859	2254.861432	-0.850319789	4.40E-41	4.03E-38	Down
ENSG00000113369.9	ARRDC3	protein_coding	838.0071419	1270.326493	0.599762858	4.15E-15	4.51E-13	Up
ENSG00000113594.10	LIFR	protein_coding	365.565615	599.4975304	0.712400692	2.30E-11	1.46E-09	Up
ENSG00000114019.15	AMOTL2	protein_coding	613.0770972	958.032944	0.643382927	1.21E-11	8.14E-10	Up
ENSG00000114251.15	WNT5A	protein_coding	352.0004434	527.6321113	0.585008342	4.58E-08	1.58E-06	Up
ENSG00000115232.14	ITGA4	protein_coding	268.6158039	434.8924468	0.693964918	1.17E-09	5.58E-08	Up
ENSG00000115318.12	LOXL3	protein_coding	3771.839004	6022.416076	0.675058787	6.23E-36	4.44E-33	Up
ENSG00000115339.14	GALNT3	protein_coding	349.8591183	230.8783606	-0.600341726	5.76E-06	0.000109249	Down
ENSG00000115414.21	FN1	protein_coding	8631.587316	14281.10973	0.726384987	9.30E-34	5.43E-31	Up
ENSG00000115457.10	IGFBP2	protein_coding	646.0247472	422.7256339	-0.610460165	2.19E-09	9.92E-08	Down
ENSG00000115525.18	ST3GAL5	protein_coding	2252.823029	1393.830285	-0.692641264	5.22E-27	1.81E-24	Down
ENSG00000115648.14	MLPH	protein_coding	2039.201106	1128.030775	-0.854044712	1.15E-41	1.23E-38	Down
ENSG00000115828.17	QPCT	protein_coding	7107.62132	3645.223779	-0.963189208	1.58E-56	5.07E-53	Down
ENSG00000116962.15	NID1	protein_coding	99.17562033	244.9039663	1.305538543	1.92E-15	2.20E-13	Up
ENSG00000117983.17	MUC5B	protein_coding	145.2867051	230.1151943	0.663968705	9.55E-06	0.000167851	Up
ENSG00000118503.18	TNFAIP3	protein_coding	853.7247352	489.6278016	-0.802949736	4.06E-20	7.55E-18	Down
ENSG00000118513.21	MYB	protein_coding	241.6374247	137.1026923	-0.817220605	2.06E-07	6.06E-06	Down
ENSG00000118515.12	SGK1	protein_coding	9617.993528	6252.255164	-0.621275251	9.16E-48	2.35E-44	Down
ENSG00000118946.12	PCDH17	protein_coding	27.89699024	92.41494077	1.728134725	2.53E-09	1.13E-07	Up
ENSG00000120215.10	MLANA	protein_coding	11244.28191	7020.962495	-0.679347005	6.72E-43	9.58E-40	Down
ENSG00000122863.6	CHST3	protein_coding	215.4555838	491.6463561	1.188352339	1.10E-20	2.18E-18	Up
ENSG00000123095.6	BHLHE41	protein_coding	2748.956645	1568.435366	-0.809523588	1.74E-41	1.71E-38	Down
ENSG00000124772.12	CPNE5	protein_coding	67.7274952	26.92846756	-1.331966083	9.13E-06	0.000161569	Down
ENSG00000125378.16	BMP4	protein_coding	85.92459023	53.34410402	-0.688676563	0.010926139	0.048180144	Down
ENSG00000125726.11	CD70	protein_coding	393.3215464	253.7018595	-0.633329418	5.96E-06	0.000112624	Down
ENSG00000125848.10	FLRT3	protein_coding	40.89166797	87.88911132	1.101676551	2.40E-05	0.000369757	Up
ENSG00000125864.14	BFSP1	protein_coding	78.20285099	123.158007	0.658329849	0.003845391	0.021868317	Up
ENSG00000126856.16	PRDM7	protein_coding	1057.772344	472.5632057	-1.162052183	1.53E-44	3.27E-41	Down
ENSG00000127220.6	ABHD8	protein_coding	221.8383879	147.0169643	-0.593972078	0.000175611	0.00193595	Down
ENSG00000127952.17	STYXL1	protein_coding	119.5582423	74.94966971	-0.67304327	0.001623961	0.011313063	Down
ENSG00000128266.9	GNAZ	protein_coding	93.39047867	140.7376322	0.592749303	0.003278744	0.019281781	Up
ENSG00000128805.15	ARHGAP22	protein_coding	221.9378603	137.2951993	-0.69326428	7.86E-06	0.000141864	Down
ENSG00000129595.14	EPB41L4A	protein_coding	93.22856835	142.6159236	0.615625102	0.00142812	0.010192235	Up
ENSG00000130203.10	APOE	protein_coding	362.4674651	184.5338796	-0.97373918	2.77E-09	1.23E-07	Down
ENSG00000130303.14	BST2	protein_coding	75.66012616	44.61750188	-0.759793804	0.005784191	0.029838853	Down
ENSG00000130513.7	GDF15	protein_coding	3856.741082	1846.170165	-1.063456088	2.17E-69	1.39E-65	Down
ENSG00000130702.15	LAMA5	protein_coding	693.4763909	454.7570251	-0.607753259	7.07E-11	4.14E-09	Down
ENSG00000132182.13	NUP210	protein_coding	293.7963041	133.5787937	-1.13864711	1.51E-15	1.75E-13	Down
ENSG00000134013.16	LOXL2	protein_coding	1755.355158	3051.762443	0.797462047	4.03E-43	6.47E-40	Up

Geneid	gene_name	gene_type	mean_norm_430	mean_norm_430_KO	log_2FoldChange	pvalue	padj	change
ENSG00000134986.14	NREP	protein_coding	71.0721422	117.6557072	0.727437345	0.00055215	0.004797017	Up
ENSG00000135116.9	HRK	protein_coding	313.5374269	192.3254176	-0.704339531	7.42E-08	2.43E-06	Down
ENSG00000135119.15	RNFT2	protein_coding	132.6629547	75.49262178	-0.815364411	0.000146413	0.001668533	Down
ENSG00000135127.12	BICDL1	protein_coding	334.2693279	198.1962404	-0.753617906	1.91E-09	8.79E-08	Down
ENSG00000135362.14	PRR5L	protein_coding	79.83790851	40.67186719	-0.973438646	0.000265188	0.002696428	Down
ENSG00000135424.19	ITGA7	protein_coding	234.8246231	125.1215492	-0.906906587	1.01E-07	3.21E-06	Down
ENSG00000136040.9	PLXNC1	protein_coding	1616.936731	925.5742077	-0.804150621	8.15E-22	1.84E-19	Down
ENSG00000137337.16	MDC1	protein_coding	64.38991769	117.8195378	0.870768773	0.002628302	0.016320369	Up
ENSG00000137460.10	FHDC1	protein_coding	264.0348614	416.9802638	0.658176806	1.29E-08	5.03E-07	Up
ENSG00000137571.11	SLCO5A1	protein_coding	232.0663519	129.5368343	-0.842354894	2.22E-07	6.47E-06	Down
ENSG00000137752.25	CASP1	protein_coding	875.0235919	392.3086183	-1.156895482	2.29E-35	1.55E-32	Down
ENSG00000137801.11	THBS1	protein_coding	6328.844181	11255.74192	0.83063661	5.59E-07	1.48E-05	Up
ENSG00000138119.17	MYOF	protein_coding	3205.201822	5480.414234	0.773818932	8.31E-06	0.000149003	Up
ENSG00000138193.17	PLCE1	protein_coding	402.3909363	722.2610569	0.844175954	6.20E-16	7.65E-14	Up
ENSG00000138650.9	PCDH10	protein_coding	117.2057525	265.845104	1.181209638	1.10E-11	7.52E-10	Up
ENSG00000138835.24	RGS3	protein_coding	218.6412032	341.6992446	0.644054701	4.27E-06	8.50E-05	Up
ENSG00000139531.13	SUOX	protein_coding	309.1513905	165.8101437	-0.895781488	5.14E-09	2.17E-07	Down
ENSG00000139915.22	MDGA2	protein_coding	87.17675705	142.4499885	0.710502762	0.00035821	0.003384791	Up
ENSG00000140522.12	RLBP1	protein_coding	364.8790086	237.2787417	-0.620417744	8.62E-07	2.14E-05	Down
ENSG00000141404.17	GNAL	protein_coding	385.3160238	192.2854313	-1.002154508	7.25E-14	6.92E-12	Down
ENSG00000141527.19	CARD14	protein_coding	173.4326189	98.30897419	-0.817516618	5.21E-06	0.000100273	Down
ENSG00000141540.11	TTYH2	protein_coding	3672.017603	2415.137029	-0.604221422	7.93E-32	3.77E-29	Down
ENSG00000143127.13	ITGA10	protein_coding	66.73974183	103.5818088	0.63398031	0.003855174	0.021908589	Up
ENSG00000143375.15	CGN	protein_coding	327.3664823	193.3943337	-0.76007309	1.35E-07	4.14E-06	Down
ENSG00000143603.19	KCNN3	protein_coding	68.84292076	151.3098734	1.135465025	8.73E-09	3.52E-07	Up
ENSG00000143702.16	CEP170	protein_coding	584.8376022	969.7880514	0.729200588	1.07E-12	8.79E-11	Up
ENSG00000143786.8	CNIH3	protein_coding	108.5653964	47.44469867	-1.19211235	2.62E-07	7.50E-06	Down
ENSG00000144218.21	AFF3	protein_coding	233.2876649	131.4299846	-0.828516307	3.54E-08	1.27E-06	Down
ENSG00000144857.15	BOC	protein_coding	498.5797234	331.4934426	-0.588810394	9.13E-09	3.66E-07	Down
ENSG00000146285.15	SCML4	protein_coding	205.6082428	81.99264041	-1.326973615	4.31E-13	3.74E-11	Down
ENSG00000147027.4	TMEM47	protein_coding	265.2109809	531.4023239	1.002128392	6.08E-19	1.05E-16	Up
ENSG00000147437.10	GNRH1	protein_coding	25.84216044	49.44243157	0.93370913	0.004769091	0.025734643	Up
ENSG00000147804.10	SLC39A4	protein_coding	386.422266	250.6159519	-0.626214986	2.78E-07	7.85E-06	Down
ENSG00000148450.13	MSRB2	protein_coding	463.2009512	291.375459	-0.669023624	6.92E-08	2.30E-06	Down
ENSG00000148735.16	PLEKHS1	protein_coding	77.00107243	245.2852644	1.67089148	2.89E-15	3.23E-13	Up
ENSG00000150551.11	LYPD1	protein_coding	29.86117173	53.99161397	0.85184528	0.007757714	0.037395563	Up
ENSG00000150687.12	PRSS23	protein_coding	1200.367471	1872.697075	0.642121539	1.30E-20	2.52E-18	Up
ENSG00000151012.13	SLC7A11	protein_coding	1772.110756	3224.753476	0.864103364	1.08E-24	3.07E-22	Up
ENSG00000151224.13	MAT1A	protein_coding	153.2358339	89.63880418	-0.770211919	0.00029342	0.002909707	Down
ENSG00000151914.22	DST	protein_coding	5126.241076	7736.784893	0.593850909	4.85E-05	0.000666872	Up
ENSG00000152128.13	TMEM163	protein_coding	498.8622529	220.4051177	-1.177255547	4.22E-24	1.15E-21	Down
ENSG00000152439.13	ZNF773	protein_coding	88.0310449	141.5113517	0.684856803	0.000491837	0.004373702	Up
ENSG00000152894.15	PTPRK	protein_coding	77.0462601	192.9666803	1.325485702	5.79E-10	2.94E-08	Up
ENSG00000152942.19	RAD17	protein_coding	123.9887198	267.7675246	1.108663543	1.29E-10	7.31E-09	Up
ENSG00000153253.20	SCN3A	protein_coding	32.73843813	61.33356638	0.907666019	0.002450798	0.015476694	Up
ENSG00000153993.14	SEMA3D	protein_coding	46.24543333	73.55155714	0.671582784	0.009896305	0.044905123	Up
ENSG00000154162.15	CDH12	protein_coding	61.08102418	121.3379222	0.992090475	7.40E-06	0.000135177	Up
ENSG00000154217.16	PITPNC1	protein_coding	1118.926112	1859.479878	0.73298496	1.49E-25	4.78E-23	Up
ENSG00000154556.20	SORBS2	protein_coding	155.3458373	327.3193357	1.075202786	6.90E-11	4.06E-09	Up
ENSG00000154639.19	CXADR	protein_coding	654.521212	392.0674401	-0.738658076	1.74E-14	1.78E-12	Down
ENSG00000154856.13	APCDD1	protein_coding	396.5576568	156.9918804	-1.335874371	1.16E-16	1.53E-14	Down
ENSG00000154864.14	PIEZO2	protein_coding	71.88852888	109.1275501	0.605931467	0.009988163	0.04520921	Up
ENSG00000155849.16	ELMO1	protein_coding	84.31107248	28.45401873	-1.56825913	4.41E-08	1.54E-06	Down
ENSG00000155850.9	SLC26A2	protein_coding	9665.138527	15749.58933	0.704530006	4.45E-37	3.36E-34	Up
ENSG00000155966.14	AFF2	protein_coding	35.16545988	63.587621	0.852761088	0.005759157	0.029745033	Up
ENSG00000156103.16	MMP16	protein_coding	3074.900034	4617.518607	0.586623215	3.71E-17	5.12E-15	Up
ENSG00000156453.14	PCDH1	protein_coding	491.358497	807.0791928	0.7158169	4.11E-14	4.02E-12	Up
ENSG00000158022.7	TRIM63	protein_coding	865.8722751	486.1897684	-0.833088804	1.10E-21	2.43E-19	Down
ENSG00000158352.18	SHROOM4	protein_coding	413.609002	626.3930116	0.599716631	1.23E-08	4.81E-07	Up
ENSG00000158747.15	NBL1	protein_coding	4542.143688	3021.529647	-0.58788895	8.14E-18	1.24E-15	Down
ENSG00000159685.11	CHCHD6	protein_coding	2778.495138	1604.71653	-0.79166379	2.76E-29	1.22E-26	Down
ENSG00000160200.18	CBS	protein_coding	104.4061231	178.1496804	0.772251505	0.000408881	0.003774651	Up
ENSG00000161249.21	DMKN	protein_coding	68.05183382	36.02113048	-0.915481717	0.001210818	0.009043779	Down
ENSG00000161970.15	RPL26	protein_coding	333.8866822	199.897193	-0.741927663	1.03E-07	3.26E-06	Down
ENSG00000162066.16	AMDHD2	protein_coding	617.9737713	405.0915871	-0.607557845	1.14E-08	4.48E-07	Down
ENSG00000162409.12	PRKAA2	protein_coding	72.32543711	111.703561	0.628203812	0.003401315	0.019866032	Up
ENSG00000162645.13	GBP2	protein_coding	54.83279145	92.84237873	0.761688356	0.002444692	0.01545277	Up
ENSG00000162733.19	DDR2	protein_coding	772.2263493	1185.132312	0.618540835	6.40E-16	7.82E-14	Up
ENSG00000162878.13	PKDCC	protein_coding	81.15352704	124.3737872	0.614396313	0.003962462	0.022334123	Up
ENSG00000162944.11	RFTN2	protein_coding	174.7604458	276.05966	0.660142157	7.82E-06	0.000141395	Up
ENSG00000163235.16	TGFA	protein_coding	526.2866094	1158.594398	1.138511728	2.09E-42	2.44E-39	Up
ENSG00000163568.16	AIM2	protein_coding	59.71365008	116.8641944	0.97216488	5.84E-05	0.000780018	Up
ENSG00000163599.18	CTLA4	protein_coding	102.8838802	64.57324837	-0.671666903	0.002849555	0.017362529	Down
ENSG00000164106.8	SCRG1	protein_coding	46.15654538	76.43149478	0.728467606	0.005270949	0.02784554	Up
ENSG00000164175.15	SLC45A2	protein_coding	4580.135189	3043.949204	-0.589218379	2.53E-27	9.03E-25	Down
ENSG00000164176.13	EDIL3	protein_coding	29.18617515	94.36016894	1.690714062	1.95E-09	8.92E-08	Up
ENSG00000164418.22	GRIK2	protein_coding	481.1266472	944.3477263	0.97297022	2.50E-23	6.28E-21	Up
ENSG00000164946.20	FREM1	protein_coding	33.6480023	73.46031981	1.130428312	0.000143294	0.001646154	Up
ENSG00000165105.10	RASEF	protein_coding	2951.464207	1752.482299	-0.752098032	1.79E-38	1.44E-35	Down
ENSG00000165238.17	WNK2	protein_coding	412.5220434	250.7625553	-0.717459118	2.86E-10	1.54E-08	Down
ENSG00000165507.9	DEPP1	protein_coding	59.03323588	127.3397325	1.11137227	3.42E-07	9.53E-06	Up
ENSG00000165626.19	BEND7	protein_coding	98.39322677	46.69885343	-1.07869313	0.000116539	0.001380388	Down
ENSG00000165948.11	IFI27L1	protein_coding	29.04200509	72.54023314	1.322661526	7.58E-06	0.000138095	Up
ENSG00000166046.11	TCP11L2	protein_coding	95.47817351	143.5962275	0.590595544	0.004589625	0.025061307	Up
ENSG00000166741.9	NNMT	protein_coding	351.675336	691.7936195	0.977426239	5.09E-21	1.05E-18	Up
ENSG00000166912.17	MTMR10	protein_coding	120.4516901	190.6011399	0.661189913	0.003405521	0.019881551	Up
ENSG00000167191.12	GPRC5B	protein_coding	4256.785674	2774.879301	-0.616975088	2.15E-27	7.86E-25	Down
ENSG00000167601.12	AXL	protein_coding	64.36208877	109.2429704	0.759910066	0.006640842	0.033255749	Up
ENSG00000168505.7	GBX2	protein_coding	251.6745049	139.7447646	-0.848519545	4.86E-08	1.68E-06	Down
ENSG00000168685.15	IL7R	protein_coding	51.63421139	121.1112492	1.227557705	1.02E-06	2.52E-05	Up
ENSG00000168772.12	CXXC4	protein_coding	46.15830576	126.9758247	1.459886671	5.89E-11	3.55E-09	Up
ENSG00000169020.10	ATP5ME	protein_coding	110.035878	61.06752154	-0.852435147	0.000278699	0.002802717	Down
ENSG00000169246.17	NPIPB3	protein_coding	107.8649578	67.3455514	-0.680248746	0.004582007	0.025051687	Down

Geneid	gene_name	gene_type	mean_norm_430	mean_norm_430_KO	log_2FoldChange	pvalue	padj	change
ENSG00000169302.16	STK32A	protein_coding	380.8029591	191.8551527	-0.986561359	3.68E-14	3.66E-12	Down
ENSG00000169306.11	IL1RAPL1	protein_coding	179.5806384	296.6512281	0.72240594	2.43E-06	5.21E-05	Up
ENSG00000169744.13	LDB2	protein_coding	234.6362791	380.7111386	0.699643556	1.24E-07	3.84E-06	Up
ENSG00000169783.13	LINGO1	protein_coding	403.9222039	259.0319078	-0.643143389	1.43E-06	3.32E-05	Down
ENSG00000169891.18	REPS2	protein_coding	126.8019022	71.45002319	-0.82375632	0.000237732	0.00246213	Down
ENSG00000170153.11	RNF150	protein_coding	430.0320642	1234.055051	1.521842927	1.91E-69	1.39E-65	Up
ENSG00000170379.21	TCAF2	protein_coding	210.8261499	351.3317582	0.738011062	2.88E-08	1.05E-06	Up
ENSG00000170396.9	ZNF804A	protein_coding	28.97099389	67.58393746	1.221401878	2.92E-05	0.000437946	Up
ENSG00000170579.19	DLGAP1	protein_coding	239.6320721	134.3460297	-0.836017604	7.69E-07	1.94E-05	Down
ENSG00000170631.15	ZNF16	protein_coding	216.8454835	348.9461499	0.685785818	8.93E-08	2.89E-06	Up
ENSG00000171224.9	FAM241B	protein_coding	122.9922731	80.06366724	-0.620753733	0.003846383	0.021868317	Down
ENSG00000171368.12	TPPP	protein_coding	764.4455342	407.1010815	-0.90888191	4.59E-22	1.07E-19	Down
ENSG00000171522.6	PTGER4	protein_coding	47.41223296	87.02176551	0.873480735	0.00050551	0.004466427	Up
ENSG00000172061.9	LRRC15	protein_coding	42.88203229	96.36168694	1.165600307	1.04E-05	0.000180486	Up
ENSG00000172260.15	NEGR1	protein_coding	11.46828177	78.86189528	2.787961996	7.31E-13	6.25E-11	Up
ENSG00000172318.6	B3GALT1	protein_coding	56.64059454	92.51807881	0.706287405	0.006007929	0.030629221	Up
ENSG00000172578.12	KLHL6	protein_coding	164.4527994	95.01967654	-0.792879024	0.000102997	0.001243326	Down
ENSG00000172817.4	CYP7B1	protein_coding	186.8406655	373.2483033	0.998058664	5.29E-12	3.88E-10	Up
ENSG00000172927.9	MYEOV	protein_coding	65.95369102	38.82305753	-0.763819099	0.008902433	0.041449935	Down
ENSG00000173114.13	LRRN3	protein_coding	56.47615506	88.33817622	0.644011521	0.007132329	0.03506592	Up
ENSG00000174473.17	GALNTL6	protein_coding	64.45058944	142.1463917	1.141901777	6.11E-08	2.06E-06	Up
ENSG00000175356.14	SCUBE2	protein_coding	220.3651264	122.4657533	-0.844342002	4.26E-06	8.50E-05	Down
ENSG00000175899.15	A2M	protein_coding	1464.307337	2564.349771	0.808631768	5.77E-32	2.85E-29	Up
ENSG00000176049.16	JAKMIP2	protein_coding	230.8762637	405.0906426	0.811213996	1.16E-11	7.91E-10	Up
ENSG00000176463.14	SLCO3A1	protein_coding	251.0155104	151.8856201	-0.726330934	6.42E-07	1.65E-05	Down
ENSG00000176771.18	NCKAP5	protein_coding	48.83147694	81.36961867	0.737308779	0.00444334	0.024449802	Up
ENSG00000178445.10	GLDC	protein_coding	421.0474652	638.9922076	0.601588082	3.88E-10	2.02E-08	Up
ENSG00000178531.6	CTXN1	protein_coding	63.04809413	38.71733969	-0.70465904	0.010455281	0.046795316	Down
ENSG00000178568.16	ERBB4	protein_coding	15.89636659	62.53271319	1.975150995	8.85E-08	2.87E-06	Up
ENSG00000179314.16	WSCD1	protein_coding	16.51710063	59.01550942	1.838030199	5.05E-07	1.35E-05	Up
ENSG00000181104.7	F2R	protein_coding	382.1025977	678.6518301	0.82824641	8.07E-18	1.24E-15	Up
ENSG00000181458.10	TMEM45A	protein_coding	570.9313376	919.1752227	0.687434694	8.11E-15	8.60E-13	Up
ENSG00000182111.9	ZNF716	protein_coding	84.48898487	131.0428176	0.633260717	0.000961991	0.007531584	Up
ENSG00000182168.16	UNC5C	protein_coding	93.94512333	329.648418	1.810446471	1.60E-28	6.61E-26	Up
ENSG00000182253.15	SYNM	protein_coding	3276.509965	5110.334316	0.641286535	3.45E-35	2.22E-32	Up
ENSG00000182256.13	GABRG3	protein_coding	109.448009	36.51008792	-1.584955912	6.75E-10	3.37E-08	Down
ENSG00000182580.3	EPHB3	protein_coding	206.4309302	332.5592335	0.689447428	1.84E-07	5.49E-06	Up
ENSG00000182612.11	TSPAN10	protein_coding	156.2270488	83.80572106	-0.896755598	2.09E-06	4.58E-05	Down
ENSG00000182667.15	NTM	protein_coding	692.0333848	1257.575322	0.861825377	1.53E-28	6.54E-26	Up
ENSG00000183054.13	RGPD6	protein_coding	37.89591855	78.52256944	1.053392048	0.000669508	0.005596749	Up
ENSG00000183098.12	GPC6	protein_coding	802.0274758	1443.702473	0.848616296	3.65E-22	8.78E-20	Up
ENSG00000183779.7	ZNF703	protein_coding	1181.604891	767.9637299	-0.620847733	6.20E-12	4.45E-10	Down
ENSG00000183873.18	SCN5A	protein_coding	103.7400649	68.44049405	-0.600732429	0.0066792	0.033401204	Down
ENSG00000184226.15	PCDH9	protein_coding	134.1805488	397.4789541	1.566599869	4.07E-28	1.58E-25	Up
ENSG00000184381.20	PLA2G6	protein_coding	744.3054102	441.6128674	-0.75279788	4.88E-16	6.14E-14	Down
ENSG00000184613.11	NELL2	protein_coding	22.26445543	78.85489115	1.830687917	9.97E-08	3.20E-06	Up
ENSG00000185304.16	RGPD2	protein_coding	25.69056738	53.06634612	1.042966622	0.005044442	0.026881346	Up
ENSG00000185442.13	FAM174B	protein_coding	131.6412082	82.10751528	-0.681169255	0.000558012	0.004838111	Down
ENSG00000185585.20	OLFML2A	protein_coding	484.6825394	929.5062619	0.939896298	9.55E-26	3.14E-23	Up
ENSG00000185614.7	INKA1	protein_coding	287.0099246	157.0499447	-0.86899966	1.76E-07	5.28E-06	Down
ENSG00000185668.8	POU3F1	protein_coding	173.6700807	108.3090178	-0.679725444	9.01E-05	0.001113525	Down
ENSG00000185737.13	NRG3	protein_coding	90.07454366	41.66118584	-1.10925286	2.71E-05	0.000412688	Down
ENSG00000186297.12	GABRA5	protein_coding	68.18340826	40.94276325	-0.736955551	0.00682225	0.033969017	Down
ENSG00000186472.20	PCLO	protein_coding	374.5344849	666.6276208	0.832167607	8.70E-15	9.15E-13	Up
ENSG00000186897.5	C1QL4	protein_coding	97.78773181	62.93497524	-0.636170069	0.006436474	0.03245298	Down
ENSG00000187135.8	VSTM2B	protein_coding	47.97113918	26.67929226	-0.849626339	0.009820505	0.044655109	Down
ENSG00000188158.17	NHS	protein_coding	42.73560605	118.8643895	1.474181306	4.31E-08	1.51E-06	Up
ENSG00000188488.14	SERPINA5	protein_coding	68.53104126	115.1120187	0.746421021	0.001253845	0.009268055	Up
ENSG00000188501.12	LCTL	protein_coding	36.45753325	62.80805736	0.784166067	0.007110216	0.034997428	Up
ENSG00000188994.14	ZNF292	protein_coding	831.1106858	1274.392753	0.616699004	1.21E-10	6.89E-09	Up
ENSG00000189184.12	PCDH18	protein_coding	76.8759072	129.2952777	0.749391607	0.000163162	0.001825369	Up
ENSG00000196154.12	S100A4	protein_coding	1250.012436	1923.007373	0.621424765	3.02E-20	5.71E-18	Up
ENSG00000196159.14	FAT4	protein_coding	120.3013616	249.3150147	1.051624473	6.69E-12	4.77E-10	Up
ENSG00000196376.11	SLC35F1	protein_coding	523.4187829	1156.516641	1.143298579	1.84E-42	2.35E-39	Up
ENSG00000196646.12	ZNF136	protein_coding	158.6884509	260.979525	0.716090914	1.09E-06	2.66E-05	Up
ENSG00000196660.12	SLC30A10	protein_coding	104.5642619	54.21869009	-0.949584701	3.79E-05	0.000542485	Down
ENSG00000197692.5	CBX3P7	processed_pseudogene	104.4546087	58.50636959	-0.833635948	0.000483079	0.004313754	Down
ENSG00000198223.18	CSF2RA	protein_coding	195.182615	109.8855353	-0.827003611	1.37E-06	3.22E-05	Down
ENSG00000198373.13	WWP2	protein_coding	2820.137313	4533.030829	0.684726994	7.74E-44	1.42E-40	Up
ENSG00000198743.7	SLC5A3	protein_coding	3947.237943	7240.816677	0.875356455	2.42E-10	1.32E-08	Up
ENSG00000198868.3	MTND4LP30	processed_pseudogene	50.84185987	27.70672896	-0.87253343	0.009173568	0.0423406	Down
ENSG00000200087.1	SNORA73B	snoRNA	89.07760113	55.92427841	-0.670990397	0.004631396	0.025235698	Down
ENSG00000204356.14	NELFE	protein_coding	354.8742113	145.8363439	-1.282922973	0.00113756	0.008639099	Down
ENSG00000204469.13	PRRC2A	protein_coding	130.6391046	50.45576617	-1.372041077	0.00686024	0.03408076	Down
ENSG00000204839.9	MROH6	protein_coding	54.8441225	30.0267027	-0.868726958	0.005018966	0.026790088	Down
ENSG00000204920.11	ZNF155	protein_coding	39.94483494	66.17311887	0.727408398	0.011350697	0.04942387	Up
ENSG00000204956.6	PCDHGA1	protein_coding	31.30547045	58.51375214	0.90284369	0.004001265	0.022479963	Up
ENSG00000205213.14	LGR4	protein_coding	992.9242569	1537.319398	0.631070502	5.99E-21	1.22E-18	Up
ENSG00000205786.8	LINC01531	lncRNA	148.0344082	56.24081737	-1.396092912	6.67E-10	3.34E-08	Down
ENSG00000206077.14	ZDHHC11B	protein_coding	358.9377557	176.3418778	-1.024817902	2.10E-15	2.39E-13	Down
ENSG00000213949.10	ITGA1	protein_coding	367.9119126	592.5085296	0.687928858	1.00E-12	8.29E-11	Up
ENSG00000218336.9	TENM3	protein_coding	1602.476669	2722.00965	0.764684358	4.66E-32	2.49E-29	Up
ENSG00000223382.6	LINC01778	lncRNA	33.15292928	62.27667606	0.908768828	0.002069332	0.013674045	Up
ENSG00000224397.9	PELATON	lncRNA	457.6642595	273.1602968	-0.744144647	5.86E-10	2.96E-08	Down
ENSG00000224660.2	SH3BP5-AS1	lncRNA	718.6093447	459.1432069	-0.64650037	1.44E-11	9.59E-10	Down
ENSG00000224934.6	GOT1-DT	lncRNA	85.56172394	133.2919726	0.640848434	0.001151988	0.008685261	Up
ENSG00000226508.1	LINC01918	lncRNA	439.6849612	213.8781487	-1.038461406	3.61E-15	3.96E-13	Down
ENSG00000227203.3	SUB1P1	processed_pseudogene	71.61064251	34.19927121	-1.065110004	0.000376139	0.003523076	Down
ENSG00000228253.1	MT-ATP8	protein_coding	11492.62467	6491.539168	-0.824107854	8.38E-09	3.39E-07	Down
ENSG00000229400.1	CNIH3-AS1	lncRNA	51.20926649	25.1087612	-1.023930975	0.003476974	0.020179345	Down
ENSG00000230082.1	PRRT3-AS1	lncRNA	112.5297579	71.3841979	-0.654589939	0.002007039	0.013351124	Down
ENSG00000231312.8	MAP4K3-DT	lncRNA	208.9154902	132.6684786	-0.654031023	2.51E-05	0.00038378	Down
ENSG00000232310.10	LINC03002	lncRNA	57.1040671	33.00320114	-0.787990475	0.010191067	0.045852655	Down

Geneid	gene_name	gene_type	mean_norm_430	mean_norm_430_KO	log_2FoldChange	pvalue	padj	change
ENSG00000233527.10	ZNF529-AS1	lncRNA	25.70516838	48.90989031	0.932346354	0.008261541	0.039147747	Up
ENSG00000233539.5	ENSG00000233539	lncRNA	83.01836683	48.44395588	-0.782870866	0.003749134	0.021497517	Down
ENSG00000234323.10	LINC01505	lncRNA	77.51867103	118.315687	0.609295543	0.00232884	0.014904579	Up
ENSG00000234362.7	LINC01914	lncRNA	51.48047066	82.40088894	0.682754037	0.010135846	0.045701247	Up
ENSG00000235172.9	LINC01366	lncRNA	131.125615	74.68232263	-0.811118357	6.67E-05	0.000871032	Down
ENSG00000237289.10	CKMT1B	protein_coding	132.4878165	80.16647533	-0.72805329	0.004071669	0.022785722	Down
ENSG00000237499.7	WAKMAR2	lncRNA	113.0577017	71.31837261	-0.666372311	0.003182098	0.018816322	Down
ENSG00000237638.3	LINC02245	lncRNA	87.75266272	48.74064239	-0.849508253	0.000650633	0.005456713	Down
ENSG00000240476.1	LINC00973	lncRNA	86.73570157	50.35527798	-0.787261322	0.002134538	0.013988962	Down
ENSG00000240695.1	DNAJC8P2	processed_pseudogene	78.37446846	48.21687976	-0.703454092	0.007613665	0.036839573	Down
ENSG00000241081.1	RPL22P2	processed_pseudogene	60.72670899	35.19190272	-0.78740969	0.007937944	0.038035733	Down
ENSG00000241945.8	PWP2	protein_coding	60.12046744	28.64853639	-1.066535658	0.001542771	0.01083571	Down
ENSG00000242083.2	RPL7AP31	processed_pseudogene	59.4853774	30.30483901	-0.970668857	0.001718511	0.01179879	Down
ENSG00000243244.7	STON1	protein_coding	129.8954779	227.4823275	0.808577039	3.31E-06	6.85E-05	Up
ENSG00000246859.3	STARD4-AS1	lncRNA	104.9549629	189.8946872	0.856753222	6.15E-07	1.59E-05	Up
ENSG00000248923.1	MTND5P11	processed_pseudogene	57.59435478	33.43179905	-0.78798374	0.009829218	0.044678899	Down
ENSG00000248964.7	ENSG00000248964	lncRNA	78.45241265	49.26833242	-0.669059645	0.008713187	0.040761072	Down
ENSG00000249992.2	TMEM158	protein_coding	484.1384686	236.6409095	-1.032863115	2.38E-17	3.36E-15	Down
ENSG00000250378.4	ENSG00000250378	lncRNA	70.18700049	34.079309	-1.041129295	0.000455696	0.004115055	Down
ENSG00000250479.9	CHCHD10	protein_coding	1351.168468	885.0390071	-0.611073124	4.94E-11	3.03E-09	Down
ENSG00000251191.8	LINC00589	lncRNA	329.8106342	190.4215266	-0.793446768	4.33E-09	1.84E-07	Down
ENSG00000254595.1	ENSG00000254595	processed_pseudogene	27.68722661	49.86109091	0.853457881	0.010604641	0.047216285	Up
ENSG00000254876.5	SUGT1P4-STRA6LP	lncRNA	52.30026959	84.72519319	0.6932456	0.007033495	0.034686137	Up
ENSG00000255248.11	MIR100HG	lncRNA	215.6394096	342.8089039	0.667657637	1.14E-07	3.57E-06	Up
ENSG00000256894.1	ENSG00000256894	lncRNA	186.5386016	115.0013073	-0.697621332	1.91E-05	0.000302508	Down
ENSG00000258645.2	HSPE1P2	processed_pseudogene	172.2702231	105.7359413	-0.70349862	0.000100568	0.001220894	Down
ENSG00000258791.9	LINC00520	lncRNA	1774.22349	1137.752565	-0.641456278	1.51E-20	2.88E-18	Down
ENSG00000260877.3	ENSG00000260877	lncRNA	88.01682539	56.58603275	-0.637077571	0.007295493	0.035663148	Down
ENSG00000260920.2	ENSG00000260920	lncRNA	31.71341589	58.72989673	0.889315197	0.003908677	0.022114703	Up
ENSG00000261036.2	ENSG00000261036	lncRNA	38.61863195	65.43004108	0.76316866	0.007429611	0.036139789	Up
ENSG00000261115.7	TMEM178B	protein_coding	138.0351206	415.1080527	1.589377209	4.85E-32	2.49E-29	Up
ENSG00000261616.1	TTC23-AS1	lncRNA	42.70865444	77.00761984	0.849843889	0.001113434	0.008486217	Up
ENSG00000266835.7	GAPLINC	lncRNA	80.80350138	46.19196034	-0.806203907	0.002460095	0.01551422	Down
ENSG00000269821.2	KCNQ1OT1	lncRNA	538.0130319	857.1325722	0.671988955	0.003033978	0.01818403	Up
ENSG00000270647.7	TAF15	protein_coding	963.6923134	2077.131842	1.107968555	0.002224024	0.014400198	Up
ENSG00000273145.1	ENSG00000273145	lncRNA	101.8390844	65.48571637	-0.638733821	0.009369191	0.042999089	Down
ENSG00000274525.1	ENSG00000274525	unprocessed_pseudogene	45.12132019	72.50949763	0.683927445	0.007894341	0.037925941	Up
ENSG00000276107.1	THBS1-IT1	lncRNA	39.54582787	69.80898261	0.815988254	0.004899727	0.026384096	Up
ENSG00000276168.1	RN7SL1	misc_RNA	1465.254072	209.4440566	-2.806553704	0.004844694	0.026098703	Down
ENSG00000276476.4	LINC00540	lncRNA	99.25670378	52.28271279	-0.92502302	0.000192566	0.002087709	Down
ENSG00000276644.5	DACH1	protein_coding	90.28859684	204.2629769	1.177402452	3.52E-12	2.67E-10	Up
ENSG00000277586.4	NEFL	protein_coding	1120.942534	628.5729139	-0.834830514	3.70E-22	8.78E-20	Down
ENSG00000279198.2	ENSG00000279198	TEC	61.64559882	26.69199828	-1.212216739	0.000104177	0.001250509	Down
ENSG00000279518.1	ENSG00000279518	TEC	41.41834145	72.98075554	0.82057501	0.003475821	0.020179345	Up
ENSG00000279970.1	ENSG00000279970	TEC	80.75880951	39.50676874	-1.027346733	0.001066084	0.00818181	Down
ENSG00000285925.1	ENSG00000285925	lncRNA	56.93005696	24.35385276	-1.226242397	0.000589747	0.00504173	Down
ENSG00000286451.1	ENSG00000286451	lncRNA	73.76671088	39.13029715	-0.912050802	0.000669935	0.005596749	Down
ENSG00000288728.2	ENSG00000288728	lncRNA	44.65105113	74.5148492	0.740794294	0.006398297	0.032298564	Up

Supplementary figures

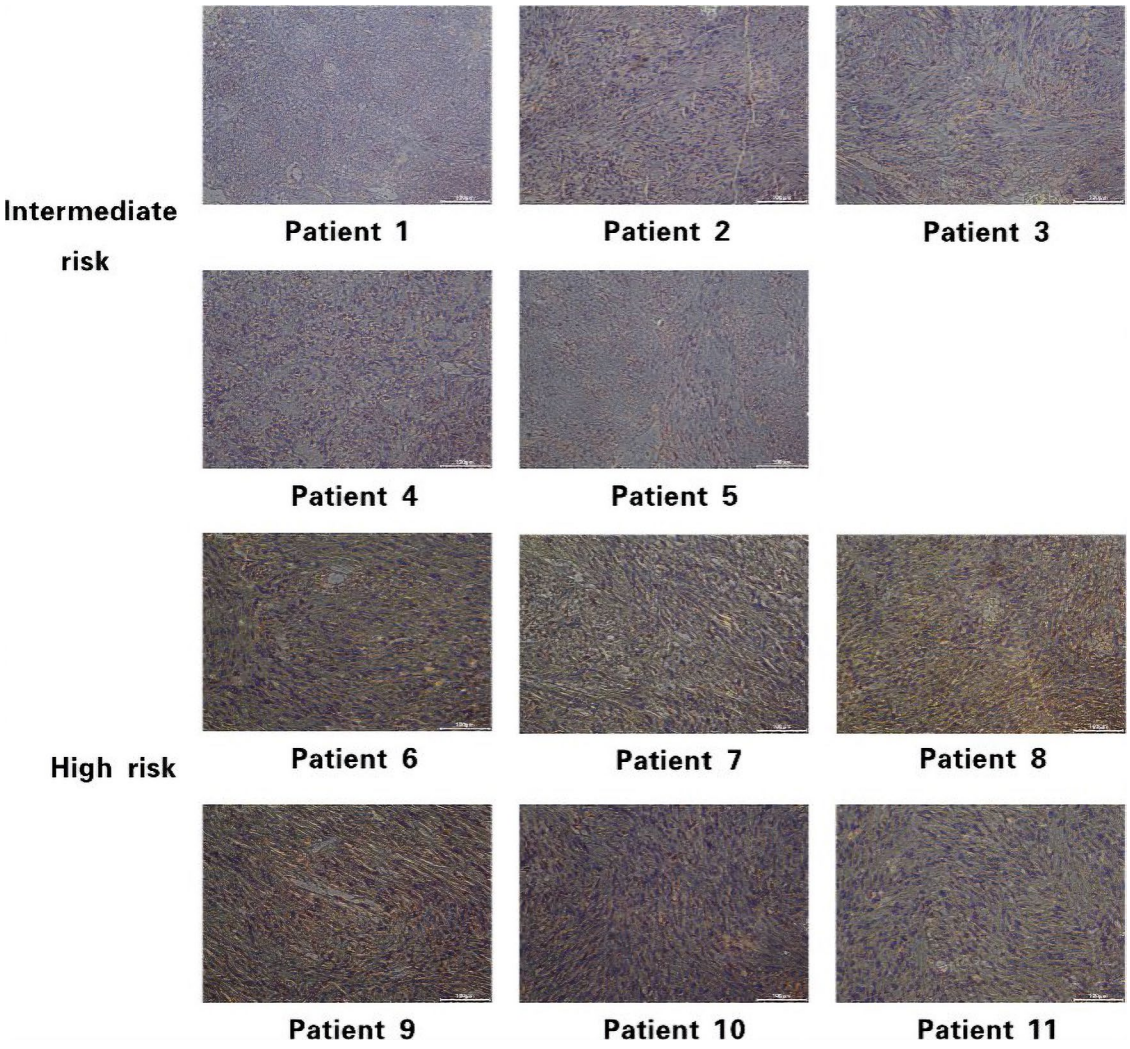

SUPPLEMENTARY FIGURE S1. Immunohistochemistry (IHC) analysis of EPHA3 in paraffin-embedded sections of tumors from 11 GIST patients, including 5 intermediate-risk and 6 high-risk cases. Original magnification, 200×; scale bar = 100 μm.

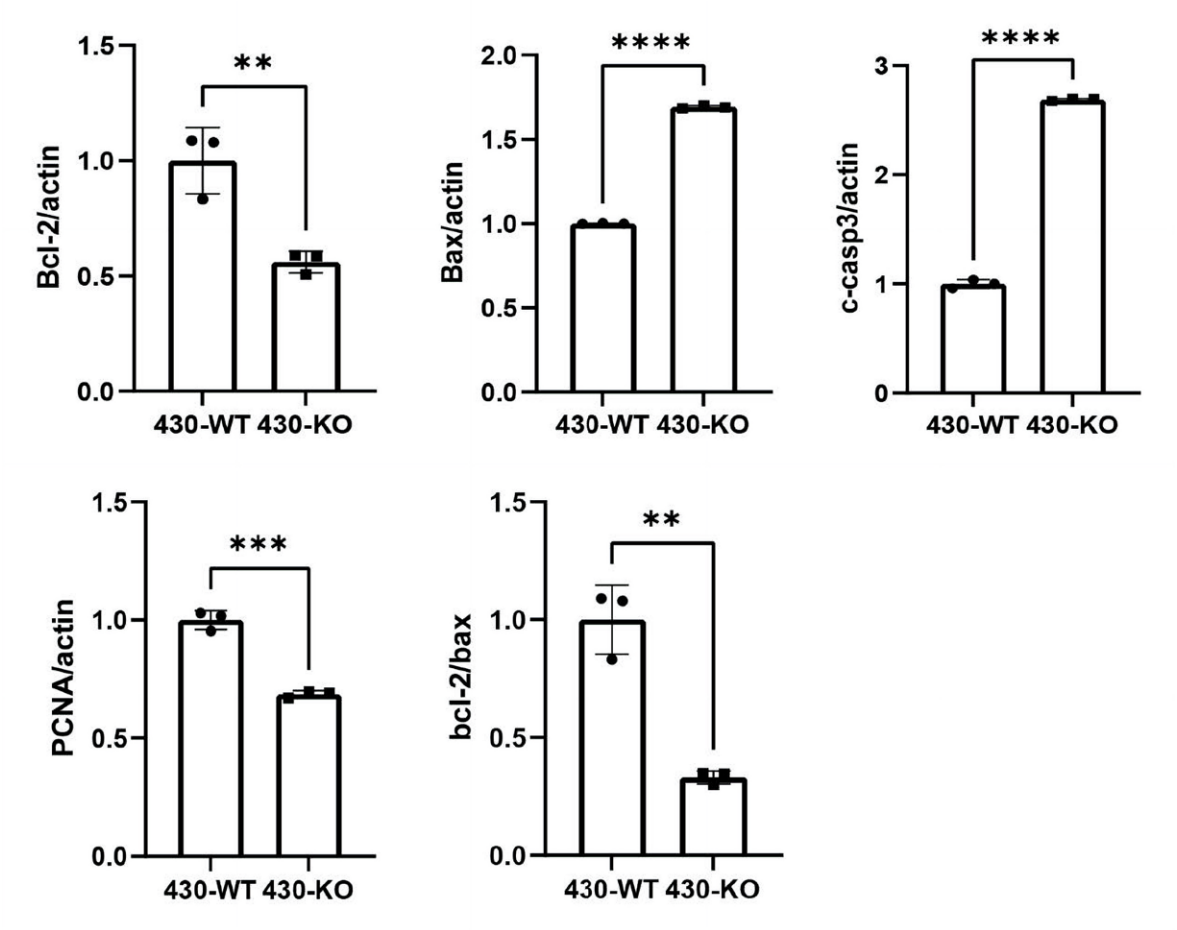

SUPPLEMENTARY FIGURE S2. Band intensities from Western blots (Figure 2A) were quantified using ImageJ (NIH). The relative expression levels of Bcl-2, Bax, PCNA, and cleaved caspase-3 were calculated by normalizing each target protein to β-actin. The Bcl-2/Bax ratio was calculated from the corresponding band intensities. Data from three independent experiments were averaged, and values were normalized to the mean of the 430-WT group, which was set to 1. Data are shown as mean ± SD from three independent experiments. Statistical significance was determined by paired t-test. *$p < 0.05$, **$p < 0.01$, ***$p < 0.001$, ****$p < 0.0001$.

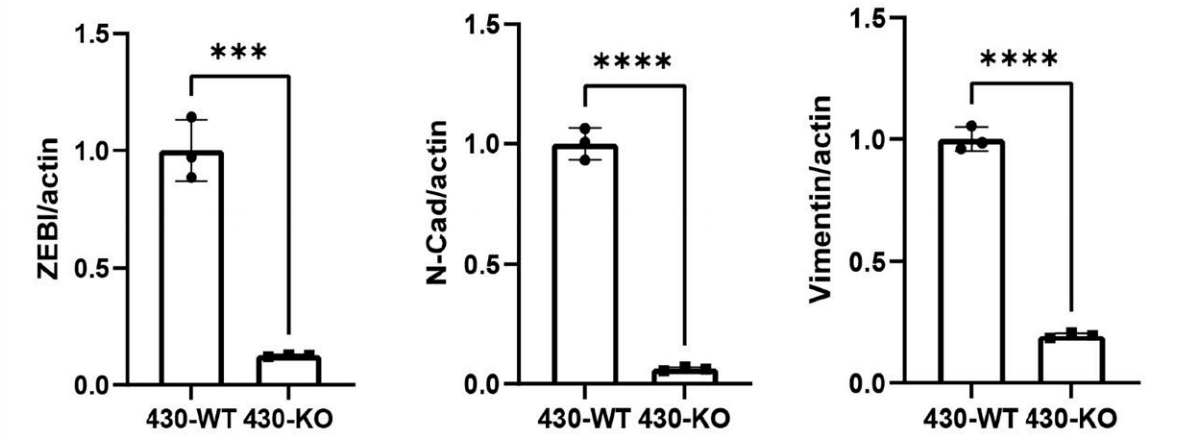

SUPPLEMENTARY FIGURE S3. Band intensities from Western blots (Figure 3D) were quantified using ImageJ (NIH). The relative expression levels of ZEB1, N-cadherin, and Vimentin were calculated by normalizing each target protein to β-actin. Data from three independent experiments were averaged, and values were normalized to the mean of the 430-WT group, which was set to 1. Data are shown as mean ± SD from three independent experiments. Statistical significance was determined by paired t-test. *$p < 0.05$, **$p < 0.01$, ***$p < 0.001$, ****$p < 0.0001$.

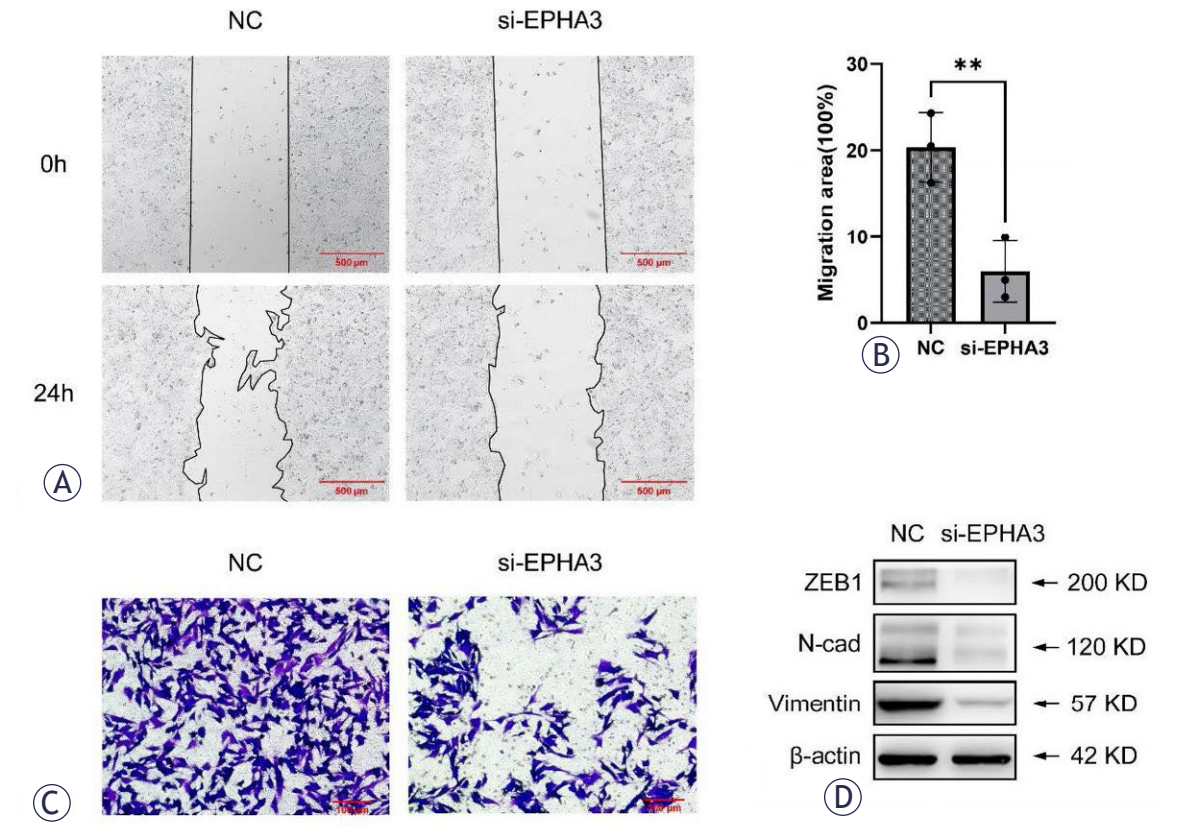

SUPPLEMENTARY FIGURE S4. EPHA3 knockdown inhibits the migration of GIST-430 cells. **(A-B)** Wound-healing assay showing the migratory capacity of GIST-430 cells transfected with negative control siRNA (NC) or si-EPHA3 at 0 and 24 h. Scale bar = 500 μm. (C) Transwell migration assay showing the migratory ability of GIST-430 cells transfected with NC or si-EPHA3. **(D)** Representative Western blot images showing the expression of EPHA3, ZEB1, N-cadherin, and Vimentin in GIST-430 cells transfected with NC or si-EPHA3, with β-actin as the loading control. Data are presented as the mean ± SD from three independent experiments, $^{**}p < 0.01$.

research article

Electrochemotherapy for cutaneous tumors combined with tumor irradiation before or after treatment: feasibility, safety, and effectiveness

Giulia Bertino[1], Marta Minuti[1], Julie Gehl[2,3], Erika Kis[4], Hadrian Nassabi[5], Michele Pio Grieco[6], Giuseppe Riva[7], Matteo Mascherini[8], Francesca De Terlizzi[9], Maja Cemazar[10], Gregor Sersa[10]

[1] Department of Otolaryngology Head and Neck Surgery, University of Pavia, IRCCS Policlinico San Matteo Foundation, Pavia, Italy
[2] Department of Clinical Oncology and Palliative Care, Zealand University Hospital, Roskilde, Denmark
[3] Department of Clinical Medicine, Faculty of Health and Medical Sciences, University of Copenhagen, Copenhagen, Denmark
[4] Department of Dermatology and Allergology, Albert Szent-Györgyi Medical School, Albert Szent-Györgyi Clinical Centre, University of Szeged, Szeged, Hungary
[5] Department of Dermatology and Plastic Surgery, SRH- Waldklinikum, Gera, Germany
[6] UOC Chirurgia Plastica e Skin Cancer Unit, IRCCS CROB Centro Riferimento Oncologico Basilicata, Rionero in Vulture (PZ), Italy
[7] Division of Otorhinolaryngology, Department of Surgical Sciences, AOU Città della Salute e della Scienza of Turin, Torino, Italy
[8] Department of Surgery, IRCCS AOM Liguria, Genoa, Italy
[9] IGEA Biophysics Lab. Carpi, Modena, Italy
[10] Department of Experimental Oncology, Institute of Oncology Ljubljana, Slovenia

Radiol Oncol 2026; 60(3): 427-435.

Received 11 August 2026
Accepted 20 August 2026

Correspondence to: Giulia Bertino, M.D., Department of Otolaryngology Head and Neck Surgery, University of Pavia, IRCCS Policlinico San Matteo Foundation, Pavia, Italy. E-mail: giulia.bertino@tin.it

Disclosure: Gregor Serša received travel grants from IGEA. No potential conflicts of interest were disclosed.

Background. Electrochemotherapy (ECT) can be performed on tumors in patients that precedes tumor irradiation or on recurrent tumors after tumor irradiation. In this study we evaluated the feasibility, safety and effectiveness of the combined ECT and tumor irradiation (radiotherapy, RT) on different tumors in the head and neck region.

Patients and methods. For the present cohort analysis, patients were selected from the Insp-ECT database, based on the following criteria: presence of head and neck lesions of any histological origin, treatment with both ECT and RT in any sequence, and a maximum interval of 12 months between the two treatments. The patients were treated with ECT followed by RT (ECT → RT) or RT followed by ECT (RT → ECT), in both cases because the first treatment resulted in incomplete response or subsequent relapse. In the case of ECT → RT the meantime interval was 5.7 months and in the case of RT → ECT 7.6 months. The minimal time interval between the treatments was 1 month.

Results. Treatment with ECT with bleomycin was feasible in all patients, treated either before or after RT. Included were 37 patients with the head and neck lesions. The combined treatment was performed predominantly on older population of patients with the age range from 50 to 96 years, median over 80 years. Importantly, in the group ECT → RT the major reason for RT was partial response (67%) after ECT. While, in the RT → ECT group the major reason for subsequent ECT was 58% of stable or progressive disease (failure to treatment). In both groups local symptoms decreased, like ulceration, odour and suppuration of tumors. In the ECT → RT group, the short-term response after 2 months was high, with 89% objective responses. In contrast, the RT → ECT group had a significantly lower rate, with 58% objective responses. At 24-month progression free survival (PFS) was 68% in the ECT → RT group and 20% in the RT → ECT group ($p = 0.0101$). The overall progression free survival Kaplan-Meier curves also differed significantly (log-rank $p = 0.0232$).

Conclusions. The combined treatment of ECT and RT is feasible, safe, and effective in elderly patients. The findings suggest that ECT may have particular value as a neoadjuvant treatment before RT, especially for bulky, ulcerated, or symptomatic lesions in this population.

Key words: cutaneous tumors; electrochemotherapy; tumor irradiation; neoadjuvant treatment; salvage therapy; tumor control

Introduction

Electrochemotherapy (ECT) is an effective local ablative therapy that utilizes application of electric pulses for efficient drug delivery into tumor cells.[1] The local potentiation of the drug, either bleomycin or cisplatin into cells provides effective tumor cell cytotoxicity. ECT has been proven in many clinical studies to be effective in local control of cutaneous as well as some deep-seated tumors.[2-12]

The Insp-ECT consortium collects clinical data on the treatment of cutaneous tumors with ECT from 48 cancer centers across Europe. The comprehensive report from this consortium reported an 85% objective response rate of the treated tumors across various tumor histotypes.[3] This response rate depends to some degree on tumor type, with melanoma being the least responsive, and on the tumor size, larger than 2 cm in diameter are less responsive. Another clinical factor influencing treatment effectiveness is previous treatment, such as chemotherapy or radiotherapy. The clinical data indicate that treatment naïve tumors respond better than previously irradiated tumors.[3]

Preclinical data indicate a radiosensitizing effect of ECT with bleomycin and cisplatin.[13-18] The systematic review by Ferioli *et al.*[19], comprehensively summarizes all the preclinical studies. The studies explored the best treatment regimen, ECT before or during the beginning of the radiation regimen resulted in pronounced tumor response. There are already some clinical reports, mainly case series, indicating that combining ECT with tumor irradiation is feasible and effective with local mild minimal side effects.[20–23]

However, if the interval between ECT and tumor irradiation extends to weeks or months, the radiosensitizing effect, which was demonstrated in preclinical studies and some clinical reports, is likely no longer present. No studies have yet examined the effectiveness of combining ECT before or after RT, with the interval between them at least one month. Therefore, the aim of this study was to evaluate the feasibility, safety, and effectiveness of combined ECT before or after RT in different tumor types, with head and neck squamous cell carcinoma (SCC) as the predominant type. In both scenarios, patients received the second therapy because of incomplete response or subsequent relapse.

Patients and methods

Data for this analysis were extracted from the Insp-ECT database, which includes contributions from 48 European centers reporting their experience with ECT. All data on patients treated with ECT are prospectively entered into a centralized online registry (https://Insp-ECT.eu) in anonymized form.

The Insp-ECT Registry contains comprehensive information on patient demographics, Eastern Cooperative Oncology Group (ECOG) performance status, disease stage, prior and concomitant oncologic treatments, as well as the location, number, size, and characteristics of cutaneous metastases. In addition, detailed data on ECT procedures (including anesthesia type and treatment parameters), treatment-related toxicities and adverse events, clinical response, pain assessment, and quality of life are systematically recorded.[3,24]

All patients provided written informed consent prior to inclusion. Data was entered prospectively by each participating center and updated over time. Each institution obtained approval from its local Ethics Committee and relevant data protection authorities. Participation in the registry required a formal signed agreement. The study was conducted in accordance with the principles of the Declaration of Helsinki.

For the present cohort analysis, patients were selected based on the following criteria: presence of head and neck lesions of any histological origin, treatment with both ECT and RT in any sequence, and a maximum interval of 12 months between the two treatments. Additional data were collected regarding treatment sequencing (ECT after RT or RT after ECT), as well as RT modality and delivered dose. Eight centers contributed to the patients' data collection: Pavia (IT), Ljubljana (SLO), Copenhagen (DK), Mainz (DE), Szeged (HU), Rionero in Vulture (IT), Torino (IT), Genova (IT).

ECT treatment

ECT was administered according to the most recent European Standard Operating Procedures (ESOPE) guidelines, as previously described.[25,26] Each participating center was responsible for defining the therapeutic strategy and making clinical decisions for individual patients, including the choice of anesthesia (general or local) based on clinical indication and patient preference.

Bleomycin was administered either intratumorally at a dose of 1000 IU/mL/cm^3 or intravenously at 15,000 IU/m^2. Electroporation was performed using the Cliniporator device (IGEA, Carpi, Italy), delivering eight pulses of 100 μs at an electric field strength of 1 kV/cm (adjusted to electrode spacing; for example, 400 V for a 4 mm electrode gap). Electrode selection was performed in accordance with standard operating procedures.[25,26]

Radiotherapy treatment

External beam radiation therapy (RT) was administered for the treatment of superficial cutaneous metastatic lesions in the head and neck region.[27,28] Treatment technique was selected at the discretion of each participating center based on lesion characteristics, anatomical location, and institutional practice. Photon-based approaches included intensity-modulated radiotherapy (IMRT) and image-guided radiotherapy (IGRT), allowing for improved dose conformity and setup accuracy, respectively.[29] In cases of superficially located lesions, electron beam radiotherapy was employed to exploit its limited penetration depth and rapid dose fall-off beyond the target volume, thereby minimizing exposure to underlying normal tissues. Details regarding the specific technique and total prescribed dose were collected and included in the analysis.

Response evaluation

Local response following ECT and/or RT was assessed 45–90 days after completion of the last treatment, according to modified Response Evaluation Criteria in Solid Tumors (RECIST).[30] Briefly, complete response (CR) was defined as the disappearance of the target lesion. Partial response (PR) was defined as a ≥30% reduction in the diameter of the target lesion. Progressive disease (PD) was defined as a ≥20% increase in lesion diameter, while stable disease (SD) was defined as neither sufficient shrinkage to qualify for PR nor sufficient increase to qualify for PD.

Up to seven cutaneous metastases per patient (including the largest lesion) were selected and recorded as target lesions.

Statistical analysis

Continuous variables were summarized using median values and ranges, while categorical variables were reported as absolute frequencies and percentages. Group comparisons for continuous variables were performed using a two-tailed heteroscedastic Student's t-test, and categorical variables were compared using the chi-square test.

Tumor control was evaluated in terms of progression-free survival (PFS), defined as the time from the first treatment (either RT or ECT) to disease progression, relapses, or last follow-up, whichever occurred first. Survival curves were estimated using the Kaplan–Meier method. One-year and 2-years local PFS rates and corresponding 95% confidence intervals (95% CI) were calculated. Differences between survival curves were assessed using the Mantel–Haenszel (log-rank) test.

All statistical analyses were performed using NCSS version 9 (NCSS, LLC, Kaysville, UT, USA). A p-value < 0.05 was considered statistically significant.

Results

Patient characteristics and treatment data

In the analysis, 37 patients with lesions in the head and neck region were included. All patients were treated at 8 European centers within the Insp-ECT group. All patients received both ECT and RT within 12 months and were listed into two groups: the "ECT → RT" group received ECT as the first treatment and RT as the subsequent treatment; the "RT → ECT" group received RT as the first treatment and ECT as the subsequent treatment.

Both groups were well matched in demographics, including number of patients, age, and nodule size (Table 1). The predominant tumor types in both groups were squamous cell carcinoma (SCC) and basal cell carcinoma (BCC), along with melanoma, breast cancer, soft tissue sarcoma, and others (Table 1). Tumors were located in the head and neck region. The nodule size was relatively large in both groups, with a mean diameter exceeding 30 mm and ranging from 2 mm to 170 mm in the largest diameter.

TABLE 1. Characteristics of the 2 groups of patients treated with combined treatment with ECT and RT

	ECT → RT (N = 18)			RT → ECT (N = 19)			P
	TYPE	**N**	**%**	**TYPE**	**N**	**%**	**Value**
DIAGNOSIS*	MM	0	0%	MM	1	5%	0.8896
	BCC	7	40%	BCC	5	26%	
	MA	1	5%	MA	2	11%	
	SCC	9	50%	SCC	9	48%	
	SAR	1	5%	SAR	1	5%	
	OTH	0	0%	OTH	1	5%	
T-STAGE	T1	3	17%	T1	6	32%	0.5381
	T2	10	56%	T2	6	32%	
	T3	1	5%	T3	4	20%	
	T4	3	17%	T4	3	16%	
	TX	1	5%	TX	0	0%	
	MEAN	**ST.DEV.**	**MEDIAN (RANGE)**	**MEAN**	**ST.DEV.**	**MEDIAN (RANGE)**	
AGE	80	10	83 (59-94)	81	13	87 (50-96)	0.7102
NODULES' SIZE (mm)	36	25	30 (14-130)	40	41	30 (2-170)	0.6513
MONTHS BETWEEN TREATMENTS	5.7	3.6	5.3 (1-12)	7.6	4.1	8 (1-12)	0.1587

BCC = basal cell carcinoma, MA = breast cancer; MM = melanoma; OTH = other; SAR = soft tissue sarcoma; SCC = squamous cell carcinoma

In ECT → RT group OTH was neoplasia of the right parotid region, in RT → ECT group OTH was Metastatic Transitional Cell Carcinoma of maxillary sinus.

The interval between the ECT → RT and RT → ECT groups were not significantly different (p = 0.1587), with mean times of 5.7 and 7.6 months, respectively (Table 1). The minimum interval was set at 1 month, which is important because we wanted to exclude patients in whom the radiosensitizing effect of ECT could be significant, due to radio sensitizing effect of bleomycin. After 1 month, bleomycin is expected to have been eluted from the ECT-treated tumors, as the anti-tumor effect of ECT should have been fully exerted by then.

The predominant type of electrodes used in ECT were linear and hexagonal array electrodes in both treatment groups. Predominant type of drug administration was intravenous, although relatively high percentage of patients in both groups received intratumoral bleomycin administration (22% and 32%, respectively) (Table 2). The dosage of bleomycin administered was according to the standard operating procedures, for either intravenous or intratumoral administration. The prescribed radiation dose did not differ significantly between the two groups, with a mean dose of 49 ± 13 Gy in the ECT → RT group and 41 ± 14 Gy in the RT → ECT group (p = 0.1853). Photon-based radiotherapy was the predominant treatment modality in both cohorts (Table 2).

The reasons for the second treatment differed between the two groups of patients. In the group of ECT → RT the major reason was partial response to ECT; therefore, tumor irradiation was performed in 67% of patients. In contrast, in the RT → ECT group of patients ECT was performed after failure of response to RT in 58% of cases (Table 3). The second treatment in both groups of patients was rarely performed because of the relapse after previous treatment. Considering this difference in the approaches the reasons also differed statistically significantly (p = 0.0423).

Feasibility and safety

In both groups of patients, the combined treatment either ECT before or after the tumor irradiation was feasible, according to the current standard operating procedures.

The treatment was also safe. In both groups the local symptoms, incidence and gravity decreased. Ulceration decreased from 67% to 44% in the ECT → RT group and from 42% to 37% in RT → ECT group. Odour decreased from 11% to 0% in the ECT → RT group and from 16% to 11% in the RT → ECT group. Suppuration decreased from 17% to 0% in the ECT → RT group and from 21% to 16% in the RT → ECT group (Figure 1).

Short-term response

Short term response was assessed at 2 months of follow-up after treatment. The distribution of response categories differed significantly between the two groups (p = 0.0383), with a higher proportion of CR and PR and no PD in the ECT → RT group (Table 4). No progressive disease was observed in the ECT → RT group, whereas PD occurred in 37% of patients in the RT → ECT group. Figure 2 illustrates the higher response rate observed with the ECT → RT sequence.

Long term response

Patients in the ECT → RT group were followed for a mean time of 23 ± 21 months (median 14, range 4-79 months). At last follow-up 7 (39%) had no evidence of disease, 5 (28%) were alive with disease, and 6 (33%) died. In the RT → ECT group the mean follow-up time was 19 ± 13 months (median 17, range 3-53). At last follow-up 7 (37%) had no evidence of disease, 6 (32%) were alive with disease and 6 (32%) died.

During follow-up period, 4 recurrences/progressions were observed in the ECT → RT group (22%) and 12 were observed in the RT → ECT group (63%), significantly higher (p = 0.0201) than the former group.

Progression free survival curves are presented in Figure 3. One-year progression free survival was 87% [C.I. 71%-100%] in the ECT → RT group and 75% [C.I. 54%-96%] in the RT → ECT group (p = 0.3819).

The recurrent tumors, which dominated in RT → ECT group, occurred after the first year and resulted in significant differences in progression free survival of the patients at 24 months as reported in Figure 3. In the ECT → RT group was 68% [C.I. 41%-95%], in the RT → ECT group it was 20% [C.I. 0%-41%] (p = 0.0101). This resulted in also significant difference (p = 0.0232) in the progression free Kaplan-Meier survival curves due to the higher progression free survival of the ECT → RT group.

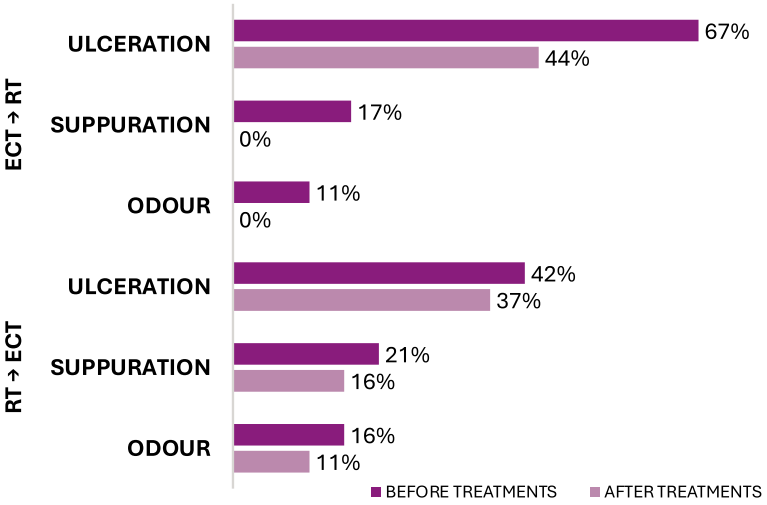

FIGURE 1. Incidence of most common local symptoms in the two groups before and after the treatments.

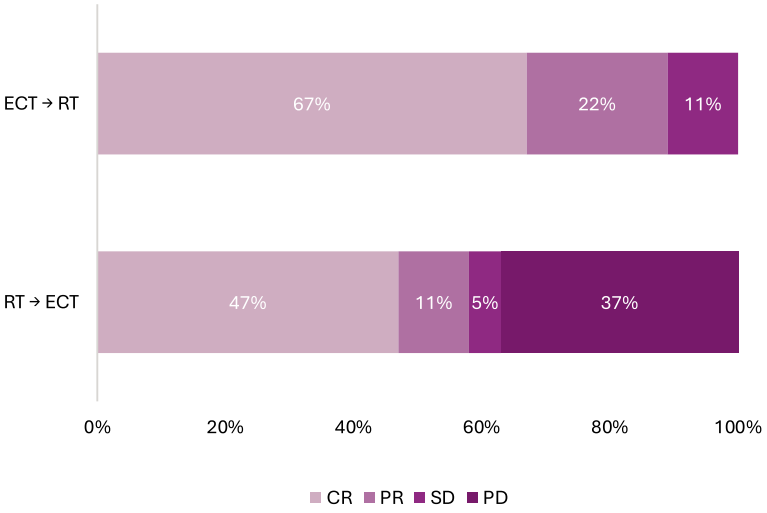

FIGURE 2. Distribution of short-term response in the 2 groups after the sequence of both treatments.

CR = complete response; PR = partial response; SD = stable disease; PD = progressive disease

Discussion

This multicenter retrospective cohort analysis demonstrates that the combination of ECT and RT, administered either before or after tumor irradiation, is feasible, safe, and clinically effective in elderly patients with head and neck cutaneous malignancies. The study specifically evaluated treatment sequences separated by at least one month, thereby minimizing the likelihood that the observed effects were attributable to the known short-term radiosensitizing properties of bleomycin-based ECT.[13,14,22] Despite the heterogeneous tumor histologies and treatment techniques, both strategies achieved meaningful local tumor control and symptom palliation.

The present results confirm previous clinical observations suggesting that ECT can be safely integrated with RT in the management of difficult-to-treat cutaneous tumors. While earlier re-

TABLE 2. Data on treatments (RT and ECT) in the two groups of patients

	ECT → RT (N = 18)			RT → ECT (N = 19)			P
	TYPE	**N**	**%**		**N**	**%**	**Value**
ELECTRODE	plate	0	0%	plate	2	11%	0.3955
	linear	8	44%	linear	8	42%	
	hexagonal	9	50%	hexagonal	9	47%	
	multiple	1	6%	multiple	0	0%	
DRUG ADMINISTERED	I.V.	14	78%	I.V.	13	68%	0.7140
	I.T.	4	22%	I.T.	6	32%	
IRRADIATION	photons	14	78%	photons	15	79%	1.000
	electrons	4	22%	electrons	4	21%	

TABLE 3. Reasons for the second treatment in the two groups of patients (p = 0.0423)

REASON FOR 2ND TREATMENT	After PR of previous treatment	After SD or PD of previous treatment	Relapse after CR of previous treatment
ECT → RT (N=18)	12	4	2
Reason for RT	67%	22%	11%
RT → ECT (N=19)	5	11	3
Reason for ECT	26%	58%	16%

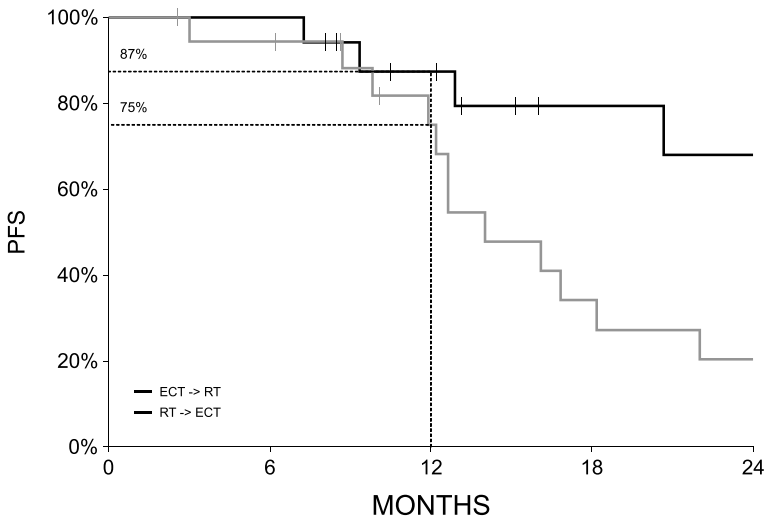

FIGURE 3. Progression free survival (PFS) Kaplan-Meier curves.

TABLE 4. Short term response in the 2 groups after the sequence of both treatments

	ECT → RT		RT → ECT		P VALUE
	N	**%**	**N**	**%**	
CR	12	67%	9	47%	0.0383
PR	4	22%	2	11%	
SD	2	11%	1	5%	
PD	0	0%	7	37%	

CR = complete response; PR = partial response; SD = stable disease; PD = progressive disease

ports mainly focused on concomitant or closely sequenced treatments designed to exploit radiosensitization[13,14,22], our study explored a different clinical scenario in which ECT and RT were combined over longer intervals. This distinction is clinically relevant because it reflects real-world treatment pathways in frail or elderly patients who often require staged therapeutic approaches. The mean interval between treatments was 5.7 months in the ECT → RT group and 7.6 months in the RT → ECT group, well beyond the expected persistence of bleomycin within treated tissues. Therefore, the improved outcomes observed in the ECT → RT cohort are unlikely to be explained solely by direct radiosensitization.

An important finding of this study is the significantly better short-term response observed when ECT preceded RT. The ECT → RT group achieved

an objective response rate of 89%, compared with 58% of patients treated with RT followed by ECT. Moreover, no progressive disease was observed in the ECT → RT cohort, whereas more than one-third of patients in the RT → ECT group experienced disease progression despite salvage ECT. These findings suggest that ECT administered neoadjuvantly before irradiation may improve local disease conditions and enhance the effectiveness of subsequent RT. It is worth mentioning that ECT as the first treatment resulted in 67% of PR and that RT was performed on down-sized tumors. Thus, tumor downsizing achieved by ECT may reduce hypoxic tumor burden, and improve dose distribution, particularly in bulky and ulcerated lesions frequently encountered in the head and neck region. On the contrary, ECT after RT may be less effective because of tumor vessels damage due to RT, and consequently lower uptake and distribution of bleomycin after intravenous administration.

The clinical role of ECT differed substantially between the two treatment groups. Although the tumor size at the time of the first treatment did not differ between the groups, in the ECT → RT cohort, ECT was predominantly used as a neoadjuvant treatment prior to RT, mainly to reduce tumor volume and improve local tumor conditions before RT; in fact, in the ECT → RT cohort, 67% of patients underwent RT after achieving a partial response to ECT, and the final objective response rate after completion of the combined treatment was 89%. In contrast, ECT in the RT → ECT group was mainly used as salvage therapy after inadequate response or failure of irradiation (SD or PD after RT), resulting in only 58% of OR after the ECT. The sequence of treatments likely contributed to the poorer outcomes observed in the RT → ECT cohort, since previously irradiated tumors are known to be more resistant to subsequent local therapies because of fibrosis, vascular damage, hypoxia, and impaired tissue healing. Previous analyses from the Insp-ECT consortium have similarly shown that treatment-naïve lesions respond better to ECT than previously irradiated tumors.[3] However, further studies on bigger cohorts of patients are needed to confirm that ECT resulted in better response than RT as the first treatment.

In addition to tumor response, both treatment strategies provided clinically meaningful symptom control. Clinically measured outcomes; reductions in ulceration, suppuration, and malodor were observed in both groups after treatment. These benefits are particularly relevant in elderly patients with advanced head and neck tumors, where local symptoms substantially impair quality of life, nutrition, communication, and social functioning. Therefore, even in patients with limited curative options, ECT combined with RT may provide important palliative benefits with acceptable tolerability.

Long-term tumor control also favored the ECT → RT sequence. Although both groups demonstrated encouraging progression-free survival (PFS), the ECT → RT group had significantly fewer recurrences and superior Kaplan–Meier PFS curves. One-year PFS reached 87% in the ECT → RT group compared with 75% in the RT → ECT group, with significantly fewer progression events overall. These findings further support the hypothesis that ECT may have particular value when integrated earlier in the local treatment strategy rather than being reserved exclusively as salvage therapy after RT failure.

The study population consisted predominantly of elderly patients, with median ages above 80 years in both cohorts. This aspect deserves particular attention because older patients are frequently poor candidates for extensive surgery or aggressive systemic therapies due to frailty and comorbidities. The good tolerability and feasibility observed in this study indicate that combined ECT and RT may represent a valuable therapeutic option for this challenging patient population. Importantly, treatment was successfully delivered across multiple European centers using standard operating procedures, supporting the reproducibility and general applicability of the approach.

Several limitations of this study should be acknowledged. First, the retrospective nature of the analysis and the relatively small sample size limit the strength of definitive conclusions. Second, the patient population was heterogeneous with respect to tumor histology, stage, RT techniques, and radiation doses. Third, the interval between ECT and RT varied considerably among patients and among groups, even if not significantly, which may have influenced treatment outcomes. Finally, because treatment allocation was not randomized, differences between groups may partially reflect underlying differences in disease biology and treatment intent, particularly the higher proportion of salvage cases in the RT → ECT cohort. This paper does not address the question whether primary treatment with ECT is more or less efficient than RT, since the database does not contain data on response rates of all patients treated with RT, only those that received ECT in addition to RT.

Nevertheless, this study provides clinically relevant evidence supporting the integration of ECT and RT in the treatment of head and neck cutaneous tumors. The findings suggest that ECT may

have particular value as a neoadjuvant treatment before RT, especially for bulky, ulcerated, or symptomatic lesions in elderly patients. Future prospective studies should further investigate optimal sequencing, timing, and patient selection criteria for combined ECT and RT protocols. In particular, the promising results observed in the ECT → RT group support the hypothesis that ECT could be intentionally incorporated into future treatment strategies as a neoadjuvant approach to improve RT effectiveness and local tumor control.

Acknowledgments

This research was partially funded by the Slovenian Research and Innovation Agency (ARIS) under program grant P3-0003.

AI disclosure

During the preparation of this paper, the authors used ChatGPT and InstaText to improve language. After using this tool/service, the authors have reviewed and edited the content as required and take full responsibility for the content of the publication.

References

1. Gehl J, Pereira PL, Cantwell CP, Deschamps F, Kocijancic A, Schmidt N, et al. Tumor ablation: emerging uses, challenges, and strategic implementation. A green paper by the Network of Expertise in Cancer (JANE-2), high tech medical resources, network on physical methods of tumor ablation. *Radiol Oncol* 2026; 60(3): 427-435.; **60:** 153-65. doi: 10.2478/raon-2026-0030
2. Marty M, Sersa G, Garbay JR, Gehl J, Collins CG, Snoj M, et al. Electrochemotherapy – an easy, highly effective and safe treatment of cutaneous and subcutaneous metastases: Results of ESOPE (European Standard Operating Procedures of Electrochemotherapy) study. *Eur J Cancer Suppl* 2006; **4:** 3-13. doi: 10.1016/j.ejcsup.2006.08.002
3. Clover AJP, de Terlizzi F, Bertino G, Curatolo P, Odili J, Campana LG, et al. Electrochemotherapy in the treatment of cutaneous malignancy: outcomes and subgroup analysis from the cumulative results from the pan-European International Network for Sharing Practice in Electrochemotherapy database for 2482 lesions in 987 patients (2008–2019). *Eur J Cancer* 2020; **138:** 30-40. doi: 10.1016/j.ejca.2020.06.020
4. Bertino G, Sersa G, De Terlizzi F, Occhini A, Plaschke CC, Groselj A, et al. European Research on Electrochemotherapy in Head and Neck Cancer (EURECA) project: Results of the treatment of skin cancer. *Eur J Cancer* 2016; **63:** 41-52. doi: 10.1016/j.ejca.2016.05.001
5. Bertino G, Minuti M, Groselj A, Jamsek C, Silvestri B, Carpene S, et al. Electrochemotherapy (ECT) in treatment of mucosal head and neck tumors. An international network for sharing practices on ECT (Insp-ECT) study group report. *Eur J Surg Oncol* 2024; **50:** 108473. doi: 10.1016/j.ejso.2024.108473
6. Campana LG, Farronato S, Hodgetts J, Odili J, Vecchiato A, Bracken A, et al. European e-Delphi process to define expert consensus on electrochemotherapy treatment indications, procedural aspects, and quality indicators in melanoma. *Brit J Surg* 2023; **110:** 818-30. doi: 10.1093/bjs/znad105
7. Campanacci L, Cevolani L, De Terlizzi F, Saenz L, Alì N, Bianchi G, et al. Electrochemotherapy is effective in the treatment of bone metastases. *Curr Oncol* 2022; **29:** 1672-82. doi: 10.3390/curroncol29030139
8. Bianchi G, Campanacci L, Ronchetti M, Donati D. Electrochemotherapy in the treatment of bone metastases: a phase II trial. *World J Surg* 2016; **40:** 3088-94. doi: 10.1007/s00268-016-3627-6
9. Deschamps F, Tselikas L, Yevich S, Bonnet B, Roux C, Kobe A, et al. Electrochemotherapy in radiotherapy-resistant epidural spinal cord compression in metastatic cancer patients. *Eur J Cancer* 2023; **186:** 62-8. doi: 10.1016/j.ejca.2023.03.012
10. Deschamps F, Tselikas L, Cazzato RL, Facchini G, Granata V, Bonnet B, et al. Electrochemotherapy in metastatic epidural spinal cord compression: a review and technical update. *Br J Radiol* 2025; **98:** 828-39. doi: 10.1093/bjr/tqae219
11. Kovács A, Bischoff P, Haddad H, Zhou W, Temming S, Schäfer A, et al. Long-term comparative study on the local tumour control of different ablation technologies in primary and secondary liver malignancies. *J Pers M* 2022; **12:** 430. doi: 10.3390/jpm12030430
12. Djokic M, Dezman R, Cemazar M, Stabuc M, Petric M, Smid LM, et al. Percutaneous image guided electrochemotherapy of hepatocellular carcinoma: technological advancement. *Radiol Oncol* 2020; **54:** 347-52. doi: 10.2478/raon-2020-0038
13. Kranjc S, Tevz G, Kamensek U, Vidic S, Cemazar M, Sersa G. Radiosensitizing effect of electrochemotherapy in a fractionated radiation regimen in radiosensitive murine sarcoma and radioresistant adenocarcinoma tumor model. *Radiat Res* 2009; **172:** 677-85. doi: 10.1667/RR1873.1
14. Kranjc S, Cemazar M, Grosel A, Sentjurc M, Sersa G. Radiosensitising effect of electrochemotherapy with bleomycin in LPB sarcoma cells and tumors in mice. *BMC Cancer* 2005; **5:** 115. doi: 10.1186/1471-2407-5-115
15. Fiorentzis M, Sokolenko EA, Bechrakis NE, Ting S, Schmid KW, Sak A, et al. Electrochemotherapy with bleomycin enhances radiosensitivity of uveal melanomas: first in vitro results in 3D cultures of primary uveal melanoma cell lines. *Cancers* 2021; **13:** 3086. doi: 10.3390/cancers13123086
16. Raeisi E, Aghamiri S, Bandi A, Rahmatpour N, Firoozabadi S, Kafi-Abad S, et al. The antitumor efficiency of combined electrochemotherapy and single dose irradiation on a breast cancer tumor model. *Radiol Oncol* 2012; **46:** 226-32. doi: 10.2478/v10019-012-0035-x
17. Todorovic V, Sersa G, Flisar K, Cemazar M. Enhanced cytotoxicity of bleomycin and cisplatin after electroporation in murine colorectal carcinoma cells. *Radiol Oncol* 2009; **43:** 264-73. doi: 10.2478/v10019-009-0037-5
18. Cemazar M, Sersa G. Recent advances in electrochemotherapy. *Bioelectricity* 2019; **1:** 204-13. doi: 10.1089/bioe.2019.0028
19. Ferioli M, Perrone AM, Buwenge M, Arcelli A, Vadala' M, Fionda B, et al. Combination of electrochemotherapy with radiotherapy: a comprehensive, systematic, PRISMA-compliant review of efficacy and potential radiosensitizing effects in tumor control. *Curr Oncol* 2023; **30:** 9895-905. doi: 10.3390/curroncol30110719
20. Gregor Sersa, Maja Cemazar, Zvonimir Rudolf, Albert P Fras. Adenocarcinoma skin metastases treated by Electrochemotherapy with cisplatin combined with radiation. *Radiol Oncol* 1999: **33:** 291-6.
21. Skarlatos I, Kyrgias G, Mosa E, Provatopoulou X, Spyrou M, Theodorou K, et al. Electrochemotherapy in cancer patients: first clinical trial in Greece. *In Vivo* 2011; **25:** 265-74. PMID: 21471545
22. G Kyrgias, E. Kostopoulou, E. Zafiriou, A. Zygogianni, J. Skarlatos, A. V. Roussaki-Schulze, K. Theodorou. Hidradenocarcinoma of the temporal area successfully treated with concomitant electrochemotherapy and radiotherapy. *Head Neck Oncol* 2013; **5:** 14.
23. Serša G, Kranjc S, Čemažar M. Improvement of combined modality therapy with cisplatin and radiation using electroporation of tumors. *Int J Radiat Oncol Biol Phys* 2000; **46:** 1037-41. doi: 10.1016/S0360-3016(99)00464-2
24. Brizio M, Ribero S, Campana LG, Clover AJP, Gehl J, Kunte C, et al. International Network for Sharing Practices on Electrochemotherapy (Insp-ECT): An Integrative Patients Treatment Consortium. In: Miklavcic D, curatore. *Handbook of Electroporation* [Internet]. Cham: Springer International Publishing; 2016 [cited 2021 Jun 3]. pp. 1–18. Available at: http://link.springer.com/10.1007/978-3-319-26779-1_95-1 doi:10.1007/978-3-319-26779-1_95-1

25. Mir LM, Gehl J, Sersa G, Collins CG, Garbay JR, Billard V, et al. Standard operating procedures of the electrochemotherapy: Instructions for the use of bleomycin or cisplatin administered either systemically or locally and electric pulses delivered by the CliniporatorTM by means of invasive or non-invasive electrodes. *Eur J Cancer Suppl* 2006; **4:** 14-25. doi: 10.1016/j.ejcsup.2006.08.003

26. Gehl J, Sersa G, Matthiessen LW, Muir T, Soden D, Occhini A, et al. Updated standard operating procedures for electrochemotherapy of cutaneous tumours and skin metastases. *Acta Oncologica* 2018; **57:** 874-82. doi: 10.1080/0284186X.2018.1454602

27. Sause WT, Cooper JS, Rush S, Ago CT, Cosmatos D, Coughlin CT, et al. Fraction size in external beam radiation therapy in the treatment of melanoma. *Int J Radiat Oncol Biol Phys* 1991; **20:** 429-32. doi: 10.1016/0360-3016(91)90053-7

28. Mittal BB. Advanced techniques in radiation therapy for head and neck cancers. *Otolaryngol Clin North Am* 1991; **24:** 1569-83. PMID: 1792085

29. Perez CA, Bradley J, Chao CKS, Grigsby PW, Mutic S, Malyapa R. Functional imaging in treatment planning in radiation therapy: a review. *Rays* 2002; **27:** 157-73. PMID: 12696245

30. Eisenhauer EA, Therasse P, Bogaerts J, Schwartz LH, Sargent D, Ford R, et al. New response evaluation criteria in solid tumours: revised RECIST guideline (version 1.1). *Eur J Cancer* 2009; **45:** 228-47. doi: 10.1016/j.ejca.2008.10.026

RADIOLOGY AND ONCOLOGY Radiology and Oncology | Ljubljana | Slovenia | www.radioloncol.com

research article

Cytoreductive surgery and hyperthermic intraperitoneal chemotherapy for colorectal peritoneal metastases: a single-institution experience

Gasper Pilko[1,2], Rok Petric[1,2]

[1] Department Surgical Oncology, Institute of Oncology Ljubljana, Ljubljana, Slovenia
[2] Medical Faculty, University of Ljubljana, Ljubljana, Slovenia

Radiol Oncol 2026; 60(3): 436-441.

Received 22 March 2026
Accepted 28 May 2026

Correspondence to: Assit. Prof. Rok Petrič, M.D., Ph.D., Department of Surgical Oncology, Institute of Oncology Ljubljana, Zaloška 2, SI-1000 Ljubljana, Slovenia, E-mail: rpetric@onko-i.si

Disclosure: No potential conflicts of interest were disclosed.

Background. Peritoneal metastases (PM) from colorectal cancer are associated with poor prognosis. Cytoreductive surgery (CRS) combined with hyperthermic intraperitoneal chemotherapy (HIPEC) has been proposed for selected patients, although its role remains debated. This study evaluates the efficacy and safety of CRS plus HIPEC in a single institution.

Patients and methods. This retrospective study included patients with colorectal PM treated with CRS and HIPEC between 2009 and 2024. Preoperative staging involved CT and/or MRI, and all cases were discussed in a multidisciplinary team. Disease burden was assessed using the Peritoneal Cancer Index (PCI), and completeness of cytoreduction (CC score) was recorded. HIPEC was performed with oxaliplatin (360 mg/m² at 42°C for 90 minutes). Overall survival (OS) was the primary endpoint; disease-free survival (DFS) and morbidity were secondary endpoints.

Results. Fifty patients (mean age 54 years) were included. Complete cytoreduction (CC-0/1) was achieved in 88% of cases, with a median PCI of 8.33. Severe complications occurred in 18% of patients, with no 30-day mortality. After a median follow-up of 34 months, median OS was 49 months; 1- and 5-year OS rates were 96% and 54%, respectively. Median DFS was 14 months. PCI, CC score, and prior surgical score (PSS) were associated with OS on univariate analysis, while PCI and CC score remained independent prognostic factors.

Conclusions. CRS plus HIPEC is a feasible and effective treatment for selected patients with colorectal PM, with acceptable morbidity. Low PCI and complete cytoreduction are key predictors of improved survival.

Key words: colorectal cancer; peritoneal metastases; cytoreductive surgery; HIPEC; peritoneal cancer index

Introduction

Colorectal cancer represents the third most common cancer and the fourth most common cause of cancer-related death worldwide.[1] The peritoneum is the second most frequent site of colon cancer metastasis.[2] Five percent of patients have synchronous peritoneal metastases (PM) at initial diagnosis and 19% develop metachronous PM after curative primary resection, with 8% being isolated metastasis.[3,4] Peritoneal metastases are associated with reduced overall survival, and, in 30–40% of cases, they are associated with significantly worse prognosis compared with non-peritoneal metastases.[5,6] Contemporary systemic chemotherapy (oxaliplatin- and irinotecan-based) with targeted

therapy attains median survival of 16.3 months for isolated PM, compared with 19.1 and 24.6 months for isolated liver and lung metastases.[6]

Recently, in selected patients, the combination of extensive cytoreductive surgery (CRS) with Hyperthermic intra-operative IntraPeritoneal Chemotherapy (HIPEC) has been reported to have a survival benefit for patients with peritoneal metastasis from colorectal cancer.[7-9] CRS aims to remove all macroscopic peritoneal disease; this is achieved by resection of tumour-coated viscera and parietal peritoneum (peritonectomy). HIPEC targets the residual microscopic lesions - intraperitoneal administration allows delivery of a higher concentration of chemotherapeutics to peritoneal disease with less systemic toxicity, while mild hyperthermia enhances the drugs' cytotoxicity and penetration into tumour nodules.[10] CRS plus HIPEC was first used to treat appendiceal mucinous neoplasm with pseudomyxoma peritonei. This technique also proved valuable for a subgroup of colorectal PM patients. In several retrospective studies, median overall survival with CRS plus HIPEC was encouraging in patients with macroscopically complete resection.[11-13] A recent meta-analysis showed that the treatment CRS plus HIPEC gives a significant survival advantage in carefully selected patients. The median overall survival was 30–63 months for colorectal PM.[14] In a Dutch phase 3 controlled trial CRS plus HIPEC was superior to systemic chemotherapy in terms of overall survival in patients in whom surgery was done only to relieve symptoms caused by bowel obstruction.[8] In specialised centres, CRS plus HIPEC can cure (*i.e.*, no evidence of disease at 5 years) around 16% of patients in whom resection is macroscopically complete.[15]

Nevertheless, controversies exist on this treatment modality. Firstly, according to some studies, it carries significant morbidity and mortality; major complications and death occurred in up to 52% and 5.8% patients in high-volume centres.[14,16] Also, the value of HIPEC on top of CRS has been questioned for colorectal PM. The results of PRODIGE-7 trial showed that combining oxaliplatin-based HIPEC with CRS had no survival advantage over optimal CRS alone, but was associated with more late complications. It is worth mentioning that both arms of PRODIGE-7 had an unexpectedly long median survival of 41 months, highlighting the benefit of complete surgical cytoreduction.[17] Current major guidelines in Europe and the United States recommend complete CRS plus HIPEC performed in experienced centres as an appropriate treatment option for selected patients with limited colorectal PM.[18]

We have started performing CRS plus HIPEC for patients with different peritoneal tumours since 2009. To our knowledge, we are the only centre in our country performing this procedure. During this time, we have performed over 100 procedures which were performed by 5 surgeons. The aim of this study is to evaluate the efficacy and safety of CRS plus HIPEC for colorectal PM in our institute.

Patients and methods

Patient selection

This study is a retrospective analysis of prospectively maintained data from patients that underwent CRS followed by HIPEC for resectable PM from colorectal cancer between 2009 and 2024. The study was approved by both Institutional Ethics and Research Boards.

All patients underwent detailed preoperative assessment including radiological and/or laparoscopic staging to estimate the extent of peritoneal dissemination and resectability of the disease. Radiological staging included thoracic, abdominal and pelvic computed tomography (CT) with intravenous contrast, and/or abdominal magnetic resonance imaging (MRI). All cases were discussed in a dedicated Multi-Disciplinary Team meeting, in which treatment options were discussed. Extra-abdominal metastases or extensive small bowel/ mesentery involvement were considered as absolute contra-indications to CRS plus HIPEC. Presence of synchronous liver metastases and a peritoneal cancer index (PCI) > 20 (either from imaging or exploratory laparotomy) were relative contraindications as they were associated with poor outcomes; under such circumstances, we only offer CRS plus HIPEC to young, fit patients who lack alternative treatment option (*e.g.* further systemic therapy is expected to be ineffective).

Procedure details

In all cases, a laparotomy was performed and the extent of peritoneal disease was calculated intraoperatively using the PCI score (a scoring system that ranges from 0 to 39, and quantifies the extent of peritoneal disease based on tumour sizes and their distribution along 13 regions within the peritoneal cavity as described by Sugarbaker *et al.*).[10] If the disease was considered to be resectable, cytoreduction was performed using tumour removal, or-

gan resections and peritonectomy techniques as described by Sugarbaker *et al.*[10] After the surgical procedure, the completeness of cytoreduction (CC) was evaluated for each patient as follows: a CC-0 score indicated no visible tumour in the peritoneal cavity; a CC-1 score indicated residual tumour size r < 2.5 mm; a CC-2 score indicated residual tumour size 2.5 mm–2.5 cm; a CC-3 score indicated a residual tumour size > 2.5 cm.[10] Patients with CC-0/CC-1 scores were considered to have undergone complete cytoreduction. Following cytoreduction, patients underwent HIPEC using the closed abdomen technique. All intestinal reconstructions were performed before closure of the abdomen, six tubes (three for inflow of the chemotherapy solution and three for outflow) were inserted and the abdomen was closed with standard abdominal closure techniques. After testing for possible leaks with normal saline 0.9%, oxaliplatin was administrated in the abdominal cavity at an intraperitoneal temperature of 42 °C at a dose 360 mg/m2 for 90 minutes.

Parameters evaluated

For each patient, demographic data, details of the course of the disease (site of primary tumour, preoperative or postoperative chemotherapy, time of diagnosis of PM, prior surgery score (PSS): PSS-0 means no prior surgery or only biopsy was made; PSS-1 limited surgery in one abdominal region; PSS-2 surgeries in two to five abdominal regions; PSS-3 extensive prior surgery > 5 regions[10] and procedural details (PCI score, CC score) were recorded. As far as the postoperative course was concerned, the length of hospital stay was recorded, while postoperative morbidity was graded according to the Clavien-Dindo classification system.[19] Overall survival was defined from the time of the surgical procedure to the date of reported death, and disease-free survival was defined from the time of the surgical procedure to the time of diagnosis of disease recurrence or progression.

Statistical analysis

Overall survival was used as the primary endpoint of this study. For categorical variables, the chi-square and Fisher's exact test were used as appropriate. Survival analysis was performed using the Kaplan–Meier method, and compared using the log-rank test. Multivariate analyses using Cox-regression models were performed in order to identify independent prognostic factors of survival. A p-value of less than 0.05 was considered statistically significant and the analysis was performed using SPSS v 20 for Windows.

TABLE 1. Patients and tumor characteristics

	N (%)
Sex	
Male	28 (56)
Female	22 (44)
Mean age, years (range)	54 (28-73)
Diagnosis of peritoneal metastases (PM)	
Synchronous to primary tumour	22 (44)
Metachronous to primary tumour	28 (56)
Systemic chemotherapy	
No chemotherapy	4 (8)
Preoperative	28 (56)
Postoperative	35 (70)
Both	17 (34)
Peritoneal Cancer Index (PCI)	
Mean (range)	8.33 (1–35)
0–8	31 (62)
9–12	9 (18)
13–39	10 (20)
Complete cytoreduction (CC-0/1)	44 (88)
Prior surgery score (PSS)	
0	33 (66)
1	6 (12)
2	9 (18)
3	2 (4)
Median duration of hospital stay, days (range)	15 (6–114)
Clavien-Dindo III/IV	9 (18)

Results

Fifty patients (28 males, 22 females) with a mean age of 54 years (range 28–73 years) were included in the analysis. 22 (44%) patients had synchronous PM and 28 (56%) patients developed PM metachronous to their primary tumour. 46 (92%) patients received chemotherapy (preoperatively or postoperatively, or both). The mean intraoperative PCI score was 8.33 (range 1–35). Complete cytoreduction (CC-0/1) was achieved in 44 (88%) procedures. The median hospital stay was 15 days (range 6-114 days). Severe complications (Clavien-Dindo III/IV) were encountered in 18% of the cases whereas the 30-day mortality rate was 0%. Patient and tumour characteristics are listed in Table 1.

After a median follow-up of 34 months (range 7–114 months), 28 (56%) patients died of the disease. Median overall survival was 49 months. 1-year and 5-year overall survival rates were 96% and 54% (Figure 1). 33 (75%) of the 44 patients who had complete cytoreduction experienced recurrence. Median disease-free survival was 14

TABLE 2. Univariate analysis, parameters affecting overall survival

	P
Sex	Not significant (NS)
Age	NS
Diagnosis of peritoneal metastases (PM)	NS
Systemic chemotherapy	NS
Peritoneal Cancer Index (PCI) score	0.001
Completeness of cytoreduction	0.042
Prior surgery score (PSS) score	0.006

months. Disease-free survival rates at 1 year was 60% whereas the 5-year disease-free survival was 14.5%.

Univariate analysis showed that the PCI score, the completeness of cytoreduction (CC score) and PSS score were correlated significantly with overall survival (Table 2).

Kaplan–Meier curve analysis showed that, when the PCI was stratified in three groups (0–8, 9–2 and 13–39), there was a statistically significant difference in survival between the three groups (p = 0.014) (Figure 2, Table 3). Notably, all patients in the 0–8 group had complete cytoreduction (CC-0/1), whereas only 60% of the patients in the 13–39 PCI group were scored as CC-0/1. Statistical analysis showed a significant correlation between the PCI score and the completeness of cytoreduction (p = 0.002).

When entered in a multivariate regression model, the PCI score (p = 0.009) and the CC score (p = 0.031) were identified as independent prognostic factors of survival, adjusted for age, sex, pre/post-operative KT, time of diagnosis of PM (synchronous/metachronous) and PSS score (Table 4).

Discussion

In the past peritoneal metastasis have been considered as a terminal incurable disease. The introduction of CRS, which consists of removal of all macroscopic disease, with the addition of HIPEC in order to eradicate any residual tumour burden, has changed the management of these patients, with significant survival benefit.[20] In selected cases of patients with colorectal PM, a median survival of up to 63 months has been reported.[7,14,21,22,23] In the present study, we report a median overall survival

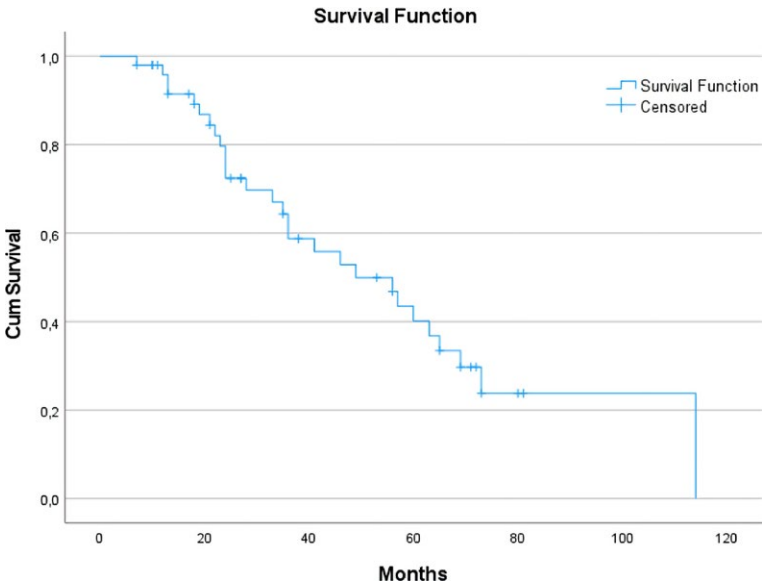

FIGURE 1. Kaplan-Meier curve: overall survival in our patient sample.

of 49 months, which is in line with OS previously reported in other studies, and supports the effectiveness of the technique.

While optimal cytoreduction is universally accepted for this treatment modality, there is still a debate about the value of HIPEC on top of CRS, largely due to the heterogeneity of drugs and pro-

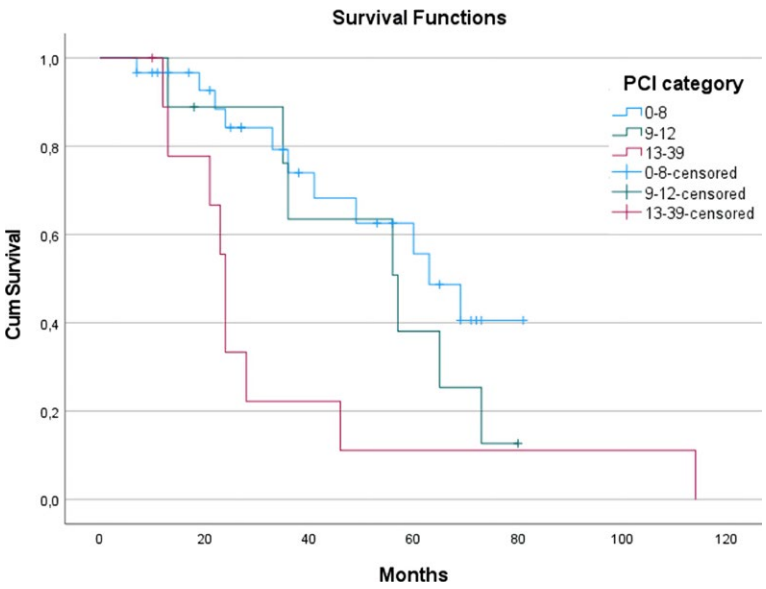

FIGURE 2. Kaplan-Meier curves: overall survival according to Peritoneal Cancer Index (PCI) score category.+

TABLE 3. Overall survival (OS) analysis according to Peritoneal Cancer Index (PCI) category

PCI score category	Number of patients	OS (median)	p
0–8	31	63	0.014
9–12	9	57	
13–39	10	24	

tocols used in HIPEC administration, plus lack of randomized trial data in the era of modern chemotherapy and targeted therapy.[24] Since a recent randomized trial showed addition of HIPEC to CRS offered survival advantage in stage III ovarian cancer[25] the negative finding of PRODIGE-7 trial was unexpected. One of the main criticisms of PRODIGE-7 trial was that the oxaliplatin based HIPEC was administered for only 30 min. In other protocols as well as in ours, HIPEC was administered for up to 120 min.[26] Other studies have shown that response to local oxaliplatin is related to duration of exposure.[27,28] Future studies of both the dose and duration of oxaliplatin-based HIPEC might produce different results. Other possible explanations for negative results of Prodige-7 trial include inappropriate choice of drug (oxaliplatin has uncertain efficacy when administered intraperitoneally) and problems in trial design (HIPEC was hypothesized to improve median OS by 18 months, on top of complete CRS; this overestimation of effect size might have obscured any potential subtle benefits of HIPEC).[29] More research efforts should be directed at identifying the optimal drug and protocol for HIPEC for colorectal PM and establishing criteria to select the subgroup that will benefit most from HIPEC.[24] Currently most Western guidelines recommend CRS plus HIPEC as a standard therapy for selected colorectal PM patients.[18,24]

TABLE 4. Multivariate analysis, independent prognostic factors of overall survival

	P
Sex	Not significant (NS)
Age	NS
Diagnosis of peritoneal metastases (PM)	NS
Systemic chemotherapy	NS
Peritoneal Cancer Index (PCI) score	0.009
Completeness of cytoreduction	0.031
Prior surgery score (PSS) score	NS

During the last decade, a lot of studies have investigated prognostic factors of outcome in patients undergoing CRS and HIPEC, in order to optimize selection of patients who will benefit more from this aggressive surgical approach.

Completeness of cytoreduction (CC-0/1) has been shown to be the most important prognostic factor, as 5-year survival in patients undergoing complete cytoreduction has been reported to be higher compared to that of patients undergoing incomplete resections.[22] In our study, patients with CC score of 0 or 1 enjoyed significantly better OS. Therefore, if incomplete cytoreduction is likely, CRS plus HIPEC should not be carried out.

The extent of peritoneal disease based on tumour sizes and their distribution along 13 regions within the peritoneal cavity (PCI score) remains another significant prognostic factor. However, the specific cut-off point associated with poor prognosis has yet to be defined, with the limit currently being between 10 and 20.[18,30] Sugarbaker *et al.* initially reported significantly higher survival (41 months) in patients with a PCI score less than 20, compared to 16 months for patients with a PCI score greater than 20.[31] Yan and Morris later showed that a PCI score ≤ 10 was a significant favourable prognostic factor.[32] In the present study, our analysis confirms that the PCI score remains a significant prognostic indicator of survival. There was a significant difference in the survival of patients according to the peritoneal tumour burden (PCI scores 0–8, 9–12 and 13–39), and PCI score of 13 or more was associated more frequently with incomplete resection.

High morbidity and mortality reported in some studies have discouraged many surgeons and oncologists from referring suitable patients for CRS plus HIPEC. With technological advances, these rates have improved to 22–34% and 0–4.1% in recent large series.[14,33] An analysis of the US national surgical database showed CRS plus HIPEC was a safer procedure than Whipple operation and esophagectomy.[34] Our results were similar, with a grade III or above complication rate of 18% and zero 30-day mortality.

Our study shows that CRS plus HIPEC offers survival benefit to patients with colorectal PM with small to moderate volume PM, with reasonable morbidity and mortality. Appropriate patient selection is the key to achieving good outcome, and complete cytoreduction is an important prognostic factor.

Acknowledgments

The authors acknowledge the financial support from the Slovenian Research and Innovation Agency (program No. P3-0289).

References

1. Siegel R, DeSantis C, Jemal A. Colorectal cancer statistics, 2014. *CA Cancer J Clin* 2014; **64:** 104-17. doi: 10.3322/caac.21220
2. Lemmens VE, Klaver YL, Verwaal VJ, Rutten HJ, Coebergh JW, de Hingh IH. Predictors and survival of synchronous peritoneal carcinomatosis of colorectal origin: a population-based study. *Int J Cancer* 2011; **128:** 2717-25. doi: 10.1002/ijc.25596
3. van Gestel YRBM, de Hingh IHJT, van Herk-Sukel MPP, van Erning FN, Beerepoot LV, Wijsman JH, et al. Patterns of metachronous metastases after curative treatment of colorectal cancer. *Cancer Epidemiol* 2014; **38:** 448-54. doi: 10.1016/j.canep.2014.04.004
4. Hashiguchi Y, Muro K, Saito Y, Ito Y, Ajioka Y, Hamaguchi T, et al. Japanese Society for Cancer of the Colon and Rectum (JSCCR) guidelines 2019 for the treatment of colorectal cancer. *Int J Clin Oncol* 2020; **25:** 1-42. doi: 10.1007/s10147-019-01485-z
5. Franko J, Shi Q, Goldman CD, Pockaj BA, Nelson GD, Goldberg RM, et al. Treatment of colorectal peritoneal carcinomatosis with systemic chemotherapy: a pooled analysis of phase III trials N9741 and N9841. *J Clin Oncol* 2012; **30:** 263-7. doi: 10.1200/JCO.2011.37.1039
6. Franko J, Shi Q, Meyers JP, Maughan TS, Adams RA, Seymour MT, et al. Prognosis of patients with peritoneal metastatic colorectal cancer given systemic therapy: analysis from the ARCAD database. *Lancet Oncol* 2016; **17:** 1709-19. doi: 10.1016/S1470-2045(16)30500-9
7. Elias D, Lefevre JH, Chevalier J, Brouquet A, Marchal F, Classe JM, et al. Complete cytoreductive surgery plus intraperitoneal chemohyperthermia with oxaliplatin for colorectal peritoneal carcinomatosis. *J Clin Oncol* 2009; **27:** 681-5. doi: 10.1200/JCO.2008.19.7160
8. Verwaal VJ, van Ruth S, de Bree E, van Sloothen GW, van Tinteren H, Boot H, et al. Randomized trial of cytoreduction and hyperthermic intraperitoneal chemotherapy versus systemic chemotherapy in colorectal carcinomatosis. *J Clin Oncol* 2003; **21:** 3737-43. doi: 10.1200/JCO.2003.04.187
9. Sugarbaker PH, Gianola FJ, Speyer JC, Wesley R, Barofsky I, Meyers CE. Intravenous versus intraperitoneal 5-fluorouracil in advanced colorectal cancer. *Surgery* 1985; **98:** 414-22. PMID: 3898450
10. Sugarbaker PH. Prevention and treatment of peritoneal metastases: a comprehensive review. *Indian J Surg Oncol* 2019; **10:** 3-23. doi: 10.1007/s13193-018-0831-6
11. Koga S, Hamazoe R, Maeta M, Shimizu N, Kanayama H, Osaki Y. Continuous hyperthermic peritoneal perfusion in rats with intraperitoneal cancer. *Cancer Res* 1984; **44:** 1840-2. PMID: 6424932
12. Elias D, Detroz B, Debaene B, Damia E, Leclercq B, Rougier R, et al. Treatment of peritoneal carcinomatosis by intraperitoneal chemo-hyperthermia: reliable and unreliable concepts. *Hepatogastroenterology* 1994; **41:** 207-13. PMID: 7959539
13. Quenet F, Goéré D, Mehta SS, Roca L, Dumont F, Hessissen M, et al. Intraperitoneal oxaliplatin with or without irinotecan during HIPEC after CRS for colorectal carcinomatosis. *Ann Surg* 2011; **254:** 294-301. doi: 10.1097/SLA.0b013e3182263933
14. Sarmiento Bonilla CI, Maldonado J, Paredes Haro HD, González Mercado ZEDA, Dunay Silva AAA, Duran SPX, et al. Evaluation of the impact of cytoreductive surgery and hyperthermic intraperitoneal chemotherapy (HIPEC) on long-term survival and morbidity profile: a systematic review. *Cureus* 2026; **18:** e106020. doi: 10.7759/cureus.106020
15. Goéré D, Malka D, Tzanis D, Gava V, Boige V, Eveno C, et al. Curative potential after complete CRS and intraperitoneal chemotherapy for colorectal carcinomatosis. *Ann Surg* 2013; **257:** 1065-71. doi: 10.1097/SLA.0b013e31827b8a3e
16. Chua TC, Yan TD, Saxena A, Morris DL. Cytoreductive surgery and HIPEC: morbidity and mortality. *Ann Surg* 2009; **249:** 900-7. doi: 10.1097/SLA.0b013e3181a45d86
17. Quénet F, Elias D, Roca L, Goéré D, Ghouti L, Pocard M, et al. Cytoreductive surgery plus HIPEC versus CRS alone for colorectal peritoneal metastases (PRODIGE 7). *Lancet Oncol* 2021; **22:** 256-66. doi: 10.1016/S1470-2045(20)30599-4
18. Van Cutsem E, Cervantes A, Adam R, Sobrero A, Van Krieken JH, Aderka D, et al. ESMO consensus guidelines for the management of patients with metastatic colorectal cancer. *Ann Oncol* 2016; **27:** 1386-422. doi: 10.1093/annonc/mdw235
19. Dindo D, Demartines N, Clavien PA. Classification of surgical complications. *Ann Surg* 2004; **240:** 205-13. doi: 10.1097/01.sla.0000133083.54934.ae
20. Spiliotis J, Kalles V, Kyriazanos I, Terra A, Prodromidou A, Raptis A, et al. CRS and HIPEC in colorectal peritoneal metastases. *Pleura Peritoneum* 2019; **4:** 20190018. doi: 10.1515/pp-2019-0018
21. Glehen O, Cotte E, Schreiber V, Sayag-Beaujard AC, Vignal J, Gilly FN. Intraperitoneal chemohyperthermia and cytoreductive surgery for colorectal peritoneal carcinomatosis. *Br J Surg* 2004; **91:** 747-54. doi: 10.1002/bjs.4474
22. Glehen O, Kwiatkowski F, Sugarbaker PH, Elias D, Levine EA, De Simone M, et al. Cytoreductive surgery combined with perioperative intraperitoneal chemotherapy for the management of peritoneal carcinomatosis from colorectal cancer. *J Clin Oncol* 2004; **22:** 3284-92. doi: 10.1200/JCO.2004.10.012
23. Shen P, Hawksworth J, Lovato J, Loggie BW, Geisinger KR, Fleming RA, et al. Cytoreductive surgery and intraperitoneal hyperthermic chemotherapy with mitomycin C for peritoneal carcinomatosis from colorectal cancer. *Ann Surg Oncol* 2004; **11:** 178-86. doi: 10.1245/ASO.2004.03.012
24. Chow FC, Yip J, Foo DC, Wei R, Choi HK, Ng KK, et al. Cytoreductive surgery and HIPEC for colorectal and appendiceal peritoneal metastases. *Asian J Surg* 2021; **44:** 221-8. doi: 10.1016/j.asjsur.2020.05.021
25. van Driel WJ, Koole SN, Sikorska K, Schagen van Leeuwen JH, Schreuder HW, Hermans RH, et al. Hyperthermic intraperitoneal chemotherapy in ovarian cancer. *N Engl J Med* 2018; **378:** 230-40. doi: 10.1056/NEJMoa1708618
26. Levine EA, Stewart JH, Shen P, Russell GB, Loggie BL, Votanopoulos KI. Intraperitoneal chemotherapy: experience with 1,000 patients. *J Am Coll Surg* 2014; **218:** 573-85. doi: 10.1016/j.jamcollsurg.2013.12.037
27. Kirstein MN, Root SA, Moore MM, Wieman KM, Williams BW, Jacobson PA, et al. Exposure-response relationships for oxaliplatin. *Anticancer Drugs* 2008; **19:** 37-44. doi: 10.1097/CAD.0b013e3282f15acb
28. Lemoine L, Thijssen E, Carleer R, Geboers K, Sugarbaker P, van der Speeten K. COBOX trial: intraperitoneal chemotherapy dosing. *J Surg Oncol* 2019; **119:** 999-1010. doi: 10.1002/jso.25442
29. Ceelen W. HIPEC with oxaliplatin for colorectal metastasis. *Eur J Surg Oncol* 2019; **45:** 400-2. doi: 10.1016/j.ejso.2018.11.513
30. Jacquet P, Sugarbaker PH. Clinical research methodologies in peritoneal carcinomatosis. *Cancer Treat Res* 1996; **82:** 359-74. doi: 10.1007/978-1-4613-1247-5_23
31. Simkens GA, Rovers KP, Nienhuijs SW, de Hingh IH. Patient selection for CRS and HIPEC. *Cancer Manag Res* 2017; **9:** 259-66. doi: 10.2147/CMAR.S119569
32. Cao C, Yan TD, Black D, Morris DL. A systematic review and meta-analysis of cytoreductive surgery with perioperative intraperitoneal chemotherapy for peritoneal carcinomatosis of colorectal origin. *Ann Surg Oncol* 2009; **16:** 2152-65. doi: 10.1245/s10434-009-0487-4
33. Newton AD, Bartlett EK, Karakousis GC. Cytoreductive surgery and hyperthermic intraperitoneal chemotherapy: a review of factors contributing to morbidity and mortality. *J Gastrointest Oncol* 2016; **7:** 99-111. doi: 10.3978/j.issn.2078-6891.2015.114
34. Foster JM, Sleightholm R, Patel A, Shostrom V, Hall B, Neilsen B, et al. Morbidity and mortality after cytoreductive surgery and hyperthermic intraperitoneal chemotherapy. *JAMA Netw Open* 2019; **2:** e187346. doi: 10.1001/jamanetworkopen.2018.7346

RADIOLOGY AND ONCOLOGY Radiology and Oncology | Ljubljana | Slovenia | www.radioloncol.com

research article

Does age have an impact on surgical and oncologic outcomes after curative resection for gastric cancer: a ten-year single-centre retrospective study

Matjaz Horvat, Stojan Potrc, Nuhi Arslani

Clinical Department of Abdominal and General Surgery, University Medical Centre Maribor, Maribor, Slovenia

Radiol Oncol 2026; 60(3): 442-449.

Received 22 January 2026
Accepted 30 April 2026

Correspondence to: Matjaž Horvat, M.D., Ph.D., Clinical Department of Abdominal and General Surgery, University Medical Centre Maribor, Ljubljanska ulica 5, 2000 Maribor, Slovenija. E-mail: matjaz.horvat@ukc-mb.si

Disclosure: No potential conflicts of interest were disclosed.

Background. Gastric cancer remains a major health burden in Slovenia, particularly among elderly patients. With increasing life expectancy, a growing number of patients aged ≥ 70 years are expected to undergo curative surgery. This study compared clinical, surgical, and oncologic outcomes between elderly (≥ 70 years) and younger (< 70 years) patients with gastric cancer.

Patients and methods. A single-center retrospective cohort study included patients who underwent curative-intent surgery for gastric adenocarcinoma between 2015 and 2024. Patients were stratified by age. Demographic data, comorbidities, tumor characteristics, surgical variables, postoperative complications (Clavien-Dindo classification), and overall survival (OS) were analyzed. Survival was assessed using the Kaplan-Meier method, and prognostic factors were evaluated using Cox proportional hazards regression.

Results. A total of 433 patients were included (229 < 70 years; 204 ≥ 70 years). Elderly patients had higher American Society of Anesthesiologists (ASA) scores and a higher incidence of major postoperative complications. R0 resection rates and surgical radicality were comparable between groups; however, elderly patients more frequently underwent subtotal gastrectomy and less extensive lymphadenectomy. Perioperative chemotherapy was more commonly administered in younger patients. Tumour characteristics and TNM stage distribution were similar between groups. Five-year OS was significantly lower in elderly patients (37.3% vs. 59.6%, $p < 0.001$).

Conclusions. Curative gastric cancer surgery should not be denied based solely on chronological age. Carefully selected elderly patients can achieve acceptable surgical and oncologic outcomes, highlighting the importance of biological age and functional status in treatment decision-making.

Key words: gastric cancer; elderly patients; curative gastrectomy; age-related outcomes

Introduction

Despite a declining incidence of gastric cancer in Slovenia over the past 60 years, its prevalence remains relatively high, with incidence rates of approximately 26.8 per 100,000 in men and 16.4 per 100,000 in women.[1,2] Approximately 60% of cases occur in individuals older than 65 years, more frequently in men than in women.[2] The overall 5-year survival rate for gastric cancer patients in Slovenia is around 28% and has shown little improvement in recent years, largely due to late-stage diagnosis.[3] According to the Statistical Office of the Republic of Slovenia, life expectancy at birth is approximately 77.7 years for men and 83.8 years for women and continues to increase.[4] Taken together, these data

suggest that the number of elderly patients with gastric cancer will rise in the future.

The European Society for Medical Oncology (ESMO) has developed several resources and guidelines to improve cancer care in elderly patients, including an accepted chronological age cut-off for defining "elderly" patients. Although biological aging is more relevant than chronological age in determining individual health status, chronological age remains a practical and widely used criterion in clinical practice. Currently, 70 years is the most commonly used cut-off in geriatric oncology.[5] Elderly patients often present with multiple comorbidities that significantly affect treatment strategies, outcomes, and quality of life.[6] In gastric cancer, delayed diagnosis, comorbidities, and atypical symptom presentation frequently result in more advanced disease at diagnosis in older patients.[7]

Although surgical resection remains the primary curative treatment, elderly patients face increased risks of postoperative complications and mortality.[7] Furthermore, chemotherapy and targeted therapies require careful consideration due to age-related declines in organ function and a higher risk of treatment-related toxicity.[8] Nevertheless, several studies have demonstrated that carefully selected, fit elderly patients can benefit from standard treatment approaches, including surgery and systemic therapy, when individualized treatment planning is applied.[8]

The aim of this study was to evaluate differences in clinical, surgical, and oncologic outcomes between elderly (≥ 70 years) and younger patients undergoing curative gastric cancer surgery and to contribute to the existing literature, which has reported inconsistent and sometimes contradictory findings.[9,10]

Patients and methods

This single-institution retrospective cohort study was conducted at the Clinical Department of Abdominal and General Surgery, University Clinical Centre Maribor, Slovenia, between January 2015 and December 2024. Patients who underwent curative-intent surgery for gastric adenocarcinoma were included. Patients were stratified into two groups according to age (< 70 years *vs.* ≥ 70 years), in line with the criteria proposed by the European Society of Medical Oncology.[5]

Demographic data, clinical findings, histopathological parameters, and clinical outcomes were retrospectively reviewed using a prospectively maintained database. Tumour topography and morphology were coded according to the International Classification of Diseases for Oncology, third edition.[11] Tumour staging was based on different editions of the Union for International Cancer Control (UICC) TNM classification, with all records subsequently harmonized to the fifth N classification.[12] Physical status was assessed using the American Society of Anesthesiologists (ASA) classification.[13] Postoperative complications were graded according to the Clavien-Dindo classification, with complications of grade III or higher included in the analysis.[14]

After surgery, patients were followed every three months during the first two years and every six months thereafter for up to five years. Follow-up evaluations included physical examination, laboratory tests, ultrasound, and, when indicated, CT, MRI, or endoscopy. Overall survival (OS) was calculated from the date of surgical resection to the date of death, using data from institution-al records and the Cancer Registry of the Republic of Slovenia.

The primary outcome was overall survival according to age group. Secondary outcomes included comparisons of surgical and pathological results and postoperative morbidity between the two groups. Statistical analysis was performed using SPSS version 30 (SPSS Inc., IBM, Chicago, USA). Categorical variables were compared using Fisher's exact test or the χ^2 test. Continuous variables were analyzed using Student's t-test or the Mann–Whitney U test, as appropriate. Independent prognostic factors were identified using Cox proportional hazards regression. Survival curves were estimated using the Kaplan–Meier method and compared with the log-rank test. The study was approved by the Ethics Committee (No: UKC-MB-KME 36/25).

Results

Between 2015 and 2024, a total of 433 patients underwent potentially curative gastric cancer resection at the University Clinical Centre Maribor. Of these, 229 patients were younger than 70 years and 204 were aged 70 years or older. Baseline demographic characteristics and preoperative clinicopathological features are summarized in Table 1. A significantly higher proportion of women was observed in the elderly group. Elderly patients also had significantly more comorbidities, as reflected

TABLE 1. Clinicopathological characteristics of the younger and elderly group

		Young (< 70years) N = 229	Elderly (≥ 70 years) N = 204	P - value
		N (%)	N (%)	
Sex	Male	169 (73.8)	130 (63.7)	
	Female	60 (26.2)	74 (36.3)	**0.024**
ASA	ASA 1, ASA2	203 (88.6)	127 (62.3)	
	ASA 3, ASA 4	26 (11.4)	77 (37.7)	**< 0.001**
Tumor site	Distal third	81 (35.4)	81 (39.7)	
	Middle third	85 (37.1)	87 (42,6)	
	Upper third	62 (27.1)	34 (16.79	
	Whole stomach	1(0.4)	2 (1)	0.069
Lauren	Intestinal	94 (48.2)	105 (61.4)	
	Diffuse	39 (20.0)	23 (13.5)	
	Mixed	60 (30.8)	42 (24.6)	0.052
	Missing data	36 (15.7)	34 (16.6)	
Tumor grading	0	1 (0.6)	0 (0.0)	
	1	19(11.0)	26 15.0)	
	2	52 (30.1)	59 (30.1)	
	3	100 (57.8	84 (48.6)	0.221
	Missing data	58 (25.3)	35 (17.1)	
Tumor diameter	mean	46.3 mm (SD 29.9)	53.2 mm(SD 32.1)	0.418

ASA = American Society of Anesthesiologists physical status classifications system; SD = standard deviation

by higher ASA scores, which were grouped as < 3 and ≥ 3 for analytical purposes.

No significant differences were observed between the groups regarding tumour location.

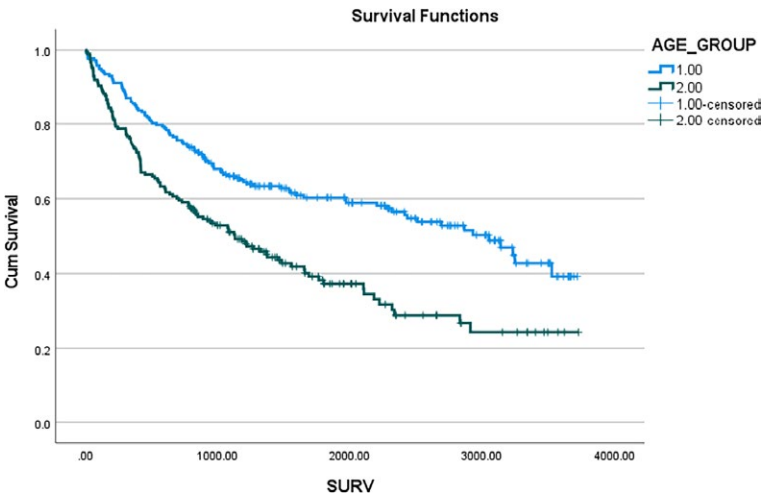

FIGURE 1. Overall survival (OS) between the younger and elderly group of patients. 1.00 represents patients < 70, 2.00 represents patients > 70.

According to the Lauren classification, the intestinal type was more common in elderly patients, although missing data were present in 15.7% of younger and 16.6% of elderly patients. Tumour grading did not differ significantly between groups. Tumour diameter was slightly larger in elderly patients (mean 53.2 mm *vs*. 46.3 mm), but this difference was not statistically significant.

Data on chemotherapy and radiotherapy are presented in Table 2. Significantly more younger patients were candidates for neoadjuvant treatment based on preoperative staging and performance status (135 *vs*. 58 patients). Consequently, all forms of neoadjuvant therapy were more frequently administered in the younger group. Adjuvant therapy was also more common in younger patients (76.9% *vs*. 55.4%), with a proportional distribution between chemotherapy and chemoradiotherapy in both groups.

Surgical procedures are detailed in Table 3. Elderly patients more frequently underwent subtotal gastrectomy, whereas total gastrectomy with distal esophagectomy was more common in younger patients. Splenectomy rates were similar, but lymphadenectomy was more extensive in younger patients (p = 0.028). R0 resection rates were high and comparable between groups (98.3% *vs*. 98.0%).

Postoperative complications were classified as Clavien-Dindo ≥ 3b or lower. Major complications were significantly more common in the elderly group. Conservative management was the most frequent approach in both groups. Interventional procedures were more common in younger patients, while reoperations were more frequent in elderly patients, although these differences were not statistically significant. Ninety-day postoperative mortality was higher in elderly patients but did not reach statistical significance.

Histopathological findings are summarized in Table 4. No significant differences were observed regarding lymphocyte infiltration, vascular invasion, tumour thrombus, extranodal infiltration, or perineural invasion. Some missing pathological data were noted. TNM stage distribution was similar between groups, with T3 being the most frequent stage. Nodal involvement did not differ significantly. Intraoperative metastases were detected in 4.4% of younger and 6.4% of elderly patients.

Overall survival data are presented in Figure 1. Five-year OS was significantly higher in younger patients (59.6%) than in elderly patients (37.3%; p < 0.001).

TABLE 2. Operation characteristics and postoperative outcome of the younger and elderly group

		Young (< 70years) N = 229	Elderly (≥ 70 years) N = 204	P - value
		N (%)	N (%)	
Type of resection	Subtotal	38 (16.6)	60 (29.4)	
	Total	132 (57.6)	108 (52.9)	
	Total + distal oesophagecgtomy	41 (17.9)	22 (10.8)	
	Proximal resection	14 (6.1)	10 (4.9)	
	Stump resection	2 (0.9)	3 (1.5)	
	Wedge resection	2 (0.9)	0 (0.0)	
	Stomach + Whipple	0 (0.0)	1 (0.5)	**0.012**
Splenectomy	No	187 (81.7)	175 (85.8)	
	Yes	42 (18.3)	29 (14.2)	0.247
Extent of lymphadenectomy	D 1	5 (2.2)	16 (7.8)	
	D 1.5	13 (5.7)	16 (7.8)	
	D 2	209 (91.3)	169 (82.8)	
	D 2.5	2 (0.9)	3 (1.5)	**0.028**
Residual tumour	R0	225 (98.3)	200 (98.0)	
	R1	2 (0.9)	3 (0.9)	
	R2	2 (0.9)	1 (0.5)	0.178
Clavien-Dindo complications classification	< 3b	206 (90.0)	171 (83.8)	
	³ 3b	23 (10)	33 (16.2)	**0.04**
Treatment of complications	None	176 (76.9)	144 (70.6)	
	Conservative	21 (9.2)	28 (13.7)	
	Interventions US guided, endoscopy	14 (6.1)	7 (3.4)	
	Surgery	18 (7.9)	25 (12.3)	0.1
Mortality (30 days)		5 (2.2)	2 (1.0)	0.275
Mortality (90 days)		10 (4.4)	17 (8.3)	0.088

Discussion

Age alone should not preclude patients from undergoing curative surgery. In this ten-year retrospective study of potentially curative gastric cancer resections, we compared surgical, pathological, and oncological outcomes between younger and elderly patients. The incidence of gastric cancer was higher in men across all age groups. Notably, the male-to-female ratio increased with advancing age, particularly after menopause, suggesting a potential protective role of oestrogen in premenopausal women.[15] In our cohort, women accounted for one quarter of cases in the younger group compared with one third in the elderly group (p = 0.024). This finding may also reflect the generally longer life expectancy of women.

Previous studies have demonstrated that higher ASA scores – particularly classes III and IV – are associated with increased postoperative complications and reduced overall survival in elderly gastric cancer patients. A retrospective study of 166 patients aged 80 years or older identified ASA class III–IV as an independent risk factor for postoperative mortality.[16] Similarly, Wakahara *et al*. reported a significantly higher incidence of postoperative cardiovascular complications among patients with ASA class III or IV, underscoring the predictive value of ASA for systemic postoperative risk. In our study, ASA class III–IV was significantly more

TABLE 3. Preoperative and postoperative chemotherapy between the groups of younger and elderly patients

		Young (< 70 years) N = 229	Elderly (≥ 70 years) N = 204	P - value
Neoadjuvant therapy	Candidate	135 (59.0)	58 (28.4)	
	Not a candidate	94 (41.0)	146 (71.6)	**< 0.001**
Type of neoadjuvant therapy	None	94 (41.0)	146 (71.6)	
	Chemo + RT	14 (2.9)	6 (4.6)	
	Chemo - FLOT	74 (32.3)	31 (15.2)	
	Chemo - EOX	47 (20.5)	21 (10.3)	**< 0.001**
Adjuvant therapy	Candidate	176 (76.9)	113 (55.4)	
	Not a candidate	53 (23.1)	91 (44.6)	**< 0.001**
Type of adjuvant therapy	None	83 (36.2)	138 (67.6)	
	Chemo	121 (52.8)	58 (28.4)	
	Chemo + RT	25 (10.9)	8 (3.9)	**< 0.001**

Chemo = chemotherapy; EOX = epirubicin + oxaliplatin + capecitabin; FLOT = 5-fluorouracil + leucovorin + oxaliplatin + docetaxel; RT = radiotherapy

frequent in the elderly group (37.7%) than in the younger group (11.4%). This difference was associated with a higher incidence of Clavien-Dindo grade ≥ 3b complications. However, no significant differences were observed in 30- or 90-day perioperative mortality, possibly due to the relatively younger age of our elderly cohort compared with those in previous studies.[17]

Tumour histology and biological behaviour vary with age. A large meta-analysis by Petrelli *et al*., including over 60,000 patients, demonstrated that the intestinal histological type is more prevalent in elderly patients and is generally associated with better differentiation and prognosis, whereas the diffuse type is more common in younger patients and is linked to poorer differentiation. Nevertheless, in elderly patients with early gastric cancer, cancer-specific survival does not appear to differ significantly between intestinal and diffuse types.[18] Yang *et al*. identified age, tumor location, differentiation, and tumour size as key predictors of overall survival in elderly patients.[19]

In our study, the middle third of the stomach was the most common tumour location in both groups. Tumour location in younger patients was relatively evenly distributed across all gastric thirds, whereas elderly patients showed a tendency toward distal tumour localization, although this difference was not statistically significant. Lauren classification in our cohort was consistent with published data, with the intestinal type accounting for approximately two thirds of cases in the elderly group. However, no significant differences were observed in tumour grading between groups. Although tumour size has been variably reported as a prognostic factor in the literature often losing significance in multivariate analyses unless lymph node evaluation is inadequate.[20-22] We found no statistically significant difference in tumour diameter, despite slightly larger tumours in the elderly group.

Surgical strategies also differed between age groups. Elderly patients more frequently underwent subtotal gastrectomy, whereas younger patients were more likely to receive total gastrectomy. In the CRITICS trial, subtotal gastrectomy was performed in 45% of patients aged ≥ 70 years compared with 39% of younger patients.[23] Similarly, in our cohort, subtotal gastrectomy was significantly more common in elderly patients (29.4% *vs*. 16.6%), despite no significant difference in tumor location. Total gastrectomy remained the most frequently performed procedure in both groups. Younger patients also underwent more extensive lymphadenectomy, with D2 dissection performed in over 90% of younger patients and over 80% of elderly patients. This difference likely reflects concerns regarding the higher risk of postoperative morbidity associated with extensive dissections in elderly patients.

Postoperative complication profiles differed between age groups when classified according to the Clavien-Dindo system. While several studies report that minor complications (grade < 3b) occur more frequently in elderly patients, the incidence of severe complications is generally comparable between age groups.[24-26] In our study, minor com-

TABLE 4. Histopathological findings between younger and elderly patients

		Young (< 70years) N = 229	Elderly (≥ 70 years) N = 204	P - value
		N (%)	N (%)	
Lymphocyte infiltration	None	68 (32.7)	60 (32.8)	
	Mild	74 (35.6)	71 (38.8)	
	Moderate	56 (26.9)	39 (21.3)	
	Severe	10 (4.8)	13 (7.1)	0.492
	Missing data	21 (9.1)	21 (10.2)	
Vascular invasion	None	173 (77.9)	138 (71.9)	
	Present	49 (22.1)	54 (28.1)	0.155
	Missing data	8 (3.4)	12 (5.8)	
Tumour thrombus	None	184 (94.8)	162 (91.0)	
	Present	10 (5.2)	16 (9.0)	0.160
	Missing data	35 (15.2)	26 (12.7)	
Extranodular infiltration	None	185 (93.4)	159 (87.8)	
	Present	13 (6.6)	22 (12.2)	0.060
	Missing data	31 8 (13.5)	23 (11.27)	
Perineura invasion	None	112 (49.8)	86 (43.4)	
	Present	113 (50.2)	111 (56.1)	0.257
	Missing data	4 (1.7)	7 (3.43)	
T stage	T0	6 (2.6)	6 (2.9)	
	Tx	0 (0.0)	1 (0.6)	
	Tis	32 14.0)	13 (6.4)	
	T1a	11 (4.8)	10 (4.9)	
	T1b	10 (4.4)	12 (5.9)	
	T2	23 (10.0)	23 (11.3)	
	T3	91 (39.7)	75 (36.8)	
	T4a	44 (19.2)	55 (27.0)	
	T4b	12 (5.2)	9 (4.49	0.200
Nodes	N0	110 (48.0)	88 (43.1)	
	N1	33 (14.4)	26 (12.7)	
	N2	39 (17.0)	37 (18.1)	
	N3a	27 (11.8)	23 (11.3)	
	N3b	20 (8.7)	30 (14.7)	0.377
	Negative nodes	110(48.0)	88 (43.1)	
	Positive nodes	119 (52.0)	116 (56.9)	0.307
Metastases	None	219 (95.6)	191 (93.6)	
	Present	10 (4.4)	13 (6.4)	0.353

plications were similarly distributed (90% in the younger group *vs*. 83.3% in the elderly group). However, severe complications (grade ≥ 3b) were significantly more frequent among elderly patients (16.2% *vs*. 10%). Management strategies were comparable across groups, with conservative treatment being the most common approach. Perioperative mortality was higher in elderly patients, particularly at 90 days, although this difference did not reach statistical significance.

Significant differences were also observed in the use of systemic therapy. Younger patients were more frequently candidates for neoadjuvant chemotherapy or chemoradiotherapy than elderly patients (59.0% *vs*. 28.4%). Given the comparable tumor characteristics between groups, this discrepancy likely reflects differences in comorbidities, functional status, and treatment tolerance. FLOT was the most commonly used neoadjuvant regimen in both groups. Prior studies have shown increased toxicity and impaired quality of life in elderly patients receiving intensive chemo-therapy, emphasizing the importance of careful patient selection.[23,27] Regarding adjuvant therapy, younger patients were more likely to receive treatment (76.9% *vs*. 55.4%), although TNM staging did not differ significantly between groups. Evidence suggests that the survival benefit of adjuvant chemotherapy is most pronounced in stage III disease, and monotherapy may offer a favourable balance between efficacy and tolerability in elderly patients.[28]

Pathological features such as lymphocytic infiltration, vascular invasion, tumor thrombus, extranodal extension, and perineural invasion did not differ significantly between groups. Nonetheless, previous studies have reported higher rates of vascular and lymphovascular invasion in patients aged ≥ 60 years.[29] Perivascular invasion is associated with aggressive tumor behavior, poorer prognosis, and significant correlations with histological subtype.[30,31]

As expected, overall survival was shorter in the elderly group, in agreement with existing clearly published data. Puhr *et al*. demonstrated similar stage-specific survival distributions across age groups.[32-34] Given the comparable tumor characteristics in our study, the reduced overall survival in elderly patients may primarily reflect a higher burden of comorbidities and shorter life expectancy. Importantly, several authors have reported comparable overall survival between younger and elderly patients when curative resection is achieved, supporting the principle that age alone should not be a contraindication to curative surgery.[35]

This study is limited by its retrospective design, with inherent risks of selection bias and inability to infer causality. Reliance on medical records introduces potential inaccuracies due to incomplete or inconsistently documented data. Missing data for key clinical variables may have introduced information bias and reduced statistical power, particularly in subgroup analyses. Finally, the single-center nature of the study limits external validity, as institutional practices and patient characteristics may not be generalizable to other settings. Prospective, multi-center studies with standardized data collection are needed to confirm these findings.

Conclusions

This ten-year retrospective study confirms that chronological age alone should not be considered a contraindication to curative surgery for gastric cancer. Although elderly patients presented with higher ASA scores and experienced more severe postoperative complications, perioperative mortality and oncologic outcomes were comparable when curative resection was achieved. Tumor characteristics and stage distribution were similar across age groups, and standard oncologic principles were maintained in selected elderly patients. The reduced overall survival observed in elderly patients appears to be driven primarily by comorbidities and limited life expectancy rather than tumor-related factors. These findings support an individualized treatment approach based on biological age, functional status, and comorbidity burden rather than chronological age. As the population continues to age, multidisciplinary assessment and tailored treatment strategies will be increasingly important.

References

1. Zadnik V, Primic Zakelj M, Lokar K, Jarm K, Ivanus U, Zagar T. Cancer burden in Slovenia with time trend analysis. *Radiol Oncol* 2017; **51:** 47-55. doi: 10.1515/raon-2017-0008
2. Zadnik V, Žagar T. SLORA: *Cancer in Slovenia*. [Internet]. Ljubljana: The Cancer Registry of Slovenia, Institute of Oncology Ljubljana. Available at: https://www.slora.si/en/home_hidden
3. Zadnik V, Zagar T, Lokar K, Tomsic S, Duratovic Konjevic A, Zakotnik B. Trends in population-based cancer survival in Slovenia. *Radiol Oncol* 2021; **55:** 42-9. doi: 10.2478/raon-2021-0003
4. Statistical Office of the Republic of Slovenia. [Internet]. Available at https://www.stat.si/statweb/en
5. Aapro MS, Schrijvers D, editors. *ESMO handbook of cancer in the senior patient*. 1st edition. New York: Informa Healthcare; 2010.
6. Marengoni A, Angleman S, Melis R, Mangialasche F, Karp A, Garmen A, et al. Aging with multimorbidity: a systematic review of the literature. *Ageing Res Rev* 2011; **10:** 430-9. doi: 10.1016/j.arr.2011.03.003
7. Joharatnam-Hogan N, Shiu KK, Khan K. Challenges in the treatment of gastric cancer in the older patient. *Cancer Treat Rev* 2020; **85:** 101980. doi: 10.1016/j.ctrv.2020.101980.
8. Kim HS, Kim JH, Kim JW, Kim BC. Chemotherapy in elderly patients with gastric cancer. *J Cancer* 2016; **7:** 88-94. doi: 10.7150/jca.13248.
9. Zhang Q, Zhang M, Hu S, Meng L, Xi J, Xu A, et al. Prevalence and risk factors of preoperative frailty in Chinese elderly inpatients with gastric and colorectal cancer undergoing surgery. *Support Care Cancer* 2022; **30:** 677-86. doi: 10.1007/s00520-021-06483-4

10. Vermillion SA, Hsu FC, Dorrell RD, Shen P, Clark CJ. Modified frailty index predicts postoperative outcomes in older gastrointestinal cancer patients. *J Surg Oncol* 2017; **115:** 997-1003. doi: 10.1002/jso.24617

11. World Health Organization. International Classification of Diseases for Oncology (ICD-O). 3rd edition. Geneva: WHO; 2000.

12. Amin MB, Edge SB, Greene FL, Byrd DR, Brookland RK, Gershenwald JE, et al., editors. *AJCC Cancer Staging Manual*. 8th edition. New York: Springer; 2017.

13. American Society of Anesthesiologists. ASA physical status classification system. 2020. [Internet]. Available at: https://www.asahq.org/standards-and-guidelines/asa-physical-status-classification-system

14. Dindo D, Demartines N, Clavien PA. Classification of surgical complications: a new proposal evaluated in 6336 patients and survey results. *Ann Surg* 2004; **240:** 205-13. doi: 10.1097/01.sla.0000133083.54934.ae

15. McNaughton SA, Bates CJ, Mishra GD. Diet quality is associated with all-cause mortality in adults aged 65 years and older. *J Nutr* 2012; **142:** 320-325. doi: 10.3945/jn.111.148692

16. Endo S, Yamatsuji T, Fujiwara Y, Higashida M, Kubota H, Matsumoto H, et al. Prognostic factors for elderly gastric cancer patients who underwent gastrectomy. *World J Surg Oncol* 2022; **20:** 10. doi: 10.1186/s12957-021-02475-0

17. Wakahara T, Ueno N, Maeda T, Kanemitsu K, Yoshikawa T, Tsuchida S, et al. Impact of gastric cancer surgery in elderly patients. *Oncology* 2018; **94:** 79-84. doi: 10.1159/000481404

18. Petrelli F, Berenato R, Turati L, Mennitto A, Steccanella F, Caporale M, et al. Prognostic value of diffuse versus intestinal histotype in patients with gastric cancer: a systematic review and meta-analysis. *J Gastrointest Oncol* 2017; **8:** 148-163. doi: 10.21037/jgo.2017.01.10

19. Yang H, Ji X, Jin C, Ji K, Jia Z, Wu X, Ji K, Jia Z, Wu X, et al. A practical nomogram for predicting the prognosis of elderly patients with gastric adenocarcinoma after gastrectomy. *Int J Gen Med* 2022; **15**: 473-88. doi: 10.2147/IJGM.S343306

20. Kunisaki C, Makino H, Takagawa R, Oshima T, Nagano Y, Kosaka T, et al. Tumor diameter as a prognostic factor in patients with gastric cancer. *Ann Surg Oncol* 2008; **15:** 1959-67. doi: 10.1245/s10434-008-9884-3

21. Yokota T, Ishiyama S, Saito T, Teshima S, Yamada Y, Iwamoto K, et al. Is tumor size a prognostic indicator for gastric carcinoma? *Anticancer Res* 2002; **22**(6B): 3673-7. PMID: 12552975

22. Xiao J, Shen K, Fan H, Wang G, Liu K, Wang Y, et al. Prognostic value of tumor size in gastric cancer: a retrospective cohort study based on the SEER database. *Int J Surg Pathol* 2023; **31:** 1273-82. doi: 10.1177/10668969231152578

23. Slagter AE, e Tudela B, van Amelsfoort RM, Sikorska K, van Sandick JW, van de Velde CJH, et al. Older versus younger adults with gastric cancer receiving perioperative treatment: results from the CRITICS trial. *Eur J Cancer* 2020; **130**:146-54. doi: 10.1016/j.ejca.2020.02.008

24. Takeuchi D, Koide N, Suzuki A, Ishizone S, Shimizu F, Tsuchiya T, et al. Postoperative complications in elderly patients with gastric cancer. *J Surg Res* 2015; **198:** 317-26. doi: 10.1016/j.jss.2015.03.095

25. Lee KG, Lee HJ, Yang JY, Oh SY, Bard S, Suh YS, et al. Risk factors associated with complication following gastrectomy for gastric cancer. *J Gastrointest Surg* 2014; **18:** 1269-77. doi: 10.1007/s11605-014-2525-1

26. Shibata C, Ogawa H, Nakano T, Koyama K, Yamamoto K, Nagao M, et al. Influence of age on postoperative complications after gastrectomy for gastric cancer. *BMC Surg* 2019; **19:** 106. doi: 10.1186/s12893-019-0573-x

27. Pak LM, Wang J. The appropriate treatment for elderly gastric cancer patients. *Art Surg* 2017; **1:** 4. doi: 10.21037/aos.2017.11.02

28. Chan WL, Liu X, Wong CK, Wong MS, Wong IY, Lam KO, et al. Adjuvant chemotherapy in older patients with gastric cancer: a population-based cohort study. *Cancers (Basel)* 2023; **15:** 3768. doi: 10.3390/cancers15153768

29. Li P, He HQ, Zhu CM, Ling YH, Hu WM, Zhang XK, et al. Prognostic significance of lymphovascular invasion in resectable gastric cancer. *BMC Cancer* 2015; **15:** 370. doi: 10.1186/s12885-015-1370-2

30. Selçukbiricik F, Tural D, Büyükünal E, Serdengeçti S. Perineural invasion as an independent prognostic factor in gastric cancer. *Asian Pac J Cancer Prev* 2012; **13:** 3149-52. doi: 10.7314/APJCP.2012.13.7.3149

31. Taghavi A, Khorsand A, Saberafsharian M, Sahabi R, Beiraghdar M, et al. Gastric cancer: correlation of histologic type with prognostic variables. *Int J Cancer Manag* 2023; **16:** e134832. doi: 10.5812/ijcm-134832

32. Puhr HC, Karner A, Taghizadeh H, Jomrich G, Schoppmann SF, Preusser M, et al. Outcome of young versus older patients with upper gastrointestinal carcinoma. *J Cancer Res Clin Oncol* 2020; **146:** 3313-22. doi: 10.1007/s00432-020-03302-x

33. Schlesinger-Raab A, Mihaljevic AL, Egert S, Emeny R, Jauch KW, Kleeff J, et al. Outcome of gastric cancer in the elderly: a population-based evaluation. *Gastric Cancer* 2016; **19:** 713-22. doi: 10.1007/s10120-015-0527-7

34. Wu C, Chen M, Huang K, Chang SC, Fang WL, Lin CH, et al. Clinicopathological characteristics and genetic alterations in younger versus older gastric cancer patients. *Aging (Albany NY)* 2020; **12:** 18137-50. doi: 10.18632/aging.103627

35. Kim HG, Lee JH, Kim DY. Prognosis of elderly patients with advanced gastric cancer without serosal invasion. *J Cancer Allied Spec* 2022; **8:** 467. doi: 10.37029/jcas.v8i2.467

RADIOLOGY AND ONCOLOGY Radiology and Oncology | Ljubljana | Slovenia | www.radioloncol.com

research article

Real-world data survival outcomes of first line immunotherapy with pembrolizumab in high expressers with stage IV non-small cell lung cancer

Vladimir Stojsic[1,2], Bojan Zaric[1,2], Petar Simurdic[1,2], Tomi Kovacevic[1,2], Darijo Bokan[1,2], Jelena Djekic Malbasa[1,2], Tatjana Sarcev[1,2], Goran Stojanovic[2,3], Daliborka Bursac[1,2], Borislava Nikolin[1,4]

[1] Faculty of Medicine, University of Novi Sad, Novi Sad, Serbia

[2] Clinic for Thoracic Oncology, Institute for Pulmonary Diseases of Vojvodina, Sremska Kamenica, Serbia

[3] Faculty of Pharmacy, University Business Academy in Novi Sad, Novi Sad, Serbia

[4] Oncology Institute of Vojvodina, Sremska Kamenica, Serbia

Radiol Oncol 2026; 60(3): 450-458.

Received 23 March 2026
Accepted 22 May 2026

Correspondence to: Prof. Bojan Zaric, M.D., Ph.D., Faculty of Medicine University of Novi Sad and Institute for Pulmonary Diseases of Vojvodina Sremska Kamenica, Serbia. E-mail: bojan.zaric@mf.uns.ac.rs

Disclosure: No potential conflicts of interest were disclosed.

Background. Pembrolizumab monotherapy is standard of care in first line treatment of patients with stage IV lung cancer and programmed death ligand 1 (PD-L1) expression ≥ 50%. Whether the higher levels of PD-L1 expression predict higher benefit from the treatment with pembrolizumab is still debatable.

Patients and methods. This trial analyzed clinical and pathological characteristics, overall response rate (ORR), and survival outcomes in patients with non-small cell lung cancer (NSCLC) and PD-L1 expression of ≥ 50% who received front line treatment with pembrolizumab in real-world setting. The aim was to evaluate does the level of expression influence survival endpoints.

Results. Fifty-one consecutive patients were evaluated in this study. The median PFS for patients in this study was 12.0 months (95% CI, 7.7–16.2 months), and the median OS was 21.0 months (95% CI, 9.6–32.3 months). Based on PD-L1 status patients were divided into two groups. First one with PD-L1 expression of 50%–79%, and the second with expression over 80%. Gender distribution between the two groups ($p = 0.029$) and difference in stage of the disease ($p = 0.039$) were statistically significant. There was no significant difference in progression free survival ($p = 0.548$) and overall survival ($p = 0.153$) between two groups.

Conclusions. This trial did not confirm relation between higher expression of PD-L1 and better survival outcomes. However, the pitfall of the trial was relatively small number of patients, so with the expansion of this real-world data (RWD) dataset future results might differ.

Key words: lung cancer; NSCLC; PD-L1; immunotherapy; pembrolizumab

Introduction

Lung cancer remains among deadliest cancers in both genders worldwide. It is the second most frequently diagnosed cancer and the leading cause of cancer-related deaths in 2022. One in ten newly diagnosed cancers worldwide is lung cancer, and one in five cancer related deaths are due to

lung cancer.[1,2] The incidence and mortality from lung cancer is twice as high in men compared to women. Male-to-female ratio, however, varies on geographic location. Five-year survival of patients with lung cancer still lingers from 10–20% globally.[2] Serbia ranks second in the world considering morbidity and mortality of lung cancer.[3] Based on the latest official data from Serbia (published in 2019), in terms of morbidity and mortality, lung cancer is first among males, while it holds second place for females, after breast cancer. According to this data, the largest number of affected individuals are aged between 65 and 69 years.

In more than 75% of patients, at the time of diagnosis, the disease is in advanced or metastatic stage. Moreover, the prognosis of lung cancer is strongly correlated with the stage of the disease, so the 5-year survival for metastatic stage (stage IV) is less than 5%.[4]

Advances in molecular biology and immunology of tumors, led to better understanding of underlying tumor growth and spread mechanisms, enabling new therapeutic options to improve survival outcomes. The turning point for development of active immunotherapies in lung cancer was understating of programmed death receptor 1 (PD-1) on T cells, and programmed death ligands 1 and 2 (PD-L1, and PD-L2) on tumors cells. That research created new class of drugs – immune check point inhibitors (ICIs).[5-9]

One of the pivotal drugs for lung cancer treatment, pembrolizumab, was initially tested in a large multicohort phase I study (KEYNOTE-001), followed by phase 2/3 study KEYNOTE-010.[10,11] Both trials defined PD-L1 expression on tumors cells as an important predictor of response to therapy. Tumors with high PD-L1 expression (defined as ≥ 50% of tumor cells with membranous expression) were more likely to respond better to pembrolizumab.[9]

Although the cut off level for low PD-L1 expression (1%–49%) and high PD-L1 expression (50%–100%) is arbitrarily created, PD-L1 represents a continuous biomarker (with a range of 0% to 100%) and has been shown through studies to correlate with the effectiveness of immunotherapy.[10-13] Theoretically, the higher the level of PD-L1 expression, the better the response to immunotherapy. There is still not enough clear and consistent data to confirm that patients with the highest level of PD-L1 expression would really have better survival outcomes on checkpoint inhibitor therapy. In clinical practice, the selection of patients with non-small cell lung cancer for immunotherapy is performed in relation to the level of PD-L1 expression. The expression of PD-L1 on the tumor cells, determined immunohistochemically (IHC), is currently the only diagnostic test approved by the Food and Drug Administration (FDA) and European Medicines Agency (EMA) for the selection of patients with non-small cell lung cancer (NSCLC) in relation to type of immunotherapy. Most investigators and physicians are aware of the imprecise connection between PD-L1 expression and survival outcomes in NSCLC, waging the benefit of treatment in relation to other, clinical and pathological prognostic factors.[14]

The effectiveness of pembrolizumab as monotherapy of metastatic NSCLC and a PD-L1 expression ≥ 50%, still needs to be additionally evaluated outside of the clinical trial setting, in real-world clinical practice - delivering real-world data for further analysis.

The primary aim of current study was to determine the duration of progression-free survival (PFS) and the duration of overall survival (OS) in patients with PD-L1 expression ≥ 50% treated with pembrolizumab immunotherapy in the first line of treatment. The trial also aimed to investigate whether there is a significant difference in clinical-pathological characteristics, progression-free survival time, and overall survival between patients with PD-L1 expression of 50%–79%and patients with PD-L1 expression of 80%–100%.

Major limitation of the trial is a smaller sample; however, it is a potential cornerstone for comparison between other smaller real-world data (RWD) datasets. While datasets expand further, evaluations might define the size of the datasets necessary for compiling real-world evidence.

Patients and methods

This retrospective study included data from 51 consecutive patients who were diagnosed with metastatic NSCLC and who started treatment in Institute for pulmonary diseases of Vojvodina in period between 1st January 2019 and 31th December 2021. Patient data were collected from the institutional lung cancer registry and available electronic medical records. Patients eligible for participation in the study were those diagnosed with metastatic-stage non-small cell lung cancer without Epidermal Growth Factor Receptor (EGFR) gene mutations and Anaplastic Lymphoma Kinase (ALK) rearrangements, with PD-L1 expression ≥ 50%, and who had received at least one cycle of

pembrolizumab monotherapy in the first line of treatment.

The study was conducted in accordance with the Declaration of Helsinki and approved by the Review and Ethics Committee of the Institute for Pulmonary Diseases of Vojvodina, Sremska Kamenica, Serbia (approval number: No 521/4 and 19-II/4 - 01.03.2023).

Clinical data were collected from the included participants, such as gender, age, smoking status, body mass index, Eastern Cooperative Oncology Group (ECOG) performance status, tumor histology, TNM disease stage, PD-L1 expression levels, duration of pembrolizumab treatment, and number of administered cycles. The radiological response to therapy was determined by experienced thoracic radiologists, by immune Response Evaluation Criteria In Solid Tumors (iRECIST) criteria version 1.1. TNM staging was done using the eighth edition TNM stage classification for lung cancer.

Progression-free survival (PFS) was defined as the time from the start of pembrolizumab treatment until the date of disease progression or death, whichever occurred first. Overall survival (OS) was defined as the time from the start of pembrolizumab treatment until death. Patients who were alive at the time of statistical analysis were censored at the date of their last contact.

PD-L1 expression was determined immunohistochemically (IHC) following institutional clinical practice and expressed as the percentage of tumor cells showing positive membrane staining. IHC assay used for analysis was Dako PD-L1 22C3 antibody. PD-L1 expression values were also collected from institutional electronic data capture system.

The data analysis included methods of descriptive and inferential statistics. Numerical attributes were presented using average values (arithmetic mean, median) and measures of variability (range, standard deviation), while categorical attributes were represented using frequencies and percentages. Univariate analysis involved $\chi 2$ tests for categorical attributes and Student's t-tests and one-way analysis of variance (ANOVA) for numerical attributes. Multivariate analysis included Cox regression and logistic regression analysis. The relationship between variables was determined using correlation analysis. The significance level of $p < 0.05$ was considered statistically significant. Event-time variables (PFS and OS) were calculated using the Kaplan-Meier method. IBM SPSS Statistics 21 software package was used for statistical data processing.

TABLE 1. Clinical characteristics of patients with NSCLC

Characteristics	Frequencies N/(%)
Gender	
Male	31 (60.2%)
Female	20 (39.8%)
Age (years)	
Average	66.8
Range	50–84
Smoking status	
Non-smokers	3 (5.9%)
Active smokers	39 (76.5%)
Former smokers	9 (17.6%)
Pack-year index	
Average	48.5
Range	0–150
Body mass index (BMI)	
Average	25.4
< 18.5	3 (5.9%)
18.5–24.9	22 (43.1%)
25.0–29.9	23 (45.1%)
30.0–34.9	1 (2.0%)
> 40.0	2 (3.9%)
ECOG performance status	
0	1 (2.0%)
1	50 (98.0%)

ECOG = Eastern Cooperative Oncology Group; NSCLC = non-small cell lung cancer

Results

This study included clinical data from patients with metastatic non-small cell lung cancer whose tumors have PD-L1 receptor expression of ≥ 50% and who received pembrolizumab as first-line treatment. Among the total of 51 patients, 31 (60.8%) were male, and 20 (39.2%) were female. The average age of the patients was 66.8 years (range 50–84 years). Most patients were smokers, accounting for 39 (76.5%). The median value of the pack-year index was 38.2 (packs per year). Regarding Body Mass Index (BMI), the average value was 25.4. Most patients fell into the normal weight group, 22 (43.1%), and the overweight group, 23 (45.1%). Almost all patients in our study had an

ECOG PS 1, 50 patients (98.0%). Clinical characteristics are given in Table 1.

Twenty-nine patients (56.9%) had tumors with non-squamous histology, all of which were classified as adenocarcinomas. Squamous cell carcinoma was confirmed in 22 patients (43.1%). In terms of TNM and disease staging, 36 patients (70.6%) were in stage IVA, while 15 patients (29.4%) were in stage IVB. The distribution of stages and histological classification is given in Table 2.

The largest number of patients had PD-L1 expression levels between 90%–100% The distribution of PD-L1 expression level is given in Table 3. Across the entire cohort, the median PD-L1 expression was 80% (range: 50–100%), and the average PD-L1 expression value was 76.5%.

All patients received the standard dose of 200 mg of pembrolizumab every three weeks until disease progression or the occurrence of unacceptable toxicity. The average duration of pembrolizumab treatment was 18.3 months (range: 2–60 months). The average number of treatment cycles with pembrolizumab was 21.3 (range: 2–61 cycles). (Table 4)

Control CT scans were performed every three months, with radiological responses evaluated according to the iRECIST 1.1 criteria. Among the patients included in this study, the majority showed stable disease (SD) as the best response to pembrolizumab therapy, accounting for 26 patients (51.0%). Radiological response, including ORR is given in Table 5.

Progression-free survival (PFS) was defined as the time from the start of pembrolizumab treatment to the date of disease progression or death, whichever occurred first. Overall survival (OS) was defined as the time from the initiation of pembrolizumab treatment to the time of death. Patients who were still alive at the time of the analysis were censored at the date of their last contact. The median progression-free survival (mPFS) for patients in this study was 12.0 months (95% CI, 7.7–16.2 months), and the median overall survival (mOS) was 21.0 months (95% CI, 9.6–32.3 months). Kaplan Meyer survival curves for PFS and OS are given in Tables 1 and 2 respectively.

Given the distribution of PD-L1 expression in this cohort, patients were divided into two groups. The median PD-L1 expression value of 80% was used as the threshold for dividing the groups, ensuring that the number of patients in each group was as balanced as possible. Thus, one group consisted of patients with tumor PD-L1 expression of 50%–80%, while the other included patients with tumor PD-L1 expression of 80%–100%. The average age of patients with PD-L1 expression values of 50%–80% was 65.4 years, while for those with PD-L1 expression values of 80%–100%, it was 68.2 years. This difference was not statistically significant (p = 0.166). In the group with PD-L1 expression below 80%, there were 19 males (76.0%) and 6 females (24.0%). In the group with PD-L1 expression of 80% or higher, there were 12 males (46.2%) and 14 females (53.8%). The difference in gender distribution between the two groups was statistically significant (p = 0.029). Most patients with PD-L1 values below 80% had a BMI of 25.0-29.9, while the majority of patients with PD-L1 values of 80% or higher had a BMI of 18.5-24.9. There was no statistically significant difference in BMI between the two groups (p = 0.394). In both groups, the majority of patients were smokers, with no statistically significant difference between groups based on smoking status (p = 0.099). Squamous and non-squamous tumor types were equally represented in both groups, and the difference in tumor type based on PD-L1 values was not statistically significant (p = 0.903). Slightly more patients with PD-L1 values below 80% were in stage IVA compared to those with PD-L1 values of 80% or higher (84.0% *vs*. 57.7%), and this difference was statistically significant (p = 0.039). Partial response (PR) was observed in 12 patients (48.0%) with PD-L1 values below 80%, while the same response was observed

TABLE 2. Pathological characteristics and TNM staging

Histological subtype of NSCLC					
Squamous					22 (43.1%)
Non-squamous (adenocarcinoma)					29 (56.9%)
TNM classification					
T		N		M	
T1a	1 (2.0%)	0	10 (19.6%)	1a	20 (41.2%)
T1b	3 (5.9%)	1	3 (5.9%)	1b	16 (31.4%)
T1c	3 (5.9%)	2	20 (39.2%)	1c	15 (27.5%)
T2a	2 (3.9%)	3	18 (35.3%)		
T2b	6 (11.8%)				
T3	7 (13.7%)				
T4	29 (56.9%)				
Stage					
IVA		IVB			
36 (70.6%)		15 (29.4%)			

NSCLC = Non-Small Cell Lung Cancer; T = Tumor; N = Node; M = Metastasis

TABLE 3. Levels of PD-L1 expression

PD-L1 expression N/(%)	
50–59%	5 (9.8%)
60–69%	11 (21.6%)
70–79%	9 (17.6%)
80–89%	13 (25.5%)
90–100%	13 (25.5%)

PD-L1 = Programmed Death-Ligand 1

TABLE 4. Duration of treatment and number of cycles with pembrolizumab

DURATION OF TREATMENT (months)	
Average	18.3
Range	2–60
NUMBER OF CYCLES WITH PEMBROLIZUMB	
Average	21.3 cycles
Range	2–61 cycles

TABLE 5. Radiological response to treatment according to the iRECIST criteria

(immuno) RADIOLOGICAL RESPONSE TO TRETMENT (iRECIST)	
Complete response (CR)	0 (0%)
Partial response (PR)	19 (37.3%)
Stable disease (SD)	26 (51.0%)
Progressive disease (PD)	6 (11.8%)
Overall response rate (ORR)	37.2%

iRECIST = (immuno) Response Evaluation Criteria In Solid Tumors

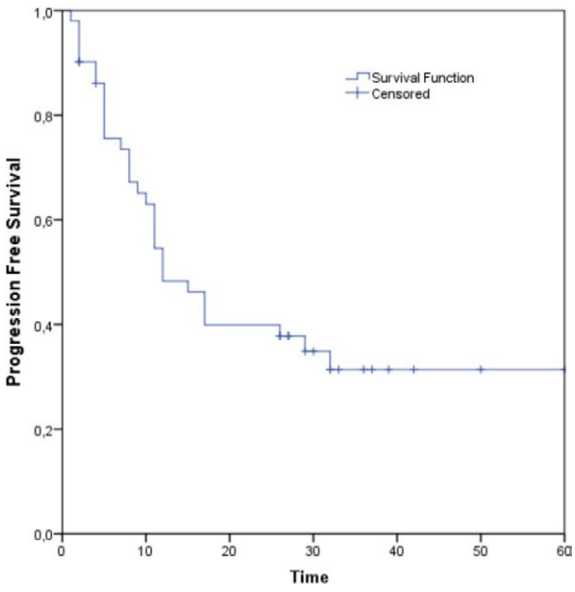

FIGURE 1. Progression free survival (PFS) for all patients evaluated in the real-world data (RWD) analysis.

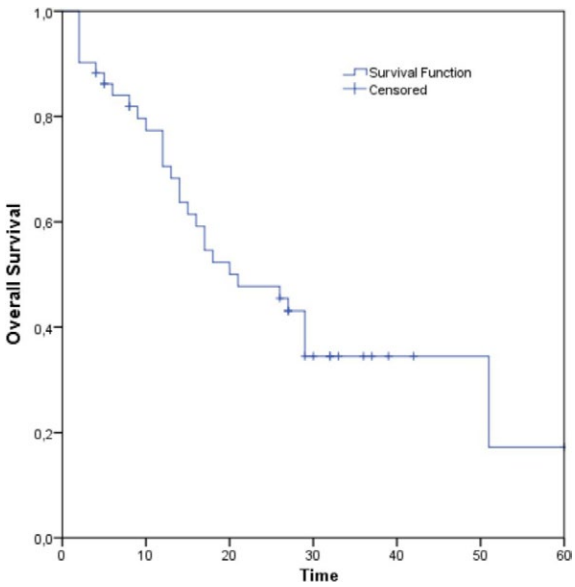

FIGURE 2. Overall survival (OS) for all patients evaluated in the real-world data (RWD) analysis.

in 7 patients (26.9%) with PD-L1 values of 80% or higher. The difference in best response between the two groups was not statistically significant (p = 0.262). Disease progression occurred in 12 patients (48.0%) with PD-L1 values below 80%, and in 15 patients (57.7%) with PD-L1 values of 80% or higher. This difference was not statistically significant (p = 0.488). In the group with PD-L1 values below 80%, there were 13 deaths (52.0%), while in the group with PD-L1 values of 80% or higher, there were 17 deaths (65.4%). Again, the difference was not statistically significant (p = 0.332). Multivariate analysis of evaluable variable is given in Table 6.

The average time to disease progression for patients with PD-L1 expression below 80% was 24.3 months, while for patients with PD-L1 expression of 80% or higher, it was 20.6 months. There is no statistically significant difference in progression free survival between two groups (p = 0.548) (Figure 3). The average overall survival for patients with PD-L1 expression of 50%–80% was 34.0 months, whereas for those with PD-L1 expression

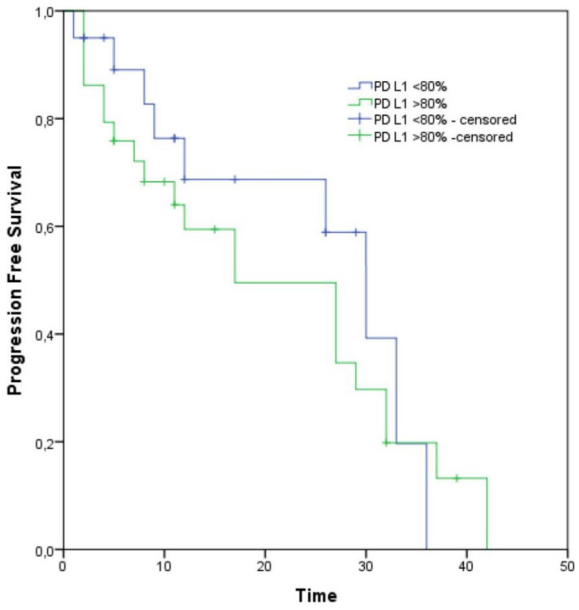

FIGURE 3. Progression Free Survival (PFS) between PD-L1 ≥ 80% group and PD-L1 < 80%; p = 0.548.

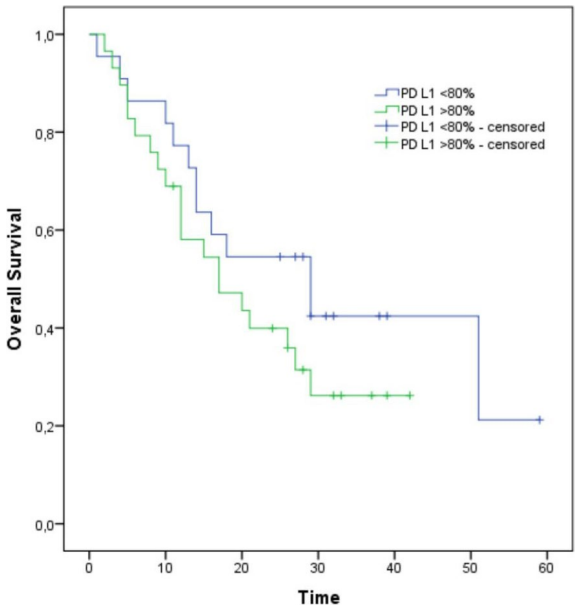

FIGURE 4. Overall Survival (OS) between PD-L1 ≥ 80% group and PD-L1 < 80%; p = 0.153

of 80%–100%, it was 22.1 months. There is no statistically significant difference in overall survival between these two groups (p = 0.153) (Figure 4). Median follow-up time was 32 months, 95%CI (29.5–34.5).

Discussion

This trial, which included 51 patients with NSCLC and PD-L1 expression ≥ 50% treated with pembrolizumab in the first-line setting, the median progression-free survival (mPFS) was 12.0 months, and the median overall survival (mOS) was 21.0 months. Among the full cohort in our study, the ORR was 37.2%. Based on a five-year follow-up result of KEYNOTE-024 study, mPFS for pembrolizumab-treated patients was 7.7 months, and mOS was 26.3 months. The objective response rate (ORR) was 46.1%.[15,16] We observed slightly higher median PFS, while median OS and ORR were somewhat lower compared to KEYNOTE-024. These discrepancies can be attributed to the design of our research, the small sample size, and the lack of precise data regarding subsequent therapies for patients who progressed after first-line pembrolizumab treatment. Additionally, in our study, as per institutional clinical practice, radiological monitoring was conducted every 12 to 16 weeks, a longer interval compared to the usual monitoring schedule in clinical trials. This might explain the slightly longer mPFS observed in our study compared to the mPFS reported in the KN-024 study. In Serbia, pembrolizumab is reimbursed for use in patients with metastatic NSCLC and PD-L1 expression ≥ 50%, and there is no cap on the number of immunotherapy cycles. However, in the clinical study design of Keynote-024, pembrolizumab was administered for a maximum of 35 cycles or earlier if disease progression, significant adverse events, or unacceptable toxicity occurred. A French research group published results of their retrospective study on first-line pembrolizumab treatment in RWD setting, for patients with metastatic NSCLC and PD-L1 expression > 50%.[17] Their study, like ours, was retrospective RWD study and lacked a control group but included more patients – 118 in total. The mPFS was slightly lower, 10.1 months, but the ORR (58.2%) was significantly higher compared to our study and the ORR observed in the KN-024 trial. Over 50% of patients in the French study showed partial responses (PR), and 2.7% had complete responses (CR). In contrast, none of our patients achieved a CR with pembrolizumab therapy, and only 37% of patients had a PR. In a multicenter retrospective study in Japan (HOPE-001) the main focus was on the efficacy and safety of pembrolizumab monotherapy in real-world practice. This study involved 213 patients predominantly consisted of older male patients (82.6% male, with a mean age of 71 years). The ORR was 51.2% with

TABLE 6. Multivariate analysis of patient characteristics in relation to PD-L1 expression

Characteristic	PD-L1 (50–79%)	PD-L1 (80–100%)	*p* value
Age (± SD)	65.4 (7.9)	68.2 (5.8)	*0.166*
Gender, N (%)			
Male	19 (76.0)	12 (46.2)	***0.029***
Female	6 (24.0)	14 (53.8)	
BMI			
< 18.5	1 (4.0)	2 (7.7)	0.394
18.5–24.9	9 (36.0)	13 (50.0)	
25.0–29.9	12 (48.0)	11 (42.3)	
30.00–34.9	1 (4.0)	0 (0.0)	
35.00–39.9	0 (0.0)	0 (0.0)	
> 40	2 (8.0)	0 (0.0)	
Smoking status, N (%)			
Nonsmokers	0 (0.0)	3 (11.5)	0.099
Smokers	22 (88.0)	17 (65.4)	
Former smokers	3 (12.0)	6 (23.1)	
Type of NSCLC, N (%)			
Squamous	11 (44.0)	11 (42.3)	0.903
Non-squamous	14 (56.0)	15 (57.7)	
Stage, N (%)			
IVa	21 (84.0)	15 (57.7)	**0.039**
IVb	4 (16.0)	11 (42.3)	
Best response, N (%)			
PR	12 (48.0)	7 (26.9)	0.262
SD	10 (40.0)	16 (61.5)	
PD	3 (12.0)	3 (11.5)	
Progression, N (%)			
No	13 (52.0)	11 (42.3)	0.488
Yes	12 (48.0)	15 (57.7)	
Outcome, N (%)			
Alive	12 (48.0)	9 (34.6)	0.332
Deceased	13 (52.0)	17 (65.4)	

BMI = Body Mass Index; NSCLC = Non-Small Cell Lung Cancer; PD-L1 = Programmed Death-Ligand 1; PD = Progressive Disease; PR = Partial Response; SD = Stable Disease; ± SD = ± Standard Deviation

median progression-free survival of 8.3 months, and the mOS of 17.8 months.[18] Our study population, even thou smaller in number, was slightly younger (mean age of 66 years) and more balanced by gender (60% male, 40% female). Regarding efficacy, the objective response rate in our study was lower than in the Japanese study; however, both mPFS (12.0 months) and mOS (21.0 months) were longer. The mPFS and mOS in Japanese study were slightly shorter also in comparison with the results from KN-024. These differences might be explained by the older patient population included in Japanise study compared to KN-024 and our research. A large European study involving 1026 patients reported an ORR of 44.5%, a mPFS of 7.9 months, and a mOS of 17.2 months.[19] This study had an ORR comparable to KN-024 but superior to our study's ORR. Notably, the European study's

mPFS and mOS were shorter than both KN-024 and our study. This difference may stem from the inclusion of patients with ECOG PS 2 (17%), ECOG PS 3 (0.4%), and patients with untreated brain metastases, which are common in everyday real-world clinical practice, but usually excluded from clinical trials. In our study, the exact metastatic disease locations were not precisely documented, representing a limitation. However, no patients with ECOG PS > 1 were included in our study, as the Republic Health Insurance Fund in Serbia only permits pembrolizumab treatment for patients with ECOG PS 0 and 1 in standard clinical practice. Despite these limitations, the efficacy of pembrolizumab in our study aligned well with findings from other real-world studies.[20,21]

Given that PD-L1 is a continuous biomarker correlating with the efficacy of immunotherapy in NSCLC patients, our study sought to determine whether patients with higher PD-L1 expression experienced better PFS and OS outcomes with first-line pembrolizumab therapy. With a median PD-L1 expression of 80% in our cohort, patients were divided into two groups: one with PD-L1 expression of 50%–80% and the other with PD-L1 expression of 80%–100%.

In a study by Aguilar *et al*. clinical outcomes were examined in NSCLC patients with very high PD-L1 expression.[21] The study conducted by Aguilar and colleagues included 187 patients with NSCLC and PD-L1 expression levels above 50%, which was three times the number of patients in our study. The ORR for the overall patient population in Aguilar's study was higher than in ours, reaching 44.4%. Median progression-free survival was only 6.5 months, while median overall survival was not reached. The median follow-up time of 12.6 months could explain the lower mPFS and the observed mOS results. In Aguilar's study, patients were divided into two groups based on PD-L1 expression to evaluate treatment outcomes in individuals with the highest PD-L1 levels. One group consisted of patients with PD-L1 expression levels of 50%–89% (N = 107), while the other included patients with levels of 90%–100% (N = 80). This division was based on the median PD-L1 expression of responders, which was 90%, contrasting with the median PD-L1 expression of 80% in our study. Both groups were well-balanced in terms of age, gender, tumor histology, smoking status, ECOG PS, and KRAS mutation status, with no statistically significant differences in clinical-pathological characteristics between them. In our research, we observed statistically significant differences in gender distribution regarding PD-L1 expression ($p = 0.029$), and patients with PD-L1 levels below 80% were more frequently in stage IVA compared to those with PD-L1 ≥ 80% (84.0% *vs*. 57.7%, $p = 0.039$). However, there were no significant differences in age, smoking status, BMI, or tumor type between the two groups in our study.

In Aguilar's study, patients with PD-L1 expression levels of 90%–100% had an ORR of 60%, while patients with PD-L1 expression levels of 50%–89% had an ORR of 32.7%. This difference was statistically significant ($p < 0.001$). Current study in our group showed no significant differences in response to pembrolizumab between the two groups, although numerically, patients with PD-L1 expression levels of 80%–100% tended to have stable disease (SD) as the best response, while patients with PD-L1 levels of 50%–80% were more likely to show partial response (PR). This result might be attributed to the smaller patient sample sizes and the different PD-L1 cutoff values used between the two studies. Aguilar's study found that mPFS was significantly longer in the PD-L1 90%–100% group compared to the PD-L1 50%–89% group (14.5 months *vs*. 4.1 months, $p < 0.01$). Similarly, mOS was significantly longer in the PD-L1 90%–100% group compared to the PD-L1 50%–89% group (not reached *vs*. 15.9 months, $p = 0.002$). Comparable results were also seen in Cortellini`s study. The median PFS and the median OS were also significantly shorter among patients with PD-L1 expression of < 90% as compared to those with a PD-L1 expression of ≥ 90%.[19] Several other studies also showed that patients with very high PD-L1 expression (PD-L1 > 90%) had a clear advantage in terms of mPFS and MOS in comparison to the patients with high PD-L1 expression (PD-L1 50%–90%).[22,23] In our study, the situation was reversed: both mPFS and mOS were longer in the PD-L1 50%–80% group, although these differences were not statistically significant. This could be explained by several factors, including the small sample size and different PD-L1 thresholds for group selection.

Even though current trial did not show significant difference in survival outcomes for patients whose tumors present expression of PD-L1 over 80% it does not necessarily mean that this prognostic factor should be neglected. The major limitations of this trial are retrospective design and smaller sample. However, that pitfall might be good starting point for piling data from smaller RWD trials, enabling direct comparison between patient populations. On the other hand, the inevitable expansion of our cohort, as well the other co-

horts currently recruiting patients in prospective parts of their trials might reveal contrasting data among larger trial population. Anyhow, all RWD data would be necessary for generating real-world evidence which might impact current treatment guidelines.

References

1. Bray F, Laversanne M, Sung H, Ferlay J, Siegel RL, Soerjomataram I, et al. Global cancer statistics 2022: GLOBOCAN estimates of incidence and mortality worldwide for 36 cancers in 185 countries. *CA Cancer J Clin* 2024; **74:** 229-63. doi: 10.3322/caac.21834
2. Siegel RL, Miller KD, Wagle NS, Jemal A. Cancer statistics, 2023. *CA Cancer J Clin* 2023; **73:** 17-48. doi: 10.3322/caac.21763
3. Goodarzi E, Sohrabivafa M, Adineh HA, Moayed L, Khazaei Z. Geographical distribution global incidence and mortality of lung cancer and its relationship with the Human Development Index (HDI); an ecology study in 2018. *WCRJ* 2019; **6:** e1354. doi: 10.32113/wcrj_20197_1354
4. Nooreldeen R, Bach H. Current and future development in lung cancer diagnosis. *Int J Mol Sci* 2021; **22:** 8661. doi: 10.3390/ijms2216866
5. Xia L, Liu Y, Wang Y. PD-1/PD-L1 Blockade Therapy in advanced non-small-cell lung cancer: current status and future directions. *Oncologist* 2019; **24(Suppl 1):** S31-41. doi: 10.1634/theoncologist.2019-IO-S1-s05
6. Francisco LM, Salinas VH, Brown KE, Vanguri VK, Freeman GJ, Kuchroo VK, et al. PD-L1 regulates the development, maintenance, and function of induced regulatory T cells. *J Exp Med* 2009; **206:** 3015-29. doi: 10.1084/jem.20090847
7. Chen L, Han X. Anti-PD-1/PD-L1 therapy of human cancer: past, present, and future. *J Clin Invest* 2015; **125:** 3384-91. doi: 10.1172/JCI80011
8. Bardhan K, Anagnostou T, Boussiotis VA. The PD1:PD-L1/2 pathway from discovery to clinical implementation. *Front Immunol* 2016; **7:** 550. doi: 10.3389/fimmu.2016.00550
9. Garon EB, Rizvi NA, Hui R, Leighl N, Balmanoukian AS, Eder JP, et al. Pembrolizumab for the treatment of non-small-cell lung cancer. *N Engl J Med* 2015; **372:** 2018-28. doi: 10.1056/NEJMoa1501824
10. Herbst RS, Baas P, Kim DW, Felip E, Perez-Gracia JL, Han JY, et al. Pembrolizumab versus docetaxel for previously treated, PD-L1-positive, advanced non-small-cell lung cancer (KEYNOTE-010): a randomised controlled trial. *Lancet* 2016; **387:** 1540-50. doi: 10.1016/S0140-6736(15)01281-7
11. Reck M, Brahmer JR. Pembrolizumab in non-small-cell lung cancer. *N Engl J Med* 2017; **376:** 997. doi: 10.1056/NEJMc1615559
12. Gandhi L, Rodríguez-Abreu D, Gadgeel S, Esteban E, Felip E, De Angelis F, et al. Pembrolizumab plus chemotherapy in metastatic non-small-cell lung cancer. *N Engl J Med* 2018; **378:** 2078-92. doi: 10.1056/NEJMoa1801005
13. Paz-Ares L, Luft A, Vicente D, Tafreshi A, Gumus M, Mazieres J, et al. Pembrolizumab plus chemotherapy for squamous non-small-cell lung cancer. *N Engl J Med* 2018; **379:** 2040-51. doi: 10.1056/NEJMoa1810865
14. Mathew M, Safyan RA, Shu CA. PD-L1 as a biomarker in NSCLC: challenges and future directions. *Ann Transl Med* 2017; **5:** 375. doi: 10.21037/atm.2017.08.04
15. Reck M, Rodriguez-Abreu D, Robinson AG, Hui R, Csoszi T, Fulop A, et al. Updated analysis of KEYNOTE-024: Pembrolizumab versus platinum-based chemotherapy for advanced non-small-cell lung cancer with PD-L1 tumor proportion score of 50% or greater. *J Clin Oncol* 2019; **37:** 537-46. doi: 10.1200/JCO.18.00149
16. Reck M, Rodríguez-Abreu D, Robinson AG, Hui R, Csőszi T, Fülop A, et al. Five-year outcomes with pembrolizumab versus chemotherapy for metastatic non-small-cell lung cancer with PD-L1 Tumor Proportion Score ≥ 50%. *J Clin Oncol* 2021; **39:** 2339-49. doi: 10.1200/JCO.21.00174
17. Amrane K, Geier M, Corre R, Léveiller G, Florence G, Lamy R, et al. First line pembrolizumab for NSCLC with PD-L1 TPS > 50% in a first French real life cohort. *Ann Oncol* 2019; **30:** v617. doi: 10.1093/annonc/mdz260
18. Tamiya M, Tamiya A, Hosoya K, Taniguchi Y, Yokoyama T, Fukuda Y, et al. Efficacy and safety of pembrolizumab as first-line therapy in advanced non-small cell lung cancer with at least 50% PD-L1 positivity: a multicenter retrospective cohort study (HOPE-001). *Invest New Drugs* 2019; **37:** 1266-73. doi: 10.1007/s10637-019-00843-y
19. Cortellini A, Tiseo M, Banna GL, Cappuzzo F, Aerts JGJV, Barbieri F, et al. Clinicopathologic Correlates of First-Line Pembrolizumab Effectiveness in Patients With Advanced NSCLC and a PD-L1 Expression of ≥ 50. *Cancer Immunol Immunother* 2020; **69:** 2209-21. doi: 10.1007/s00262-020-02613-9
20. Velcheti V, Chandwani S, Chen X, Pietanza MC, Piperdi B, Burke T. Outcomes of first-line pembrolizumab monotherapy for PD-L1-positive (TPS ≥ 50%) metastatic NSCLC at US oncology practices. *Immunotherapy* 2019; **11:** 1541-54. doi: 10.2217/imt-2019-0177
21. Aguilar EJ, Ricciuti B, Gainor JF, Kehl KL, Kravets S, Dahlberg S, et al. Outcomes to first-line pembrolizumab in patients with non-small-cell lung cancer and very high PD-L1 expression. *Ann Oncol* 2019; **30:** 1653-59. doi: 10.1093/annonc/mdz288
22. Shah M, Marmarelis ME, Mamtani M, Hennessy S. Association between survival and very high versus high PD-L1 expression in patients receiving pembrolizumab as first-line treatment for advanced non-small cell lung cancer. *Clin Lung Cancer* 2022; **23:** 731-6. doi: 10.1016/j.cllc.2022.07.003
23. Ricciuti B, Elkrief A, Lin J, Zhang J, Alessi JV, Lamberti G, et al. Three-year overall survival outcomes and correlative analyses in patients with NSCLC and high (50%–89%) versus very high (≥ 90 %) programmed death-ligand 1 expression treated with first-line pembrolizumab or cemiplimab. *JTO Clin Res Rep* 2024; **5:** 100675. doi: 10.1016/j.jtocrr.2024.100675

research article

Analysis of the effects of individualized nutrition and physical activities on body composition during the treatment of breast cancer patients

Rok Blaz[1], Masa Kovac[1], Nada Rotovnik Kozjek[2]

[1] University of Ljubljana, Medical Faculty, Ljubljana, Slovenia

[2] Institute of Oncology Ljubljana, Department for Clinical Nutrition, Ljubljana, Slovenia

Radiol Oncol 2026; 60(3): 459-470.

Received 10 February 2026
Accepted 2 June 2026

Correspondence to: Prof. Nada Rotovnik Kozjek, M.D., Ph.D., Institute of Oncology Ljubljana, Department for Clinical Nutrition, Zaloska 2, SI-1000 Ljubljana, Slovenia. E-mail: nkozjek@onko-i.si

Disclosure: No potential conflicts of interest were disclosed.

Background. Malnutrition and loss of skeletal muscle mass are common in breast cancer patients and represent negative prognostic factors. Combined nutrition and exercise interventions may help preserve body composition during treatment. The aim of this study was to evaluate the effects of a targeted nutritional and exercise intervention on body composition, assessed by Bioelectrical Impedance Analysis (BIA), in breast cancer patients undergoing treatment, stratified by baseline nutritional status according to the Global Leadership Initiative on Malnutrition (GLIM) criteria.

Patients and methods. In this retrospective analysis of the OREH pilot study, 287 patients were included in the intervention group and 194 in the control group. All patients underwent BIA measurements at baseline, 6 months, and 12 months. Malnourished patients (GLIM-positive) in both groups received individualized nutritional counseling as standard care. GLIM-negative patients in the intervention group received preventive nutritional counseling via online lectures. All intervention group patients participated in supervised group exercise. Differences in BIA parameters (fat-free mass index, phase angle, fat mass, total body water, and body mass index) between the 3rd and 1st measurements were compared using Welch's t-test, with p-values adjusted by the Bonferroni-Holm method.

Results. No statistically significant differences in body composition parameters were observed between the intervention and control groups over the 12-month follow-up period. The adjusted p-value for fat-free mass index (FFMI) was 0.2 in GLIM-positive patients and 1.0 in GLIM-negative patients. A trend toward greater FFMI increase was observed in GLIM-positive patients in the intervention group compared to controls (mean difference 0.30; 95% CI 0.05–0.54; unadjusted p = 0.017), but this did not remain significant after correction for multiple comparisons.

Conclusions. The combined nutritional and exercise intervention did not significantly improve BIA-derived body composition parameters. However, the trend toward FFMI improvement in GLIM-positive patients receiving individualized nutritional counseling suggests that personalized approaches may be more effective than group-based interventions. Future studies should incorporate individualized nutrition and resistance training programs to optimize body composition outcomes in breast cancer patients.

Key words: individualized nutrition; physical activity; body composition; breast cancer; bioelectrical impedance analysis; GLIM criteria

Introduction

Breast cancer is one of the most common cancers among women and represents a major public health challenge worldwide. The World Health Organization estimates that in 2022, approximately 2.3 million women were diagnosed with breast cancer and 670,000 died from the disease, making it the most common cancer in women in 157 of 185 countries.[1,2] In Slovenia, breast cancer is the most frequently diagnosed cancer in women, with 1,660 new cases, 470 deaths, and 7,128 five-year prevalent cases reported in 2022.[1,3] The national screening program DORA has achieved nationwide coverage with participation rates consistently above 70%, and registry-based evaluations have demonstrated that women undergoing organized screening have lower cancer stage at diagnosis and significantly better five-year net survival.[4,5]

Malnutrition is a prevalent and clinically consequential complication in cancer patients undergoing active treatment. It is defined as a state of energy and protein deficiency leading to unfavorable changes in body composition and impaired physiological function.[6] A more severe manifestation is cancer cachexia – a multifactorial syndrome characterized by ongoing loss of skeletal muscle mass, with or without fat mass depletion, that cannot be fully reversed by conventional nutritional support.[6] Cachexia develops through complex pathophysiological mechanisms, including systemic inflammation driven by pro-inflammatory cytokines, accelerated proteolysis (the enzymatic breakdown of muscle proteins), and anabolic resistance (the diminished capacity of skeletal muscle to respond to anabolic stimuli such as protein ingestion or exercise).[6,7] These processes are exacerbated by inflammatory factors released during cancer growth and are further intensified by chemotherapy and surgical treatment.[8] Additional contributing factors include comorbidities, treatment-related side effects (anemia, loss of appetite, nausea, vomiting, diarrhea, oral ulcers, taste changes, and dysphagia), and cessation of physical activity.[9] Collectively, these factors lead to quantitative and qualitative muscle loss, increased frailty, higher mortality, and decreased quality of life.[10-13]

Body composition has emerged as a critical prognostic factor in cancer patients.[14] Fat-free mass (FFM) represents metabolically active tissues, including muscles, bones, and visceral organs, and its loss is associated with higher mortality, poor clinical outcomes, and worse well-being.[14] Importantly, body mass index (BMI) alone fails to capture compositional changes, as patients may develop sarcopenic obesity. Sarcopenic obesity represents the simultaneous loss of muscle mass and gain of fat mass during treatment, characterized by reduced fat-free mass index (FFMI 15 kg/m^2 for women, 17 kg/m^2 for men) with normal or increased body weight.[15] Bioelectrical Impedance Analysis (BIA) is a simple, non-invasive method for assessing body composition that can be used at the bedside.[14] BIA measures tissue impedance when an electric current passes through the body: at lower frequencies, the current bypasses cell membranes, providing an estimate of extracellular water, while at higher frequencies it penetrates cell membranes, allowing assessment of total body water (TBW).[14] From these measurements, FFM, fat mass (FM), and phase angle can be calculated. Phase angle, obtained directly from BIA measurements, reflects cell membrane integrity and the ratio of intracellular to extracellular water. It is a reliable indicator of body cell mass, is strongly associated with muscle strength, and has high prognostic value in cancer patients.[16] However, since BIA is an indirect method, its reliability depends on certain conditions, including homogeneous tissue composition, stable fluid balance, and BMI between 16 and 34 kg/m^2, which may not always be met in hospitalized or chronically ill patients.[16]

The role of nutrition and exercise interventions in mitigating treatment-related body composition changes has gained increasing attention. Personalized nutrition is an important component of managing malnutrition in cancer patients, as standard dietary recommendations are not appropriate for oncology patients whose nutritional requirements differ from those of healthy adults.[10] A daily protein intake of at least 1 g/kg body weight from high-quality sources is recommended.[10] However, nutritional interventions alone are insufficient to fully prevent loss of body mass. Planned physical activity improves cardiorespiratory, neuromuscular, and immune system function, and has positive psychological effects.[12] Exercise increases gene expression of myogenic factors, activates mitochondrial biogenesis, reduces systemic inflammation and oxidative stress, counteracts cancer-induced anabolic suppression, and promotes protein synthesis.[13] At least 150 minutes of moderate-intensity or 75 minutes of vigorous-intensity exercise per week is recommended for breast cancer patients, with resistance exercises advised at least two to three times per week to maintain or increase muscle function and mass.[9]

The assessment of nutritional status in cancer patients begins with screening for nutritional risk using validated tools such as the Nutritional Risk Screening 2002 (NRS 2002).[17] If a patient is found to be at nutritional risk, the diagnosis of malnutrition can be established using the Global Leadership Initiative on Malnutrition (GLIM) criteria.[18] The GLIM criteria have been validated in clinical settings, demonstrating their ability to predict adverse clinical outcomes and response to nutritional treatment.[19]

Despite growing evidence supporting nutrition and exercise interventions in oncology, important knowledge gaps remain. Few studies have evaluated individualized, combined nutrition and exercise interventions targeting body composition specifically in breast cancer patients undergoing active treatment. Furthermore, the interaction between baseline nutritional status defined by GLIM criteria and intervention response remains poorly characterized. Preliminary data from a pilot study on individualized comprehensive rehabilitation in breast cancer patients in Slovenia suggested potential benefits, but definitive evidence is lacking.[20]

The aim of this study was to evaluate the effects of a targeted online nutrition sessions and supervised exercise intervention on body composition parameters assessed by BIA in breast cancer patients undergoing treatment, stratified by baseline nutritional status according to GLIM criteria.

Patients and methods

Study design and participants

The study was conducted as part of the Pilot Study on Individualized Comprehensive Rehabilitation of Breast Cancer Patients (OREH Study) at the Institute of Oncology Ljubljana (OIL), between 2019 and 2022.[20] A total of 600 patients were enrolled, with 301 assigned to the control group and 299 to the intervention group. Due to incomplete BIA measurements, the final sample consisted of 287 patients in the intervention group and 194 patients in the control group.

The intervention group included women aged 25 to 65 years diagnosed with breast cancer, treated at OIL, with permanent residence within the regional units of the Health Insurance Institute of Slovenia (ZZZS), Ljubljana or Kranj.[20] The control group comprised women with breast cancer aged 25 to 65 years, with permanent residence within the ZZZS regional units of Nova Gorica, Koper, Novo Mesto, Krško, Ljubljana, or Kranj.[20]

Intervention

A permanent reference point was established at OIL by a coordination nurse, who served as the central contact person to provide guidance and support during treatment. The comprehensive rehabilitation program included online workshops and off-site services delivered in collaboration with the University Rehabilitation Institute Soča, the Institute for Medical Rehabilitation at the University Medical Center Ljubljana, and Health Promotion Centers within community health centers.[20] Approval for the study was granted by the National Medical Ethics Committee of the Republic of Slovenia (reference number: 0120-264/2024-2711-3).

Online activities for patients in the intervention group included:

1. Clinical nutrition lectures (five series, each consisting of three one-hour sessions) delivered by clinical dietitians from the Clinical Nutrition Unit of OIL (average attendance per session: 31 participants).
2. Supervised group exercise sessions, conducted twice weekly for 30 minutes under the supervision of kinesiologists from the Faculty of Sport (average attendance: 25 participants).
3. Yoga sessions, conducted once weekly under the supervision of a physiotherapist (average attendance: 35 participants).

Nutritional assessment and management

All patients in both groups were screened for nutritional risk using the NRS 2002 tool.[17] Patients identified as at nutritional risk underwent diagnostic assessment using the GLIM criteria, which require at least one phenotypic criterion (unintentional weight loss, low BMI, or reduced FFMI) and at least one etiologic criterion (reduced dietary intake or disease burden/inflammation) for the diagnosis of malnutrition.[18,21] All patients diagnosed with malnutrition (GLIM-positive) in both groups were referred for individualized nutritional management, which represents the standard clinical practice at OIL.[21]

Body composition measurements

In both groups, body composition measurements were performed using BIA at baseline (measurement 1), at 6 months (measurement 2), and at 12 months (measurement 3). Measurements were obtained with a Bodystat Quadscan 4000 device. The

TABLE 1. Baseline demographic and clinical characteristics of participants

		Intervention	Control	p
N		**287**	**194**	
Cancer stage [%]				0.398
	0	5 (1.7)	4 (2.1)	
	1	121 (42.2)	86 (44.3)	
	2	114 (39.7)	64 (33.0)	
	3	30 (10.5)	30 (15.5)	
	4	17 (5.9)	10 (5.2)	
Living environment [%]				0.001
	urban	157 (54.7)	78 (40.2)	
	suburban	48 (16.7)	30 (15.5)	
	rural	82 (28.6)	86 (44.3)	
Social status [%]				0.836
	upper class	4 (1.4)	3 (1.5)	
	upper middle class	44 (15.3)	25 (12.9)	
	middle class	205 (71.4)	141 (72.7)	
	working class	33 (11.5)	23 (11.9)	
	lower class	1 (0.3)	1 (0.5)	
	no data	0 (0.0)	1 (0.5)	
Age at baseline (years) ± SD		51.28 +/- 9.11	51.19 +/- 8.76	0.909
Nutritional Risk Screening (NRS) [%]		122 (42.5)	90 (46.4)	0.455
NRS – points [%]				
	0	165 (57.5)	104 (53.6)	
	1	90 (31.4)	66 (34.0)	
	2	13 (4.5)	12 (6.2)	
	3	7 (2.4)	4 (2.1)	
	4	1 (0.3)	0 (0.0)	
	no data	11 (3.8)	8 (4.1)	
GLIM -positive [%]		60 (20.9)	52 (26.8)	0.164
Obesity = 1 [%] [BMI ≥ 30 kg/m²]		61 (21.3)	41 (21.1)	1.000

BMI = body mass index; GLIM = Global Leadership Initiative on Malnutrition; NRS 2002 = Nutritional Risk Screening 2002; SD = standard deviation; WHO = World Health Organization

following parameters were monitored: BMI (kg/m²), FFMI (kg/m²), phase angle (degrees), TBW (%), and FM (%).

Statistical analysis

Continuous variables were summarized as means and standard deviations, and categorical variables as frequencies and percentages. Baseline demographic and clinical characteristics were compared between the intervention and control groups using the chi-square test or Fisher's exact test for categorical variables, as appropriate, and Welch's two-sample t-test for continuous variables. The primary outcome was the change in body composition parameters between the third and first measurement. The analyzed BIA parameters were fat-free mass index, body mass index, total body water, fat mass, and phase angle. Positive values indicated an increase between baseline and the

TABLE 2. Descriptive statistics (mean ± SD) for Bioelectrical Impedance Analysis (BIA) parameters at each measurement time point, stratified by GLIM status

		GLIM negative		GLIM positive	
Parameter	**Meas.**	**Intervention**	**Control**	**Intervention**	**Control**
Phase angle (°)	1	5.4 +/-0.7	5.5 +/-0.6	5.2 +/-1.3	5.2 +/-0.6
	2	4.9 +/-0.6	5 +/-0.6	4.8 +/-0.6	4.7 +/-0.7
	3	5 +/-0.7	5.2 +/-0.7	4.9 +/-0.7	4.9 +/-0.6
FFMI (kg/m²)	1	17.1 +/-1.5	17.2 +/-1.3	15 +/-1.7	15 +/-1.6
	2	17.2 +/-1.7	17.2 +/-1.5	15.5 +/-1.8	15.4 +/-1.8
	3	17 +/-1.6	17.1 +/-1.4	15.4 +/-1.6	15.1 +/-1.5
Fat mass (%)	1	36.5 +/-7.5	36.6 +/-7	30.3 +/-7.4	30.4 +/-8.5
	2	36.3 +/-7.1	36.6 +/-7	31.4 +/-6.7	30.3 +/-6.3
	3	37 +/-6.8	37.1 +/-7.1	32.4 +/-8.4	31.3 +/-6.5
TBW (%)	1	47.6 +/-5	47.6 +/-4.9	53.6 +/-5.7	54 +/-6.1
	2	48 +/-5	47.8 +/-4.8	52.8 +/-4.9	53.6 +/-5.4
	3	47.5 +/-4.7	47.4 +/-4.9	51.5 +/-5.3	53.2 +/-5.8

FFMI = fat-free mass index; GLIM = Global Leadership Initiative on Malnutrition; TBW = total body water Meas. = Measurement; Measurement 1 = baseline; Measurement 2 = 6 months; Measurement 3 = 12 months

third measurement. Changes in BIA parameters were compared between the intervention and control groups using Welch's two-sample t-test, separately for GLIM-negative and GLIM-positive patients. To account for multiple comparisons across BIA parameters and GLIM subgroups, p-values were adjusted using the Bonferroni-Holm method. All tests were two-sided, and adjusted p-values below 0.05 were considered statistically significant. Missing data was not imputed because the proportion of missing observations was low (3.4% across all outcome variables and measurement points). Missing outcome data were handled using pairwise deletion. Statistical analyses were performed using R software.

Results

Baseline characteristics

The study included 481 female patients aged 25 to 65 years (287 intervention, 194 control). The mean age at baseline was 51.3 ± 7.1 years in the intervention group and 51.2 ± 7.3 years in the control group, with no statistically significant difference (p = 0.909). Baseline demographic and clinical characteristics are presented in Table 1.

Baseline characteristics were largely similar between groups. There were no statistically significant differences in cancer stage (p = 0.398), social status (p = 0.836), nutritional risk by NRS 2002 (p = 0.455), GLIM-defined malnutrition (20.9% *vs.* 26.8%; p = 0.164), or obesity prevalence (21.3% *vs.* 21.1%; p = 1.000). However, the living environment differed significantly between groups, with a higher proportion of urban participants in the intervention group (54.7%) compared to the control group (40.2%), and a higher proportion of rural participants in the control group (44.3% *vs.* 28.6%; p = 0.001).

Among patients screened with NRS 2002, 42.5% of the intervention group and 46.4% of the control group were identified as at nutritional risk (p = 0.455). The distribution of NRS scores was similar between groups, with the majority scoring 0 (no risk) or 1 point

Body composition measurements

Descriptive statistics for BIA parameters at each measurement time point, stratified by GLIM status and group allocation, are presented in Table 2. Measurement time points correspond to baseline (measurement 1), 6 months (measurement 2), and 12 months (measurement 3). In GLIM-negative patients, FFMI remained relatively stable across all three measurements in both groups (intervention: 17.1, 17.2, 17.0 kg/m²; control: 17.2, 17.2, 17.1 kg/m²). Phase angle decreased from baseline to 6 months in both groups (intervention: 5.4 to 4.9; control: 5.5

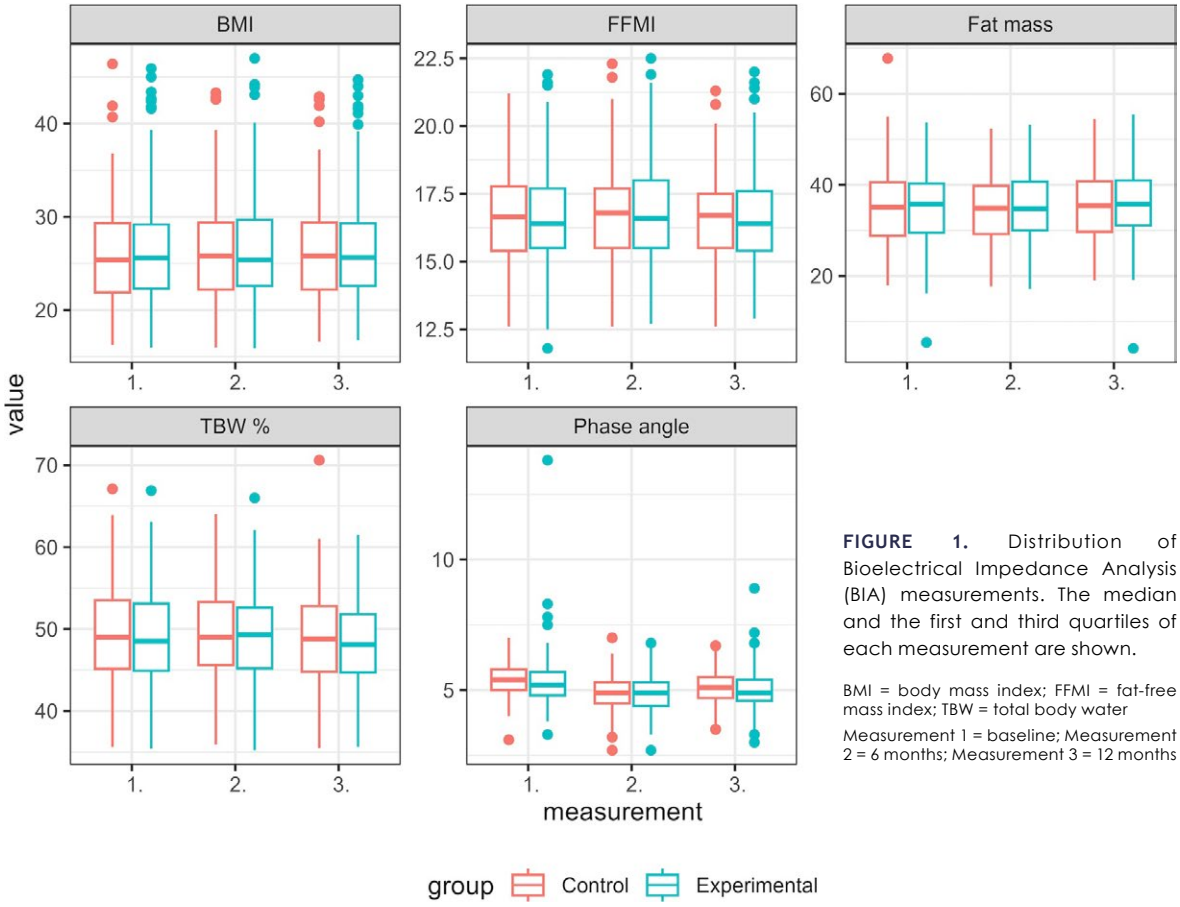

FIGURE 1. Distribution of Bioelectrical Impedance Analysis (BIA) measurements. The median and the first and third quartiles of each measurement are shown.

BMI = body mass index; FFMI = fat-free mass index; TBW = total body water

Measurement 1 = baseline; Measurement 2 = 6 months; Measurement 3 = 12 months

to 5.0), with partial recovery at 12 months (intervention: 5.0; control: 5.2). Fat mass percentage and TBW remained largely unchanged.

In GLIM-positive patients, FFMI increased from baseline to 6 months in both groups (intervention: 15.0 to 15.5 kg/m²; control: 15.0 to 15.4 kg/m²), with the intervention group maintaining a slightly higher value at 12 months (15.4 *vs.* 15.1 kg/m²). Phase angle decreased similarly in both groups from baseline to 6 months (intervention: 5.2 to 4.8; control: 5.2 to 4.7), with partial recovery at 12 months (both groups: 4.9). Fat mass percentage increased progressively in both groups, with a greater increase in the intervention group (30.3 to 32.4%) compared to controls (30.4 to 31.3%). TBW decreased in both groups, with a more pronounced decrease in the intervention group (53.6 to 51.5%) compared to controls (54.0 to 53.2%). The distribution of BIA measurements at each time point is shown in Figure 1.

Comparison of body composition changes between groups

To assess the effect of the intervention, the difference between the 3rd (12 months) and 1st (baseline) measurements was calculated for each parameter. The mean difference and 95% confidence interval are presented in Figure 2, stratified by GLIM status and group allocation.

Differences between groups were tested using Welch's t-test (Table 3). After adjustment for multiple comparisons using the Bonferroni-Holm method, none of the differences reached statistical significance. In GLIM-negative patients, no meaningful differences were observed between the intervention and control groups for any parameter: FFMI (mean difference −0.03; adjusted p = 1.0), BMI (−0.17; adjusted p = 1.0), TBW (0.19; adjusted p = 1.0), FM (0.05; adjusted p = 1.0), and phase angle (0.02; adjusted p = 1.0).

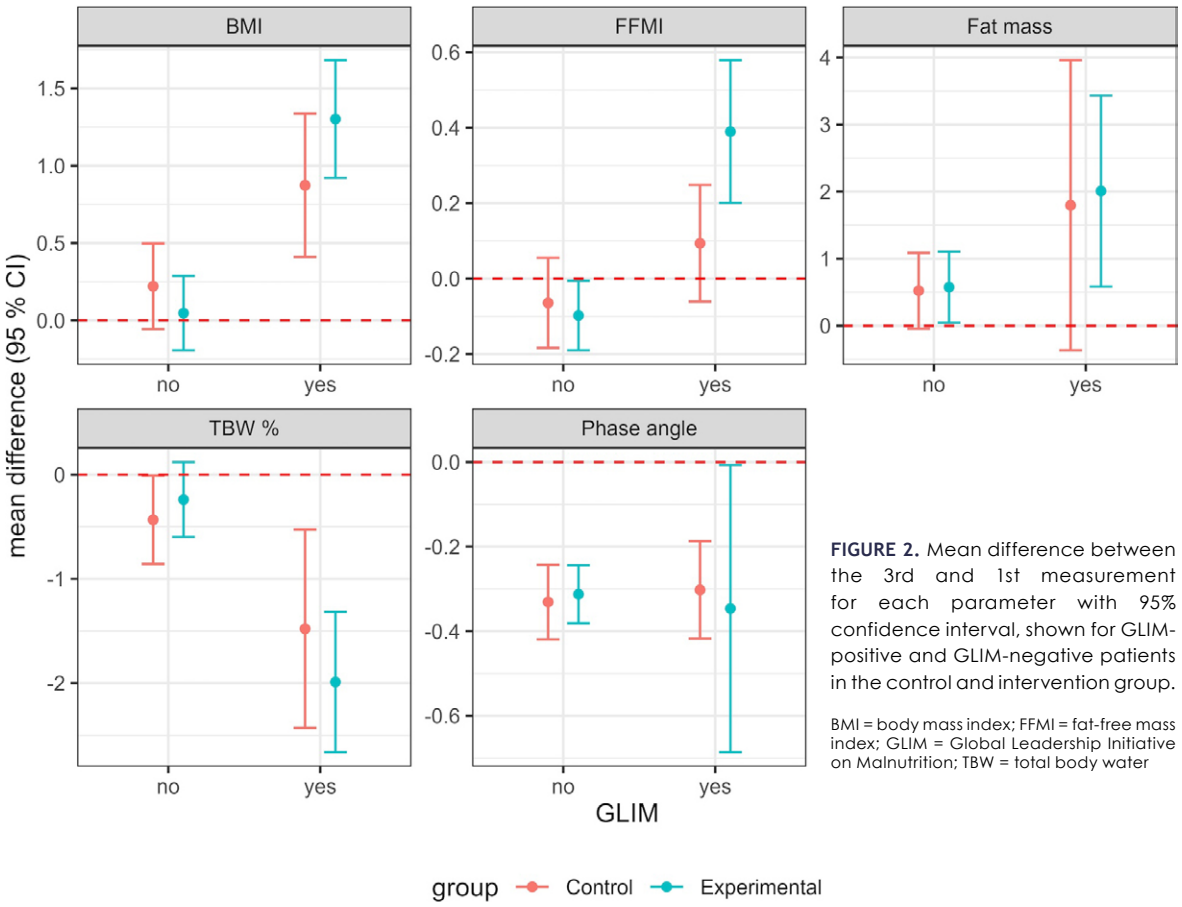

FIGURE 2. Mean difference between the 3rd and 1st measurement for each parameter with 95% confidence interval, shown for GLIM-positive and GLIM-negative patients in the control and intervention group.

BMI = body mass index; FFMI = fat-free mass index; GLIM = Global Leadership Initiative on Malnutrition; TBW = total body water

In GLIM-positive patients, the intervention group showed a greater increase in FFMI compared to controls (mean difference 0.30; 95% CI 0.05–0.54; unadjusted p = 0.017), but this did not remain significant after Bonferroni-Holm correction (adjusted p = 0.2). No significant differences were observed for BMI (0.43; adjusted p = 1.0), TBW (−0.51; adjusted p = 1.0), FM (0.21; adjusted p = 1.0), or phase angle (−0.25; adjusted p = 1.0).

Discussion

This study evaluated the effects of a combined nutritional and exercise intervention on body composition in breast cancer patients undergoing treatment, stratified by baseline nutritional status according to GLIM criteria. The main findings were that: (1) the intervention did not produce statistically significant improvements in any BIA-derived body composition parameter over the 12-month follow-up; (2) a trend toward greater FFMI increase was observed in GLIM-positive patients in the intervention group (mean difference 0.30; unadjusted p = 0.017), although this did not survive correction for multiple comparisons; and (3) both GLIM-positive and GLIM-negative patients experienced a decline in phase angle during treatment, regardless of group allocation.

Interpretation of body composition findings

The absence of statistically significant body composition improvements in the overall cohort, despite the multimodal intervention design, warrants careful interpretation. Several mechanistic and practical factors may explain this finding. First, the catabolic effects of cancer treatment-mediated by pro-inflammatory cytokines and tumor-

TABLE 3. Comparison of body composition changes (3rd−1st measurement) between intervention and control groups, stratified by GLIM status

Parameter	GLIM	Mean difference (intervention – control)	t-value	Diference	p-value	Adjusted p-value	Lower limit	Higher limit
FFMI	0	-0.03	-0.44	270.1	0.662	1.0	-0.18	0.12
FFMI	1	0.30	2.43	104.0	0.017	0.2	0.05	0.54
BMI	0	-0.17	-0.94	295.1	0.350	1.0	-0.54	0.19
BMI	1	0.43	1.44	96.4	0.154	1.0	-0.16	1.02
TBW	0	0.19	0.69	284.9	0.492	1.0	-0.36	0.75
TBW	1	-0.51	-0.88	83.6	0.380	1.0	-1.66	0.64
FM	0	0.05	0.13	309.8	0.894	1.0	-0.72	0.82
FM	1	0.21	0.16	84.2	0.869	1.0	-2.35	2.78
phase angle (°)	0	0.02	0.33	257.8	0.744	1.0	-0.09	0.13
phase angle (°)	1	-0.25	-0.25	67.1	0.806	1.0	-0.04	0.31

BMI = body mass index (kg/m²); FM = fat mass (%); FFMI = fat-free mass index (kg/m²); GLIM = Global Leadership Initiative on Malnutrition; TBW = total body water (%)

derived factors – may have overwhelmed the anabolic stimulus provided by nutrition and exercise. Systemic inflammation drives accelerated proteolysis and impairs muscle protein synthesis even in the presence of adequate nutritional intake, a hallmark feature distinguishing cachexia from simple starvation.[6,7] Second, the exercise component of the intervention (twice-weekly 30-minute group sessions plus weekly yoga) may have been insufficient in intensity and individualization to produce measurable changes in muscle mass. This interpretation is supported by the comparison with Short *et al.*, who demonstrated a statistically significant increase in phase angle using a more intensive 12-week program comprising 45 minutes of resistance training, 30 minutes of aerobic exercise, and 15 minutes of stretching, three times per week.[22] Third, treatment-related side effects likely limited adherence to nutritional targets, reducing effective protein and energy intake below prescribed levels.[9,10]

These findings are consistent with those of van der Werf *et al.*, who monitored muscle mass changes using CT imaging in patients with metastatic colorectal cancer over a 12-week chemotherapy period and likewise found no statistically significant differences between intervention and control groups despite individualized dietary counseling.[23] Similarly, Pérez-Bilbao *et al.* reported heterogeneous effects of combined exercise and diet interventions in breast cancer patients, with outcomes depending on intervention type, timing, and patient characteristics.[24]

GLIM-stratified analysis

The observation that FFMI increased in GLIM-positive patients in both groups, with a greater increase in the intervention group (mean difference 0.30), while it slightly decreased in GLIM-negative patients, is clinically noteworthy despite not reaching statistical significance after correction for multiple comparisons. This differential response may reflect the fact that GLIM-positive patients, who received individualized nutritional counseling as standard care in both groups, benefited more from targeted individualized nutritional support than GLIM-negative patients who received only group-based lectures.

These findings align with those of Kaegi-Braun *et al.*, who confirmed the strong prognostic value of GLIM-defined malnutrition for predicting adverse clinical outcomes and suggested – although not statistically significantly – that nutritional intervention may reduce unfavorable consequences among GLIM-positive patients.[19] Similarly, Jiang *et al.* demonstrated that nutritional support in geriatric inpatients classified by GLIM criteria yielded greater improvements in BMI, handgrip strength, and calf circumference among patients at risk of malnutrition compared to well-nourished patients, suggesting that individualized nutritional support is more effective in malnourished populations.[25] The EFFECT trial by Schuetz *et al.* further demonstrated that individualized nutritional support in medical inpatients at nutritional risk significantly improved clinical outcomes, reinforcing the con-

cept that baseline nutritional status modifies intervention response.[26]

Altogether, these findings collectively highlight the importance of routine nutritional screening and diagnosis using GLIM criteria, particularly in vulnerable patient populations, and suggest that individualized rather than group-based nutritional approaches may be necessary to achieve meaningful body composition improvements.

Phase angle

Phase angle decreased in both groups across GLIM subgroups, with no statistically significant differences between intervention and control groups (adjusted p = 1.0). The decline in phase angle during treatment likely reflects the catabolic effects of chemotherapy on cellular integrity, consistent with the findings of Schmidt *et al*., who investigated the effect of 12-week resistance training on phase angle in 158 breast cancer patients and similarly found no statistically significant intervention effect.[27]

However, other studies have demonstrated that more intensive exercise programs can improve phase angle. Short *et al.* reported a significant increase in phase angle following a 12-week individualized rehabilitation program in breast cancer survivors.[22] Escriche-Escuder *et al.* similarly demonstrated phase angle improvement after a 12-week exercise program that included twice-weekly resistance training and twice-weekly endurance sessions.[28] These results suggest that exercise intensity and the inclusion of resistance training are critical determinants of phase angle response, and that the exercise component in the present study may have been insufficient to counteract treatment-induced cellular deterioration.

Phase angle has been established as a reliable prognostic marker in cancer patients, with low values associated with higher mortality and worse clinical outcomes.[16,27] Pereira *et al.* demonstrated that TBW and the ratio of extracellular to intracellular water independently predict mortality in hospitalized oncology patients.[29] The clinical relevance of even modest phase angle changes underscores the importance of incorporating this parameter into routine nutritional monitoring.

BMI and fat mass

Both BMI and fat mass percentage increased in the intervention and control groups, with a greater increase observed among GLIM-positive patients. However, no statistically significant differences were found between subgroups (adjusted p = 1.0). These findings are consistent with those of Ligibel *et al*., who observed nonsignificant reductions in body mass, body fat, and waist circumference in breast cancer patients receiving supervised resistance exercise and aerobic training.[30]

Importantly, BMI and fat mass alone are insufficient indicators of treatment prognosis. Treatment outcomes in oncology patients are more closely related to individual body composition than to BMI.[14] Simillis *et al.* demonstrated a U-shaped relationship between BMI and survival in colorectal cancer surgery patients, with both very low (18.5 kg/m²) and very high (> 35 kg/m²) BMI associated with worse outcomes, while overweight patients (BMI 25–30 kg/m²) had the best survival.[31] This further supports the use of body composition parameters such as FFMI and phase angle rather than BMI alone for prognostic assessment.

Total body water

TBW decreased in both groups and across GLIM subgroups, with a more pronounced decrease in GLIM-positive patients. No statistically significant differences were observed between groups (adjusted p = 1.0). Since TBW is strongly correlated with FFM – in healthy individuals, FFM contains approximately 73% of total body water, changes in TBW may partially reflect changes in lean tissue mass.[32] The more pronounced TBW decrease in GLIM-positive patients, despite their FFMI increase, may reflect shifts in fluid distribution related to treatment effects or changes in fat mass composition rather than true lean tissue loss.

Comparison with individualized intervention studies

The contrast between the present study's null findings and the positive results reported in studies using individualized approaches is instructive. Mlakar-Mastnak *et al.* demonstrated that individualized nutritional intervention by a clinical dietitian in patients at risk of malnutrition in Slovenian primary healthcare produced statistically significant increases in phase angle, FFMI, and BMI after six months.[21,33] That intervention consisted of four individual consultations over six months with tailored plans based on each patient's energy, macro-, and micronutrient needs.[21] The present study's nutritional program for GLIM-negative patients in the intervention group consisted of group work-

shops with very low average attendance (31 participants per session), suggesting that group-based approaches may be insufficient to achieve meaningful behavior and nutritional change.

Furthermore, Champ *et al*. reported that resistance exercise has a greater effect on maintaining or increasing muscle mass in cancer patients compared to aerobic exercise alone.[34] The present study's exercise component lacked an individualized resistance training component, which may have limited its effectiveness. Incorporating individualized resistance training, as recommended by current evidence, could potentially improve outcomes in future studies.[9,12,13]

Strengths and limitations

This study has several strengths. The 12-month follow-up period is longer than most previous studies, which typically implemented interventions over 12 weeks.[22,23,27,28] BIA is a practical, safe, and cost-effective method for body composition assessment compared to DXA, CT, or MRI.[34] The stratification by GLIM criteria provides novel insights into the interaction between baseline nutritional status and intervention response.

However, several limitations must be acknowledged. First, complete data for all three measurements were not available for all OREH study participants, reducing the sample size from 600 to 481 and potentially introducing selection bias. Second, the proportion of patients with obesity (BMI ≥ 30 kg/m^2) was approximately 21% in both groups; BIA may not be sufficiently accurate in these patients, potentially underestimating fat mass and overestimating FFM.[35,36] However, a study comparing BIA and DXA for monitoring FFM changes in cancer patients found 100% sensitivity and 90% specificity for detecting FFM reductions greater than 5%, supporting BIA as a suitable method for detecting clinically meaningful changes.[35] Third, attendance at intervention workshops was very low (average 25–35 participants per session), and individual attendance tracking was not available, making it impossible to determine the effective intervention dose. Fourth, the significant baseline imbalance in living environment ($p = 0.001$) represents a potential source of confounding, as urban versus rural residence may affect access to intervention resources, dietary patterns, and physical activity opportunities. Fifth, the study design was retrospective, limiting the ability to establish causality. Sixth, the exercise component lacked individualization and dedicated resistance training, which may have reduced its effectiveness. Finally, chemotherapy regimen heterogeneity introduced unmeasured variability in catabolic stress.

Clinical implications and future directions

Based on these results and supporting evidence from the literature, several recommendations can be made for future individualized rehabilitation programs for breast cancer patients.[37] First, routine nutritional screening using NRS 2002 followed by GLIM diagnostic assessment should be standard practice, as baseline nutritional status appears to modify intervention response.[17,18,19] Second, nutritional interventions should be individualized with concrete goals for energy and protein intake for all patients, not only those diagnosed with malnutrition, as the EFFECT trial demonstrated that individualized nutritional support significantly reduces mortality in at-risk patients.[26] Third, exercise programs should include resistance training at least two to three times per week, as evidence consistently demonstrates that resistance exercise is more effective than aerobic exercise alone for preserving or increasing muscle mass in cancer patients.[9,12,33] Fourth, intervention adherence should be tracked individually to enable accurate assessment of effectiveness. Fifth, future studies should consider longer intervention durations, larger sample sizes with adequate statistical power, and multicenter designs to improve generalizability.

Conclusions

In this study, a combined nutritional and physical activity program did not produce statistically significant improvements in BIA-derived body composition parameters (FFMI, phase angle, fat mass, TBW, and BMI) over 12 months in breast cancer patients undergoing treatment. The intervention, which included group-based nutrition lectures and supervised exercise without individualized resistance training, was insufficient to prevent treatment-related body composition changes. However, a trend toward greater FFMI improvement in GLIM-positive patients, who received individualized nutritional counseling as standard care, suggests that personalized nutritional approaches may be more effective than group-based interventions. Based on these findings and supporting evidence, future programs should incorporate individualized nutrition counseling with

specific energy and protein targets for all patients, structured resistance training, and systematic adherence monitoring to optimize body composition outcomes in breast cancer patients.

Acknowledgements

Special thanks goes to the mentor of this research paper, Assoc. Prof. Dr. Nada Rotovnik Kozjek, M.D., for her guidance, advice, and support during the preparation of this research project. We would also like to thank Prof. Dr. Nikola Bešić, M.D., for his valuable advice regarding data collection and the writing of the paper.

We sincerely thank Denis Mastnak Mlakar, clinical dietitian, for her professional guidance and assistance in using the RedCap program.

Our sincere gratitude also goes to Dr. Bor Vratanar for performing the statistical analysis, helping with data interpretation and providing numerous ideas for improving the paper.

Finally, we would like to thank everyone else who, in any way, contributed with their help, advice or support for the completion of this research project.

This study received no specific funding. It represents a secondary analysis of data collected within the project V3-1906 funded by the Slovenian Research and Innovation Agency (ARIS).

AI disclosure

During the preparation of this manuscript, the authors used Chat GPT to improve readability and language. After using this tool, the authors reviewed and edited the content as necessary and take full responsibility for the content of the manuscript.

References

1. Zadnik V, Primic Žakelj M, Zagar T, Krajc M, Repse-Fokter A, Pompe kirn V, et al. *Cancer in Slovenia 2020* [Internet]. Ljubljana: Institute of Oncology Ljubljana, Epidemiology and Cancer Registry; 2022. Raport No. 65. [cited 2026 jan 15]. Available at: https://www.onkoi.si/fileadmin/onko/datoteke/rrs/lp/letno_porocilo_2020.pdf
2. Kim J, Harper A, McCormack V, Sung H, Houssami N, Morgan E, et al. Global patterns and trends in breast cancer incidence and mortality across 185 countries. *Nat Med* 2025; **31:** 1154-62. doi: 10.1038/s41591-025-03502-3
3. Ferlay J, Ervik M, Lam F, Laversanne M, Colombet M, Mery L, et al. *Global cancer observatory: cancer today* [Internet]. Lyon, France: International Agency for Research on Cancer; 2024. [cited 2026 jan 16]. Available at: https://gco.iarc.who.int/media/globocan/factsheets/populations/705-slovenia-fact-sheet.pdf
4. Jarm K, Kadivec M, Šval C, Hertl K, Primic Žakelj M, Dean PB, et al. Quality assured implementation of Slovenian breast cancer screening programme. *Plos One* 2021; **16:** e0258343. doi: 10.1371/journal.pone.0258343
5. Tomšič S, Žagar T, Mihor A, Mlakar M, Lokar K, Jarm K, et al. Prognostic factors and outcomes in women with breast cancer in Slovenia in relation to step-wise implementation of organized screening. *Plos One* 2022; **17:** e0278384. doi: 10.1371/journal.pone.0278384
6. Rotovnik Kozjek N, Tonin G, Puzigaća L, Veninšek G, Pirkmajer S, Košir Božič T, et al. [Terminology of clinical nutrition: nutritional disorders and nutrition related conditions] [Slovenian]. *Zdrav Vestn* 2023; **92:** 356-70. doi: 10.6016/ZdravVestn.3446
7. Paulussen KJM, McKenna CF, Beals JW, Wilund KR, Salvador AF, Burd NA. Anabolic resistance of muscle protein turnover comes in various shapes and sizes. *Front Nutr* 2021; **8:** 615849. doi: 10.3389/fnut.2021.615849
8. Martin A, Gallot YS, Freyssenet D. Molecular mechanisms of cancer cachexia-related loss of skeletal muscle mass: data analysis from preclinical and clinical studies. *J Cachexia Sarcopenia Muscle* 2023; **14**: 1150-67. doi: 10.1002/jcsm.13073
9. Milliron BJ, Packel L, Dychtwald D, Klobodu C, Pontiggia L, Ogbogu O, et al. When eating becomes torturous: understanding nutrition-related cancer treatment side effects among individuals with cancer and their caregivers. *Nutrients* 2022; **14:** 356. doi: 10.3390/nu14020356
10. Arends J, Bachmann P, Baracos V, Barthelemy N, Bertz H, Bozzetti F, et al. ESPEN guidelines on nutrition in cancer patients. *Clin Nutr* 2017; **36:** 11-48. doi: 10.1016/j.clnu.2016.07.015
11. Invernizzi M, Venetis K, Sajjadi E, Piciotti R, de Sire A, Fusco N. Understanding the biology of volumetric muscle loss for an individualized exercise rehabilitation approach in breast cancer patients. *Curr Opin Pharmacol* 2021; **58:** 27-34. doi: 10.1016/j.coph.2021.03.007
12. Pedersen BK, Saltin B. Exercise as medicine - evidence for prescribing exercise as therapy in 26 different chronic diseases. *Scand J Med Sci Sports* 2015; **25:** Suppl 3: 1-72. doi: 10.1111/sms.12581
13. Tsitkanou S, Murach KA, Washington TA, Greene NP. Exercise counteracts the deleterious effects of cancer cachexia. *Cancers (Basel)* 2022; **14:** 2512. doi: 10.3390/cancers14102512
14. Thibault R, Genton L, Pichard C. Body composition: why, when and for who? *Clin Nutr* 2012; **31:** 435-47. doi: 10.1016/j.clnu.2011.12.011
15. Donini LM, Busetto L, Bischoff SC, Cederholm T, Ballesteros-Pomar MD, Batsis JA, et al. Definition and diagnostic criteria for sarcopenic obesity: ESPEN and EASO consensus statement. *Clin Nutr* 2022; **41:** 990-1000. doi: 10.1016/j.clnu.2021.11.014
16. Martins PC, Alves Junior CAS, Silva AM, Silva DAS. Phase angle and body composition: a scoping review. *Clin Nutr ESPEN* 2023; **56:** 237-50. doi: 10.1016/j.clnesp.2023.05.015
17. Kondrup J, Rasmussen HH, Hamberg O, Stanga Z; Ad Hoc ESPEN Working Group. Nutritional risk screening (NRS 2002): a new method based on an analysis of controlled clinical trials. *Clin Nutr* 2003; **22:** 321-36. doi: 10.1016/s0261-5614(02)00214-5
18. Cederholm T, Jensen GL, Correia MITD, Gonzalez MC, Fukushima R, Higashiguchi T, et al. GLIM criteria for the diagnosis of malnutrition - a consensus report from the global clinical nutrition community. *Clin Nutr* 2019; **38:** 1-9. doi: 10.1016/j.clnu.2018.08.002
19. Kaegi-Braun N, Boesiger F, Tribolet P, Gomes F, Kutz A, Hoess C, et al. Validation of modified GLIM criteria to predict adverse clinical outcome and response to nutritional treatment: a secondary analysis of a randomized clinical trial. *Clin Nutr* 2022; **41:** 795-804. doi: 10.1016/j.clnu.2022.02.009
20. Bešić N, Kurir Borovčić M, Žagar T, Zadravec Zaletel L. [Pilot study on individualized comprehensive rehabilitation for breast cancer patients, 2019–2022]. [Slovenian]. OREH study; Research Project V3-1906): final report. Institute of Oncology Ljubljana; 2023.
21. Mlakar-Mastnak D, Kogovšek K, Rotovnik Kozjek N, Jordan T. [Clinical pathway for nutritional support at the Institute of Oncology Ljubljana]. [Slovenian]. Ljubljana: Institute of Oncology Ljubljana, Department for Clinical Nutrition; 2016. [cited 2026 Jan 15]. Available at: https://www.onko-i.si/fileadmin/onko/datoteke/Strokovna_knjiznica/klinicne_poti/Klinicna_pot_prehranske_podpore_na_Onkoloskem_institutu_Ljubljana_2016.pdf
22. Short T, Teranishi-Hashimoto C, Yamada PM. Exercise-based cancer rehabilitation program improves phase angle in breast cancer survivors. *Int J Exerc Sci* 2022; **15:** 1444-56. doi: 10.70252/OOAQ4294

23. van der Werf A, Langius JAE, Beeker A, Ten Tije AJ, Vulink AJ, Haringhuizen A, et al. The effect of nutritional counseling on muscle mass and treatment outcome in patients with metastatic colorectal cancer undergoing chemotherapy: a randomized controlled trial. *Clin Nutr* 2020; **39:** 3005-13. doi: 10.1016/j.clnu.2020.01.009

24. Pérez-Bilbao T, Alonso-Dueñas M, Peinado AB, San Juan AF. Effects of combined interventions of exercise and diet or exercise and supplementation on breast cancer patients: a systematic review. *Nutrients* 2023; **15:** 1013. doi: 10.3390/nu15041013

25. Jiang S, Chen X, Ma L, Guo Q, Luo L, Wang Y, et al. Evaluating the effect of nutritional support in geriatric inpatients classified by the GLIM criteria. *J Nutr Health Aging* 2025; **29:** 100585. doi: 10.1016/j.jnha.2025.100585

26. Schuetz P, Fehr R, Baechli V, Geiser M, Deiss M, Gomes F, et al. Individualised nutritional support in medical inpatients at nutritional risk: a randomised clinical trial. *Lancet* 2019; **393:** 2312-21. doi: 10.1016/S0140-6736(18)32776-4

27. Schmidt ME, Chong M, Klassen O, Wiskemann J, Steindorf K. Longitudinal associations of bioelectrical phase angle and fatigue in breast cancer patients. *Int J Cancer* 2023; **153:** 1192-200. doi: 10.1002/ijc.34630

28. Escriche-Escuder A, García-Almeida JM, Vegas-Aguilar IM, Pajares B, Alba E, Trinidad-Fernández M, et al. Effect of a 12-week exercise program on phase angle in women with breast cancer. *Support Care Cancer* 2025; **33:** 398. doi: 10.1007/s00520-025-09443-4

29. da Costa Pereira JP, Santana Costa JH, Gomes de Miranda BL, Aires IO, de Andrade Gomes DA, de Almeida Paula H, et al. Prognostic value of overhydration and bioelectrical impedance vector on short- and long-term outcomes in hospitalized patients with cancer. *Clin Nutr* 2024; **43:** 756-64. doi: 10.1016/j.clnu.2024.01.025

30. Ligibel JA, Chen W, Keshaviah A, Adloff K, Partridge A, Salinardi T, et al. The impact of an exercise intervention on body composition, fat distribution, and weight in breast cancer survivors. *J Clin Oncol* 2006; **24(18 Suppl):** 590. doi: 10.1200/jco.2006.24.18_suppl.590

31. Simillis C, Taylor B, Ahmad A, Lal N, Afxentiou T, Powar MP, et al. A systematic review and meta-analysis assessing the impact of body mass index on long-term survival outcomes after surgery for colorectal cancer. *Eur J Cancer* 2022; **172:** 237-51. doi: 10.1016/j.ejca.2022.05.018

32. Genton L, Hans D, Kyle UG, Pichard C. Dual-energy X-ray absorptiometry and body composition: differences between devices and comparison with reference methods. *Nutrition* 2002; **18:** 66-70. doi: 10.1016/s0899-9007(01)00700-6

33. Mlakar-Mastnak D, Blaž Kovač M, Terčelj M, Uhan S, Majdič N, Rotovnik Kozjek N. Effectiveness of nutritional intervention led by clinical dietitian in patients at risk of malnutrition at the primary healthcare level in Slovenia - evaluation study. *Zdr Varst* 2024; **63:** 81-8. doi: 10.2478/sjph-2024-0012

34. Champ CE, Peluso C, Carpenter DJ, Rosenberg J, Velasquez F, Annichine A, et al. EXERT-BC: prospective study of an exercise regimen after treatment for breast cancer. *Sports Med Int Open* 2024; **8:** a21930922. doi: 10.1055/a-2193-0922

35. Wells JCK, Williams JE, Fewtrell M, Singhal A, Lucas A, Cole TJ. A simplified approach to analysing bio-electrical impedance data in epidemiological surveys. *Int J Obes (Lond)* 2007; **31:** 507-14. doi: 10.1038/sj.ijo.0803441

36. Branco MG, Mateus C, Capelas ML, Pimenta N, Santos T, Mäkitie A, et al. Bioelectrical impedance analysis (BIA) for the assessment of body composition in oncology: a scoping review. *Nutrients* 2023; **15:** 4792. doi: 10.3390/nu15224792

37. Chen LK, Liu LK, Woo J, Assantachai P, Auyeung TW, Bahyah KS, et al. Sarcopenia in Asia: consensus report of the Asian Working Group for Sarcopenia. *J Am Med Dir Assoc* 2014; **15:** 95-101. doi: 10.1016/j.jamda.2013.11.025

Radiol Oncol 2026; 60(3): 307-322.
doi: 10.2478/raon-2026-0040

Netermična ablacija in vnos zdravilnih učinkovin z elektroporacijo. Indikacije, ki presežejo zdravljenje raka in srčnih bolezni

Miklavčič D, Cindrič H, Davalos RV, Deschamps F, Gehl J, Kos B, Kramar P, Kuhelj D, Meijerink MR, Soden D, Štabuc M, Serša G

Izhodišča. Pri obravnavi in zdravljenju na osnovi elektroporacije uporabljamo kratke visokonapetostne električne pulze, ki začasno povečajo prepustnost celične membrane. Na ta način omogočamo povečan vnos zdravilnih učinkovin neposredno v celice in netermično ablacijo mehkih tkiv. Med elektroporacijske terapije trenutno uvrščamo predvsem elektrokemoterapijo in ireverzibilno elektroporacijo za zdravljenje raka, ter gensko elektrotransfekcijo. Omenjena zdravljenja, predvsem prvi dve v klinični praksi uporabljamo že več kot tri desetletja, vendar je njihova uporaba v primerjavi s termičnimi ablacijskimi metodami še vedno omejena. Nasprotno pa se je srčna ablacija z elektroporacijo *(angl. pulsed field ablation)* po prvi odobritvi klinične naprave decembra 2023 v ZDA hitro uveljavila in doživela razcvet v klinični praksi.

Zaključki. V tem preglednem članku najprej podajamo kratek pregled trenutno uveljavljenih elektroporacijskih terapij v onkologiji in pri zdravljenju srčnih aritmij. Nato posebno pozornost namenimo novim terapevtskim pristopom, ki presegajo uveljavljene onkološke in kardiološke indikacije: endoskopski terapiji z elektroporacijo za zdravljenje sladkorne bolezni tipa 2, bronhialni reoplastiki za zdravljenje kroničnega bronhitisa, elektrosklerotерapiji z bleomicinom za zdravljenje žilnih malformacij, ablaciji z nanosekundnimi električnimi pulzi za zdravljenje benignih tvorb v ščitnici ter genski elektrotransfekciji. Nazadnje navedemo ključne ovire za širšo uveljavitev elektroporacije v klinični praksi, vključno s pomanjkanjem randomiziranih kliničnih raziskav, odsotnostjo validiranih postopkov za načrtovanje zdravljenja, neopredeljenim sistemom povračila stroškov v Evropi in neizdelano standardizacijo. Predlagamo ukrepe za pospešitev kliničnega prenosa.

Radiol Oncol 2026; 60(3): 323-331.
doi: 10.2478/raon-2026-0036

Zdravljenje s hadroni pri terapiji lokalnih ponovitev raka danke. Sistematski pregled

Perpar A, Georg P, Šečerov Ermenc A

Izhodišča. Rak debelega črevesa in danke je pogosto rakavo obolenje. Napredek kombiniranega zdravljenja je izboljšal izide. Približno 2–10 % bolnikov doživi lokalno ponovitev bolezni tudi po optimalni terapiji. V takšnih primerih je zdravljenje izbire reševalna kirurgija, vendar je pri posteriornih in lateralnih ponovitvah bolezni operacija povezana z visokim morbiditetnim tveganjem. Nekateri recidivi ostanejo neresektabilni tudi po neoadjuvantnem zdravljenju.

Materiali in metode. V sistematskem pregledu literature smo iskali raziskave o zdravljenju z obsevanjem z namenom ozdravitve, vključujoč konformno obsevanje s fotoni, stereotaktično obsevanje (*angl. stereotactic body radiation therapy*, SBRT) ter zdravljenje s hadroni. Namen pregleda je bilo opredeliti vlogo terapije s hadroni pri zdravljenju bolnikov z neresektabilnimi in inoperabilnimi lokalnimi recidivi raka danke, kjer je znižanje stadija bolezni po neoadjuvantnem zdravljenju manj verjetno. Pri teh bolnikih predstavlja obsevanje edino možno zdravilno terapijo.

Rezultat. Opredelili smo 32 raziskav, ki so izpolnjevale merila za našo analizo. SBRT in zdravljenje s hadroni sta dovoljevala obsevanje tarče z bistveno višjimi dozami brez sočasnega povečanega tveganja za zaplete zdravljenja.

Zaključki. Ablativni tehniki obsevanja, kot so stereotaktično obsevanje in zdravljenje s hadroni, pri neresektabilnih in inoperabilnih lokalnih ponovitvah raka danke lahko omogočata zdravljenje z namenom ozdravitve. Tako predstavljata alternativo kirurškemu zdravljenju. SBRT je primerna pri majhnih lokalnih in regionalnih ponovitvah bolezni, medtem ko zdravljenje s hadroni lahko uporabimo pri večjih ponovitvah in kompleksnejših oblik, ki segajo v več anatomskih predelov. Potrebne so nadaljnje raziskave, s katerimi bi omogočili razvrščanje bolnikov za najprimernejše obsevanje z namenom ozdravitve.

Radiol Oncol 2026; 60(3): 332-338.
doi: 10.2478/raon-2026-0023

Klinični pomen elementov v sledovih kot potencialnih bioloških označevalcev za diagnozo in napoved odziva na sistemsko zdravljenje pri gastrointestinalnih rakih

Reberšek M, Milačič Ščančar R, Ščančar J, Hribernik N

Izhodišča. Rak prebavil je eden najpogostejših rakov na svetu in je v napredovalem stanju še vedno neozdravljiv. Trenutno uporabljeni biološki označevalci imajo omejeno diagnostično vrednost za zgodnje odkrivanje bolezni in ponovitve, zato obstaja velika potreba po bolj občutljivih in specifičnih označevalcih za zgodnejšo diagnozo. Elementi v sledovih delujejo v številnih fizioloških in presnovnih procesih v človeškem telesu, njihova deregulacija homeostaze pa je vključena v karcinogenezo različnih vrst raka, vključno z rakom prebavil. V več bazičnih in predkliničnih preskušanj so ugotovili pomen elementov v sledovih in njihovo vlogo v bioloških celičnih procesih. Nedavne klinične raziskave z retrospektivnimi analizami pa kažejo, da je lahko povečanje ali zmanjšanje elementov v sledovih v telesu povezano z nastankom in razvojem številnih vrst raka, zato je kvantitativno dinamično določanje koncentracij elementov v sledovih v serumu med zdravljenjem in spremljanjem nova možnost za spremljanje učinkovitosti zdravljenja in za napovedovanje poteka bolezni.

Zaključki. Elementi v sledovih lahko služijo kot potencialni napovedni biološki označevalci za diagnozo in napoved odziva na sistemsko zdravljenje.

Radiol Oncol 2026; 60(3): 339-345.
doi: 10.2478/raon-2026-0045

Časovno opredeljeno vzorčenje sline kot nov zanesljiv biološki označevalec za ocenjevanje vnosa joda

Oblak A, Imperl J, Kolar M, Marolt G, Krhin B, Zaletel K, Gaberšček S

Izhodišča. Jod je esencialna sestavina ščitničnih hormonov, zato je zadosten vnos joda ključen za ustrezno delovanje ščitnice. Merjenje koncentracije joda v urinu je priporočena metoda za ocenjevanje vnosa joda na ravni populacije, vendar ima določene pomanjkljivosti. Jod izločamo z urinom in tudi s slino. Namen raziskave je bil ugotoviti, ali bi merjenje koncentracije joda v slini (*angl. salivary iodine concentration,* SLIC) lahko nadomestilo merjenje koncentracije joda v urinu oziroma celo zlati standard merjenja–izločanje joda v 24-urnem urinu. Ocenili smo tudi vpliv časa odvzema vzorca sline na vrednosti SLIC.

Subjekti in metode. V raziskavo smo vključili odrasle prostovoljce, ki so v skladu s strogim protokolom na isti dan doma zbrali 24-urni vzorec urina in vzorce sline. Koncentracijo joda v urinu in SLIC pred in po obrokih smo določili z metodo Sandell-Kolthoff, katere rezultati so primerljivi z metodo masne spektrometrije z induktivno sklopljeno plazmo.

Rezultati. Raziskava je zajela 104 zdravih udeležencev, pri katerih so bili vsi biološki vzorci uspešno in v celoti zbrani. Pomembno je, da nihče od njih ni jemal zdravil za zdravljenje bolezni ščitnice ali prehranskih dopolnil z jodom ter da nihče ni imel bolezni ščitnice. Ugotovili smo zelo dobro korelacijo med vrednostmi SLIC, izmerjenimi 60 in 120 minut po prvem in drugem obroku ter 30 minut po drugem, tretjem in četrtem obroku ter izločanjem joda v 24-urnem urinu ($P > 0,05$).

Zaključki. Ugotovili smo odlično korelacijo med vrednostmi SLIC in izločanje joda v 24-urnem urinu, pri čemer so bile vrednosti SLIC odvisne od časa odvzema vzorca in/ali števila zaužitih obrokov. Meritev SLIC bi lahko nadomestila meritev joda v 24-urnem urinu in predstavlja pomemben ter potencialen nov biološki označevalec za ocenjevanje vnosa joda.

Radiol Oncol 2026; 60(3): 346-355.
doi: 10.2478/raon-2026-0047

Vzorci ponovitve bolezni, ugotovljeni s pomočjo PET/CT z 18F-FDG, in izidi preživetja pri raku požiralnika. Izkušnje terciarnega centra

Kotur M, Odalović S, Petrović J, Pantić N, Grozdić Milojević I, Sobić Šaranović D, Sabljak P, Artiko V

Izhodišča. Namen raziskave je bil oceniti razlike med tremi skupinami bolnikov s sumom na ponovitev bolezni raka požiralnika na podlagi izvidov pozitronske emisijske tomografije/računalniške tomografije z 18F-fluorodeoksiglukozo (18F-FDG PET/CT). Ovrednotili smo polkvantitativne in kvantitativne parametre PET/CT ter serumske tumorske označevalce in oceniti njihov vpliv na preživetje brez napredovanja bolezni in na celokupno preživetje.

Bolniki in metode. V retrospektivno kohortno raziskavo smo vključili 77 bolnikov s pozitivnimi izvidi 18F-FDG PET/CT v obdobju od januarja 2014 do decembra 2025. Na podlagi izvidov 18F-FDG PET/CT smo bolnike razvrstili v tri skupine: G1 (posamezna lokoregionalna ponovitev bolezni), G2 (posamezne metastaze) in G3 (sočasna lokoregionalna ponovitev bolezni in metastaze). Med skupinami smo primerjali polkvantitativne in kvantitativne parametre preiskave 18F-FDG PET/CT, histopatološke značilnosti ter vrednosti tumorskih označevalcev v krvi. Pred analizo preživetja smo bolnike razvrstili v skupino z nizko in skupino z visoko vrednostjo glede na srednjo vrednost posameznega parametra.

Rezultati. Povišane vrednosti karcinoembrionalnega antigena (CEA) so bile znatno pogostejše v skupinah G2 in G3 v primerjavi s skupino G1 (p = 0,005), medtem ko pri vrednostih karbohidratnega antigena 19-9 (CA19-9) nismo ugotovili statistično pomembne razlike (p = 0,280). Med tremi skupinami smo ugotovili statistično pomembne razlike v vseh analiziranih parametrih 18F-FDG PET/CT, najvišje vrednosti pa so bile v skupini G3. Bolniki z nižjimi vrednostmi največjega standardiziranega prevzema radiofarmaka (*angl. maximal standardized uptake values*, SUVmax) in srednje vrednosti SUV (*angl.* SUVmean) so imeli statistično pomembno daljše preživetje brez napredovanja bolezni in celokupno preživetje. Prav tako so bile nižje vrednosti tumorskega volumna (*angl. metabolic tumor volume*, MTV) in celokupne vrednosti glikolize v leziji (*angl. total lesion glycolysis*, TLG) povezane s statistično pomembno daljšim preživetjem brez napredovanja bolezni in tudi daljšim celokupnim preživetjem, čeprav pri slednjem nismo ugotovili statistične pomembnosti.

Zaključki. Raziskave, v katerih so bolnike razvrščali glede na posamezne lokoregionalne ponovitve bolezni, posamezne metastaze in kombinacijo obojih na podlagi 18F-FDG PET/CT, so še vedno omejene. Rezultati zgoraj opisane raziskave kažejo, da lahko vzorci širjenja bolezni ter polkvantitativni in kvantitativni parametri 18F-FDG PET/CT predstavljajo pomembno napovedno vrednost pri bolnikih z rakom požiravnika.

Radiol Oncol 2026; 60(3): 356-366.
doi: 10.2478/raon-2026-0043

Morfološke značilnosti in semikvantitativni parametri dinamično kontrastno ojačanega magnetnoresonančnega slikanja (DCE-MRI) dojk, ki so povezane z napredovanjem v invazivni karcinom. Ugotovitve pri biopsijsko potrjenem duktalnem karcinomu *in situ* (DCIS) dojk

Urban V, Milošević Z, Bukumirić Z, Obradović K, Adžić N, Pavlović-Stanković D, Petković I, Šović I, Jovanić I, Spurnić I

Izhodišča. Namen raziskave je bil opredeliti slikovne napovedne dejavnike napredovanja v invazivni karcinom pri bolnicah z biopsijsko potrjenim duktalnim karcinomom *in situ* (DCIS), na podlagi morfoloških značilnosti in semikvantitativnih parametrov, pridobljenih z dinamičnim kontrastno ojačanim magnetnoresonančnim slikanjem dojk (*angl. dynamic contrast-enhanced breast magnetic resonance imaging,* DCE-MRI).

Bolniki in metode. V raziskavo smo vključili 90 zaporednih bolnic z biopsijsko potrjenim DCIS, pri katerih smo ugotovili pozitivne izvide, pridobljene s preiskavo standardnega celostnega protokola DCE-MRI dojk, in smo nato dokončno histopatološko potrdili diagnozo s kirurško ekscizijo. Bolnice, pri katerih smo pooperativno dokazali invazivni karcinom, smo primerjali s tistimi, kjer invazivnega karcinoma nismo ugotovili. Analizirali smo morfološke značilnosti (tip lezije, velikost, multifokalnost/multicentričnost, značilnosti T2-poudarjenih (T2W) slik in posnetke s turbo inverzijsko obnovitvijo in prikazom magnitude signala (*angl. turbo inversion recovery magnitude*, TIRM) ter razčlenili semikvantitativne parametre (izpiranje, največjo stopnjo ojačitve, pozno fazo časovno-intenzitetne krivulje *[angl. delayed phase of the time-intensity curve*, TIC], čas do največje ojačitve [*angl. time to peak*, TTP] in pozitivni integral ojačitve [*angl. positive enhancement integral*, PEI]).

Rezultati. Pri 55 bolnicah (61,1 %) nismo ugotovili invazivnega karcinoma, pri 35 bolnicah (38,9 %) pa smo invazivni karcinom našli ob pooperativni histopatološki preiskavi. Bolnice z invazivnim karcinom so imele pogosteje ne-masne ojačitve (*angl. non-mass enhancement*, NME) v kombinaciji z masno lezijo, večjo velikost lezije, multifokalno ali multicentrično bolezen, hiperintenzivnost na sekvenci T2W/TIRM, hitrejši dotok kontrastnega sredstva, višjo najvišjo stopnjo ojačitve, vzorce TIC z višjim vrhom ojačitve, platojem in izpiranjem, višji PEI ter krajši TTP. Multivariatna analiza je kot neodvisne napovednike invazivnega raka prepoznala NME v kombinaciji z maso, značilnosti pozne faze TIC in hiperintenzivnost TIRM.

Zaključki. Raziskava je potrdila, da lahko napovedni modeli, ki vključujejo morfološke značilnosti in semikvantitativne parametre DCE-MRI dojk, razvrstijo bolnice z biopsijsko potrjenim DCIS glede na verjetnost napredovanja v invazivni karcinom. Hiperintenzivnost na sekvencah TIRM se je izkazala kot eden od treh neodvisnih napovednikov invazivnega karcinoma in, kolikor nam je znano, doslej v tem kontekstu še ni bila opisana.

Radiol Oncol 2026; 60(3): 367-377.
doi: 10.2478/raon-2026-0029

Ali obstaja povezava med razmerjem intenzivnosti signalov pri 3T-MRI in molekularnimi podtipi raka dojke?

Tao Y, Chao H, Ren Y, Zheng W, Chen Y, Du L, Li H, Cui F

Izhodišča. Namen raziskave je bil preveriti, ali razmerje intenzivnosti signala (*angl. signal intensity ratio*, SIR) v tumorju in drugi kazalniki, pridobljeni z magnetno resonanco 3T, nudijo informacije v zvezi z molekularnimi podtipi raka dojke.

Bolniki in metode. Med januarjem 2022 in avgustom 2025 smo 256 bolnic z rakom dojke pregledali z MRI 3T. Morfološke značilnosti MRI in kvantitativne parametre (SIR T1, SIR T2, povprečni navidezni difuzijski koeficient (*angl. apparent diffusion coefficient*, ADC) iz difuzijsko uteženega slikanja [*angl. diffusion-weighted imaging*, DWI] ter premer tumorja) smo primerjali in izmerili glede na molekularne podtipe. Uporabili smo logistično regresijo, da bi ugotovili povezane parametre MRI in določili kombinirane parametre. Na koncu smo naredili analizo karakteristike delovanja sprejemnika (*angl. receiver operating characteristic*, ROC), da bi preverili diagnostično moč multivariatnega logističnega regresijskega modela.

Rezultati. V raziskavo smo vključili 263 lezij. Trojno negativni podtip je pokazal najvišjo vrednost SIR T2 in najnižjo vrednost SIR T1 ($p < 0,05$). Povprečne vrednosti ADC so bile najnižje pri trojno negativnem podtipu in najvišje pri podtipu, kjer so celice prekomerno izražale humani epidermalni rastni dejavnik (celice z receptorji HER2+) ($p < 0,001$). Premer tumorja pri podtipu HER2+ je bil najmanjši, pri trojno negativnem podtipu pa največji ($p < 0,001$). Neodvisni vplivni dejavniki so bili višji SIR T2 ($p = 0,017$) in večji premer tumorja ($p = 0,011$), povezana s trojno negativnem podtipom; SIR T1 ($p = < 0,01$) pa je bil edini kvantitativni parameter, povezan s podtipom HER2+. Kombinirani parameter (povprečna ADC + premer tumorja) je dosegel največjo površino pod krivuljo ROC (*angl. area under the ROC curve*, AUC) (AUC = 0,781) za ločevanje luminalnega A podtipa

Zaključki. Kvantitativni parametri MRI so povezani z molekularnimi podtipi raka dojke. Kombinirani parametri, ki vključujejo SIR T1 in SIR T2, kažejo potencialno diagnostično uporabnost pri razlikovanju tumorskih podtipov s HER2+, oziroma trojno negativnih podtipov. SIR T1 in SIR T2 lahko obogatita kvantitativne deskriptorje iz MRI dojk.

Radiol Oncol 2026; 60(3): 378-393.
doi: 10.2478/raon-2026-0037

Diagnostična uspešnost z difuzijsko uteženim slikanjem celotnega telesa pri določanju stadija raka požiralnika. Primerjalna raziskava s PET-CT

Xu X, Yu R, Ma Q, Yin T, Chen H, Qian Y, Li H, Qi R, Xu Y

Izhodišča. Natančno predoperativno določanje stadija je ključnega pomena za načrtovanje zdravljenja in za predvidevanje poteka bolezni pri raku požiralnika. Pozitronska emisijska tomografija v kombinaciji s računalniško tomografijo (PET-CT) je trenutno najnatančnejša metoda za določanje stadija, medtem ko je pomen difuzijsko obteženega slikanja celotnega telesa (*angl. whole-body diffusion-weighted imaging*, WB-DWI) – tehnike funkcionalne magnetne resonance (MRI) brez sevanja – še vedno nejasna. Namen raziskave je bil neposredno primerjati diagnostično natančnost WB-DWI in PET-CT in pri začetni diagnozi bolnikov z rakom požiralnika in smo zato primerjali natančnost obeh metod pri določitvi stadija TNM.

Bolniki in metode. Zbrali smo podatke 96 bolnikov z rakom požiralnika, ki smo jih med januarjem 2023 in januarjem 2025 v Ljudski bolnišnici Haian slikovno in patomorfološko diagnosticirali. Motilne dejavnike med skupinama smo uravnotežili z metodo ujemanja na podlagi nagnjenostnega indeksa (*angl. Propensity Score Matching*, PSM). Na ta način smo oblikovali obe kohorti: skupino WB-DWI (n = 32) in skupino PET-CT (n = 32). S pooperativno patološko preiskavo in/ali kliničnim 6-mesečnim sledenjem bolnikov smo ocenili: natančnost stadijev T, občutljivost/specifičnost pri odkrivanju patoloških bezgavk (stadij N) in oddaljenih metastaz (stadiji M) ter natančnost stadijev v celoti, razmerje med signalom in šumom na sliki, trajanje preiskave ter ujemanje med opazovalci (vrednost Kappa). Izračunali smo občutljivost, specifičnost, pozitivno napovedno vrednost, negativno napovedno vrednost in natančnost. Diagnostična zmogljivost smo analizirali z uporabo krivulj ROC, površine pod krivuljo (*angl. area under the curve,* AUC) pa smo primerjali z DeLongovim testom.

Rezultati. WB-DWI in PET-CT sta pri raku požiralnika pokazala primerljivo celokupno natančnost pri določanju stadija (84,4 % proti 87,5 %, $p > 0,05$). Pri določanju stadija N je PET-CT pokazal višjo občutljivost (90,6 % proti 78,1 %, $p < 0,05$), medtem ko sta obe metodi pokazali enako specifičnost (87,5 %). Pri odkrivanju oddaljenih metastaz je PET-CT pokazal nekoliko višje stopnje odkrivanja in natančnost kot WB-DWI, čeprav razlike niso bile statistično pomembne. WB-DWI je pokazal nižjo natančnost pri določanju stadija T (71,9 % proti 84,4 %, $p < 0,05$). Slike WB-DWI so pokazale statistično pomembno nižje razmerje signal-šum kot PET-CT ($p < 0,01$), vendar je bilo trajanje preiskave krajše in je pokazalo ujemanje med opazovalci (Kappa > 0,60, $p < 0,001$).

Zaključki. Metoda WB-DWI kaže primerljivo celokupno natačnost kot PET-CT pri določanju stadija raka požiralnika. Čeprav sta njena občutljivost in natančnost nekoliko nižji, sta zaradi odsotnosti sevanja, ter visoke specifičnosti primerna dopolnitev ali alternativa preiskavi PET-CT za določene skupine bolnikov. Ti izsledki omogočajo podlago za optimalne klinične odločitve.

Radiol Oncol 2026; 60(3): 394-401.
doi: 10.2478/raon-2026-0039

Primerjava vizualne in avtomatizirane ocene CT-perfuzije za napoved izida pri bolnikih z možgansko kapjo v sprednjem krvnem obtoku, zdravljenih z mehansko trombektomijo

Rigler I, Gspan T, Longo A, Pretnar Oblak J

Izhodišča. Prognostična vrednost vizualne ocene CT-perfuzije (CTP) pri napovedovanju kliničnega izida je bila že dokazana pri bolnikih z ishemično možgansko kapjo, zdravljenih z mehansko trombektomijo (MT). Kljub temu je avtomatizirana analiza CTP postala prevladujoča metoda vrednotenja perfuzije v klinični praksi. Namen raziskave je bil primerjati prognostično natančnost vizualnega ocenjevanja perfuzijskih kart CTP z avtomatizirano analizo CTP pri napovedovanju kliničnega izida pri bolnikih z možgansko kapjo v sprednjem krvnem obtoku, zdravljenih z MT.

Bolniki in metode. Retrospektivno smo analizirali zaporedne bolnike z zaporo velike možganske arterije v sprednjem krvnem obtoku, zdravljene z MT. Izhodiščno slikanje je vključevalo nativni CT možganov, CT angiografijo (CTA) z oceno kolateralnega obtoka ter CTP. Karte časa do vrha perfuzije (*time to peak*, TTP) smo vizualno ocenili po štiristopenjski ordinalni lestvici glede na ocenjeni delež penumbre. Avtomatizirano analizo CTP smo izvedli s programom syngo.via (SYV) z uporabo privzetih nastavitev ter rezultate razvrstili po primerljivi ordinalni lestvici. Primarni opazovani dogodek je bil ugoden funkcionalni izid po 90 dneh, opredeljen kot modificirana Rankinova lestvica (mRS) ≤ 3.

Rezultati. V raziskavo smo vključili 579 bolnikov. Ujemanje med vizualno in avtomatizirano oceno CTP je bilo zmerno ($\kappa = 0{,}36$). Obe metodi sta bili statistično značilno povezani z ugodnim funkcionalnim izidom ($p < 0{,}01$), pri čemer je vizualno ocenjevanje pokazalo nekoliko močnejšo povezanost (Pearson $\chi^2 = 30$ proti 22). V multivariatnih modelih je vizualna ocena CTP ostala neodvisen napovedni dejavnik, medtem ko je avtomatizirana analiza CTP po vključitvi ocene kolateralnega obtoka izgubila statistično značilnost.

Zaključki. Vizualno ocenjevanje perfuzijskih kart TTP je pokazalo nekoliko boljšo prognostično zmogljivost kot avtomatizirana analiza CTP s programom SYV. Vizualna ocena CTP je preprosto, dostopno in klinično uporabno orodje tako za odločanje o zdravljenju kot za napovedovanje kliničnega izida pri bolnikih z možgansko kapjo v sprednjem krvnem obtoku, zdravljenih z mehansko trombektomijo.

Radiol Oncol 2026; 60(3): 402-415.
doi: 10.2478/raon-2026-0049

Imunska aktivacija, ki jo povzroča luciferaza, preprečuje nastanek ortotopičnega osteosarkoma K7M2luc pri miših BALB/c

Kupčič S, Kamenšek U, Čemažar M, Lampreht Tratar U

Izhodišča. Uporaba mišjih ortotopskih tumorskih modelov zahteva uporabo celic, ki izražajo luciferazo, kar omogoča *in vivo* bioluminiscenčno slikanje. Vendar luciferaza lahko sproži imunski odziv, ki ovira nastanek tumorja.

Materiali in metode. V celice K7M2 divjega tipa (*angl. wild-type*, wt) smo vnesli gen za luciferazo in ovrednotili njihovo rast *in vitro*. Nato smo celice ortotopično vsadili v miši BALB/c in ob neuspešnem nastanku tumorja preučili sistemske in lokalne mehanizme za zaviranje rasti tumorja.

Rezultati. Vse preučevane celične linije so imele primerljiv čas podvojitve *in vitro* pri 24 in 48 urah. Kljub temu se je linija K7M2luc E5 razlikovala od linij K7M2luc A7 in K7M2 wt po precej višji stopnji proliferacije po 72 urah (35-krat, 15-krat in 17-krat). *In vivo* nobena od obeh celičnih linij, ki sta izražali luciferazo, ni uspela tvoriti tumorjev, medtem ko je imela linija K7M2 wt 100-odstotno stopnjo uspešnosti. Da bi raziskali vzrok, smo preučili sistemsko in lokalno celično posredovano imunost. Miši v skupinah K7M2luc A7 in K7M2luc E5 so imele višjo spremembo v številu (5 ± 0,8 in 6 ± 1,05) splenocitov, ki izločajo GrB, v primerjavi z naivnimi mišmi (1 ± 0,2). V mikrookolju kosti so skupine z luciferazo pokazale povečano število celic, ki izločajo GrB, in $CD8^+$ T-celic v primerjavi z mišmi K7M2 wt in naivnimi mišmi.

Zaključki. Rezultati opisane raziskave kažejo, da luciferaza aktivira odzive citotoksičnih T-celic, ki so sposobne eliminirati vsajene celice. Nastanek tumorja se je ponovno vzpostavil pri imunodeficientnih miših brez $CD8^+$ celic, kar potrjuje imunsko posredovano zavrnitev.

Radiol Oncol 2026; 60(3): 416-426.
doi: 10.2478/raon-2026-0042

Gen *EPHA3*, katerega ekspresija je povečana v histoloških podtipih gastrointestinalnih stromalnih tumorjev z visokim tveganjem, spodbuja napredovanje GIST

Wei H, Zhao J, Wang H, Guo L, Liu Y, Wang C, Yang L, Qi Z, Tian W, Cao L, Gao Y

Izhodišča. Namen raziskave je bil proučiti ekspresijo in funkcionalno vlogo receptorja EPH A3 (EPHA3) v gastrointestinalnih stromalnih tumorjih (GIST) z visokim tveganjem ter njegov morebitni pomen pri napredovanju tumorja.

Materiali in metode. Opravili smo imunohistokemično (IHC) analizo za oceno ekspresije *EPHA3* v pilotni kohorti kliničnih vzorcev GIST z različnimi stopnjami tveganja. Biološke funkcije EPHA3 *in vitro* smo ocenili z uporabo testov EdU, tvorbe kolonij, apoptoze, celjenja ran in testom *transwell* (*angl. Transwell assay*) v celicah GIST-430 z izklopljenim genom *EPHA3*. Poleg tega smo uporabili analizo sekveniranja RNK (*angl. sequencing RNA*, RNA-seq), da bi prepoznali različno izražene gene in povezane signalne poti po izklopitvi *EPHA3*.

Rezultati. Ugotovili smo, da je izražanje *EPHA3* povečano v vzorcih GIST z visokim tveganjem v primerjavi z vzorci GIST z zmernim tveganjem. Testi izgube funkcije so pokazali, da je izklopitev EPHA3 *in vitro* zavirala celično proliferacijo in migracijo, hkrati pa spodbujala apoptozo. Analiza obogatitve signalnih poti je nakazala, da je izražanje *EPHA3* povezano s celično adhezijo, interakcijo z ekstracelularnim matriksom in fenotipskim preoblikovanjem, povezanim z mezenhimalnim tkivom.

Zaključki. Ugotovitve raziskave kažejo, da je izražanje gena *EPHA3* pri GIST-ih z visokim tveganjem povečano in da ta gen prispeva k agresivnemu celičnemu vedenju *in vitro*. Preliminarni podatki v raziskavi kažejo, da bi gen *EPHA3* lahko imel vlogo pri malignem napredovanju GIST-ov, čeprav je potrebno njegovo klinično uporabnost kot biološkega označevalca še dodatno potrditi v večjih kohortah

Radiol Oncol 2026; 60(3): 427-435.
doi: 10.2478/raon-2026-0051

Elektrokemoterapija kožnih tumorjev v kombinaciji z obsevanjem tumorja pred ali po zdravljenju. Izvedljivost, varnost in učinkovitost

Bertino G, Minuti M, Gehl J, Kis E, Nassabi H, Grieco MP, Riva G, Mascherini M, De Terlizzi F, Čemažar M, Serša G

Izhodišča. Elektrokemoterapijo (ECT) lahko pri bolnikih izvedemo pred obsevanjem tumorja ali pri ponovitvi bolezni po predhodnem obsevanju. V raziskavi smo ocenili izvedljivost, varnost in učinkovitost kombiniranega zdravljenja z ECT in obsevanjem tumorja (radioterapijo, RT) pri različnih tumorjih v predelu glave in vratu.

Bolniki in metode. Za kohortno analizo smo bolnike izbrali iz podatkovne zbirke *Insp-ECT* na podlagi naslednjih meril: prisotnost lezij na glavi in vratu katerega koli histološkega izvora, zdravljenje z ECT in RT v poljubnem zaporedju ter največ 12-mesečni razmik med obema zdravljenjema. Bolnike smo zdravili z ECT, ki ji je sledila RT (ECT → RT) ali z RT, ki ji je sledila ECT (RT → ECT), v obeh primerih je bil razlog, ker prvo zdravljenje ni privedlo do popolnega odziva. Časovni razmik v primeru ECT → RT je znašal 5,3 meseca, v primeru RT → ECT pa 7,6 meseca. Najkrajši časovni razmik med zdravljenjema je bil en mesec.

Rezultati. Zdravljenje z ECT z bleomicinom je bilo izvedljivo pri vseh bolnikih, ne glede na to, ali smo jih zdravili pred ali po RT. V raziskavo smo vključili 37 bolnikov z lezijami na glavi in vratu. Kombinirano zdravljenje smo izvedli predvsem pri starejših bolnikih, starih od 59 do 96 let, s srednjo starostjo nad 80 let. Pomembno je, da je bil v skupini ECT → RT glavni razlog za RT delni odziv (67 %) po ECT. V skupini RT → ECT pa je bil glavni razlog za naknadno ECT v 58 % primerih stagnacija ali napredovanje bolezni. V obeh skupinah so se zmanjšali lokalni simptomi, kot so razjede, neprijeten vonj in gnojenje tumorjev. V skupini ECT → RT je bil kratkoročni odziv po 2 mesecih visok, saj smo zabeležili 88 % objektivnih odgovorov. Nasprotno pa je bil v skupini RT → ECT ta delež znatno nižji in je znašal 58 %. Dolgoročni odzivi, merjeni po 2 letih spremljanja z preživetjem brez napredovanja bolezni, so bili prav tako znatno višji v skupini ECT → RT (68 %) v primerjavi s skupino RT → ECT (20 %). To je privedlo do znatno boljšega celokupnega preživetja brez napredovanja bolezni v skupini ECT → RT (p = 0,0232).

Zaključki. Kombinirano zdravljenje z ECT in RT je izvedljivo, varno in učinkovito pri starejših bolnikih. Rezultati kažejo, da ima lahko ECT poseben pomen kot neoadjuvantno zdravljenje pred RT, zlasti pri obsežnih, ulceriranih ali simptomatskih lezijah v tej populaciji.

Radiol Oncol 2026; 60(3): 436-441.
doi: 10.2478/raon-2026-0041

Citoredukcija in hipertermična intraperitonealna kemoterapija pri peritonealnih zasevkih kolorektalnega raka. Izkušnje terciarne ustanove

Pilko G, Petrič R

Izhodišča. Peritonealni zasevki kolorektalnega raka so povezani s slabo napovedjo poteka bolezni. Citoreduktivna kirurgija v kombinaciji s hipertermično intraperitonealno kemoterapijo (HIPEC) je ena od možnosti zdravljenja pri izbranih bolnikih, vendar njena vloga ostaja predmet razprav. Namen raziskave je bil oceniti učinkovitost in varnost citoredukcije v kombinaciji s HIPEC Na Onkološkem inštitutu Ljubljana.

Bolniki in metode. V retrospektivno raziskavo smo vključili bolnike s peritonealnimi zasevki kolorektalnega raka, ki smo jih zdravili s citoredukcijo in postopkom HIPEC med leti 2009 in 2024. Pri vseh bolnikih smo preoperativno naredili preiskavi računalniško tomografijo in/ali magnetno resonanco ter vsakega bolnika obravnavali na multidisciplinarnem konziliju. Obseg bolezni smo ocenili z indeksom peritonealne karcinomatoze (*angl. Peritoneal Cancer Index*, PCI), popolnost citoredukcije pa z indeksom popolnosti citoredukcije (*angl. completeness of cytoreduction*, CC). HIPEC smo izvedli z oksaliplatinom (360 mg/m² pri 42 °C 90 minut). Primarni opazovani izid raziskave je bilo celokupno preživetje, sekundarna izida pa preživetje brez znakov bolezni in pooperativna obolevnost.

Rezultati. V raziskavo smo vključili 50 bolnikov (povprečna starost 54 let). Popolno citoredukcijo (CC-0/1) smo dosegli v 88 % primerov, srednji PCI pa je znašal 8,33. Hudi zapleti so se pojavili pri 18 % bolnikov, 30-dnevne umrljivosti ni bilo. Po srednjem obdobju spremljanja, ki je trajalo 34 mesecev, je bilo srednje celokupno preživetje 49 mesecev; eno- in petletno preživetje sta znašali 96 % in 54 %. Srednje preživetje brez znakov bolezni je bilo 14 mesecev. V univariatni analizi so bili PCI, CC in indeks predhodnih kirurških posegov (*angl. prior surgical score*, PSS) povezani s celokupnim preživetjem, v multivariatni analizi pa sta PCI in CC ostala neodvisna napovedna dejavnika.

Zaključki. Citoredukcija v kombinaciji s postopkom HIPEC predstavlja učinkovito metodo zdravljenja pri skrbno izbranih bolnikih s peritonealnimi zasevki kolorektalnega raka in s sprejemljivo stopnjo zapletov. Nizek PCI in popolna citoredukcija sta ključna napovednika boljšega preživetja.

Radiol Oncol 2026; 60(3): 442-449.
doi: 10.2478/raon-2026-0044

Ali starost vpliva na kirurške in onkološke izide po kurativni resekciji pri raku želodca. Desetletna retrospektivna raziskava terciarnega centra

Horvat M, Potrč S, Arslani N

Izhodišča. Rak želodca ostaja v Sloveniji veliko breme za zdravstveni sistem, zlasti med starejšimi bolniki. Zaradi vse daljše življenjske dobe pričakujemo, da bomo vedno več bolnikov, starih 70 let ali več, zdravili kirurško z namenom ozdravitve. V raziskavi smo primerjali klinične, kirurške in onkološke izide med starejšimi (≥ 70 let) in mlajšimi (< 70 let) bolniki z rakom želodca.

Bolniki in metode. V monocentrično retrospektivno kohortno raziskavo smo vključili bolnike, ki smo jih med letoma 2015 in 2024 operirali zaradi adenokarcinoma želodca z namenom ozdravitve. Bolnike smo razvrstili po starosti. Analizirani smo demografske podatke, spremljajoče bolezni, značilnosti tumorja, kirurške spremenljivke, pooperativne zaplete (uporabili klasifikacijo Clavien-Dindo) in celokupno preživetje. Preživetje smo ocenjevali s pomočjo metode Kaplan-Meier, napovedne dejavnike preživeta pa s Coxovo regresijo sorazmernih tveganj.

Rezultati. Vključili smo skupno 433 bolnikov (229 < 70 let; 204 ≥ 70 let). Starejši bolniki so imeli višje stopnje preoperativnega stanja po lestvici Ameriškega združenja anesteziologov (ASA) in večjo pogostnost hudih pooperativnih zapletov. Delež resekcij R0 in delež radikalnosti kirurškega posega sta bila primerljiva med skupinama, vendar smo pri starejši bolniki pogosteje naredili subtotalno gastrektomijo in manj obsežno limfadenektomijo. Perioperativno kemoterapijo so pogosteje prejeli mlajši bolniki. Značilnosti tumorja in porazdelitev stopenj TNM so bile podobne med obema skupinama. Petletno celokupno preživetje je bilo znatno nižje pri starejših bolnikih (37,3 % proti 59,6 %, p < 0,001).

Zaključki. Zgolj kronološka starost bolnika ne bi smela biti razlog za zavrnitev operacije raka želodca z namenom ozdravitve. Pri skrbno izbranih starejših bolnikih je mogoče doseči sprejemljive kirurške in onkološke izide, kar poudarja pomen biološke starosti in funkcionalnega stanja pri odločanju o zdravljenju.

Radiol Oncol 2026; 60(3): 450-458.
doi: 10.2478/raon-2026-0050

Preživetje bolnikov z napredovalim nedrobnoceličnim pljučnim rakom IV. stadija in visoko izraženostjo PD-L1, ki so prejeli pembrolizumab kot zdravljenje prvega reda. Podatki iz vsakodnevne klinične prakse

Stojšić V, Zarić B, Simurdić P, Kovačević T, Bokan D, Djekić Malbaša J, Šarčev T, Stojanović G, Bursać D, Nikolin B

Izhodišča. Monoterapija s pembrolizumabom je standardno zdravljenje prve izbire pri bolnikih z rakom pljuč IV. stadija in izraženostjo liganda programirane celične smrti 1 (*angl. programmed death ligand 1*, PD-L1) ≥ 50 %. Ali višja stopnja izraženosti PD-L1 napoveduje večjo korist zdravljenja s pembrolizumabom, ostaja predmet razprav.

Bolniki in metode. V raziskavi smo analizirali klinične in patohistološke značilnosti, celokupni delež odgovorov ter izide preživetja pri bolnikih z nedrobnoceličnim rakom pljuč in izraženostjo PD-L1 ≥ 50 %, ki so v okviru vsakodnevne klinične prakse prejeli prvi red zdravljenja s pembrolizumabom. Namen raziskave je bil ugotoviti, ali stopnja izraženosti PD-L1 vpliva na kazalnike preživetja.

Rezultati. V raziskavo smo vključili 51 zaporednih bolnikov z nedrobnoceličnim rakom pljuč. Srednje preživetja brez napredovanja bolezni je bilo 12,0 meseca (95 % interval zaupanja [IZ] 7,7–16,2 meseca), srednje celokupno preživetje pa 21,0 meseca (95 % IZ 9,6–32,3 meseca). Glede na izraženost PD-L1 smo bolnike razdelili v dve skupini: v prvo skupino tiste z izraženostjo PD-L1 50–79 %, v drugo pa z izraženostjo > 80 %. Med skupinama sta bili statistično značilni razliki v porazdelitvi spola (p = 0,029) in stadiju bolezni (p = 0,039). Med skupinama ni bilo statistično značilnih razlik v preživetju brez napredovanja bolezni (p = 0,548) ali celokupnem preživetju (p = 0,153).

Zaključki. Raziskava ni potrdila povezave med višjo izraženostjo PD-L1 in boljšimi izidi preživetja. Omejitev raziskave je bilo razmeroma majhno število bolnikov, zato bi se lahko v prihodnje rezultati razlikovali, če bo analiza zajela večje število bolnikov z večjim naborom podatkov iz vsakodnevne klinične prakse.

Radiol Oncol 2026; 60(3): 459-470.
doi: 10.2478/raon-2026-0046

Analiza učinkov individualizirane prehrane in telesne dejavnosti na telesno sestavo med zdravljenjem bolnic z rakom dojk

Blaž R, Kovač M, Rotovnik Kozjek N

Izhodišča. Podhranjenost in izguba skeletne mišične mase sta pri bolnicah rakom dojk pogosti ter predstavljata negativna prognostična dejavnika. Kombinirani prehranski in vadbeni ukrepi lahko med zdravljenjem prispevajo k ohranjanju telesne sestave. Namen raziskave je bil oceniti učinke ciljno usmerjene prehranske in gibalne intervencije na telesno sestavo, določeno z bioelektrično impedančno analizo (BIA), pri bolnicah z rakom dojk med zdravljenjem, razvrščenih glede na izhodiščno prehransko stanje po merilih Global Leadership Initiative on Malnutrition (GLIM).

Bolnice in metode. V retrospektivno analizo pilotne študije OREH je bilo vključenih 287 bolnic v intervencijski skupini in 194 bolnic v kontrolni skupini. Pri vseh bolnicah so bile meritve z BIA opravljene ob vključitvi v raziskavo ter po 6 in 12 mesecih. Podhranjene bolnice (GLIM-pozitivne) v obeh skupinah so v okviru standardne obravnave prejele individualizirano prehransko svetovanje. GLIM-negativne bolnice v intervencijski skupini so prejele preventivno prehransko svetovanje prek spletnih predavanj. Vse bolnice v intervencijski skupini so sodelovale v nadzorovani skupinski telesni vadbi. Razlike v parametrih BIA (indeks puste telesne mase – FFMI, fazni kot, maščobna masa, skupna telesna voda in indeks telesne mase) med tretjo in prvo meritvijo so bile primerjane z Welchovim t-testom, pri čemer so bile vrednosti *p* prilagojene po metodi Bonferroni–Holm.

Rezultati. Med intervencijsko in kontrolno skupino v 12-mesečnem obdobju spremljanja niso bile ugotovljene statistično značilne razlike v parametrih telesne sestave. Prilagojena vrednost *p* za FFMI je znašala 0,2 pri GLIM-pozitivnih bolnicah in 1,0 pri GLIM-negativnih bolnicah. Pri GLIM-pozitivnih bolnicah v intervencijski skupini je bil opažen trend večjega povečanja FFMI v primerjavi s kontrolno skupino (povprečna razlika 0,30; 95 % interval zaupanja 0,05–0,54; neprilagojena vrednost $p = 0,017$), vendar po popravku zaradi večkratnih primerjav ta razlika ni ostala statistično značilna.

Zaključki. Kombinirana prehranska in vadbena intervencija ni pomembno izboljšala parametrov telesne sestave, določenih z BIA. Kljub temu trend izboljšanja FFMI pri GLIM-pozitivnih bolnicah, ki so prejele individualizirano prehransko svetovanje, nakazuje, da so lahko prilagojeni pristopi učinkovitejši od skupinskih intervencij. Prihodnje raziskave bi morale vključevati individualizirane prehranske programe in programe vadbe za moč, da bi optimizirali izide telesne sestave pri bolnicah z rakom dojk.

Fundacija ''Docent dr. J. Cholewa''
je neprofitno, neinstitucionalno in nestrankarsko
združenje posameznikov, ustanov in organizacij, ki želijo
materialno spodbujati in poglabljati raziskovalno
dejavnost v onkologiji.

Dunajska 106
1000 Ljubljana
IBAN: SI56 0203 3001 7879 431

PR/BSI/BEN/2026/005

TANTUM VERDE®

benzidaminijev klorid

Za lajšanje bolečine in oteklin v ustni votlini in žrelu, ki so posledica radiomukozitisa

Bistvene informacije iz Povzetka glavnih značilnosti zdravila

Tantum Verde 1,5 mg/ml oralno pršilo, raztopina
Tantum Verde 3 mg/ml oralno pršilo, raztopina

Sestava 1,5 mg/ml: 1 ml raztopine vsebuje 1,5 mg benzidaminijevega klorida, kar ustreza 1,34 mg benzidamina. V enem razpršku je 0,17 ml raztopine. En razpršek vsebuje 0,255 mg benzidaminijevega klorida, kar ustreza 0,2278 mg benzidamina. **Sestava 3 mg/ml:** 1 ml raztopine vsebuje 3 mg benzidaminijevega klorida, kar ustreza 2,68 mg benzidamina. V enem razpršku je 0,17 ml raztopine. En razpršek vsebuje 0,51 mg benzidaminijevega klorida, kar ustreza 0,4556 mg benzidamina. **Terapevtske indikacije:** Samozdravljenje: Lajšanje bolečine in oteklin pri vnetju v ustni votlini in žrelu, ki so lahko posledica okužb in stanj po operaciji. Po nasvetu in navodilu zdravnika: Lajšanje bolečine in oteklin v ustni votlini in žrelu, ki so posledica radiomukozitisa. **Odmerjanje in način uporabe:** Uporaba: 2- do 6-krat na dan (vsake 1,5 do 3 ure). Odmerjanje 1,5 mg/ml: Odrasli: 4 do 8 razpršков 2- do 6-krat na dan. Pediatrična populacija: Mladostniki, stari od 12 do 18 let: 4-8 razpršков 2- do 6-krat na dan. Otroci od 6 do 12 let: 4 razprški 2- do 6-krat na dan. Otroci, mlajši od 6 let: 1 razpršek na 4 kg telesne mase; do največ 4 razprške 2- do 6-krat na dan. Odmerjanje 3 mg/ml: Odrasli: 2 do 4 razprški 2- do 6-krat na dan. Pediatrična populacija: Mladostniki, stari od 12 do 18 let: 2 do 4 razprški 2- do 6-krat na dan. Otroci od 6 do 12 let: 2 razprška 2- do 6-krat na dan. Otroci, mlajši od 6 let: 1 razpršek na 8 kg telesne mase; do največ 2 razprška 2- do 6-krat na dan. Starejši bolniki, bolniki z jetrno okvaro in bolniki z ledvično okvaro: niso potrebni posebni previdnostni ukrepi. Trajanje zdravljenja ne sme biti daljše od 7 dni. Način uporabe: Za orofaringealno uporabo. Zdravilo se razprši v usta in žrelo. **Kontraindikacije:** Preobčutljivost na učinkovino ali katero koli pomožno snov. **Posebna opozorila in previdnostni ukrepi:** Pri nekaterih bolnikih lahko resne bolezni povzročijo ustne/žrelne ulceracije. Če se simptomi v treh dneh ne izboljšajo, se mora bolnik posvetovati z zdravnikom ali zobozdravnikom, kot je primerno. Uporaba benzidamina ni priporočljiva za bolnike s preobčutljivostjo na salicilno kislino ali druga nesteroidna protivnetna zdravila. Pri bolnikih, ki imajo ali so imeli bronhialno astmo, lahko pride do bronhospazma. Pri takih bolnikih je potrebna previdnost.
To zdravilo vsebuje 13,6 mg alkohola (etanola) v enem razpršku (0,17 ml), kar ustreza manj kot 0,34 ml piva oziroma 0,14 ml vina. Majhna količina alkohola v zdravilu ne bo imela nobenih opaznih učinkov. To zdravilo vsebuje metilparahidroksibenzoat (E218). Lahko povzroči alergijske reakcije (lahko zapoznele). To zdravilo vsebuje manj kot 1 mmol (23 mg) natrija v enem razpršku (0,17 ml), kar v bistvu pomeni 'brez natrija'. Zdravilo vsebuje aromo poprove mete z benzilalkoholom, cinamilalkoholom, citralom, citronelolom, geraniolom, izoevgenolom, linalolom, evgenolom in D-limonen, ki lahko povzročijo alergijske reakcije.
Zdravilo z jakostjo 3 mg/ml vsebuje makrogolglicerol hidroksistearat 40. Lahko povzroči želodčne težave in drisko.
Medsebojno delovanje z drugimi zdravili in druge oblike interakcij: Študij medsebojnega delovanja niso izvedli. **Plodnost, nosečnost in dojenje**: Nosečnost: Ni kliničnih podatkov o uporabi zdravila Tantum Verde med nosečnostjo. V tretjem trimesečju nosečnosti lahko sistemska uporaba zaviralcev prostaglandin-sintetaze povzroči kardiopulmonalno in ledvično toksičnost pri plodu. Ob koncu nosečnosti se lahko pri materi in otroku podaljša čas krvavitve, porod pa se lahko zakasni. Ni znano, ali je sistemska izpostavljenost zdravilu Tantum Verde, dosežena po topikalni uporabi, lahko škodljiva za zarodek ali plod. Zato se Tantum Verde med nosečnostjo ne sme uporabljati, razen če je to nujno potrebno. Če se uporablja, mora biti odmerek čim manjši, trajanje zdravljenja pa čim krajše. Dojenje: O uporabi benzidamina pri doječih ženskah ni zadostnih podatkov. Izločanja v mleko niso preučevali. Glede učinkov na dojenje (glejte poglavje 5.3), študije na živalih niso zadostne. Možno tveganje za ljudi ni znano. Uporaba zdravila Tantum Verde med dojenjem ni priporočljiva. Plodnost: S študijami reproduktivne funkcije so ugotovili, da benzidamin nima učinka na plodnost in ne vpliva na sposobnost razmnoževanja. **Vpliv na sposobnost vožnje in upravljanja strojev:** Zdravilo v priporočenem odmerku nima vpliva na sposobnost vožnje in upravljanja strojev. **Neželeni učinki:** Neznana pogostnost (ni mogoče oceniti iz razpoložljivih podatkov): anafilaktične reakcije, preobčutljivostne reakcije, odrevenelost, laringospazem, suha usta, navzea in bruhanje, oralna hipestezija, angioedem, fotosenzitivnost, pekoč občutek v ustih. Neposredno po uporabi se lahko pojavi občutek odrevenelosti v ustih in v žrelu. Ta učinek se pojavi zaradi načina delovanja zdravila in po kratkem času izgine.
Način in režim izdaje zdravila: BRp-Izdaja zdravila je brez recepta v lekarnah in specializiranih prodajalnah. **Imetnik dovoljenja za promet:** Aziende Chimiche Riunite Angelini Francesco – A.C.R.A.F. S.p.A., Viale Amelia 70, 00181 Rim, Italija.
Datum zadnje revizije besedila: 1,5 mg/ml oralno pršilo, raztopina 06. 11. 2025 in 3 mg/ml oralno pršilo, raztopina 24. 11. 2025.

Pred svetovanjem ali izdajo preberite celoten Povzetek glavnih značilnosti zdravila.

Samo za strokovno javnost.
Datum priprave informacije: julij 2026
Odgovoren za trženje: Bonifar d.o.o.

ANGELINI

REŽIM ZDRAVLJENJA, KI GA PRIPOROČAJO SMERNICE[1-5]

SEZITE DLJE

z zdraviloma Imfinzi in Imjudo

rGC/GEJC

Perioperativno zdravljenje adenokarcinoma želodca ali gasteroezofagealnega prehoda v 1. liniji:

IMFINZI® + FLOT[6]

VEČ KOT 2/3 BOLNIKOV ŽIVIH PO 3 LETIH z režimom IMFINZI + FLOT kot neoadjuvantno in adjuvantno zdravljenje, ki mu sledi adjuvantna monoterapija z zdravilom IMFINZI v primerjavi z FLOT + placebo[7]

HR = 0,78 (95 % IZ; 0,63-0,96)

uHCC

Zdravljenje neresektabilnega hepatoceličnega karcinoma v 1. liniji:

IMFINZI® + IMJUDO®[6, 8]

2X VEČ BOLNIKOV ŽIVIH PO 6 LETIH z zdraviloma IMFINZI + IMJUDO v primerjavi s sorafenibom[9]

HR = 0,76 (95 % IZ; 0,65-0,89)

aBTC

Zdravljenje napredovalega raka biliarnega trakta:

IMFINZI® + gem-cis[6]

več kot 2x več bolnikov živih po 4 letih z zdravilom IMFINZI + gem-cis v primerjavi s samo kemoterapijo[10]

HR = 0,74 (95 % IZ; 0,63 - 0,87)

aBTC = napredovali rak biliarnega trakta; FLOT = 5-FU, levkovorin, oksaliplatin, docetaksel; gem+cis = gemcitabin in cisplatin; rGC/GEJC = operabilni rak želodca ali gastroezofagealnega prehoda; uHCC = neoperabilni rak hepatoceličnega karcinoma; 1L = prva linija; IZ = interval zaupanja;HR = razmerje obetov.

1. Vogel A, et al. Hepatocellular carcinoma: ESMO Clinical Practice Guideline for diagnosis, treatment and follow-up. Ann Oncol. 2025 May;36(5):491–506. **2.** NCCN Guidelines Hepatocellular Carcinoma Version 2.2025, October 22, 2025. www.NCCN.org. **3.** Vogel, A., et al. Biliary tract cancer: ESMO Clinical Practice Guideline for diagnosis, treatment and follow-up. Annals of Oncology 34.2 (2023): 127–140. doi: 10.1016/j.annonc.2022.10.506. **4.** NCCN Guidelines Biliary Tract Cancers Version 2.2025, July 2, 2025, NCCN.org. **5.** Onkopedia Guidelines, Gastric Cancer. Status: August 2025. Onlive available at: https://www.onkopedia.com/en/onkopedia/guidelines/gastric-cancer/@@guideline/html/index.html. Last access: 11/2025. **6.** Povzetek glavnih značilnosti zdravila IMFINZI, marec 2026. **7.** Tabernero J, et al. Final overall survival and the association of pathological outcomes with event-free survival in MATTERHORN: a randomised, Phase 3 study of durvalumab plus 5-fluorouracil, leucovorin, oxaliplatin and docetaxel in resectable gastric / gastroesophageal junction adenocarcinoma [presentation]. Presented at: ESMO Congress 2025; October 17 – 21, 2025; Berlin, Germany. **8.** Povzetek glavnih značilnosti zdravila IMJUDO, avgust 2025. **9.** Rimassa L, et al. Five-year overall survival update from the HIMALAYA study of tremelimumab plus durvalumab in unresectable HCC. Journal of Hepatology, https://doi.org/10.1016/j.jhep.2025.03.033. **10.** Oh DY, et al. Durvalumab plus chemotherapy in advanced biliary tract cancer: 3-year overall survival update from the phase III TOPAZ-1 study. J Hepatol. 2025 May 15:S0168-8278(25)02201-9. doi: 10.1016/j.jhep.2025.05.003.

IMJUDO® tremelimumab
Koncentrat za raztopino za infundiranje 20 mg/ml

IMFINZI® durvalumab
Koncentrat za raztopino za infundiranje 50 mg/ml

AstraZeneca

SKRAJŠAN POVZETEK GLAVNIH ZNAČILNOSTI ZDRAVILA

Imfinzi 50 mg/ml koncentrat za raztopino za infundiranje

SESTAVA: 1 ml koncentrata za raztopino za infundiranje vsebuje 50 mg durvalumaba. Ena viala z 2,4 ml koncentrata vsebuje 120 mg durvalumaba. Ena viala z 10 ml koncentrata vsebuje 500 mg durvalumaba. **INDIKACIJE**: **Nedrobnocelični pljučni rak (NSCLC)** Zdravilo IMFINZI je v kombinaciji s kemoterapijo na osnovi platine indicirano kot neoadjuvantno zdravljenje in nato kot samostojno adjuvantno zdravljenje pri odraslih z operabilnim nedrobnoceličnim pljučnim rakom (NSCLC – non-small cell lung cancer), ki imajo veliko tveganje za ponovitev in nimajo mutacij EGFR ali preureditev ALK. Zdravilo IMFINZI je kot samostojno zdravljenje indicirano za zdravljenje lokalno napredovalega, neoperabilnega nedrobnoceličnega pljučnega raka (NSCLC – non small cell lung cancer) pri odraslih, ki imajo tumorje z ≥ 1 % izraženostjo PD-L1 na tumorskih celicah in pri katerih bolezen ni napredovala po kemoradioterapiji na osnovi platine. Zdravilo IMFINZI je v kombinaciji s tremelimumabom in kemoterapijo na osnovi platine indicirano za prvo linijo zdravljenja odraslih z metastatskim NSCLC brez senzibilizirajočih mutacij EGFR ali pozitivnih mutacij ALK. **Drobnocelični pljučni rak (SCLC)** Zdravilo IMFINZI je kot samostojno zdravljenje indicirano za zdravljenje odraslih bolnikov z drobnoceličnim pljučnim rakom v omejenem stadiju (LS-SCLC - limited-stage small cell lung cancer), pri katerih bolezen ni napredovala po kemoradioterapiji na osnovi platine. Zdravilo IMFINZI je v kombinaciji z etopozidom in bodisi karboplatinom bodisi cisplatinom indicirano za prvo linijo zdravljenja odraslih z razsejanim drobnoceličnim pljučnim rakom (ES- SCLC – extensive stage small cell lung cancer). **Rak biliarnega trakta (RBT)** Zdravilo IMFINZI je v kombinaciji z gemcitabinom in cisplatinom indicirano za prvo linijo zdravljenja odraslih z neoperabilnim ali metastatskim rakom biliarnega trakta (RBT). **Hepatocelularni karcinom (HCK)** Zdravilo IMFINZI je kot samostojno zdravljenje indicirano za prvo linijo zdravljenja odraslih z napredovalim ali neoperabilnim hepatocelularnim karcinomom (HCK). Zdravilo IMFINZI je v kombinaciji s tremelimumabom indicirano za prvo linijo zdravljenja odraslih z napredovalim ali neoperabilnim hepatocelularnim karcinomom (HCK). **Rak endometrija** Zdravilo IMFINZI je v kombinaciji s karboplatinom in paklitakselom indicirano za prvo linijo zdravljenja odraslih s primarno napredovalim ali ponovljenim rakom endometrija, ki so kandidati za sistemsko zdravljenje, kateremu sledi vzdrževalno zdravljenje z: • zdravilom IMFINZI kot monoterapijo pri raku endometrija z okvaro MMR v tumorju (dMMR - Mismatch Repair Deficient) • zdravilom IMFINZI v kombinaciji z olaparibom pri raku endometrija brez okvare MMR v tumorju (pMMR - Mismatch Repair Proficient). **Mišično invazivni rak sečnega mehurja** Zdravilo IMFINZI v kombinaciji z gemcitabinom in cisplatinom kot neoadjuvantno zdravljenje, ki mu po radikalni cistektomiji sledi zdravilo IMFINZI kot adjuvantno zdravljenje v monoterapiji, je indicirano za zdravljenje odraslih z operabilnim mišično invazivnim rakom sečnega mehurja (MIBC). **Adenokarcinom želodca ali gastroezofagealnega prehoda (GC/GEJC)** Zdravilo IMFINZI je v kombinaciji s kemoterapijo FLOT kot neoadjuvantno in adjuvantno zdravljenje, ki mu sledi adjuvantna monoterapija z zdravilom IMFINZI, indicirano za zdravljenje odraslih z operabilnim adenokarcinomom želodca ali gastroezofagealnega prehoda. **ODMERJANJE IN NAČIN UPORABE**: Zdravljenje mora uvesti in nadzorovati zdravnik, ki ima izkušnje na področju zdravljenja raka. **Odmerjanje: Priporočeni odmerek zdravila Imfinzi pri *samostojnem zdravljenju*** pri lokalno napredovalem NSCLC je 10 mg/kg na 2 tedna ali 1500 mg na 4 tedne do napredovanja bolezni, nesprejemljivih toksičnih učinkov ali največ 12 mesecev, pri LS-SCLC 1500 mg na 4 tedne do napredovanja bolezni, nesprejemljivih toksičnih učinkov ali največ 24 mesecev, pri HCK 1500 mg na 4 tedne do napredovanja bolezni ali do nesprejemljivih toksičnih učinkov. **Priporočeni odmerek zdravila Imfinzi pri *kombiniranem zdravljenju*** za operabilni NSCLC je 1500 mg v kombinaciji s kemoterapijo na osnovi platine na 3 tedne do 4 cikle pred operacijo, nato samostojno zdravljenje s 1500 mg na 4 tedne do 12 ciklov po operaciji. Trajanje zdravljenja v neoadjuvantni fazi je do napredovanja bolezni, ki onemogoča definitivno operacijo ali do nesprejemljivih toksičnih učinkov, v adjuvantni fazi pa do ponovitve bolezni, nesprejemljivih toksičnih učinkov ali največ 12 ciklov po operaciji; za metastatski NSCLC je med kemoterapijo s platino: 1500 mg v kombinaciji s 75 mg tremelimumaba in kemoterapijo na osnovi platine na 3 tedne (21 dni) 4 cikle (12 tednov), po kemoterapiji s platino: 1500 mg na 4 tedne kot monoterapija in vzdrževalno zdravljenje s pemetreksedom (na podlagi histologije) na 4 tedne, peti odmerek 75 mg tremelimumaba je treba dati 16. teden skupaj z zdravilom Imfinzi. Trajanje zdravljenja je do napredovanja bolezni ali nesprejemljivih toksičnih učinkov. Pri ES-SCLC je priporočeni odmerek zdravila Imfinzi 1500 mg v kombinaciji s kemoterapijo na 3 tedne (21 dni) 4 cikle in nato 1500 mg na 4 tedne kot samostojno zdravljenje do napredovanja bolezni ali nesprejemljivih toksičnih učinkov. Pri RBT je priporočeni odmerek zdravila Imfinzi 1500 mg v kombinaciji s kemoterapijo na 3 tedne (21 dni) do 8 ciklov, nato po 1500 mg na 4 tedne kot samostojno zdravljenje do napredovanja bolezni ali nesprejemljivih toksičnih učinkov. Pri HCK je priporočeni odmerek 1500 mg zdravila Imfinzi v kombinaciji s 300 mg tremelimumaba v enem odmerku 1. dan 1. cikla, nato zdravilo Imfinzi kot monoterapija na 4 tedne do napredovanja bolezni ali nesprejemljivih toksičnih učinkov. Pri raku endometrija je priporočeni odmerek 1120 mg zdravila Imfinzi v kombinaciji s karboplatinom in paklitakselom na 3 tedne (21 dni) minimalno 4 cikle in največ 6 ciklov, nato pa 1500 mg zdravila Imfinzi na 4 tedne kot monoterapija (bolnice z dMMR) ali v kombinaciji s 300 mg olapariba dvakrat na dan (bolnice s pMMR) do napredovanja bolezni ali nesprejemljivih toksičnih učinkov. Pri MIBC je priporočeni odmerek zdravila Imfinzi 1500 mg v kombinaciji s kemoterapijo na 3 tedne v 4 ciklih pred operacijo, nato pa 1500 mg na 4 tedne kot monoterapija do 8 ciklov po operaciji. Trajanje zdravljenja je v neoadjuvantni fazi do napredovanja bolezni, ki onemogoča definitivno operacijo ali do nesprejemljivih toksičnih učinkov, v adjuvantni fazi pa do ponovitve bolezni, nesprejemljivih toksičnih učinkov ali največ 8 ciklov po operaciji. Pri GC/GEJC je priporočeni odmerek zdravila Imfinzi 1500 mg v kombinaciji s kemoterapijo FLOT na 4 tedne do 2 cikla pred operacijo, nato pa 1500 mg s kemoterapijo FLOT na 4 tedne do 2 cikla in potem kot monoterapija s 1500 mg na 4 tedne do 10 ciklov, skupno do 12 ciklov po operaciji. Trajanje zdravljenja je v neoadjuvantni fazi do napredovanja bolezni, ki onemogoča definitivno operacijo ali do nesprejemljivih toksičnih učinkov, v adjuvantni fazi do napredovanja ali ponovitve bolezni, nesprejemljivih toksičnih učinkov ali največ 12 ciklov po operaciji. **Način uporabe:** Zdravilo Imfinzi je namenjeno za intravensko uporabo. Dati ga je treba kot raztopino za intravensko infundiranje v obdobju 1 ure. Če je zdravilo Imfinzi uporabljeno v kombinaciji s kemoterapijo, je treba dati zdravilo Imfinzi pred kemoterapijo na isti dan. Če je zdravilo Imfinzi uporabljeno v kombinaciji s tremelimumabom in kemoterapijo na osnovi platine, je treba najprej dati tremelimumab, ki mu v istem dnevu sledita zdravilo Imfinzi in nato kemoterapija na osnovi platine. Če je zdravilo Imfinzi uporabljeno v kombinaciji s petim odmerkom tremelimumaba in vzdrževalnim zdravljenjem s pemetreksedom 16. teden, je treba najprej dati tremelimumab, ki mu v istem dnevu sledita zdravilo Imfinzi in potem vzdrževalno zdravljenje s pemetreksedom. Zdravilo Imfinzi, tremelimumab in kemoterapijo na osnovi platine je treba dati v ločenih intravenskih infuzijah. Če je zdravilo Imfinzi uporabljeno v kombinaciji s tremelimumabom, je treba dati tremelimumab pred zdravilom Imfinzi na isti dan. Zdravilo Imfinzi in tremelimumab je treba dati v ločenih intravenskih infuzijah. **KONTRAINDIKACIJE**: Preobčutljivost na učinkovino (učinkovine) ali katero koli pomožno snov. **POSEBNA OPOZORILA IN PREVIDNOSTNI UKREPI**: Za domnevne imunsko pogojene neželene učinke je treba opraviti ustrezno ovrednotenje za potrditev etiologije ali izključitev drugih etiologij. Glede na resnost neželenega učinka je treba uporabo zdravila Imfinzi ali zdravilo Imfinzi v kombinaciji s tremelimumabom prekiniti ali trajno ukiniti. Začeti je treba zdravljenje s kortikosteroidi ali endokrino terapijo. Pri dogodkih, ki zahtevajo zdravljenje s kortikosteroidi, in po izboljšanju na ≤ 1. stopnjo, je treba začeti z zmanjševanjem kortikosteroida in ga zmanjševati v obdobju vsaj 1 meseca. Če pride do poslabšanja ali pa če ni izboljšanja, je treba razmisliti o povečanju odmerka kortikosteroidov in/ali o dodatni uporabi sistemskih imunosupresivov. Pri bolnikih, ki so prejemali zdravilo Imfinzi, zdravilo Imfinzi v kombinaciji s tremelimumabom ali zdravilo Imfinzi v kombinaciji s kemoterapijo na osnovi platine, ki mu sledi zdravilo Imfinzi v kombinaciji z olaparibom ali v kombinaciji s kemoterapijo, sta se pojavila imunsko pogojeni pnevmonitis ali intersticijska bolezen pljuč. Pri bolnikih, zdravljenih z radioterapijo pljuč, je pogost radiacijski pnevmonitis in klinična slika pnevmonitisa in radiacijskega pnevmonitisa je zelo podobna. Bolnike je treba spremljati glede znakov in simptomov pnevmonitisa ali radiacijskega pnevmonitisa. Pri bolnikih, ki so prejemali zdravilo Imfinzi ali zdravilo Imfinzi v kombinaciji s tremelimumabom ali v kombinaciji s kemoterapijo, se je pojavil imunsko pogojeni hepatitis, imunsko pogojeni kolitis, imunsko pogojene hipotiroidizem, hipertiroidizem in tiroiditis, imunsko pogojena adrenalna insuficienca, imunsko pogojena sladkorna bolezen tipa 1, imunsko pogojeni hipofizitis/hipopituitarizem, imunsko pogojeni nefritis, imunsko pogojeni izpuščaj, imunsko pogojeni miokarditis, drugi imunsko pogojeni neželeni učinki (miastenija gravis, transverzni mielitis, miozitis, polimiozitis, rabdomioliza, meningitis, encefalitis, Guillain-Barréjev sindrom, imunska trombocitopenija, imunsko pogojeni artritis, uveitis in neinfektivni cistitis), z infundiranjem povezane reakcije. Pri bolnikih, ki so prejemali zdravilo Imfinzi v kombinaciji s tremelimumabom in kemoterapijo ali v kombinaciji s kemoterapijo, se je pojavil imunsko pogojeni pankreatitis. Pri bolnikih z že obstoječo avtoimunsko boleznijo podatki iz opazovalnih študij kažejo na povečano tveganje za imunsko pogojene neželene učinke po terapiji z zaviralci imunske kontrolne točke v primerjavi z bolniki brez obstoječe avtoimunske bolezni. Poleg tega so bili pogosti izbruhi osnovne obstoječe avtoimunske bolezni, vendar je bila večina blagih in obvladljivih. Za bolezen specifični previdnostni ukrepi (RBT): Bolnike z RBT (zlasti tiste z biliarno opornico) je treba natančno nadzorovati glede holangitisa ali okužb biliarnega trakta tako pred uvedbo zdravljenja kot redno med zdravljenjem. Za zdravljenje specifičen previdnostni ukrep (zdravilo Imfinzi v kombinaciji z olaparibom pri raku endometrija): Hematotoksičnost: Med vzdrževalnim zdravljenjem z olaparibom v kombinaciji z zdravilom Imfinzi, po zdravljenju z zdravilom Imfinzi v kombinaciji s kemoterapijo na osnovi platine so poročali o čisti aplaziji rdečih krvnih celic (PRCA – Pure Red Cell Aplasia) in avtoimunski hemolitični anemiji (AIHA - Autoimmune Haemolytic Anemia). Če je PRCA ali AIHA potrjena, je treba zdravljenje z zdravilom Imfinzi in olaparibom prenehati. Metastatski NSCLC: Podatkov o starejših bolnikih (≥ 75 let), zdravljenih z zdravilom Imfinzi v kombinaciji s tremelimumabom in kemoterapijo na osnovi platine, je malo. Morebitno korist/tveganje te sheme je priporočljivo skrbno pretehtati za vsakega bolnika posebej. **MEDSEBOJNO DELOVANJE Z DRUGIMI ZDRAVILI**: Razen fizioloških odmerkov sistemskih kortikosteroidov (≤ 10 mg na dan prednizona ali ekvivalenta) pred uvedbo durvalumaba ni priporočljivo uporabljati sistemskih kortikosteroidov ali imunosupresivov, ker lahko vplivajo na farmakodinamično aktivnost in učinkovitost durvalumaba. Vendar pa je mogoče kortikosteroide ali druge imunosupresive uporabiti po začetku zdravljenja z durvalumabom za zdravljenje imunsko pogojenih neželenih učinkov. Z durvalumabom niso izvedli formalnih farmakokinetičnih (PK) študij medsebojnega delovanja zdravil. Primarni poti odstranjevanja durvalumaba sta katabolizem beljakovin preko retikuloendotelijskega sistema oziroma tarčno posredovano odstranjevanje, zato ni pričakovati presnovnih medsebojnih delovanj med zdravili. **PLODNOST, NOSEČNOST IN DOJENJE**: Ženske v rodni dobi morajo med zdravljenjem z durvalumabom in vsaj še 3 mesece po zadnjem odmerku durvalumaba uporabljati učinkovito kontracepcijo. Podatkov o uporabi durvalumaba pri nosečnicah ni. Glede na mehanizem delovanja durvalumab lahko vpliva na vzdrževanje nosečnosti; v alogenskem modelu nosečnosti pri miših je bilo ugotovljeno, da moteno signaliziranje PD-L1 poveča izgubo plodov. Pri nosečnici uporabljeni durvalumab lahko škoduje plodu in ga ni priporočljivo uporabljati med nosečnostjo in pri ženskah v rodni dobi, ki ne uporabljajo učinkovite kontracepcije med zdravljenjem in vsaj še 3 mesece po zadnjem odmerku. Ni znano, ali se durvalumab pri človeku izloča v materino mleko. Pri človeku protitelesa lahko prehajajo v materino mleko, a možnost absorpcije in škode za novorojenčka ni znana. Toda možnega tveganja za dojenega otroka ni mogoče izključiti. Odločiti se je treba, ali naj ženska prekine z dojenjem ali naj prekine zdravljenje z durvalumabom oziroma sploh ne začne zdravljenja z njim, pri čemer je treba upoštevati koristi dojenja za otroka in koristi zdravljenja za žensko. Podatkov o možnih vplivih durvalumaba na plodnost pri človeku ali živalih ni. **NEŽELENI UČINKI**: Ugotovitve o varnosti zdravila Imfinzi pri samostojnem zdravljenju temeljijo na kumulativnih podatkih 4642 bolnikov z več vrstami tumorjev. Zdravilo Imfinzi so uporabljali v odmerku 10 mg/kg na 2 tedna, 20 mg/kg na 4 tedne ali 1500 mg/kg na 4 tedne. Najpogostejši neželeni učinki (> 10 %) so bili kašelj/produktiven kašelj (18,1 %), driska (15,1 %), izpuščaj (15,0 %), artralgija (12,4 %), zvišana telesna temperatura (12,5 %), bolečine v trebuhu (11,8 %), okužbe zgornjih dihal (11,8 %), srbenje (11,1 %) in hipotiroidizem (11,6 %). Podatki o varnosti zdravila Imfinzi v kombinaciji s kemoterapijo temeljijo na kumulativnih podatkih 2244 bolnikov iz 6 študij (TOPAZ-1, CASPIAN, DUO-E, AEGEAN, NIAGARA in MATTERHORN). Najpogostejši (> 10 %) neželeni učinki so bili nevtropenija (44,6 %), navzea (42,4 %), utrujenost (41,2 %), anemija (37,4 %), driska (27,5 %), zaprtje (26,7 %), zmanjšanje apetita (24,0 %), alopecija (22,0 %), periferna nevropatija (21,6 %), trobmocitopenija (19,7 %), izpuščaj (19,7 %), bruhanje (18,8 %), bolečine v trebuhu (17,9 %), zvišana telesna temperatura (15,2 %), levkopenija (14,9 %), pruritus (12,5 %), hipotiroidizem (11,1 %), artralgija (10,9 %), kašelj/produktiven kašelj (10,8 %) in zvišana aspartat-aminotransferaza/zvišana alanin-aminotransferaza (10,5 %). Izsledki o varnosti zdravila Imfinzi v kombinaciji s 75 mg tremelimumaba in kemoterapijo temeljijo na podatkih 330 bolnikov z metastatskim NSCLC. Najpogostejši (> 20 %) neželeni učinki so bili anemija (49,7 %), navzea (41,5 %), nevtropenija (41,2 %), utrujenost (36,1 %), izpuščaj (25,8 %), trombocitopenija (24,5 %) in driska (21,5 %). Izsledki o varnosti zdravila Imfinzi v kombinaciji z enkratnim odmerkom 300 mg tremelimumaba temeljijo na združenih podatkih 462 bolnikov s HCK iz študije HIMALAYA in še ene študije pri bolnikih s HCK, študija 22. Najpogostejši neželeni učinki (> 10 %) so bili izpuščaj (32,5 %), srbenje (25,5 %), driska (25,3 %), bolečine v trebuhu (19,7 %), zvišana aspartat aminotransferaza/zvišana alanin aminotransferaza (18,0 %), zvišana telesna temperatura (13,9 %), hipotiroidizem (13,0 %), kašelj/produktiven kašelj (10,8 %), periferni edemi (10,4 %) in zvišana lipaza (10,0 %). Varnost zdravila Imfinzi v kombinaciji s kemoterapijo na osnovi platine, ki ji sledi zdravilo Imfinzi v kombinaciji s 300 mg olapariba dvakrat na dan, temelji na podatkih 238 bolnic z rakom endometrija. Najpogostejši (> 20 %) neželeni učinki so bili anemija (61,8 %), navzea (54,6 %), utrujenost (54,2 %), periferna nevropatija (51,7 %), alopecija (50,8 %), nevtropenija (39,5 %), zaprtje (32,8 %), trombocitopenija (29,8 %), driska (28,2 %), bruhanje (25,6 %), artralgija (24,4 %), izpuščaj (23,5 %), bolečine v trebuhu (23,5 %), zmanjšan apetit (23,1 %) in levkopenija (20,2 %). **VRSTA IN VSEBINA OVOJNINE**: 2,4 ml (skupno 120 mg durvalumaba) koncentrata v stekleni viali iz stekla tipa 1 z elastomernim zamaškom in sivo snemno aluminijsko zaporo. Pakiranje vsebuje 1 vialo. 10 ml (skupno 500 mg durvalumaba) koncentrata v stekleni viali iz stekla tipa 1 z elastomernim zamaškom in belo snemno aluminijsko zaporo. Pakiranje vsebuje 1 vialo. **NAČIN IZDAJANJA ZDRAVILA**: H - Predpisovanje in izdaja zdravila je le na recept. **DATUM REVIZIJA BESEDILA**: 12.3.2026 (SI-3708) **IMETNIK DOVOLJENJA ZA PROMET**: AstraZeneca AB, S-151 85, Sodertalje, Švedska **Pred predpisovanjem, prosimo, preberite celoten povzetek glavnih značilnosti zdravila.** Dodatne informacije so na voljo pri družbi AstraZeneca UK Limited, Podružnica v Sloveniji, Verovškova 55, Ljubljana, telefon +386 1 51 35 600.

SKRAJŠAN POVZETEK GLAVNIH ZNAČILNOSTI ZDRAVILA

▼Za to zdravilo se izvaja dodatno spremljanje varnosti. Tako bodo hitreje na voljo nove informacije o njegovi varnosti. Zdravstvene delavce naprošamo, da poročajo o katerem koli domnevnem neželenem učinku zdravila. Glejte poglavje 4.8, kako poročati o neželenih učinkih.

IMJUDO 20 mg/ml koncentrat za raztopino za infundiranje

SESTAVA: En mililiter koncentrata za raztopino za infundiranje vsebuje 20 mg tremelimumaba. Ena viala z 1,25 ml koncentrata vsebuje 25 mg tremelimumaba. Ena viala s 15 ml koncentrata vsebuje 300 mg tremelimumaba. INDIKACIJE: Zdravilo IMJUDO je v kombinaciji z durvalumabom indicirano za prvo linijo zdravljenja odraslih z napredovalim ali neresektabilnim karcinomom jetrnih celic (hepatocelularnim karcinomom – HCK). Zdravilo IMJUDO je v kombinaciji z durvalumabom in kemoterapijo na osnovi platine indicirano za prvo linijo zdravljenja odraslih z metastatskim nedrobnoceličnim rakom pljuč (non-small cell lung cancer – NSCLC) brez senzibilizirajočih mutacij EGFR ali pozitivnih mutacij ALK. ODMERJANJE IN NAČIN UPORABE: Zdravljenje mora uvesti in nadzorovati zdravnik, ki ima izkušnje na področju zdravljenja raka. Odmerjanje: Zdravilo IMJUDO se daje v 1-urni intravenski infuziji. ***Pri HCK, ki je napredoval ali je neresektabilen*** je priporočeno odmerjanje 300 mg zdravila IMJUDO v enkratnem odmerku v kombinaciji s 1500 mg durvalumaba 1. dan 1. cikla, nato monoterapija z durvalumabom na 4 tedne do napredovanja bolezni ali nesprejemljivih toksičnih učinkov. ***Pri metastatskem NSCLC*** je priporočeno odmerjanje med kemoterapijo s platino: 75 mg v kombinaciji s 1500 mg durvalumaba in kemoterapijo na osnovi platine na 3 tedne (21 dni) 4 cikle (12 tednov). Po kemoterapiji s platino: 1500 mg durvalumaba na 4 tedne in vzdrževalno zdravljenje s pemetreksedom na podlagi histologije na 4 tedne. Peti odmerek 75 mg zdravila IMJUDO je treba dati 16. teden, obenem s 6. odmerkom durvalumaba. V primeru napredovanja bolezni ali nesprejemljive toksičnosti lahko bolniki dobijo manj kot pet odmerkov zdravila IMJUDO v kombinaciji s 1500 mg durvalumaba in kemoterapijo na osnovi platine. Med zdravljenjem z zdravilom IMJUDO v kombinaciji z durvalumabom odmerkov ni priporočljivo povečevati ali zmanjševati. Pri posameznem bolniku se lahko glede na varnost in prenašanje pokaže potreba po odložitvi zdravljenja ali njegovem prenehanju. Smernice za obravnavanje imunsko pogojenih neželenih učinkov so opisane v preglednici 2 SmPC. *Posebne populacije:* Starejšim bolnikom (starim ≥ 65 let) odmerka ni treba prilagoditi. Podatkov o bolnikih, z metastatskim NSCLC, starih 75 let ali več, je malo. Bolnikom z blago ali zmerno okvaro ledvic odmerka zdravila IMJUDO ni treba prilagoditi. Podatkov o bolnikih s hudo okvaro ledvic je premalo, da bi lahko sklepali o tej populaciji. Bolnikom z blago ali zmerno okvaro jeter odmerka zdravila IMJUDO ni treba prilagoditi. Pri bolnikih s hudo okvaro jeter zdravilo IMJUDO ni raziskano. *Pediatrična populacija*: Varnost in učinkovitost zdravila IMJUDO za HCK in NSCLC pri otrocih in mladostnikih, mlajših od 18 let, nista ugotovljeni. Podatkov ni na voljo. Izven odobrenih indikacij so zdravilo IMJUDO v kombinaciji z durvalumabom proučevali pri otrocih, starih od 1 do 17 let, z nevroblastomom, solidnim tumorjem in sarkomom, vendar rezultati študije niso omogočili zaključka, da koristi takšne uporabe odtehtajo tveganja. Način uporabe: Zdravilo IMJUDO je namenjeno za intravensko uporabo, apliciramo ga v obliki 1-urne intravenske infuzije, po razredčenju. ***Če je zdravilo IMJUDO uporabljeno v kombinaciji z durvalumabom***, je treba zdravilo IMJUDO dati kot ločeno intravensko infuzijo pred durvalumabom na isti dan. Za informacije o uporabi durvalumaba glejte povzetek glavnih značilnosti za durvalumab. ***Če je zdravilo IMJUDO uporabljeno v kombinaciji z durvalumabom in kemoterapijo na osnovi platine***, je treba najprej dati zdravilo IMJUDO, potem durvalumab in nato kemoterapijo na osnovi platine na dan odmerjanja. Kadar je zdravilo IMJUDO uporabljeno kot peti odmerek v kombinaciji z durvalumabom in vzdrževalnim zdravljenjem s pemetreksedom 16. teden, je treba najprej dati zdravilo IMJUDO, potem durvalumab in nato vzdrževalno zdravljenje s pemetreksedom na dan odmerjanja. Zdravilo IMJUDO, durvalumab in kemoterapija na osnovi platine se dajejo v ločenih intravenskih infuzijah. Zdravilo IMJUDO in durvalumab se oba dajeta po 1 uro. Za informacije o dajanju kemoterapije na osnovi platine glejte povzetek glavnih značilnosti zadevnega zdravila. Za informacije o dajanju pemetrekseda glejte povzetek glavnih značilnosti pemetrekseda. Za vsako infuzijo je treba uporabiti ločene infuzijske vreče in filtre. V 1. ciklu mora zdravilu IMJUDO slediti durvalumab; njegovo dajanje se začne približno 1 uro (in največ 2 uri) po koncu infundiranja zdravila IMJUDO. Infundiranje kemoterapije na osnovi platine se mora začeti približno 1 uro (in največ 2 uri) po koncu infundiranja durvalumaba. Če med 1. ciklom ni klinično pomembnih težav, je mogoče po zdravnikovi presoji naslednje cikle durvalumaba dati takoj po zdravilu IMJUDO, čas med koncem infundiranja durvalumaba in začetkom kemoterapije pa je mogoče skrajšati na 30 minut. KONTRAINDIKACIJE: Preobčutljivost na učinkovino ali katero koli pomožno snov. POSEBNA OPOZORILA IN PREVIDNOSTNI UKREPI: Z namenom izboljšanja sledljivosti bioloških zdravil je treba jasno zabeležiti ime in številko serije uporabljenega zdravila. Pri bolnikih, ki so prejemali tremelimumab v kombinaciji z durvalumabom ali z durvalumabom in kemoterapijo, so se pojavili imunsko pogojeni pnevmonitis ali intersticijska bolezen pljuč, imunsko pogojeni hepatitis, imunsko pogojeni kolitis ali driska, hipotiroidizem, hipertiroidizem in tiroiditis, imunsko pogojena nadledvična insuficienca, imunsko pogojena sladkorna bolezen tipa 1, ki se lahko najprej pokaže z diabetično ketoacidozo, ki je lahko smrtna, če ni odkrita zgodaj, imunsko pogojeni hipofizitis ali hipopituitarizem, imunsko pogojeni nefritis, imunsko pogojen izpuščaj ali dermatitis (vključno s pemfigoidom), imunsko pogojeni miokarditis, ki je lahko smrten, imunsko pogojeni pankreatitis. Lahko se pojavijo še drugi potencialno imunsko pogojeni neželeni učinki; miastenija gravis, miozitis, polimiozitis, meningitis, encefalitis, Guillain-Barréjev sindrom, imunska trombocitopenija, neinfekcijski cistitis, imunsko pogojeni artritis, uveitis in revmatična polimialgija. Bolnike je treba spremljati glede znakov in simptomov z infundiranjem povezanih reakcij. Pri bolnikih, ki so prejemali tremelimumab v kombinaciji z durvalumabom, so poročali o hudih z infundiranjem povezanih reakcijah. Za starejše bolnike (≥ 75 let), zdravljene s tremelimumabom v kombinaciji z durvalumabom in kemoterapijo na osnovi platine pri metastatskem NSCLC, je podatkov malo, pri vsakem bolniku je treba individualno skrbno razmisliti o možnih koristih in tveganjih te sheme. Zdravilo vsebuje manj kot 1 mmol (23 mg) natrija na odmerek, kar v bistvu pomeni »brez natrija«. MEDSEBOJNO DELOVANJE Z DRUGIMI ZDRAVILI: Sistemski kortikosteroidi oziroma imunosupresivi lahko vplivajo na farmakodinamično aktivnost in učinkovitost tremelimumaba, zato jih pred uvedbo tremelimumaba ni priporočljivo uporabljati; izjema so fiziološki odmerki sistemskih kortikosteroidov (≤ 10 mg/dan prednizona ali ekvivalenta). Vendar pa se kortikosteroide ali druge imunosupresive lahko uporabi po uvedbi tremelimumaba za zdravljenje imunsko pogojenih neželenih učinkov. Formalnih farmakokinetičnih študij medsebojnega delovanja zdravil s tremelimumabom niso izvedli. Ker sta glavni poti odstranjevanja tremelimumaba katabolizem beljakovin prek retikuloendotelijskega sistema ali tarčno posredovana razgradnja, presnovnih medsebojnih delovanj z zdravili ni pričakovati. Farmakokinetično medsebojno delovanje zdravil s tremelimumabom v kombinaciji z durvalumabom in kemoterapijo na osnovi platine so ocenili v študiji POSEIDON. Med sočasnim zdravljenjem niso ugotovili nobenih klinično pomembnih medsebojnih delovanj med tremelimumabom, durvalumabom, nab-paklitakselom, gemcitabinom, pemetreksedom, karboplatinom ali cisplatinom. PLODNOST, NOSEČNOST IN DOJENJE: ***Ženske v rodni dobi*** morajo med zdravljenjem s tremelimumabom in vsaj še 3 mesece po zadnjem odmerku tremelimumaba uporabljati učinkovito kontracepcijo. Podatkov o uporabi tremelimumaba ***pri nosečnicah*** ni. Glede na mehanizem delovanja in prenos humanega IgG2 skozi placento, lahko tremelimumab vpliva na ohranitev nosečnosti in bi v primeru uporabe pri nosečnici lahko škodoval plodu. Študije na živalih ne kažejo neposrednih ali posrednih škodljivih učinkov glede vpliva na razmnoževanje. Zdravila IMJUDO ni priporočljivo uporabljati med nosečnostjo in pri ženskah v rodni dobi, ki ne uporabljajo učinkovite kontracepcije med zdravljenjem in vsaj še 3 mesece po zadnjem odmerku. O prisotnosti tremelimumaba v materinem mleku pri človeku, o njegovi absorpciji in vplivih na dojenega dojenčka ali o vplivih na nastajanje mleka ni podatkov. Znano je, da se humani IgG2 izločajo v materino mleko. Tveganje za nerojenega otroka ni mogoče izključiti. Med zdravljenjem z zdravilom IMJUDO je treba ***dojenje*** prekiniti, bolnica pa še vsaj 3 mesece po zadnjem odmerku ne sme dojiti. Podatkov o možnih vplivih tremelimumaba na ***plodnost*** pri človeku ali živalih ni. NEŽELENI UČINKI: Zdravilo IMJUDO v kombinaciji z durvalumabom: Izsledki o varnosti 300 mg tremelimumaba v enkratnem odmerku v kombinaciji z durvalumabom temeljijo na združenih podatkih 462 bolnikov s HCK (»skupina s HCK«) iz študije HIMALAYA in še ene študije pri bolnikih s HCK, Študije 22. Najpogostejši neželeni učinki (> 10 %) so bili izpuščaj (32,5 %), srbenje (25,5 %), driska (25,3 %), bolečine v trebuhu (19,7 %), zvišana aspartat-aminotransferaza/zvišana alanin-aminotransferaza (18,0 %), zvišana telesna temperatura (13,9 %), hipotiroidizem (13,0 %), kašelj/produktiven kašelj (10,8 %) in periferni edemi (10,4 %). Najpogostejši (> 3%) hudi neželeni učinki (≥ 3. stopnje po NCI CTCAE) so bili zvišana aspartat-aminotransferaza/zvišana alanin-aminotransferaza (8,9 %), zvišana lipaza (7,1 %), zvišana amilaza (4,3 %) in driska (3,9 %). Najpogostejši (> 2%) resni neželeni učinki so bili kolitis (2,6 %), driska (2,4 %) in pljučnica (2,2 %). Pogostnost prenehanj zdravljenja zaradi neželenih učinkov je bila 6,5 %. Neželena učinka, ki sta najpogosteje povzročila prenehanje zdravljenja, sta bila hepatitis (1,5 %) in zvišana aspartat-aminotransferaza/zvišana alanin-aminotransferaza (1,3 %). Zdravilo IMJUDO v kombinaciji z durvalumabom in kemoterapijo: Informacije o varnosti tremelimumaba, uporabljenega v kombinaciji z durvalumabom in kemoterapijo, temeljijo na podatkih 330 bolnikov z metastatskim NSCLC. Najpogostejši (> 10 %) neželeni učinki so bili anemija (49,7 %), navzea (41,5 %), nevtropenija (41,2 %), utrujenost (36,1 %), zmanjšan apetit (28,2 %), izpuščaj (25,8 %), trombocitopenija (24,5 %), driska (21,5 %), levkopenija (19,4 %), zaprtje (19,1 %), bruhanje (18,2 %), zvišana aspartat-aminotransferaza/zvišana alanin-aminotransferaza (17,6 %), zvišana telesna temperatura (16,1 %), okužbe zgornjih dihal (15,5 %), pljučnica (14,8 %), hipotiroidizem (13,3%), artralgija (12,4 %), kašelj/produktivni kašelj (12,1 %) in srbenje (10,9 %). Najpogostejši (> 3 %) hudi neželeni učinki (≥ 3. stopnje po NCI CTCAE) so bili nevtropenija (23,9 %), anemija (20,6 %), pljučnica (9,4 %), trombocitopenija (8,2 %), levkopenija (5,5 %), utrujenost (5,2 %), zvišana lipaza (3,9 %) in zvišana amilaza (3,6 %). Najpogostejši (> 2 %) resni neželeni učinki so bili pljučnica (11,5 %), anemija (5,5 %), trombocitopenija (3 %), kolitis (2,4 %), driska (2,4 %), zvišana telesna temperatura (2,4 %) in febrilna nevtropenija (2,1 %). Zaradi neželenih učinkov so tremelimumab prenehali uporabljati pri 4,5 % bolnikov. Najpogostejša neželena učinka, ki sta povzročila prenehanje zdravljenja, sta bila pljučnica (1,2 %) in kolitis (0,9 %). Zaradi neželenih učinkov so uporabo tremelimumaba začasno prekinili pri 40,6 % bolnikov. Najpogostejši neželeni učinki, ki so povzročili začasno prekinitev uporabe, so bili nevtropenija (13,6 %), trombocitopenija (5,8 %), levkopenija (4,5 %), driska (3,0 %), pljučnica (2,7 %), zvišana aspartat-aminotransferaza/zvišana alanin-aminotransferaza (2,4 %), utrujenost (2,4 %), zvišana lipaza (2,4 %), kolitis (2,1 %), hepatitis (2,1 %) in izpuščaj (2,1 %). VRSTA IN VSEBINA OVOJNINE: Na voljo sta dve velikosti pakiranja zdravila IMJUDO: ***1,25 ml koncentrata (skupno 25 mg tremelimumaba)*** v viali iz stekla tipa I z elastomernim zamaškom in vijolično snemno aluminijsko zaporo. Velikost pakiranj: 1 viala z enim odmerkom. ***15 ml koncentrata (skupno 300 mg tremelimumaba)*** v viali iz stekla tipa I z elastomernim zamaškom in temno modro snemno aluminijsko zaporo. Velikost pakiranj: 1 viala z enim odmerkom. NAČIN IZDAJANJA ZDRAVILA: H DATUM REVIZIJE BESEDILA: 4.8.2025, SI-3777 IMETNIK DOVOLJENJA ZA PROMET: AstraZeneca AB, S-151 85, Sodertalje, Švedska Pred predpisovanjem, prosimo, preberite celoten povzetek glavnih značilnosti zdravila. Dodatne informacije so na voljo pri družbi AstraZeneca UK Limited, Podružnica v Sloveniji, Verovškova 55, Ljubljana, telefon +386 1 51 35 600.

SKRAJŠAN POVZETEK GLAVNIH ZNAČILNOSTI ZDRAVILA

Calquence 100 mg trde kapsule
Calquence 100 mg filmsko obložene tablete

SESTAVA: Ena trda kapsula vsebuje 100 mg akalabrutiniba. Ena filmsko obložena tableta vsebuje 100 mg akalabrutiniba (v obliki akalabrutinibijevega maleata). Akalabrutinib je selektiven zaviralec Brutonove tirozin kinaze.
INDIKACIJE: Zdravilo Calquence je kot monoterapija ali v kombinaciji z obinutuzumabom indicirano za zdravljenje odraslih bolnikov s predhodno nezdravljeno kronično limfocitno levkemijo. Zdravilo Calquence je v kombinaciji z venetoklaksom, z obinutuzumabom ali brez njega, indicirano za zdravljenje odraslih bolnikov s predhodno nezdravljeno kronično limfocitno levkemijo. Zdravilo Calquence je kot monoterapija indicirano za zdravljenje odraslih bolnikov s kronično limfocitno levkemijo, ki so predhodno prejemali vsaj eno zdravljenje. Zdravilo Calquence je v kombinaciji z bendamustinom in rituksimabom (BR) indicirano za zdravljenje odraslih bolnikov s predhodno nezdravljenim limfomom plaščnih celic (MCL - mantle cell lymphoma), ki niso primerni za avtologno presaditev matičnih celic. Zdravilo Calquence je kot monoterapija indicirano za zdravljenje odraslih bolnikov s ponovitvijo ali z neodzivno obliko limfoma plaščnih celic (MCL - mantle cell lymphoma), ki predhodno niso bili zdravljeni z zaviralcem Brutonove tirozin kinaze (BTK).
ODMERJANJE IN NAČIN UPORABE: Zdravljenje s tem zdravilom mora uvesti in nadzorovati zdravnik, ki ima izkušnje z uporabo zdravil za zdravljenje raka. Priporočeni odmerek zdravila Calquence v monoterapiji ali v kombinaciji z drugimi zdravili je 100 mg akalabrutiniba dvakrat na dan (to ustreza skupnemu dnevnemu odmerku 200 mg). Odmerni interval zdravila Calquence je približno 12 ur. Zdravilo Calquence v monoterapiji ali v kombinaciji z obinutuzumabom: Zdravljenje v monoterapiji ali v kombinaciji z obinutuzumabom je treba nadaljevati do napredovanja bolezni ali nesprejemljive toksičnosti. Zdravilo Calquence v kombinaciji z venetoklaksom, z obinutuzumabom ali brez njega: Zdravljenje v kombinaciji z venetoklaksom, z obinutuzumabom ali brez njega, je treba nadaljevati do napredovanja bolezni, nesprejemljive toksičnosti ali dokončanja 14 ciklov zdravljenja (vsak cikel traja 28 dni). Zdravilo Calquence je treba dati 1. dan 1. cikla in ga uporabljati skupno 14 ciklov. Venetoklaks je treba dati 1. dan 3. cikla in skupno 12 ciklov, najprej v odmerku 20 mg in nato s tedenskim povečevanjem na 50 mg, 100 mg, 200 mg in končno 400 mg. Če je zdravilo Calquence uporabljeno v kombinaciji z venetoklaksom in obinutuzumabom, je treba obinutuzumab uporabiti v odmerku 100 mg 1. dan 2. cikla, čemur sledi 900 mg, uporabljenih 1. ali 2. dan. Uporabite 1000 mg obinutuzumaba 8. in 15. dan 2. cikla, nato pa 1000 mg 1. dan 3. do 7. cikla. Obinutuzumab se uporablja skupno 6 ciklov. Zdravilo Calquence v kombinaciji z bendamustinom in rituksimabom: Zdravilo Calquence je treba dati 1. dan 1. cikla (vsak cikel traja 28 dni) do napredovanja bolezni ali pojava nesprejemljive toksičnosti. Bendamustin je treba dati v odmerku 90 mg/m2 1. in 2. dan vsakega cikla, skupaj 6 ciklov. Rituksimab je treba dati v odmerku 375 mg/m2 1. dan vsakega cikla, skupaj 6 ciklov. Bolniki, ki po prvih 6 ciklih dosežejo odziv (delen odziv [PR partial response] ali popoln odziv [CR complete response]), lahko prejemajo rituksimab kot vzdrževalno zdravljenje v odmerku 375 mg/m2 1. dan vsakega drugega cikla največ 12 dodatnih odmerkov z začetkom v 8. ciklu in do 30. cikla.
Informacije o priporočenih prilagoditvah odmerka zdravila Calquence v monoterapiji ali v kombinaciji z drugimi zdravili v primeru neželenih učinkov ≥ 3. stopnje in pri uporabi z zaviralci ali induktorji CYP3A in zdravili za zmanjšanje izločanja želodčne kisline najdete v povzetku glavnih značilnosti zdravila. Starejšim bolnikom odmerka ni treba prilagoditi. Kliničnih študij pri bolnikih z okvaro ledvic niso izvedli. Bolnike z blago ali zmerno okvaro ledvic so zdravili v kliničnih študijah zdravila Calquence. Bolnikom z blago ali zmerno okvaro odmerka ni treba prilagoditi. Pri bolnikih s hudo okvaro ledvic se zdravilo Calquence lahko uporabi le, če koristi odtehtajo tveganje; te bolnike je treba skrbno spremljati glede znakov toksičnosti. Podatkov o bolnikih s hudo okvaro ledvic in bolnikih na dializi ni. Bolnikom z blago ali zmerno okvaro jeter odmerka ni treba prilagoditi. Vendar je treba bolnike z zmerno okvaro jeter natančno spremljati glede znakov toksičnosti. Zdravila Calquence ni priporočljivo uporabljati pri bolnikih s hudo okvaro jeter. Bolniki s hudimi srčno žilnimi boleznimi niso bili vključeni v klinične študije zdravila Calquence. Varnost in učinkovitost zdravila Calquence pri otrocih in mladostnikih v starosti od 0 do 18 let nista bili dokazani. Zdravilo Calquence je namenjeno za peroralno uporabo. Kapsule ali tablete je treba zaužiti cele z vodo, vsak dan ob približno istem času, s hrano ali brez nje. Kapsul ali tablet se ne sme gristi, raztapljati ali odpirati.
KONTRAINDIKACIJE: Preobčutljivost za zdravilno učinkovino ali katerokoli pomožno snov.
OPOZORILA IN PREVIDNOSTNI UKREPI: Krvavitve: Pri bolnikih s hematološkimi malignomi, ki so bili zdravljeni z zdravilom Calquence v monoterapiji ali v kombinaciji z drugimi zdravili so se pojavile večje krvavitve, vključno s krvavitvami v osrednjem živčevju in gastrointestinalnimi krvavitvami, v nekaterih primerih s smrtnim izidom. Ti dogodki so se pojavili tako pri bolnikih s trombocitopenijo kot tudi pri tistih brez nje. Na splošno pa so bile krvavitve manj hudi dogodki, ki so vključevali podplutbe in petehije. Bolniki, ki prejemajo antitrombotična zdravila, imajo večje tveganje za krvavitve. Varfarina ali drugih antagonistov vitamina K se ne sme uporabljati sočasno z zdravilom Calquence. Razmislite o koristih in tveganjih zadržanja zdravila Calquence vsaj 3 dni pred kirurškim posegom in po njem. Okužbe: Pri bolnikih s hematološkimi malignomi, ki so bili zdravljeni z zdravilom Calquence v monoterapiji ali v kombinaciji z drugimi zdravili, so se pojavile resne okužbe (bakterijske, virusne ali glivične), vključno s smrtnimi primeri. Te okužbe so se večinoma pojavile brez nevtropenije; o nevtropeničnih okužbah so poročali pri 10,1 % bolnikov, ki so prejemali monoterapijo in pri 26,8 % bolnikov, ki so prejemali kombinirano zdravljenje. Pojavile so se okužbe zaradi reaktivacije virusa hepatitisa B (HBV) in virusa herpesa zostra (HZV), aspergiloza in progresivna multifokalna levkoencefalopatija (PML). Reaktivacija virusov: Pri bolnikih, ki so prejemali zdravilo Calquence, so poročali o primerih reaktivacije hepatitisa B. Med uporabo zdravila Calquence v okviru predhodnega ali sočasnega imunosupresivnega zdravljenja so poročali o primerih progresivne multifokalne levkoencefalopatije (PML), vključno s primeri s smrtnim izidom. Zdravniki morajo PML upoštevati v diferencialni diagnostiki pri bolnikih, ki imajo nove nevrološke, kognitivne ali vedenjske znake ali simptome, oziroma se jim ti znaki ali simptomi poslabšajo. V primeru suma na PML je treba zdravljenje z zdravilom Calquence prekiniti, dokler PML ni izključena. Citopenije: Pri bolnikih s hematološkimi malignomi, ki so bili zdravljeni z zdravilom Calquence v monoterapiji ali v kombinaciji z drugimi zdravili, so se med zdravljenjem pojavile citopenije 3. ali 4. stopnje, vključno z nevtropenijo, anemijo in trombocitopenijo. Drugi primarni malignomi: Pri bolnikih s hematološkimi malignomi, ki so bili zdravljeni z zdravilom Calquence v monoterapiji ali v kombinaciji z drugimi zdravili, so se pojavili drugi primarni malignomi, vključno s kožnim in nekožnim rakom. O kožnem raku so poročali pogosto. Atrijska fibrilacija: Pri bolnikih s hematološkimi malignomi, ki so bili zdravljeni z zdravilom Calquence v monoterapiji ali v kombinaciji z drugimi zdravili, se je pojavila atrijska fibrilacija/undulacija. Sindrom tumorske lize: Med zdravljenjem z zdravilom Calquence so poročali o sindromu tumorske lize. Bolnike z domnevnim tveganjem za sindrom tumorske lize (npr. bolnike z izhodiščno obsežno boleznijo) je treba oceniti glede možnega tveganja za ta sindrom in jih natančno spremljati, kot je klinično indicirano. Intersticijska bolezen pljuč/pnevmonitis: Pri bolnikih, ki so bili zaradi limfoma plaščnih celic (MCL) zdravljeni z zdravilom Calquence v kombinaciji z bendamustinom in rituksimabom, so poročali o intersticijski bolezni pljuč/pnevmonitisu. Bolnike je treba spremljati glede pljučnih simptomov, ki nakazujejo intersticijsko bolezen pljuč/pnevmonitis (npr. kašelj, dispneja ali hipoksija) in intersticijsko bolezen pljuč/pnevmonitis obravnavajte, kot je klinično indicirano.
MEDSEBOJNO DELOVANJE Z DRUGIMI ZDRAVILI: Sočasna uporaba močnih zaviralcev CYP3A in zdravila Calquence lahko poveča izpostavljenost akalabrutinibu in tako poveča tveganje za toksične učinke. Nasprotno pa lahko sočasna uporaba induktorjev CYP3A zmanjša izpostavljenost akalabrutinibu in tako pomeni tveganje za nezadostno učinkovitost. Sočasni uporabi z močnimi zaviralci CYP3A se je treba izogniti. Če bo uporaba teh zaviralcev kratkotrajna (npr. antiinfektivna zdravila do sedem dni), je treba zdravljenje z zdravilom Calquence prekiniti. V primeru uporabe zmernega zaviralca CYP3A je treba bolnike skrbno spremljati glede znakov toksičnosti. Sočasni uporabi z močnimi induktorji CYP3A4 se je treba izogibati zaradi tveganja za nezadostno učinkovitost. Tablete akalabrutiniba je mogoče jemati sočasno z zdravili za zmanjšanje izločanja želodčne kisline (zaviralci protonske črpalke, antagonisti receptorjev H2, antacidi), za razliko od kapsul akalabrutiniba, pri katerih je privzem z zdravili za zmanjšanje izločanja kisline moten. Ker zaviralci protonske črpalke učinkujejo dolgo časa, je mogoče, da časovna ločitev odmerkov zaviralcev protonske črpalke ne odpravi medsebojnega delovanja, zato se je treba sočasni uporabi s kapsulami akalabrutiniba izogniti.
NEŽELENI UČINKI: Med bolniki, ki so prejemali zdravilo Calquence v monoterapiji, so bili najpogosteje poročani neželeni učinki katere koli stopnje okužba, driska, glavobol, mišično skeletna bolečina, podplutbe, kašelj, artralgija, utrujenost, navzea in izpuščaj. Najpogosteje poročani neželeni učinki ≥ 3. stopnje so bili okužba, levkopenija, nevtropenija, anemija, drug primarni malignom in trombocitopenija. Med bolniki, ki so prejemali zdravilo Calquence v kombinaciji z obinutuzumabom, so bili najpogosteje poročani neželeni učinki katere koli stopnje okužba, mišično skeletna bolečina, driska, glavobol, levkopenija, nevtropenija, kašelj, utrujenost, artralgija, navzea, omotica in zaprtje. Najpogosteje poročani neželeni učinki ≥ 3. stopnje so bili levkopenija, nevtropenija, okužba, trombocitopenija in anemija. Med bolniki, ki so prejemali zdravilo Calquence v kombinaciji z venetoklaksom, so bili najpogosteje poročani neželeni učinki katere koli stopnje okužbe, nevtropenija, glavobol, podplutbe, driska in mišično skeletna bolečina. Najpogosteje poročani neželeni učinek ≥ 3. stopnje je bil nevtropenija. Med bolniki, ki so prejemali zdravilo Calquence v kombinaciji z venetoklaksom in obinutuzumabom, so bili najpogosteje poročani neželeni učinki katere koli stopnje okužbe, nevtropenija, glavobol, podplutbe, driska, navzea in mišično skeletna bolečina. Najpogosteje poročana neželena učinka ≥ 3. stopnje sta bila nevtropenija in trombocitopenija. Med bolniki, ki so bili zdravljeni z zdravilom Calquence v kombinaciji z bendamustinom in rituksimabom, so bili najpogostejši neželeni učinki zdravila katere koli stopnje nevtropenija, navzea, izpuščaj, driska, mišično skeletna bolečina, glavobol, utrujenost, bruhanje, zaprtje, anemija in trombocitopenija. Najpogosteje zabeleženi neželeni učinki zdravila ≥ 3. stopnje so bili nevtropenija, izpuščaj, trombocitopenija, anemija, pljučnica, drug primarni malignom, hipertenzija in drug primarni malignom izključujoč nemelanomskega kožnega raka.
Od bolnikov, zdravljenih z zdravilom Calquence v kombinaciji z venetoklaksom, so o hudih okužbah (≥ 3. stopnje) poročali pri 12,4 % bolnikov (najpogosteje so poročali o COVID 19 ali pljučnici zaradi COVID 19). Okužbe s smrtnim izidom so se pojavile pri 3,1 % bolnikov (najpogosteje so poročali o COVID 19 ali pljučnici zaradi COVID 19). Od bolnikov, zdravljenih z zdravilom Calquence v kombinaciji z venetoklaksom in obinutuzumabom, so o hudih okužbah (≥ 3. stopnje) poročali pri 23,6 % bolnikov (najpogosteje so poročali o COVID 19 ali pljučnici zaradi COVID 19). Okužbe s smrtnim izidom so se pojavile pri 5,6 % bolnikov (najpogosteje so poročali o COVID 19 ali pljučnici zaradi COVID 19). Med bolniki, zdravljenimi z monoterapijo zdravila Calquence, so o prenehanju zdravljenja zaradi neželenih učinkih poročali pri 14,6 % bolnikov. Ti glavni neželeni učinki so vključevali pljučnico, trombocitopenijo in drisko. O zmanjšanju odmerka zaradi neželenih učinkov so poročali pri 5,9 % bolnikov. Ti glavni neželeni učinki so vključevali reaktivacijo hepatitisa B, sepso in drisko. Med bolniki, zdravljenimi z zdravilom Calquence v kombinaciji z obinutuzumabom, so o prenehanju zdravljenja z zdravilom Calquence zaradi neželenih učinkov poročali pri 10,8 % bolnikov. Ti glavni neželeni učinki so vključevali pljučnico, trombocitopenijo in drisko. O zmanjšanju odmerka zaradi neželenih učinkov so poročali pri 6,7 % bolnikov. Ti glavni neželeni učinki so vključevali nevtropenijo, drisko in bruhanje. Med bolniki, zdravljenimi z zdravilom Calquence v kombinaciji z venetoklaksom, so o prenehanju zdravljenja z zdravilom Calquence zaradi neželenih učinkov poročali pri 7,6 % bolnikov, o zmanjšanju odmerka zdravila Calquence zaradi neželenih učinkov pa pri 5,8 % bolnikov. Med glavnimi neželenimi učinki, ki so vodili v prenehanje zdravljenja, sta bila pljučnica zaradi COVID 19 in COVID 19, neželeni učinek, ki je vodil v zmanjšanje odmerka, pa je bil nevtropenija. Med bolniki, zdravljenimi z zdravilom Calquence v kombinaciji z venetoklaksom in obinutuzumabom, so o prenehanju zdravljenja z zdravilom Calquence zaradi neželenih učinkov poročali pri 13,7 % bolnikov, o zmanjšanju odmerka zdravila Calquence zaradi neželenih učinkov pa pri 6,3 % bolnikov. Med glavnimi neželenimi učinki, ki so vodili v prenehanje zdravljenja, sta bila pljučnica zaradi COVID 19 in COVID 19, neželeni učinek, ki je vodil v zmanjšanje odmerka, pa je bil nevtropenija. Med bolniki, zdravljenimi z zdravilom Calquence v kombinaciji z bendamustinom in rituksimabom, so o prenehanju zdravljenja z zdravilom Calquence zaradi neželenih učinkov poročali pri 42,8 % bolnikov. Ti glavni neželeni učinki so vključevali COVID 19, pljučnico zaradi COVID 19, nevtropenijo in pljučnico. O zmanjšanju odmerka zaradi neželenih učinkov so poročali pri 10,1 % bolnikov. Ti glavni neželeni učinki so vključevali nevtropenijo in navzeo.
POSEBNA NAVODILA ZA SHRANJEVANJE: Posebna navodila za shranjevanje niso potrebna.
VRSTA IN VSEBINA OVOJNINE: Calquence 100 mg trde kapsule: Aluminij/aluminijski pretisni omoti s simboli sonca/lune, vsebujejo 6 ali 8 trdih kapsul. Škatle s 56 ali 60 kapsulami. Calquence 100 mg filmsko obložene tablete: Aluminij/aluminijska pakiranja pretisnih omotov s simboli sonca/lune, vsebujejo 8 ali 10 filmsko obloženih tablet. Škatle s 56 ali 60 tabletami. Na trgu morda ni vseh navedenih pakiranj.
NAČIN IZDAJANJA ZDRAVILA: Rp/Spec - Predpisovanje in izdaja zdravila je le na recept s posebnim režimom.
DATUM REVIZIJE BESEDILA: maj 2026 SI-5187
IMETNIK DOVOLJENJA ZA PROMET: AstraZeneca AB, S-151 85, Sodertalje, Švedska

Pred predpisovanjem, prosimo, preberite celoten povzetek glavnih značilnosti zdravila.
Dodatne informacije so na voljo pri družbi AstraZeneca UK Limited, Podružnica v Sloveniji, Verovškova 55, Ljubljana.

KLL = kronična limfocitna levkemija; MCL = (*angl. Mantle Cell Lymphoma*) limfom plaščnih celic.
Literatura: 1. Povzetek glavnih značilnosti zdravila Calquence, maj 2026.

AstraZeneca
Dodatne informacije so na voljo pri družbi Astrazeneca UK Limited,
Podružnica v Sloveniji, Verovškova 55, Ljubljana. Tel. (01) 51 35 600

Samo za strokovno javnost. Datum priprave: avgust 2026. SI-5670

CALQUENCE
(akalabrutinib) 100 mg tablete

KEYTRUDA SC

(pembrolizumab) raztopina za injiciranje

KEYTRUDA SC raztopina za injiciranje je odobrena za subkutano uporabo kot samostojno ali kombinirano zdravljenje pri odraslih bolnikih v vseh odobrenih indikacijah zdravila KEYTRUDA.[1]

Keytruda SC omogoča:[1]

HITRO SUBKUTANO APLIKACIJO[a]
~ 1 minuta pri Q3W
~ 2 minuti pri Q6W

DALJŠI INTERVAL ODMERJANJA
s shemo odmerjanja Q6W

MAJHEN VOLUMEN INJEKCIJE
2,4 ml pri Q3W
4,8 ml pri Q6W

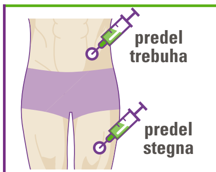

2 MESTI INJICIRANJA

[a] Ne upošteva vseh vidikov zdravljenja. Dejanska dolžina bivanja v kliniki se lahko razlikuje.
Za več informacij o odmerjanju in načinu uporabe za posamezne indikacije glejte Povzetek glavnih značilnosti zdravila

Okrajšave: Q3W = vsake tri tedne; **Q6W** = vsakih šest tednov.
Vir: 1. Povzetek glavnih značilnosti zdravila KEYTRUDA

SKRAJŠAN POVZETEK GLAVNIH ZNAČILNOSTI ZDRAVILA
Pred predpisovanjem, prosimo, preberite celoten Povzetek glavnih značilnosti zdravila!
Ime zdravila: KEYTRUDA 25 mg/ml koncentrat za raztopino za infundiranje; KEYTRUDA 395 mg raztopina za injiciranje; in KEYTRUDA 790 mg raztopina za injiciranje vsebujejo pembrolizumab. Pomožna snov z znanim učinkom: polisorbat. **Terapevtske indikacije:** Zdravilo KEYTRUDA je kot samostojno zdravljenje indicirano za zdravljenje: odraslih in mladostnikov, starih 12 let ali več, z napredovalim (neoperabilnim ali metastatskim) melanomom; za adjuvantno zdravljenje odraslih in mladostnikov, starih 12 let ali več, z melanomom v stadiju IIB, IIC ali III, in sicer po popolni kirurški odstranitvi; za adjuvantno zdravljenje odraslih z nedrobnoceličnim pljučnim rakom, ki imajo visoko tveganje za ponovitev bolezni po popolni kirurški odstranitvi in kemoterapiji na osnovi platine; metastatskega nedrobnoceličnega pljučnega raka (NSCLC) v prvi liniji zdravljenja pri odraslih, ki imajo tumorje z ≥ 50 % izraženostjo PD-L1 (TPS) in brez pozitivnih tumorskih mutacij EGFR ali ALK; lokalno napredovalega ali metastatskega NSCLC pri odraslih, ki imajo tumorje z ≥ 1 % izraženostjo PD-L1 (TPS) in so bili predhodno zdravljeni z vsaj eno shemo kemoterapije, bolniki s pozitivnimi tumorskimi mutacijami EGFR ali ALK so pred prejemom zdravila KEYTRUDA morali prejeti tudi tarčno zdravljenje; odraslih in pediatričnih bolnikov, starih 3 leta ali več, s ponovljenim ali neodzivnim klasičnim Hodgkinovim limfomom (cHL), pri katerih avtologna presaditev matičnih celic (ASCT) ni bila uspešna, ali po najmanj dveh predhodnih zdravljenjih kadar ASCT ne pride v poštev kot možnost zdravljenja; lokalno napredovalega ali metastatskega urotelijskega raka pri odraslih, predhodno zdravljenih s kemoterapijo, ki je vključevala platino; lokalno napredovalega ali metastatskega urotelijskega raka pri odraslih, ki niso primerni za zdravljenje s kemoterapijo, ki vsebuje cisplatin in imajo tumorje z izraženostjo PD-L1 ≥ 10, ocenjeno s kombinirano pozitivno oceno (CPS); ponovljenega ali metastatskega ploščatoceličnega raka glave in vratu (HNSCC) pri odraslih, ki imajo tumorje z ≥ 50 % izraženostjo PD-L1 (TPS), in pri katerih je bolezen napredovala med zdravljenjem ali po zdravljenju s kemoterapijo, ki je vključevala platino; za adjuvantno zdravljenje odraslih z rakom ledvičnih celic s povišanim tveganjem za ponovitev bolezni po nefrektomiji, ali po nefrektomiji in kirurški odstranitvi metastatskih lezij, za zdravljenje odraslih z MSI-H (microsatellite instability-high) ali dMMR (mismatch repair deficient) kolorektalnim rakom v naslednjih terapevtskih okoliščinah: prva linija zdravljenja metastatskega kolorektalnega raka; zdravljenje neoperabilnega ali metastatskega kolorektalnega raka po predhodnem kombiniranem zdravljenju, ki je temeljilo na fluoropirimidinu; in za zdravljenje MSI-H ali dMMR tumorjev pri odraslih z: napredovalim ali ponovljenim rakom endometrija, pri katerih je bolezen napredovala med ali po predhodnem zdravljenju, ki je vključevalo platino, v katerih koli terapevtskih okoliščinah, in ki niso kandidati za kurativno operacijo ali obsevanje; neoperabilnim ali metastatskim rakom želodca, tankega črevesa ali biliarnega trakta, pri katerih je bolezen napredovala med ali po vsaj enem predhodnem zdravljenju. Zdravilo KEYTRUDA je kot samostojno zdravljenje ali v kombinaciji s kemoterapijo s platino in 5-fluorouracilom (5-FU) indicirano za prvo linijo zdravljenja metastatskega ali neoperabilnega ponovljenega ploščatoceličnega raka glave in vratu pri odraslih, ki imajo tumorje z izraženostjo PD-L1 s CPS ≥ 1. Zdravilo KEYTRUDA je v kombinaciji s kemoterapijo, ki vključuje platino, indicirano za neoadjuvantno zdravljenje, in v nadaljevanju kot samostojno zdravljenje za adjuvantno zdravljenje odraslih z operabilnim nedrobnoceličnim pljučnim rakom, ki imajo visoko tveganje za ponovitev bolezni; v kombinaciji s pemetreksedom in kemoterapijo na osnovi platine je indicirano za prvo linijo zdravljenja metastatskega neploščatoceličnega NSCLC pri odraslih, pri katerih tumorji nimajo pozitivnih mutacij EGFR ali ALK; v kombinaciji s karboplatinom in bodisi paklitakselom bodisi nab-paklitakselom je indicirano za prvo linijo zdravljenja metastatskega ploščatoceličnega NSCLC pri odraslih; v kombinaciji s pemetreksedom in kemoterapijo na osnovi platine je indicirano za prvo linijo zdravljenja pri odraslih z neoperabilnim neepiteloidnim malignim mezoteliomom plevre; v kombinaciji z enfortumab vedotinom je indicirano za neoadjuvantno zdravljenje, in v nadaljevanju po radikalni cistektomiji za adjuvantno zdravljenje pri odraslih z operabilnim mišično invazivnim rakom sečnega mehurja (MIBC - muscle invasive bladder cancer), ki niso primerni za zdravljenje s kemoterapijo, ki vsebuje cisplatin; v kombinaciji z enfortumab vedotinom je indicirano za prvo linijo zdravljenja neoperabilnega ali metastatskega urotelijskega raka pri odraslih; kot samostojno zdravljenje je indicirano za neoadjuvantno zdravljenje operabilnega lokalno napredovalega ploščatoceličnega raka glave in vratu, in v nadaljevanju kot adjuvantno zdravljenje v kombinaciji z radioterapijo s sočasnim dajanjem cisplatina ali brez njega, ter nato kot samostojno zdravljenje pri odraslih, ki imajo tumorje z izraženostjo PD-L1 s CPS ≥ 1; v kombinaciji z aksitinibom ali v kombinaciji z lenvatinibom je indicirano za prvo linijo zdravljenja napredovalega raka ledvičnih celic (RCC) pri odraslih; v kombinaciji s kemoterapijo s platino in fluoropirimidinom je indicirano za prvo linijo zdravljenja lokalno napredovalega neoperabilnega ali metastatskega raka požiralnika pri odraslih, ki imajo tumorje z izraženostjo PD-L1 s CPS ≥ 10; v kombinaciji s kemoterapijo za neoadjuvantno zdravljenje, in v nadaljevanju kot samostojno adjuvantno zdravljenje po kirurškem posegu, je indicirano za zdravljenje odraslih z lokalno napredovalim trojno negativnim rakom dojk ali trojno negativnim rakom dojk v zgodnjem stadiju z visokim tveganjem za ponovitev bolezni; v kombinaciji s kemoterapijo je indicirano za zdravljenje lokalno ponovljenega neoperabilnega ali metastatskega trojno negativnega raka dojk pri odraslih, ki imajo tumorje z izraženostjo PD-L1 s CPS ≥ 10 in predhodno niso prejeli kemoterapije za metastatsko bolezen; v kombinaciji s karboplatinom in paklitakselom je indicirano za prvo linijo zdravljenja primarno napredovalega ali ponovljenega raka endometrija (EC) pri odraslih, ki so kandidati za sistemsko zdravljenje; v kombinaciji z lenvatinibom je indicirano za zdravljenje napredovalega ali ponovljenega raka endometrija pri odraslih z napredovalo boleznijo med ali po predhodnem zdravljenju s kemoterapijo, ki je vključevala platino, v katerih koli terapevtskih okoliščinah, in ki niso kandidati za kurativno operacijo ali obsevanje; v kombinaciji s kemoradioterapijo (zdravljenje z zunanjim obsevanjem, ki mu sledi brahiterapija) je indicirano za zdravljenje lokalno napredovalega raka materničnega vratu v stadiju III - IVA po FIGO 2014 pri odraslih, ki niso prejeli predhodne definitivne terapije; v kombinaciji s kemoterapijo, z bevacizumabom ali brez njega, je indicirano za zdravljenje persistentnega, ponovljenega ali metastatskega raka materničnega vratu pri odraslih bolnicah, ki imajo tumorje z izraženostjo PD-L1 s CPS ≥ 1; v kombinaciji s trastuzumabom, fluoropirimidinom in kemoterapijo, ki vključuje platino, je indicirano za prvo linijo zdravljenja lokalno napredovalega neoperabilnega ali metastatskega HER2-pozitivnega adenokarcinoma želodca ali gastroezofagealnega prehoda pri odraslih, ki imajo tumorje z izraženostjo PD-L1 s CPS ≥ 1; v kombinaciji s fluoropirimidinom in kemoterapijo, ki vključuje platino, je indicirano za prvo linijo zdravljenja lokalno napredovalega neoperabilnega ali metastatskega HER2-negativnega adenokarcinoma želodca ali gastroezofagealnega prehoda pri odraslih, ki imajo tumorje z izraženostjo PD-L1 s CPS ≥ 1; v kombinaciji z gemcitabinom in cisplatinom je indicirano za prvo linijo zdravljenja lokalno napredovalega neoperabilnega ali metastatskega raka biliarnega trakta pri odraslih; v kombinaciji s paklitakselom, z bevacizumabom ali brez njega, je indicirano za zdravljenje na platino odpornega epitelijskega raka jajčnikov, jajcevodov ali primarnega peritonealnega karcinoma pri odraslih bolnicah, ki imajo tumorje z izraženostjo PD-L1 s CPS ≥ 1 in so prejele eno ali dve predhodni shemi sistemskega zdravljenja. **Odmerjanje in način uporabe:** Bolniki, ki prejemajo pembrolizumab intravensko, lahko preidejo na subkutani pembrolizumab ob naslednjem predvidenem odmerku. Bolniki, ki prejemajo pembrolizumab subkutano, lahko preidejo na intravenski pembrolizumab ob naslednjem predvidenem odmerku. Testiranje PD-L1: Če je navedeno v indikaciji, je treba izbiro bolnika za zdravljenje z zdravilom KEYTRUDA na podlagi izraženosti PD-L1 tumorja potrditi z validirano preiskavo. Testiranje MSI/MMR: Če je navedeno v indikaciji, je treba izbiro bolnika za zdravljenje z zdravilom KEYTRUDA na podlagi MSI-H/dMMR statusa tumorja potrditi z validirano preiskavo. Odmerjanje: Priporočeni odmerek zdravila KEYTRUDA pri odraslih je bodisi 200 mg na 3 tedne ali 400 mg na 6 tednov, apliciran z intravensko infuzijo v 30 minutah. Priporočeni odmerek zdravila KEYTRUDA za samostojno zdravljenje pri pediatričnih bolnikih s cHL, starih 3 leta ali več, ali bolnikih z melanomom, starih 12 let ali več, je 2 mg/kg telesne mase (do največ 200 mg) na 3 tedne, apliciran z intravensko infuzijo v 30 minutah. Priporočeni odmerek zdravila KEYTRUDA raztopina za injiciranje pri odraslih in pri mladostnikih z melanomom ali cHL, starih 12 let ali več in s telesno maso več kot 40 kg, je bodisi: 395 mg na 3 tedne v subkutani injekciji, ki traja 1 minuto, ali 790 mg na 6 tednov v subkutani injekciji, ki traja 2 minuti. Za uporabo v kombinaciji glejte povzetke glavnih značilnosti zdravil sočasno uporabljenih zdravil. Bolnike je treba zdraviti do napredovanja bolezni ali nesprejemljivih toksičnih učinkov (in do maksimalnega trajanja zdravljenja, če je le to določeno za indikacijo). Pri adjuvantnem zdravljenju melanoma, NSCLC ali RCC je treba zdravilo uporabljati do ponovitve bolezni, pojava nesprejemljivih toksičnih učinkov oziroma mora zdravljenje trajati do enega leta. Za neoadjuvantno in adjuvantno zdravljenje operabilnega NSCLC morajo bolniki neoadjuvantno prejeti zdravilo KEYTRUDA v kombinaciji s kemoterapijo, in sicer 4 odmerke po 200 mg ali 395 mg na 3 tedne ali 2 odmerka po 400 mg ali 790 mg na 6 tednov ali do napredovanja bolezni, ki izključuje definitivni kirurški poseg, ali do pojava nesprejemljivih toksičnih učinkov, čemur sledi adjuvantno zdravljenje z zdravilom KEYTRUDA kot samostojnim zdravljenjem, in sicer 13 odmerkov po 200 mg ali 395 mg na 3 tedne ali 7 odmerkov po 400 mg ali 790 mg na 6 tednov ali do ponovitve bolezni ali do pojava nesprejemljivih toksičnih učinkov. Bolniki, pri katerih pride do napredovanja bolezni, ki izključuje definitivni kirurški poseg, ali do nesprejemljivih toksičnih učinkov, povezanih z zdravilom KEYTRUDA kot neoadjuvantnim zdravljenjem v kombinaciji s kemoterapijo, ne smejo prejeti zdravila KEYTRUDA kot samostojnega zdravljenja za adjuvantno zdravljenje. Za neoadjuvantno in adjuvantno zdravljenje bolnikov z MIBC, ki niso primerni za zdravljenje s cisplatinom, morajo bolniki neoadjuvantno prejeti zdravilo KEYTRUDA v kombinaciji z enfortumab vedotinom, in sicer 3 odmerke po 200 mg na 3 tedne ali 3 odmerke po 395 mg na 3 tedne ali do napredovanja bolezni, ki izključuje radikalno cistektomijo, ali do pojava nesprejemljivih toksičnih učinkov, čemur sledi adjuvantno zdravljenje z zdravilom KEYTRUDA v kombinaciji z enfortumab vedotinom, in sicer 14 odmerkov po 200 mg na 3 tedne ali 14 odmerkov po 395 mg na 3 tedne ali 7 odmerkov po 400 mg na 6 tednov ali 7 odmerkov po 790 mg na 6 tednov ali do ponovitve bolezni ali do pojava nesprejemljivih toksičnih učinkov. Za neoadjuvantno in adjuvantno zdravljenje operabilnega lokalno napredovalega HNSCC morajo bolniki prejeti zdravilo KEYTRUDA neoadjuvantno kot samostojno zdravljenje, in sicer 2 odmerka po 200 mg ali 395 mg na 3 tedne ali 1 odmerek po 400 mg ali 790 mg ali do napredovanja bolezni, ki izključuje definitivni kirurški poseg, ali do pojava nesprejemljivih toksičnih učinkov, čemur sledi adjuvantno zdravljenje z zdravilom KEYTRUDA v kombinaciji z radioterapijo s sočasnim dajanjem cisplatina ali brez njega, in sicer 3 odmerki po 200 mg ali 395 mg na 3 tedne ali 2 odmerka po 400 mg ali 790 mg na 6 tednov, čemur sledi samostojno zdravljenje z zdravilom KEYTRUDA, in sicer 12 odmerkov po 200 mg ali 395 mg na 3 tedne ali 6 odmerkov po 400 mg ali 790 mg na 6 tednov oziroma do ponovitve bolezni ali pojava nesprejemljivih toksičnih učinkov. Bolniki, pri katerih pride do napredovanja bolezni, ki izključuje definitivni kirurški poseg, ali do nesprejemljivih toksičnih učinkov, povezanih s samostojnim zdravljenjem z zdravilom KEYTRUDA kot neoadjuvantnim zdravljenjem, ne smejo prejeti zdravila KEYTRUDA v kombinaciji z radioterapijo s sočasnim dajanjem cisplatina ali brez njega za adjuvantno zdravljenje. Za neoadjuvantno in adjuvantno zdravljenje TNBC morajo bolniki neoadjuvantno prejeti zdravilo KEYTRUDA v kombinaciji s kemoterapijo, in sicer 8 odmerkov po 200 mg ali 395 mg na 3 tedne ali 4 odmerke po 400 mg ali 790 mg na 6 tednov, ali do napredovanja bolezni, ki izključuje definitivni kirurški poseg, ali do pojava nesprejemljivih toksičnih učinkov, čemur sledi adjuvantno zdravljenje z zdravilom KEYTRUDA kot samostojnim zdravljenjem, in sicer 9 odmerkov po 200 mg ali 395 mg na 3 tedne ali 5 odmerkov po 400 mg ali 790 mg na 6 tednov ali do ponovitve bolezni ali pojava nesprejemljivih toksičnih učinkov. Bolniki, pri katerih pride do napredovanja bolezni, ki izključuje definitivni kirurški poseg, ali do nesprejemljivih toksičnih učinkov povezanih z zdravilom KEYTRUDA kot neoadjuvantnim zdravljenjem v kombinaciji s kemoterapijo, ne smejo prejemati zdravila KEYTRUDA kot samostojnega zdravljenja za adjuvantno zdravljenje. Za lokalno napredovalega raka materničnega vratu morajo bolnice prejeti zdravilo KEYTRUDA sočasno s kemoradioterapijo, čemur sledi samostojno zdravljenje z zdravilom KEYTRUDA. Zdravilo KEYTRUDA se lahko daje v odmerku 200 mg ali 395 mg na 3 tedne ali 400 mg ali 790 mg na 6 tednov do napredovanja bolezni, pojava nesprejemljivih toksičnih učinkov ali do 24 mesecev. Če je aksitinib uporabljen v kombinaciji s pembrolizumabom, se lahko razmisli o povečanju odmerka aksitiniba nad začetnih 5 mg v presledkih šest tednov ali več. V primeru uporabe v kombinaciji z lenvatinibom je treba zdravljenje z enim ali obema zdraviloma prekiniti, kot je primerno. Uporabo lenvatiniba je treba zadržati, odmerek zmanjšati ali prenehati z uporabo, v skladu z navodili v povzetku glavnih značilnosti zdravila za lenvatinib, in sicer za kombinacijo s pembrolizumabom. Pri bolnikih starih ≥ 65 let, bolnikih z blago do zmerno okvaro ledvic, bolnikih z blago ali zmerno okvaro jeter prilagoditev odmerka ni potrebna. *Odložitev odmerka ali ukinitev zdravljenja:* Zmanjšanje odmerka zdravila KEYTRUDA ni priporočljivo. Za obvladovanje neželenih učinkov je treba uporabo zdravila KEYTRUDA zadržati ali ukiniti, prosimo, glejte celoten Povzetek glavnih značilnosti zdravila. Način uporabe: Pomembno je preveriti nalepko viale in tako zagotoviti pripravo in uporabo pravilne, bolniku predpisane oblike zdravila (intravenske ali subkutane), da se zmanjša tveganje za napake pri uporabi zdravila. **Zdravilo KEYTRUDA koncentrat za raztopino za infundiranje je namenjeno le za intravensko uporabo. Zdravilo KEYTRUDA koncentrat za raztopino za infundiranje ni namenjeno za subkutano uporabo.** Zdravilo KEYTRUDA koncentrat za raztopino za infundiranje je treba dajati z infuzijo, ki traja 30 minut. Intravenske oblike zdravila KEYTRUDA se ne sme dajati s hitro infuzijo ali z bolusno injekcijo. Zdravila KEYTRUDA koncentrat za raztopino za infundiranje se ne sme zamenjati s subkutano obliko pembrolizumaba in obratno, ker imata različne priporočene odmerke in poti uporabe. **Zdravilo KEYTRUDA raztopina za injiciranje je namenjeno le za subkutano uporabo. Zdravila KEYTRUDA raztopina za injiciranje se ne sme dajati intravensko.** Zdravila KEYTRUDA raztopina za injiciranje se ne sme zamenjati z intravensko obliko pembrolizumaba in obratno, ker imata različne priporočene odmerke in poti uporabe. Zdravilo KEYTRUDA raztopina za injiciranje je namenjeno le za subkutano injiciranje v stegno ali trebuh. Mesta injiciranja menjajte pri vsakem naslednjem injiciranju. Med zdravljenjem z zdravilom KEYTRUDA raztopina za injiciranje ne dajajte drugih zdravil za subkutano uporabo na isto mesto kot zdravilo KEYTRUDA raztopina za injiciranje. Če se zdravilo KEYTRUDA uporablja kot del kombiniranega zdravljenja skupaj z intravensko kemoterapijo, je treba zdravilo KEYTRUDA aplicirati prvo. Če se zdravilo KEYTRUDA uporablja kot del kombiniranega zdravljenja skupaj z enfortumab vedotinom, je treba zdravilo KEYTRUDA aplicirati po enfortumab vedotinu, kadar sta uporabljena na isti dan. **Kontraindikacije**: Preobčutljivost na učinkovino ali katero koli pomožno snov. **Povzetek posebnih opozoril, previdnostnih ukrepov, interakcij in neželenih učinkov:** Imunsko pogojeni neželeni učinki (pnevmonitis, kolitis, hepatitis, nefritis, endokrinopatije, neželeni učinki na kožo in drugi): Pri bolnikih, ki so prejemali pembrolizumab, so se pojavili imunsko pogojeni neželeni učinki, vključno s hudimi in smrtnimi primeri. Večina imunsko pogojenih neželenih učinkov, ki so se pojavili med zdravljenjem s pembrolizumabom, je bila reverzibilnih in so jih obvladali s prekinitvami uporabe pembrolizumaba, uporabo kortikosteroidov in/ali podporno oskrbo. Pojavijo se lahko tudi po zadnjem odmerku pembrolizumaba in hkrati prizadanejo več organskih sistemov. V primeru suma na imunsko pogojene neželene učinke je treba poskrbeti za ustrezno oceno za potrditev etiologije oziroma izključitev drugih vzrokov. Glede na izrazitost neželenega učinka je treba zadržati uporabo pembrolizumaba in uporabiti kortikosteroide – za natančna navodila, prosimo, glejte Povzetek glavnih značilnosti zdravila Keytruda. Zdravljenje s pembrolizumabom lahko poveča tveganje za zavrnitev pri prejemnikih presadkov čvrstih organov. Pri bolnikih, ki so prejemali pembrolizumab, so poročali o hudih z infuzijo povezanih reakcijah, vključno s preobčutljivostjo in anafilaksijo. Pembrolizumab se iz obtoka odstrani s katabolizmom, zato presnovnih medsebojnih delovanj zdravil ni pričakovati. Uporabi sistemskih kortikosteroidov ali imunosupresivov pred uvedbo pembrolizumaba se je treba izogibati, ker lahko vplivajo na farmakodinamično aktivnost in učinkovitost pembrolizumaba. Vendar pa je kortikosteroide ali druge imunosupresive mogoče uporabiti za zdravljenje imunsko pogojenih neželenih učinkov. Kortikosteroide je mogoče uporabiti tudi kot premedikacijo, če je pembrolizumab uporabljen v kombinaciji s kemoterapijo, kot antiemetično profilakso in/ali za ublažitev neželenih učinkov, povezanih s kemoterapijo. Ženske v rodni dobi morajo med zdravljenjem s pembrolizumabom in vsaj še 4 mesece po zadnjem odmerku pembrolizumaba uporabljati učinkovito kontracepcijo, med nosečnostjo in dojenjem se ga ne sme uporabljati. Varnost pembrolizumaba pri samostojnem zdravljenju so v kliničnih študijah ocenili pri 7631 bolnikih, ki so imeli različne vrste raka, s štirimi odmerki (2 mg/kg telesne mase na 3 tedne, 200 mg na 3 tedne in 10 mg/kg telesne mase na 2 ali 3 tedne). V tej populaciji bolnikov je mediani čas opazovanja znašal 8,5 meseca (v razponu od 1 dneva do 39 mesecev), najpogostejši neželeni učinki zdravljenja s pembrolizumabom pa so bili utrujenost (31 %), diareja (22 %) in navzea (20 %). Večina poročanih neželenih učinkov pri samostojnem zdravljenju je bila po izrazitosti 1. ali 2. stopnje. Najresnejši neželeni učinki so bili imunsko pogojeni neželeni učinki in hude z infuzijo povezane reakcije. Pojavnost imunsko pogojenih neželenih učinkov pri uporabi pembrolizumaba samega za adjuvantno zdravljenje je znašala 37 % za vse stopnje in 9 % od 3. do 5. stopnje, pri metastatski bolezni pa 25 % za vse stopnje in 6 % od 3. do 5. stopnje. Pri adjuvantnem zdravljenju niso zaznali nobenih novih imunsko pogojenih neželenih učinkov. Varnost pembrolizumaba pri kombiniranem zdravljenju s kemoterapijo, RT ali CRT so ocenili pri 7015 bolnikih z različnimi vrstami raka, ki so v kliničnih študijah prejemali pembrolizumab v odmerkih 200 mg, 2 mg/kg telesne mase ali 10 mg/kg telesne mase na vsake 3 tedne oziroma 400 mg na vsakih 6 tednov. V tej populaciji bolnikov so bili najpogostejši neželeni učinki naslednji: anemija (51 %), navzea (50 %), utrujenost (36 %), diareja (35 %), zaprtost (32 %), bruhanje (27 %) in zmanjšanje apetita (26 %). Pojavnost neželenih učinkov 3. do 5. stopnje je pri bolnikih z NSCLC pri kombiniranem zdravljenju s pembrolizumabom znašala 69 % in pri zdravljenju samo s kemoterapijo 61 %, pri bolnikih s HNSCC pri kombiniranem zdravljenju s pembrolizumabom (kemoterapija ali RT s kemoterapijo ali brez nje) 80 % in pri zdravljenju s kemoterapijo v kombinaciji s cetuksimabom ali RT s kemoterapijo ali brez nje 79 %, pri bolnikih z rakom požiralnika pri kombiniranem zdravljenju s pembrolizumabom 86 % in pri zdravljenju samo s kemoterapijo 83 %, pri bolnikih s TNBC pri kombiniranem zdravljenju s pembrolizumabom 80 % in pri zdravljenju samo s kemoterapijo 77 %, pri bolnicah z rakom materničnega vratu pri kombiniranem zdravljenju s pembrolizumabom (kemoterapija z ali brez bevacizumaba ali v kombinaciji s CRT) 77 % in pri zdravljenju s kemoterapijo z ali brez bevacizumaba ali samostojno s CRT 71 %, pri bolnikih z rakom želodca pri kombiniranem zdravljenju s pembrolizumabom (kemoterapija z ali brez trastuzumaba) 74 % in pri kemoterapiji v kombinaciji z ali brez trastuzumaba 68 %, pri bolnikih z rakom biliarnega trakta pri kombiniranem zdravljenju s pembrolizumabom 85 % in pri samostojni kemoterapiji 84 %, pri bolnicah z EC pri kombiniranem zdravljenju s pembrolizumabom 59 % in pri samostojni kemoterapiji 46 %, pri bolnikih z malignim mezoteliomom plevre pri kombiniranem zdravljenju s pembrolizumabom 44 % in pri samostojni kemoterapiji 30 %, in pri bolnicah z rakom jajčnikov pri kombiniranem zdravljenju s pembrolizumabom (kemoterapija z ali brez bevacizumaba) 83 % in pri zdravljenju s kemoterapijo z ali brez bevacizumaba 71 %. Varnost pembrolizumaba v kombinaciji z aksitinibom ali lenvatinibom pri napredovalem RCC in v kombinaciji z lenvatinibom pri napredovalem EC so ocenili pri skupno 1456 bolnikih z napredovalim RCC ali napredovalim EC, ki so v kliničnih študijah prejemali 200 mg pembrolizumaba na 3 tedne skupaj s 5 mg aksitiniba dvakrat na dan ali z 20 mg lenvatiniba enkrat na dan, kot je bilo ustrezno. V teh populacijah bolnikov so bili najpogostejši neželeni učinki diareja (58 %), hipertenzija (54 %), hipotiroidizem (46 %), utrujenost (41 %), zmanjšan apetit (40 %), navzea (40 %), artralgija (30 %), bruhanje (28 %), zmanjšanje telesne mase (28 %), disfonija (28 %), bolečine v trebuhu (28 %), proteinurija (27 %), sindrom palmarno-plantarne eritrodizestezije (26 %), izpuščaj (26 %), stomatitis (25 %), zaprtost (25 %), mišično-skeletna bolečina (23 %), glavobol (23 %) in kašelj (21 %). Neželenih učinkov od 3. do 5. stopnje je bilo pri bolnikih z RCC med uporabo pembrolizumaba v kombinaciji z aksitinibom ali lenvatinibom 80 % in med uporabo sunitiniba samega 71 %. Pri bolnicah z EC je bilo neželenih učinkov od 3. do 5. stopnje med uporabo pembrolizumaba v kombinaciji z lenvatinibom 89 % in med uporabo kemoterapije same 73 %. Varnost pembrolizumaba v kombinaciji z enfortumab vedotinom so ocenili pri 564 bolnikih z neoperabilnim ali metastatskim urotelijskim rakom, ki so prejemali 200 mg pembrolizumaba 1. dan in 1,25 mg/kg enfortumab vedotina 1. in 8. dan vsakega 21-dnevnega ciklusa. Na splošno so opazili, da je bila pojavnost neželenih učinkov za pembrolizumab v kombinaciji z enfortumab vedotinom višja kot pri samostojnem zdravljenju s pembrolizumabom, kar odraža prispevek enfortumab vedotina in daljšega trajanja kombiniranega zdravljenja. Neželeni učinki so bili na splošno podobni neželenim učinkom, ki so jih opazili pri bolnikih, ki so prejemali pembrolizumab ali enfortumab vedotin kot samostojno zdravljenje. Pojavnost makulopapuloznega izpuščaja vseh stopenj je bila 36 % (10 % od 3. do 4. stopnje), kar je višje, kot je bilo opaženo pri samostojnem zdravljenju s pembrolizumabom. Na splošno so bile pogostnosti neželenih učinkov višje pri bolnikih, starih ≥ 65 let, v primerjavi z bolniki, starimi < 65 let, predvsem za resne neželene učinke (56,3 % pri bolnikih, starih ≥ 65 let, in 35,3 % pri bolnikih, starih < 65 let) in učinke ≥ 3. stopnje (80,3 % pri bolnikih, starih ≥ 65 let, in 64,2 % pri bolnikih, starih < 65 let), podobno kot opažanja pri primerjalni kemoterapiji. Varnost pembrolizumaba v kombinaciji z enfortumab vedotinom so ocenili pri 167 bolnikih z MIBC, ki so prejemali 200 mg pembrolizumaba 1. dan in 1,25 mg/kg enfortumab vedotina 1. in 8. dan vsakega 21-dnevnega ciklusa kot neoadjuvantno zdravljenje in v nadaljevanju po radikalni cistektomiji kot adjuvantno zdravljenje. Na splošno so opazili, da je bila pojavnost neželenih učinkov pri pembrolizumabu v kombinaciji z enfortumab vedotinom višja kot pri samostojnem zdravljenju s pembrolizumabom, kar odraža prispevek enfortumab vedotina. Neželeni učinki so bili na splošno podobni neželenim učinkom, opaženim pri bolnikih z neoperabilnim ali metastatskim urotelijskim rakom, ki so bili zdravljeni s pembrolizumabom v kombinaciji z enfortumab vedotinom. Za celoten seznam neželenih učinkov, prosimo, glejte celoten Povzetek glavnih značilnosti zdravila. Za dodatne informacije o varnosti v primeru uporabe pembrolizumaba v kombinaciji glejte povzetke glavnih značilnosti zdravila za posamezne komponente kombiniranega zdravljenja. **Način in režim izdaje zdravila:** H – Predpisovanje in izdaja zdravila je le na recept, zdravilo se uporablja samo v bolnišnicah. **Imetnik dovoljenja za promet z zdravilom:** Merck Sharp & Dohme B.V., Waarderweg 39, 2031 BN Haarlem, Nizozemska.

MSD

itovebi
inavolisib 3 mg • 9 mg filmsko obložene tablete

Roche

Odločilna prva poteza

pri zdravljenju PIK3CA mutiranega raka dojk[1]

Itovebi

- v kombinaciji s palbociklibom in fulvestrantom
- v prvi liniji zdravljenja bolnikov z ER - pozitivnim, HER 2 - negativnim lokalno napredovalim ali razsejanim rakom dojk
- s prisotno mutacijo PIK3CA

+7 mesecev mOS[2]

34,0 proti 27,0 mesecev
Stratificirano razmerje ogroženosti = 0,67
(95 % IZ: 0,48–0,94) *p*=0,02

>2× podaljšana mPFS*[2]

17,2 proti 7,3 mesece
Stratificirano razmerje ogroženosti = 0,42
(95 % IZ: 0,32–0,55)

Zdravilo še ni krito iz obveznega zdravstvenega zavarovanja.

* posodobljena analiza PFS (mediana sledenja 34, 2 meseca)

EMA - Evropska agencija za zdravila; **mOS** - mediana celokupnega preživetja; **mPFS** - mediana preživetja brez napredovanja bolezni; **IZ** - interval zaupanja

Reference: 1. Povzetek glavnih značilnosti zdravila Itovebi, dostopano avgusta 2026 na:https://ec.europa.eu/health/documents/community-register/2025/20250718166598/anx_166598_sl.pdf. **2.** Jhaveri KL, Im S-A, Saura C, et al. N Engl J Med. 2025; 393: 151-61, dostopano avgusta 2026 na: https://www.nejm.org/doi/10.1056/NEJMoa2501796?url_ver=Z39.88-2003&rfr_id=ori:rid:crossref.org&rfr_dat=cr_pub%20%200pubmed

▽ Za to zdravilo se izvaja dodatno spremljanje varnosti, kar označuje navzdol obrnjen črn trikotnik. Tako bodo hitreje na voljo nove informacije o njegovi varnosti. Sami lahko k temu prispevate s poročanjem o katerem koli domnevnem neželenem učinku zdravila. Prosimo, da o domnevnih neželenih učinkih, ki jih opazite pri zdravljenju z zdravilom Itovebi, poročate Nacionalnemu centru za farmakovigilanco prek spletnega obrazca ali na drug način naveden na spletni strani JAZMP (www.jazmp.si/humana-zdravila/farmakovigilanca/porocanje-o-nezelenih-ucinkih-zdravil/).

Ime zdravila: Itovebi 3 mg filmsko obložene tablete / 9 mg filmsko obložene tablete. **Kakovostna in količinska sestava:** Ena filmsko obložena tableta vsebuje 3 mg / 9 mg inavolisiba. *Pomožna snov z znanim učinkom:* Ena filmsko obložena tableta vsebuje 22 mg / 66 mg laktoze. **Terapevtske indikacije:** Zdravilo Itovebi je v kombinaciji s palbociklibom in fulvestrantom indicirano za zdravljenje odraslih bolnikov z lokalno napredovalim ali razsejanim rakom dojk s prisotno mutacijo PIK3CA, ki je pozitiven na estrogenske receptorje (ER-pozitiven) in HER2-negativen, po ponovitvi bolezni med adjuvantnim endokrinim zdravljenjem ali v 12 mesecih po koncu adjuvantnega endokrinega zdravljenja. Pri bolnikih, ki so v okviru (neo)adjuvantnega zdravljenja prejemali zaviralce CDK 4/6, mora od prenehanja zdravljenja z zaviralcem CDK 4/6 do ponovitve bolezni preteči najmanj 12 mesecev. Pri ženskah pred menopavzo/v perimenopavzi in moških je treba endokrino zdravljenje kombinirati z agonistom LHRH (LHRH – Luteinising Hormone-Releasing Hormone). **Odmerjanje in način uporabe:** Priporočeni odmerek zdravila Itovebi je 9 mg peroralno enkrat na dan s hrano ali brez nje. Zdravilo Itovebi je treba dajati v kombinaciji s palbociklibom in fulvestrantom. Zdravljenje žensk pred menopavzo ali v perimenopavzi in moških z zdravilom Itovebi mora vključevati tudi agonist LHRH v skladu z lokalno klinično prakso. Način uporabe: Zdravilo Itovebi se jemlje peroralno. Tablete se lahko jemljejo s hrano ali brez nje. Tablete je treba pogoltniti cele in jih ni dovoljeno žvečiti, zdrobiti, raztopiti ali deliti. **Kontraindikacije:** Preobčutljivost na učinkovino ali katero koli pomožno snov. **Posebna opozorila in previdnostni ukrepi:** Hiperglikemija: Pri bolnikih z anamnezo sladkorne bolezni bo med zdravljenjem z zdravilom Itovebi morda potrebno okrepljeno antihiperglikemično zdravljenje in pogostejše spremljanje ravni glukoze na tešče. Zdravljenja z zdravilom Itovebi se ne sme pričeti, dokler se ravni glukoze na tešče ne optimizirajo. Pri bolnikih, zdravljenih z zdravilom Itovebi, so pogosto poročali o hiperglikemiji. Zabeležili so primere hude hiperglikemije, vključno s ketoacidozo s smrtnimi zapleti. Pred začetkom zdravljenja z zdravilom Itovebi je treba bolnike seznaniti z znaki in simptomi hiperglikemije in jim naročiti, naj nemudoma obvestijo zdravstvenega delavca v primeru pojava teh simptomov. Pred in med zdravljenjem je treba vzdrževati optimalno hidracijo. Pri bolnikih je treba pred zdravljenjem z zdravilom Itovebi in v rednih intervalih med zdravljenjem preverjati raven glukoze na tešče ali raven glukoze v krvi na tešče in vrednost HbA_{1c}. Pri bolnikih, ki imajo dejavnike tveganja za hiperglikemijo ali pri katerih se pojavi hiperglikemija, je treba razmisliti o spremljanju ravni glukoze na tešče v domačem okolju. Pri bolnikih z dejavniki tveganja za hiperglikemijo je smiselno razmisliti o premedikaciji z metforminom. Vse bolnike je treba poučiti o spremembah življenjskega sloga. Stomatitis: Pri bolnikih, zdravljenih z zdravilom Itovebi, so poročali o stomatitisu. Glede na izrazitost stomatitisa se lahko odmerjanje zdravila Itovebi prekine, zmanjša ali dokončno ukine. Bolnikom je treba svetovati, naj ob prvih znakih stomatitisa začnejo z izpiranjem ust z ustno vodo, ki vsebuje kortikosteroide, in naj se izogibajo ustnim vodam, ki vsebujejo alkohol ali peroksid, saj z njihovo uporabo stanje lahko poslabšajo. Smiselno je svetovati tudi spremembe v prehrani. Uporaba pri bolnikih, ki so predhodno prejemali zaviralec CDK4/6: Podatkov o učinkovitosti kombinacije zdravila Itovebi, palbocikliba in fulvestranta je zelo malo pri bolnikih, ki so predhodno prejemali zaviralec CDK4/6 kot del neoadjuvantnega ali adjuvantnega zdravljenja. Učinkovitost je lahko pri takih bolnikih manjša. Laktoza: Bolniki z redko dedno intoleranco za galaktozo, odsotnostjo encima laktaze ali malabsorpcijo glukoze/galaktoze ne smejo jemati tega zdravila. **Medsebojno delovanje z drugimi zdravili in druge oblike interakcij:** Zaviralci in induktorji CYP: Rezultati kliničnih študij kažejo, da za nastanek prevladujočih presnovkov inavolisiba niso odgovorni encimi CYP in da je glavna presnovna pot hidroliza. To kaže na majhno verjetnost klinično pomembnega medsebojnega delovanja med inavolisibom in zaviralci ali induktorji CYP. Substrati CYP: Inavolisib inducira CYP3A in je časovno odvisen zaviralec CYP3A *in vitro*. Zato je treba inavolisib uporabljati previdno v kombinaciji z občutljivimi substrati CYP3A4 z ozkim terapevtskim oknom, saj lahko inavolisib poveča ali zmanjša sistemsko izpostavljenost tem substratom. Poleg tega inavolisib inducira CYP2B6, CYP2C8, CYP2C9 in CYP2C19 *in vitro*. Zato je treba inavolisib uporabljati previdno v kombinaciji z občutljivimi substrati teh encimov z ozkim_terapevtskim oknom, saj lahko inavolisib zmanjša sistemsko izpostavljenost tem substratom in posledično zmanjša učinkovitost. **Neželeni učinki:** Najpogostejši neželeni učinki pri bolnikih, ki so prejemali zdravilo Itovebi, so bili hiperglikemija, stomatitis, driska, trombocitopenija, utrujenost, anemija, navzea, zmanjšan apetit, izpuščaj, glavobol, zmanjšanje telesne mase, bruhanje in okužbe sečil. Najpogostejši resni neželeni učinki, o katerih so poročali pri bolnikih, ki so prejemali zdravilo Itovebi, so bili anemija, driska in okužbe sečil. Neželeni učinki, zaradi katerih je bilo treba zdravljenje z zdravilom Itovebi dokončno ukiniti, so bili hiperglikemija, stomatitis, zvišanje ALT in zmanjšanje telesne mase. Poročanje o domnevnih neželenih učinkih: Poročanje o domnevnih neželenih učinkih zdravila po izdaji dovoljenja za promet je pomembno. Omogoča namreč stalno spremljanje razmerja med koristmi in tveganji zdravila. Od zdravstvenih delavcev se zahteva, da poročajo o katerem koli domnevnem neželenem učinku zdravila na: Javna agencija Republike Slovenije za zdravila in medicinske pripomočke, Sektor za farmakovigilanco, Nacionalni center za farmakovigilanco, Slovenčeva ulica 22, SI-1000 Ljubljana, Tel: +386 (0)8 2000 500, Faks: +386 (0)8 2000 510, e-pošta: h-farmakovigilanca@jazmp.si, spletna stran: www.jazmp.si. Za zagotavljanje sledljivosti zdravila je pomembno, da pri izpolnjevanju obrazca o domnevnih neželenih učinkih zdravila navedete številko serije biološkega zdravila. **Režim izdaje zdravila:** Rp/Spec. **Imetnik dovoljenja za promet:** Roche Registration GmbH, Emil-Barell-Strasse 1, 79639 Grenzach-Wyhlen, Nemčija. Za podrobnejše informacije glejte celoten Povzetek glavnih značilnosti zdravila. **Verzija: 1.0/25**

DODATNE INFORMACIJE SO NA VOLJO PRI:
Roche farmacevtska družba d.o.o., Stegne 13G, Ljubljana

Samo za strokovno javnost.
M-SI-00001489 (v 2.0). Datum priprave informacije: avgust 2026

▼TIBSOVO® 250 mg filmsko obložene tablete: PERSONALIZIRANO ZDRAVLJENJE ZA VEČJO KORIST

Pri predhodno zdravljenih bolnikih s holangiokarcinomom (CCA) in prisotno mutacijo IDH1 R132 Tibsovo (ivosidenib) omogoča:

- podaljšanje mPFS v primerjavi s placebom in 63-% zmanjšanje tveganja za napredovanje bolezni ali smrt (p<0,0001)[1]
- dvakrat daljši mOS v primerjavi s placebom in 51-% zmanjšanje tveganja za smrt (p<0,001; RPSFT-prilagojeni)[2]
- obvladljiv profil varnosti.[1-3]

Omogočite svojim bolnikom s CCA in prisotno mutacijo IDH1 R132 TARČNO ZDRAVLJENJE z zdravilom TIBSOVO®

▼Za to zdravilo se izvaja dodatno spremljanje varnosti. Tako bodo hitreje na voljo nove informacije o njegovi varnosti. Zdravstvene delavce naprošamo, da poročajo o katerem koli domnevnem neželenem učinku zdravila.

1. Abou-Alfa GK et al. Lancet Oncol. 2020;21:796-807. 2. Zhu AX et al. JAMA Oncol. 2021;7:1669-1677. 3. Povzetek glavnih značilnosti zdravila Tibsovo 250 mg filmsko obložene tablete, februar 2026.

SKRAJŠAN POVZETEK GLAVNIH ZNAČILNOSTI ZDRAVILA Tibsovo 250 mg filmsko obložene tablete

▼ Za to zdravilo se izvaja dodatno spremljanje varnosti. Tako bodo hitreje na voljo nove informacije o njegovi varnosti. Zdravstvene delavce naprošamo, da poročajo o katerem koli domnevnem neželenem učinku zdravila.

SESTAVA*: Ena filmsko obložena tableta vsebuje 250 mg ivosideniba. **TERAPEVTSKE INDIKACIJE*:** V kombinaciji z azacitidinom za zdravljenje odraslih bolnikov z novoodkrito akutno mieloično levkemijo (AML) s prisotno mutacijo izocitrat dehidrogenaze-1 (IDH1) R132, ki niso primerni za standardno indukcijsko kemoterapijo. V monoterapiji za zdravljenje odraslih bolnikov z lokalno napredovalim ali metastatskim holangiokarcinomom (CCA) s prisotno mutacijo IDH1 R132, ki so bili predhodno zdravljeni z vsaj eno predhodno linijo sistemske terapije. **ODMERJANJE IN NAČIN UPORABE***: Zdravljenje je treba začeti pod nadzorom zdravnika, ki ima izkušnje z uporabo zdravil za zdravljenje raka. Bolniki morajo imeti pred začetkom jemanja zdravila Tibsovo z ustreznim diagnostičnim testom potrjeno mutacijo IDH1 R132. Pred uvedbo zdravljenja in med zdravljenjem je treba posneti EKG in oceniti celotno krvno sliko in biokemijske izvide krvi. Interval QT, popravljen glede na srčni utrip (QTc), mora biti pred uvedbo zdravljenja manj kot 450 ms. Priporočeni odmerek pri AML: 500 mg ivosideniba (2 x 250-mg tableta) peroralno enkrat na dan enkrat dnevno na 1. do 28. dan vsakega cikla. Ivosidenib je treba začeti na 1. dan 1. cikla zdravljenja v kombinaciji z azacitidinom v odmerku 75 mg/m^2 telesne površine, intravensko ali subkutano, enkrat dnevno na 1. do 7. dan vsakega 28dnevnega cikla. Priporočljivo je, da bolniki prejmejo vsaj 6 ciklov zdravljenja. Priporočeni odmerek pri holangiokarcinomu: 500 mg ivosideniba (2 x 250-mg tableta) peroralno enkrat na dan. Bolniki 2 uri pred in še 1 uro po jemanju tablet ne smejo uživati hrane. Priporočene so prilagoditve odmerka pri sočasni uporabi z zmernimi ali močnimi zaviralci CYP3A4 in za obvladovanje diferenciacijskega sindroma, levkocitoze, podaljšanja intervala QTc ter neželenih učinkov 3. ali višje stopnje. **KONTRAINDIKACIJE*:** Preobčutljivost na učinkovino ali katero koli pomožno snov, sočasna uporaba z močnimi induktorji CYP3A4 ali dagibatranom (glejte Interakcije), prirojeni sindrom podaljšanega intervala QT, nenadna smrt ali polimorfna ventrikularna aritmija v družinski anamnezi, interval QT/QTc > 500 ms ne glede na metodo popravka. **OPOZORILA*:** Sindrom diferenciacije pri bolnikih z AML: Brez zdravljenja je sindrom diferenciacije lahko življenje ogrožajoč ali smrten. Bolniki morajo biti obveščeni o znakih in simptomih sindroma diferenciacije. Treba jim je svetovati, naj se ob pojavu le-teh takoj posvetujejo z zdravnikom ter naj imajo vedno pri sebi opozorilno kartico za bolnika. Prekinite zdravljenje z zdravilom Tibsovo, če hudi znaki/simptomi vztrajajo več kot 48 ur po uvedbi sistemskih kortikosteroidov. Podaljšanje intervala QTc: Nepravilnosti je treba obravnavati takoj. V primeru značilne simptomatike je treba posneti EKG, kot je to klinično indicirano. V primeru hudega bruhanja in/ali driske je treba oceniti nepravilnosti serumskih elektrolitov. Bolnike je treba obvestiti o tveganju za podaljšanje intervala QT, njegovih znakih in simptomih (palpitacije, omotica, sinkopa ali celo srčni zastoj) in jim svetovati da takoj obvestijo zdravnika, če se ti pojavijo. Pri zdravljenju bolnikov je potrebna previdnost in pozorno spremljanje glede podaljšanja intervala QTc, če ni mogoča uporaba drugega ustreznega zdravljenja namesto zdravil, za katera je znano, da podaljšajo interval QTc, ali zmernih oz. močnih zaviralcev CYP3A4. Pozorno je treba spremljati bolnike s kongestivnim srčnim popuščanjem, elektrolitskimi motnjami oz. če je za obvladovanje znakov/simptomov sindroma diferenciacije klinično indicirano dajanje furosemida. Zdravljenje je treba dokončno ukiniti, če bolniki razvijejo podaljšanje intervala QTc z znaki ali simptomi življenje ogrožajoče aritmije. Ivosidenib je treba pri bolnikih, ki imajo znižane vrednosti albumina oz. imajo majhno telesno maso, uporabljati s previdnostjo. Huda ledvična okvara: previdnost pri uporabi in skrbno spremljanje. Jetrna okvara: zdravilo je treba uporabljati previdno pri bolnikih z zmerno in s hudo jetrno okvaro (Child-Pugh razreda B in C) in to skupino bolnikov je treba skrbno spremljati. Zdravilo Tibsovo je treba pri bolnikih z blago jetrno okvaro uporabljati previdno (Child-Pugh razred A). Pomožne snovi: vsebuje laktozo in natrij (v bistvu ‚brez natrija'). **INTERAKCIJE*:** Kontraindicirano: močni induktorji encima CYP3A4; dabigatran. Ni priporočljivo: zmerni ali močni zaviralci CYP3A4; zdravila, za katera je znano, da podaljšujejo interval QTc; substrati OAT3 ali OATP1B1/1B3; substrati CYP3A4, CYP2B6, CYP2C8 ali CYP2C9 z ozkim terapevtskim indeksom, ali substrati CYP2C19; itrakonazol ali ketokonazol; substrati UGT. Previdnostni ukrepi: hormonski kontraceptivi. **PLODNOST*. NOSEČNOST*:** Uporaba ni priporočljiva. **DOJENJE*:** Med zdravljenjem in še vsaj 1 mesec po zadnjem odmerku je treba prenehati z dojenjem. **KONTRACEPCIJA*: Ženske v rodni dobi morajo pred začetkom zdravljenja z zdravilom Tibsovo opraviti test nosečnosti ter se morajo med zdravljenjem izogibati zanositvi.** Med zdravljenjem in še vsaj 1 mesec po zadnjem odmerku je treba uporabljati učinkovito kontracepcijo. **VPLIV NA SPOSOBNOST VOŽNJE IN UPRAVLJANJA STROJEV*:** Blag vpliv. Utrujenost in omotico je treba upoštevati pri oceni bolnikove sposobnosti vožnje in upravljanja strojev. **NEŽELENI UČINKI*: Pri AML:** Zelo pogosti: sindrom diferenciacije, levkocitoza, trombocitopenija, nevtropenija, nespečnost, glavobol, omotica, bruhanje, bolečina v okončinah, artralgija, bolečina v hrbtu, podaljšanje intervala QT. Pogosti: levkopenija, periferna nevropatija, orofaringealna bolečina. **Pri CCA:** Zelo pogosti: anemija, zmanjšan apetit, periferna nevropatija, glavobol, ascites, diareja, bruhanje, navzea, bolečina v trebuhu, izpuščaj, utrujenost, zvišanje aspartat aminotransferaze, zvišanje bilirubina. Pogosti: holestatična zlatenica, hiperbilirubinemija, padec, podaljšanje intervala QT, zvišanje alanin aminotransferaze, zmanjšanje števila belih krvnih celic, zmanjšanje števila trombocitov. **PREVELIKO ODMERJANJE*:** Ni na voljo specifičnega antidota. Bolnike je treba skrbno spremljati in jim zagotoviti ustrezno podporno nego. **FARMAKODINAMIČNE LASTNOSTI*:** Ivosidenib je zaviralec mutiranega encima IDH1. Mutirana oblika IDH1 pretvarja alfa-ketoglutarat (α-KG) v 2-hidroksiglutarat (2-HG), ki blokira celično diferenciacijo in spodbuja tumorigenezo tako pri hematoloških kot pri nehematoloških malignih boleznih. Mehanizem delovanja ivosideniba pri posameznih indikacijah še ni povsem pojasnjen, razen sposobnosti zaviranja 2-HG in obnavljanja celične diferenciacije. **PAKIRANJE*:** Pakiranje vsebuje 60 filmsko obloženih tablet. **NAČIN PREDPISOVANJA IN IZDAJE ZDRAVILA: Rp/Spec - Predpisovanje in izdaja zdravila je le na recept zdravnika specialista ustreznega področja medicine ali od njega pooblaščenega zdravnika. DATUM ZADNJE REVIZIJE BESEDILA: 24. 02. 2026. Imetnik dovoljenja za promet:** Les Laboratoires Servier, 50, rue Carnot, 92284 Suresnes cedex, Francija. ***Pred predpisovanjem preberite celoten povzetek glavnih značilnosti zdravila. Celoten povzetek glavnih značilnosti zdravila in podrobnejše informacije so na voljo pri: Servier Pharma d.o.o., Podmilščakova ulica 24, 1000 Ljubljana, www.servier.si.**

Zdravilo je na slovenskem trgu na voljo v tuji ovojnini. Navodilo za uporabo v slovenskem jeziku je priloženo ovojnini skupaj z opozorilno kartico za bolnika. Opozorilna kartica je namenjena bolnikom z AML, ki jim je bilo predpisano zdravilo Tibsovo, da zagotovi dodatne informacije glede pomembnega ugotovljenega tveganja sindroma diferenciacije (objavljena je tudi na spletni strani JAZMP: http://www.jazmp.si/dokumenti/). Informacije o zdravilu v slovenskem jeziku so dostopne na uradni spletni strani www.cbz.si.

▼TIBSOVO®
250 mg filmsko obložene tablete
(ivosidenib)

SERVIER
moved by you

TIB CCA AD C2 2025-26 Samo za strokovno javnost.
Datum priprave informacije: marec 2026.

Instructions for authors

The editorial policy

Radiology and Oncology is an international, peer-reviewed, open access, multidisciplinary journal publishing original scientific and review articles in radiology, oncology and related biomedical fields.

The journal covers diagnostic and interventional radiology, oncologic imaging, nuclear medicine, radiotherapy, clinical oncology, experimental oncology, radiobiology, medical physics, radiation protection and related translational research. Manuscripts addressing broader scientific, clinical or methodological topics relevant to radiology, oncology and cancer research may also be considered, provided that they fall within the journal's scope.

Radiology and Oncology welcomes submissions from authors worldwide and aims to promote the international exchange of scientifically sound, ethically conducted and clinically or translationally relevant research. The journal publishes original scientific articles and review articles. Case reports are not accepted.

Submitted manuscripts must be original, must not have been published previously and must not be under consideration for publication elsewhere. Authors are responsible for the accuracy, integrity and ethical compliance of the submitted work. Accepted and published articles may be reused only in accordance with the applicable Creative Commons licence and proper citation requirements.

Submission of the manuscript

Manuscripts must be submitted through the journal's online submission system, Editorial Manager, available through the journal website: https://www.radioloncol.com. Manuscripts must be written in English and prepared in accordance with these Instructions for Authors. Use of the journal manuscript template is strongly recommended at initial submission. Where applicable, submissions must also include alternative text (alt text) for all figures, charts, diagrams, images and other non-text elements, as described below.

In case of technical problems with the online submission system, please contact Sašo Trupej at *saso.trupej@computing.si*. For editorial questions, please contact the Editor at *gsersa@onko-i.si*.

Submitted manuscripts undergo initial editorial screening for completeness, suitability for the journal's aims and scope, adherence to ethical requirements and compliance with the journal's basic submission requirements. Manuscripts that are incomplete, outside the scope of the journal or not compliant with the journal's requirements may be returned to the authors for correction or declined without external peer review.

Manuscripts considered suitable for peer review are sent to independent expert reviewers. Radiology and Oncology uses a single-blind peer review model: reviewers know the identities of the authors, while reviewer identities are not disclosed to the authors. Authors are asked to suggest 3–4 potential reviewers in the cover letter; however, these suggestions are not binding, and the final selection of reviewers is the editor's responsibility.

Based on the reviewers' comments and the editor's assessment, the editorial decision may be to request revisions, accept the submission or decline the submission. The editorial board may request scientific, structural, language, grammatical or stylistic revisions when necessary. There are no separate submission or peer-review charges. Article processing/publication charges are described below.

Before production of the accepted article, authors will be asked to submit the final version of the manuscript using the journal template and fully compliant with these Instructions for Authors. This includes correct document structure, complete figure captions, properly formatted tables, alternative text for all non-text elements and references formatted according to the journal's required style, including DOI or PMID where available.

All accepted articles are subject to a publication fee of 1500 EUR plus VAT. Exceptionally, a waiver or reduction of the publication fee may be negotiated with the editorial office at the time of manuscript submission.

Manuscripts submitted by multiple authors are reviewed on the assumption that all listed authors meet the journal's authorship requirements, approve the submitted manuscript, agree to its submission and are accountable for the integrity and accuracy of the work. The corresponding author is responsible for communication with the journal and for keeping all co-authors informed throughout the submission, review and production process.

Open access policy

Articles are published online as open access on the journal website and on the reference-global.com platform: https://reference-global.com/journal/RAON. Published articles are also permanently archived in the Digital Repository of Slovenian Research Organizations (DiRROS): https://dirros.openscience.si/ and in the Digital Library of Slovenia (dLib.si): https://www.dlib.si/.

Radiology and Oncology supports open access to research data. Authors are encouraged to make the data underlying their published article available in a recognized public, institutional or subject repository, unless restricted by ethical, legal, privacy, confidentiality or intellectual property considerations. Where data cannot be openly shared, authors should state the reason and describe any available controlled-access arrangements.

The journal may provide technical support for depositing research data in the DiRROS repository. Deposited data may receive a catalogue entry and a persistent DOI identifier. Authors retain the rights to their research data and should cite deposited datasets in the reference list, where applicable.

Preparation of manuscripts

Radiology and Oncology considers manuscripts prepared in accordance with the International Committee of Medical Journal Editors (ICMJE) Recommendations for the Conduct, Reporting, Editing and Publication of Scholarly Work in Medical Journals, which supersede the former "Uniform Requirements for Manuscripts Submitted to Biomedical Journals". Direct link: https://www.icmje.org/recommendations/.

Authors are encouraged to follow relevant reporting guidelines, where applicable, including CONSORT for randomized trials (https://www.consort-spirit.org/), PRISMA for systematic reviews and meta-analyses (https://www.prisma-statement.org/prisma-2020), STROBE for observational studies (https://www.strobe-statement.org/) and ARRIVE for animal research (https://arriveguidelines.org/arrive-guidelines).

The manuscript should be written in grammatically and stylistically correct English. Abbreviations should be avoided. If their use is necessary, they should be explained at the first time mentioned in the main text. The technical data should conform to the SI system. The manuscript, excluding the references, tables, figures and figure legends, must not exceed 5000 words. The total number of figures and tables is limited to 8. The text should be organized into the following sections: Introduction, Materials/Patients and Methods, Results, and Discussion with Conclusions. Exceptionally, the Results and Discussion sections may be combined. Each section should start on a new page, and all pages should be numbered consecutively using Arabic numerals. For ease of review, manuscripts should be submitted as single-column, 1.5 spacing with numbered lines. Use of the journal manuscript template is strongly recommended at initial submission. Manuscripts submitted without the template may still be considered for peer review if they meet the journal's basic submission requirements. After acceptance, authors may be required to submit a final version prepared in the journal template and fully compliant with these Instructions for Authors, including correct document structure, use of predefined styles, accessible tables, descriptive hyperlinks and alternative text for all non-text elements.

The manuscript template is available in Editorial Manager and on the Radiology and Oncology website under Submission Preparation Checklist and Paradigm website.

The Title page should include a concise and informative title, followed by the full name(s) of the author(s); the institutional affiliation of each author; the name and address of the corresponding author (including telephone number and institutional e-mail address), and an abbreviated title (not exceeding 60 characters).

The title page should be followed by an abstract page. The abstract should not exceed 250 words and should summarize the rationale for the study, the experimental or methodological approach, the major findings, including specific data where appropriate, and the principal conclusions. Structured abstracts are required. Abbreviations should be avoided in the abstract; if their use is unavoidable, they must be defined at first use within the abstract. Authors should provide 3–6 keywords for indexing purposes. Slovenian-speaking authors are requested to provide the title and abstract in Slovenian in a separate file.

The text of the research article should then proceed as follows:

- *Introduction* should summarize the rationale for the study or observation, cite only essential references, and clearly state the aim of the study.
- *Materials/Patients and methods* should provide sufficient information to allow the study or experiments to be repeated. New methods should be described in detail.
- *Results* should be presented clearly and concisely without repeating the data shown in figures and tables. Emphasis should be placed on clear and precise presentation of the results and their significance in relation to the aim of the investigation.
- *Discussion* should interpret the results rather than simply repeat them, explain their significance, and draw conclusions. It should discuss the results in the context of previously published work. Include Conclusions sub-section at the end of Discussion.

Charts, Illustrations, Images and Tables

Charts, illustrations, images and tables must be numbered consecutively and referred to in the text. The preferred location of each chart, illustration, image or table should be indicated in the manuscript.

Charts, illustrations and images submitted electronically must be of sufficient quality for publication. Illustrations and charts should preferably be prepared as vector graphics, created in CMYK colour space, using Century Gothic as the preferred font, and saved in .AI, .EPS or .PDF format. Images should be at least 2,000 pixels on the longer side and saved in .TIF format at maximum quality. Colour charts, illustrations and images are encouraged and are published without additional charge.

Figures, charts and diagrams should not rely on colour alone to convey information. Where relevant, authors should use labels, symbols, patterns or other visual distinctions in addition to colour.

Any information that could identify a patient must be removed or masked in images, unless written informed consent for publication has been obtained.

Tables should be typed double-spaced, with a descriptive title. Where appropriate, units of measurement should be included in column headings. Tables should be submitted as editable text and not as images. Use the table style provided in the manuscript template and ensure the header row is marked as a repeating header row (Table → Row → Repeat as header in Word), not just formatted to look like one. Tables should include clearly identifiable header rows and should avoid merged or split cells where possible.

Figures and tables may be uploaded as separate files.

Alternative text

Alternative text (alt text) allows readers using screen readers, or those who cannot otherwise see a figure, to understand what it shows. As the author, you know your figures best, so this description should come from you rather than the editorial team. This is required as part of our publisher's accessibility policy.

For accessibility, all figures, charts, diagrams, images and other non-text elements should be accompanied by alternative text (alt text). Alt text should briefly describe the essential visual information needed to understand the figure in the context of the manuscript. It should not simply repeat the figure caption and should not begin with phrases such as "image of" or "picture of". If the figure is fully described in the caption or in the main text, the alt text may state "See caption" or "See main text". For complex figures, charts or diagrams, authors should also provide a longer description where short alt text isn't sufficient.

This requirement applies to manuscripts submitted from 1 September 2026. Submit alt text together with your manuscript, in the figure list or manuscript template, alongside the figure number, caption, and (where needed) long description. Authors whose manuscripts are currently under review and are subsequently accepted will also be asked to provide alt text for their figures before publication.

Abbreviations

All non-standard abbreviations used in the manuscript should be listed alphabetically in a table titled 'Abbreviations', placed at the end of the main text, before the reference list. Each entry should give the abbreviation followed by its full term.

References

References must be numbered consecutively in the order in which they first appear in the text. Reference numbers should be cited in the text as superscript Arabic numerals.[1-4]

Authors are responsible for the accuracy and completeness of their references.

References to the Abstracts and Letters to the Editor must be identified as such. Papers in preparation, manuscripts submitted for publication, unpublished observations and personal communications should not be included in the reference list. If essential, such information may be cited in the appropriate place in the text.

References should follow Vancouver/NLM style (Index Medicus). DOI numbers should be included where available. PMID may be included when a DOI is not available.

All authors should be listed when there are six or fewer authors. When there are seven or more authors, list the first six authors followed by "et al.".

For websites, online guidelines, legal documents and other non-journal sources, references should include the responsible author or organization, title, indication that the source is available online, year or date of publication or update where available, date accessed, and URL.

Examples of references for journal articles[1,2], books[3] and book chapters[4] are provided below:

Jesenko T, Omerzel M, Heller LC, Cemazar M. Between defence and delivery: the DNA sensing response to gene electrotransfer. *Radiol Oncol* 2025; **59:** 467-76. doi: 10.2478/raon-2025-0063

Markovic G, Resnik N, Janev A, Zupancic D, Grubelnik G, Debeljak M, et al. The role of focal adhesion kinase in bladder cancer: translation from in vitro to ex vivo human urothelial carcinomas. *Radiol Oncol* 2025; **59:** 349-67. doi: 10.2478/raon-2025-0052

Hall EJ, Giaccia AJ. *Radiobiology for the radiologist*. 8th ed. Philadelphia: Wolters Kluwer; 2019.

Hall EJ, Giaccia AJ. Cancer biology. In: Pecarich Lauren, editor. *Radiobiology for the radiologist*. Philadelphia: Wolters Kluwer; 2019. p. 274-309.

Authorization for the use of human participants or experimental animals

When reporting research involving human participants, human biological material or identifiable human data, authors must state that the study was conducted in accordance with the principles of the Declaration of Helsinki: https://www.wma.net/policies-post/wma-declaration-of-helsinki/.

The manuscript must include the name of the approving ethics committee or institutional review board, the approval number where available, and a statement confirming that informed consent was obtained where required. Clinical trials must include the clinical trial registration number.

Patient privacy must be protected. Identifying information, including names, initials, hospital numbers, images or other details that could identify a patient, must not be published unless scientifically necessary and unless written informed consent for publication has been obtained.

Retrospective clinical studies must be approved by an accredited institutional review board, committee for medical ethics or other equivalent body, unless formal exemption has been granted. These statements should appear in the Materials and Methods section.

Research involving animals must be conducted in accordance with applicable national and institutional regulations and with Directive 2010/63/EU on the protection of animals used for scientific purposes: https://eur-lex.europa.eu/eli/dir/2010/63/oj/eng.

Authors must state the name of the committee approving the animal experiments and confirm that all experiments were performed in accordance with relevant regulations. Measures taken to minimize animal suffering and reduce the number of animals used should be described where appropriate.

These statements should appear in the Materials and Methods section or, for contributions without this section, within the main text or in the captions of relevant figures or tables.

License to Publish and Copyright

For publication of accepted articles, authors are required to complete and submit the journal's License to Publish. A properly completed License to Publish, signed by the corresponding author on behalf of all authors, must be submitted as one scanned file by e-mail to gsersa@onko-i.si for each accepted manuscript.

Authors who publish with Radiology and Oncology retain the copyright to their published articles and agree to make their work available under the applicable Creative Commons licence.

Since Issue 4, 2022, articles published in Radiology and Oncology have been distributed under the terms of the Creative Commons Attribution 4.0 International License (CC BY 4.0). Under this licence, users are permitted to copy, share, distribute, reproduce, adapt and build upon the published work in any medium or format, including for commercial purposes, provided that appropriate credit is given to the original author(s), the original publication in Radiology and Oncology is cited, a link to the licence is provided, and any changes made are indicated.

Reuse of the published work must comply with the terms of the CC BY 4.0 licence. Any reuse, adaptation or redistribution must be properly attributed and must not be presented as approved by the author(s), the journal or the publisher. Users must not add legal or technical restrictions that would prevent others from using the work under the same licence terms.

Further information on the CC BY 4.0 licence is available here:

https://creativecommons.org/licenses/by/4.0/.

For articles published before Issue 4, 2022, the applicable licence and copyright terms should be confirmed from the individual published article, issue, archive record or publishing agreement applicable at the time of publication.

Conflict of interest

Authors must disclose all real, potential or perceived conflicts of interest that could influence, or be perceived to influence, the submitted work. Conflicts of interest include financial and non-financial relationships, including employment, consultancies, stock ownership, honoraria, patents, grants, personal relationships, academic competition or institutional affiliations.

The conflict-of-interest statement must be included in the manuscript and/or cover letter. If there are no conflicts of interest, this should be stated explicitly. Authors may use the ICMJE Disclosure of Interest form: https://icmje.org/disclosure-of-interest/. Editors and reviewers must decline handling or reviewing a manuscript if a conflict of interest prevents an objective assessment.

Funding

Authors must disclose all sources of financial support for the reported work, including grant numbers and the names of funding bodies. This information must appear in a separate statement titled 'Funding', placed before the Acknowledgments section. If no external funding was received, authors should state: 'This research received no external funding.'

Use and disclosure of AI and AI-assisted technologies in scientific writing

When authors use artificial intelligence (AI) and AI-assisted technologies in the writing process, the following principles apply:

AI and AI-assisted technologies may be used to improve readability and language. They must not replace the authors' primary responsibility for scientific reasoning, data analysis, interpretation of data and drawing valid conclusions.

AI and AI-assisted technologies must be used under human supervision and control. Authors must carefully review and edit any AI-generated output, as such tools may produce content that appears authoritative but may be incorrect, incomplete, biased or misleading.

AI and AI-assisted technologies must not be listed as authors or co-authors and must not be cited as authors. Authorship carries responsibilities and accountability that can only be attributed to humans.

Authors must disclose the use of AI and AI-assisted technologies in the manuscript, as described below. An appropriate disclosure statement should appear in the published paper. Authors remain fully responsible and accountable for the accuracy, integrity and originality of the content of the manuscript.

Disclosure notes:

Authors must disclose the use of AI and AI-assisted technologies in the writing process by adding a statement to the main manuscript file at the time of submission. The statement should be placed at the end of the manuscript, before the reference list, in a separate section titled 'AI Use Statement'.

This disclosure requirement does not apply to the use of basic tools for checking grammar, spelling, formatting or references; however, the use of AI or AI-assisted technologies for generating, rewriting, summarizing, translating or substantially editing manuscript text must be disclosed.

Suggested statement:

"During the preparation of this manuscript, the author(s) used [NAME TOOL / SERVICE] for [PURPOSE]. After using this tool/service, the author(s) reviewed and edited the content as necessary and take full responsibility for the content of the manuscript."

Page proofs

Page proofs will be sent by e-mail to the corresponding author. The corresponding author is responsible for checking the proofs carefully and returning a list of essential corrections to the editorial office **within three business days of receipt**.

Only essential corrections of typographical, grammatical or production errors are permitted at this stage. Substantive changes to the manuscript are not allowed after acceptance unless specifically approved by the editor.

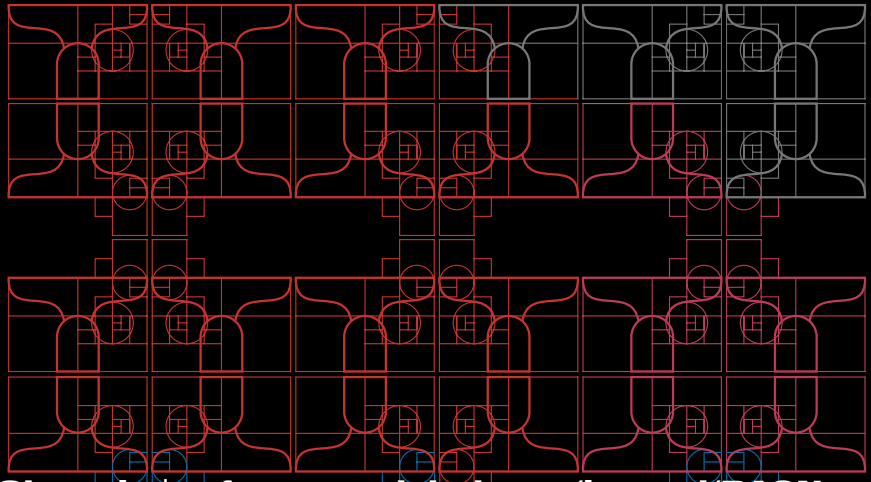

Radiology and Oncology | Ljubljana | Slovenia | reference-global.com/journal/RAON

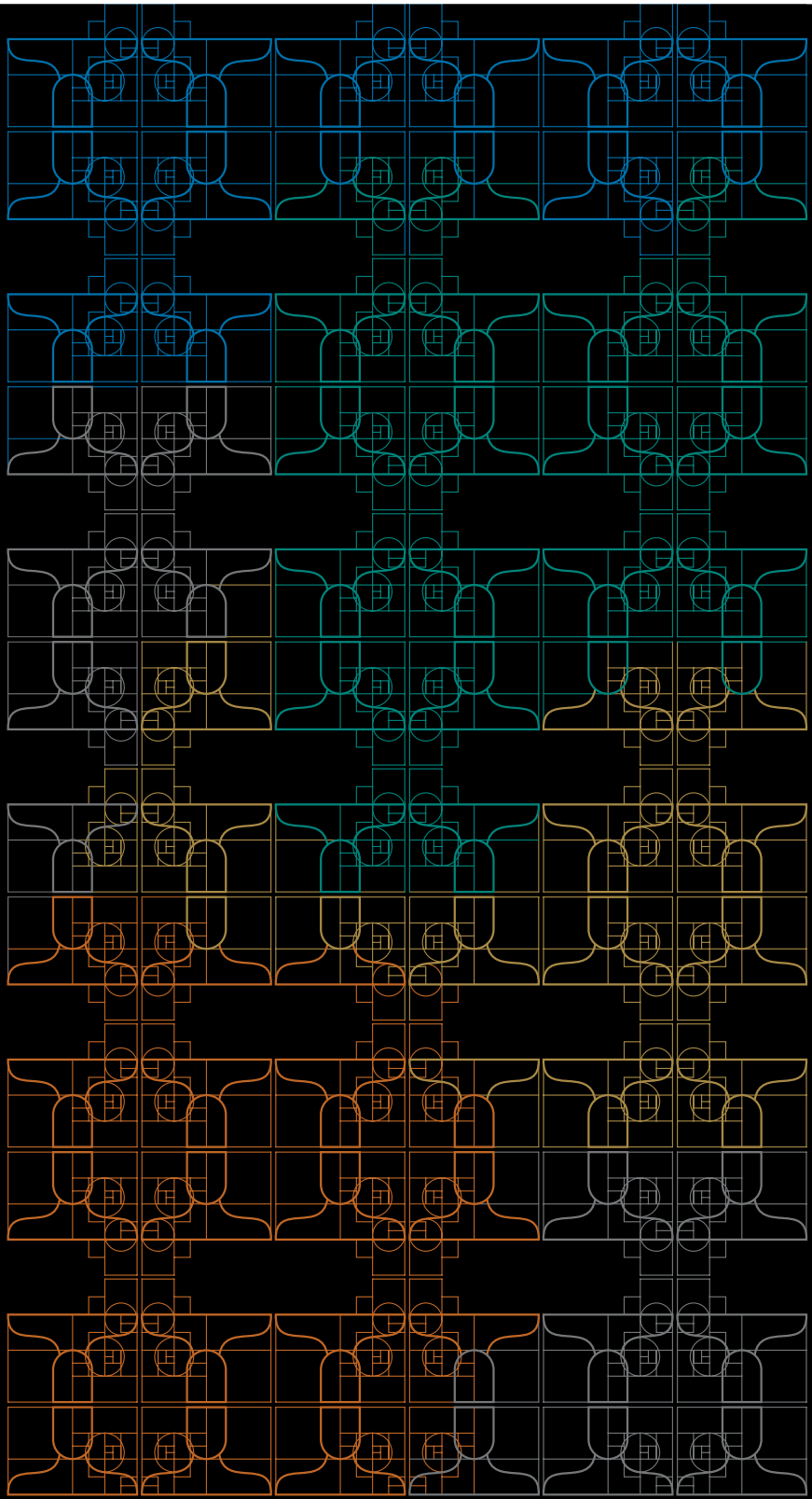

ISSN 1318 - 2099